ASSESSING MICROGLIAL FUNCTION AND IDENTITY

EDITED BY: Rosa Chiara Paolicelli and Amanda Sierra
PUBLISHED IN: Frontiers in Immunology, Frontiers in Neurology and Frontiers in Molecular Neuroscience

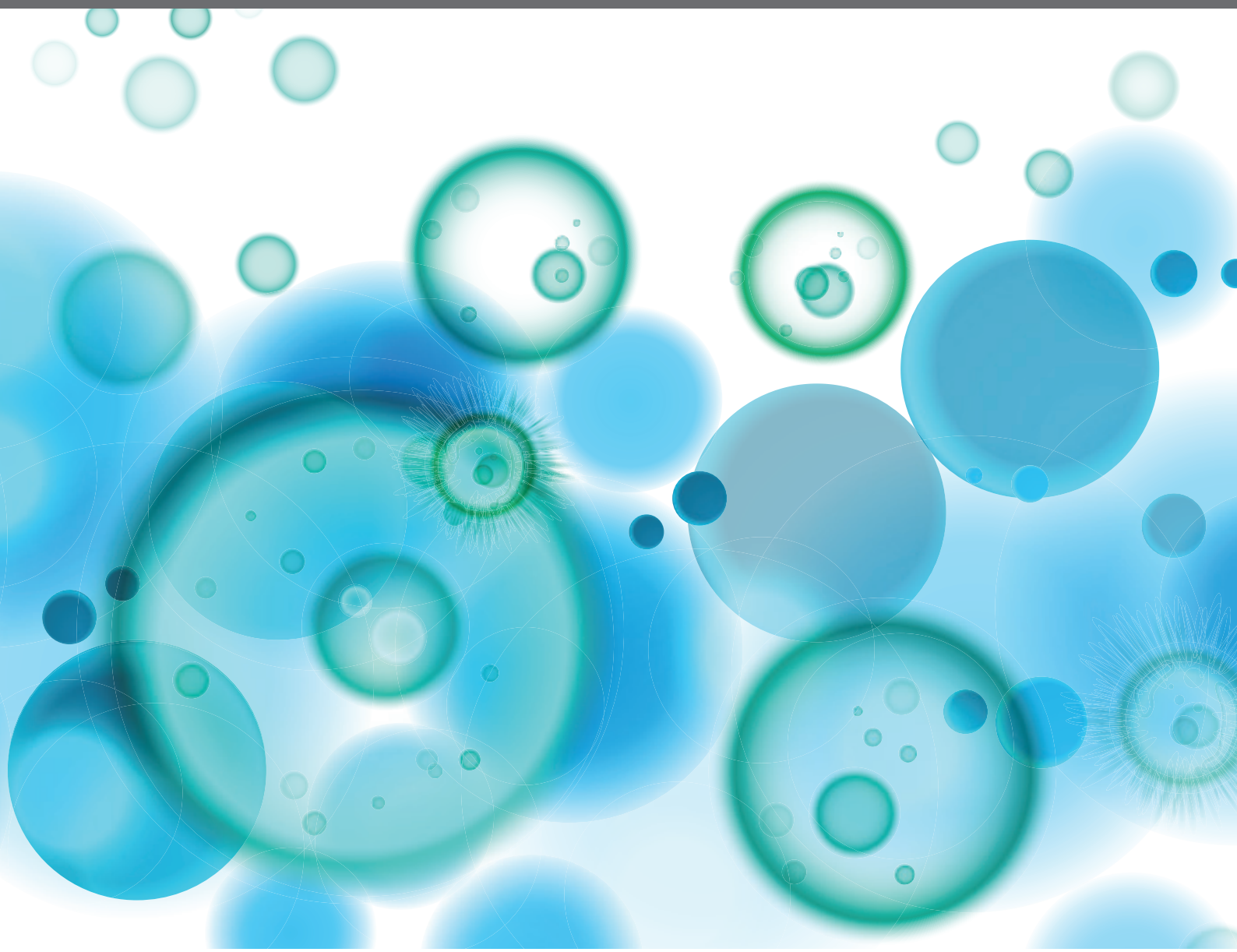

frontiers Research Topics

ISSN 1664-8714
ISBN 978-2-88974-291-2
DOI 10.3389/978-2-88974-291-2

About Frontiers

Frontiers is more than just an open-access publisher of scholarly articles: it is a pioneering approach to the world of academia, radically improving the way scholarly research is managed. The grand vision of Frontiers is a world where all people have an equal opportunity to seek, share and generate knowledge. Frontiers provides immediate and permanent online open access to all its publications, but this alone is not enough to realize our grand goals.

Frontiers Journal Series

The Frontiers Journal Series is a multi-tier and interdisciplinary set of open-access, online journals, promising a paradigm shift from the current review, selection and dissemination processes in academic publishing. All Frontiers journals are driven by researchers for researchers; therefore, they constitute a service to the scholarly community. At the same time, the Frontiers Journal Series operates on a revolutionary invention, the tiered publishing system, initially addressing specific communities of scholars, and gradually climbing up to broader public understanding, thus serving the interests of the lay society, too.

Dedication to Quality

Each Frontiers article is a landmark of the highest quality, thanks to genuinely collaborative interactions between authors and review editors, who include some of the world's best academicians. Research must be certified by peers before entering a stream of knowledge that may eventually reach the public - and shape society; therefore, Frontiers only applies the most rigorous and unbiased reviews.
Frontiers revolutionizes research publishing by freely delivering the most outstanding research, evaluated with no bias from both the academic and social point of view. By applying the most advanced information technologies, Frontiers is catapulting scholarly publishing into a new generation.

What are Frontiers Research Topics?

Frontiers Research Topics are very popular trademarks of the Frontiers Journals Series: they are collections of at least ten articles, all centered on a particular subject. With their unique mix of varied contributions from Original Research to Review Articles, Frontiers Research Topics unify the most influential researchers, the latest key findings and historical advances in a hot research area! Find out more on how to host your own Frontiers Research Topic or contribute to one as an author by contacting the Frontiers Editorial Office: frontiersin.org/about/contact

ASSESSING MICROGLIAL FUNCTION AND IDENTITY

Topic Editors:
Rosa Chiara Paolicelli, University of Lausanne, Switzerland
Amanda Sierra, Achucarro Basque Center for Neuroscience, Spain

Citation: Paolicelli, R. C., Sierra, A., eds. (2022). Assessing Microglial Function and Identity. Lausanne: Frontiers Media SA. doi: 10.3389/978-2-88974-291-2

Table of Contents

frontiers in Immunology

EDITORIAL
published: 20 December 2021
doi: 10.3389/fimmu.2021.824866

Editorial: Assessing Microglial Function and Identity

Amanda Sierra[1,2,3*] *and Rosa Chiara Paolicelli*[4*]

[1] Achucarro Basque Center for Neuroscience, Glial Cell Biology Lab, Leioa, Spain, [2] Department of Neuroscience, University of the Basque Country EHU/UPV, Leioa, Spain, [3] Ikerbasque Foundation, Bilbao, Spain, [4] Department of Biomedical Sciences, University of Lausanne, Lausanne, Switzerland

Keywords: microglia, methods, central nervous system (CNS), disease, neuroimmunology and neuropathology

Editorial on the Research Topic

Assessing Microglial Function and Identity

Microglia are the immune cells of the central nervous system. They are, however, a unique type of macrophage, as they arise from primitive myeloid progenitors in the embryonic yolk sac and do not repopulate from bone marrow-derived monocytes (1–3). In addition, they are instructed by brain activity and their highly motile processes contact all elements of the brain parenchyma (4–6). Over the past decades, a number of novel functions besides their classical immunological roles have been discovered, underscoring the importance of these cells in health and disease (7).

The field of microglia research is evolving at a rapid pace due to the equally fast development of both *in vitro* and *in vivo* methods and methodologies to label, visualize, and manipulate them. These tools include novel antibodies, viral vectors and transgenic mice specifically targeting microglia in invertebrate, rodent and primate models, as well as imaging tools for longitudinal analysis in humans. Validation of *in vitro* models of human microglia, including cells generated from induced pluripotent stem cells and organoids, will also push the field towards translational applications. Another important front is the development of drugs and nanomaterials that allow the selective manipulation of specific microglial functions. Finally, computational and modeling approaches, alongside with integrative –omics (epigenetic, transcriptomic, proteomic, and metabolomic) will come to maturity and help us understand the impact of microglia in brain physiology.

In this Research Topic we have collected 15 manuscripts, including original papers as well as literature reviews, that discuss the major methods currently available to investigate different aspects of microglial biology. These papers focus on methods to culture mouse and human microglia (Hernández et al., Hedegaard et al., Reich et al.) and to study microglia *in vivo* using live imaging tools (Eme-Scolan and Dando, Andoh and Koyama). Another set of papers pay attention to the microglial state characterized by transcriptomic and proteomic studies (Hsiao et al., Glasnović et al. , Miedema et al., Alsema et al.). Finally, a series of papers deal with microglial biology, including the study of autophagy (Plaza-Zabala et al.); and microglial function, including their role in synapse remodeling (Brioschi et al., Morini et al.) and as therapeutic targets in disease (Chen et al., Liu et al., Aires et al.).

In vitro and *ex vivo* methods are essential for investigating specific aspects and properties of microglial biology. Hernández et al. describe a novel protocol for inducing microglial reactivity to protein extract of injured rat spinal cord, and provide a comprehensive characterization, including morphology, phagocytic capacity and cytokine profile. Major efforts have been recently put into the development of human-induced Pluripotent Stem Cell (hiPSC) models to derive microglia from

OPEN ACCESS

Edited and reviewed by:
Robert Weissert,
University of Regensburg, Germany

***Correspondence:**
Amanda Sierra
amanda.sierra@ehu.eus
Rosa Chiara Paolicelli
rosachiara.paolicelli@unil.ch

Specialty section:
This article was submitted to Multiple Sclerosis and Neuroimmunology, a section of the journal Frontiers in Immunology

Received: *29 November 2021*
Accepted: *30 November 2021*
Published: *20 December 2021*

Citation:
Sierra A and Paolicelli RC (2021) Editorial: Assessing Microglial Function and Identity. Front. Immunol. 12:824866. doi: 10.3389/fimmu.2021.824866

patients. The relevance of such models for investigating human diseases is unquestioned; however, the establishment of related protocols and functional assays is often challenged by reproducibility and scalability issues. Hedegaard et al. review the current methods available to generate hiPSC-derived microglia and discuss areas for improvement, advantages and limitations. By establishing a new type of hiPSC-derived microglia, Reich et al. investigate the regulatory role of TREM2, and provide a detailed characterization of the functional microglial properties affected by TREM2 loss of function.

Microglia are extremely sensitive to external stimuli and able to rapidly change their state in response to perturbations in the brain environment. This remarkable ability of microglia calls for the need of developing more and more advanced techniques and tools for studying them *in situ*, and catching their dynamic behavior. Eme-Scolan and Dando provide an overview on the current tools and approaches for studying microglia *in vivo*, highlighting advantages and limitations. In detail, Andoh and Koyama review different experimental systems available for live imaging and discuss some of the molecular mechanisms underlying microglial dynamics.

Insights into relevant molecular pathways regulating microglial states are provided in two distinct reviews, which systematically analyze publicly available transcriptomic data, to discuss the role of G-protein-coupled-receptors (GPCRs) and the RANKL/RANK/OPG (RRO) axis (Hsiao et al., and Glasnović et al., respectively). Both works highlight the therapeutic potential of these signaling pathways for targeting microglial dysfunction in brain disease. A number of studies in this collection examine the emerging roles of microglia in pathology, discussing the microglial profile, by complementary angles, in a variety of neurodegenerative disorders. Miedema et al. highlight the importance of microglial heterogeneity, reviewing high-resolution transcriptomic and proteomic approaches to assess microglia in multiple sclerosis. Using acute human *post-mortem* brain samples, Alsema et al. investigate the microglial transcriptome of Alzheimer's disease (AD) and non-demented (ND) elderly, reporting a core similarity between AD and ND donors.

Understanding microglial physiology is essential to appraise their role from development to aging and disease. One key process is autophagy, which is in charge or recycling intracellular organelles. Plaza-Zabala et al. propose a two-step model to assess autophagy in microglia, and offer a detailed method to determine autophagosome formation, degradation and net turnover, which will help understand the role of autophagy in healthy and diseased microglia. Microglia-mediated synapse elimination has received growing attention in the last years, both in physiological and pathological contexts. Novel methodological approaches are continuously developed to meet the need for accurate investigation and quantification of this process. Brioschi et al. propose a novel technical approach for the assessment of synaptic engulfment by microglia, based on flow cytometry, and provide quantification of synapse engulfment in microglia acutely isolated from the developing mouse brain, and from the brain of mouse models of neurodegeneration. The current methods available to investigate microglial phagocytosis of neuronal and synaptic structures are extensively reviewed by Morini et al., who focus on critical developmental time windows, and discuss the implication of specific ligand-receptor crosstalk.

Further implications of microglia in the diseased brain are discussed by Chen et al., with a special focus on neuromyelitis optica (NMO), an autoantibody-triggered disease affecting the spinal cord and the optic nerve. Liu et al. examine the complex roles of microglia in intracerebral hemorrhage, revising the distinct phenotypes and dynamic profiles associated with functional responses upon the hemorrhagic event. Age-related impairments in microglial function are discussed by Aires et al., who provide evidence for CD22 blockage as a potential therapeutic approach for restoring microglial ramification and surveillance capacity, notably reduced in the ageing brain.

Taken all together, the manuscripts gathered in this Research Topic strongly emphasize the heterogeneity and complexity of microglia, and their multifaceted roles in the healthy and diseased CNS. These studies also highlight the undisputed importance of carefully reporting the spatial and temporal coordinates when describing microglial profiles and associated functions, to facilitate data integration and interpretation across studies.

In conclusion, we hope this collection of systematic reviews and original methods may serve as a reference for the field, and may promote a culture of exchange for synergistically improve the current techniques available to assess microglial identity and function.

AUTHOR CONTRIBUTIONS

AS and RCP both contributed to this editorial by resuming the results of all scientific manuscripts included in the Research Topic. All authors contributed to the article and approved the submitted version.

FUNDING

This work was supported by the Spanish Ministry of Science and Innovation CompetitivenessMCIN/AEI/10.13039/501100011033 (https://www.ciencia.gob.es/) and FEDER "A way to make Europe" (RTI2018-099267-B-I00 and RYC-2013-12817), a Tatiana Foundation Award (P-048-FTPGB 2018), and a Basque Government Department of Education project (PIBA 2020_1_0030;http://www.euskadi.eus/basque-government/department-education/) to AS; by grants from the Synapsis Foundation - Alzheimer Research Switzerland ARS, the Swiss National Science Foundation (SNSF 310030_197940) and the European Research Council (ERC StGrant REMIND 804949) to RCP.

REFERENCES

1. Ginhoux F, Greter M, Leboeuf M, Nandi S, See P, Gokhan S, et al. Fate Mapping Analysis Reveals That Adult Microglia Derive From Primitive Macrophages. *Science* (2010) 330:841–5. doi: 10.1126/science.1194637
2. Goldmann T, Wieghofer P, Müller PF, Wolf Y, Varol D, Yona S, et al. A New Type of Microglia Gene Targeting Shows TAK1 to be Pivotal in CNS Autoimmune Inflammation. *Nat Neurosci* (2013) 16:1618–26. doi: 10.1038/nn.3531
3. Yona S, Kim K-W, Wolf Y, Mildner A, Varol D, Breker M, et al. Fate Mapping Reveals Origins and Dynamics of Monocytes and Tissue Macrophages Under Homeostasis. *Immunity* (2013) 38:79–91. doi: 10.1016/j.immuni.2012.12.001
4. Davalos D, Grutzendler J, Yang G, Kim JV, Zuo Y, Jung S, et al. ATP Mediates Rapid Microglial Response to Local Brain Injury In Vivo. *Nat Neurosci* (2005) 8 (6):752–8. doi: 10.1038/nn1472
5. Nimmerjahn A, Kirchhoff F, Helmchen F. Resting Microglial Cells are Highly Dynamic Surveillants of Brain Parenchyma In Vivo. *Science* (2005) 308 (5726):1314–8. doi: 10.1126/science.1110647
6. Cserép C, Pósfai B, Lénárt N, Fekete R, László ZI, Lele Z, et al. Microglia Monitor and Protect Neuronal Function Through Specialized Somatic Purinergic Junctions. *Science* (2020) 367(6477):528–37. doi: 10.1126/science.aax6752
7. Sierra A, Paolicelli RC, Kettenmann H. Cien Años De Microglía: Milestones in a Century of Microglial Research. *Trends Neurosci* (2019) 42(11):778–92. doi: 10.1016/j.tins.2019.09.004

Conflict of Interest: The authors declare that the research was conducted in the absence of any commercial or financial relationships that could be construed as a potential conflict of interest.

frontiers in Molecular Neuroscience

ORIGINAL RESEARCH
published: 29 September 2020
doi: 10.3389/fnmol.2020.00149

Detection of Synaptic Proteins in Microglia by Flow Cytometry

*Simone Brioschi[1,2], Paolo d'Errico[3], Lukas S. Amann[1,4], Hana Janova[5], Sonja M. Wojcik[6], Melanie Meyer-Luehmann[3], Lawrence Rajendran[7], Peter Wieghofer[8], Rosa C. Paolicelli[7,9] and Knut Biber[1]**

[1]Faculty of Biology, University of Freiburg, Freiburg, Germany, [2]Department of Psychiatry, University of Freiburg Medical Center, Freiburg, Germany, [3]Department of Neurology, University of Freiburg Medical Center, Freiburg, Germany, [4]Institute of Neuropathology, University of Freiburg Medical Center, Freiburg, Germany, [5]Department of Clinical Neuroscience, Max Planck Institute of Experimental Medicine, Göttingen, Germany, [6]Department of Molecular Neurobiology, Max Planck Institute of Experimental Medicine, Göttingen, Germany, [7]Institute for Regenerative Medicine, University of Zürich, Zürich, Switzerland, [8]Institute of Anatomy, Leipzig University, Leipzig, Germany, [9]Department of Biomedical Sciences, University of Lausanne, Lausanne, Switzerland

A growing body of evidence indicates that microglia actively remove synapses *in vivo*, thereby playing a key role in synaptic refinement and modulation of brain connectivity. This phenomenon was mainly investigated in immunofluorescence staining and confocal microscopy. However, a quantification of synaptic material in microglia using these techniques is extremely time-consuming and labor-intensive. To address this issue, we aimed to quantify synaptic proteins in microglia using flow cytometry. With this approach, we first showed that microglia from the healthy adult mouse brain contain a detectable level of VGLUT1 protein. Next, we found more than two-fold increased VGLUT1 immunoreactivity in microglia from the developing brain (P15) as compared to adult microglia. These data indicate that microglia-mediated synaptic pruning mostly occurs during the brain developmental period. We then quantified the VGLUT1 staining in microglia in two transgenic models characterized by pathological microglia-mediated synaptic pruning. In the 5xFAD mouse model of Alzheimer's disease (AD) microglia exhibited a significant increase in VGLUT1 immunoreactivity before the onset of amyloid pathology. Moreover, conditional deletion of TDP-43 in microglia, which causes a hyper-phagocytic phenotype associated with synaptic loss, also resulted in increased VGLUT1 immunoreactivity within microglia. This work provides a quantitative assessment of synaptic proteins in microglia, under homeostasis, and in mouse models of disease.

Keywords: microglia, synaptic pruning, VGLUT1, 5xFAD model, TDP-43 conditional knock-out

OPEN ACCESS

Edited by:
Marie-Eve Tremblay,
University of Victoria, Canada

Reviewed by:
Zsuzsanna Callaerts-Vegh,
KU Leuven, Belgium
Tsuneya Ikezu,
Boston University, United States

****Correspondence:***
Knut Biber
knut.biber@abbvie.com

Received: *11 May 2020*
Accepted: *16 July 2020*
Published: *29 September 2020*

Citation:
Brioschi S, d'Errico P, Amann LS, Janova H, Wojcik SM, Meyer-Luehmann M, Rajendran L, Wieghofer P, Paolicelli RC and Biber K (2020) Detection of Synaptic Proteins in Microglia by Flow Cytometry. Front. Mol. Neurosci. 13:149. doi: 10.3389/fnmol.2020.00149

INTRODUCTION

Microglia originate through primitive hematopoiesis in the yolk sac and colonize the brain rudiment during embryonic development (Ginhoux et al., 2010; Schulz et al., 2012; Kierdorf et al., 2013). During the perinatal period, microglia acquire a highly ramified morphology and appear evenly distributed throughout the brain parenchyma (Ginhoux and Prinz, 2015). Microglia *in vivo* are extremely motile cells exhibiting continuous extension and retraction of their finely ramified processes, thus performing a ceaseless immunological surveillance of the surrounding

environment (Davalos et al., 2005; Nimmerjahn et al., 2005; Hanisch and Kettenmann, 2007). Moreover, microglia support the formation and consolidation of neural circuits in the developing brain (Parkhurst et al., 2013; Ueno et al., 2013; Squarzoni et al., 2014; Zhan et al., 2014; Miyamoto et al., 2016). Under homeostasis, microglia constantly interact with synaptic inputs (Wake et al., 2009; Tremblay et al., 2010), thus mediating a fine-tuning of the synaptic activity (Kettenmann et al., 2013). Importantly, during brain development microglia enact displacement/removal of synaptic inputs, thus actively contributing to synaptic pruning (Stevens et al., 2007; Paolicelli et al., 2011; Schafer et al., 2012; Filipello et al., 2018; Lehrman et al., 2018). Very recently, abnormal synaptic refinement by microglia was also reported in various mouse models of neurological disorders (Hong et al., 2016; Lui et al., 2016; Schafer et al., 2016; Vasek et al., 2016; Paolicelli et al., 2017; Shi et al., 2017; Di Liberto et al., 2018). A full elucidation of this mechanism will provide a deeper understanding of the dynamics of brain development, as well as of neurodevelopmental and neurodegenerative disorders (Neniskyte and Gross, 2017; Salter and Stevens, 2017). At present, further progress in this field of research is hampered by the lack of standardized techniques allowing an accurate estimation of synaptic material in microglia. To our knowledge, all the available data are essentially generated with microscopy-based approaches, such as confocal imaging and electron microscopy (EM; Schafer et al., 2012; Bisht et al., 2016; Sipe et al., 2016). Modern microscopy provides a qualitative appraisal of synaptic proteins inside of microglia, yet for a fast and unbiased quantification, microscopy-based techniques have some drawbacks. In particular, the spatial resolution of confocal microscopy may be insufficient to resolve microglial and synaptic structures when they are less than few hundreds of nanometers apart from each other (Weinhard et al., 2018). Given these technical limitations, the development of alternative approaches is currently in high demand (Sierra et al., 2013). In the present work, we used flow cytometry intracellular staining to quantify VGLUT1, which is a marker for glutamatergic synapses, in microglia acutely isolated from different mouse models. In flow cytometry, VGLUT1 immunoreactivity was detected in microglia, but not in other extra-parenchymal $CD45^{hi}$ brain macrophages. We then provided evidence that VGLUT1 is localized inside microglial cells and is not due merely to adhesion of synaptic proteins on the cell surface. Interestingly, significantly increased VGLUT1 immunoreactivity was found in microglia from juvenile mice (post-natal day 15) than in microglia from adult mice (12-week-old), supporting the hypothesis that synaptic pruning occurs primarily in brain development. Similarly, microglia from 2-month-old 5xFAD mice exhibited higher VGLUT1 staining compared to wild-type controls, indicating increased pruning of glutamatergic synapses at the early stages of amyloid pathology. Last, augmented VGLUT1 was also found in TDP43-deficient microglia, which was previously shown to exhibit an hyper-phagocytic phenotype (Paolicelli et al., 2017). By providing a quantitative assessment, our data consolidate previous evidence concerning the uptake of synaptic material by microglia in various mouse models of brain disease.

MATERIALS AND METHODS

Animals and Ethics

All animal experiments were performed with the permission of the local authorities of the Regional Council of Freiburg (Regierungspräsidium) and the animal welfare committee of the University of Freiburg, and with approval of the animal care and use committees of the Swiss Cantonal Veterinary Office. All mice used here (including wild-type, *Cx3cr1*$^{GFP/+}$, *Vglut1*$^{-/-}$, *5xTgFAD* and *Cx3cr1*$^{CreERT2/+}$;*Tardbp*$^{flox/flox}$) were bred on a C57BL/6J background and maintained under specific pathogen-free conditions, in a temperature- and humidity-controlled facility with a 12 h light-dark cycle. Food and water were available *ad libitum*. To minimize gender-dependent heterogeneity of amyloid pathology in *5xTgFAD* mice, males only were used. *5xTgFAD* and wild-type control mice were analyzed at the age of 2 months, therefore prior to the amyloid-plaques formation. For all the other experiments both genders were used, and mice were analyzed at the age of either 2 months or post-natal day 15 (P15). The generation and characterization of the *Vglut1* knock-out line used here were previously described (Wojcik et al., 2004). *Vglut1* knock-out mice and control wild-type littermates were analyzed at the age of P15–P17 because of the premature death owing to *Vglut1*-deficiency. To induce the recombination of the *Tardbp* floxed allele in microglia, *Cx3cr1*$^{CreERT2/+}$;*Tardbp*$^{flox/flox}$ mice (TDP-43 conditional knockout) underwent 5 i.p. injections 24 h apart of corn oil-dissolved Tamoxifen (1.5 mg/mouse/day; Sigma–Aldrich, Buchs, Switzerland). Tamoxifen treatment began at P30 and mice were sacrificed at P90. Importantly, the insertion of the *Cre* transgene downstream of the *Cx3cr1* promoter disrupts expression of the endogenous *Cx3cr1* gene. Given the risk of experimental bias due to the monoallelic expression of *Cx3cr1*, we used *Cx3cr1*$^{CreERT2/+}$;*Tardbp*$^{+/+}$ littermates as the wild-type control. The same tamoxifen treatment was applied on both *Cx3cr1*$^{CreERT2/+}$;*Tardbp*$^{flox/flox}$ and *Cx3cr1*$^{CreERT2/+}$;*Tardbp*$^{+/+}$ mice to normalize possible drug-related effects.

Immunofluorescence

Mice were deeply anesthetized through intraperitoneal (i.p.) injection of ketamine hydrochloride (Ketavet, Pfizer; dosage 300 mg/kg body weight) and xylazine (Rompun, Bayer HealthCare; dosage 30 mg/kg body weight). Mice were then intracardially perfused with ice-cold PBS. Dissected brains were fixed in 4% PFA (paraformaldehyde) overnight at 4°C and subsequently cryoprotected in 30% sucrose solution for 48 h at 4°C. Frozen whole brains were cut into 60 μm thick coronal sections. Free-floating sections were pre-incubated for 2 h at room temperature with blocking solution (PBS + 5% horse serum and 0.5% Triton X-100) and subsequently incubated 48 h at 4°C with the primary antibody solution (PBS + 1% horse serum and 0.5% Triton X-100). Sections were then washed and incubated overnight at 4°C with secondary (fluorochrome-conjugated)

Antibody	Product	Clone	Host	Dilution
Anti-Iba1	Wako Chemicals, 019-19741	Polyclonal	Rabbit	1:500
Anti-CD68	Bio-Rad, MCA1957GA	FA-11	Rat	1:200
Anti-VGLUT1	Merck Millipore, MAB5502	3C10.2	Mouse	1:500
Anti-NeuN Alexa-488	Merck Millipore, MAB377	A60	Mouse	1:1,000
Anti-Amyloid-Beta	Biolegend, Sig-39320	6E10	Mouse	1:1,000
Anti-Mouse Alexa-488	Life Technologies, A21202	Polyclonal	Donkey	1:1,000
Anti-Rat Alexa-488	Abcam, ab150153	Polyclonal	Donkey	1:1,000
Anti-Mouse Alexa-555	Thermo Fisher Scientific, A-21424	Polyclonal	Goat	1:1,000
Anti-Mouse Alexa-568	Life Technologies, A11004	Polyclonal	Goat	1:1,000
Anti-Rabbit Alexa-647	Life Technologies, A31573	Polyclonal	Donkey	1:1,000

Antibody	Product	Clone	Host	Dilution
Anti-CD11b BV421	Biolegend, 101235	M1/70	Rat	1:200
Anti-CD45 APC	eBioscience, 17-0451-82	30-F11	Rat	1:200
Anti-VGLUT1 PE	Merck Millipore, FCMAB335PE	3C10.2	Mouse	0.5 μg/test
Anti-VGLUT1 Oyser550	Synaptic Systems, 135303C3	Polyclonal	Rabbit	0.5 μg/test
Anti-Synaptophysin	Merck Millipore, MAB5258-20UG	SY38	Mouse	0.5 μg/test
IgG1 K Isotype Control PE	eBioscience, 12-4714-42	P3.6.2.8.1	Mouse	0.5 μg/test
Anti-HA Tag Oyser550	Synaptic Systems, 245003C3	Polyclonal	Rabbit	0.5 μg/test

antibody and DAPI for nuclear staining (1:4,000, Sigma). After washing sections were mounted with ProLong Diamond Antifade Mounting Medium (Thermo Fisher Scientific).

Amyloid-β immunostaining was performed on 25 μm thick coronal sections. Free-floating sections were incubated overnight with the anti-Aβ 6E10 primary antibody (1:1,000, Biolegend). Staining with the secondary (fluorochrome-conjugated) antibody was performed for 2 h at room temperature. Dense-core plaques were stained with Thiazine-red (2 μM, Sigma) for 5 min at room temperature. Sections were then counterstained with DAPI (1:10,000, Sigma) and mounted with fluorescence mounting medium (DAKO).

Confocal Imaging

Immunostained 60 μm thick brain cryosections were analyzed by confocal laser scanning ZEISS LSM 510 META microscope. z-stack images were obtained with either 25×/0.8 NA or 63×/1.4 NA oil-immersion objectives (Zeiss). Microscope settings: 1.6 μs pixel dwell, resolution 2,048 × 2,048 pixels, averaging number 4, *z*-step 0.5 μm, unidirectional acquisition mode, color depth 12 bit. Confocal images were initially deconvolved with Huygens Professional software[1] using default parameter settings and subsequently analyzed using IMARIS software version 7.5.3[2]. Amyloid-β covered area was calculated with ImageJ using the default auto-threshold. Manual threshold adjustments were applied if necessary. Quantification of the VGLUT1+ synaptic inputs was carried out using the Imaris spot-detection tool. The automatic detection algorithm was set to identify all VGLUT1+ spots with a diameter ≥1 μm. For thresholding, 10% of dimmest spots were excluded.

STED Microscopy

STED images were acquired utilizing STEDYCON technology (Abberior Instruments GmbH) installed on a ZEISS LSM 510 META confocal microscope carrying a 100×1.45 NA oil-immersion objectives (Zeiss). Immunofluorescent labeling for Iba1 and VGLUT1 was carried out as described above. Anti-mouse-Star580 and anti-rabbit-StarRED (diluted 1:100) were used as secondary (fluorochrome-conjugated) antibodies. Secondary antibodies were a kind gift from Dr. Janina Hanne of Abberior Instruments GmbH[3]. Raw images were deconvolved with Huygens Professional software and analyzed in IMARIS 7.5.3 software.

Flow Cytometry

After intracardiac perfusion with ice-cold PBS, brains were harvested and slowly homogenized with a tissue potter and filtered through a 70 μm strainer. Myelin was then removed by centrifugation on 30% percoll gradient. Brain pellets were sequentially stained with live/dead staining and for the microglial surface markers CD11b and CD45. Subsequently, stained samples were fixed and permeabilized using the BD Cytofix/Cytoperm kit. Eventually, we performed intracellular staining for the desired synaptic marker. Samples were acquired on BD FACS Canto II (BD Bioscience) flow cytometer. Raw data were analyzed with FlowJo v10 (BD Bioscience). See the protocol for a more detailed description of the method.

Statistics

Graphs and statistics were produced using the Graph-Pad Prism 5 software package. Statistical difference between two groups was determined by either a two-tailed unpaired Student's *t*-test or two-tailed Mann–Whitney *U*-test. To test for normal distribution, the Kolmogorov–Smirnov test was used. When the data passed the normality test ($\alpha = 0.05$), the *p*-value was determined with the unpaired Student's *t*-test. When the data did not pass the normality test ($\alpha = 0.05$), or the *N* size was too small, the *p*-value was determined with the Mann–Whitney *U*-test. The exact *p*-values were reported. Data are shown as the mean value ± SEM.

[1]https://svi.nl

[2]https://www.bitplane.com

[3]https://www.abberior-instruments.com

RESULTS

VGLUT1 Inclusions Can Be Found in Adult Hippocampal Microglia Under Homeostasis

In the adult mouse brain, microglia constantly engage contacts with the surrounding neuronal dendrites (**Supplementary Figure S1A**) and this phenomenon is apparently driven by neuronal activity (Wake et al., 2009; Tremblay et al., 2010; Stowell et al., 2019). We analyzed the brain of 12-week-old mice by confocal imaging, looking for evidence of synaptic engulfment in microglia. Immunostaining for Iba1 (a marker for microglia) and VGLUT1 (a marker for glutamatergic pre-synaptic inputs) showed that microglial processes often overlap with glutamatergic synapses in both cortex and dentate gyrus (**Figure 1A**). To exclude possible bias due to a non-specific staining, we tested the used anti-VGLUT1 antibody on *Vglut1* knock-out (*Vglut1*$^{-/-}$) mice (**Figure 1B**, **Supplementary Figure S1B**). Confocal imaging in the cortex and dentate gyrus shows that the used antibody did not produce detectable staining in *Vglut1*$^{-/-}$ mice (**Figure 1C**). Moreover, VGLUT1 staining in Thy1-EGFP mice showed that VGLUT1 synapses are localized in proximity to the neuronal dendrites (**Supplementary Figure S1C**). These data together indicate that the used anti-VGLUT1 antibody was specific for glutamatergic synapses. We, therefore, decided to focus on VGLUT1 as a synaptic marker of interest.

In the hippocampus of 12-week-old mice, we could occasionally observe the presence of VGLUT1 immunoreactivity localized within the microglial cytoplasm (**Figure 1D**). Intracellular localization of VGLUT1 staining was confirmed by 3D cell reconstruction (**Figures 1E,F**). Such inclusions were found in both microglial processes (**Supplementary Figure S1D**) and cell bodies (**Supplementary Figure S1E**). The presence of VGLUT1 staining inside microglia was further confirmed by STED microscopy (**Figures 1G,H**) and 3D cell reconstruction (**Figure 1I**). To determine whether VGLUT1 inclusions in microglia stemmed from phagocytosis of synapses we performed triple staining for Iba1, VGLUT1, and CD68 (a marker for phagolysosomes in macrophages). Our images show that VGLUT1 inclusions in microglia colocalized with phagosomes (**Figures 1J,K**). Moreover, 3D reconstruction of the CD68-positive surface confirmed that the VGLUT1 inclusions were located within the phagosomes (**Figure 1L**), indicating that glutamatergic pre-synaptic inputs were taken up by phagocytosis.

Although immunofluorescence staining may help appreciate the presence of glutamatergic synaptic proteins in microglia, we concluded that confocal imaging does not grant enough resolution power to reliably discriminate between the synapses that are truly engulfed and those that are simply juxtaposed to the microglial processes. Indeed, a recent work suggested caution to use confocal imaging to investigate synaptic pruning (Weinhard et al., 2018). As an alternative and complementary approach, we used flow cytometry to assess and quantify VGLUT1 immunoreactivity in microglia.

Flow Cytometry Allows for Relative Quantification of VGLUT1 Immunoreactivity in Microglia From the Adult Healthy Brain

We first tested whether VGLUT1 staining could be reliably quantified in adult microglia by flow cytometry. To do so, we performed intracellular staining for VGLUT1 on brain homogenates from 12-week-old *Cx3cr1*$^{GFP/+}$ mice (gating strategy in **Supplementary Figure S2**). We then gated separately microglia (CD11b^{+}CD45^{lo} population) and brain's non-myeloid cells (CD11b^{-}CD45^{-} population; **Figure 2A**). Microglia exhibited a weak yet detectable immunoreactivity for VGLUT1. By contrast, the brain's non-myeloid cells were strongly positive for VGLUT1 (**Figure 2B**). Importantly, no VGLUT1 signal could be detected in the spleen homogenate, indicating that the used antibody did not cross-react with antigens outside the CNS (**Supplementary Figure S3A**). We then quantified VGLUT1 immunoreactivity in microglia by comparing VGLUT1-stained vs. isotype control samples (**Figure 2C**). Doing so, we could detect an average of 12.4% (±1.3%) VGLUT1-positive microglial cells in our samples (**Figure 2D**). However, this method of quantification is obviously biased by the manual gating. To provide an unbiased relative quantification of the VGLUT1 immunoreactivity (hereafter VGLUT1 IR) among different cell types, we normalized VGLUT1 Mean-Fluorescence-Intensity (MFI) to the isotype MFI in each population of interest (MFI VGLUT1: MFI Isotype, hereafter "n-MFI"). Using this formula, VGLUT1 nMFI was determined in both microglia and CD11b^{+}CD45^{hi} macrophages (CD45^{hi} MPs) separately (**Figure 2E**). The CD45^{hi} MPs population comprises extra-parenchymal myeloid cells (mostly perivascular, meningeal, and choroid plexus macrophages) which are not in direct contact with the brain's parenchyma (Kierdorf et al., 2019; Brioschi et al., 2020) and therefore should not be positive for VGLUT1. Indeed, microglia exhibited a VGLUT1 n-MFI = 4.3 ± 0.5 (meaning 4.3-fold increased MFI compared to the isotype), while no signal was detected in CD45^{hi} MPs (n-MFI = 1.2 ± 0.1; **Figures 2F,F1**). Similar results were obtained staining for the pre-synaptic marker Synaptophysin (SYN; n-MFI in microglia = 2.6 ± 0.5; n-MFI in CD45^{hi} MPs = 1.1 ± 0.1; **Figures 2G,G1**). Overall, these data indicate that different synaptic markers can be detected and quantified in microglia, but not in CD45^{hi} MPs, which served as an internal control (**Figure 2H**). To rule out possible bias due to unspecific staining, we performed an additional VGLUT1 staining using a different antibody clone, which yielded similar n-MFI values (n-MFI in microglia = 5.4 ± 0.7; **Figure 2I**). Additionally, we compared VGLUT1 IR between hippocampal and cortical microglia from 12-week-old mice. We found that microglia from hippocampus exhibit a slight, yet significant, increase of VGLUT1 n-MFI (5.5 ± 0.5) compared to microglia from cortex (3.9 ± 0.2; **Supplementary Figure S3B**). These data indicate that VGLUT1 IR in microglia varies depending on the brain region. In summary, this flow cytometry-based approach allowed for relative quantification of synaptic proteins in microglia from the adult healthy brain.

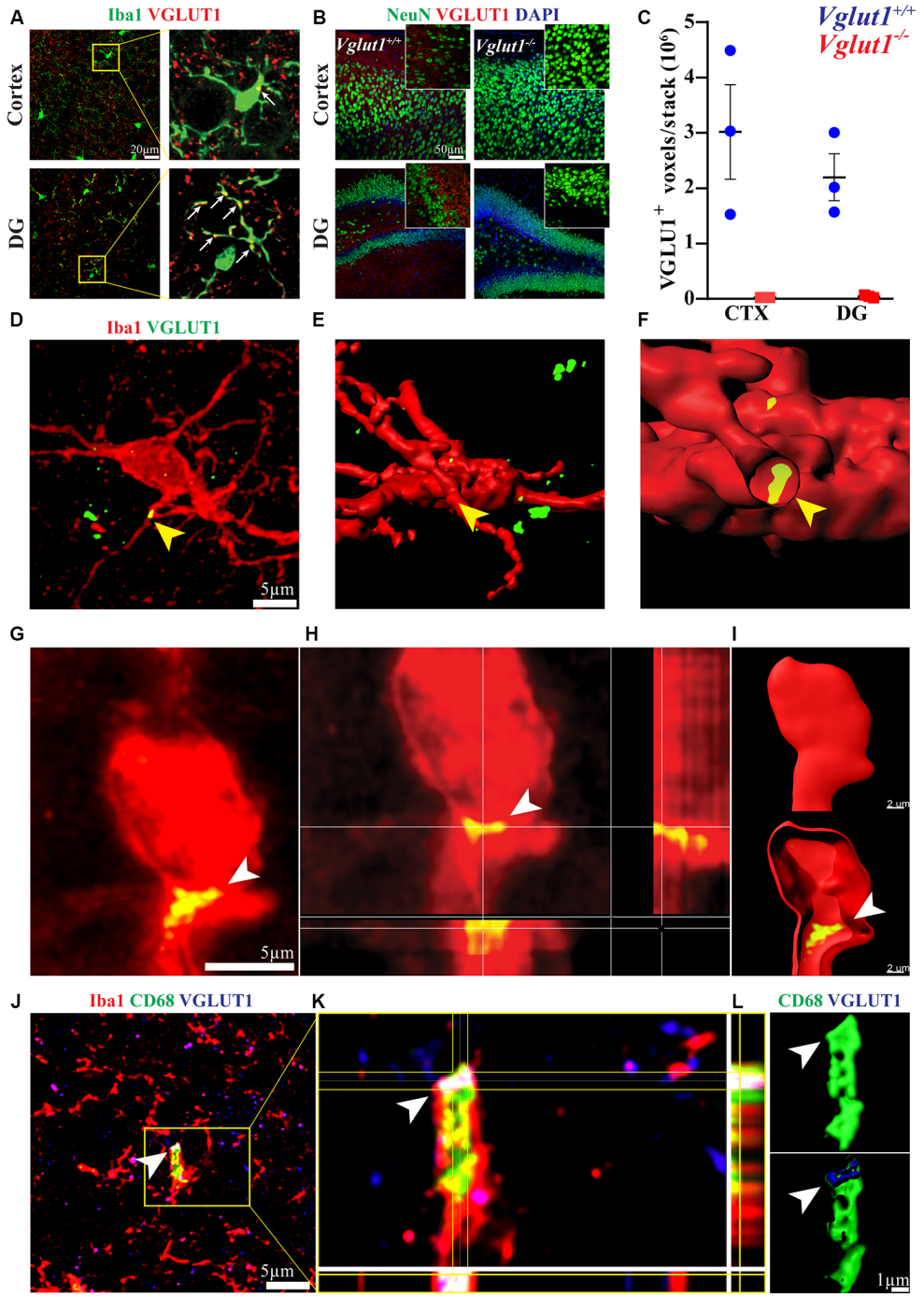

FIGURE 1 | VGLUT1 inclusions can be found in adult hippocampal microglia under homeostasis. **(A)** In immunohistochemistry, frequent overlaps between Iba1 and VGLUT1 signals can be detected in the brain cortex and dentate gyrus (DG). **(B)** Anti-VGLUT1 staining in cortex and dentate gyrus (DG) from both *Vglut1*$^{+/+}$ (wild-type) and *Vglut1*$^{-/-}$ (knock-out) littermates. **(C)** Quantification of the VGLUT1-positive voxels per stack in cortex (CTX) and dentate gyrus (DG) of both *Vglut1*$^{+/+}$ and *Vglut1*$^{-/-}$ mice (*N* = 3 mice per group, two sections per mouse; data from a single experiment). **(D)** Microglial cell at the CA1 hippocampus exhibiting a VGLUT1 inclusion overlapping with a process (yellow arrowhead). **(E)** 3D cell reconstruction of the same microglial cell displayed in panel **(D)**. **(F)** Application of a clipping surface on the 3D reconstruction discloses the presence of a VGLUT1 inclusion within the microglial process (yellow arrowhead). **(G)** STED image of a microglial cell in the CA1 exhibiting a VGLUT1 inclusion (white arrowhead). **(H)** Orthogonal projection of the imaged in panel **(J)** showing the intracellular localization of the VGLUT1 staining. **(I)** 3D reconstruction of the cell in panel **(J)** showing the intracellular localization of the VGLUT1 staining. **(J)** A confocal image of a microglial cell body exhibiting VGLUT1 inclusion overlapping with a CD68^{+} phagosome (scale bar 5 µm). **(K)** Orthogonal projection of the inset area. Note the colocalization between VGLUT1 and CD68 staining (white spot in the centre of the crosshair). **(L)** 3D reconstruction of both CD68 (green) and VGLUT1 (blue) signals showing that the VGLUT1 inclusion is perfectly encased within the microglial phagosomes (white arrowhead).

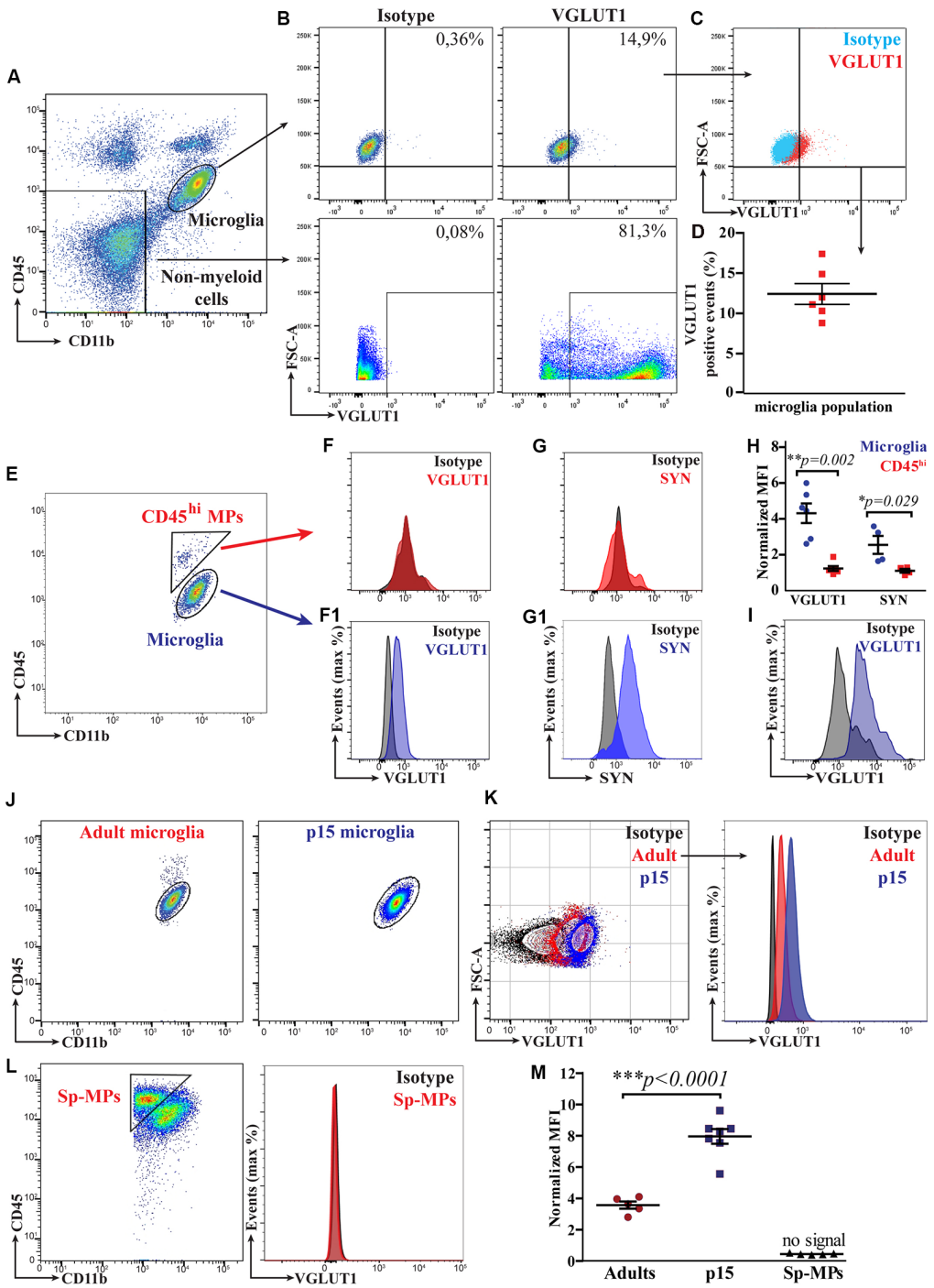

FIGURE 2 | Flow cytometry allows for a relative quantification of VGLUT1 immunoreactivity in microglia from both the adult and the developing mouse brain. **(A)** FACS plot displaying the gates for both microglia ($CD11b^{+}CD45^{lo}$ population) and brain's non-myeloid cells ($CD11b^{-}CD45^{-}$ population). **(B)** FACS plot showing VGLUT1 immunoreactivity in both microglia and brain's non-myeloid cells. **(C)** Microglia from VGLUT1-stained samples exhibit a positive staining, as compared to isotype control. **(D)** Percentage of the VGLUT1-positive microglia, fluorescence of the isotype control is used as baseline ($N = 6$ mice, pooled data from two independent experiments). **(E)** FACS plot displaying both microglia ($CD11b^{+}CD45^{lo}$ population) and CD45hi MPs ($CD11b^{+}CD45^{hi}$ population). **(F)** Fluorescence peak of the VGLUT1 staining in $CD45^{hi}$ MPs. **(F1)** Fluorescence peak of the VGLUT1 staining in microglia (anti-VGLUT1-PE, Merck Millipore FCMAB335PE, clone 3C10.2). **(G)** Fluorescence peak of the Synaptophysin staining in $CD45^{hi}$ MPs. **(G1)** Fluorescence peak of the Synaptophysin staining in microglia. **(H)** n-MEAN-FLUORESCENCE-INTENSITY (MFI) for VGLUT1 and Synaptophysin in both microglia and $CD45^{hi}$ MPs (VGLUT1 $N = 6$ mice per group, pooled data from two independent experiments; Mann–Whitney U-test; $^{**}p = 0.002$. Synaptophysin $N = 4$ mice per group, data from a single experiment; Mann–Whitney U-test unpaired; $^{*}p = 0.029$). **(I)** Fluorescence peak of the VGLUT1 staining in microglia using an alternative antibody clone conjugated with a different dye

(*Continued*)

FIGURE 2 | Continued
(anti-VGLUT1-Oyster550, Synaptic Systems 135303C3, polyclonal). **(J)** FACS plot displaying microglia from either adult (12-week-old) or P15 mice. **(K)** Comparison of the VGLUT1 immunoreactivity between adult and P15 microglia. **(L)** VGLUT1 staining was not detectable in splenic macrophages (Sp-MPs). **(M)** VGLUT1 n-MFI in microglia from P15 and adult brain, Sp-MPs served as a negative control (adult $N = 5$ mice per group, P15 $N = 7$ mice per group, Sp-MPs $N = 5$ mice per group, data from a single experiment; unpaired *t*-test; $^{***}p < 0.0001$).

VGLUT1 Immunoreactivity in Microglia Is Intracellular

To prove that the observed VGLUT1 IR in microglia was derived from a specific intracellular staining, we performed a control experiment treating brain homogenates with either FACS buffer or permeabilization buffer. In principle, without permeabilization, the antibody does not cross the cell membrane, resulting in a lack of intracellular staining. For this experiment, we prepared brain homogenates from *Cx3cr1*$^{GFP/+}$ mice, which were split equally into two separate tubes. Half of the sample was stained for VGLUT1 in FACS buffer, while the other half was stained using a permeabilization buffer. In flow cytometry, we gated both microglia ($CX_3CR1^+CD11b^+CD45^{lo}$) and non-microglial cells ($CX_3CR1^-CD11b^-CD45^-$) separately (**Supplementary Figure S3C**). In samples incubated with FACS buffer microglia did not exhibit detectable VGLUT1 IR, which was instead present using the permeabilization buffer (**Supplementary Figure S3D**). This difference was even more remarkable in the non-myeloid cells (**Supplementary Figure S3E**). Focusing on microglia, we measured a VGLUT1 n-MFI = 0.9 ± 0.1 using FACS buffer, and n-MFI = 6.8 ± 0.9 with the permeabilization buffer (**Supplementary Figure S3F**). This experiment showed that membrane permeabilization increased VGLUT1 IR in microglia of ∼7-fold (**Supplementary Figure S3G**). To summarize, the permeabilization of the cell membrane was necessary for successful detection of VGLUT1 in microglia, hence, we concluded that the stained synaptic protein was located within intracellular compartments.

P15 Microglia Exhibit Increased VGLUT1 Immunoreactivity as Compared to Adult Microglia

Early post-natal development is a critical period for brain maturation and synapse remodeling (Tau and Peterson, 2010). Recent literature has provided evidence that, in the early post-natal brain, microglia contribute to maturation of neural circuits by refining synaptic connections (Paolicelli et al., 2011; Schafer et al., 2012; Filipello et al., 2018). We hence aimed to quantify VGLUT1 staining in microglia from the developing brain (at postnatal day 15, P15) using flow cytometry (**Figure 2J**). We found that VGLUT1 IR was increased in microglia from P15 as compared to adult mice (**Figure 2K**). As expected, no VGLUT1 IR was detected in either splenic macrophages (Sp-MPs; **Figure 2L**) or $CD45^{hi}$ MPs (not shown). According to our quantification, we measured 2.2-fold increased VGLUT1 n-MFI in P15 microglia (8.0 ± 0.5) compared to adult microglia (3.6 ± 0.2; **Figure 2M**). These data indicate that VGLUT1-positive microglia can be found in both the adult and the juvenile mouse brain. However, microglia during the post-natal brain development display a significantly higher VGLUT1 immunoreactivity, suggestive of an increased uptake of glutamatergic synapses in this period.

Microglia Exhibit Increased VGLUT1 Immunoreactivity at Early Stages of Amyloid Pathology

As main pathological hallmarks, Alzheimer's disease (AD) is characterized by extracellular deposition of amyloid-β and intracellular accumulation of phospho-Tau. Alongside, AD brains feature a progressive loss of neurons and synapses (Ziegler-Waldkirch and Meyer-Luehmann, 2018). Interestingly, an increase of microglia-mediated synaptic pruning was recently indicated as an early pathophysiological event in a mouse model of AD before full-blown amyloid pathology (Hong et al., 2016). We then hypothesized that microglia may exhibit increased content of VGLUT1 protein at early stages of amyloid-β (Aβ) deposition. To test this hypothesis, we compared VGLUT1 IR in microglia from a mouse model of AD and wild-type controls. For this experiment, we decided to rely on the *5xTgFAD* (hereafter FAD+) mouse line crossed with the *Cx3cr1*$^{GFP/+}$ line to help visualize microglia during amyloid pathology. In mice carrying the FAD mutations, amyloid plaques typically start to develop in the subiculum at 2 months and in the hippocampus 4 months after birth. Nonetheless, intraneuronal $A\beta_{42}$ and synaptic degeneration can be observed at earlier time points (Oakley et al., 2006). Importantly, amyloid pathology does not involve the cerebellum. First, we assessed the presence of the amyloid plaques in the cortex of 2 months old and 7 months old FAD+ mice using both the 6E10 antibody (staining for human APP) and the thiazine-red staining (staining for fibrillar Aβ). Confocal imaging showed that, at 2 months of age, no obvious amyloid deposits can be observed. By contrast, several amyloid plaques surrounded by plaque-associated microglia are clearly visible at 7 months (**Figure 3A**). This data indicates that FAD+ mice at age of 2 months do not exhibit signs of obvious amyloid pathology. We then analyzed VGLUT1 IR in microglia from the cortex of 2 months old FAD+ and FAD− (wild-type) mice, while microglia from the cerebellum were used as a negative control (**Figure 3B**). Our flow cytometry analysis revealed a slight, but significant, increase of the VGLUT1 n-MFI in cortical microglia from FAD+ compared to FAD− mice (6.8 ± 0.4 and 5.1 ± 0.2, respectively; **Figure 3C**). By contrast, cerebellar microglia did not show any significant difference between FAD+ and FAD− mice (5.8 ± 0.4 and 5.1 ± 0.3, respectively; **Figure 3D**). In immunohistochemistry, we assessed the overall density of VGLUT1 synapses in both cortex (**Supplementary Figure S4A**) and cerebellum (**Supplementary Figure S4B**) of 2 months old FAD+ and FAD− mice. Our quantification revealed a mild loss of VGLUT1 synapses in the cortex of FAD+ mice as compared to wild-type controls (**Supplementary Figure S4C**). Although the observed difference did not reach the statistical significance ($p = 0.2$), we can cautiously suggest that there is a tendency

towards a loss of glutamatergic synapses at the age of 2 months. As expected, no difference in density of VGLUT1 synapses was found in the cerebellum (**Supplementary Figure S4**). To further corroborate these data, we assessed the number of VGLUT1-positive events in the cortical non-myeloid cells ($CX_3CR1^-CD11b^-CD45^-$ population) using flow cytometry (**Supplementary Figure S4E**). Consistently with the previous observation, a significant reduction (−19% ± 0.04) of the VGLUT1-positive events was found in the cortex of 2 months old FAD+ mice in comparison to wild-type mice (**Supplementary Figure S4F**). In summary, FAD+ mice display a (mild) loss of cortical glutamatergic synapses before the formation of amyloid plaques. At the very same time, cortical microglia exhibit increased immunoreactivity for VGLUT1, suggesting increased engulfment of glutamatergic synapses at early stages of amyloid pathology.

Microglia Exhibit Increased VGLUT1 Immunoreactivity After Conditional TDP-43 Deletion

Recent work described augmented phagocytosis in microglia lacking the *Tardbp* gene, encoding for the RNA-DNA binding-protein TDP-43. The depletion of TDP-43 in microglia caused increased phagocytosis of amyloid-β, but also promoted loss of VGLUT1 synapses, probably because of augmented synaptic pruning (Paolicelli et al., 2017). As an additional benchmark for our quantification method, we decided to compare VGLUT1 IR between TDP-43-deficient and wild-type microglia. Mice selectively lacking TDP-43 in microglia were generated by crossing *Cx3cr1*^{CreERT2} mice with *Tardbp*$^{flox/flox}$ mice (Parkhurst et al., 2013; Paolicelli et al., 2017; **Figure 3E**). In principle, this conditional Tamoxifen-inducible mouse model allows to specifically delete loxP-flanked genes in parenchymal microglia and other long-lived CNS-associated macrophages (Goldmann et al., 2013, 2016; Wieghofer et al., 2015). To further explore the presence of VGLUT1 protein in highly phagocytic microglia, we assessed the VGLUT1 IR in both *Cx3cr1*^{CreERT2};*Tardbp*$^{+/+}$ and *Cx3cr1*^{CreERT2};*Tardbp*$^{flox/flox}$ littermates (hereafter wild-type and TDP-43 cKO, respectively). Starting at P30, all mice underwent daily injections of Tamoxifen on five consecutive days to induce Cre-mediated recombination. Successful ablation of TDP-43 in microglia from *Tardbp*$^{flox/flox}$ carriers was previously demonstrated (Paolicelli et al., 2017). After 8 weeks, mice were euthanized, and brains were analyzed by flow cytometry (experimental plan in **Figure 3F**). Unlike wild-type mice, in the TDP-43 cKO group, we could observe the presence of two distinct sub-populations of microglia differing in CD11b intensity (**Figure 3G**). To explain this phenomenon, we hypothesize that some microglial cells failed to recombine both *Tardbp* alleles, thus generating two populations with different CD11b expression level. Whether or not this difference in CD11b expression is caused by an incomplete recombination of the *Tardbp*$^{flox/flox}$ locus remains to be established. Besides this unexpected finding, TDP-43 cKO microglia exhibited a remarkable increase of VGLUT1 IR (**Figure 3H**). Our quantification showed a significant increase of VGLUT1 n-MFI in TDP-43 cKO microglia as compared to wild-type (4.2 ± 0.1 and 3.1 ± 0.2, respectively; **Figure 3I**). Again, VGLUT1 IR was not detectable in $CD45^{hi}$ MPs (not shown). These data support previous evidence that TDP-43 ablation in microglia leads to increased engulfment of glutamatergic synapses (Paolicelli et al., 2017).

DISCUSSION

The first evidence of microglia displacing synapses from neuronal cell bodies was presented approximately 50 years ago (Blinzinger and Kreutzberg, 1968). Over the last decade, the scientific community has witnessed a growing interest in this topic (Tremblay et al., 2010; Paolicelli et al., 2011; Schafer et al., 2012). In the mouse brain, the first 2 weeks of postnatal development are accompanied by a peak in synaptic turnover, with intense *de novo* synapse formation and synapse elimination. Microglia critically contribute to the removal of exuberant and unnecessary synapses generated across this period, playing an important role in synaptic pruning. To date, the molecular cues implicated in this process are largely unknown and it is possible that different brain cells, other than microglia, secrete factors modulating this process (Bialas and Stevens, 2013; Vainchtein et al., 2018). It has been so far shown that a microglia-mediated synaptic pruning occurs during brain development, while evidence of synaptic pruning in the healthy adult brain is still lacking.

We first sought evidence of colocalization between the pre-synaptic marker VGLUT1 and microglial cytoplasm in the hippocampus of adult mice by confocal imaging. Our confocal and STED images disclosed the presence of the pre-synaptic protein VGLUT1 within microglial processes and cell bodies. Moreover, such VGLUT1 inclusions were often colocalized with the phagosomes, indicating that synaptic pruning may still occur in the hippocampus during adulthood. To provide a quantitative appraisal of the VGLUT1 protein in microglia we assessed VGLUT1 immunoreactivity in the $CD11b^+CD45^{lo}$ population by flow cytometry. Our data show that microglia in the adult brain contain a detectable amount of VGLUT1 protein, which can be successfully stained and quantified *via* fluorescence intensity. Using this approach, we could also show that microglia from the developing brain contain more than two times the amount of VGLUT1 found in adult microglia.

Next, we aimed to quantify VGLUT1 in microglia from two pathological models. First, we assessed the VGLUT1 staining in microglia from the 5xFAD mouse model of AD. We found that cortical microglia exhibit a significant increase of immunoreactivity for VGLUT1 in 2 months old 5xFAD mice as compared to wild-types. This suggests that microglia may account, at least partially, for the synaptic degeneration observed in the early stages of the pathology (Hong et al., 2016; Shi et al., 2017). Microglia may remove injured/dysfunctional glutamatergic synapses at early stages of amyloid pathology *via* synaptic pruning. Alternatively, we may hypothesize that Aβ-related toxicity causes a loss of glutamatergic synapses, debris of which is rapidly scavenged by neighboring microglia. These two scenarios are not mutually exclusive, and

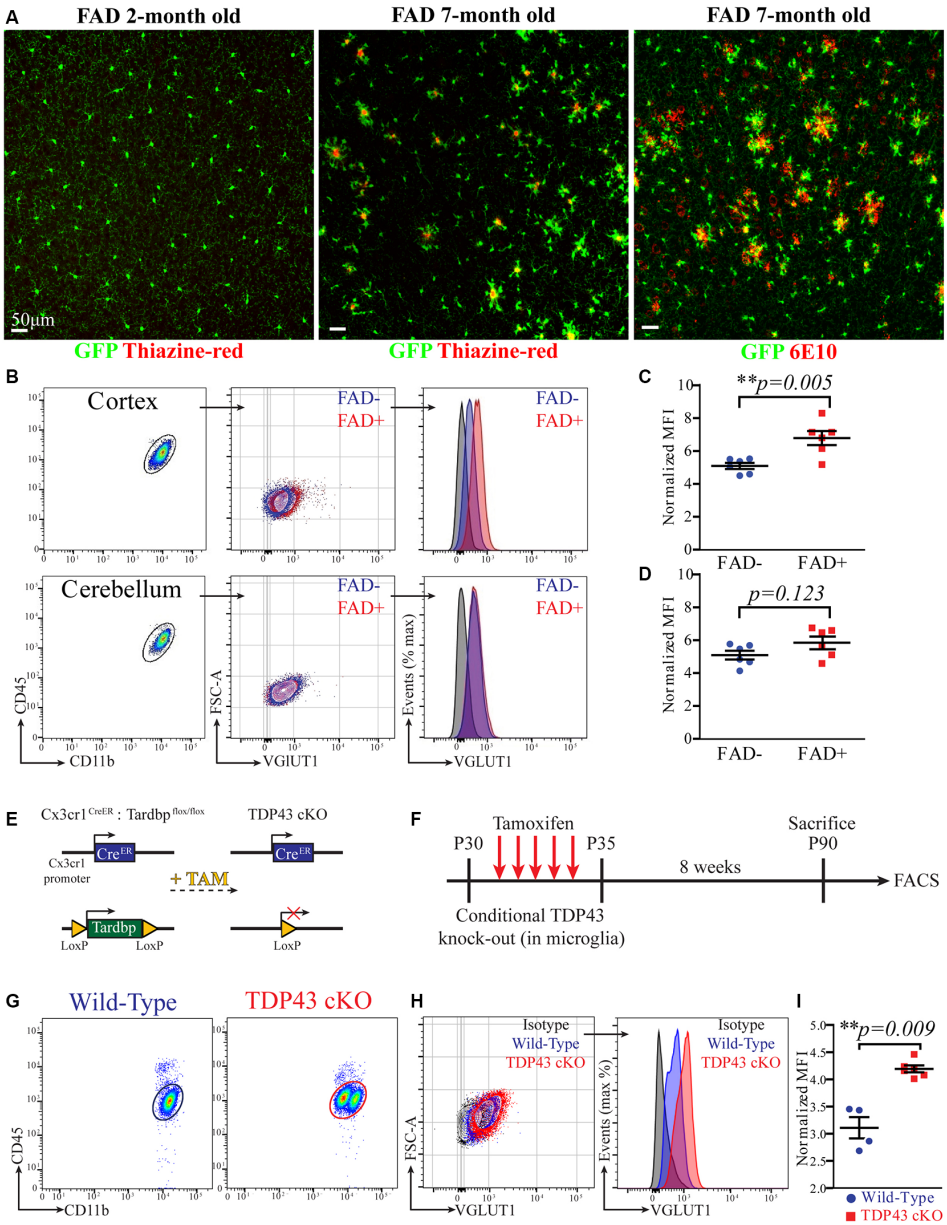

FIGURE 3 | Microglia exhibit increased VGLUT1 immunoreactivity at early stages of amyloid pathology and after conditional TDP-43 deletion. **(A)** Confocal imaging in the cortex of 2-month-old and 7-month-old *5xFAD* × *Cx3cr1GFP/+* mice stained with either thiazine-red or the 6E10 antibody. Representative of three mice per group. **(B)** FACS plot of microglia extracted from either cortex or cerebellum. A comparison of the VGLUT1 IR between FAD+ and FAD− mice is displayed. **(C)** VGLUT1 n-MFI in cortical microglia from either FAD− or FAD+ mice (*N* = 6 mice per group; pooled data from two independent experiments; unpaired *t*-test; $^{**}p = 0.005$). **(D)** VGLUT1 n-MFI in cerebellar microglia from either FAD− or FAD+ mice (*N* = 6 mice per group; pooled data from two independent experiments; unpaired *t*-test; non-significant difference). **(E)** Scheme of the conditional *Tardbp* knock-out in microglia. **(F)** Scheme of the experimental design. **(G)** FACS plot displaying microglia from wild-type and TDP-43 cKO mice. Note that TDP-43 cKO microglia appeared as two distinct populations. **(H)** VGLUT1 IR in microglia from wild-type and TDP-43 cKO mice. **(I)** VGLUT1 nMFI in TDP-43 cKO microglia compared to wild-type microglia (wild-type *N* = 4 mice, TDP-43 cKO *N* = 6 mice, data from a single experiment; Mann–Whitney *U*-test; $^{**}p = 0.009$).

further studies are needed to determine whether microglia are directly involved in the synaptic loss observed under AD-like pathology.

Last, we assessed the presence of VGLUT1 protein in microglia from the *Cx3cr1*^{CreERT2};*Tardbp*$^{flox/flox}$ mouse line. As recently described, conditional TDP-43 deletion in microglia (TDP-43 cKO) induces a highly phagocytic phenotype, which develops alongside the loss of VGLUT1 synapses from the cortical parenchyma (Paolicelli et al., 2017). In flow cytometry, we could detect a significant increase in VGLUT1 immunoreactivity in TDP-43 cKO microglia, suggesting augmented pruning of glutamatergic synapses. This

evidence further corroborates (and integrates) the previously published data, indicating that the synaptic loss observed in this transgenic mouse is likely contributed by exaggerated synaptic pruning.

The quantification of synaptic proteins in microglia by flow cytometry certainly provides some advantages compared to the traditional microscopy techniques, such as a much faster acquisition and analysis of the experimental data. Nevertheless, there are some important caveats to keep in mind: (1) Application of this technique is limited by the availability of antibodies specific for synapses and, at the same time, suitable for flow cytometry staining. (2) Flow cytometry requires tissue homogenization with loss of the structural and anatomical information of the brain's parenchyma, that is otherwise preserved in histology. (3) Using flow cytometry, we are unable to provide a direct visualization of the VGLUT1 immunoreactivity in microglia, which would help determine the exact localization of the VGLUT1 inclusions. (4) The presented data do not provide experimental proof that microglia actively prune synapses from the neuronal dendrites as opposed to "simply" scavenging synaptic debris within the brain parenchyma. (5) This method is not specific for synaptic proteins; indeed, we could also detect immunoreactivity for GFAP, MAP2, and NeuN in microglia (not shown), possibly owing to the uptake of dead cells in the brain.

It is important to note that, in this study, VGLUT1 immunoreactivity was never found in $CD45^{hi}$ (extra-parenchymal) macrophages or splenic macrophages, indicating that the staining did not produce non-specific labeling of myeloid antigens. Moreover, we provided evidence that the observed VGLUT1 immunoreactivity was intracellular and not merely due to adhesion of VGLUT1 proteins to the cell surface.

In conclusion, with this study, we aimed to perform relative quantification of the synaptic protein VGLUT1 in microglia during brain development, adulthood, and neurodegeneration using flow cytometry. This work corroborates previous evidence, mostly based on imaging techniques, providing a methodological framework for quantitative assessment which may help investigate microglia-mediated synapse elimination. A better understanding of the pathological synaptic pruning will help design novel therapies for neurodevelopmental and neurodegenerative disorders.

DATA AVAILABILITY STATEMENT

All datasets presented in this study are included in the article/**Supplementary Material**.

ETHICS STATEMENT

The animal study was reviewed and approved by committee of the University of Freiburg/Swiss Cantonal Veterinary Office.

AUTHOR CONTRIBUTIONS

SB designed the experiments, performed the experiments and wrote the manuscript. PD'E, LA, HJ, PW and RP performed the experiments. SW, MM-L, LR and KB provided animals and/or materials. All authors edited the manuscript. PW, RP and KB supervised the project.

FUNDING

The work of KB and SB was supported by German Research Council (DFG); Grant numbers: BI 668/2-2 and BI 668/5-1. RP was supported by Synapsis Foundation Alzheimer Research Switzerland ARS and by the European Research Council (ERC Starting Grant REMIND 804949).

ACKNOWLEDGMENTS

We warmly thank Evan Balmuth (Tufts University, Medford, USA) for the careful proofreading of the manuscript. We also thank Dr. Roland Nitschke and his team [Life Imaging Center, Center for Biological Systems Analysis (ZBSA), Albert-Ludwigs-University, Freiburg, Germany] for their precious assistance concerning imaging techniques and data analysis.

SUPPLEMENTARY MATERIAL

The Supplementary Material for this article can be found online at: https://www.frontiersin.org/articles/10.3389/fnmol.2020.00149/full#supplementary-material.

FIGURE S1 | (A) Confocal image in the hippocampus of a Thy.1-eGFP mouse with anti-Iba1 staining showing the interactions between microglial processes and neuronal dendrites (white arrowheads). A GFP^+ inclusion within the microglial cytoplasm is also visible (yellow arrowhead). **(B)** Immunohistochemistry in the mouse cortex for Iba1 (green) and VGLUT1 (red). Diffuse VGLUT1 staining is present in wild-type (*Vglut1*$^{+/+}$), but not in the knock-out (*Vglut1*$^{-/-}$) brain. **(C)** VGLUT1 synapses (red) were found in proximity to Thy1-GFP neurons (green). 3D reconstruction highlights the close contact between VGLUT1 synapses and the neuronal dendrites. **(D)** A microglial cell in the CA1 exhibiting a VGLUT1 inclusion within a process (white box and yellow arrowhead). **(E)** A microglial cell in the CA1 exhibiting VGLUT1 inclusions in the cell body (white box and yellow arrowhead).

FIGURE S2 | Gating strategy for microglia, brain $CD45^{hi}$ MPs and splenic MPs. Cells were hierarchically gated as follows: $CD11b^+$ brain's myeloid cells → single cells → viable cells → GFP^+ or GFP^- (depending on the presence of the *Cx3cr1*$^{GFP/+}$ transgene) → $CD11b^+CD45^{lo}$ population (microglia) and $CD11b^+CD45^{hi}$ population ($CD45^{hi}$ MPs). Representative gating strategy for **(A)** wild-type brain, **(B)** *Cx3cr1*$^{GFP/+}$ brain, and **(C)** spleen.

FIGURE S3 | (A) VGLUT1 immunoreactivity is present in the brain tissue, but not in the spleen. **(B)** VGLUT1 n-MFI in microglia from either cortex or hippocampus ($N = 6$ mice per group; pooled data from two independent experiments; unpaired *t*-test; $^*p = 0.0149$). **(C)** FACS plot showing all brain cells from *Cx3cr1*$^{GFP/+}$ mice, gated as $CD11b^+$ and $CD11b^-$ populations. **(D)** Microglia were gated as $CD11b^+CX_3CR1^+CD45^{lo}$ population. **(E)** Non-myeloid cells were gated as $CD11b^-CX_3CR1^-CD45^-$ population. VGLUT1 IR in either gate was detectable only in presence of permeabilization buffer. **(F)** VGLUT1 n-MFI in microglia stained with either FACS buffer or permeabilization buffer ($N = 4$ samples per group; data from a single experiment; Mann–Whitney *U*-test; $^*p < 0.028$). **(G)** VGLUT1 MFI fold-change between non-permeabilized and permeabilized microglia (four samples per group).

FIGURE S4 | (A) Iba1 (red) and VGLUT1 (green) staining in the cortex of FAD− and FAD+ mice at the age of 2 months. **(B)** Iba1 (red) and VGLUT1 (green) staining in the cerebellum of FAD− and FAD+ mice at the age of 2 months. **(C)**

Quantification of VGLUT1+ puncta per field (100 μm^2) in the cortex of FAD− and FAD+ mice at 2 months (N = 3 mice per group, average of two sections per mouse; data from a single experiment; Mann–Whitney U-test; non-significant difference). **(D)** Quantification of VGLUT1+ puncta per field (100 μm^2) in the cerebellum of FAD− and FAD+ mice at 2 months (N = 3 mice per group, average of two sections per mouse; data from a single experiment; Mann–Whitney U-test; non-significant difference). **(E)** VGLUT1 immunoreactivity in the non-myeloid cells (CD11b−CD45−) from the cortex of either FAD− and FAD+ mice at 2 months. **(F)** Percentage of the VGLUT1-positive events in the brain's non-myeloid cells (gated as in panel **E**) were measured. The plot displays the fold change in the FAD+ group (N = 4 mice per group; data from a single experiment; Mann–Whitney U-test; $^*p < 0.029$).

REFERENCES

Bialas, A. R., and Stevens, B. (2013). TGF-β signaling regulates neuronal C1q expression and developmental synaptic refinement. *Nat. Neurosci.* 16, 1773–1782. doi: 10.1038/nn.3560

Bisht, K., Sharma, K. P., Lecours, C., Gabriela Sánchez, M., El Hajj, H., Milior, G., et al. (2016). Dark microglia: a new phenotype predominantly associated with pathological states. *Glia* 64, 826–839. doi: 10.1002/glia.22966

Blinzinger, K., and Kreutzberg, G. (1968). Displacement of synaptic terminals from regenerating motoneurons by microglial cells. *Z. Zellforsch. Mikrosk. Anat.* 85, 145–157. doi: 10.1007/bf00325030

Brioschi, S., Zhou, Y., and Colonna, M. (2020). Brain parenchymal and extraparenchymal macrophages in development, homeostasis, and disease. *J. Immunol.* 204, 294–305. doi: 10.4049/jimmunol.1900821

Davalos, D., Grutzendler, J., Yang, G., Kim, J. V., Zuo, Y., Jung, S., et al. (2005). ATP mediates rapid microglial response to local brain injury *in vivo*. *Nat. Neurosci.* 8, 752–758. doi: 10.1038/nn1472

Di Liberto, G., Pantelyushin, S., Kreutzfeldt, M., Page, N., Musardo, S., Coras, R., et al. (2018). Neurons under T cell attack coordinate phagocyte-mediated synaptic stripping. *Cell* 175, 458.e19–471.e19. doi: 10.1016/j.cell.2018.07.049

Filipello, F., Morini, R., Corradini, I., Zerbi, V., Canzi, A., Michalski, B., et al. (2018). The microglial innate immune receptor TREM2 is required for synapse elimination and normal brain connectivity. *Immunity* 48, 979.e8–991.e8. doi: 10.1016/j.immuni.2018.04.016

Ginhoux, F., Greter, M., Leboeuf, M., Nandi, S., See, P., Gokhan, S., et al. (2010). Fate mapping analysis reveals that adult microglia derive from primitive macrophages. *Science* 330, 841–845. doi: 10.1126/science.1194637

Ginhoux, F., and Prinz, M. (2015). Origin of microglia: current concepts and past controversies. *Cold Spring Harb. Perspect. Biol.* 7:a020537. doi: 10.1101/cshperspect.a020537

Goldmann, T., Wieghofer, P., Jordão, M. J. C., Prutek, F., Hagemeyer, N., Frenzel, K., et al. (2016). Origin, fate and dynamics of macrophages at central nervous system interfaces. *Nat. Immunol.* 17, 797–805. doi: 10.1038/ni.3423

Goldmann, T., Wieghofer, P., Müller, P. F., Wolf, Y., Varol, D., Yona, S., et al. (2013). A new type of microglia gene targeting shows TAK1 to be pivotal in CNS autoimmune inflammation. *Nat. Neurosci.* 16, 1618–1626. doi: 10.1038/nn.3531

Hanisch, U.-K. K., and Kettenmann, H. (2007). Microglia: active sensor and versatile effector cells in the normal and pathologic brain. *Nat. Neurosci.* 10, 1387–1394. doi: 10.1038/nn1997

Hong, S., Beja-Glasser, V. F., Nfonoyim, B. M., Frouin, A., Li, S., Ramakrishnan, S., et al. (2016). Complement and microglia mediate early synapse loss in Alzheimer mouse models. *Science* 352, 712–716. doi: 10.1126/science.aad8373

Kettenmann, H., Kirchhoff, F., and Verkhratsky, A. (2013). Microglia: new roles for the synaptic stripper. *Neuron* 77, 10–18. doi: 10.1016/j.neuron.2012.12.023

Kierdorf, K., Erny, D., Goldmann, T., Sander, V., Schulz, C., Gomez Perdiguero, E., et al. (2013). Microglia emerge from erythromyeloid precursors *via* Pu.1- and Irf8-dependent pathways. *Nat. Neurosci.* 16, 273–280. doi: 10.1038/nn.3318

Kierdorf, K., Masuda, T., Jordão, M. J. C., and Prinz, M. (2019). Macrophages at CNS interfaces: ontogeny and function in health and disease. *Nat. Rev. Neurosci.* 20, 547–562. doi: 10.1038/s41583-019-0201-x

Lehrman, E. K., Wilton, D. K., Litvina, E. Y., Welsh, C. A., Chang, S. T., Frouin, A., et al. (2018). CD47 protects synapses from excess microglia-mediated pruning during development. *Neuron* 100, 120.e6–134.e6. doi: 10.1016/j.neuron.2018.09.017

Lui, H., Zhang, J., Makinson, S. R., Cahill, M. K., Kelley, K. W., Huang, H. Y., et al. (2016). Progranulin deficiency promotes circuit-specific synaptic pruning by microglia *via* complement activation. *Cell* 165, 921–935. doi: 10.1016/j.cell.2016.04.001

Miyamoto, A., Wake, H., Ishikawa, A. W., Eto, K., Shibata, K., Murakoshi, H., et al. (2016). Microglia contact induces synapse formation in developing somatosensory cortex. *Nat. Commun.* 7:12540. doi: 10.1038/ncomms12540

Neniskyte, U., and Gross, C. T. (2017). Errant gardeners: glial-cell-dependent synaptic pruning and neurodevelopmental disorders. *Nat. Rev. Neurosci.* 18, 658–670. doi: 10.1038/nrn.2017.110

Nimmerjahn, A., Kirchhoff, F., and Helmchen, F. (2005). Resting microglial cells are highly dynamic surveillants of brain parenchyma *in vivo*. *Science* 308, 1314–8. doi: 10.1126/science

Oakley, H., Cole, S. L., Logan, S., Maus, E., Shao, P., Craft, J., et al. (2006). Intraneuronal β-amyloid aggregates, neurodegeneration, and neuron loss in transgenic mice with five familial Alzheimer's disease mutations: potential factors in amyloid plaque formation. *J. Neurosci.* 26, 10129–10140. doi: 10.1523/JNEUROSCI.1202-06.2006

Paolicelli, R. C., Bolasco, G., Pagani, F., Maggi, L., Scianni, M., Panzanelli, P., et al. (2011). Synaptic pruning by microglia is necessary for normal brain development. *Science* 333, 1456–1458. doi: 10.1126/science.1202529

Paolicelli, R. C., Jawaid, A., Henstridge, C. M., Valeri, A., Merlini, M., Robinson, J. L., et al. (2017). TDP-43 depletion in microglia promotes amyloid clearance but also induces synapse loss. *Neuron* 95, 297.e6–308.e6. doi: 10.1016/j.neuron.2017.05.037

Parkhurst, C. N., Yang, G., Ninan, I., Savas, J. N., Yates, J. R., Lafaille, J. J., et al. (2013). Microglia promote learning-dependent synapse formation through brain-derived neurotrophic factor. *Cell* 155, 1596–1609. doi: 10.1016/j.cell.2013.11.030

Salter, M. W., and Stevens, B. (2017). Microglia emerge as central players in brain disease. *Nat. Med.* 23, 1018–1027. doi: 10.1038/nm.4397

Schafer, D. P., Heller, C. T., Gunner, G., Heller, M., Gordon, C., Hammond, T., et al. (2016). Microglia contribute to circuit defects in Mecp2 null mice independent of microglia-specific loss of Mecp2 expression. *eLife* 5:e15224. doi: 10.7554/eLife.15224

Schafer, D. P., Lehrman, E. K., Kautzman, A. G., Koyama, R., Mardinly, A. R., Yamasaki, R., et al. (2012). Microglia sculpt postnatal neural circuits in an activity and complement-dependent manner. *Neuron* 74, 691–705. doi: 10.1016/j.neuron.2012.03.026

Schulz, C., Gomez Perdiguero, E., Chorro, L., Szabo-Rogers, H., Cagnard, N., Kierdorf, K., et al. (2012). A lineage of myeloid cells independent of Myb and hematopoietic stem cells. *Science* 336, 86–90. doi: 10.1126/science.1219179

Shi, Q., Chowdhury, S., Ma, R., Le, K. X., Hong, S., Caldarone, B. J., et al. (2017). Complement C3 deficiency protects against neurodegeneration in aged plaque-rich APP/PS1 mice. *Sci. Transl. Med.* 9:eaaf6295. doi: 10.1126/scitranslmed.aaf6295

Sierra, A., Abiega, O., Shahraz, A., and Neumann, H. (2013). Janus-faced microglia: beneficial and detrimental consequences of microglial phagocytosis. *Front. Cell. Neurosci.* 7:6. doi: 10.3389/fncel.2013.00006

Sipe, G. O., Lowery, R. L., Tremblay, M.-È., Kelly, E. A., Lamantia, C. E., and Majewska, A. K. (2016). Microglial P2Y12 is necessary for synaptic plasticity in mouse visual cortex. *Nat. Commun.* 7:10905. doi: 10.1038/ncomms10905

Squarzoni, P., Oller, G., Hoeffel, G., Pont-Lezica, L., Rostaing, P., Low, D., et al. (2014). Microglia modulate wiring of the embryonic forebrain. *Cell Rep.* 8, 1271–1279. doi: 10.1016/j.celrep.2014.07.042

Stevens, B., Allen, N. J., Vazquez, L. E., Howell, G. R., Christopherson, K. S., Nouri, N., et al. (2007). The classical complement cascade mediates CNS synapse elimination. *Cell* 131, 1164–1178. doi: 10.1016/j.cell.2007.10.036

Stowell, R. D., Sipe, G. O., Dawes, R. P., Batchelor, H. N., Lordy, K. A., Whitelaw, B. S., et al. (2019). Noradrenergic signaling in the wakeful state inhibits microglial surveillance and synaptic plasticity in the mouse visual cortex. *Nat. Neurosci.* 22, 1782–1792. doi: 10.1038/s41593-019-0514-0

Tau, G. Z., and Peterson, B. S. (2010). Normal development of brain circuits. *Neuropsychopharmacology* 35, 147–168. doi: 10.1038/npp.2009.115

Tremblay, M. È., Lowery, R. L., and Majewska, A. K. (2010). Microglial interactions with synapses are modulated by visual experience. *PLoS Biol.* 8:e1000527. doi: 10.1371/journal.pbio.1000527

Ueno, M., Fujita, Y., Tanaka, T., Nakamura, Y., Kikuta, J., Ishii, M., et al. (2013). Layer V cortical neurons require microglial support for survival during postnatal development. *Nat. Neurosci.* 16, 543–551. doi: 10.1038/nn.3358

Vainchtein, I. D., Chin, G., Cho, F. S., Kelley, K. W., Miller, J. G., Chien, E. C., et al. (2018). Astrocyte-derived interleukin-33 promotes microglial synapse engulfment and neural circuit development. *Science* 359, 1269–1273. doi: 10.1126/science.aal3589

Vasek, M. J., Garber, C., Dorsey, D., Durrant, D. M., Bollman, B., Soung, A., et al. (2016). A complement-microglial axis drives synapse loss during virus-induced memory impairment. *Nature* 534, 538–543. doi: 10.1038/nature18283

Wake, H., Moorhouse, A. J., Jinno, S., Kohsaka, S., and Nabekura, J. (2009). Resting microglia directly monitor the functional state of synapses *in vivo* and determine the fate of ischemic terminals. *J. Neurosci.* 29, 3974–3980. doi: 10.1523/JNEUROSCI.4363-08.2009

Weinhard, L., Di Bartolomei, G., Bolasco, G., Machado, P., Schieber, N. L., Neniskyte, U., et al. (2018). Microglia remodel synapses by presynaptic trogocytosis and spine head filopodia induction. *Nat. Commun.* 9:1228. doi: 10.1038/s41467-018-03566-5

Wieghofer, P., Knobeloch, K. P., and Prinz, M. (2015). Genetic targeting of microglia. *Glia* 63, 1–22. doi: 10.1002/glia.22727

Wojcik, S. M., Rhee, J. S., Herzog, E., Sigler, A., Jahn, R., Takamori, S., et al. (2004). An essential role for vesicular glutamate transporter 1 (VGLUT1) in postnatal development and control of quantal size. *Proc. Natl. Acad. Sci. U S A* 101, 7158–7163. doi: 10.1073/pnas.0401764101

Zhan, Y., Paolicelli, R. C., Sforazzini, F., Weinhard, L., Bolasco, G., Pagani, F., et al. (2014). Deficient neuron-microglia signaling results in impaired functional brain connectivity and social behavior. *Nat. Neurosci.* 17, 400–406. doi: 10.1038/nn.3641

Ziegler-Waldkirch, S., and Meyer-Luehmann, M. (2018). The role of glial cells and synapse loss in mouse models of Alzheimer's disease. *Front. Cell. Neurosci.* 12:473. doi: 10.3389/fncel.2018.00473

Conflict of Interest: The authors declare that the research was conducted in the absence of any commercial or financial relationships that could be construed as a potential conflict of interest.

frontiers in Immunology

MINI REVIEW
published: 07 October 2020
doi: 10.3389/fimmu.2020.583647

Tools and Approaches for Studying Microglia *In vivo*

Elisa Eme-Scolan[1,2] *and Samantha J. Dando*[2]*

[1] École Normale Supérieure de Lyon, Université Claude Bernard Lyon I, Université de Lyon, Lyon, France, [2] Faculty of Health, Centre for Immunology and Infection Control, School of Biomedical Sciences, Queensland University of Technology (QUT), Brisbane, QLD, Australia

Microglia are specialized resident macrophages of the central nervous system (CNS) that have important functions during neurodevelopment, homeostasis and disease. This mini-review provides an overview of the current tools and approaches for studying microglia *in vivo*. We focus on tools for labeling microglia, highlighting the advantages and limitations of microglia markers/antibodies and reporter mice. We also discuss techniques for imaging microglia *in situ*, including *in vivo* live imaging of brain and retinal microglia. Finally, we review microglia depletion approaches and their use to investigate microglial function in CNS homeostasis and disease.

Keywords: microglia, central nervous system, brain, retina, reporter mice, microglia homeostatic genes, microglia imaging, microglia depletion

OPEN ACCESS

Edited by:
Amanda Sierra, Achucarro Basque Center for Neuroscience, Spain

Reviewed by:
Souvarish Sarkar, Brigham and Women's Hospital and Harvard Medical School, United States
Rishein Gupta, University of Texas at San Antonio, United States

***Correspondence:**
Samantha J. Dando
samantha.dando@qut.edu.au

Specialty section:
This article was submitted to Multiple Sclerosis and Neuroimmunology, a section of the journal Frontiers in Immunology

Received: *15 July 2020*
Accepted: *24 August 2020*
Published: *07 October 2020*

Citation:
Eme-Scolan E and Dando SJ (2020) Tools and Approaches for Studying Microglia In vivo. Front. Immunol. 11:583647. doi: 10.3389/fimmu.2020.583647

INTRODUCTION

The CNS (comprising the brain parenchyma, spinal cord, and neural retina) is populated with specialized resident macrophages called microglia. Microglia are derived from yolk sac progenitors (1) and are long lived cells that are maintained within the CNS through *in situ* self-renewal (2). Microglia continuously survey their surroundings via highly motile processes (3) and are exquisitely programmed to respond to changes in their microenvironment. In response to injury, infection or inflammation, microglia become "activated" and can shift into numerous functional states to elicit innate immune responses. In addition to performing immune functions, microglia are intimately involved in neurodevelopment and maintaining homeostasis of the healthy CNS. Some of their "non-immune" functions include: phagocytosing apoptotic/dead neural cells and debris (4); supporting neurogenesis, neuronal development and neural circuit assembly (5–7); inducing synapse formation (8); maintaining synaptic structure and function (9); synaptic pruning (10, 11); and maintaining neurons via the formation of somatic junctions (12).

The heterogeneous states of activated microglia exist on a continuum ranging from neuroprotective to neurotoxic/pathogenic (13). There is increasing evidence, largely from animal studies, that uncontrolled activated microglia contribute to the pathogenesis of a range of neurological and ocular diseases, including Alzheimer's disease (AD) (14), multiple sclerosis (15), Parkinson's disease (16), Huntington's disease (17), Amyotrophic Lateral Sclerosis (ALS) (18), neuromyelitis optica (19) and autoimmune uveitis (20). However, protective disease-associated microglia have also been described in AD and ALS (21), and may also exist in retinal degeneration (22). Despite the ongoing debate regarding the protective vs. pathogenic role of microglia, they are clearly involved in a wide range of CNS diseases and display a high level of plasticity.

Microglia are the subject of intense research efforts; however, there are several challenges associated with studying these cells. *Challenge 1*: microglia cultured *in vitro* do not recapitulate *in vivo* microglia in their physiological environment. Although important advances have been made to develop new microglia culture methods, including serum-free culture conditions and iPSC-derived microglia [reviewed in (23–25)], *in vitro* approaches that reflect microglia within their immune-privileged neural environment are still lacking. *Challenge 2*: when studying microglia *in vivo*, manipulation of the CNS (for example, preparing brain slices) can lead to injury and subsequent microglia activation (26), which is a limitation for studying microglia in their physiological state. *Challenge 3*: microglia share overlapping markers with other myeloid cells (27). It is essential to differentiate microglia from border-associated macrophages (BAMs), which reside within the meninges, choroid plexus and perivascular spaces of the brain, and the choroid that lies adjacent to the retina. Similarly, microglia must also be distinguished from circulating myeloid cells that infiltrate the CNS during neuroinflammation.

In recent years, significant progress has been made to address these challenges by developing new cellular and molecular tools for microglia research. In this mini-review we discuss the current "microglia tool kit" for *in vivo* research (summarized in **Figure 1** and **Table 1**), and how recently developed approaches can be used to overcome some of the above challenges.

TOOLS FOR LABELING MICROGLIA IN THE CNS

Markers and Antibodies

Immunohistochemistry and flow cytometry are common techniques in neuroimmunology. Traditionally, Iba-1 antibodies have been used to label/stain microglia using immunohistochemistry; however, Iba-1 is also expressed by BAMs and subsets of peripheral myeloid cells (28, 29). During neuroinflammation, peripheral Iba-1^{+} myeloid cells that invade the CNS adopt a similar morphology to activated microglia (30), therefore microglia cannot be definitively distinguished from infiltrating leukocytes based solely on Iba-1 expression. Microglia also express several other markers that are common to BAMs and peripheral myeloid cells, including CD45, CD11b, CD68, Cx3cr1, F4/80, and CSF1R (31). Using flow cytometry, it is possible to distinguish microglia from other leukocytes based on their unique expression profile of selected surface markers. For example, microglia in the healthy CNS express low/intermediate levels of CD45, whereas BAMs and peripheral immune cells are CD45^{hi}. Whether microglia retain low/intermediate CD45 expression during neuroinflammation is debated and appears to be disease- and CNS region-dependent. O'Koren et al. reported that retinal microglia retain a CD45^{lo} phenotype in a light injury model and can be distinguished from infiltrating myeloid cells based on their unique CD45^{lo}

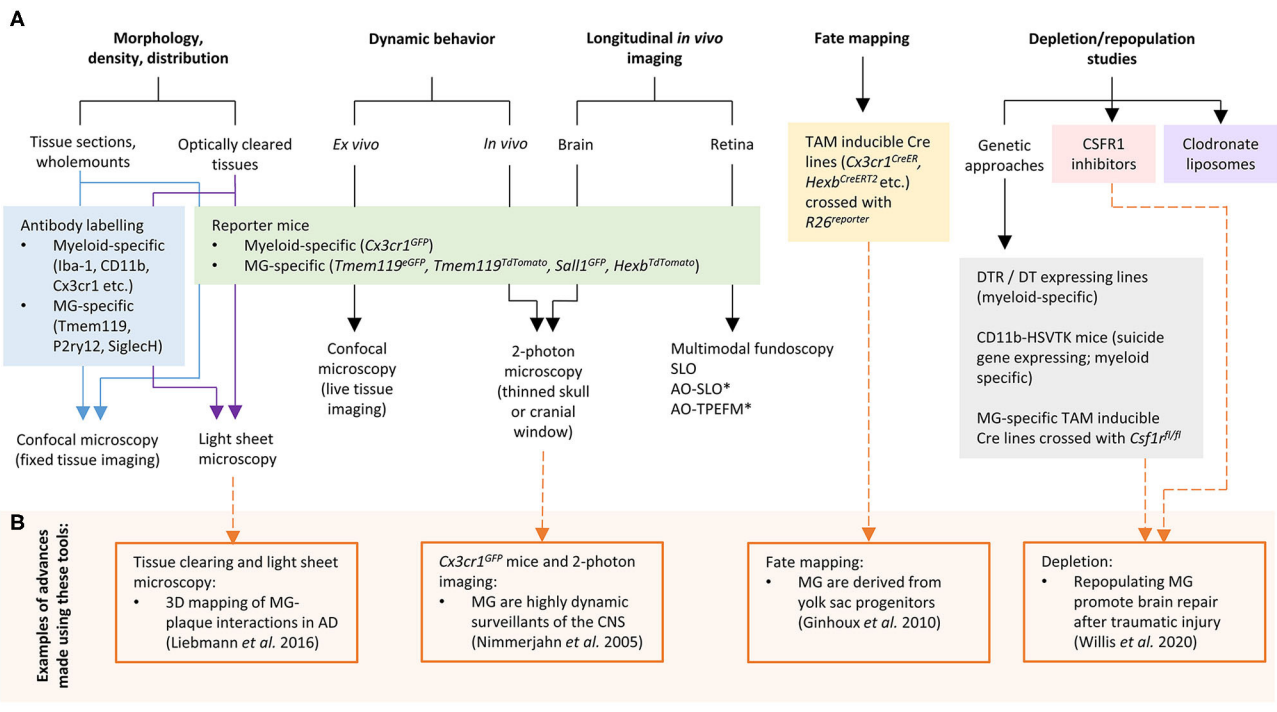

FIGURE 1 | (A) Tools and approaches for studying microglia *in vivo*. **(B)** Examples of advances in microglia research that have been made using these tools. AD, Alzheimer's disease; AO, adaptive optics; CSF1R, colony stimulating factor 1 receptor; DT, diphtheria toxin; DTR, diphtheria toxin receptor; MG, microglia; SLO, scanning laser ophthalmoscopy; TPEFM, two-photon excitation fluorescence microscopy. *can also be used for *in vivo* retinal microglia dynamic behavior studies.

TABLE 1 | Advantages, limitations, and applications of tools to study microglia *in vivo*.

	Advantages	Limitations	Applications for studying MG *in vivo*
LABELING MG			
Myeloid markers (Iba-1, Cx3cr1, CD45, CD11b)	Antibodies widely available; most work well in fixed tissue sections and whole mounts.	Also expressed by BAMs and peripheral immune cells.	Phenotyping (e.g., analysis of MG density, distribution, morphology, marker co-expression, cell interactions).
MG-specific markers (Tmem119, P2RY12, FCRLS, SiglecH, HexB)	Expression restricted to MG in healthy brain. Highly expressed by MG in steady state.	Expression may be decreased by MG during disease. Tmem119 expression may not be restricted to MG in the diseased retina. Few commercially available antibodies.	
***Cx3cr1* reporter mice** *Cx3cr1*^{GFP}; *Cx3cr1*^{CreER}:*R26* ^{Reporter}	GFP or Cre under control of *Cx3cr1* promoter, which is highly expressed in homeostatic MG. *Cx3cr1*^{GFP} mice available on C57Bl/6 and BALB/c background. *Cx3cr1*^{CreER}:*R26* ^{Reporter} mice: Temporary labeling of peripheral myeloid cells; irreversible labeling of MG.	*Cx3cr1*^{GFP}: BAMs and peripheral immune cells also labeled. Heterozygous *Cx3cr1*^{GFP} mice may have partially impaired Cx3cl1-Cx3cr1 signaling compared to WT mice. *Cx3cr1*^{CreER}:*R26* ^{Reporter}: BAMs also labeled.	*Cx3cr1*^{GFP}: Phenotyping. Homozygous *Cx3cr1*^{GFP} mice can be used to study effects of full *Cx3cr1* deletion. *Cx3cr1*^{CreER}:*R26* ^{Reporter}: Fate mapping MG in development, disease, and aging.
"Next generation" MG reporter mice *Tmem119*^{Reporter}, *Sall1*^{GFP}, *Hexb*^{TdTomato} *Tmem119/Sall1/Hexb/P2ry12*^{CreER}:*R26* ^{Reporter}	Higher specificity for MG compared to *Cx3cr1* lines. Hexb reporter stably expressed during neurodegeneration and demyelination.	Non-specific recombination can occur in some Cre lines, resulting in subsets of BAMs and glia also being labeled. Fluorescent reporter expression may be decreased during disease.	Phenotyping (fluorescent reporter lines); fate mapping in development, disease, and aging (Cre lines).
IMAGING MG			
Confocal microscopy (Fixed tissues)	High resolution 3D datasets generated by collecting optical Z sections through tissue. Many laboratories have access to confocal microscopes through core facilities.	Most confocal microscopes have limited imaging depth: requires specimen to be sectioned (brain) or microdissected (retina). Image acquisition can be slow. Photobleaching of tissue can occur. Cannot study dynamic behavior of MG in fixed tissues. Fixation may affect MG morphology.	Imaging fluorescently labeled microglia in fixed brain/spinal cord/retinal sections or whole mounts.
Tissue clearing and light sheet microscopy (Fixed tissues)	Can perform rapid 3D reconstructions of optically cleared tissues (deep imaging). Eliminates requirement for histological sectioning. Large variety of tissue clearing methods for mouse brain and eye; some compatible with antibody labeling and endogenous fluorescent reporters.	Not all research facilities have access to light sheet microscopes and specialized objectives. Some hydrophobic tissue clearing methods quench fluorescent reporter signals.	Imaging fluorescently labeled microglia in fixed, optically cleared tissues ("global" tissue imaging).
***In vivo* live imaging** Two-photon microscopy (brain) Multimodal fundoscopy, SLO, AO-SLO (retina)	Imaging MG in live animals.	Specialized instrumentation required; not available in all research facilities. High level of technical expertise required. Microglia process dynamics are increased in anesthetized mice compared to awake mice. Cranial window or thinned skull preparation required for brain two-photon imaging. Not all brain regions are accessible using two-photon imaging.	Imaging dynamic MG behavior *in vivo* (study MG tissue surveillance functions). *In vivo* longitudinal imaging of MG. *In vivo* cellular interactions.

(Continued)

TABLE 1 | Continued

	Advantages	Limitations	Applications for studying MG *in vivo*
DEPLETING MG			
Clodronate liposomes	Effective for short-term depletion studies.	MG depletion requires intracerebral or intravitreal injection (break "immune privilege" due to physical trauma). Likely to also deplete BAMs. Off-target effects.	Depletion of MG to determine their functions in development, homeostasis or disease. Study MG repopulation.
CSF1R inhibitors (PLX3397, PLX5662)	Cross the blood-brain/blood-retina barrier and can be administered orally. 90–99% MG depletion after 21 days treatment. Can be used for sustained MG depletion studies. MG repopulate quickly after cessation of treatment.	Not MG-specific	
Genetic approaches *Cx3cr1*^{CreER}*:R26*^{iDTR} *Iba1-tTA::DTA*$^{tetO/tetO}$ *CD11b-HSVTK* *Siglech*$^{DTR/DTR}$ *Sall1*^{CreER}*Csf1r*$^{fl/fl}$ *Hexb*$^{CreERT2/CreERT2}$*Csf1r*$^{fl/fl}$	*Siglech*$^{DTR/DTR}$, *Sall1*^{CreER}*Csf1r*$^{fl/fl}$ and *Hexb*$^{CreERT2/CreERT2}$*Csf1r*$^{fl/fl}$ mice enable precise depletion of MG (BAMs or circulating leukocytes not targeted). High levels of MG depletion (>90%) can be achieved in *Cx3cr1*^{CreER}*:R26*^{iDTR}, *Iba1-tTA::DTA*$^{tetO/tetO}$ and *CD11b-HSVTK* mice.	Depletion requires injections of either tamoxifen, DT or ganciclovir. *Cx3cr1*^{CreER}*:R26*^{iDTR}, *Iba1-tTA::DTA*$^{tetO/tetO}$ and *CD11b-HSVTK* mice do not enable MG-specific depletion (BAMs and subsets of circulating myeloid cells also depleted) Depletion less efficient in *Hexb*$^{CreERT2/CreERT2}$*Csf1r*$^{fl/fl}$ mice.	

AO, adaptive optics; BAMs, border-associated macrophages; CSF1R, colony stimulating factor 1 receptor; DT, diphtheria toxin; MG, microglia; SLO, scanning laser ophthalmoscopy.

CD11c^{lo} F4/80^{lo} I-A/I-E^{-} signature (32). In contrast, Plemel et al. demonstrated that spinal cord microglia increased CD45 expression in a demyelination model and suggested that classical markers (such as CD45 and Cx3cr1) are less sensitive for distinguishing activated microglia from infiltrating myeloid cells in this model (33). Therefore, more recent studies have focused on identifying microglia-specific markers that can reliably distinguish microglia from other leukocytes during health and disease.

Bulk RNA-seq studies have identified several highly expressed genes that constitute the "microglia homeostatic signature" (28, 34–36). These signature genes, including *Tmem119*, *P2ry12*, *Olfml3*, *Hexb*, *Fcrls*, *Siglech*, *Tgfbr1*, *Gpr34*, *Sall1,* and others, have been the basis for the development of a range of new tools for microglia research in recent years, including microglia-specific antibodies. Tmem119 antibodies were developed by Bennett et al. for specific labeling of microglia using immunohistochemistry and flow cytometry (37). Tmem119 is expressed by mouse and human microglia but not BAMs or peripheral immune cells, and commercially available Tmem119 antibodies are now widely used. Butovsky et al. generated antibodies to P2ry12 and FCRLS, and showed that these distinguished mouse microglia from infiltrating myeloid cells (34). Furthermore, Konishi et al. reported that SiglecH antibodies specifically labeled microglia in the mouse brain but not BAMs or infiltrating monocytes (38). Microglia signature genes have also recently been used as targets for single molecule fluorescence *in situ* hybridization (smFISH) using RNAscope assays. Hammond et al. used smFISH (alongside single cell RNA-seq) to study microglia throughout the mouse lifespan and demonstrated that (i) microglia universally expressed FCRLS and (ii) diverse subtypes of microglia with unique spatial gene expression signatures exist in the developing, aged, and injured mouse brain (39).

The development of microglia-specific antibodies is useful for labeling these cells during homeostatic conditions. However, these markers may not be reliable for the identification of microglia during development and disease. For example, embryonic microglia do not express Tmem119, and expression of this protein by all microglia does not occur until postnatal day 14 in mice (37). This limits the use of Tmem119 antibodies during development and early postnatal stages. Furthermore, Tmem119 immunoreactivity may not be restricted to microglia in the diseased retina, as Su et al. reported that other cell types (such as Müller cells) may become Tmem119^{+} in a choroidal neovascularization model (40). Although further studies are required to validate these findings in other experimental models, Tmem119 antibodies should be used cautiously in the diseased retina. Moreover, microglial homeostatic genes including *Tmem119*, *P2ry12,* and *Siglech* are reported to be downregulated in CNS diseases (21, 41, 42), which may further limit their use. This is likely to be disease-dependent however, as some studies have shown stable expression of microglia homeostatic genes during disease (43). Given the range of markers and antibodies that can be used to identify microglia, the choice of targets needs to be carefully considered for each research question.

Reporter Mice

The fractalkine receptor gene *Cx3cr1* is the basis of several reporter mouse lines that are widely used in microglia research. In $Cx3cr1^{GFP}$ mice, microglia express GFP under the control of the *Cx3cr1* promoter (44). Homeostatic microglia express high levels of Cx3cr1 and are therefore strongly GFP^{+}, which is extremely useful for identifying microglia within tissues. One limitation of these mice is that they are either heterozygous ($Cx3cr1^{GFP/+}$) or deficient ($Cx3cr1^{GFP/GFP}$) for *Cx3cr1*, and therefore neuron-microglia communication (mediated by Cx3cl1-Cx3cr1 signaling) is impaired compared to wild type mice, which can lead to reduced cognitive and synaptic function (45). Another important caveat is that Cx3cr1 is also expressed by BAMs, peripheral monocytes, DCs and NK cells (44), therefore GFP expression is not restricted to microglia. In contrast, tamoxifen inducible $Cx3cr1^{CreER}$ mice crossed with $R26^{Reporter}$ mice are a useful tool to distinguish microglia and CNS-infiltrating myeloid cells (32, 46). In these mice, CreER is constitutively expressed under the control of the *Cx3cr1* promoter, whereas $R26^{Reporter}$ expression is dependent on Cre recombination. Upon tamoxifen administration, Cre is activated in Cx3cr1 expressing cells and a stop codon controlling $R26^{Reporter}$ expression is excised, resulting in $Cx3cr1^{+}$ cells becoming $R26^{Reporter+}$ (i.e., both tissue resident macrophages and circulating myeloid cells express $R26^{Reporter}$). Due to the temporary activation of Cre and the turnover of circulating myeloid cells, several weeks after tamoxifen induction blood-borne myeloid cells lose $R26^{Reporter}$ expression. In contrast, $R26^{Reporter}$ labeling is irreversible in long-lived tissue resident macrophages, including microglia (32, 46). However, BAMs are also long-lived resident cells that retain expression of the tamoxifen-induced reporter using this $Cx3cr1^{CreER}$ approach (47), and additional means are required to distinguish microglia from BAMs.

Recently described reporter mice have taken advantage of microglia-specific signature genes. $Tmem119^{eGFP}$ (48), $Tmem119^{TdTomato}$ (49), $Sall1^{GFP}$ (50, 51), and $Hexb^{TdTomato}$ (52) mice are knock-in strains in which expression of fluorescent reporter proteins is largely restricted to microglia. Although *Tmem119*, *Sall1,* and other microglia signature genes are typically downregulated during CNS disease, mouse microglia were recently reported to maintain stable *Hexb* expression in models of neurodegeneration and demyelination, suggesting that $Hexb^{TdTomato}$ mice may be suitable for consistent bright labeling of microglia in both homeostasis and CNS disease (52). In addition to the $Cx3cr1^{CreER}$ mice described above, several other tamoxifen inducible Cre lines now also exist for microglia fate mapping and genetic manipulation. These include $Tmem119^{CreERT2}$ (48), $Sall1^{CreER}$ (50), $Hexb^{CreERT2}$ (52) and $P2ry12^{CreER}$ (53). Although these mouse strains have a much higher specificity for microglia compared to $Cx3cr1^{CreER}$ mice, they still have some limitations. For example, $Tmem119^{CreERT2}$ and $P2ry12^{CreER}$ mice are not 100% microglia specific as recombination also occurs in some BAM subsets after tamoxifen administration. In addition, recombination is detected in glial cells in $Sall1^{CreER}$ mice (52, 54). Of the available tamoxifen inducible Cre lines, $Hexb^{CreERT2}$ mice are reported to have the highest microglia specificity, although not all microglia are targeted (brain region dependent) and recombination also occurs in a very small percentage of perivascular macrophages (52). Despite these limitations, these "next generation" reporter mice are an excellent resource for the neuroimmunology research community.

TECHNIQUES FOR IMAGING MICROGLIA *IN SITU*

Confocal Microscopy of Fixed and Fresh Tissue

The ability to label microglia using the above approaches enables researchers to visualize these cells *in situ*. Confocal laser scanning microscopy is frequently used to image fluorescently labeled microglia in tissue sections (fixed), retinal wholemounts (fixed or fresh) and organotypic brain slices (fresh) to investigate microglial density, morphology, distribution, cellular interactions and dynamic behavior. However, there are limitations to these approaches. Fixation obviously preserves the tissue but makes it impossible to study the dynamism of microglia. Fixation procedures can also have effects on microglia morphology (55), which may confound some experiments. On the other hand, the dynamic behavior of microglia can be observed in fresh retinal wholemounts (56) and brain slices (57) but as tissues are placed in artificial medium for live imaging, microglia are likely to sense perturbations within their environment. In addition, the process of preparing brain slices and retinal wholemounts for live imaging can cause physical trauma. Therefore, microglia observed using live *ex vivo* approaches may not recapitulate their *in vivo* physiological counterparts.

Tissue Clearing and Light Sheet Microscopy

Tissue clearing techniques coupled with light sheet microscopy can be used to visualize microglia within intact transparent CNS tissues. Tissue clearing methods [reviewed in detail in (58)] make tissues transparent, resulting in minimal light scattering and enabling deep imaging and 3D reconstruction of tissues (including brains and eyes). This allows unbiased global investigation of tissues and eliminates the requirement to perform histological sectioning, which is a major advantage of this technique. A range of tissue clearing methods (including hydrophobic, hydrophilic and hydrogel-based methods) can be used to "clear" fixed CNS tissues (58, 59). Depending on the clearing method, tissues can be labeled with antibodies, nanobodies and lectins prior to clearing for visualization of cells and structures of interest. For example, Liebmann et al. used iDISCO clearing and Iba-1 immunolabeling to reconstruct the 3D interactions between brain microglia, vasculature and amyloid-β plaques in a mouse model of Alzheimer's disease (60). Some hydrophobic tissue clearing methods [such as

3DISCO (61)] rapidly quench fluorescent reporter protein signals; however, several hydrophilic and hydrogel-based clearing approaches effectively preserve endogenous fluorescence and can be used to image microglia in fluorescent reporter mice (described above). For instance, Xu et al. developed the FACT tissue clearing method and applied this to *Cx3cr1*^{YFP} mouse brains for deep imaging of YFP^{+} microglia (62). Using this method, the authors detected fluorescent signal to a Z depth of ∼800 μm although the signal intensity was markedly diminished after ∼550 μm (62).

Unlike the brain, the eye is naturally transparent. However, the retinal pigment epithelium, the interface between the retinal photoreceptors and the choroid, is highly melanized (darkly pigmented), which remains a challenge for standard clearing methods. Specialized clearing techniques including EyeCi (63), DEEP-Clear (64), and EyeDISCO (65) were developed to address this issue and enable light sheet imaging of retinas within intact eyeballs. However, to the best of our knowledge these techniques have not yet been used for retinal microglia studies.

In vivo Live Imaging of Microglia

Two-photon microscopy is a powerful technique that allows unparalleled imaging of microglia in live animals. Time-lapse *in vivo* two-photon imaging of *Cx3cr1*^{GFP} mouse brains led to the seminal discovery that microglia are highly dynamic surveillants that constantly extend and retract their processes during homeostasis (3). Several studies have since used two-photon imaging to study microglial dynamism in CNS disease models and aging (66–68). Most two-photon microglia imaging studies are performed on mice under general anesthesia through either a cranial window or thinned skull preparation [reviewed in detail in (69)]. The major advantage of this approach is that it is performed in live animals and therefore the cells are observed within their physiological environment. However, there are some important limitations. Firstly, microglial arbor, surveillance territory and process dynamics are increased in anesthetized mice compared to awake mice (70, 71) and methods to image microglia in awake mice may be required for some studies. Secondly, cranial window surgery and skull thinning procedures can induce CNS damage and subsequent microglial activation (69). Thirdly, not all brain regions are accessible using this approach. It remains difficult to image deep brain regions, therefore most two-photon studies are performed on cortical microglia. Using *Hexb*^{TdTomato} mice, Masuda et al. demonstrated that it is possible to perform time lapse *in vivo* two-photon imaging of microglia to a depth of 500 μm from the surface of the brain (52).

Specialized tools are available for *in vivo* live imaging of retinal microglia. Multimodal fundoscopy and scanning laser ophthalmoscopy (SLO) enable longitudinal studies of microglia in fluorescent reporter mice (72, 73) but these methods do not have sufficient resolution for examination of microglia fine process morphology or dynamic behavior, nor do they provide any depth information. Adaptive optics (AO) is a recent advancement that corrects optical aberrations and significantly improves resolution. When combined with SLO, AO-SLO enables microglia within distinct retinal layers to be resolved *in vivo* (74). Miller et al. demonstrated that AO-SLO can be used to quantify the 3D distribution, morphology and dynamism of microglia within individual layers of the *Cx3cr1*^{GFP} mouse retina (75). More recently, Qin et al. developed an adaptive optics two-photon excitation fluorescence microscopy (AO-TPEFM) system that provides further improvements in the resolution of *in vivo* retinal microglia imaging (76). Combined with microglia-specific fluorescent reporter mice, AO-SLO and AO-TPEFM imaging will be useful tools to examine *in vivo* longitudinal changes in microglia in retinal diseases.

In vivo microglia imaging in humans remains challenging due to a lack of specific tools but positron emission tomography (PET) combined with 18-kDa translocator protein (TPSO)-binding radioligands is used to non-specifically assess microglial activation and neuroinflammation in patients *in vivo* (77, 78). The use of this clinical neuroimaging technique in multiple sclerosis patients has been reviewed previously (77) and will not be discussed here.

TOOLS FOR DEPLETING MICROGLIA

Clodronate Liposomes

To attribute *in vivo* functions to microglia, depletion studies are often required. One approach to deplete microglia *in vivo* involves clodronate liposomes. Clodronate liposomes are phagocytosed by macrophages and subsequently released into the cytosol, where clodronate inhibits mitochondrial ADP/ATP translocase and induces macrophage apoptosis (79). To deplete microglia, clodronate liposomes are injected intracerebrally (80, 81) or intravitreally (82) to bypass the blood-brain/blood-retina barrier. This approach is effective for short-term microglia depletion; however, intracerebral injections can induce physical trauma and break "immune privilege" of the CNS (83). Moreover, off-target effects may occur (84), and control liposomes (that do not contain clodronate) have been shown to non-specifically activate microglia (85). Intracerebral delivery of clodronate liposomes is also likely to deplete BAMs (in particular, perivascular macrophages), although the specificity of depletion following intracerebral administration of clodronate liposomes has not been investigated to the best of our knowledge. In contrast, intraventricular injection of clodronate liposomes results in selective depletion of BAMs and not microglia (86).

CSF1R Inhibitors

CSF1R inhibitors are effective for microglia depletion, as adult microglia depend on CSF1R for survival (87). Unlike CSF1R antibodies and clodronate liposomes, CSF1R inhibitors are small molecules that readily cross the blood-brain/blood-retina barrier and can be administered orally, either by oral gavage or mixed within standard rodent chow. PLX3397 and PLX5662 are the most commonly used CSF1R inhibitors for microglia depletion as these have high potency (PLX3397)

(87) and high brain penetrance (PLX5662) (88). CSF1R inhibitors are effective to achieve long-term, sustained microglial depletion *in vivo*. However, this approach does not eliminate 100% of microglia. For example, PLX3397 depletes 90–99% of microglia from the mouse brain after 21 days of treatment (89). Microglial repopulation begins after CSF1R inhibitor treatment ceases, and it is thought that repopulating microglia are generated from the few microglial cells that are not eliminated by the treatment (72). In the mouse retina, repopulated microglia display similar dynamism to endogenous microglia, suggesting that repopulated microglia restore homeostatic tissue surveillance (72). Interestingly, the adult mouse brain only has capacity for a single microglia repopulation event, as following repeated PLX3397 depletion cycles microglia fail to repopulate the brain (90). Using PLX3397 depletion, Spangenberg et al. reported that microglial elimination improved contextual memory deficits in a mouse model (5xFAD) of Alzheimer's disease (91). Further studies demonstrated that sustained PLX5662 microglia depletion impaired plaque formation in 5xFAD mice (88, 92). As such, CSF1R inhibitors are being investigated as a potential treatment option for CNS diseases (93). However, studies involving CSF1R depletion strategies must be interpreted cautiously, as CSF1R inhibitors also likely target BAMs and some peripheral immune populations (93).

Genetic Approaches

Microglia depletion can also be achieved with genetic approaches. In $Cx3cr1^{CreER}$:$R26^{iDTR}$ mice, microglia and other long-lived resident immune cells (but not circulating myeloid cells) express the diphtheria toxin receptor (DTR) following tamoxifen administration. Upon exposure to diphtheria toxin (DT), ∼99% of microglia are depleted within 1 day, and low numbers of microglia are maintained in the CNS for up to 7 days post-DT (46). *Iba1-tTA::DTA*$^{tetO/tetO}$ mice also take advantage of a DT system. In these mice, selective expression of DT occurs in Iba-1$^+$ cells after withdrawal of doxycycline. This results in ∼90% depletion of microglia (94); however, Iba-1$^+$ BAMs and peripheral myeloid cells are also likely to be targeted in these mice. Depletion systems based on the *CD11b* promoter also broadly target myeloid cells and are not microglia specific. In *CD11b-HSVTK* mice, expression of the suicide gene *HSVTK* is driven by the *CD11b* promoter. After administration of the drug ganciclovir, HSVTK converts ganciclovir to a toxic compound, which induces apoptosis of CD11b$^+$ cells. Intracerebroventricular infusion of ganciclovir achieves high levels (<90%) of microglia depletion; however, this is short-lived as microglia robustly repopulate the CNS within 2 weeks of ganciclovir treatment (95).

Genetic depletion systems targeting microglia-specific genes offer a more precise approach to microglia elimination without affecting BAMs and circulating myeloid cells. Using $Siglech^{DTR/DTR}$ mice, Konishi et al. reported that ∼80–85% of Iba-1$^+$ CD206$^-$ microglia were depleted in the cortex and area postrema following intraperitoneal DT injection. In contrast, the numbers of perivascular macrophages, meningeal macrophages and infiltrating monocytes following nerve injury were unaffected (38). Tamoxifen inducible Cre lines also exist for specific microglia depletion, including $Sall1^{CreER}Csf1r^{fl/fl}$ and $Hexb^{CreERT2/CreERT2}Csf1r^{fl/fl}$ mice. In these strains, the conditional *Csf1r* allele is deleted by tamoxifen inducible Cre expressed from the *Sall1* or *Hexb* locus (50, 52). Whilst these strains specifically target microglia (and not BAMs or circulating myeloid cells), recombination appears to be less efficient that other genetic depletion systems. For example, in $Hexb^{CreERT2/CreERT2}Csf1r^{fl/fl}$ mice only 60% of microglia are depleted after tamoxifen injection (52). Moreover, in $Sall1^{CreER}Csf1r^{fl/fl}$ mice small numbers of Sall1$^+$ CD45$^-$ cells in the adult kidney and liver are also depleted (50). Whilst tamoxifen-induced depletion of these cells in adult mice does not result in overt inflammation in the serum, spleen, liver, and kidneys (50), it is possible there may be other effects in these peripheral organs.

CONCLUSION

Researchers have previously applied traditional immunological approaches to study microglia the CNS. Thanks to rapid advances in the neuroimmunology field, we now have a suite of tools and techniques for microglia research. The discovery of microglia-specific signature genes has elevated the choice of markers, antibodies and reporter mice for studying these cells *in vivo*. However, further research to identify microglia-specific markers that are stably expressed during neuroinflammation is required. The combination of microglia-specific labeling, powerful *in vivo* imaging, and precise depletion approaches is already accelerating discoveries relating to microglial biology. These tools provide opportunities to investigate microglial function and phenotype *in vivo,* and to understand the spatial and disease-dependent heterogeneity of these multitasking, multifunctional cells.

AUTHOR CONTRIBUTIONS

EE-S and SD conceived and researched data for the article and wrote the review. All authors contributed to the article and approved the submitted version.

FUNDING

SD was supported by an Australian Research Council DECRA (DE180101075).

ACKNOWLEDGMENTS

The authors thank Dr. Antoine Corbin and Dr. Rejane Rua for insightful discussions and comments on early drafts of the manuscript, and the Master de Biologie of the École Normale Supérieure de Lyon for their support and guidance.

REFERENCES

1. Ginhoux F, Greter M, Leboeuf M, Nandi S, See P, Gokhan S, et al. Fate mapping analysis reveals that adult microglia derive from primitive macrophages. *Science.* (2010) 330:841–5. doi: 10.1126/science.1194637
2. Ajami B, Bennett JL, Krieger C, Tetzlaff W, Rossi FMV. Local self-renewal can sustain CNS microglia maintenance and function throughout adult life. *Nat Neurosci.* (2007) 10:1538–43. doi: 10.1038/nn2014
3. Nimmerjahn A, Kirchhoff F, Helmchen F. Resting microglial cells are highly dynamic surveillants of brain parenchyma *in vivo*. *Science.* (2005) 308:1314–8. doi: 10.1126/science.1110647
4. Márquez-Ropero M, Benito E, Plaza-Zabala A, Sierra A. Microglial corpse clearance: lessons from macrophages. *Front Immunol.* (2020) 11:506. doi: 10.3389/fimmu.2020.00506
5. Wallace J, Lord J, Dissing-Olesen L, Stevens B, Murthy VN. Microglial depletion disrupts normal functional development of adult-born neurons in the olfactory bulb. *eLife.* (2020) 9:e50531. doi: 10.7554/eLife.50531
6. Squarzoni P, Oller G, Hoeffel G, Pont-Lezica L, Rostaing P, Low D, et al. Microglia modulate wiring of the embryonic forebrain. *Cell Rep.* (2014) 8:1271–9. doi: 10.1016/j.celrep.2014.07.042
7. Diaz-Aparicio I, Paris I, Sierra-Torre V, Plaza-Zabala A, Rodríguez-Iglesias N, Márquez-Ropero M, et al. Microglia actively remodel adult hippocampal neurogenesis through the phagocytosis secretome. *J Neurosci.* (2020) 40:1453–82. doi: 10.1523/JNEUROSCI.0993-19.2019
8. Miyamoto A, Wake H, Ishikawa AW, Eto K, Shibata K, Murakoshi H, et al. Microglia contact induces synapse formation in developing somatosensory cortex. *Nat Commun.* (2016) 7:12540. doi: 10.1038/ncomms12540
9. Wang X, Zhao L, Zhang J, Fariss RN, Ma W, Kretschmer F, et al. Requirement for microglia for the maintenance of synaptic function and integrity in the mature retina. *J Neurosci.* (2016) 36:2827–42. doi: 10.1523/JNEUROSCI.3575-15.2016
10. Paolicelli RC, Bolasco G, Pagani F, Maggi L, Scianni M, Panzanelli P, et al. Synaptic pruning by microglia is necessary for normal brain development. *Science.* (2011) 333:1456–8. doi: 10.1126/science.1202529
11. Tremblay M-È, Lowery RL, Majewska AK. Microglial interactions with synapses are modulated by visual experience. *PLOS Biol.* (2010) 8:e1000527. doi: 10.1371/journal.pbio.1000527
12. Cserép C, Pósfai B, Lénárt N, Fekete R, László ZI, Lele Z, et al. Microglia monitor and protect neuronal function through specialized somatic purinergic junctions. *Science.* (2020) 367:528–37. doi: 10.1126/science.aax6752
13. Hellwig S, Heinrich A, Biber K. The brain's best friend: microglial neurotoxicity revisited. *Front Cell Neurosci.* (2013) 7:71. doi: 10.3389/fncel.2013.00071
14. Shi Y, Manis M, Long J, Wang K, Sullivan PM, Remolina Serrano J, et al. Microglia drive APOE-dependent neurodegeneration in a tauopathy mouse model. *J Exp Med.* (2019) 216:2546–61. doi: 10.1084/jem.20190980
15. Voet S, Prinz M, van Loo G. Microglia in central nervous system inflammation and multiple sclerosis pathology. *Trends Mol Med.* (2019) 25:112–23. doi: 10.1016/j.molmed.2018.11.005
16. Guo M, Wang J, Zhao Y, Feng Y, Han S, Dong Q, et al. Microglial exosomes facilitate α-synuclein transmission in Parkinson's disease. *Brain.* (2020) 143:1476–97. doi: 10.1093/brain/awaa090
17. Crapser JD, Ochaba J, Soni N, Reidling JC, Thompson LM, Green KN. Microglial depletion prevents extracellular matrix changes and striatal volume reduction in a model of Huntington's disease. *Brain.* (2020) 143:266–88. doi: 10.1093/brain/awz363
18. Christoforidou E, Joilin G, Hafezparast M. Potential of activated microglia as a source of dysregulated extracellular microRNAs contributing to neurodegeneration in amyotrophic lateral sclerosis. *J Neuroinflamm.* (2020) 17:135. doi: 10.1186/s12974-020-01822-4
19. Chen T, Lennon VA, Liu YU, Bosco DB, Li Y, Yi M-H, et al. Astrocyte-microglia interaction drives evolving neuromyelitis optica lesion. *J Clin Invest.* (2020) 130:4025–38. doi: 10.1172/JCI134816
20. Okunuki Y, Mukai R, Nakao T, Tabor SJ, Butovsky O, Dana R, et al. Retinal microglia initiate neuroinflammation in ocular autoimmunity. *Proc Natl Acad Sci USA.* (2019) 116:9989–98. doi: 10.1073/pnas.1820387116
21. Keren-Shaul H, Spinrad A, Weiner A, Matcovitch-Natan O, Dvir-Szternfeld R, Ulland TK, et al. A unique microglia type associated with restricting development of Alzheimer's disease. *Cell.* (2017) 169:1276–90.e17. doi: 10.1016/j.cell.2017.05.018
22. Yu C, Roubeix C, Sennlaub F, Saban DR. Microglia versus monocytes: distinct roles in degenerative diseases of the retina. *Trends Neurosci.* (2020) 43:433–49. doi: 10.1016/j.tins.2020.03.012
23. Guttenplan KA, Liddelow SA. Astrocytes and microglia: models and tools. *J Exp Med.* (2019) 216:71–83. doi: 10.1084/jem.20180200
24. Timmerman R, Burm SM, Bajramovic JJ. An overview of *in vitro* methods to study microglia. *Front Cell Neurosci.* (2018) 12:242. doi: 10.3389/fncel.2018.00242
25. Hasselmann J, Blurton-Jones M. Human iPSC-derived microglia: a growing toolset to study the brain's innate immune cells. *Glia.* (2020) 68:721–39. doi: 10.1002/glia.23781
26. Stence N, Waite M, Dailey ME. Dynamics of microglial activation: a confocal time-lapse analysis in hippocampal slices. *Glia.* (2001) 33:256–66. doi: 10.1002/1098-1136(200103)33:3<256::AID-GLIA1024>3.0.CO;2-J
27. McMenamin PG, Saban DR, Dando SJ. Immune cells in the retina and choroid: two different tissue environments that require different defenses and surveillance. *Prog Retin Eye Res.* (2019) 70:85–98. doi: 10.1016/j.preteyeres.2018.12.002
28. Chiu IM, Morimoto ETA, Goodarzi H, Liao JT, O'Keeffe S, Phatnani HP, et al. A neurodegeneration-specific gene-expression signature of acutely isolated microglia from an amyotrophic lateral sclerosis mouse model. *Cell Rep.* (2013) 4:385–401. doi: 10.1016/j.celrep.2013.06.018
29. Dando SJ, Kazanis R, Chinnery HR, McMenamin PG. Regional and functional heterogeneity of antigen presenting cells in the mouse brain and meninges. *Glia.* (2019) 67:935–49. doi: 10.1002/glia.23581
30. Miró-Mur F, Pérez-de-Puig I, Ferrer-Ferrer M, Urra X, Justicia C, Chamorro A, et al. Immature monocytes recruited to the ischemic mouse brain differentiate into macrophages with features of alternative activation. *Brain Behav Immun.* (2016) 53:18–33. doi: 10.1016/j.bbi.2015.08.010
31. Dando SJ, Naranjo Golborne C, Chinnery HR, Ruitenberg MJ, McMenamin PG. A case of mistaken identity: CD11c-eYFP + cells in the normal mouse brain parenchyma and neural retina display the phenotype of microglia, not dendritic cells. *Glia.* (2016) 64:1331–49. doi: 10.1002/glia.23005
32. O'Koren EG, Mathew R, Saban DR. Fate mapping reveals that microglia and recruited monocyte-derived macrophages are definitively distinguishable by phenotype in the retina. *Sci Rep.* (2016) 6:20636. doi: 10.1038/srep20636
33. Plemel JR, Stratton JA, Michaels NJ, Rawji KS, Zhang E, Sinha S, et al. Microglia response following acute demyelination is heterogeneous and limits infiltrating macrophage dispersion. *Sci Adv.* (2020) 6:eaay6324. doi: 10.1126/sciadv.aay6324
34. Butovsky O, Jedrychowski MP, Moore CS, Cialic R, Lanser AJ, Gabriely G, et al. Identification of a unique TGF-β-dependent molecular and functional signature in microglia. *Nat Neurosci.* (2014) 17:131–43. doi: 10.1038/nn.3599
35. Gautier EL, Shay T, Miller J, Greter M, Jakubzick C, Ivanov S, et al. Gene-expression profiles and transcriptional regulatory pathways that underlie the identity and diversity of mouse tissue macrophages. *Nat Immunol.* (2012) 13:1118–28. doi: 10.1038/ni.2419
36. Hickman SE, Kingery ND, Ohsumi TK, Borowsky ML, Wang L, Means TK, et al. The microglial sensome revealed by direct RNA sequencing. *Nat Neurosci.* (2013) 16:1896–905. doi: 10.1038/nn.3554
37. Bennett ML, Bennett FC, Liddelow SA, Ajami B, Zamanian JL, Fernhoff NB, et al. New tools for studying microglia in the mouse and human CNS. *Proc Natl Acad Sci USA.* (2016) 113:E1738–46. doi: 10.1073/pnas.1525528113
38. Konishi H, Kobayashi M, Kunisawa T, Imai K, Sayo A, Malissen B, et al. Siglec-H is a microglia-specific marker that discriminates microglia from CNS-associated macrophages and CNS-infiltrating monocytes. *Glia.* (2017) 65:1927–43. doi: 10.1002/glia.23204
39. Hammond TR, Dufort C, Dissing-Olesen L, Giera S, Young A, Wysoker A, et al. Single-cell RNA sequencing of microglia throughout the mouse lifespan and in the injured brain reveals complex cell-state changes. *Immunity.* (2019) 50:253–71.e6. doi: 10.1016/j.immuni.2018.11.004

40. Su N, März S, Plagemann T, Cao J, Schnittler H-J, Eter N, et al. Occurrence of transmembrane protein 119 in the retina is not restricted to the microglia: an immunohistochemical study. *Trans Vis Sci Tech.* (2019) 8:29. doi: 10.1167/tvst.8.6.29
41. Holtman IR, Raj DD, Miller JA, Schaafsma W, Yin Z, Brouwer N, et al. Induction of a common microglia gene expression signature by aging and neurodegenerative conditions: a co-expression meta-analysis. *Acta Neuropathol Commun.* (2015) 3:31. doi: 10.1186/s40478-015-0203-5
42. Butovsky O, Weiner HL. Microglial signatures and their role in health and disease. *Nat Rev Neurosci.* (2018) 19:622–635. doi: 10.1038/s41583-018-0057-5
43. van der Poel M, Ulas T, Mizee MR, Hsiao C-C, Miedema SSM, Adelia, et al. Transcriptional profiling of human microglia reveals grey–white matter heterogeneity and multiple sclerosis-associated changes. *Nat Commun.* (2019) 10:1139. doi: 10.1038/s41467-019-08976-7
44. Jung S, Aliberti J, Graemmel P, Sunshine MJ, Kreutzberg GW, Sher A, et al. Analysis of fractalkine receptor CX3CR1 function by targeted deletion and green fluorescent protein reporter gene insertion. *Mol Cell Biol.* (2000) 20:4106–14. doi: 10.1128/MCB.20.11.4106-4114.2000
45. Rogers JT, Morganti JM, Bachstetter AD, Hudson CE, Peters MM, Grimmig BA, et al. CX3CR1 deficiency leads to impairment of hippocampal cognitive function and synaptic plasticity. *J Neurosci.* (2011) 31:16241–50. doi: 10.1523/JNEUROSCI.3667-11.2011
46. Parkhurst CN, Yang G, Ninan I, Savas JN, Yates JR, Lafaille JJ, et al. Microglia promote learning-dependent synapse formation through brain-derived neurotrophic factor. *Cell.* (2013) 155:1596–609. doi: 10.1016/j.cell.2013.11.030
47. Goldmann T, Wieghofer P, Jordão MJC, Prutek F, Hagemeyer N, Frenzel K, et al. Origin, fate and dynamics of macrophages at central nervous system interfaces. *Nat Immunol.* (2016) 17:797–805. doi: 10.1038/ni.3423
48. Kaiser T, Feng G. Tmem119-EGFP and Tmem119-CreERT2 transgenic mice for labeling and manipulating microglia. *eNeuro.* (2019) 6:ENEURO.0448-18.2019. doi: 10.1523/ENEURO.0448-18.2019
49. Ruan C, Sun L, Kroshilina A, Beckers L, De Jager P, Bradshaw EM, et al. A novel Tmem119-tdTomato reporter mouse model for studying microglia in the central nervous system. *Brain Behav Immun.* (2020) 83:180–91. doi: 10.1016/j.bbi.2019.10.009
50. Buttgereit A, Lelios I, Yu X, Vrohlings M, Krakoski NR, Gautier EL, et al. Sall1 is a transcriptional regulator defining microglia identity and function. *Nat Immunol.* (2016) 17:1397–406. doi: 10.1038/ni.3585
51. Takasato M, Osafune K, Matsumoto Y, Kataoka Y, Yoshida N, Meguro H, et al. Identification of kidney mesenchymal genes by a combination of microarray analysis and Sall1-GFP knockin mice. *Mech Dev.* (2004) 121:547–57. doi: 10.1016/j.mod.2004.04.007
52. Masuda T, Amann L, Sankowski R, Staszewski O, Lenz M, d'Errico P, et al. Novel Hexb-based tools for studying microglia in the CNS. *Nat Immunol.* (2020) 21:802–15. doi: 10.1038/s41590-020-0774-6
53. McKinsey GL, Lizama CO, Keown-Lang AE, Niu A, Santander N, Larpthaveesarp A, et al. A new genetic strategy for targeting microglia in development and disease. *eLife.* (2020) 9:e54590. doi: 10.7554/eLife.54590
54. Chappell-Maor L, Kolesnikov M, Grozovski J, Kim J-S, Shemer A, Haimon Z, et al. Comparative analysis of CreER transgenic mice for the study of brain macrophages – a case study. *Immunology.* (2019) 50:353–62. doi: 10.1101/725218
55. Cătălin B, Stopper L, Bălşeanu T-A, Scheller A. The *in situ* morphology of microglia is highly sensitive to the mode of tissue fixation. *J Chem Neuroanat.* (2017) 86:59–66. doi: 10.1016/j.jchemneu.2017.08.007
56. Lee JE, Liang KJ, Fariss RN, Wong WT. *Ex vivo* dynamic imaging of retinal microglia using time-lapse confocal microscopy. *Invest Ophthalmol Vis Sci.* (2008) 49:4169–76. doi: 10.1167/iovs.08-2076
57. Dailey ME, Eyo U, Fuller L, Hass J, Kurpius D. Imaging microglia in brain slices and slice cultures. *Cold Spring Harbor Protoc.* (2013) 2013:pdb.prot079483-pdb.prot079483. doi: 10.1101/pdb.prot079483
58. Ueda HR, Ertürk A, Chung K, Gradinaru V, Chédotal A, Tomancak P, et al. Tissue clearing and its applications in neuroscience. *Nat Rev Neurosci.* (2020) 21:61–79. doi: 10.1038/s41583-019-0250-1
59. Wan P, Zhu J, Xu J, Li Y, Yu T, Zhu D. Evaluation of seven optical clearing methods in mouse brain. *NPH.* (2018) 5:035007. doi: 10.1117/1.NPh.5.3.035007
60. Liebmann T, Renier N, Bettayeb K, Greengard P, Tessier-Lavigne M, Flajolet M. Three-dimensional study of Alzheimer's disease hallmarks using the iDISCO clearing method. *Cell Rep.* (2016) 16:1138–52. doi: 10.1016/j.celrep.2016.06.060
61. Ertürk A, Becker K, Jährling N, Mauch CP, Hojer CD, Egen JG, et al. Three-dimensional imaging of solvent-cleared organs using 3DISCO. *Nat Protoc.* (2012) 7:1983–95. doi: 10.1038/nprot.2012.119
62. Xu N, Tamadon A, Liu Y, Ma T, Leak RK, Chen J, et al. Fast free-of-acrylamide clearing tissue (FACT)—an optimized new protocol for rapid, high-resolution imaging of three-dimensional brain tissue. *Sci Rep.* (2017) 7:9895 doi: 10.1038/s41598-017-10204-5
63. Henning Y, Osadnik C, Malkemper EP. EyeCi: optical clearing and imaging of immunolabeled mouse eyes using light-sheet fluorescence microscopy. *Exp Eye Res.* (2019) 180:137–45. doi: 10.1016/j.exer.2018.12.001
64. Pende M, Vadiwala K, Schmidbaur H, Stockinger AW, Murawala P, Saghafi S, et al. A versatile depigmentation, clearing, and labeling method for exploring nervous system diversity. *Sci Adv.* (2020) 6:aba0365. doi: 10.1126/sciadv.aba0365
65. Vigouroux RJ, Cesar Q, Chédotal A, Nguyen-Ba-Charvet KT. Revisiting the role of Dcc in visual system development with a novel eye clearing method. *eLife.* (2020) 9:e51275. doi: 10.7554/eLife.51275
66. Bayerl SH, Niesner R, Cseresnyes Z, Radbruch H, Pohlan J, Brandenburg S, et al. Time lapse *in vivo* microscopy reveals distinct dynamics of microglia-tumor environment interactions—a new role for the tumor perivascular space as highway for trafficking microglia. *Glia.* (2016) 64:1210–26. doi: 10.1002/glia.22994
67. Drost N, Houtman J, Cseresnyés Z, Niesner R, Rinnenthal J-L, Miller KR, et al. The Amyloid-beta rich CNS environment alters myeloid cell functionality independent of their origin. *Sci Rep.* (2020) 10:7152. doi: 10.1038/s41598-020-63989-3
68. Füger P, Hefendehl JK, Veeraraghavalu K, Wendeln A-C, Schlosser C, Obermüller U, et al. Microglia turnover with aging and in an Alzheimer's model via long-term *in vivo* single-cell imaging. *Nat Neurosci.* (2017) 20:1371–6. doi: 10.1038/nn.4631
69. Hierro-Bujalance C, Bacskai BJ, Garcia-Alloza M. *In vivo* imaging of microglia with multiphoton microscopy. *Front Aging Neurosci.* (2018) 10:218. doi: 10.3389/fnagi.2018.00218
70. Liu YU, Ying Y, Li Y, Eyo UB, Chen T, Zheng J, et al. Neuronal network activity controls microglial process surveillance in awake mice via norepinephrine signaling. *Nat Neurosci.* (2019) 22:1771–81. doi: 10.1038/s41593-019-0511-3
71. Stowell RD, Sipe GO, Dawes RP, Batchelor HN, Lordy KA, Whitelaw BS, et al. Noradrenergic signaling in the wakeful state inhibits microglial surveillance and synaptic plasticity in the mouse visual cortex. *Nat Neurosci.* (2019) 22:1782–92. doi: 10.1038/s41593-019-0514-0
72. Zhang Y, Zhao L, Wang X, Ma W, Lazere A, Qian H, et al. Repopulating retinal microglia restore endogenous organization and function under CX3CL1-CX3CR1 regulation. *Sci Adv.* (2018) 4:eaap8492. doi: 10.1126/sciadv.aap8492
73. Chen X, Kezic JM, Forrester JV, Goldberg GL, Wicks IP, Bernard CC, et al. *In vivo* multi-modal imaging of experimental autoimmune uveoretinitis in transgenic reporter mice reveals the dynamic nature of inflammatory changes during disease progression. *J Neuroinflamm.* (2015) 12:17. doi: 10.1186/s12974-015-0235-6
74. Zawadzki RJ, Zhang P, Zam A, Miller EB, Goswami M, Wang X, et al. Adaptive-optics SLO imaging combined with widefield OCT and SLO enables precise 3D localization of fluorescent cells in the mouse retina. *Biomed Opt Exp.* (2015) 6:2191–210. doi: 10.1364/BOE.6.002191
75. Miller EB, Zhang P, Ching K, Pugh EN, Burns ME. *in vivo* imaging reveals transient microglia recruitment and functional recovery of photoreceptor signaling after injury. *Proc Natl Acad Sci USA.* (2019) 116:16603–12. doi: 10.1073/pnas.1903336116
76. Qin Z, He S, Yang C, Yung JS-Y, Chen C, Leung CK-S, et al. Adaptive optics two-photon microscopy enables near-diffraction-limited and functional retinal imaging *in vivo*. *Light Sci Appl.* (2020) 9:79. doi: 10.1038/s41377-020-0317-9
77. Airas L, Nylund M, Rissanen E. Evaluation of microglial activation in multiple sclerosis patients using positron emission tomography. *Front Neurol.* (2018) 9:181. doi: 10.3389/fneur.2018.00181

78. Conen S, Gregory CJ, Hinz R, Smallman R, Corsi-Zuelli F, Deakin B, et al. Neuroinflammation as measured by positron emission tomography in patients with recent onset and established schizophrenia: implications for immune pathogenesis. *Mol Psychiatry.* (2020). doi: 10.1038/s41380-020-0829-y. [Epub ahead of print].
79. Lehenkari PP, Kellinsalmi M, Näpänkangas JP, Ylitalo KV, Mönkkönen J, Rogers MJ, et al. Further insight into mechanism of action of clodronate: inhibition of mitochondrial ADP/ATP translocase by a nonhydrolyzable, adenine-containing metabolite. *Mol Pharmacol.* (2002) 61:1255–62. doi: 10.1124/mol.61.5.1255
80. Faustino JV, Wang X, Johnson CE, Klibanov A, Derugin N, Wendland MF, et al. Microglial cells contribute to endogenous brain defenses after acute neonatal focal stroke. *J Neurosci.* (2011) 31:12992–3001. doi: 10.1523/JNEUROSCI.2102-11.2011
81. Andreou KE, Soto MS, Allen D, Economopoulos V, de Bernardi A, Larkin JR, et al. Anti-inflammatory microglia/macrophages as a potential therapeutic target in brain metastasis. *Front Oncol.* (2017) 7:251. doi: 10.3389/fonc.2017.00251
82. Todd L, Palazzo I, Suarez L, Liu X, Volkov L, Hoang TV, et al. Reactive microglia and IL1β/IL-1R1-signaling mediate neuroprotection in excitotoxin-damaged mouse retina. *J Neuroinflamm.* (2019) 16:118. doi: 10.1186/s12974-019-1505-5
83. Forrester JV, McMenamin PG, Dando SJ. CNS infection and immune privilege. *Nat Rev Neurosci.* (2018) 19:655–71. doi: 10.1038/s41583-018-0070-8
84. Han X, Li Q, Lan X, EL-Mufti L, Ren H, Wang J. Microglial depletion with clodronate liposomes increases proinflammatory cytokine levels, induces astrocyte activation, and damages blood vessel integrity. *Mol Neurobiol.* (2019) 56:6184–96. doi: 10.1007/s12035-019-1502-9
85. Zelinka CP, Scott MA, Volkov L, Fischer AJ. The reactivity, distribution and abundance of Non-Astrocytic Inner Retinal Glial (NIRG) cells are regulated by microglia, acute damage, and IGF1. *PLoS ONE.* (2012) 7:e44477. doi: 10.1371/journal.pone.0044477
86. Polfliet MMJ, Goede PH, van Kesteren-Hendrikx EML, van Rooijen N, Dijkstra CD, van den Berg TK. A method for the selective depletion of perivascular and meningeal macrophages in the central nervous system. *J Neuroimmunol.* (2001) 116:188–95. doi: 10.1016/S0165-5728(01)00282-X
87. Elmore MRP, Najafi AR, Koike MA, Dagher NN, Spangenberg EE, Rice RA, et al. Colony-stimulating factor 1 receptor signaling is necessary for microglia viability, unmasking a microglia progenitor cell in the adult brain. *Neuron.* (2014) 82:380–97. doi: 10.1016/j.neuron.2014.02.040
88. Spangenberg E, Severson PL, Hohsfield LA, Crapser J, Zhang J, Burton EA, et al. Sustained microglial depletion with CSF1R inhibitor impairs parenchymal plaque development in an Alzheimer's disease model. *Nat Commun.* (2019) 10:1–21. doi: 10.1038/s41467-019-11674-z
89. Han J, Harris RA, Zhang X-M. An updated assessment of microglia depletion: current concepts and future directions. *Mol Brain.* (2017) 10:25. doi: 10.1186/s13041-017-0307-x
90. Najafi AR, Crapser J, Jiang S, Ng W, Mortazavi A, West BL, et al. A limited capacity for microglial repopulation in the adult brain. *Glia.* (2018) 66:2385–96. doi: 10.1002/glia.23477
91. Spangenberg EE, Lee RJ, Najafi AR, Rice RA, Elmore MRP, Blurton-Jones M, et al. Eliminating microglia in Alzheimer's mice prevents neuronal loss without modulating amyloid-β pathology. *Brain.* (2016) 139:1265–81. doi: 10.1093/brain/aww016
92. Casali BT, MacPherson KP, Reed-Geaghan EG, Landreth GE. Microglia depletion rapidly and reversibly alters amyloid pathology by modification of plaque compaction and morphologies. *Neurobiol Dis.* (2020) 142:104956. doi: 10.1016/j.nbd.2020.104956
93. Han J, Zhu K, Zhang X-M, Harris RA. Enforced microglial depletion and repopulation as a promising strategy for the treatment of neurological disorders. *Glia.* (2019) 67:217–31. doi: 10.1002/glia.23529
94. Takeda A, Shinozaki Y, Kashiwagi K, Ohno N, Eto K, Wake H, et al. Microglia mediate non-cell-autonomous cell death of retinal ganglion cells. *Glia.* (2018) 66:2366–84. doi: 10.1002/glia.23475
95. Varvel NH, Grathwohl SA, Baumann F, Liebig C, Bosch A, Brawek B, et al. Microglial repopulation model reveals a robust homeostatic process for replacing CNS myeloid cells. *Proc Natl Acad Sci USA.* (2012) 109:18150–5. doi: 10.1073/pnas.1210150109

Conflict of Interest: The authors declare that the research was conducted in the absence of any commercial or financial relationships that could be construed as a potential conflict of interest.

frontiers in Molecular Neuroscience

REVIEW
published: 22 October 2020
doi: 10.3389/fnmol.2020.583811

High-Resolution Transcriptomic and Proteomic Profiling of Heterogeneity of Brain-Derived Microglia in Multiple Sclerosis

Anneke Miedema†, Marion H. C. Wijering†, Bart J. L. Eggen‡ and Susanne M. Kooistra‡*

Section Molecular Neurobiology, Department of Biomedical Sciences of Cells and Systems, University Medical Center Groningen, University of Groningen, Groningen, Netherlands

Microglia are important for central nervous system (CNS) homeostasis and first to respond to tissue damage and perturbations. Microglia are heterogeneous cells; in case of pathology, microglia adopt a range of phenotypes with altered functions. However, how these different microglia subtypes are implicated in CNS disease is largely unresolved. Multiple sclerosis (MS) is a chronic demyelinating disease of the CNS, characterized by inflammation and axonal degeneration, ultimately leading to neurological decline. One way microglia are implicated in MS is through stimulation of remyelination. They facilitate efficient remyelination by phagocytosis of myelin debris. In addition, microglia recruit oligodendrocyte precursor cells (OPCs) to demyelinated areas and stimulate remyelination. The development of high-resolution technologies to profile individual cells has greatly contributed to our understanding of microglia heterogeneity and function under normal and pathological conditions. Gene expression profiling technologies have evolved from whole tissue RNA sequencing toward single-cell or nucleus sequencing. Single microglia proteomic profiles are also increasingly generated, offering another layer of high-resolution data. Here, we will review recent studies that have employed these technologies in the context of MS and their respective advantages and disadvantages. Moreover, recent developments that allow for (single) cell profiling while retaining spatial information and tissue context will be discussed.

Keywords: multiple sclerosis, microglia, heterogeneity, spatial, sequencing

OPEN ACCESS

Edited by:
Rosa Chiara Paolicelli, University of Lausanne, Switzerland

Reviewed by:
Antje Kroner, Medical College of Wisconsin, United States
Madhuvika Murugan, Newark College of Engineering, New Jersey Institute of Technology, United States

****Correspondence:***
Susanne M. Kooistra
s.m.kooistra@umcg.nl

†These authors share first authorship

‡These authors share last authorship

Received: *15 July 2020*
Accepted: *23 September 2020*
Published: *22 October 2020*

Citation:
Miedema A, Wijering MHC, Eggen BJL and Kooistra SM (2020) High-Resolution Transcriptomic and Proteomic Profiling of Heterogeneity of Brain-Derived Microglia in Multiple Sclerosis. Front. Mol. Neurosci. 13:583811. doi: 10.3389/fnmol.2020.583811

Abbreviations: ALS, amyotrophic lateral sclerosis; ATAC-seq, assay for transposase-accessible chromatin sequencing; BBB, blood–brain barrier; CC, corpus callosum; CHIP-seq, chromatin immunoprecipitation sequencing; CITE-seq, cellular indexing of transcriptomes and epitopes by sequencing; CNS, central nervous system; CyTOF, cytometry by time-of-flight; EAE, experimental-autoimmune encephalomyelitis; ELISA, enzyme-linked immunosorbent assay; FACS, fluorescent-activated cell sorting; FF, fresh frozen; FPE, formalin-fixed paraffin-embedded; FISH, fluorescent *in situ* hybridization; FISSEQ, fluorescent *in situ* sequencing; GM, gray matter; GML, gray matter lesion; GO, Gene ontology; GWAS, genome-wide association study; HD, Huntington's disease; HE, hematoxylin and eosin; ICP, inductively coupled argon plasma; IHC, immunohistochemistry; ISH, *in situ* hybridization; ISS, *in situ* sequencing; LCM, laser capture microdissection; LPC, lysolecithin; LPS, lipopolysaccharide; MERFISH, multiplexed error-robust fluorescent in situ hybridization; MRI, magnetic resonance imaging; MS, multiple sclerosis; NAGM, normal-appearing gray matter; NAWM, normal-appearing white matter; OPC, oligodendrocyte precursor cell; PMD, postmortem delay; qPCR, quantitative polymerase chain reaction; RCA, rolling circle amplification; REAPseq, RNA expression and protein sequencing assay; ROS, reactive oxygen species; RRMS, relapsing–remitting multiple sclerosis; scRNAseq, single-cell RNA sequencing; smFISH, single-molecule fluorescent *in situ* hybridization; SNP, single-nucleotide polymorphisms; snRNAseq, single-nucleus RNA sequencing; ST, spatial transcriptomics; TLR, toll-like receptor; UMI, unique molecular identifier; WM, white matter; WML, white matter lesion.

INTRODUCTION

Multiple sclerosis (MS) is a common chronic neurodegenerative disease of the central nervous system (CNS) affecting 2.5 million people worldwide. MS symptoms include muscle weakness and spasms, movement difficulties, optic problems, fatigue, and acute or chronic pain (Koriem, 2016). In MS, demyelination contributes to axonal loss and gives rise to a neuroinflammatory environment. This provokes an immune response involving infiltrating immune cells and CNS-resident glial cells, including microglia, the innate immune cells of the CNS. Under homeostatic circumstances, microglia scan their surroundings with ramified processes and protect the nervous system from neural damage and inflammation. During pathology, microglia change their phenotype toward immune-reactive microglia. Morphologically, immune-reactive microglia acquire a more amoeboid morphology with retracted processes and secrete proinflammatory cytokines to aim for attenuated disease progression. A range of microglia phenotypes have been reported, possibly with distinct molecular and functional signatures, although these have not yet been fully elucidated.

In MS, demyelinated areas can be classified as preactive, active, chronic active, inactive, and remyelinated lesions, based on the degree of inflammation, demyelination, and axonal degeneration (Kuhlmann et al., 2017). This lesion heterogeneity is associated with alterations in microglia phenotype and functionality, giving rise to different microglia subtypes. However, the exact role and functions of different microglia subtypes in MS and other CNS diseases are largely unresolved. In addition, under healthy conditions, several factors contribute to microglial heterogeneity, for example the CNS region where the microglia reside in. Different subtypes of microglia are found in gray matter (GM) versus white matter (WM) (Anderson et al., 2007; McKay et al., 2007; van der Poel et al., 2019). Considerable variation in microglia subtypes and density has been described between brain regions as well. Lawson et al. (1990) reported variation in the density of microglia processes with a more than fivefold difference between brain regions. Furthermore, density variation was even observed within one brain region (Lawson et al., 1990), illustrating the importance of regional analysis. Why certain brain areas have a higher microglia density than others is not yet understood. In addition to microglia heterogeneity within an individual, microglia also differ between species and between male and female individuals, which until now mainly has been studied in mice and humans (Lenz et al., 2013; Torres-Platas et al., 2014; Galatro et al., 2017; Gosselin et al., 2017; Hanamsagar et al., 2017; Guneykaya et al., 2018; Villa et al., 2018; Geirsdottir et al., 2019). Furthermore, differences in the microglia transcriptome are observed when comparing microglia from various brain regions, and it has been shown that these regions are non-uniformly affected by aging (Grabert et al., 2016). Recently, high-resolution transcriptomic analysis, such as single-cell and single-nucleus sequencing, has contributed to a better understanding of microglia heterogeneity during development, in health, and disease (Keren-Shaul et al., 2017; Mathys et al., 2017; Brioschi et al., 2019; Hammond et al., 2019; Schirmer et al., 2019; Masuda et al., 2020).

Although these studies provided important insights and identified novel microglia subtypes, spatial information of the analyzed cells in their tissue of origin is lacking. In the past few years, technologies for the generation of gene expression that combine spatial information with gene expression data have been improved. Furthermore, single-cell proteomic methods, such as cellular indexing of transcriptomes and epitopes by sequencing (CITE-seq), are evolving. These methods will provide more insight into (regional) microglia heterogeneity under healthy circumstances and in case of CNS disease. Here, we will review recent studies in the context of MS that have implemented such methods and discuss their respective advantages and disadvantages.

MICROGLIA IN MS

Multiple sclerosis is a heterogeneous disease in which different types of lesions are located in the CNS, with high variability in the number and type of lesions not only between patients but also within patients (Minneboo et al., 2005; Metz et al., 2014). Disease severity correlates with a higher lesion load (number of lesions per brain area), a higher number of chronic active lesions, and a higher proportion of foamy microglia/macrophages (Luchetti et al., 2018). Different cell types are involved in MS; a continuous cross-talk of astrocytes, oligodendrocytes, microglia, and neurons takes place within the brain. One of the key functions of oligodendrocytes is the production of myelin to ensheath axons for neurotrophic support and to facilitate optimal action potential transduction through the CNS (Kuhn et al., 2019). However, under pathological circumstances, these CNS cell–cell interactions are affected. Disturbances in the homeostatic environment initially lead to the activation of microglia, which is necessary for debris and pathogen clearance, repair, and formation of new cells to restore homeostasis (Peferoen et al., 2013). Also in MS, microglia get activated and migrate to the place of injury to clear debris, contribute to the repair of tissues/cells, and interact with surrounding neurons and astrocytes while secreting anti-inflammatory factors to dampen stress and promote remyelination (Luo et al., 2017; Prinz et al., 2019; Voet et al., 2019). However, activated microglia can also secrete proinflammatory factors that affect neighboring cells, including oligodendrocytes, resulting in oligodendrocyte death and production of poor-quality myelin sheaths (Luo et al., 2017; Masuda et al., 2020). In turn, oligodendrocytes produce chemokines, cytokines, and chaperokines, while astrocytes secrete proinflammatory genes, chemokines, and growth factors to control microglia activity, phagocytosis, and migration (Jha et al., 2019), illustrating a complex signaling network between cells during MS pathology.

White Matter Microglia Lose Their Homeostatic Profile Upon Neuroinflammation Associated With MS Lesions

Neuroinflammation in the CNS is associated with a loss of the homeostatic microglia profile, which has been observed in various neuroinflammatory diseases (Dubbelaar et al., 2018). Beaino et al. (2017) have shown that, in mice, the local neuroinflammatory environment affects microglia activity by downregulating the expression of the homeostatic microglia marker *P2ry12*. Using human microglia *in vitro*, they identified that a proinflammatory environment decreases *P2RY12* expression (Beaino et al., 2017). This is supported by data that show a decrease in the level of P2RY12 in normal-appearing white matter (NAWM) and minimal P2RY12 immunoreactivity in active lesions in postmortem human MS tissue (Zrzavy et al., 2017). The same pattern of expression was seen for the homeostatic microglia marker *TMEM119* (Zrzavy et al., 2017; Van Wageningen et al., 2019). Interestingly, *P2RY12* reappeared in mixed active–inactive white matter lesions. This study revealed that messenger RNA (mRNA) levels of *P2RY12* and *TMEM119* are regulated by interleukin-4 (IL-4) and interferon-gamma (IFNγ). In contrast to white matter lesions (WMLs) and NAWM, levels of *P2RY12* and *TMEM119* did not differ between gray matter lesions (GMLs) and normal-appearing gray matter (NAGM). This could be explained by the lower number of lymphocytes observed within GMLs compared to WMLs, as lymphocytes secrete inflammatory mediators such as IL-4 and IFNγ and thus indirectly regulate *P2RY12* and *TMEM119* expression (Van Wageningen et al., 2019).

Microglia in MS Lesion Pathology

Lesions are often classified by the presence/absence of certain proteins to indicate de- or remyelination and/or inflammation. To classify these lesions, immunohistochemistry (IHC) can be performed using the inflammation markers human leukocyte antigen DR isotype (HLA-DR) and/or CD68 and a myelin marker, such as myelin proteolipid protein 1 (PLP1). Preactive lesions can be recognized by nodules of activated microglia (elevated levels of HLA-DR and CD68) in the absence of demyelination (van Horssen et al., 2012). These clusters of activated microglia express, e.g., tumor necrosis factor alpha (TNFα) and interleukin-10 (IL-10), which both play a role in cell survival, while IL-10 exerts also anti-inflammatory effects and is important for neurogenesis (Zhou et al., 2009; van Horssen et al., 2012; Pereira et al., 2015). Within these lesions, microglia have a ramified morphology and express the homeostatic markers P2RY12 and TMEM119, reflecting a (partly) homeostatic state (**Figure 1**).

In the healthy brain, oligodendrocytes and myelin are depositories of iron, an essential element for the regulation of myelination and oxidative phosphorylation (Hametner et al., 2013). However, in active MS lesions, oligodendrocytes are vulnerable to the inflammatory environment and, when damaged, release iron into the extracellular space, leading to the generation of reactive oxygen species (ROS) and uptake of iron by microglia and macrophages. Active lesions are characterized by a demyelinated core, containing an abundance of foamy myelin-containing microglia within the lesion. Another hallmark of active lesions is disruption of the blood–brain barrier (BBB), combined with leukocyte infiltration into the CNS (Kuhlmann et al., 2017; Grajchen et al., 2018). As a consequence, reactive microglia start synthesizing ROS, resulting in local oxidative stress, DNA damage, and neurotoxicity (Hametner et al., 2013, 2018; Yauger et al., 2019). These iron-laden microglia have the tendency to stay in this proinflammatory state, impairing clearance of myelin debris, making it harder for oligodendrocytes to migrate toward the lesion site and, as a result, complicating remyelination processes (Mairuae et al., 2011; Lee et al., 2019). Compared to active lesions, mixed active/inactive (chronic active) lesions contain significantly fewer infiltrated immune cells (**Figure 1**). Chronic active lesions can be recognized by a rim of HLA-DR-positive cells surrounding the demyelinated area. These reactive microglia contain phagocytosed iron and other phagocytosed products such as myelin and neuronal debris, which contribute to their amoeboid phenotype (Gillen et al., 2018). Dal-Bianco et al. (2017) visualized these lesions using magnetic resonance imaging (MRI) and showed that lesions with an iron-positive microglia/macrophage rim have a higher probability to expand than lesions with an iron-negative rim, which often become smaller, probably due to remyelination. This could indicate that, in lesions with iron-positive rims, remyelination is impaired (Dal-Bianco et al., 2017). Over time, the infiltrated immune cells disappear, resulting in a chronic silent lesion (inactive lesion). The majority of microglia in inactive lesions are positive for the homeostatic marker P2RY12, but these cells also still express proinflammatory factors (**Figure 1**) (Beaino et al., 2017; Zrzavy et al., 2017).

Remyelination in MS

Cells from the oligodendrocyte lineage are important for remyelination within lesions. Remyelinated lesions show microglia polarization from a proinflammatory state toward an anti-inflammatory phenotype, necessary for the initiation of remyelination (Miron et al., 2013). First, a proinflammatory state is initiated to clear myelin debris and to stimulate oligodendrogenesis in newly formed lesions. When lesions expand, phagocytes acquire a more anti-inflammatory state and produce factors (IL-4, IL13, and IL-10) required for OPC differentiation (Butovsky et al., 2006; Miron et al., 2013; Cunha et al., 2020). This results in the de- and remyelinated regions that are often detected in/around active lesions. In remyelinated lesions, the so-called shadow plaques, iron accumulation is absent, suggesting that microglia present in these lesions have the capacity to clear myelin debris, enabling the maturation of OPCs, which results in the ability to remyelinate axons (Lampron et al., 2015; Dal-Bianco et al., 2017). In support of this notion, impeding myelin clearance through deletion of *Cx3cr1*, a receptor involved in microglia–neuron crosstalk, resulted in inefficient remyelination of axons (Lampron et al., 2015). Overall, microglia are very dynamic, and the environmental heterogeneity between and within MS lesions is associated with different microglia responses. Moreover, iron-positive

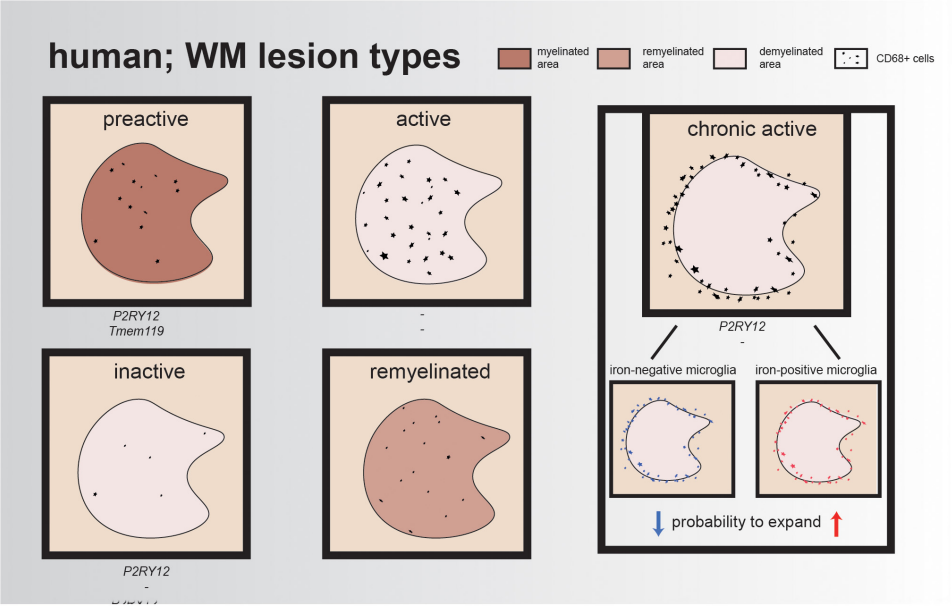

FIGURE 1 | Illustrative overview of different human WM lesion types. Preactive lesions express the homeostatic microglia markers P2RY12 and TMEM119, while expression of these markers is minimal/absent in active lesions and reappears in chronic active lesions and inactive lesions; for remyelinated lesions, the expression of these genes remains unidentified. In each lesion type, CD68+ cells are represented, either within the lesion or at the rim of the lesion. The rim of chronic active lesions can either contain iron-positive microglia/macrophages resulting in a higher probability for lesion expansion or iron-negative microglia/macrophages, which often results in smaller lesions over time.

microglia/macrophages that form a rim around the lesion could impair the remyelination process, resulting in slowly expanding lesions rather than shrinkage of the lesion.

HETEROGENEITY OF MICROGLIA IN THE CNS

For a long time, research focused on WM pathology, as it was considered the main pathological characteristic of MS. However, demyelination and lesion formation is not restricted to the WM and also occurs in the GM (Petiet et al., 2016). In the last decades, studies expanded to include the GM due to advances in visualization technologies and IHC. Similar to WM lesions, cortical GM lesions can be subdivided into different lesion types: leukocortical (lesions that extend in subcortical WM), intracortical (lesions that do not extend to subcortical WM or the surface of the brain), and subpial lesions (lesions that extend to the surface of the brain). It has been shown that WM lesion load is related to cortical lesions; leukocortical and intracortical lesions correlated with the incidence of chronic active lesions, reactive site load, and the proportion of remyelinated lesions. However, no correlation was detected between WM lesion load and subpial lesions, indicating that subpial lesion formation is initiated by different underlying processes than in leukocortical and intracortical lesions (Luchetti et al., 2018). Interestingly, subpial lesion formation is often located close to sites of meningeal inflammation, which might contribute to GM lesion pathology (Howell et al., 2011). Moreover, differences in microglial phenotype, as well as transcriptomic differences, have been observed between species and male and female. Here, we focus on WM/GM microglial heterogeneity and microglial differences between species and sex (summarized in **Figure 2**).

Microglia Are Heterogenous Across Brain Regions and Differ in WM Compared to GM Tissue

Microglia are present in both the WM and GM; however, these microglia are phenotypically different. Previous studies reported that microglia differ in density, morphology, and transcriptomic signature throughout the CNS, which could contribute to the difference in lesion pathology observed in WM versus GM (Lawson et al., 1990; Savchenko et al., 1997; Mittelbronn et al., 2001; de Haas et al., 2008; Böttcher et al., 2019; van der Poel et al., 2019; Van Wageningen et al., 2019). Furthermore, it has been observed that microglia show a region-specific gene expression profile; GM microglia were enriched for genes involved in type-I IFN responses, while WM microglia expressed high levels of genes involved in the nuclear factor kappa B (Nf-κb) pathway (van der Poel et al., 2019). Transcriptional differences were also observed in NAWM compared to NAGM; NAWM microglia increased the coexpression of genes involved in glycolysis and metal ion homeostasis (*ABCB6*, *CCR2*, *LPAR6*, *SDC1*, and *SLC25A37*), whereas in NAGM, microglia increased the coexpression of genes associated with lysosomal pathway, lipid catabolism, and foam cell differentiation (*ASAH1*, *CTSD*, *SCARB2*, *ABHD2*, and *LPL*).

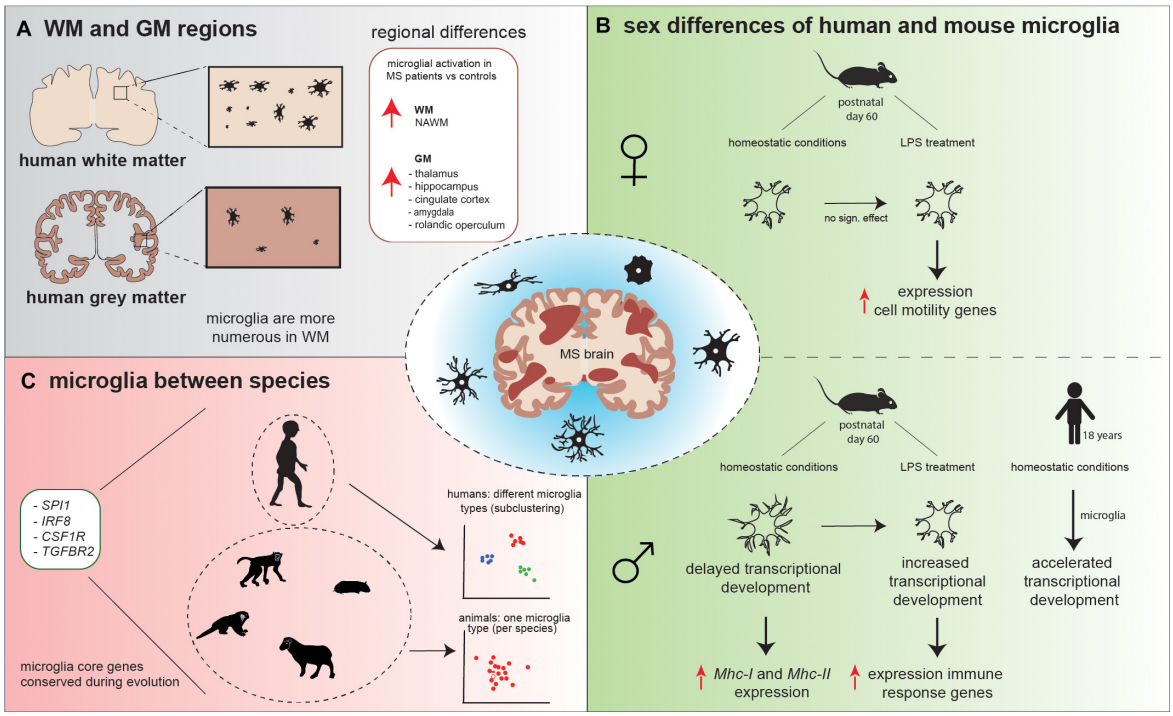

FIGURE 2 | Schematic overview of microglial heterogeneity **(A)** in WM versus GM regions, **(B)** between human and mouse male and female microglia, and **(C)** between species. **(A)** Microglia in WM are more numerous compared to GM. Microglial activation is observed in NAWM, while in GM, microglial activation is conserved to specific areas. **(B)** Under homeostatic conditions, mouse male microglia have a higher process volume, process area, number of branches, and number of intersections compared to female microglia. These male microglia appeared to be delayed in the transcriptional development compared to female microglia and show increased expression of *Mhc-I* and *Mhc-II*. LPS treatment decreased male microglial total process volume and area, whereas in female individual, no significant effect of LPS on microglia morphology was observed. In response to LPS, male microglia increased their transcriptional development to a level that was comparable to the transcriptional development in female microglia observed prior to the LPS challenge and increased expression of immune response genes, while female microglia increased the expression of cell motility genes. In opposite, homeostatic human male microglia have an accelerated transcriptional development in comparison to female microglia. **(C)** *Spi1*, *Irf8*, *Csf1r*, and *Tgfbr2* are core microglial genes that are conserved during evolution, since these genes were strongly expressed in human, macaque, marmoset, sheep, mouse, and hamster. Human microglia subcluster into different microglial types, while mouse, macaque, marmoset, hamster, and sheep microglia grouped mainly into one microglia type, based on their gene expression profiles.

Generally, microglia are more numerous in human WM than in GM (**Figure 2**) (Mittelbronn et al., 2001), which is in contrast to mice, where microglia numbers are higher in the GM (Kondo and Duncan, 2009; Lawson et al., 1990). However, microglia density is not homogeneous between specific WM and GM regions. In mice, the highest microglial density was detected in the frontal cortex, olfactory bulb, basal ganglia, and substantia nigra (regions low in myelin), while intermediate microglial density was detected in the cerebral cortex, thalamus, and hypothalamus, and microglial density was the lowest in the brainstem, cerebellum, and fiber tracts (myelin-rich regions) (Lawson et al., 1990). To determine whether microglia from WM or GM respond differently to the same lesion type, Cătălin et al. (2013) induced local tissue damage in both the WM (spine) and GM (cortex) with high-power laser pulses. The morphological response of WM and GM microglia did not differ upon this damaging cue. Although no difference in microglia morphology was identified, the speed at which microglia processes extended toward the lesion site (μm/min) was faster in WM compared to GM (Cătălin et al., 2013). Furthermore, Verdonk et al. (2016) used a Cx3cr1:GFP/++ model (mice in which the Cx3cr1 promoter drives expression of a GFP reporter gene) and treated one group with lipopolysaccharide (LPS). Twenty-four hours after LPS treatment, Verdonk et al. (2016) observed morphological differences in brain-derived microglia between the two groups; the cell body and cytoplasm area were significantly larger in microglia from the LPS group compared to controls. Interestingly, in both the LPS and control group, the cytoplasm area was significantly larger in the cerebellum compared to frontal cortex, hippocampus, and striatum. No significant differences were observed in cytoplasm area between these last three brain regions (Verdonk et al., 2016). Summarized, microglia are not uniformly distributed throughout the WM and GM brain regions. Microglia change their phenotype in response to immunomodulatory stimuli; however, differences are observed between brain regions.

Regional Differences in a Cuprizone Mouse Model

Cuprizone mouse models are frequently used to study de- and remyelination in WM and, to a lesser extent, in GM. Cuprizone is a toxic compound that induces oligodendrocyte death, resulting in robust demyelination. Mice on a cuprizone diet for a limited

time are used as a model to resemble de- and remyelination in MS. Extensive demyelination occurs within the corpus callosum (CC); however, also GM areas such as the cortex are affected by demyelination (Skripuletz et al., 2008). A previous study from Gudi et al. (2009) showed that microglia start to accumulate in the CC 3 weeks after the start of the cuprizone diet and reach their peak at 4.5 weeks of treatment. In addition, a significant increase in the number of activated microglia was identified within the cortex; however, the increase was much lower compared to microglia accumulation within the CC (Gudi et al., 2009). Interestingly, heterogeneity in microglial distribution throughout the cortex was observed; at 3 weeks of cuprizone treatment, microglia mostly resided in cortical layer V, while at 4–4.5 weeks of treatment, microglia were equally distributed through both cortical layers V and VI. At weeks 5–5.5, the highest microglia number was observed in cortical layer VI, while at all these timepoints, demyelination was present in all cortical layers. Oligodendrocytes were also higher in number in these two layers of the cortex 4.5 weeks after the start of the cuprizone diet (Gudi et al., 2009). Cortical layers V and VI are most densely myelinated and are in proximity to the CC, which is one of the regions most affected by demyelination induced by cuprizone, possibly explaining the increase in microglia in these GM regions (Gudi et al., 2009; Tomassy et al., 2014). Another observation was increased microglial proliferation in both the CC and cortex during the demyelination phase. However, the number of proliferating cells decreased again during remyelination in both the WM and GM (Gudi et al., 2009). In MS lesions, remyelination is more extensive in the GM than in the WM, and the remyelination process occurs at a higher speed, which could be due to the higher number of OPCs present in GM lesions compared to WM lesions (Chang et al., 2012). Most cuprizone studies include young mice that receive a cuprizone diet for 5 weeks to investigate remyelination. In aged mice (6 months of age), 5 weeks cuprizone treatment did not result in complete demyelination; however, complete demyelination was achieved following 6.5 weeks of cuprizone treatment (0.4% cuprizone) with high accumulation of microglia within the CC. Interestingly, these mice showed incomplete remyelination, with increased numbers of microglia and prolonged microglial activation in the CC, even 3.5 weeks after withdrawal of cuprizone, which could suggest that aged microglia are less capable of phagocytosing debris, resulting in the delayed and incomplete remyelination seen in aged cuprizone mice (Gingele et al., 2020). Thus, when studying MS pathology, the use of an aged cuprizone mouse model should be considered, as this offers more reliable insights in de- and remyelination processes than the young cuprizone mouse model that is most commonly used.

Microglia Differences Between Species

To study MS, cuprizone and EAE mouse models are commonly applied (Torkildsen et al., 2008; Constantinescu et al., 2011). However, animal models do not fully approximate or recapitulate human disease and pathology. First of all, when comparing mice to humans, we should take into account that the environment laboratory mice reside in is clean and controlled, while for humans, the environment changes frequently and contains microbes that could cause infections. Furthermore, genetic variation and environmental factors contribute to donor variation, while mice are generally inbred and most factors are held constant throughout an experiment. Here, we will discuss the differences in microglia phenotype and transcriptomic signature between species, with a focus on mice and humans.

Gosselin et al. (2017) compared mouse and human microglial transcriptomic data. Mice and humans showed an extensive overlap in microglial gene expression patterns (Pearson's $r = 0.806$), although, genes involved in the regulation of the complement system and brain structure development were expressed at a higher level by human microglia (Gosselin et al., 2017).

Recently, a microglial gene expression profiling study of eight species across evolution—human, macaque, marmoset, sheep, mouse, hamster, chicken, and zebrafish—using a combined single-cell and bulk sequencing approach, was reported (Geirsdottir et al., 2019). Since chicken and zebrafish microglia showed evolutionary distance to the other six species, these two species were excluded from further analysis allowing the characterization of subtle microglial changes between mammalian species. Hierarchical clustering showed that the macaque transcriptomic signature was most similar to the human transcriptomic signature. Interestingly, all six species abundantly expressed *SPI1*, *IRF8*, *CSF1R*, and *TGFBR2*, genes with a critical role in microglial development, suggesting that these genes are core microglial genes that are conserved during evolution (**Figure 2**). In total, 163 genes were detected that were both conserved and specific for microglia. Moreover, it was observed that human microglia subcluster into different microglia types, based on their gene expression profiles, while mouse, macaque, marmoset, hamster, and sheep microglia grouped mainly into one type (**Figure 2**). One such human microglial subtype was identified by high expression of inflammatory genes, which could be a result of the effect of aging (Geirsdottir et al., 2019).

Our group previously reported that natural aging affects microglia differently in mice and humans. Just a small number of gene expression changes induced by aging are shared between mice and human microglia, and quite a few genes show opposite expression patterns (Galatro et al., 2017). Of note, although microglia age differently under healthy conditions, upon damage or disease, mouse and human microglia show very similar responses (Holtman et al., 2015b). The aging-related differences in expression patterns might be the result of external (signaling) factors, but also intrinsically, microglia could be dictated to express different genes upon aging. One of the processes possibly affecting microglia aging is their turnover rate. The microglia population is locally maintained by self-renewal. In adult rodents, it is unequal throughout the CNS and appeared to be higher in the dentate gyrus, where microglial proliferation declines faster with age compared to other brain regions. This could lead to an earlier-reached state of microglial senescence in this brain region, as a result of the Hayflick limit, which describes that cells have a finite capacity to divide due to telomere shortening; most cells divide around 40–60 times (Hayflick, 1965; Askew et al., 2017). This could explain the significant decrease in microglial proliferation rate that was observed in the dentate gyrus during

aging. In humans, microglial proliferation rate has been estimated to be 2.9× higher compared to rodents (Askew et al., 2017). Furthermore, humans have a much longer lifespan than mice. When studying age-related brain diseases, it is important to take these differences into account, as they might influence the translational value from studies in mice to the human situation.

Microglial Sex Differences

Women are at a two to three times higher risk to develop MS and suffer from more frequent relapses than men (Tremlett et al., 2008; Sellner et al., 2011). It was observed that MS characteristics are, among others, related to sex differences (Ribbons et al., 2015; Luchetti et al., 2018). In relapsing–remitting MS (RRMS), male individuals progress significantly faster than female individuals (Ribbons et al., 2015). In male individuals, a higher incidence of chronic active lesions was observed compared to female individuals. In addition, cortical lesions occurred more frequently in male than in female individuals. However, a direct relationship was observed between the presence of cortical lesions and disease severity in female individuals, while, interestingly, no such relation was observed in male individuals. Another observation was that the presence of chronic active lesions positively correlated with disease severity and lesion load (Luchetti et al., 2018), which could explain why in RRMS patients, a faster progression is observed in male compared to female patients.

So far, most research has focused on sex differences in T-cell immune responses in MS (Kodama and Gan, 2019). However, sex-specific differences have also been described for microglia. During embryonic and early postnatal development, mouse male and female microglia develop in a similar way based on gene transcription analysis (Hanamsagar et al., 2017). Microglia transcriptionally and morphologically reach a mature state at postnatal day 14, where they resemble homeostatic microglia from adult mice (Bennett et al., 2016; Matcovitch-Natan et al., 2016). However, in adult mice, it was observed that the increase in developmentally regulated genes during normal development is delayed in male microglia compared to female microglia, which can be used as an indicator for developmental maturation (Hanamsagar et al., 2017). When early adult mice were injected with LPS 2 h prior to isolation, changes in morphology, as well as at the transcriptional level, were observed in microglia. LPS treatment decreased male microglial total process volume and area, which was inversely correlated with gene expression changes normally associated with microglial developmental maturity. In female individuals, no significant effect of LPS on microglial total process volume and area was observed (**Figure 2**) (Hanamsagar et al., 2017). In addition, sex-specific gene expression responses were identified; male microglia adapted their expression of developmentally regulated genes to a level that was comparable to the expression of these genes in female microglia observed prior to the LPS challenge. LPS treatment increased the expression of immune response genes in male microglia, while in female microglia, cell motility genes were highly expressed (**Figure 2**). Female mice go through cyclic hormonal changes; however, different phases of the estrous cycle did not result in altered gene expression in microglia (Hanamsagar et al., 2017).

Interestingly, in humans, male microglia have an accelerated transcriptional development compared to female microglia (**Figure 2**) (Hanamsagar et al., 2017). Hanamsagar et al. (2017) hypothesized that this mouse–human difference could be a result of the relatively sterile environment that mice reside in. They postulated that males could be more susceptible to infectious agents during development than females, stimulating the transcriptomic development (Hanamsagar et al., 2017).

Morphological differences were observed when comparing microglia in early adult male and female mice (Lenz et al., 2013; Hanamsagar et al., 2017; Guneykaya et al., 2018; Villa et al., 2018). Differences in microglial process volume, process area, number of branches, and number of intersections were observed, which were all increased in males compared to females (**Figure 2**) (Hanamsagar et al., 2017). Guneykaya et al. (2018) also describe an increase in microglial density in the cortex, hippocampus, and amygdala in 13-week-old male mice. Furthermore, an increase in microglial soma size was seen in these three brain areas in adult male mice. These findings suggest that male microglia are in a more primed state and are prepared to directly react to immunomodulatory stimuli. This is supported by a higher expression of proteins involved in toll-like receptor (TLR) pathways found in male microglia, as determined by mass spectrometry-based proteomics (Guneykaya et al., 2018). In addition, *NF-κB* transcription activity was 2.4-fold higher in adult male microglia, also indicating a higher responsiveness to immunological stimuli (Villa et al., 2018). Thereby, adult male microglia have a higher antigen-presenting potential than adult female microglia. Using flow cytometry analysis, male microglia showed higher expression of *Mhc-I* in the hippocampus and amygdala, whereas *Mhc-II* expression was increased in the cortex, compared to the expression of *Mhc-I* and *Mhc-II* in female microglia (Guneykaya et al., 2018).

The different functional properties and the lower transcriptomic developmental state of human female microglia could be one of the factors contributing to the higher risk of MS in female individuals. In the last years, research groups have studied sex-specific features of microglia and their response to immunomodulatory stimuli. However, less is known about the effect of sex differences in microglia in disease and if these differences contribute to the development and progression of neurodegenerative diseases, such as MS.

Analysis of Neuroinflammation in the Brain

In addition to the differences observed in microglial morphology in WM and GM, microglia change their phenotype during neuroinflammation. One method to analyze neuroinflammation is translocator protein (TSPO) positron emission tomography (PET) imaging. TSPO is present at the mitochondrial membrane, with increased expression in reactive astrocytes and proinflammatory microglia/macrophages (Chechneva and Deng, 2016; Beckers et al., 2018; Singhal et al., 2019). Under normal conditions, TSPO is expressed only at low levels in the GM in humans (Vowinckel et al., 1997; Banati, 2002). Using experimental-autoimmune encephalomyelitis (EAE), a

mouse model for MS, Vowinckel et al. (1997) showed high concentrations of TSPO in the inflamed WM of EAE mice. In MS patients, significant differences in the uptake of a radioligand for TSPO were identified in specific regions of cortical GM areas compared to healthy controls; a recent study by Singhal et al. (2019) detected an increase in radioligand uptake in the hippocampus, amygdala, posterior cingulate, midcingulate, and rolandic operculum, indicating higher levels of microglial activation in these GM areas compared to healthy controls (**Figure 2**). However, microglia activation in total cortical GM did not differ from healthy controls (Singhal et al., 2019). A similar approach was used by Datta et al. (2017). Datta et al. (2017) detected that radioligand uptake predominantly occurred in the thalamus and that MS patients showed higher radioligand binding to TSPO in this region than healthy controls. Furthermore, an increase in radioligand uptake was identified in NAWM, compared to healthy WM (Datta et al., 2017), which is supported by Van Wageningen et al. (2019) who observed a decrease in the homeostatic gene expression of *P2RY12* and *TMEM119* in microglia, suggesting a shift toward reactive microglia.

All things considered, it is important to keep in mind that microglia are heterogenous in both WM and GM areas. Throughout the CNS, microglia show differences in density, morphology, and transcriptomic signature, with the latter being described more in detail in Chapter "Transcriptomic Profiling, an Initial Step Toward Understanding MS Heterogeneity." In MS, higher levels of microglia activation can be found in a number of specific GM areas, while microglia activation levels are more or less homogeneous throughout the WM. Based on their gene expression profile, these human microglia subcluster into different microglial types, while in other species, microglia subcluster into only one microglial type. Moreover, male human microglia appeared to be more mature than female microglia, while interestingly, this is the other way around in mice. These male mice microglia have a more primed phenotype and a higher antigen-presenting potential than female mice microglia, and when responding to immunomodulatory stimuli, they push their transcriptomic signature to a more mature state. However, the question why some brain areas show higher microglial density and/or morphology compared to other brain areas still need to be answered.

TRANSCRIPTOMIC PROFILING, AN INITIAL STEP TOWARD UNDERSTANDING MS HETEROGENEITY

Low-Resolution Transcriptomic Profiling of Human MS Tissue

Transcriptomic profiling of human MS postmortem brain tissues initially was performed using microarrays and bulk RNA sequencing approaches, which mainly resulted in information about neuronal cells, simply because neurons are more abundant than glial cells (Zheng et al., 2018). Therefore, combinations with laser capture microdissection (LCM), fluorescent-activated cell sorting (FACS), and region-specific analysis were applied to decrease sample heterogeneity. These studies identified gene signatures of active lesions (immune-related genes), which differ from the inactive lesion signature (apoptosis, stress-related genes) (Mycko et al., 2004; Elkjaer et al., 2019). An LCM-microarray study of chronic MS lesions detected increased expression of genes encoding for heat-shock proteins (HSP) in a region-dependent manner. Differences in specific *HSP* gene expression were observed between the margin and the center of the lesions, compared to NAWM. This lesion margin and center heterogeneity is potentially regulated by heat shock factor four (HSF4) (Mycko et al., 2012). In addition, inactive lesions increased expression of genes related to extracellular matrix components and steroid metabolism, while the rim of active lesions expressed genes related to lipid metabolism and lysosome signaling, including genes encoding for scavenger receptors (*OLR1*, *CD68*, *MSR1*, *CXCL16*), which are potential mediators of early demyelination (**Figure 3**) (Hendrickx et al., 2017). The role of lipid metabolism in early MS pathogenesis has been further elucidated, where lipid metabolism-related genes (*LPL*, *EEPD1*, *CHI3L1*) were enriched in NAWM compared to CWM (van der Poel et al., 2019). Besides lesion-specific profiles, a region-specific gene signature of the choroid plexus was identified, characterized by increased expression of hypoxia-related, neuroprotective, and secretory genes (Rodríguez-Lorenzo et al., 2020). Taken together, high molecular complexity is detected between lesion types, where the immune system and lipid metabolism are major processes linked with active lesions and apoptosis, while stress response and extracellular matrix changes are related to inactive lesions.

High-Resolution Transcriptomic Profiling

Bulk transcriptomic profiling contributed to MS research, although its resolution by the analysis of pools of cells, masking cellular heterogeneity. Currently, a broad spectrum of sequencing technologies is available to analyze single cells (scRNAseq, see **Figure 3** for an overview). Two types of amplification strategies can be distinguished: protocols that measure full-length complementary DNA (cDNA) molecules (SMART-seq2) (Picelli et al., 2014) and protocols that measure the 3′ or 5′ end of cDNA molecules linked to a unique molecular identifier (UMI) (MARS-seq, STRT, CEL-seq2, Dropseq, and inDrops). The use of UMIs massively increase the throughput; however, it decreases sensitivity, which remains higher in sequencing full-length cDNA. Combinations with microfluidics and droplet-based sequencing platforms (Fluidigm C1, Chromium-10X genomics and Indrop-Cellbio) created easy-to-use library preparation protocols. The advantages and disadvantages of these protocols are reviewed by See et al. (2018). For human CNS tissue, it is logistically challenging to obtain a viable single-cell population from fresh tissue prior to sequencing; therefore, some alternatives can be considered. If a sufficient number of cells can be obtained, possibilities exist to use a fixation buffer such as methanol, allowing temporal storage of single-cell suspensions at −80°. However, not all cells will recover from this process, and it should be tested if these buffers are suitable for glia cells (Chen et al., 2018; Böttcher et al., 2019). Instead of analyzing

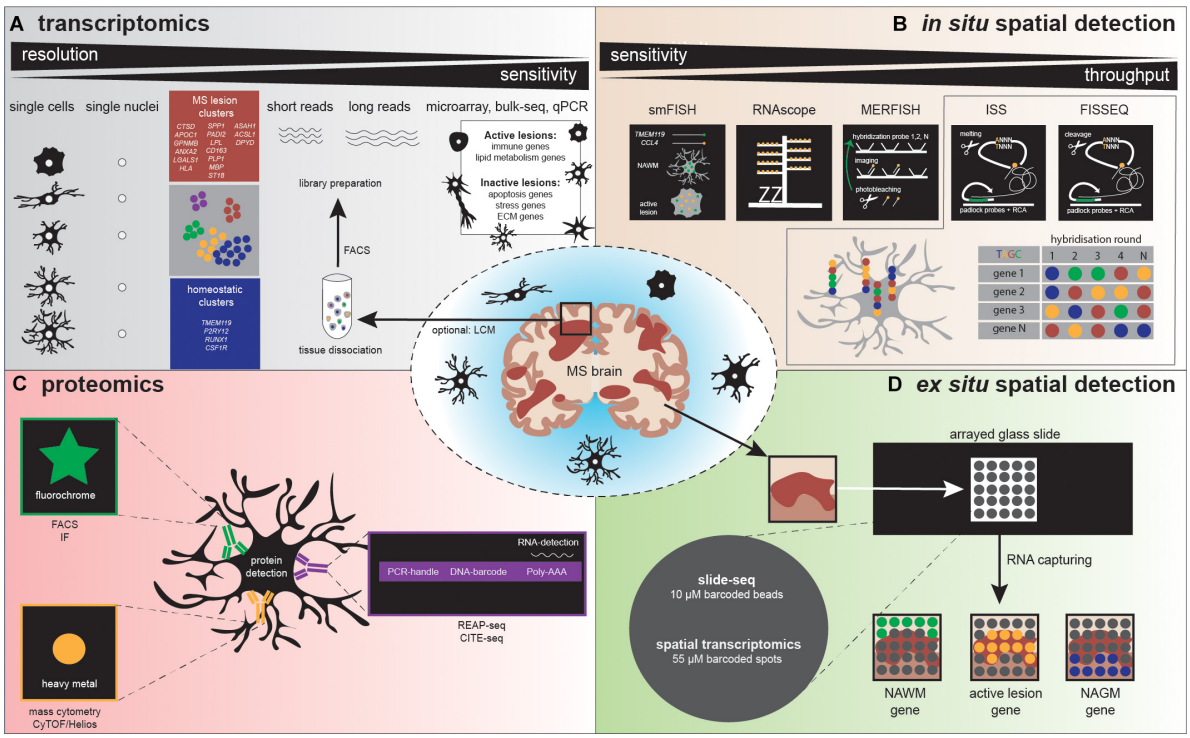

FIGURE 3 | Illustration depicts various methodologies to detect microglia heterogeneity, **(A)** distinguished in transcriptomics, **(B)** *in situ* spatial detection, **(C)** proteomics, and **(D)** *ex situ* spatial detection. **(A)** After tissue dissociation and often FACS analysis, a library can be prepared to detect microglia heterogeneity. Sequencing detects heterogeneity at high (single cell/nucleus) resolution, but sensitivity is low, compared to microarray, bulk-seq, and qPCR. Several studies already detected homeostatic and MS-associated microglia clusters, characterized by the genes depicted in the blue and red squares, respectively. **(B)** The golden standard methods using a single probe (smFISH) and a probe with amplifiers (RNAscope) are followed by high-throughput *in situ* detection of genes, via multiple rounds of probe hybridization, cleavage, imaging, and finally sequence decoding. **(C)** Standardly applied proteomic methods use antibodies containing fluorophores to detect a protein, while high-throughput proteomics methodologies make use of antibodies labeled with heavy metals (mass cytometry) or DNA barcodes (REAP-seq/CITE-seq). REAP-seq and CITE-seq antibodies also contain an RNA binding site for simultaneous RNA detection. **(D)** A tissue section is placed on a barcoded slide with beads (slide-seq) or spots (spatial transcriptomics), which allows to explore regional gene expression in MS lesions.

cells, individual nuclei isolated from fresh or frozen tissue can be profiled, a technique referred to as single nucleus RNA sequencing (snRNAseq) (Krishnaswami et al., 2016). The nuclear transcriptome of microglia has been reported to reflect the cellular transcriptome under homeostatic conditions and also following an LPS challenge (Gerrits et al., 2020).

Microglia Subtypes

Recently, high-resolution transcriptomic profiling (**Figure 3**) confirmed the existence of molecularly distinct microglia subtypes, with potentially specific functionalities (Keren-Shaul et al., 2017; Mathys et al., 2017; Geirsdottir et al., 2019; Hammond et al., 2019; Jordão et al., 2019; Masuda et al., 2019; Schirmer et al., 2019). To date, dynamics of microglial subtypes have been studied under homeostasis and during development, aging, and various neurodegenerative disease conditions in human and mouse models [including cuprizone and EAE, (de)(re)myelination and inflammation model for MS, respectively] (reviewed by Masuda et al., 2020). Complexity in microglial subtypes is increased in disease compared to homeostatic conditions and is highly influenced by the brain microenvironment. The availability of an extensive amount of transcriptomic profiles facilitated the separation of microglia from CNS-associated and blood-derived macrophages in gene expression datasets, based on marker genes (Jordão et al., 2019). scRNAseq/snRNAseq studies of microglia derived from human postmortem brain tissue from MS donors are scarce and only available with a limited number of donors and cells. However, CNS single-cell data are highly relevant for understanding MS pathogenesis. Masuda et al. were first to sequence individual CD45-positive cells isolated from MS brain tissue. Within their dataset, clustering analysis of 1,180 control microglia and 422 MS microglia identified 7 distinct clusters, all characterized by expression of *TMEM119* and *P2RY12*, referred to as microglia core genes. Controls mainly consisted of three clusters with high expression of microglia core genes linked to homeostatic functions. Homeostatic cluster four was present in controls and MS; this cluster decreased microglia core genes and increased cytokine and chemokine gene expression, referred to as preactivated microglia. In MS, three clusters were more abundant. The first cluster had increased expression of *CTSD*, *APOC1*, *GPNMB*, *ANXA2*, and *LGALS1*, while the second cluster was enriched for *HLA* genes related to antigen presentation, and the third cluster expressed genes that could

be involved in demyelination: *SPP1*, *PADI2*, and *LPL* (Masuda et al., 2019). Recently, the first single-nuclei sequencing study in MS has been performed. In total, 1,524 MS microglia nuclei were compared to 159 control microglia nuclei. Hierarchical clustering distinguished microglia with homeostatic (*P2RY12*, *RUNX1*, *CSF1R*), MS-specific (activation markers, complement factors, *MHC-II* and lipid genes: *ASAH1*, *ACSL1*, *DPYD*), and phagocytosis- and oligodendrocytes-associated genes (*CD163*, *PLP1*, *MBP*, and *ST18*) (Schirmer et al., 2019). These studies indicate that unique gene expression changes occur in MS in specialized microglial subtypes. It is still unclear which factors initiate these gene expression changes and what is the exact functional role of these subtypes in MS. However, these studies provide us with candidate genes to be studied in more detail with functional assays, which likely contributes to future understanding of MS pathology. Taken together, high-resolution transcriptomic studies revealed microglia landscapes, showing the complexity of subtypes in a spatial and temporal manner. Extended information about transcriptional profiling of astrocytes, oligodendrocytes, and neurons in MS is available in **Box 1**.

SPATIAL DETECTION COULD PROVIDE NEW INSIGHTS IN REGIONAL HETEROGENEITY

High-resolution transcriptomics technologies have made it possible to study the entire transcriptome at the level of an individual cell. These methods are highly relevant for understanding MS pathogenesis, as they can detect differentially expressed genes in the affected tissue and potentially identify novel cell subtypes. However, these technologies require disruption of the tissue for the isolation of cells or nuclei from the tissue, and as a consequence, spatial context is lost. However, spatial context is important in understanding cell functioning in health and during pathology. Thus, techniques that allow spatial detection could provide added value when studying (regional) heterogeneity to further elucidate pathogenic features (**Figure 3**).

In situ Hybridization Assays

In 1969, *in situ* hybridization (ISH) was pioneered by Pardue et al., and this was followed by the invention of fluorescent probes around 10 years later (Pardue and Gall, 1969; Rudkin and Stollar, 1977). (Fluorescence) *in situ* hybridization [(F)ISH] is a technique that uses labeled DNA or RNA probes to target a specific DNA or RNA sequence within a histological section, thus indicating gene expression at a spatial level. A problem that arose with this technique was that single molecules could only be detected in regions with a low background signal. In 1998, single-molecule FISH (smFISH) was developed by Femino et al. (1998). smFISH includes probes labeled with five fluorochromes that target multiple regions of the transcript, resulting in a higher fluorescence signal, allowing specific detection of single molecules (Femino et al., 1998). However, the use of probes consisting of five different fluorochromes was associated with a high risk of both false-positive and false-negative outcomes. Furthermore, these heavily labeled probes were difficult to develop (Femino et al., 1998; Asp et al., 2020). Raj et al. (2008) optimized smFISH. The technique uses 40 probes, each coupled to a single fluorochrome, resulting in more accurate mRNA counts (Raj et al., 2008). Hammond et al. (2019) studied microglial RNA expression patterns in mice during development, in old age, and after brain injury. Following demyelination injury by lysolecithin (LPC) injection, this research group used smFISH to determine the organization of microglia within these demyelinated lesions. Three probes were used for smFISH to label the microglial marker *Fcrls* and chemokines *Ccl4* and *Cxcl10*. smFISH confirmed an increase in Fc receptor-like molecules+ (Fcrls+) microglia and showed higher *Apoe* expression after LPC injection compared to control mice. Furthermore, smFISH identified a spatial distribution of *Ccl4* and *Cxcl10* within the lesion; both chemokines were expressed only in small specific parts of the demyelinated area, and in most of the cases, the chemokine expression colocalized with *Fcrls*+ microglia. In human MS active lesions, also an increase in *CCL4* expression was observed, mostly in TMEM119+ microglia (**Figure 3**) (Hammond et al., 2019). Another study investigated regional GM heterogeneity by studying neuronal gene expression in the different layers of the cortex, to further elucidate MS pathology (Schirmer et al., 2019). Using smFISH, probes for simultaneous detection of two to three genes of interest were included, and gene expression was measured in cortical GM, adjacent subcortical WM lesion areas, and controls. smFISH showed a decrease in upper-layer neuronal marker *CUX2* in completely and incompletely demyelinated cortical MS lesions, while expression of the interneuronal marker *VIP* was maintained. Furthermore, smFISH confirmed the increase in the neuronal cell stress markers *PPIA* and *NORAD*, which were mainly upregulated in demyelinated cortical MS lesions (Schirmer et al., 2019). A similar approach to smFISH is RNAscope. RNAscope uses target-specific double Z probes that target the mRNA. Then, amplifiers and different labels (chromogenic or fluorescent) can be added to these Z probes. Targeted mRNA transcripts are detected as dots, each dot representing a single copy of the mRNA. Compared to smFISH, RNAscope probes amplify signals while simultaneously suppressing the background noise (Wang et al., 2012).

In (sm)FISH, the number of fluorescent probes is generally limited to three due to limitations of fluorescent microscopy, such as the use of band- and long-pass filters (Lukumbuzya et al., 2019). Multiplexed error-robust FISH (MERFISH), a technique that was developed in 2015 allows for the detection of multiple probes. MERFISH uses multiple rounds of hybridization and imaging, with a different probe for each RNA molecule (**Figure 3**) (Chen et al., 2015). These probes label the RNA with a specific combination of readout sequences, resulting in "barcodes" assigned to the RNAs of interest. The barcodes are then read out by the use of fluorescent probes that target the RNA sequences. The higher the number of rounds, the higher the copy number of genes that can be measured simultaneously. To adjust for detection errors that exponentially increase with the number of rounds, error-robust encoding schemes were added that detect and correct errors to improve accuracy and sensitivity (Chen et al., 2015; Strell et al., 2019). A recent study

BOX 1 | MS-associated cell subtypes.

Besides microglia, transcriptional profiling of other CNS cell types may contribute to understanding MS pathogenesis. Microglia interact with oligodendrocytes (Peferoen et al., 2013), astrocytes (Wheeler et al., 2020; Vainchtein and Molofsky, 2020), and neurons (Pósfai et al., 2019). In addition, in these cell types, transcriptional changes have been observed in human MS tissues. First of all, reactive *GFAP*-positive astrocytes are already transcriptionally distinct in MS NAWM tissue compared to controls. In MS NAWM, astrocytes are involved in responses to iron, oxidative stress, and immune responses, and they secrete factors for neuronal survival (Waller et al., 2016). Importantly, all above cell types are involved in (de)(re)myelination and immune signaling, which are the main processes that are altered in MS (Domingues et al., 2016; Molina-Gonzalez and Miron, 2019). In addition, recruitment of peripheral immune cells during MS pathogenesis is mediated by oligodendrocyte apoptosis and microglia immune activation (Chrzanowski et al., 2019). Therefore, high-resolution transcriptomic profiling of all cell types potentially involved in MS are relevant to understand MS pathology. Oligodendrocyte lineage cells are the actual suppliers of myelin, which was for a long term described as their only function as a pool of cells. However, high-resolution transcriptomics changed this passive view into a dynamic view, where oligodendrocyte lineage cells display heterogeneity across brain regions (Marques et al., 2016), throughout development (Perlman et al., 2020) and during the course of MS pathology (Jäkel et al., 2019; Schirmer et al., 2019; Yeung et al., 2019). As an example, Yeung et al. (2019) identified subsets of disease-specific oligodendrocyte lineage cells in EAE mice. One EAE-associated subtype was characterized by increased expression of *Mhc-II* and interferon-responsive genes, suggesting an active immune-modulatory role (Yeung et al., 2019). Functionally, they proved *in vitro* that Mhc-II-positive oligodendrocyte lineage cells performed phagocytosis (Yeung et al., 2019). Brain tissues from MS donors also contained MHC-II-positive oligodendrocyte lineage cells, and therefore, phagocytosis by these cells is likely involved in MS pathology. Others investigated human subcortical MS lesions, wherein a myelinating oligodendrocyte subtype increased the expression of genes associated with cellular stress (*HSP90AA1*, *FAIM2*, *ATF4*, and *UBB*), while myelin gene expression was reduced (*BCAS1*, *SGMS1*, *KCNJ10*, *SEMA6A*, and *GLDN*) (Schirmer et al., 2019). snRNAseq of various WM lesions derived from five MS donors generated a transcriptomic landscape consisting of six human oligodendrocytes subtypes. The frequency of each subtype differed within MS lesions and compared to control WM (Jäkel et al., 2019). In a similar approach that focused on astrocytes in EAE, astrocyte heterogeneity was detected and an EAE-associated astrocyte subtype, driven by increased *Mafg* and reduced *Nrf2* expression, was defined. This subtype was also present in 60% of the examined transcriptomic profiles of MS donors. In addition, immunohistochemistry showed that MAFG protein expression was increased in active human MS lesions, while NRF2 proteins already decreased in NAWM compared to controls. MAFG decreases the expression of NRF2, which is a negative regulator of inflammation and oxidative stress. Thus, when less NRF2 is available, inflammation is no longer inhibited. MAFG interacts with MAT2α to block anti-inflammatory pathways. Therefore, inflammatory responses increase due to this specific astrocyte subtype (Wheeler et al., 2020). In human tissue, isolation of astrocytes is technically challenging and, so far, has not resulted in the isolation of intact cells; therefore, analysis of astrocyte nuclei derived from frozen MS tissues is a major improvement. Nuclei sequencing resulted in a nuclear profile specific to subcortical WM (*SLC1A2*) and cortical GM (*CD44*) astrocytes, where all astrocyte populations expressed the marker *RFX4*. In the rim of active MS lesions, an increase in reactive astrocyte genes was observed (*BCL6*, *FOS*, *EDNRB*, *LINC01088*) (Schirmer et al., 2019). Schirmer et al. (2019) sequenced single nuclei of all CNS cell types, but their population consisted mainly of neurons. *CUX2* expressing upper-layer excitatory projection neurons (EN-L2-3A/B) showed major gene expression differences between MS and control donors and trajectory analysis defined a link with chronic inactive lesions. Functionally, *CUX2*-positive neurons were annotated with gene ontology (GO) terms related to oxidative stress, mitochondrial dysfunction, and cell death. Therefore, *CUX2*-positive neurons are sensitive to cell damage, and especially, this neuronal subtype is reduced in MS compared to other, preserved neuronal subtypes (Schirmer et al., 2019).

investigated the role of astrocyte heterogeneity and regulation in MS (Wheeler et al., 2020). This group identified an astrocyte population characterized by an increase in MAFG expression and a decrease in NRF2 expression in EAE and MS. In addition, MERFISH revealed that these *Mafg*+ astrocytes were in close proximity to granulocyte-macrophage colony-stimulating factor *Gm-csf*+ T cells (Wheeler et al., 2020). Thus, MERFISH adds value when spatially investigating the (co-) expression of a high number of RNAs of interest simultaneously.

Spatial *in situ* Sequencing Techniques

Fluorescent *in situ* sequencing (FISSEQ) is a method that was first described by Mitra et al. (2003). First of all, a library with molecules of linear DNA is generated. Each of these molecules contain one variable region that is linked to two constant regions. These constant regions allow primer binding during an amplification step. In-gel amplification of this library results in so-called polonies (polymerase colonies). During FISSEQ, the polonies are denatured, and sequencing primers hybridize to the template (**Figure 3**). Next, sequencing is performed by different cycles in which single fluorescent nucleotides are added and imaged (Mitra et al., 2003). In 2014, the next-generation of FISSEQ was developed (Lee et al., 2014). This technique allows the use of both fresh-frozen (FF) tissue and formalin-fixed paraffin-embedded (FFPE) tissue. First, the fixed tissue is tagged with random hexamers, followed by reverse transcription and cDNA amplification. Next, these cDNA amplicons are cross-linked *in situ* and sequenced. Each base is visualized in one color, resulting in certain barcodes that can be mapped to the genome. There is no need to select candidate genes as this method captures all of the mRNA and thus can localize the RNA whole transcriptome. Other advantages of this technology are high sensitivity and high throughput. Furthermore, FISSEQ can be applied to intact cells and tissues, avoiding sectioning. However, low-abundant targets are not detected by FISSEQ, as the mRNA to cDNA conversion efficiency is limited (Lee et al., 2014, 2015).

In situ sequencing (ISS) was first described in 2013 (Ke et al., 2013). The ISS procedure starts with reverse transcription of mRNA to cDNA, followed by the hybridization of padlock probes to the cDNA strand (**Figure 3**). Two approaches were developed: gap-targeted sequencing and barcode-targeted sequencing. Both approaches are followed by rolling-circle amplification and sequencing by ligation, which makes it possible to sequence small RNA fragments, within cells, and tissue sections. For gap-targeted sequencing, one extra DNA polymerase step has to be taken to fill the gap. The barcode-targeted sequencing approach uses a padlock probe containing a barcode. During sequencing by ligation, anchor primers are hybridized next to the targeted sequence. Then, sequencing probes containing a fluorescent label for one specific nucleotide bind to the anchor primers, allowing the decoding of the gap sequence or the barcode (Ke et al., 2013). In 2017, CARTANA commercialized ISS (barcode-targeted sequencing approach) promising the simultaneous detection of 600 target genes. To increase the detection sensitivity for low-abundant targets, multiple probes could be assigned to one target, as was performed by Chen et al. for the microglial gene *Itgam*

(Chen et al., 2020). In this study, ISS was used as a validation method for spatial transcriptomics (ST), discussed below. ISS was performed in a mouse model for Alzheimer's disease to determine if certain gene expression patterns could be localized to specific cell types. They observed that microglia were the main cell type responsible for expressing plaque-induced genes. Eighteen of these plaque-induced genes overlapped with disease-associated microglia (DAM) genes, which are also increased in MS mouse models (Krasemann et al., 2017). ISS thus could bring us new insights in MS pathology at a spatial single-cell level. Moreover, low-abundancy problems could be solved using multiple probes for one target.

Spatial *ex situ* Sequencing Techniques

Another approach to profile gene expression while retaining spatial tissue information is spatial transcriptomics. ST was first reported by Ståhl et al. (2016) and was improved by 10X Genomics in 2019 under the name "10X Visium" with an increase in resolution. ST and 10X Visium make use of special glass slides containing barcoded mRNA-capturing probes printed in spots (**Figure 3**). All probes within one spot have the same spatial barcode. First, samples are fixed on the glass slide followed by hematoxylin and eosin (HE) staining and imaging. Next, the tissue is permeabilized, which allows RNA binding to the barcoded mRNA-capturing probes. This barcode will be incorporated into the cDNA during reverse transcription. The last step is library preparation and sequencing (Salmén et al., 2018). ST and 10X Visium thus combine histology and transcriptomics. An advantage of these techniques is that prior knowledge of certain genes is not needed, as the 200 million probes within a spot capture all of the mRNA in a tissue section. However, the resolution does not yet approach the single-cell level; the spots have a diameter of 100 μm (ST) or 55 μm (10X Visium), and thus, multiple cells (depending on the tissue type) are captured within each spot. The use of ST could be of interest when analyzing different lesion types in MS. Several studies already analyzed gene expression profiles of different MS lesions, for example by bulk-RNA sequencing or single-cell sequencing (Mycko et al., 2004; Elkjaer et al., 2019; Schirmer et al., 2019). ST/10X Visium retains spatial information by staining and imaging the tissue prior to tissue permeabilization. The spatial barcode makes it possible to map gene expression patterns back to their original location within the tissue section (**Figure 3**). ST/10X Visium thus could add insights in spatial gene expression profiles within the lesions itself or where the lesion transitions to NAWM. A limitation of ST technology is that it is not suitable for detection of low abundant targets, which is true for the majority of microglial genes. Furthermore, only a relatively small tissue section can be analyzed, as the mRNA-capturing probes lay in squares of around 6 × 6 mm (ST) or 8 × 8 mm (10X Visium) (Salmén et al., 2018).

A similar approach to ST/10X Visium is slide-seq, which was developed in 2019. Slide-seq also uses glass slides containing barcoded beads (**Figure 3**). These barcodes refer to a position on the glass slide, which makes it possible to map gene expression back to the imaged tissue section. However, in contrast to ST/10X Visium, adjacent tissue sections are used for staining and imaging, which could decrease the specificity when including heterogeneous tissues. A major advantage of slide-seq is that the barcoded beads have a resolution of 10 μm and can detect gene expression with approximate single-cell resolution (Rodriques et al., 2019; Asp et al., 2020). Furthermore, it takes about 3 h to process the tissue, while this is around 8 h for 10X Visium (for both techniques, this excludes imaging and quality control time) (Rodriques et al., 2019). However, slide-seq is not yet commercially available.

In summary, in the last few decades, different techniques have been developed that make use of spatial gene expression analysis. Methods that allow for spatial detection could provide information about heterogeneity of cells and genes within tissue sections, interactions between cells, and their function and cellular composition. These findings could contribute to novel insights in the underlying mechanisms of pathologies, which are crucial in the process to identify novel therapeutic targets. Depending on the study and its aim, it is important to keep in mind the advantages and disadvantages of the spatial technologies as sensitivity, resolution, and throughput differ between the spatial assays and could lead to wrong interpretation of research outcomes.

PREANALYTICAL FACTORS TO CONSIDER DURING MICROGLIA TRANSCRIPTOMICS PROFILING

Both high-resolution transcriptomics and spatial detection methods measure RNA levels. In addition, high-resolution transcriptomics requires isolation of microglial cells. It remains largely unclear how preanalytical factors such as RNA quality, postmortem delay (PMD), and microglia isolation methods exactly influence the microglial transcriptome. These preanalytical factors vary between labs, and standard procedures are lacking. In order to obtain a pure microglia cell population, mechanical or enzymatic tissue dissociation methods are required, followed by FACS or magnetic bead sorting. Alternatively, in mice, microglia-specific RNA molecules can be captured using RiboTag or PAPERCLIP technologies (Hwang et al., 2017; Haimon et al., 2018). Analysis of microglia gene expression by RiboTag identified that changes can occur upon microglia isolation, where proinflammatory genes are significantly upregulated due to dissociation at 37°C (Haimon et al., 2018). The PAPERCLIP technology has the advantage that microglia cells represent a more native state because alternative polyadenylation does not affect microglial gene expression profiles (Hwang et al., 2017). Furthermore, microglia can be obtained via LCM-guided single-cell isolation. However, the microglia transcriptome appeared to be different when comparing LCM- and FACS-isolated microglia, where LCM-isolated microglia are not a pure microglial population, since 50% neuronal and oligodendroglial transcripts were also detected (Solga et al., 2015). In mice, tissue dissociation steps can be skipped using the genetic cTag-PAPERCLIP or Ribotag model for microglia isolation, which more accurately reflects the microglia transcriptome (Hwang et al., 2017). Of note,

spatial detection methodologies are always independent of microglia isolation procedures, therefore reflecting *in vivo* microglia more accurately; of course, the effect of PMD still remains. The Netherlands Brain Bank isolated microglia cells of 100 donors, including MS donors who, in general, have a longer PMD compared to controls, since an extended autopsy protocol was applied for MS donors using MRI to select lesions. RNA isolation and quantitative PCR (qPCR) were performed on microglial cells isolated from these donors. Surprisingly, there was no effect of PMD on microglial cell yield, while cerebrospinal fluid pH had a positive correlation with the yield (Mizee et al., 2017). Next, a high RNA integrity number, reflecting no RNA degradation within the tissues, is an important factor to generate reliable and reproducible gene expression datasets. In brain tissue, RNA quality of controls has been reported to be significantly higher than in disease conditions, but overall RNA quality was independent of PMD up to 36 h (White et al., 2018). In addition, RNA quality is independent of storage time (White et al., 2018; Shah et al., 2019). RNA quality differences within one dataset might mask biologically relevant information. Computationally, it is possible to correct for RNA quality using a linear model framework (Gallego Romero et al., 2014). However, tissue selection based on RNA quality is an important step prior to downstream analysis. To summarize, RNA quality and microglia isolation procedures have larger effects on gene expression than the PMD. However, only a minimal amount of studies investigated the effect of PMD on gene expression; so far, these studies did not use high-throughput gene expression technologies.

PROTEOMIC STUDIES TO DECODE CELLULAR HETEROGENEITY

Proteomics is the study of the entire proteome in a cell, tissue, or organism. The proteome is dynamic and subject to posttranslational modifications, protein–protein interactions, synthesis, and degradation (Chandramouli and Qian, 2009; Aslam et al., 2017). Techniques to analyze specific proteins are Western blotting and enzyme-linked immunosorbent assay (ELISA); however, these allow the analysis of just a few proteins at a time (Aslam et al., 2017). Coons et al. (1941) were the first to use IHC in their study for the spatial detection of protein epitopes within a tissue section. Already in the 1990s, HLA-DR stainings were performed to study antigen representation in NAWM from MS patients compared to controls (Hayes et al., 1988). IHC is a technique that is still used; however, over the years, new methods have been developed for protein detection that allow a higher throughput or are combined with transcriptomics.

One protein detection technique with a higher throughput is mass cytometry. This technique is a combination of flow cytometry and mass spectrometry. Instruments to measure mass cytometry are cytometry by time-of-flight (CyTOF), CyTOF2, and the most recent one, Helios. Both sensitivity and throughput increased with each generation of instruments. Mass cytometry requires single-cell suspensions, which are incubated in a pool of antibodies conjugated to a unique, stable heavy-metal isotope (**Figure 3**). These isotopes are used as reporters, capable of measuring the gene expression of specific targets. Next, nebulized droplets are introduced into the inductively coupled argon plasma (ICP). Here, ions are liberated, and cells are atomized. Ions are filtered in the quadripole, which allows only the heavy-metal reporter ions to be distinguished by their variation in mass and to be quantified by CyTOF(2) or Helios. Up to 45 parameters can be detected, which is a large improvement compared to the 8–12 parameters that can be detected by flow cytometry (Bendall et al., 2012; Spitzer and Nolan, 2016). Mass cytometry does not only allow for the detection of proteins and their expression levels; also posttranslational modifications and proteolytic products can be determined. For example, the technique is able to measure phosphorylated (activated) states of proteins, which could provide insights in cellular behavior (Spitzer and Nolan, 2016). Mass cytometry thus contributes to the decoding of cellular heterogeneity. Ajami et al. (2018) used cell cytometry to characterize myeloid populations in EAE and other models for neurodegenerative diseases [Huntington's disease (HD) and amyotrophic lateral sclerosis (ALS)]. Using CyTOF, Ajami et al. (2018) identified two CD11b+ myeloid populations in the healthy brain, while an extra CD11b+ myeloid population was detected in the CNS of EAE mice and in HD and ALS models. The first population (population A) was characterized by a CD317+ MHC-II–CD39lowCD86- profile; the second population (population B) was CD317+ MHC-II–CD39hiCD86+; and the third (population C) was CD317+MHC-II+CD39hiCD86+, indicating that populations B and C consisted of activated microglia. Furthermore, CD11c was only expressed by population C. During EAE progression, population C expanded, while in chronic EAE and in the recovery phase, a decrease in the number of cells in population C was observed. CyTOF revealed coexpression of granulocyte-macrophage colony-stimulating factor (GM-CSF) and TNFα in most of the cells in population C during EAE onset and peak of disease, while in HD and ALS models, the percentage of cells expressing these cytokines was low or absent. Another interesting observation was an increase in the expression of the signaling molecules pCREB and pMAPKAPK2 in populations B and C during the onset and subsequently during the peak of EAE. In addition, CyTOF revealed that CD49d (α4 integrin) and CD49a (α5 integrin) were only expressed on peripheral monocyte populations and not on CNS resident myeloid populations. Blocking CD49a expression attenuated EAE, highlighting the potential of CD49a as a therapeutic target (Ajami et al., 2018). This study confirms that mass cytometry is an interesting method to consider when studying cellular heterogeneity, as it is a single-cell method that can distinguish different populations based on (co)expression levels of transcription factors, signaling molecules, cytokines, and other proteins in a specific cell type.

Mass cytometry has a throughput of around thousand cells per seconds, which is much lower compared to flow cytometry, making the technique time consuming. Furthermore, as cells are ionized and atomized during mass cytometry and thus fully shattered, it is not possible to sort cells and collect them for further analysis (Bandura et al., 2009; Spitzer and Nolan, 2016).

New methods, such as cellular indexing of transcriptomes and epitopes by sequencing (CITE-seq) and RNA expression and protein sequencing assay (REAP-seq), have been developed that measure both cell-surface protein and gene expression levels in the same individual cell (**Figure 3**). Both techniques use DNA-barcoded antibodies to tag proteins of interest. These barcodes are unique oligonucleotides that contain an amplification primer and sequencing handle. After cell lysis, reverse transcription, and preamplifications steps, library preparation can be performed followed by single-cell sequencing (Peterson et al., 2017; Stoeckius et al., 2017). The difference between the two techniques is the way the antibody is conjugated to the DNA sequence. In CITE-seq, antibodies are conjugated to streptavidin, which is non-covalently bound to the oligonucleotide, while in REAP-seq, the antibody and oligonucleotide are conjugated by covalent bonds (Peterson et al., 2017; Todorovic, 2017). At the moment, both techniques are not able to detect intracellular proteins; however, due to the conjugation of antibody and barcode by covalent bonds, REAP-seq has potential for intracellular labeling of proteins in the future (Peterson et al., 2017). At present, up to 82 antibodies can be multiplexed at the same time, although it is likely that this number will increase as CITE-seq and REAP-seq are not obstructed by signal collision as is the case in flow and mass cytometry (Stoeckius et al., 2017).

Taken together, proteomic studies are of importance when investigating underlying mechanisms of diseases, as mRNA gene expression levels do not always reflect protein expression levels due to posttranslational modifications, protein trafficking, localizations, and protein–protein interactions. Mass cytometry could provide insights, as it is able to determine posttranslational modification and proteolysis products. On the other hand, since REAP-seq and CITE-seq can measure cell-surface protein and gene expression levels in parallel, they could also contribute to a better understanding of cell functioning and/or cellular heterogeneity.

DISCUSSION: COMPARISON OF TRANSCRIPTOMICS, SPATIAL DETECTION, AND PROTEOMIC METHODOLOGIES. WHICH METHOD SHOULD I USE?

Wide availability of (novel) technologies makes it challenging to choose the most appropriate method to apply to answer specific scientific questions. Here, we provide an overview of important properties per technology, which can facilitate the decision-making process (**Table 1** and **Supplementary Figure 1**). All sequencing-based technologies are unbiased, facilitating novel discovery, since there is no need to preselect candidate genes.

High sensitivity is a major advantage of low-resolution transcriptomics. Increasing resolution and throughput generally decreases sensitivity (20%) due to a lower library complexity, which is a major drawback of high-resolution transcriptomics, and only allows the detection of variations in the most abundantly expressed genes. Sequencing methodologies differ in sequencing of whole transcripts (long reads) or sequencing of a small part of the transcript: the 3′ or 5′ end (short read). Short-read sequencing is not suitable to detect splicing variants and has a higher error rate, making annotating genes to the genome more complex compared to long-read sequencing. Therefore, long-read sequencing is more sensitive compared to short-read sequencing. However, in terms of examining heterogeneity and identifying microglia subtypes, high resolution is absolutely required. High-resolution transcriptomics is possible at the single-cell or single-nucleus level. snRNAseq has certain advantages above scRNAseq; first, nuclear RNA molecules can be obtained from frozen archived tissue samples, which can be very precisely classified for example into MS lesion types with matching HLA-DR scores. Furthermore, cell isolation and sorting is not required, which are the main factors causing cellular stress, which in turn can slightly change the transcriptome. Some cell subtypes are more vulnerable to cellular stress than others; therefore, nuclear RNA most likely represents a more reliable ratio of cell subtypes. Second, nuclear RNA molecules reflect active transcription, which might result in a more accurate view of the condition of interest. snRNAseq of microglia or other less abundant cell types benefits from enrichment strategies to obtain sufficient numbers for in-depth analysis. So far, studies have used a direct microglial enrichment strategy based on IRF8 sorting (van der Poel et al., 2019) or an indirect strategy by selecting a NEUN/OLIG2 negative population to select against major cell types of the brain: neurons and oligodendrocytes (Gerrits et al., 2020). Both single-cell and single-nuclei sequencing require extensive validation experiments to prove the existence and functionality of the detected subtypes, since spatial information is lacking.

Cell shape and localization often reflect functionality, which is already an old concept in biology. Therefore, spatial detection methods offer great possibilities to examine heterogeneity and functionality at the same time in a region specific manner, by using *ex situ* (spatial transcriptomics, slide-seq) or *in situ* (FISSEQ, MERFISH, ISS) technologies, reviewed here (Lee, 2017; Lein et al., 2017). However, can we obtain similar resolution and throughput as in single-cell/single-nuclei sequencing? Not at the moment. The resolution of *ex situ* spatial detection is 55 μM (1–10 cells/spot) for a commercially available method from 10X Genomics (Visium), as resolution is limited by printing distinguishable barcodes (Ståhl et al., 2016; Salmén et al., 2018; Gregory et al., 2020). That level of resolution could cause problems if your goal is to determine the contribution of the microglial transcriptome for a specific condition or disease, since microglia comprise only 10% of all brain cell types and since specific microglial subtypes are expected to represent an even smaller percentage. Compared to astrocyte and oligodendrocyte populations, these subsets likely provide too few RNA molecules to be detected and visualized in spatial transcriptomics in the mouse brain (**Figure 4**). Solving this issue would require higher resolution, higher sensitivity, and better computational deconvolution strategies. In comparison, slide-seq uses barcoded beads to increase the resolution to 10 μM (one to two cells/bead) and detection of genes is unbiased, although standardized description of the protocol

TABLE 1 | Comparison transcriptomics and proteomics technologies.

Target	Technology	Resolution (μM)	Sensitivity	Time needed to run method	Nr of targets detected simultaneously	Costs	Spatial context preserved	Requires candidate genes/ proteins	Suitable for low abundant targets	Tissue type	Commercially available	Brief description of the chemistry	References methods
RNA	Microarray	–	++	+	++ (>100 genes)	+	N	Y	Y	F, FF	Low Input Quick Amp Labeling Kit (Agilent)	Barcoded microfluidic chip	Mycko et al., 2004; Hendrickx et al., 2017; Zheng et al., 2018
	BULKseq	–	+++	+++	+++	+	N	N	N	F, FF. FFPE	Lexogen QuantSeq 3' mRNA-Seq kit, KAPA Stranded mRNA-Seq kit, NEB Next Ultra Directional RNA Library Prep Kit from Illumina	OligoDT primers or beads combined with barcode or UMI	Niu et al., 2019; Geirsdottir et al., 2019; Elkjaer et al., 2019; van der Poel et al., 2019; Rodríguez-Lorenzo et al., 2020
	LCMseq	+++	+++ (LCM-bulk seq) + (LCM-scRNAseq)	–	+++	+	Y	N	N	FF, FFPE, stained tissues	N	Infrared or ultraviolet guided laser capture microdis-section	Mycko et al., 2012; Shrestha et al., 2014; Datta et al., 2015; Guillot et al., 2015; Waller et al., 2016; Nichterwitz et al., 2016; Shrestha et al., 2017; Hendrickx et al., 2017; Foley et al., 2019

(Continued)

TABLE 1 | Continued

Target	Technology	Resolution (μM)	Sensitivity	Time needed to run method	Nr of targets detected simultaneously	Costs	Spatial context preserved	Requires candidate genes/ proteins	Suitable for low abundant targets	Tissue type	Commercially available	Brief description of the chemistry	References methods
	scRNAseq - Full length cDNA	+++	–	++	+++	++	N	N	Y	F	N	OligoDT primer, template switching and tagmentation UMI and barcoded full length cDNA	Picelli et al., 2014; Mathys et al., 2017
	scRNAseq - 3′/5′ end cDNA	+++	–	+++	+++	++	N	N	Y	F	10X Genomics (chromium)	Microfluicic partitioning, UMI and barcoded 3/5 prime cDNA	Keren-Shaul et al., 2017; Geirsdottir et al., 2019; Hammond et al., 2019; Jordão et al., 2019; Masuda et al., 2019
	snRNAseq	+++	–	+++	+++	++	N	N	Y	F, FF	10X Genomics (chromium)	Microfluicic partitioning, UMI and barcoded 3/5 prime cDNA	Krishnaswami et al., 2016; Schirmer et al., 2019; Gerrits et al., 2020
	Spatial transcriptomics	–	–	++	+++	++	Y	N	N	FF	10X Genomics (Visium)	OligoDT probes barcoded on slide	Ståhl et al., 2016; Asp et al., 2017; Salmén et al., 2018; Gregory et al., 2020

(Continued)

TABLE 1 | Continued

Target	Technology	Resolution (μM)	Sensitivity	Time needed to run method	Nr of targets detected simultaneously	Costs	Spatial context preserved	Requires candidate genes/ proteins	Suitable for low abundant targets	Tissue type	Commercially available	Brief description of the chemistry	References methods
	Slide-seq	+++	−	+	++	+	Y	N	N	FF	N	Barcoded microparticles on a rubber-coated glass coverslip	Eisenstein, 2019; Rodriques et al., 2019
	ISS	+++	Unknown	−	+	Unknown	Y	Y	N* *only possible if you extend the nr of probes per target	FF, FX	N	Padlock probes	Ke et al., 2013; Maïno et al., 2019
	ISS - Next generation ISS (CARTANA)	+++	−	−	++	+++	Y	Y	N* *only possible if you extend the nr of probes per target	FF, FFPE, FX	CARTANA	Padlock probes	CARTANA AB. 2020 URL: https://www.cartana.se/
	FISSEQ	+++	—	—	++	+	Y	N	N	FF, FFPE	ReadCoor Inc.	RNA is converted into cross-linked cDNA amplicons	Mitra et al., 2003; Lee et al., 2015
	MERFISH	+++	++	+	++	+	Y	Y	Y	FF	N (upcoming; Vizgen)	Probes	Chen et al., 2015; Xia et al., 2019; Wheeler et al., 2020
	smFISH	+++	+++	−	−	++	Y	Y	Y	FF, FFPE	PixelBioTech GmbH, Biosearch Technologies, Inc	Probes	Femino et al., 1998; Raj et al., 2008; Asp et al., 2017; Hammond et al., 2019; Schirmer et al., 2019

(Continued)

TABLE 1 | Continued

Target	Technology	Resolution (μM)	Sensitivity	Time needed to run method	Nr of targets detected simultaneously	Costs	Spatial context preserved	Requires candidate genes/ proteins	Suitable for low abundant targets	Tissue type	Commercially available	Brief description of the chemistry	References methods
	RNAscope	+++	+++	+++	—	+	Y	Y	Y (RNA-scope 2.0)	FF, FFPE, FX	ACD Bio	Target-specific double Z probes	Wang et al., 2012 Advanced Cell Diagnostics, Inc. 2020. URL: https: //acdbio.com/
Protein	Mass cytometry	+++	+++	+++	–	–	N	Y	N	F, FF, FFPE, FX	Novus Biologicals, Miltenyi Biotec, etc.	Antibodies conjugated to a heavy-metal isotope	Bendall et al., 2012; Spitzer and Nolan, 2016; Ajami et al., 2018
	IHC	+++	Depending on antibody/fixation method	++	—	–	Y	Y	N	F, FF, FFPE, FX	Y	Antibodies	Coons et al., 1941; van Horssen et al., 2012; Peferoen et al., 2015; Kuhlmann et al., 2017; Zrzavy et al., 2017; Van Wageningen et al., 2019
RNA and Protein	CITE-seq and Reap-seq	+++	+	++	Proteins; + Genes ++	+	N	Y candidate proteins	Y	F, FF, FX	Totalseq - Biolegend, Fluidigm	Cell-surface antibodies linked to oligonucleotide barcodes	Peterson et al., 2017; Baron et al., 2018; Stoeckius et al., 2017 Fluidigm 2020. URL: https://www. fluidigm.com/

F, fresh; FF, fresh frozen; FFPE, formalin-fixed paraffin embedded; FX, fixed tissue samples. Technologies were compared on several parameters indicated by the following scoring range: – – –, – –, –, +, ++, +++, corresponding to very low, low, below average, average, high, very high, respectively. Other characteristics were indicated by Y, yes or N, no, referring to the presence or absence.

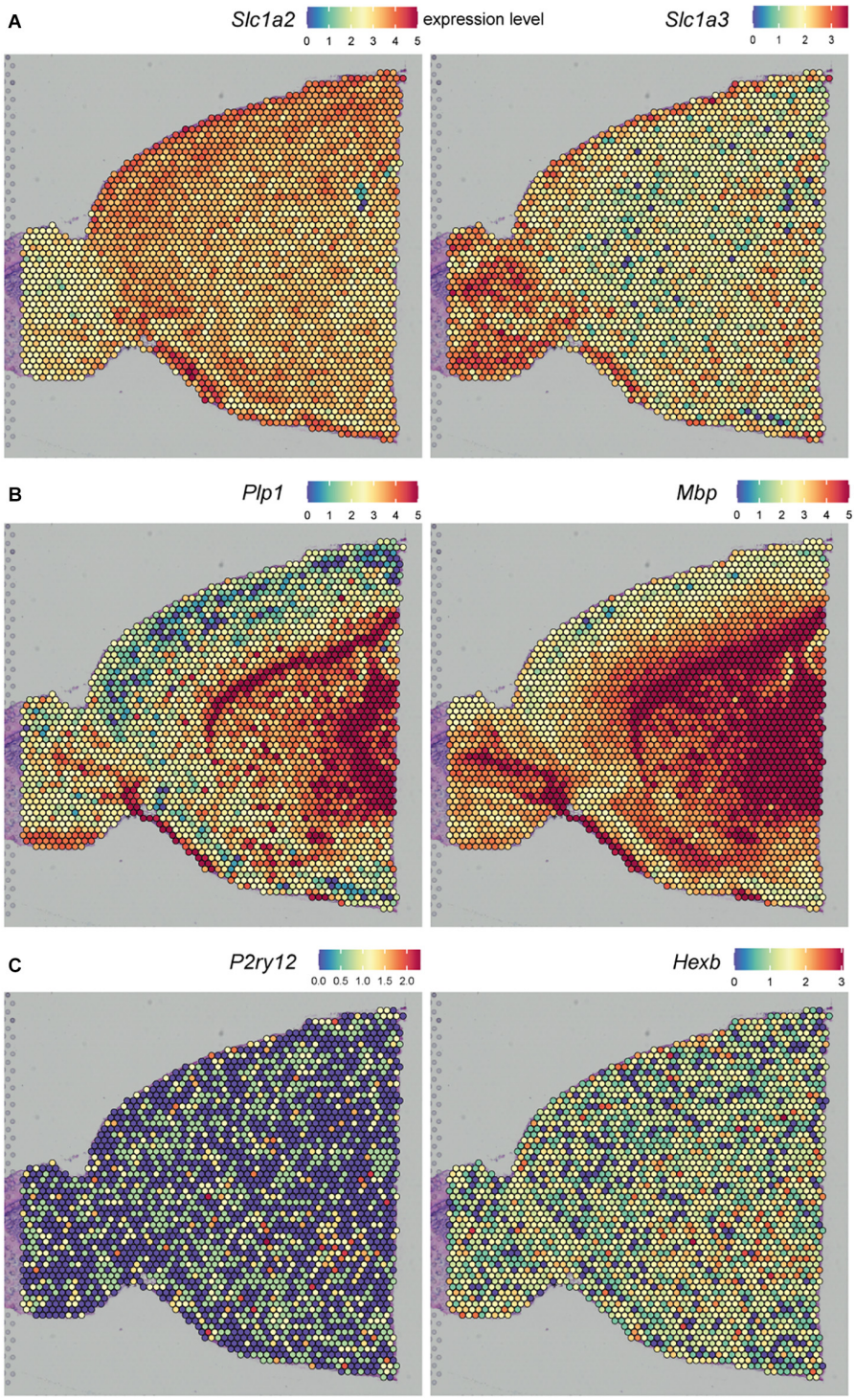

FIGURE 4 | Spatial gene expression of **(A)** astrocyte, **(B)** oligodendrocytes, and **(C)** microglia-cell-specific marker genes, visualized in sagittal anterior control mouse brain. Dataset obtained from 10X Genomics.

is not available yet (Rodriques et al., 2019). Throughput of all spatial detection methodologies is limited by imaging speed; therefore, measuring the complete tissue section is often not possible or very expensive. *In situ* spatial detection methods are very suitable for regional validation of target genes in a cell-specific manner. ISS by CARTANA (Ke et al., 2013; Maïno et al., 2019) is a very promising and easy-to-use methodology, where individual genes are targeted by barcoded padlock probes, which

is a more sensitive methodology compared to unbiased *in situ* approaches including FISSEQ (Lee et al., 2015). More specifically, the sensitivity of ST (7%), ISS (10%), and FISSEQ (0,005%) are all lower compared to single-cell or single-nuclei sequencing (20%). Other disadvantages of ISS are limited throughput and limited detected targets (up to 90 genes) restricted to predetermined target genes, and the design of novel padlock probes is costly. However, the next generation ISS allows detection of up to 600 genes and does not use padlock probes.

Proteomics technologies have some advantages above transcriptomic technologies. Proteomics is generally easier to apply because proteins are more stable than RNA molecules, although this might not be true for all posttranslational modifications. Most proteomics technologies are also cheaper compared to transcriptomics; however, exceptions are, for example, CyTOF, which requires the production of many antibodies. mRNA expression does not always predict protein expression levels in a cell. Therefore, proteomics could contribute to important insights in cell functioning. This will be a major advantage when the study goal is to find new effective drugs, since most therapeutics target proteins and not the mRNA, which makes proteomics crucial for drug development. For example, with a proteomic strategy, Ajami et al. (2018) discovered CD49a as a potential new drug target for MS. Furthermore, proteins are often adapted with posttranslational modifications such as phosphorylation, lipidation, and glycosylation, resulting in, for example, active forms of a protein with slightly changed folding or conformation. Proteomics technologies are able to distinguish the phosphorylated (active) state of a protein, from the non-phosphorylated (inactive) state (Spitzer and Nolan, 2016), which is highly important for biological data interpretation and cannot be detected with transcriptomics. High-throughput proteomic methodologies, such as REAP-seq and CITE-seq, can perform proteome and transcriptome analysis simultaneously, which allows to compare the levels of both molecules in one biological sample. Despite these major advantages, there are also disadvantages to this type of proteomics technique; often, not all proteins can be detected easily, and some technologies can only detect extracellular and not intracellular proteins. Moreover, protocols for proteomic methodologies are not commercially available, thus requiring more skills to robustly perform these technologies. Furthermore, proteomics can often detect a lower number of targets simultaneously compared to transcriptomics; however, this is expected to increase in the future.

FUTURE PERSPECTIVES

The recent advances in high-resolution gene and protein expression profiling of microglia in MS have contributed to the identification of MS signatures in microglia subtypes; it makes researchers aware of the heterogeneity present in MS tissues. Future studies should take this heterogeneity into account by analyzing the different lesion types and GM/WM independently. This selective approach is likely to result in more information about MS-associated microglia subtypes. Currently, specific markers to isolate these MS-associated microglia subtypes individually are lacking. The field would remarkably benefit from isolating these disease-associated subtypes and perform more functional assays in order to elucidate their exact role in MS. Moreover, creating a landscape of cell (sub)type specific datasets allows studying interactions between cell (sub)types, for example ligand receptor mapping (Cabello-Aguilar et al., 2020). Furthermore, it can help to identify the drivers behind spatial heterogeneity; is this solely determined by the environment or do cell intrinsic mechanisms also play a role? In the context of MS, this information can be linked with genome-wide association studies (GWAS), which provide information about single-nucleotide polymorphisms (SNPs) associated with higher MS risk (Patsopoulos et al., 2019).

Finally, to facilitate the extraction of biologically relevant information from these large datasets, public platforms should be generated to share datasets produced by different research groups, stratified by disease, region, and cell (sub)types. Three existing RNA sequencing databases are GOAD—now Brain-sat (Holtman et al., 2015a), Brain RNA-seq (Zhang et al., 2014), and Neuroexpresso (Mancarci et al., 2017), which can be used to obtain glial-cell-type specific information. Currently, region specific information is lacking in these databases. For analysis of distinct regions, the mouse (Erö et al., 2018) or human brain atlas (Sunkin et al., 2013) can be used to annotate brain regions in spatial transcriptomics datasets. The Allen Brain Atlas already extended their anatomic data with genomic data, combining microarray, ISH, and MRI datasets. Future databases should be extended with protein and spatial information. The next step would be to integrate such a database with information about chromatin states associated with transcription regulation, such as chromatin accessibility (ATAC-seq), specific histone marks (CHIP-seq), or interactions within the genome and chromatin conformation capture technologies (Hi-C, PLAC-seq). Recently, an MS study by Factor et al. (2020) showed that this type of analysis can result in valuable information, as this study showed that the enhancer elements regulating *BRD3* and *HEXIM1* are directly associated with an MS risk gene and that these enhancers were dysregulated in MS, contributing to remyelination failure. Region and cell (sub)type specific profiling, as reviewed here, can be applied to diseases where cellular heterogeneity is an important factor in disease progression. In addition, it would allow for the identification and targeting of (pathogenic) cellular subsets. These specific pathogenic subtypes can potentially be reprogrammed into a homeostatic or more beneficial state via targeted drugs or treatments. Thus, the use of these novel technologies will result in better insights in MS disease pathogenesis and potentially contribute to the identification of novel targets to treat MS.

AUTHOR CONTRIBUTIONS

AM and MW wrote the manuscript and designed the figures. BE and SK revised the manuscript. All the authors contributed to the article and approved the submitted version.

FUNDING

AM and SK are supported by a fellowship from the Dutch MS Research Foundation (# 16-947). MW is supported by a grant from the Dutch MS Research Foundation (#18-733c). AM and MW are supported by grants from "Stichting de Cock-Hadders" (2019-47 and 2020-14, respectively). Research in the BJLE lab is supported by grants from the Dutch MS Research Foundation (#18-733c, #18-1002 MS, #20-1085, "VriendenLoterij" project MSCNN, 16-972 MS).

SUPPLEMENTARY MATERIAL

The Supplementary Material for this article can be found online at: https://www.frontiersin.org/articles/10.3389/fnmol.2020.583811/full#supplementary-material

REFERENCES

Ajami, B., Samusik, N., Wieghofer, P., Ho, P. P., Crotti, A., Bjornson, Z., et al. (2018). Single-cell mass cytometry reveals distinct populations of brain myeloid cells in mouse neuroinflammation and neurodegeneration models. *Nat. Neurosci.* 21, 541–551. doi: 10.1038/s41593-018-0100-x

Anderson, A. C., Anderson, D. E., Bregoli, L., Hastings, W. D., Kassam, N., Lei, C., et al. (2007). Promotion of tissue inflammation by the immune receptor Tim-3 expressed on innate immune cells. *Science* 318, 1141–1143. doi: 10.1126/science.1148536

Askew, K., Li, K., Olmos-Alonso, A., Garcia-Moreno, F., Liang, Y., Richardson, P., et al. (2017). Coupled proliferation and apoptosis maintain the rapid turnover of microglia in the adult brain. *Cell Rep.* 18, 391–405. doi: 10.1016/j.celrep.2016.12.041

Aslam, B., Basit, M., Nisar, M. A., Khurshid, M., and Rasool, M. H. (2017). Proteomics: technologies and their applications. *J. Chromatogr. Sci.* 55, 182–196. doi: 10.1093/chromsci/bmw167

Asp, M., Bergenstråhle, J., and Lundeberg, J. (2020). Spatially resolved transcriptomes – next generation tools for tissue exploration. *BioEssays* 42:1900221. doi: 10.1002/bies.201900221

Asp, M., Salmén, F., Ståhl, P. L., Vickovic, S., Felldin, U., Navarro, J. F., et al. (2017). Spatial detection of fetal marker genes expressed at low level in adult human heart tissue. *Sci. Rep.* 7:12941. doi: 10.1038/s41598-017-13462-5

Banati, R. B. (2002). Visualising microglial activation in vivo. *Glia* 40, 206–217. doi: 10.1002/glia.10144

Bandura, D. R., Baranov, V. I., Ornatsky, O. I., Antonov, A., Kinach, R., Lou, X., et al. (2009). Mass cytometry: technique for real time single cell multitarget immunoassay based on inductively coupled plasma time-of-flight mass spectrometry. *Anal. Chem.* 81, 6813–6822. doi: 10.1021/ac901049w

Beaino, W., Janssen, B., Kooij, G., van der Pol, S. M. A., van Het Hof, B., van Horssen, J., et al. (2017). Purinergic receptors P2Y12R and P2X7R: potential targets for PET imaging of microglia phenotypes in multiple sclerosis. *J. Neuroinflamm.* 14, 1–16. doi: 10.1186/s12974-017-1034-z

Beckers, L., Ory, D., Geric, I., Declercq, L., Koole, M., Kassiou, M., et al. (2018). Increased expression of translocator protein (TSPO) marks pro-inflammatory microglia but does not predict neurodegeneration. *Mol. Imaging Biol.* 20, 94–102. doi: 10.1007/s11307-017-1099-1

Bendall, S. C., Nolan, G. P., Roederer, M., and Chattopadhyay, P. K. (2012). A deep profiler's guide to cytometry. *Trends Immunol.* 33, 323–332. doi: 10.1016/j.it.2012.02.010

Bennett, M. L., Bennett, F. C., Liddelow, S. A., Ajami, B., Zamanian, J. L., Fernhoff, N. B., et al. (2016). New tools for studying microglia in the mouse and human CNS. *Proc. Natl. Acad. Sci. U.S.A.* 113, E1738–E1746. doi: 10.1073/pnas.1525528113

Böttcher, C., Schlickeiser, S., Sneeboer, M. A. M., Kunkel, D., Knop, A., Paza, E., et al. (2019). Human microglia regional heterogeneity and phenotypes determined by multiplexed single-cell mass cytometry. *Nat. Neurosci.* 22, 78–90. doi: 10.1038/s41593-018-0290-2

Brioschi, S., Peng, V., and Colonna, M. (2019). Fifty shades of microglia. *Trends Neurosci.* 42, 440–443. doi: 10.1016/j.tins.2019.03.010

Butovsky, O., Ziv, Y., Schwartz, A., Landa, G., Talpalar, A. E., Pluchino, S., et al. (2006). Microglia activated by IL-4 or IFN-γ differentially induce neurogenesis and oligodendrogenesis from adult stem/progenitor cells. *Mol. Cell. Neurosci.* 31, 149–160. doi: 10.1016/j.mcn.2005.10.006

Cabello-Aguilar, S., Alame, M., Kon-Sun-Tack, F., Fau, C., Lacroix, M., and Colinge, J. (2020). SingleCellSignalR: inference of intercellular networks from single-cell transcriptomics. *Nucleic Acids Res.* 48:e55. doi: 10.1093/nar/gkaa183

Cătălin, B., Mitran, S., Albu, C., and Iancău, M. (2013). Comparative aspects of microglia reaction in white and gray matter. *Curr. Health Sci. J.* 39, 151–154.

Chandramouli, K., and Qian, P.-Y. (2009). Proteomics: challenges, techniques and possibilities to overcome biological sample complexity. *Hum. Genomics Proteom.* 2009:239204. doi: 10.4061/2009/239204

Chang, A., Staugaitis, S. M., Dutta, R., Batt, C. E., Easley, K. E., Chomyk, A. M., et al. (2012). Cortical remyelination: a new target for repair therapies in multiple sclerosis. *Ann. Neurol.* 72, 918–926. doi: 10.1002/ana.23693

Chechneva, O. V., and Deng, W. (2016). Mitochondrial translocator protein (TSPO), astrocytes and neuroinflammation. *Neural Regen. Res.* 11, 1056–1057. doi: 10.4103/1673-5374.187027

Chen, J., Cheung, F., Shi, R., Zhou, H., Lu, W., Candia, J., et al. (2018). PBMC fixation and processing for Chromium single-cell RNA sequencing. *J. Transl. Med.* 16, 1–11. doi: 10.1186/s12967-018-1578-4

Chen, K. H., Boettiger, A. N., Moffitt, J. R., Wang, S., and Zhuang, X. (2015). Spatially resolved, highly multiplexed RNA profiling in single cells. *Science* 348, 1360–1363. doi: 10.1126/science.aaa6090

Chen, W.-T., Lu, A., Craessaerts, K., Pavie, B., Sala Frigerio, C., Corthout, N., et al. (2020). Spatial transcriptomics and *in situ* sequencing to study Alzheimer's disease. *Cell* 182, 976–991. doi: 10.1016/j.cell.2020.06.038

Chrzanowski, U., Bhattarai, S., Scheld, M., Clarner, T., Fallier-Becker, P., Beyer, C., et al. (2019). Oligodendrocyte degeneration and concomitant microglia activation directs peripheral immune cells into the forebrain. *Neurochem. Int.* 126, 139–153. doi: 10.1016/j.neuint.2019.03.005

Constantinescu, C. S., Farooqi, N., O'Brien, K., and Gran, B. (2011). Experimental autoimmune encephalomyelitis (EAE) as a model for multiple sclerosis (MS). *Br. J. Pharmacol.* 164, 1079–1106. doi: 10.1111/j.1476-5381.2011.01302.x

Coons, A. H., Creech, H. J., and Jones, R. N. (1941). Immunological properties of an antibody containing a fluorescent group. *Proc. Soc. Exp. Biol. Med.* 47, 200–202.

Cunha, M. I, Su, M., Cantuti-Castelvetri, L., Müller, S. A., Schifferer, M., Djannatian, M., et al. (2020). Pro-inflammatory activation following demyelination is required for myelin clearance and oligodendrogenesis. *J. Exp. Med.* 217:e20191390. doi: 10.1084/jem.20191390

Dal-Bianco, A., Grabner, G., Kronnerwetter, C., Weber, M., Höftberger, R., Berger, T., et al. (2017). Slow expansion of multiple sclerosis iron rim lesions: pathology and 7 T magnetic resonance imaging. *Acta Neuropathol.* 133, 25–42. doi: 10.1007/s00401-016-1636-z

Datta, G., Colasanti, A., Kalk, N., Owen, D., Scott, G., Rabiner, E. A., et al. (2017). 11C-PBR28 and 18F-PBR111 detect white matter inflammatory heterogeneity in multiple sclerosis. *J. Nuclear Med.* 58, 1477–1482. doi: 10.2967/jnumed.116.187161

Datta, S., Malhotra, L., Dickerson, R., Chaffee, S., Sen, C. K., and Roy, S. (2015). Laser capture microdissection: Big data from small samples. *Histol. Histopathol.* 30, 1255–1269. doi: 10.14670/HH-11-622

de Haas, A. H., Boddeke, H. W. G. M., and Biber, K. (2008). Region-specific expression of immunoregulatory proteins on microglia in the healthy CNS. *Glia* 56, 888–894. doi: 10.1002/glia.20663

Domingues, H. S., Portugal, C. C., Socodato, R., and Relvas, J. B. (2016). Oligodendrocyte, astrocyte, and microglia crosstalk in myelin development, damage, and repair. *Front. Cell Dev. Biol.* 4:71. doi: 10.3389/fcell.2016.00071

Dubbelaar, M. L., Kracht, L., Eggen, B. J. L., and Boddeke, E. W. G. M. (2018). The kaleidoscope of microglial phenotypes. *Front. Immunol.* 9:1753. doi: 10.3389/fimmu.2018.01753

Eisenstein, M. (2019). Companies seek slice of spatial imaging market. *Nat. Biotechnol.* 37, 490–491. doi: 10.1038/d41587-019-00011-w

Elkjaer, M. L., Frisch, T., Reynolds, R., Kacprowski, T., Burton, M., Kruse, T. A., et al. (2019). Molecular signature of different lesion types in the brain white matter of patients with progressive multiple sclerosis. *Acta Neuropathol. Commun.* 7, 1–17. doi: 10.1186/s40478-019-0855-7

Erö, C., Gewaltig, M. O., Keller, D., and Markram, H. (2018). A cell atlas for the mouse brain. *Front. Neuroinform.* 12:84. doi: 10.3389/fninf.2018.00084

Factor, D. C., Barbeau, A. M., Allan, K. C., Scacheri, P. C., Tesar, P. J., Corradin, O., et al. (2020). Cell type-specific intralocus interactions reveal oligodendrocyte mechanisms in ms article cell type-specific intralocus interactions reveal oligodendrocyte mechanisms in MS. *Cell* 181, 382–395.e21. doi: 10.1016/j.cell.2020.03.002

Femino, A. M., Fay, F. S., Fogarty, K., and Singer, R. H. (1998). Visualization of single RNA transcripts in situ. *Science* 280, 585–590. doi: 10.1126/science.280.5363.585

Foley, J. W., Zhu, C., Jolivet, P., Zhu, S. X., Lu, P., Meaney, M. J., et al. (2019). Gene expression profiling of single cells from archival tissue with laser-capture microdissection and Smart-3SEQ. *Genome Res.* 29, 1816–1825. doi: 10.1101/gr.234807.118

Galatro, T. F., Holtman, I. R., Lerario, A. M., Vainchtein, I. D., Brouwer, N., Sola, P. R., et al. (2017). Transcriptomic analysis of purified human cortical microglia reveals age-associated changes. *Nat. Neurosci.* 20, 1162–1171. doi: 10.1038/nn.4597

Gallego Romero, I., Pai, A. A., Tung, J., and Gilad, Y. (2014). RNA-seq: impact of RNA degradation on transcript quantification. *BMC Biol.* 12:42. doi: 10.1186/1741-7007-12-42

Geirsdottir, L., David, E., Keren-Shaul, H., Weiner, A., Bohlen, S. C., Neuber, J., et al. (2019). Cross-species single-cell analysis reveals divergence of the primate microglia program. *Cell* 179, 1609–1622.e16. doi: 10.1016/j.cell.2019.11.010

Gerrits, E., Heng, Y., Boddeke, E. W. G. M., and Eggen, B. J. L. (2020). Transcriptional profiling of microglia; current state of the art and future perspectives. *Glia* 68, 740–755. doi: 10.1002/glia.23767

Gillen, K. M., Mubarak, M., Nguyen, T. D., and Pitt, D. (2018). Significance and in vivo detection of iron-laden microglia in white matter multiple sclerosis lesions. *Front. Immunol.* 9:255. doi: 10.3389/fimmu.2018.00255

Gingele, S., Henkel, F., Heckers, S., Moellenkamp, T. M., Hümmert, M. W., Skripuletz, T., et al. (2020). Delayed demyelination and impaired remyelination in aged mice in the cuprizone model. *Cells* 9:945. doi: 10.3390/cells9040945

Gosselin, D., Skola, D., Coufal, N. G., Holtman, I. R., Schlachetzki, J. C. M., Sajti, E., et al. (2017). An environment-dependent transcriptional network specifies human microglia identity. *Science* 356, 1248–1259. doi: 10.1126/science.aal3222

Grabert, K., Michoel, T., Karavolos, M. H., Clohisey, S., Kenneth Baillie, J., Stevens, M. P., et al. (2016). Microglial brain regionâ 'dependent diversity and selective regional sensitivities to aging. *Nat. Neurosci.* 19, 504–516. doi: 10.1038/nn.4222

Grajchen, E., Hendriks, J. J. A., and Bogie, J. F. J. (2018). The physiology of foamy phagocytes in multiple sclerosis. *Acta Neuropathol. Commun.* 6:124. doi: 10.1186/s40478-018-0628-8

Gregory, J. M., McDade, K., Livesey, M. R., Croy, I., Marion de Proce, S., Aitman, T., et al. (2020). Spatial transcriptomics identifies spatially dysregulated expression of GRM3 and USP47 in amyotrophic lateral sclerosis. *Neuropathol. Appl. Neurobiol.* 72, 1–17. doi: 10.1111/nan.12597

Gudi, V., Moharregh-Khiabani, D., Skripuletz, T., Koutsoudaki, P. N., Kotsiari, A., Skuljec, J., et al. (2009). Regional differences between grey and white matter in cuprizone induced demyelination. *Brain Res.* 1283, 127–138. doi: 10.1016/j.brainres.2009.06.005

Guillot, F., Garcia, A., Salou, M., Brouard, S., Laplaud, D. A., and Nicot, A. B. (2015). Transcript analysis of laser capture microdissected white matter astrocytes and higher phenol sulfotransferase 1A1 expression during autoimmune neuroinflammation. *J. Neuroinflammation* 12:130. doi: 10.1186/s12974-015-0348-y

Guneykaya, D., Ivanov, A., Hernandez, D. P., Haage, V., Wojtas, B., Meyer, N., et al. (2018). Transcriptional and translational differences of microglia from male and female brains. *Cell Rep.* 24, 2773–2783.e6. doi: 10.1016/j.celrep.2018.08.001

Haimon, Z., Volaski, A., Orthgiess, J., Boura-Halfon, S., Varol, D., Shemer, A., et al. (2018). Re-evaluating microglia expression profiles using RiboTag and cell isolation strategies /631/1647/2017 /631/1647/2017/2079 technical-report. *Nat. Immunol.* 19, 636–644. doi: 10.1038/s41590-018-0110-6

Hametner, S., Dal Bianco, A., Trattnig, S., and Lassmann, H. (2018). Iron related changes in MS lesions and their validity to characterize MS lesion types and dynamics with Ultra-high field magnetic resonance imaging. *Brain Pathol.* 28, 743–749. doi: 10.1111/bpa.12643

Hametner, S., Wimmer, I., Haider, L., Pfeifenbring, S., Brück, W., and Lassmann, H. (2013). Iron and neurodegeneration in the multiple sclerosis brain. *Ann. Neurol.* 74, 848–861. doi: 10.1002/ana.23974

Hammond, T. R., Dufort, C., Dissing-Olesen, L., Giera, S., Young, A., Wysoker, A., et al. (2019). Single-cell RNA sequencing of microglia throughout the mouse lifespan and in the injured brain reveals complex cell-state changes. *Immunity* 50, 253–271.e6. doi: 10.1016/j.immuni.2018.11.004

Hanamsagar, R., Alter, M. D., Block, C. S., Sullivan, H., Bolton, J. L., and Bilbo, S. D. (2017). Generation of a microglial developmental index in mice and in humans reveals a sex difference in maturation and immune reactivity. *Glia* 65, 1504–1520. doi: 10.1002/glia.23176

Hayes, G. M., Woodroofe, M. N., and Cuzner, M. L. (1988). Microglia express MHC class II in normal and demyelinating human white matter. *Ann. N. Y. Acad. Sci.* 540, 501–503. doi: 10.1111/j.1749-6632.1988.tb27150.x

Hayflick, L. (1965). The limited in vitro lifetime of human diploid cell strains. *Exp. Cell Res.* 37, 614–636. doi: 10.1016/0014-4827(65)90211-9

Hendrickx, D. A. E., van Scheppingen, J., van der Poel, M., Bossers, K., Schuurman, K. G., van Eden, C. G., et al. (2017). Gene expression profiling of multiple sclerosis pathology identifies early patterns of demyelination surrounding chronic active lesions. *Front. Immunol.* 8:1810. doi: 10.3389/fimmu.2017.01810

Holtman, I. R., Noback, M., Bijlsma, M., Duong, K. N., van der Geest, M. A., Ketelaars, P. T., et al. (2015a). Glia open access database (GOAD): a comprehensive gene expression encyclopedia of glia cells in health and disease. *Glia* 63, 1495–1506. doi: 10.1002/glia.22810

Holtman, I. R., Raj, D. D., Miller, J. A., Schaafsma, W., Yin, Z., Brouwer, N., et al. (2015b). Induction of a common microglia gene expression signature by aging and neurodegenerative conditions: a co-expression meta-analysis. *Acta Neuropathol. Commun.* 3:31. doi: 10.1186/s40478-015-0203-5

Howell, O. W., Reeves, C. A., Nicholas, R., Carassiti, D., Radotra, B., Gentleman, S. M., et al. (2011). Meningeal inflammation is widespread and linked to cortical pathology in multiple sclerosis. *Brain* 134, 2755–2771. doi: 10.1093/brain/awr182

Hwang, H. W., Saito, Y., Park, C. Y., Blachère, N. E., Tajima, Y., Fak, J. J., et al. (2017). cTag-PAPERCLIP reveals alternative polyadenylation promotes cell-type specific protein diversity and shifts araf isoforms with microglia activation. *Neuron* 95, 1334–1349.e5. doi: 10.1016/j.neuron.2017.08.024

Jäkel, S., Agirre, E., Mendanha Falcão, A., van Bruggen, D., Lee, K. W., Knuesel, I., et al. (2019). Altered human oligodendrocyte heterogeneity in multiple sclerosis. *Nature* 566, 543–547. doi: 10.1038/s41586-019-0903-2

Jha, M. K., Jo, M., Kim, J. H., and Suk, K. (2019). Microglia-astrocyte crosstalk: an intimate molecular conversation. *Neuroscientist* 25, 227–240. doi: 10.1177/1073858418783959

Jordão, M. J. C., Sankowski, R., Brendecke, S. M., Locatelli, S. G., Tai, Y. H., Tay, T. L., et al. (2019). Neuroimmunology: single-cell profiling identifies myeloid cell subsets with distinct fates during neuroinflammation. *Science* 363:eaat7554. doi: 10.1126/science.aat7554

Ke, R., Mignardi, M., Pacureanu, A., Svedlund, J., Botling, J., Wählby, C., et al. (2013). In situ sequencing for RNA analysis in preserved tissue and cells. *Nat. Methods* 10, 857–860. doi: 10.1038/nmeth.2563

Keren-Shaul, H., Spinrad, A., Weiner, A., Matcovitch-Natan, O., Dvir-Szternfeld, R., Ulland, T. K., et al. (2017). A unique microglia type associated with restricting development of Alzheimer's disease. *Cell* 169, 1276–1290.e17. doi: 10.1016/j.cell.2017.05.018

Kodama, L., and Gan, L. (2019). Do microglial sex differences contribute to sex differences in neurodegenerative diseases? *Trends Mol. Med.* 25, 741–749. doi: 10.1016/j.molmed.2019.05.001

Kondo, Y., and Duncan, I. D. (2009). Selective reduction in microglia density and function in the white matter of colony-stimulating factor-1-deficient mice. *J. Neurosci. Res.* 87, 2686–2695. doi: 10.1002/jnr.22096

Koriem, K. M. M. (2016). Multiple sclerosis: new insights and trends. *Asian Pac. J. Trop. Biomed.* 6, 429–440. doi: 10.1016/j.apjtb.2016.03.009

Krasemann, S., Madore, C., Cialic, R., Baufeld, C., Calcagno, N., El Fatimy, R., et al. (2017). The TREM2-APOE pathway drives the transcriptional phenotype of dysfunctional microglia in neurodegenerative diseases. *Immunity* 47, 566–581.e9. doi: 10.1016/j.immuni.2017.08.008

Krishnaswami, S. R., Grindberg, R. V., Novotny, M., Venepally, P., Lacar, B., Bhutani, K., et al. (2016). Using single nuclei for RNA-seq to capture the transcriptome of postmortem neurons. *Nat. Protoc.* 11, 499–524. doi: 10.1038/nprot.2016.015

Kuhlmann, T., Ludwin, S., Prat, A., Antel, J., Brück, W., and Lassmann, H. (2017). An updated histological classification system for multiple sclerosis lesions. *Acta Neuropathol.* 133, 13–24. doi: 10.1007/s00401-016-1653-y

Kuhn, S., Gritti, L., Crooks, D., and Dombrowski, Y. (2019). Oligodendrocytes in development, myelin generation and beyond. *Cells* 8:1424.

Lampron, A., Larochelle, A., Laflamme, N., Préfontaine, P., Plante, M. M., Sánchez, M. G., et al. (2015). Inefficient clearance of myelin debris by microglia impairs remyelinating processes. *J. Exp. Med.* 212, 481–495. doi: 10.1084/jem.20141656

Lawson, L. J., Perry, V. H., Dri, P., and Gordon, S. (1990). Heterogeneity in the distribution and morphology of microglia in the normal adult mouse brain. *Neuroscience* 39, 151–170. doi: 10.1016/0306-4522(90)90229-W

Lee, J. H. (2017). Quantitative approaches for investigating the spatial context of gene expression. *Wiley Interdiscip. Rev.* 9, 17–19. doi: 10.1002/wsbm.1369

Lee, J. H., Daugharthy, E. R., Scheiman, J., Kalhor, R., Amamoto, R., Peters, D. T., et al. (2014). Highly multiplexed subcellular RNA sequencing *in situ*. *Science* 343, 1360–1364. doi: 10.1126/science.1250212

Lee, J. H., Daugharthy, E. R., Scheiman, J., Kalhor, R., Ferrante, T. C., Terry, R., et al. (2015). Fluorescent *in situ* sequencing (FISSEQ) of RNA for gene expression profiling in intact cells and tissues. *Nat. Protoc.* 10, 442–458. doi: 10.1038/nprot.2014.191

Lee, N. J., Ha, S. K., Sati, P., Absinta, M., Nair, G., Luciano, N. J., et al. (2019). Potential role of iron in repair of inflammatory demyelinating lesions. *J. Clin. Invest.* 129, 4365–4376. doi: 10.1172/JCI126809

Lein, E., Borm, L. E., and Linnarsson, S. (2017). The promise of spatial transcriptomics for neuroscience in the era of molecular cell typing. *Science* 358, 64–69. doi: 10.1126/science.aan6827

Lenz, K. M., Nugent, B. M., Haliyur, R., and McCarthy, M. M. (2013). Microglia are essential to masculinization of brain and behavior. *J. Neurosci.* 33, 2761–2772. doi: 10.1523/JNEUROSCI.1268-12.2013

Luchetti, S., Fransen, N. L., van Eden, C. G., Ramaglia, V., Mason, M., and Huitinga, I. (2018). Progressive multiple sclerosis patients show substantial lesion activity that correlates with clinical disease severity and sex: a retrospective autopsy cohort analysis. *Acta Neuropathol.* 135, 511–528. doi: 10.1007/s00401-018-1818-y

Lukumbuzya, M., Schmid, M., Pjevac, P., and Daims, H. (2019). A multicolor fluorescence in situ hybridization approach using an extended set of fluorophores to visualize microorganisms. *Front. Microbiol.* 10:1383. doi: 10.3389/fmicb.2019.01383

Luo, C., Jian, C., Liao, Y., Huang, Q., Wu, Y., Liu, X., et al. (2017). The role of microglia in multiple sclerosis. *Neuropsychiatr. Dis. Treat.* 13, 1661–1667. doi: 10.2147/NDT.S140634

Maïno, N., Hauling, T., Cappi, G., Madaboosi, N., Dupouy, D. G., and Nilsson, M. (2019). A microfluidic platform towards automated multiplexed in situ sequencing. *Sci. Rep.* 9, 1–10. doi: 10.1038/s41598-019-40026-6

Mairuae, N., Connor, J. R., and Cheepsunthorn, P. (2011). Increased cellular iron levels affect matrix metalloproteinase expression and phagocytosis in activated microglia. *Neurosci. Lett.* 500, 36–40. doi: 10.1016/j.neulet.2011.06.001

Mancarci, B. O., Toker, L., Tripathy, S. J., Li, B., Rocco, B., Sibille, E., et al. (2017). Cross-laboratory analysis of brain cell type transcriptomes with applications to interpretation of bulk tissue data. *eNeuro* 4:ENEURO.0212-17.2017. doi: 10.1523/ENEURO.0212-17.2017

Marques, S., Zeisel, A., Codeluppi, S., van Bruggen, D., Falcǎo, A. M., Xiao, L., et al. (2016). Oligodendrocyte heterogeneity in the mouse juvenile and adult central nervous system. *Science* 352, 1326–1329. doi: 10.1126/science.aaf0784

Masuda, T., Sankowski, R., Staszewski, O., Böttcher, C., Amann, L., Sagar, S. C., et al. (2019). Spatial and temporal heterogeneity of mouse and human microglia at single-cell resolution. *Nature* 566, 388–392. doi: 10.1038/s41586-019-0924-x

Masuda, T., Sankowski, R., Staszewski, O., and Prinz, M. (2020). Microglia heterogeneity in the single-cell era. *Cell Rep.* 30, 1271–1281. doi: 10.1016/j.celrep.2020.01.010

Matcovitch-Natan, O., Winter, D. R., Giladi, A., Aguilar, S. V., Spinrad, A., Sarrazin, S., et al. (2016). Microglia development follows a stepwise program to regulate brain homeostasis. *Science* 353:aad8670. doi: 10.1126/science.aad8670

Mathys, H., Adaikkan, C., Gao, F., Young, J. Z., Manet, E., Hemberg, M., et al. (2017). Temporal tracking of microglia activation in neurodegeneration at single-cell resolution. *Cell Rep.* 21, 366–380. doi: 10.1016/j.celrep.2017.09.039

McKay, S. M., Brooks, D. J., Hu, P., and McLachlan, E. M. (2007). Distinct types of microglial activation in white and grey matter of rat lumbosacral cord after mid-thoracic spinal transection. *J. Neuropathol. Exp. Neurol.* 66, 698–710. doi: 10.1097/nen.0b013e3181256b32

Metz, I., Weigand, S. D., Popescu, B. F. G., Frischer, J. M., Parisi, J. E., Guo, Y., et al. (2014). Pathologic heterogeneity persists in early active multiple sclerosis lesions. *Ann. Neurol.* 75, 728–738. doi: 10.1002/ana.24163

Minneboo, A., Uitdehaag, B. M. J., Ader, H. J., Barkhof, F., Polman, C. H., and Castelijns, J. A. (2005). Patterns of enhancing lesion evolution in multiple sclerosis are uniform within patients. *Neurology* 65, 56–61. doi: 10.1212/01.wnl.0000167538.24338.bb

Miron, V. E., Boyd, A., Zhao, J. W., Yuen, T. J., Ruckh, J. M., Shadrach, J. L., et al. (2013). M2 microglia and macrophages drive oligodendrocyte differentiation during CNS remyelination. *Nat. Neurosci.* 16, 1211–1218. doi: 10.1038/nn.3469

Mitra, R. D., Shendure, J., Olejnik, J., Krzymanska-Olejnik, E., and Church, G. M. (2003). Fluorescent in situ sequencing on polymerase colonies. *Anal. Biochem.* 320, 55–65. doi: 10.1016/S0003-2697(03)00291-4

Mittelbronn, M., Dietz, K., Schluesener, H. J., and Meyermann, R. (2001). Local distribution of microglia in the normal adult human central nervous system differs by up to one order of magnitude. *Acta Neuropathol.* 101, 249–255. doi: 10.1007/s004010000284

Mizee, M. R., Miedema, S. S. M., van der Poel, M., Adelia, Schuurman, K. G., van Strien, M. E., et al. (2017). Isolation of primary microglia from the human post-mortem brain: effects of ante- and post-mortem variables. *Acta Neuropathol. Commun.* 5:16. doi: 10.1186/s40478-017-0418-8

Molina-Gonzalez, I., and Miron, V. E. (2019). Astrocytes in myelination and remyelination. *Neurosci. Lett.* 713:134532. doi: 10.1016/j.neulet.2019.134532

Mycko, M. P., Brosnan, C. F., Raine, C. S., Fendler, W., and Selmaj, K. W. (2012). Transcriptional profiling of microdissected areas of active multiple sclerosis lesions reveals activation of heat shock protein genes. *J. Neurosci. Res.* 90, 1941–1948. doi: 10.1002/jnr.23079

Mycko, M. P., Papoian, R., Boschert, U., Raine, C. S., and Selmaj, K. W. (2004). Microarray gene expression profiling of chronic active and inactive lesions in multiple sclerosis. *Clin. Neurol. Neurosurg.* 106, 223–229. doi: 10.1016/j.clineuro.2004.02.019

Nichterwitz, S., Chen, G., Aguila Benitez, J., Yilmaz, M., Storvall, H., Cao, M., et al. (2016). Laser capture microscopy coupled with Smart-seq2 for precise spatial transcriptomic profiling. *Nat. Commun.* 7:12139. doi: 10.1038/ncomms12139

Niu, J., Tsai, H. H., Hoi, K. K., Huang, N., Yu, G., Kim, K., et al. (2019). Aberrant oligodendroglial–vascular interactions disrupt the blood–brain barrier, triggering CNS inflammation. *Nat. Neurosci.* 22, 709–718. doi: 10.1038/s41593-019-0369-4

Pardue, M. L., and Gall, J. G. (1969). Molecular hybridization of radioactive DNA to the DNA of cytological preparations. *Proc. Natl. Acad. Sci. U.S.A.* 64, 600–604.

Patsopoulos, N. A., Baranzini, S. E., Santaniello, A., Shoostari, P., Cotsapas, C., Wong, G., et al. (2019). Multiple sclerosis genomic map implicates peripheral immune cells and microglia in susceptibility. *Science* 365:eaav7188. doi: 10.1126/science.aav7188

Peferoen, L., Kipp, M., van der Valk, P., van Noort, J. M., and Amor, S. (2013). Oligodendrocyte-microglia cross-talk in the central nervous system. *Immunology* 141, 302–313. doi: 10.1111/imm.12163

Peferoen, L. A. N., Vogel, D. Y. S., Ummenthum, K., Breur, M., Heijnen, P. D. A. M., Gerritsen, W. H., et al. (2015). Activation status of human microglia is dependent on lesion formation stage and remyelination in multiple sclerosis. *J. Neuropathol. Exp. Neurol.* 74, 48–63. doi: 10.1097/NEN.0000000000000149

Pereira, L., Font-Nieves, M., Van den Haute, C., Baekelandt, V., Planas, A. M., and Pozas, E. (2015). IL-10 regulates adult neurogenesis by modulating ERK and STAT3 activity. *Front. Cell. Neurosci.* 9:57. doi: 10.3389/fncel.2015.00057

Perlman, K., Couturier, C. P., Yaqubi, M., Tanti, A., Cui, Q. L., Pernin, F., et al. (2020). Developmental trajectory of oligodendrocyte progenitor cells in the human brain revealed by single cell RNA sequencing. *Glia* 68, 1291–1303. doi: 10.1002/glia.23777

Peterson, V. M., Zhang, K. X., Kumar, N., Wong, J., Li, L., Wilson, D. C., et al. (2017). Multiplexed quantification of proteins and transcripts in single cells. *Nat. Biotechnol.* 35, 936–939. doi: 10.1038/nbt.3973

Petiet, A., Aigrot, M. S., and Stankoff, B. (2016). Gray and white matter demyelination and remyelination detected with multimodal quantitative mri analysis at 11.7T in a chronic mouse model of multiple sclerosis. *Front. Neurosci.* 10:491. doi: 10.3389/fnins.2016.00491

Picelli, S., Faridani, O. R., Björklund, ÅK., Winberg, G., Sagasser, S., and Sandberg, R. (2014). Full-length RNA-seq from single cells using Smart-seq2. *Nat. Protoc.* 9, 171–181. doi: 10.1038/nprot.2014.006

Pósfai, B., Cserép, C., Orsolits, B., and Dénes, Á (2019). New insights into microglia–neuron interactions: a neuron's perspective. *Neuroscience* 405, 103–117. doi: 10.1016/j.neuroscience.2018.04.046

Prinz, M., Jung, S., and Priller, J. (2019). Microglia biology: one century of evolving concepts. *Cell* 179, 292–311. doi: 10.1016/j.cell.2019.08.053

Raj, A., van den Bogaard, P., Rifkin, S. A., van Oudenaarden, A., and Tyagi, S. (2008). Imaging individual mRNA molecules using multiple singly labeled probes. *Nat. Methods* 5, 877–879. doi: 10.1038/nmeth.1253

Ribbons, K. A., McElduff, P., Boz, C., Trojano, M., Izquierdo, G., Duquette, P., et al. (2015). Male sex is independently associated with faster disability accumulation in relapse-onset MS but not in primary progressive MS. *PLoS One* 10:e0122686. doi: 10.1371/journal.pone.0122686

Rodríguez-Lorenzo, S., Ferreira Francisco, D. M., Vos, R., Van Het Hof, B., Rijnsburger, M., Schroten, H., et al. (2020). Altered secretory and neuroprotective function of the choroid plexus in progressive multiple sclerosis. *Acta Neuropathol. Commun.* 8, 1–13. doi: 10.1186/s40478-020-00903-y

Rodriques, S. G., Stickels, R. R., Goeva, A., Martin, C. A., Murray, E., Vanderburg, C. R., et al. (2019). Slide-seq: a scalable technology for measuring genome-wide expression at high spatial resolution. *Science* 363, 1463–1467. doi: 10.1126/science.aaw1219

Rudkin, G. T., and Stollar, B. D. (1977). High resolution detection of DNA–RNA hybrids in situ by indirect immunofluorescence. *Nature* 265, 472–473.

Salmén, F., Ståhl, P. L., Mollbrink, A., Navarro, J. F., Vickovic, S., Frisén, J., et al. (2018). Barcoded solid-phase RNA capture for spatial transcriptomics profiling in mammalian tissue sections. *Nat. Protoc.* 13, 2501–2534. doi: 10.1038/s41596-018-0045-2

Savchenko, V. L., Nikonenko, I. R., Skibo, G. G., and McKanna, J. A. (1997). Distribution of microglia and astrocytes in different regions of the normal adult rat brain. *Neurophysiology* 29, 343–351. doi: 10.1007/BF02463354

Schirmer, L., Velmeshev, D., Holmqvist, S., Kaufmann, M., Werneburg, S., Jung, D., et al. (2019). Neuronal vulnerability and multilineage diversity in multiple sclerosis. *Nature* 573, 75–82. doi: 10.1038/s41586-019-1404-z

See, P., Lum, J., Chen, J., and Ginhoux, F. (2018). A single-cell sequencing guide for immunologists. *Front. Immunol.* 9:2425. doi: 10.3389/fimmu.2018.02425

Sellner, J., Kraus, J., Awad, A., Milo, R., Hemmer, B., and Stüve, O. (2011). The increasing incidence and prevalence of female multiple sclerosis-A critical analysis of potential environmental factors. *Autoimmun. Rev.* 10, 495–502. doi: 10.1016/j.autrev.2011.02.006

Shah, S. G., Rashid, M., Verma, T., Ludbe, M., Khade, B., Gera, P. B., et al. (2019). Establishing a correlation between RIN and A260/280 along with the multivariate evaluation of factors affecting the quality of RNA in cryopreserved cancer bio-specimen. *Cell Tissue Banking* 20, 489–499. doi: 10.1007/s10561-019-09782-7

Shrestha, B., Ge, S., and Pachter, J. S. (2014). Resolution of central nervous system astrocytic and endothelial sources of CCL2 gene expression during evolving neuroinflammation. *Fluids Barriers CNS* 11:6. doi: 10.1186/2045-8118-11-6

Shrestha, B., Jiang, X., Ge, S., Paul, D., Chianchiano, P., and Pachter, J. S. (2017). Spatiotemporal resolution of spinal meningeal and parenchymal inflammation during experimental autoimmune encephalomyelitis. *Neurobiol. Dis.* 108, 159–172. doi: 10.1016/j.nbd.2017.08.010

Singhal, T., O'Connor, K., Dubey, S., Pan, H., Chu, R., Hurwitz, S., et al. (2019). Gray matter microglial activation in relapsing vs progressive MS: a [F-18]PBR06-PET study. *Neurology* 6:e587. doi: 10.1212/NXI.0000000000000587

Skripuletz, T., Lindner, M., Kotsiari, A., Garde, N., Fokuhl, J., Linsmeier, F., et al. (2008). Cortical demyelination is prominent in the murine cuprizone model and is strain-dependent. *Am. J. Pathol.* 172, 1053–1061. doi: 10.2353/ajpath.2008.070850

Solga, A. C., Pong, W. W., Walker, J., Wylie, T., Magrini, V., Apicelli, A. J., et al. (2015). RNA-sequencing reveals oligodendrocyte and neuronal transcripts in microglia relevant to central nervous system disease. *Glia* 63, 531–548. doi: 10.1002/glia.22754

Spitzer, M. H., and Nolan, G. P. (2016). Mass cytometry: single cells, many features. *Cell* 165, 780–791. doi: 10.1016/j.cell.2016.04.019

Ståhl, P. L., Salmén, F., Vickovic, S., Lundmark, A., Navarro, J. F., Magnusson, J., et al. (2016). Visualization and analysis of gene expression in tissue sections by spatial transcriptomics. *Science* 353, 78–82. doi: 10.1126/science.aaf2403

Stoeckius, M., Hafemeister, C., Stephenson, W., Houck-Loomis, B., Chattopadhyay, P. K., Swerdlow, H., et al. (2017). Simultaneous epitope and transcriptome measurement in single cells. *Nat. Methods* 14, 865–868. doi: 10.1038/nmeth.4380

Strell, C., Hilscher, M. M., Laxman, N., Svedlund, J., Wu, C., Yokota, C., et al. (2019). Placing RNA in context and space–methods for spatially resolved transcriptomics. *FEBS J.* 286, 1468–1481. doi: 10.1111/febs.14435

Sunkin, S. M., Ng, L., Lau, C., Dolbeare, T., Gilbert, T. L., Thompson, C. L., et al. (2013). Allen brain atlas: an integrated spatio-temporal portal for exploring the central nervous system. *Nucleic Acids Res.* 41, D996–D1008. doi: 10.1093/nar/gks1042

Todorovic, V. (2017). Single-cell RNA-seq–now with protein. *Nat. Methods* 14, 1028–1029. doi: 10.1038/nmeth.4488

Tomassy, G. S., Berger, D. R., Chen, H., Kasthuri, N., Hayworth, K. J., Vercelli, A., et al. (2014). Distinct profiles of myelin distribution along single axons of pyramidal neurons in the neocortex. *Science* 344, 319–324. doi: 10.1126/science.1249766

Torkildsen, O., Brunborg, L. A., Myhr, K. M., and Bø, L. (2008). The cuprizone model for demyelination. *Acta Neurol. Scand.* 117(SUPPL. 188), 72–76. doi: 10.1111/j.1600-0404.2008.01036.x

Torres-Platas, S. G., Comeau, S., Rachalski, A., Bo, G. D., Cruceanu, C., Turecki, G., et al. (2014). Morphometric characterization of microglial phenotypes in human cerebral cortex. *J. Neuroinflamm.* 11, 1–13. doi: 10.1186/1742-2094-11-12

Tremlett, H., Zhao, Y., Joseph, J., Devonshire, V., Adams, D., Craig, D., et al. (2008). Relapses in multiple sclerosis are age- and time-dependent. *J. Neurol. Neurosurg. Psychiatry* 79, 1368–1374. doi: 10.1136/jnnp.2008.145805

Vainchtein, I. D., and Molofsky, A. V. (2020). Astrocytes and microglia: in sickness and in health. *Trends Neurosci.* 43, 144–154. doi: 10.1016/j.tins.2020.01.003

van der Poel, M., Ulas, T., Mizee, M. R., Hsiao, C. C., Miedema, S. S. M., Adelia, et al. (2019). Transcriptional profiling of human microglia reveals grey–white matter heterogeneity and multiple sclerosis-associated changes. *Nat. Commun.* 10, 1–13. doi: 10.1038/s41467-019-08976-7

van Horssen, J., Singh, S., van der Pol, S., Kipp, M., Lim, J. L., Peferoen, L., et al. (2012). Clusters of activated microglia in normal-appearing white matter show signs of innate immune activation. *J. Neuroinflamm.* 9, 1–9. doi: 10.1186/1742-2094-9-156

Van Wageningen, T. A., Vlaar, E., Kooij, G., Jongenelen, C. A. M., Geurts, J. J. G., and Van Dam, A. M. (2019). Regulation of microglial TMEM119 and P2RY12 immunoreactivity in multiple sclerosis white and grey matter lesions is dependent on their inflammatory environment. *Acta Neuropathol. Commun.* 7, 1–16. doi: 10.1186/s40478-019-0850-z

Verdonk, F., Roux, P., Flamant, P., Fiette, L., Bozza, F. A., Simard, S., et al. (2016). Phenotypic clustering: a novel method for microglial morphology analysis. *J. Neuroinflamm.* 13:153. doi: 10.1186/s12974-016-0614-7

Villa, A., Gelosa, P., Castiglioni, L., Cimino, M., Rizzi, N., Pepe, G., et al. (2018). Sex-specific features of microglia from adult mice. *Cell Rep.* 23, 3501–3511. doi: 10.1016/j.celrep.2018.05.048

Voet, S., Prinz, M., and van Loo, G. (2019). Microglia in central nervous system inflammation and multiple sclerosis pathology. *Trends Mol. Med.* 25, 112–123. doi: 10.1016/j.molmed.2018.11.005

Vowinckel, E., Reutens, D., Becher, B., Verge, G., Evans, A., Owens, T., et al. (1997). PK11195 binding to the peripheral benzodiazepine receptor as a marker of microgila activation in multiple sclerosis and experimental autoimmune encephalomyelitis. *J. Neurosci. Res.* 50, 345–353.

Waller, R., Woodroofe, M. N., Wharton, S. B., Ince, P. G., Francese, S., Heath, P. R., et al. (2016). Gene expression profiling of the astrocyte transcriptome in multiple sclerosis normal appearing white matter reveals a neuroprotective role. *J. Neuroimmunol.* 299, 139–146. doi: 10.1016/j.jneuroim.2016.09.010

Wang, F., Flanagan, J., Su, N., Wang, L. C., Bui, S., Nielson, A., et al. (2012). RNAscope: a novel in situ RNA analysis platform for formalin-fixed, paraffin-embedded tissues. *J. Mol. Diagn.* 14, 22–29. doi: 10.1016/j.jmoldx.2011.08.002

Wheeler, M. A., Clark, I. C., Tjon, E. C., Li, Z., Zandee, S. E. J., Couturier, C. P., et al. (2020). MAFG-driven astrocytes promote CNS inflammation. *Nature* 578, 593–599. doi: 10.1038/s41586-020-1999-0

White, K., Yang, P., Li, L., Farshori, A., Medina, A. E., and Zielke, H. R. (2018). Effect of postmortem interval and years in storage on RNA quality of tissue at a repository of the NIH NeuroBioBank. *Biopreserv. Biobank.* 16, 148–157. doi: 10.1089/bio.2017.0099

Xia, C., Fan, J., Emanuel, G., Hao, J., and Zhuang, X. (2019). Spatial transcriptome profiling by MERFISH reveals subcellular RNA compartmentalization and cell cycle-dependent gene expression. *Proc. Natl. Acad. Sci. U.S.A.* 116, 19490–19499. doi: 10.1073/pnas.1912459116

Yauger, Y. J., Bermudez, S., Moritz, K. E., Glaser, E., Stoica, B., and Byrnes, K. R. (2019). Iron accentuated reactive oxygen species release by NADPH oxidase in activated microglia contributes to oxidative stress in vitro. *J. Neuroinflamm.* 16, 1–15. doi: 10.1186/s12974-019-1430-7

Yeung, M. S. Y., Djelloul, M., Steiner, E., Bernard, S., Possnert, G., Brundin, L., et al. (2019). Disease-specific oligodendrocyte lineage cells arise in multiple sclerosis. *Nat. Med.* 566, 538–542. doi: 10.1038/s41586-018-0842-3

Zhang, Y., Chen, K., Sloan, S. A., Bennett, M. L., Scholze, A. R., O'Keeffe, S., et al. (2014). An RNA-sequencing transcriptome and splicing database of glia, neurons, and vascular cells of the cerebral cortex. *J. Neurosci.* 34, 11929–11947. doi: 10.1523/JNEUROSCI.1860-14.2014

Zheng, W., Chen, Y., Chen, H., Xiao, W., Liang, Y. J., Wang, N., et al. (2018). Identification of key target genes and biological pathways in multiple sclerosis brains using microarray data obtained from the Gene Expression Omnibus database. *Neurol. Res.* 40, 883–891. doi: 10.1080/01616412.2018.1497253

Zhou, Z., Peng, X., Insolera, R., Fink, D. J., and Mata, M. (2009). Interleukin-10 provides direct trophic support to neurons. *J. Neurochem.* 110, 1617–1627. doi: 10.1111/j.1471-4159.2009.06263.x

Zrzavy, T., Hametner, S., Wimmer, I., Butovsky, O., Weiner, H. L., and Lassmann, H. (2017). Loss of "homeostatic" microglia and patterns of their activation in active multiple sclerosis. *Brain* 140, 1900–1913. doi: 10.1093/brain/awx113

Conflict of Interest: The authors declare that the research was conducted in the absence of any commercial or financial relationships that could be construed as a potential conflict of interest.

frontiers in Molecular Neuroscience

ORIGINAL RESEARCH
published: 28 October 2020
doi: 10.3389/fnmol.2020.00134

Profiling Microglia From Alzheimer's Disease Donors and Non-demented Elderly in Acute Human Postmortem Cortical Tissue

Astrid M. Alsema[1†], Qiong Jiang[1†], Laura Kracht[1†], Emma Gerrits[1], Marissa L. Dubbelaar[1], Anneke Miedema[1], Nieske Brouwer[1], Elly M. Hol[2], Jinte Middeldorp[2], Roland van Dijk[2], Maya Woodbury[3], Astrid Wachter[4], Simon Xi[3], Thomas Möller[3], Knut P. Biber[4], Susanne M. Kooistra[1], Erik W. G. M. Boddeke[1,5‡] and Bart J. L. Eggen[1‡]*

[1]Department of Biomedical Sciences of Cells and Systems, Section Molecular Neurobiology, University of Groningen, University Medical Center Groningen, Groningen, Netherlands, [2]Department of Translational Neuroscience, UMC Utrecht Brain Centre, University Medical Centre Utrecht, University Utrecht, Utrecht, Netherlands, [3]Foundational Neuroscience Center, AbbVie Inc., Cambridge, MA, United States, [4]Neuroscience Discovery, AbbVie Deutschland GmbH and Co. KG, Ludwigshafen, Germany, [5]Department of Cellular and Molecular Medicine, Center for Healthy Ageing, University of Copenhagen, Copenhagen, Denmark

OPEN ACCESS

Edited by:
Amanda Sierra, Achucarro Basque Center for Neuroscience, Spain

Reviewed by:
Jose P. Lopez-Atalaya, Consejo Superior de Investigaciones Científicas (CSIC), Spain
Tuan Leng Tay, University of Freiburg, Germany

***Correspondence:**
Bart J. L. Eggen
b.j.l.eggen@umcg.nl

[†]These authors have contributed equally to this work

[‡]These authors share senior authorship

Received: *06 February 2020*
Accepted: *06 July 2020*
Published: *28 October 2020*

Citation:
Alsema AM, Jiang Q, Kracht L, Gerrits E, Dubbelaar ML, Miedema A, Brouwer N, Hol EM, Middeldorp J, van Dijk R, Woodbury M, Wachter A, Xi S, Möller T, Biber KP, Kooistra SM, Boddeke EWGM and Eggen BJL (2020) Profiling Microglia From Alzheimer's Disease Donors and Non-demented Elderly in Acute Human Postmortem Cortical Tissue. Front. Mol. Neurosci. 13:134. doi: 10.3389/fnmol.2020.00134

Microglia are the tissue-resident macrophages of the central nervous system (CNS). Recent studies based on bulk and single-cell RNA sequencing in mice indicate high relevance of microglia with respect to risk genes and neuro-inflammation in Alzheimer's disease (AD). Here, we investigated microglia transcriptomes at bulk and single-cell levels in non-demented elderly and AD donors using acute human postmortem cortical brain samples. We identified seven human microglial subpopulations with heterogeneity in gene expression. Notably, gene expression profiles and subcluster composition of microglia did not differ between AD donors and non-demented elderly in bulk RNA sequencing nor in single-cell sequencing.

Keywords: Alzheimer's disease, microglia, single-cell RNA sequencing, barcoded Smart-seq2, human

INTRODUCTION

Alzheimer's disease (AD), one of the most prevalent age-related neurodegenerative disorders, is characterized by extracellular deposition of β-amyloid protein (Aβ) and intraneuronal neurofibrillary tangles in the neocortex (Hyman and Trojanowski, 1997).

Functional changes occurring in microglia cells have been proposed as an important factor in AD pathology (Zhang et al., 2013; Mhatre et al., 2015). AD single nucleotide polymorphism heritability was recently found to be highly enriched in microglia enhancers (Nott et al., 2019). Multiple genes associated with increased susceptibility for sporadic AD are preferentially expressed in microglia, including *APOE*, *CR1*, *CD33*, *INPP5D*, *PLCG2*, *MS4A6A*, and *TREM2* (Ulrich et al., 2014; Sarlus and Heneka, 2017). In AD mouse models, microglia have been implicated in Aβ seeding, Aβ plaques are surrounded by activated microglia, microglia protrusions physically interact with insoluble Aβ aggregates, and microglia around Aβ plaques undergo transcriptional changes (Rogers and Lue, 2001; Kamphuis et al., 2016; Keren-Shaul et al., 2017; Krasemann et al., 2017; Venegas et al., 2017; Yin et al., 2017). Sustained depletion of microglia in 5xFAD mice prevents Aβ plaque formation in parenchymal tissue and rather shows Aβ accumulation in the brain vasculature (Spangenberg et al., 2019). The functional changes occurring in microglia during AD pathology seem to be diverse (Friedman et al., 2018), and the exact role that microglia play in AD pathology is still unknown.

Many efforts have been made in AD mouse models to identify subpopulations of microglia that are associated with AD pathology. A subpopulation of microglia associated with neurodegeneration was discovered by Krasemann et al. (2017) that was associated with Aβ plaques and triggered by the phagocytosis of apoptotic neurons. This transcriptional phenotype was characterized by increased *Spp1*, *Itgax*, *Axl*, *Lilrb4*, *Clec7a*, *Ccl2*, *Csf1*, and *Apoe* and decreased *P2ry12*, *Tmem119*, *Olfml3*, *Csf1r*, *Rhob*, *Cx3cr1*, *Tgfb1*, *Mef2a*, *Mafb*, and *Sall1* expression levels (Krasemann et al., 2017). At the same time, a highly similar gene expression change, associated with microglia surrounding Aβ plaques was reported by Keren-Shaul et al. (2017), termed disease-associated microglia (DAMs). Using single-cell RNA-sequencing (scRNAseq) these DAMs were subdivided into two sequential stages, a *Trem2*-independent stage, marked by increased expression of *Tyrobp*, *Apoe*, and *B2m* and decreased expression of homeostatic genes, followed by a *Trem2*-dependent activation stage marked by induction of genes involved in lipid metabolism and phagocytosis (*Trem2, Spp1, Itgax, Axl, Lilrb4, Clec7a, Cts7, Ctsl, Lpl, Cd9, Csf1, Ccl6, Cd68*, and more). Sala Frigerio et al. (2019) described a microglia subpopulation in AppNL-G-F mice that appears in response to Aβ deposition and shares gene expression changes with DAMs. They identified mutually exclusive subtypes of activated response microglia overlapping with DAMs and, in addition, an independent subtype of interferon response microglia.

Studies investigating human microglia subtypes are limited, probably due to the technical and logistical difficulties of isolating pure, viable microglia from acute human brain tissue. Olah et al. (2018) investigated acutely isolated single human microglia from donors with a large variety of neuropathological backgrounds. They observed 23 clusters of microglia, where 5 out of 23 clusters were enriched for DAM signature genes. However, the neuropathological background of donors was too diverse to associate the observed changes with AD. Mathys et al. (2019) used single-nucleus sequencing and subclustered ∼2,400 microglia of 48 donors. The study was focused on cell-type specific responses to AD development, and profiling of ∼50 microglia per donor was insufficient to fully define microglia diversity in AD.

In this study, we aimed to identify transcriptomic changes in human microglia at the end stage of AD by applying both bulk and scRNAseq of microglia acutely isolated from postmortem central nervous system (CNS) tissue. We isolated and sequenced a pure population of microglia after CD11B+CD45+-based FACS sorting and investigated effects of sex, brain region, and diagnosis.

MATERIALS AND METHODS

Human Brain Specimens

Autopsy brain specimens from the superior parietal lobe (LPS) and the superior frontal gyrus (GFS) were obtained from 25 donors of the Netherlands Brain Bank (NBB)[1] and two donors of the NeuroBiobank of the Institute Born-Bunge (NBB-IBB, Wilrijk, Antwerp, Belgium, ID: BB190113). All donors have given informed consent for autopsy and use of their brain tissue for research purposes. The performed procedures and research protocols were approved by the corresponding ethical committees of the NBB. On average, the autopsies were performed within 6 h after death. Detailed information about brain specimens used for bulk and scRNAseq can be found in **Supplementary Tables S1**, **S2**, respectively.

Microglia Isolation and Sorting

Microglia were isolated as described previously (Galatro et al., 2017a,b) with minor modifications. All procedures were performed on ice and all centrifugation steps were performed at 4°C. The tissue was homogenized by mechanical dissociation using a glass Dounce homogenizer in Medium A (HBSS (Gibco, 14170-088) containing 15 mM HEPES (Lonza, BE17-737E) and 0.6% glucose (Sigma–Aldrich, G8769) and was filtered through a 300- and 106-μm sieve. Homogenate was centrifuged at 220× *g* for 10 min, and myelin and other lipids were removed through two Percoll gradient centrifugation steps. A 100% Percoll solution was prepared consisting of 90% Percoll (GE Healthcare, UK) and 10% 10× HBSS (Gibco, 14180-046), from which the dilutions were prepared. First, cells were resuspended in 24.5% (vol/vol) Percoll in Medium A. A layer of PBS was added, and the gradient was centrifuged at 950× *g* for 20 min with reduced acceleration speed and brakes off. After the supernatant was removed, cells were resuspended in 60% (vol/vol) Percoll in 1× HBSS (Gibco, 14170-088), and a layer of 30% (vol/vol) Percoll in 1× HBSS (Gibco,) and PBS, respectively, were added and centrifuged at 800× *g* for 25 min (acc: 4, brake: 0). The cells in between the 30%/60% Percoll layer were collected and washed in 1× HBSS (Gibco, 14175-053) and pelleted at 600× *g* for 10 min.

Cells were incubated with antihuman Fc receptor (0.005 μg/ml eBioscience, 14-9161-73) for 10 min in Medium A without phenol red (HBSS, Gibco, 14170-053) containing 15 mM HEPES (Lonza, BE17-737E), 0.6% glucose (Sigma–Adrich, St. Louis, MO, USA, G8769), 1 mM EDTA (Invitrogen, 15575-038), followed by incubation with FITC antihuman CD45 (5 μg/ml, BioLegend, 304006) and PE antihuman CD11B (3.75 μg/ml, BioLegend, 301306). Prior to sorting, DAPI (0.15 μg/ml, Biolegend, 422801) and eBioscience DRAQ5 (2 μM, Thermo Fisher Scientific, Waltham, MA, USA, 63351) were added. Single, viable microglia defined as DAPI−, DRAQ5+, CD45+, and CD11B+ were FACS sorted on a Beckman Coulter MoFlo XDP or Astrios. Microglial subpopulations might be reflected by a slight difference in CD45 and CD11B expression. Since only scRNAseq allows for the disentanglement of microglial subpopulations, we applied a broader CD45+CD11B+ gate to collect microglia for scRNAseq and a narrower CD45+CD11B+ gate for bulk RNA sequencing (bulk RNAseq).

For bulk microglia RNAseq, microglia were sorted into low-retention Eppendorf tubes (Sigma–Adrich, St. Louis, MO, USA, Z666548-250EA) containing 200 μl RNA later (Qiagen, 76104). Following centrifugation at 4°C and 5,000× *g* for 10 min, supernatant was carefully removed, and microglia were resuspended in 350 μl RLTplus lysis buffer (Qiagen, 1053393) and stored at −80°C. For barcoded 3' single-cell sequencing,

[1]https://www.brainbank.nl/

15,792 single microglia were collected in 384-well PCR plates containing cell lysis buffer [0.2% Triton (Sigma–Adrich, St. Louis, MO, USA, T9284), 4 U RNAse inhibitor (Takara, 2313A), 10 mM dNTPs (Thermo Fisher Scientific, Waltham, MA, USA, #R0193), and 10 μM barcoded oligo-dT primer] and were stored for maximally 1 month at −80°C until further processing. For 10× Genomics Chromium single-cell RNA sequencing, approximately 25,000 single microglia were sorted from each sample (2018-135, 2019-010) into low-retention Eppendorf tubes (Sigma, Z666548-250EA) containing 5 μl Medium A and were immediately processed with the Single Cell 3' Reagent Kit v2 (10× Genomics). FACS data was analyzed with FlowJo (Becton, Dickinson and Company).

Bulk Microglia RNA Sequencing Library Preparation

Total RNA was extracted from the bulk sorted microglia samples using the RNeasy Plus Micro kit (Qiagen, 74034) according to the manufacturer's protocol. RNA quality and quantity were determined with the Experion RNA HighSens Analysis Kit (Bio-Rad, #7007105). All 25 RNA samples, with RIN values varying between 5.1 and 9.9, were enriched for poly(A) + messenger RNA using NEXTflex Poly(A) Beads (BIOO Scientific, #NOVA-512980) according to the manufacturer's protocol, and 14 μl of this mRNA-enriched poly(A)-tailed RNA was used as the input for the NEXTflex Rapid Directional qRNA-Seq kit (BIOO Scientific, #NOVA-5130-04). Library preparation was performed according to the manufacturer's protocol. Quality and concentration of libraries from individual samples were assessed using the High Sensitivity dsDNA kit (Agilent, 067-4626) on a 2100 Bioanalyzer (Agilent) and a Qubit 2.0 Fluorometer (Life Technologies). Subsequently, individual libraries were combined into two sequencing pools of 13 samples each with equal molar input, and 75 bp paired-end sequencing was performed on an Illumina NextSeq 500 system. PhiX was added at 5% to both pools as an internal control before sequencing.

Single-Cell RNA Sequencing Library Preparation

The scRNAseq library preparation method that was used here is based on the Smart-seq2 protocol by Picelli et al. (2014) with the modification of obtaining 3' instead of full-length RNA/cDNA libraries as in Uniken Venema et al. (2019). After cell lysis and barcoded poly-dT primer annealing (73°C, 3 min), RNA was reversed transcribed (RT) based on the template switching oligo mechanism using 0.1 μM biotinylated barcoded template switching oligo (BC-TSO, 5'-AAGCAGTGGTATCAACGC AGAGTACATrGrG+G-biotin-3'), 25 U SmartScribe reverse transcriptase, first-strand buffer, and 2 mM DTT (Takara, 639538), 1 U RNAse inhibitor (Takara, 2313A), and 1 M betaine (Sigma–Aldrich, B0300-5VL) with the following PCR program: (1) 42°C, 90 min; (2) 11 cycles of 50°C, 2 min, 42°C, 2 min; (3) 70°C, 15 min. To account for amplification bias and to allow multiplexing of cells, the barcoded poly-dT primer contains a cell-specific barcode and a unique molecular identifier (UMI) and a known sequence that is used as a primer-binding site during the first amplification step. This same primer-binding site is linked to the BC-TSO, enabling the use of one primer pair (custom primer) during the first amplification. After the RT reaction, primer-dimers and small fragments were removed by 0.5 U Exonuclease (GE Healthcare, E70073Z) treatment for 1 h at 42°C. cDNA libraries were amplified with KAPA Hifi HotStart ReadyMix (KAPA Biosystems, KK2602) and custom PCR primer (5′-AAGCAGTGGTATCAACGCAGAGT-3′) with the following PCR program: 98°C, 3 min, 25 cycles of 98°C, 20 s, 67°C, 15 s, 72°C, 6 min; 72°C, 5 min. cDNA libraries of 84 cells were multiplexed, and short fragments were eliminated by Agencourt Ampure XP beads (Beckman Coulter, A63880, ratio of 0.8:1 beads to library volume). The quality of multiplexed cDNA libraries was examined with a 2100 Bioanalyzer (Agilent) according to the manufacturer's protocol. cDNA libraries with an average size of 1.5–2 kb were tagmented and indexed during a second PCR amplification step with the Illumina Nextera XT DNA preparation kit (Illumina, FC-131-1024). Tagmentation was performed according to the manufacturer's protocol with an input of 500 pg cDNA and amplicon tagment mix for 5 min at 55°C. The tagmentation reaction was stopped using neutralize tagment buffer. Next, tagmented cDNA was amplified with Nextera PCR master mix, the Nextera indices (12 pool-specific indices, Illumina, FC-131-2001) and 10 μM P5-TSO hybrid primer (5′-AATGATACGGCGACCACC GAGATCTACACGCCTGTCCGCGGAAGCAGTGGTATC AACGCAGAGT*A*C-3′) with the following PCR program: (1) 72°C, 3 min; (2) 95°C, 30 s; (3) 10 cycles of 95°C, 10 s, 55°C, 30 s, 72°C, 30 s; and (4) 72°C, 5 min. Tagmented cDNA libraries were purified by a 0.6:1 ratio of Agencourt Ampure XP beads (Beckman Coulter, A63880) to library volume. The quality and concentration of tagmented cDNA libraries were determined with a 2100 Bioanalyzer (Agilent). cDNA pools with an average size of 300–600 bp were multiplexed using a balanced design with pools from 10 different donors (in total, 840 cells) per sequencing run. In other words, cells from each donor were distributed over several sequencing runs to avoid potential batch effects. To eliminate short fragments, the final superpool was gel-purified from 2% agarose gel (Invitrogen, 10135444) with the Zymoclean Gel DNA Recovery kit (Zymo Research, D4007). The concentration was determined using a 2100 Bioanalyzer (Agilent) and Qubit 3.0 (ThermoFisher Scientific) according to the manufacturer's protocol. Pools were loaded on an Ilumina NextSeq at a final concentration of 2 pM with a 7% spike in PhiX DNA; 0.3 μM BC read 1 primer (5′-GCCTGTCCGCGGAAGCAGTGGTATCAACGCAGAG TAC-3′) was used for the sequencing run. The libraries were sequenced on an Illumina NextSeq 500 system with an average sequencing depth of 26 million reads per pool. The exact number of cell barcodes per pool varied, but approximately ∼350,000 raw reads per cell were sequenced. After read alignment, exonic read count, and deduplication, this resulted in an average of 19,050 UMIs per cell.

10× Genomics Chromium Single-Cell 3' Library Construction

The scRNAseq barcoded libraries were constructed according to the instructions of the Single-Cell 3' Reagent Kits v2 (10×

Genomics). Briefly, cells were loaded into a slot of a Chromium chip and GEMs were incubated in a thermal cycler to generate barcoded cDNA. After amplification, the cDNA was fragmented and processed for sequencing by ligating adapters and sample indices. The libraries were sequenced on an Illumina NextSeq 500 system with an average sequencing depth of ∼42,500 raw reads per cell; this resulted in an average of 629 UMIs per cell.

Immunohistochemistry

Immunohistochemistry was performed as described previously (Yin et al., 2017). Briefly, 16 μm sections of PFA-fixed human brain tissue were vacuum-dried, post-fixated for 10 min with 4% PFA, and washed with PBS. Heat-induced antigen retrieval was performed in sodium citrate solution (pH 6.0) for 10 min in a microwave. Endogenous peroxidase was blocked by incubating the slides in 0.3% H_2O_2 for 30 min. After three washing steps with PBS, primary antibodies against IBA1 (WAKO, 019-19741, 1:1,000), Phospho-TAU (Thermo Fisher Scientific, Waltham, MA, USA, MN1020, clone AT8, 1:750), and Beta-Amyloid (Dako, M0872, 1:100) were diluted in Bright Diluent (ImmunoLogic, BD09-500) to prevent background staining and incubated overnight at 4°C. After three washing steps in PBS, secondary biotinylated horse antimouse IgG antibody (0.000125 mg/ml Vector BA-2001) was incubated for 1 h at room temperature. The tissue sections were washed three times in PBS. The signal was amplified with avidin-biotin complexes (Vectastain Elite ABC-HRP, Vector, PK-6100) for 30 min at RT and visualized with 3,3′-diaminobenzidine (Sigma–Adrich, St. Louis, MO, USA, D-5637). Additionally, after the phospho-TAU staining, we performed a crystal violet counterstaining. The slides were dehydrated with an ethanol series (50%, 70%, 80%, 90%, 2× 96%, and 3× 100% ethanol) and air-dried for 30 min prior to mounting a coverslip with DePeX (Serva, 18243). Imaging was performed with a Hamamatsu Nanozoomer at 40x magnification.

Preprocessing of RNA-Sequencing Data

For bulk samples, NEXTflex barcodes (nine base pairs) were stripped from the sequence. Sequencing reads were then aligned with HISAT2 (version 2.1.0; Kim et al., 2015) to the GRCh38.92 reference genome with Ensembl annotation. Further processing with samtools (version 1.9) and Picard Tools (version 1.140) included sorting, read group assignment, verification of mate pair information, and marking of duplicates. Reads were further quantified using featureCounts (Subread version 1.6.2; Liao et al., 2014) and based on NEXTflex barcodes deduplicated with a bash script developed by BIOO Scientific (version 2, release date 11/1/14) to eliminate PCR duplicates.

Reads from bc-Smart-seq2 single cells were demultiplexed with UMI-tools (version 0.5.3; Smith et al., 2017). A cell barcode whitelist was used to filter barcodes for downstream processing. Cell barcodes and the UMI from each read were extracted to the read name of the sequence using the UM-tools *extract* function. Reads were single-end aligned with HISAT2 (version 2.1.0) to the GRCh38.91 reference genome with Ensembl annotation using default parameters, followed by sorting and indexing of BAM files. Primary counts were quantified with featureCounts (version 1.6.0) using the flag -primary. PCR duplicates were removed, and unique molecules were counted per gene and per cell using the UMI-tools function *count* (Smith et al., 2017). Nine pools in which less than 10% of total sequenced reads were assigned to features were excluded.

Reads from 10× Genomics Chromium single cells were demultiplexed and aligned with Cell Ranger to the GRCh38 genome with Ensembl transcriptome annotation using default parameters. Barcode filtering was performed with the R package DropletUtils using a threshold of >100 UMIs per barcode (Griffiths et al., 2018).

Downstream Analysis

Samples were sequenced with a median of 32 million total reads, 25 million uniquely mapped reads, and 20 million exonic reads. The sequencing depth fulfilled the ENCODE Consortium guidelines for RNA sequencing experiments with the aim to investigate the similarity between transcriptional profiles of polyA+ samples (The ENCODE Consortium, 2016). A data-adaptive flag method (George and Chang, 2014) was applied to remove lowly expressed genes. Only genes with an expression level higher than three counts per million (CPM) in at least two samples were included in the analysis. After both gene-filtering steps, the average library size was 3.8 M counts (standard deviation ±2.2 M) for downstream analysis. Counts per million (CPM) were calculated as (counts gene *i*/sample library size) × 10^6. For plotting gene expression in boxplots and heat maps $\log_2$(CPM + 1) was used. For **Figure 1B**, cell type markers from three independent data sets (Lake et al., 2016; Galatro et al., 2017a; Zhong et al., 2018) were combined, and the top 25 most abundant genes were plotted. Principal component analysis was computed on rlog transformed counts of the top 500 most variable genes using the *prcomp* function. We applied upper quartile normalization to adjust for library size with *calcNormFactors* function of edgeR (version 3.28.1; Robinson et al., 2010). For the design matrix of the within-subject comparison of the brain region, we used the factors "Brain Region" and "Donor." For the between-subject comparison between the sexes, we included "Sex" while controlling for "Age." For the between-subject comparison of donor conditions, we used the factor "Donor Group" (CTR, CTR+, AD) while controlling for variables "Age" and "Sex." The brain regions (LPS and GFS) were analyzed separately for between-subject comparisons. Differences between groups were tested with likelihood ratio tests as implemented in edgeR, resulting in FDR values. For a subset of significantly altered genes, we observed a large absolute increase in predictive log fold changes (logFC) computed by edgeR compared to regular log fold changes computed by subtracting average $\log_2$CPMs between groups. We opted to report the most conservative of the two, in this case the regular logFC. Thresholds were set at FDR<0.05 and abs(logFC)>1 to define differentially expressed genes.

For bc-Smart-seq2 single cells, approximately 25% of the cells were filtered out during preprocessing. To remove empty cells while respecting variation across donors, we set a threshold for each donor individually, removing cells with library sizes exceeding median of log(total counts) ±3 median absolute

deviation (MAD). In addition, cells with more than 3,000 unique genes and were considered doublets (genes per cell median 520; MAD ± 276) and were excluded. Cells with >10% mitochondrial transcripts were excluded. Genes not detected in at least three cells were removed. Downstream analysis started with 14 donors and 9,764 cells for clustering analysis. After filtering, we detected a median of 13,441 UMIs and median 513 unique genes per cell. We clustered a median of 714 cells per donor for bc-Smart-seq2 data. Raw counts were normalized by total expression per cell, scaled by 10,000, and log-transformed with the CRAN package Seurat (version 3.1.5; Butler et al., 2018). We used the mean variability method to select highly variable genes (HVGs). Briefly, this method identifies variable genes while controlling for the strong relation between gene variability and gene average expression. We allowed lowly expressed genes in the highly variable gene list, since some disease-associated genes (e.g., *TREM2, TYROBP, CTSD*) are biologically relevant but also lowly expressed. These extra ∼600 lowly expressed HVGs did not change clustering results and were included in the final clustering analysis. The number of detected genes, ribosomal, and mitochondrial content per cell were regressed out as they were considered unwanted sources of variation. In addition, smaller technical variations due to sequencing superpool or i7 sample index were regressed out. We used the first 15 principal components for PCA-Louvain clustering as implemented by Seurat (version 3.1.4). Cluster resolution was set at 0.5 since seven clusters was the most stable cluster number when considering resolutions from 0.1 to 2.0. Resolutions above 0.5 were investigated and did not give AD-associated subclusters. Cluster-enriched genes were identified using logistic regression as implemented in Seurat's *FindAllMarkers* function with default thresholds and only.pos = TRUE. Gene ontology enrichment (GO) for cluster-enriched genes was computed against the human genome as background ("org.Hs.eg.db" version 3.10.0) using ClusterProfiler (version 3.14.3; Yu et al., 2012) with *p*-value cutoff of 0.01 and q-value cutoff of 0.05.

10× Genomics Chromium single cells were analyzed for each donor individually. Low-quality cells with >10% mitochondrial gene (MT) content were removed in donor 2018-135. Donor 2019-010 had very high cell quality, so a >5% MT threshold was applied. Duplicate cells were filtered by setting an upper UMI threshold that was based on the multiplet rate as mentioned in the 10× Genomics user guide. Genes not detected in at least three cells were removed. We analyzed 3079 single cells for MCI donor 2019-010 and 2,881 single cells for AD donor 2018-135. We regressed out total UMI count, ribosomal, and mitochondrial content per cell. The first 20 principal components were used for PCA-Louvain clustering. Each donor was analyzed individually. To gain sufficient detail to detect small subpopulations within one donor, the cluster resolution was set at 0.6 for each donor. Cluster-enriched genes were identified using logistic regression implemented in Seurat's *FindAllMarkers* function with default thresholds and only.pos = TRUE.

Gene Set Analysis

Raw counts were normalized by total expression per cell, scaled by 10,000, and log transformed. The DAM gene set used here consists of the top 500 most significantly increased mouse genes between *microglia3* and *microglia1* from Keren-Shaul et al. (2017) subsetting to genes expressed and detectable in human single microglia. The neurodegeneration-related gene set consists of the 126 human genes from Friedman et al. (2018), reported in Data S4 as myeloid activation "neurodegeneration-related." For the single-nucleus gene set, 77 cluster marker genes from *microglia1* cluster reported by Mathys et al. (2019) were used. Gene set score was defined as average expression of genes in a set per cell. Next, the mean gene set score in any cluster was calculated and compared to the mean of all other clusters. To compare gene set cluster means we used linear regression with gene set score as dependent variable and independent variables cell library size (*z*-transformed), number of detected genes per cell (z-transformed), donor, and the cluster number as categorical variable. *P*-values were adjusted with a Bonferroni correction. Visualizations were made with the R package "ggplot2."

RESULTS

Isolation of Pure Microglia From Acute Postmortem Brain Tissue

To investigate transcriptomic changes in microglia during AD, bulk and single-cell RNA sequencing (scRNAseq) were performed. Postmortem tissue samples of the superior parietal lobe (LPS) and superior frontal gyrus (GFS) were obtained from 27 donors (**Supplementary Tables S1**, **S2**). The samples were classified into three experimental groups based on a clinical diagnostic report provided by the Netherlands Brain Bank/NeuroBiobank Born-Bunge and immunohistochemical analysis of Aβ and hyperphosphorylated tau (PHF-tau): CTR (no dementia, absence of Aβ plaques and PHF-tau, $n = 6$), CTR with plaques (CTR+, no dementia, presence of Aβ plaques and/or PHF-tau, $n = 9$), and AD (dementia, AD diagnosis, presence of Aβ plaques and/or PHF-tau, $n = 11$). One donor diagnosed with mild cognitive impairment (MCI) and presence of Aβ and PHF-tau plaques was included as well. Representative images of immunohistochemical Aβ and PHF-tau stainings of donor CNS tissues are shown in **Supplementary Figure S1**. The stratification of CTR and CTR+ donors ensured that the CTR group was free of undiagnosed AD donors. Microglia were isolated from mechanically dissociated tissue using fluorescence-activated cell sorting (FACS) of single, viable CD11B and CD45 positive cells. Twenty-five microglia samples (13 LPS and 12 GFS) from 17 donors were sequenced as bulk samples, and 14 LPS samples from 14 donors were single-cell sequenced (bc-Smart-seq2 and 10× Genomics; **Figure 1A**). Four donors (1 CTR, 3 CTR+) were included in both single-cell and bulk cohorts. A pure microglia population was obtained based on the expression of known microglia marker genes and the absence of expression of genes associated with other CNS cell types (**Figure 1B**). Cell type–specific genes were selected based on previously published gene expression profiles of adult human microglia (Galatro et al., 2017a), early human prefrontal cortex cell types (Zhong et al., 2018), and human CNS nuclei (Lake et al., 2016).

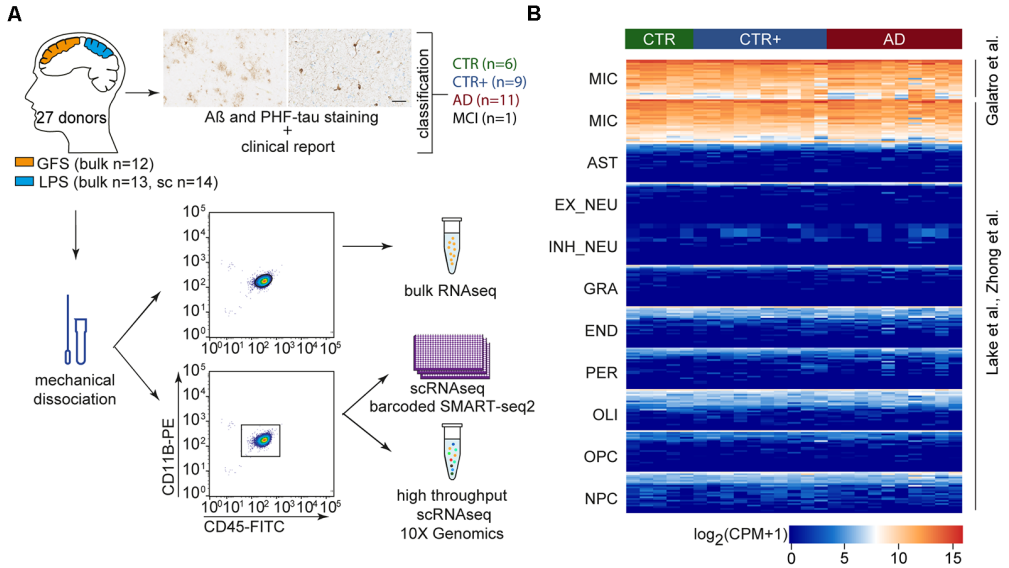

FIGURE 1 | Microglia gene expression profiling of four groups of donors from acute postmortem human brain tissue. **(A)** Tissue samples from GFS and LPS were classified into four experimental groups (CTR, CTR+, AD, MCI) based on Aβ and PHF-tau immunohistological stainings and the clinical report of the donor (scale bar = 50 μm). Microglia were mechanically isolated and collected by CD11B+CD45+ -based FACS sorting. Sorted microglia were used for bulk or single-cell sequencing (barcoded Smartseq2 and 10× Genomics sequencing techniques). **(B)** Heat map depicting $\log_2$ CPM expression of cell type-specific markers in bulk-sorted microglia, as previously published in different data sets (Lake et al., 2016; Galatro et al., 2017a; Zhong et al., 2018). Abbreviations: AD, clinically diagnosed Alzheimer's Disease; AST, astrocytes; Aβ, amyloid beta; CPM, counts per million; CTR, Control; CTR+, Control with Aβ plaques and/or hyperphosphorylated tau; END, endothelial cells; EX_NEU, excitatory neurons; GFS, superior frontal gyrus; GRA, granulocytes; IN_NEU, inhibitory neurons; LPS, superior parietal lobe; MCI, mild cognitive impairment; MIC, microglia; NPC, Neural Progenitor Cells; OLI, oligodendrocytes; OPC, Oligodendrocyte Precursor Cells; PER, pericytes; PHF-tau, hyperphosphorylated tau; scRNAseq, single-cell RNA sequencing.

No Differences in Bulk RNA Sequencing Profiles of Microglia Between CTR, CTR With Plaques (CTR+), and AD Donors

To investigate general transcriptional characteristics of microglia in AD, we bulk sorted and transcriptionally profiled microglia from CTR (n = 3), CTR+ (n = 7) and AD (n = 7) samples. The CTR, CTR+, and AD samples had comparable sequencing depth (**Supplementary Figures S2A–C**) and fulfilled the recommended sequencing depth of ENCODE Consortium guidelines. In addition, median RNA integrity numbers were ∼8–9, indicating high RNA quality (**Supplementary Figure S2D**). Thus, bulk gene expression profiles of microglia were likely not influenced by quality metrics, such as sequencing depth and RIN value.

Principal component analysis (PCA) revealed no clear segregation between donor groups (**Figure 2A**). Variation in the first principal component could potentially be attributed to individual gene expression differences between donors. The second principal component showed segregation of microglia samples on sex and age but not on brain region.

To further examine the effect of sex, male and female microglia samples from GFS (female n = 5, male n = 7) and LPS (female n = 6, male n = 7) were compared while accounting for the effect of age. Besides the expected expression differences of genes located on sex chromosomes, two genes in GFS and seven genes in LPS, which were localized on autosomal chromosomes, were differentially expressed in microglia from male compared to female donors. None of the differentially expressed genes located on autosomal chromosomes overlapped between the GFS and LPS (**Supplementary Table S3**). This suggests that, besides the expression of genes located on sex chromosomes, microglia gene expression profiles of males and females are similar.

Gene expression differences between microglia from frontal and parietal brain regions were assessed for eight donors, and a within-subject comparison was performed. Expression of four genes (*CST7, HBEGF*, *JAML*, *TREM1*) was increased in LPS compared to GFS, and one long noncoding RNA (*AC011451.1*) was decreased in LPS compared to GFS (**Supplementary Figure S3**, **Supplementary Table S4**). This indicates that the bulk gene expression profiles of microglia isolated from frontal (GFS) and parietal (LPS) brain regions are very similar in terms of gene expression.

To assess the effect of AD, we compared microglia from the AD group to the CTR/CTR+ group. The effect of age and sex in the AD-CTR/CTR+ comparison was accounted for, because subtle effects were visible in the PCA. LPS- and GFS-derived microglia were analyzed separately.

Microglia from the AD group were compared to the CTR group. In GFS microglia, the expression level of one gene was significantly increased (CTR n = 2, AD n = 6), but this was one finding using a small reference group (CTR n = 2). In LPS, no significant gene expression changes were detected (CTR

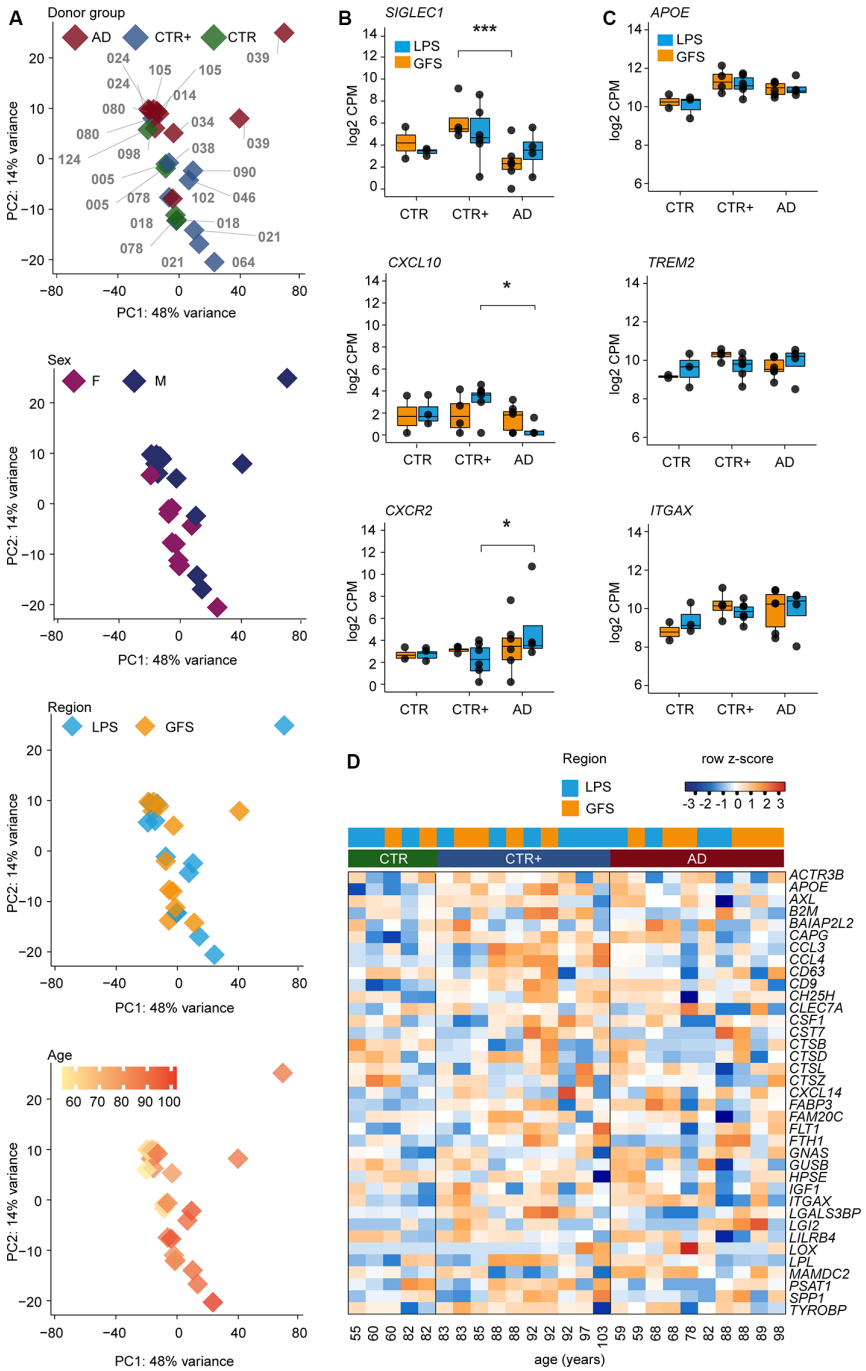

FIGURE 2 | Transcriptomic analysis of microglia populations isolated from CTR, CTR+, and AD donors. **(A)** Principal component analysis (PCA) of RNA-sequencing data from acutely isolated microglia illustrating the effect of donor (each sample is indicated with a donor label), donor groups, sex, brain region, and age. **(B)** Differentially expressed genes between AD and CTR+ donors (likelihood ratio test, *SIGLEC1* ***FDR = 0.002, *CXCL10* *FDR = 0.02 and *CXCR2* *FDR = 0.02). **(C)** Selected examples of expression levels (log_2 CPM) of disease-associated microglia genes in bulk microglia samples. **(D)** Heat map depicting expression of most abundant disease-associated microglia genes in bulk microglia samples from three donor groups in row z scores of log_2 CPM values. Donors are ordered by age (young to old) within the donor group. Abbreviations: AD, Alzheimer's Disease; CPM, counts per million; CTR, Control; CTR+, Control with Aβ plaques and/or hyperphosphorylated tau; F, female; M, male; GFS, superior frontal gyrus; LPS, superior parietal lobe.

n = 3, AD n = 4; **Supplementary Table S5**). Therefore, no gene expression differences were observed between the CTR and AD group.

Next, microglia from the AD group were compared to the CTR+ group. In GFS (CTR+ n = 4, AD n = 6), the expression level of four genes was increased, and 13 genes were decreased in

AD. For example, expression of the phagocytic marker *SIGLEC1* (Bogie et al., 2018) was decreased in AD compared to CTR+ microglia (**Figure 2B**, **Supplementary Table S5**). In LPS (CTR+ $n = 6$, AD $n = 4$), five genes were less expressed in AD compared to CTR+ microglia, including *CXCL10* (**Figure 2B**, **Supplementary Table S5**). *CXCL10* has been implicated in AD studies with contrasting results. *CXCL10* protein levels were reported to be increased in AD donors in prefrontal cortical tissue (Bradburn et al., 2018). However, *CXCL10* protein levels were increased in MCI donors but not in severe AD donors in the cerebral spinal fluid (Galimberti et al., 2006). Expression of 20 genes was increased in the LPS of AD compared to CTR+ microglia, including chemokine receptors *CXCR1* and *-2* (**Figure 2B**, **Supplementary Table S5**). Several studies claim that *CXCR2* could augment AD pathology in mouse models and that deficiency in *CXCR2* decreases amyloid-beta deposition (Xia and Hyman, 2002; Bakshi et al., 2011; Veenstra and Ransohoff, 2012; Ryu et al., 2015). All gene expression differences detected between AD and CTR+ microglia were restricted to either the GFS or the LPS brain region (**Supplementary Table S5**).

In 5xFAD mice, a subset of microglia is reported that emerges with increasing amyloid pathology. These disease-associated microglia (DAMs) progressively express a specific set of genes, associated with lipid metabolism and phagocytosis (Keren-Shaul et al., 2017). Expression levels of the most significantly increased genes in the mouse DAM cluster, including *APOE*, *TREM2*, *ITGAX*, were investigated in our bulk human microglia data set and did not differ between control- and AD-derived human microglia in both LPS and GFS regions (**Figures 2C,D**, **Supplementary Table S5**).

To summarize, although some gene expression changes were detected in CTR+ compared to AD bulk microglia, microglia transcriptomes from AD and CTR donors did not significantly differ.

Single-Cell Gene Expression Profiling Identifies Seven Subsets of Microglia but No AD-Associated Subpopulation

AD-associated gene expression changes might occur in only a small subpopulation of microglia that are in closer proximity to Aβ plaques. In bulk RNAseq, gene expression changes in such a microglial subpopulation might remain undetected as bulk RNAseq provides the average gene expression profile of all microglia in a sample. To address this possibility, we employed scRNAseq to assess AD-associated gene expression changes in individual microglia. Microglia derived from the LPS region were analyzed with a median of 714 cells per donor from four CTR, five CTR+, one donor with MCI, and four AD donors. Clustering analysis identified seven microglia subsets, indicating heterogeneity in microglia transcriptomes (**Figure 3A**). The sequencing depth and number of uniquely detected genes were variable between donors (**Supplementary Figures S4A,B**), but comparable across clusters (**Supplementary Figures S4D,E**). The percentage of mitochondrial transcripts detected were comparable across donors and clusters except for the smallest cluster 6 ($n = 29$ cells; **Supplementary Figures S4C,F**). Each donor contributed cells to most clusters, including the larger clusters 0–2 (**Figure 3B**). The absence of the formation of donor-specific clusters indicates that cluster formation was likely not influenced by donor-specific effects. The expression of cell type–specific markers across all clusters showed that all analyzed cells were microglia (*ITGAX*) without contamination of neurons (*RBFOX3*), oligodendrocytes (*MOG*), astrocytes (*GFAP*), circulating monocytes (*CCR2*), and erythrocytes (*HBA1*; **Figure 3C**).

Differential gene expression analysis between any cluster compared to all other clusters was used to identify cluster-enriched genes (**Supplementary Table S6**). The small clusters 3–6 contained relatively few cells of the total microglia population (0.3%–1.6%) and were marked by a very low number of unique cluster-enriched genes (**Supplementary Table S6**). Notably, cluster-enriched genes in the small clusters were expressed in more than 75% of the cells in the small clusters, whereas cluster-enriched genes were detected in ∼30% of the cells in the large clusters 0–2. In addition, expression levels of cluster-enriched genes were higher in the smaller clusters than in the larger clusters (**Figure 3D**, **Supplementary Table S7**). This very frequent expression of few genes with strong enrichment could have resulted in the formation of the smaller clusters 3–6. The small clusters showed a unique enrichment for *SMIM11A* and *-B* (cluster 3); *MEF2C*, *GPR89A*, and *-B* (cluster 4); *SERF1A* and *-B* (cluster 5); and *FRG1* and *FRG1CP* (cluster 6; **Figure 3D**, **Supplementary Tables S6**, **S7**). Gene ontology (GO) enrichment analysis revealed no biological annotation associated with the small clusters.

Microglia in cluster 0 were uniquely enriched in the genes *AXL, CLEC7A, CYBB* (**Figure 3D**, **Supplementary Tables S6**, **S7**). These genes were associated with a hyper-responsive inflammatory phenotype conserved in aging and neurodegenerative-related mouse models that is involved in functions, such as phagocytosis (Holtman et al., 2015). In addition, microglia in cluster 0 were uniquely enriched in cytoskeleton-related genes (*FGD2, ACTB, SRGAP2*; **Figure 3D**, **Supplementary Tables S6**, **S7**). These genes were associated with GO terms involved in locomotion, endocytosis, and filopodium assembly (**Supplementary Figure S5**, **Supplementary Table S8**). Microglia in cluster 1 uniquely expressed genes involved in transcriptional activity (*ZNF302, NEAT1*, and *ANKRD11*; **Figure 3D**, **Supplementary Tables S6**, **S7**), and the associated GO terms included RNA splicing (**Supplementary Figure S5**, **Supplementary Table S8**). Microglia in cluster 2 were uniquely enriched in genes associated with neurodegenerative diseases (*TREM2*, *GLUL*, *S100A*; Keren-Shaul et al., 2017; Krasemann et al., 2017; Cristóvaõ and Gomes, 2019) and immune activated microglia (*CD63*, *HLA* genes, *CD14*, *TSPO*; Beschorner et al., 2002; Kamphuis et al., 2016; Beckers et al., 2018) and in ribosomal genes (*RPL* genes; **Figure 3D**, **Supplementary Tables S6**, **S7**). Associated GO terms included protein targeting and active immune response (**Supplementary Figure S5**, **Supplementary Table S8**). Cells of all clusters showed higher expression of DAM genes compared to homeostatic microglia markers (**Figure 3D**, **Supplementary Table S7**).

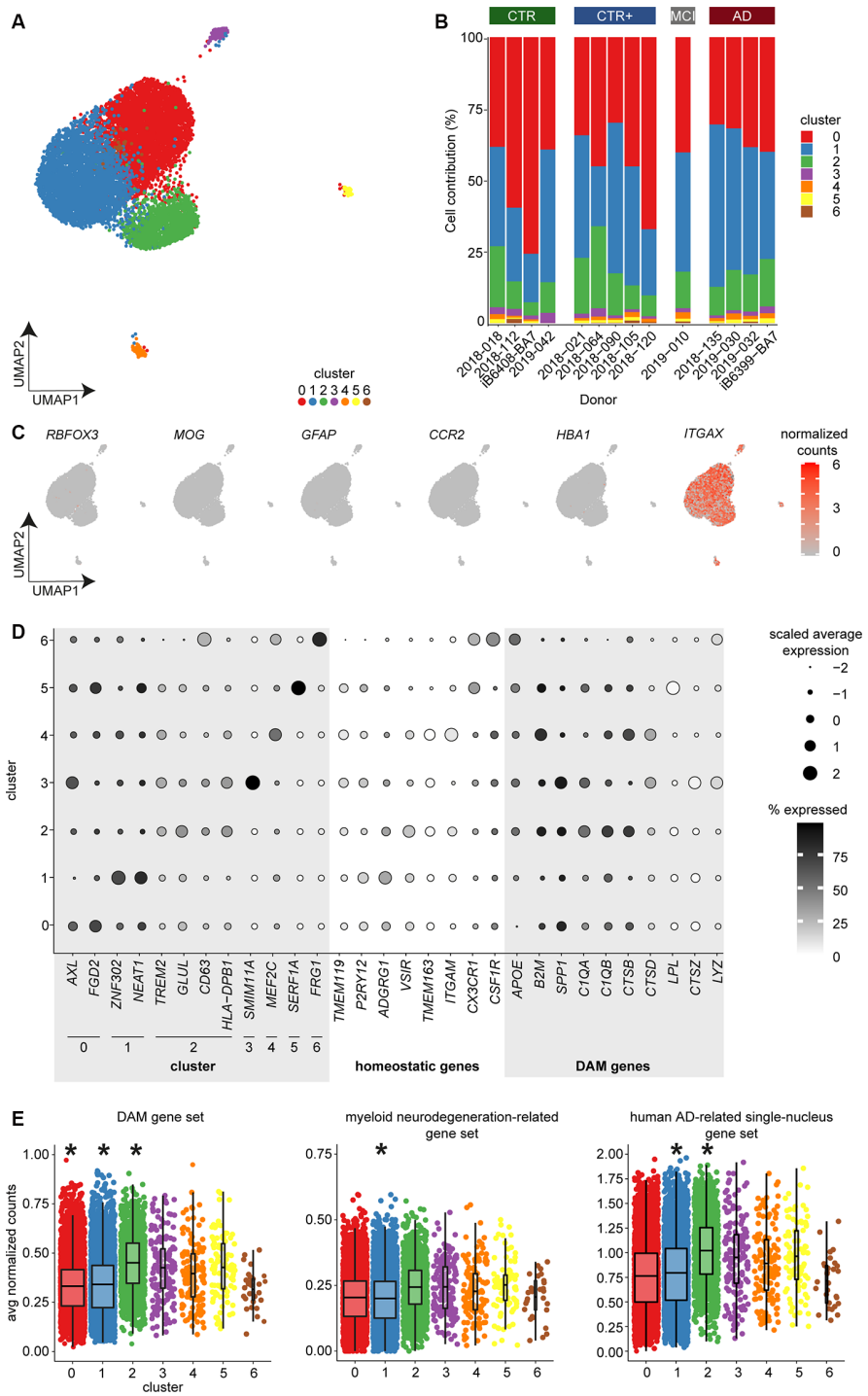

FIGURE 3 | Single-cell expression profiling of microglia identified seven subsets of microglia but no AD-associated cluster using bc-Smart-seq2. **(A)** UMAP visualization and unsupervised clustering of microglia derived from AD (n = 4), MCI (n = 1), CTR+ (n = 5), and CTR (n = 4) donors. Colors represent cluster identity. **(B)** Cluster contribution normalized to donor. **(C)** Expression of cell type–specific markers for neurons (*RBFOX3*), oligodendrocytes (*MOG*), astrocytes (*GFAP*), circulating monocytes (*CCR2*), erythrocytes (*HBA1*), and microglia (*ITGAX*). **(D)** Dot plot visualizing scaled average expression and the percentage of cells expressing the indicated genes. **(E)** Average expression of the mouse DAM (Keren-Shaul et al., 2017), myeloid neurodegeneration-related (Friedman et al., 2018), and human AD-related single-nucleus (Mathys et al., 2019) gene sets per cell across clusters (multiple linear regression with Bonferroni correction, *indicate p-value < 0.001). Horizontal lines in the boxplots represent the mean; the lower and upper hinges represent the 25th and 75th percentiles. Abbreviations: AD, Alzheimer's Disease; avg, average; CPM, counts per million; CTR, Control; CTR+, Control with Aβ plaques and/or hyperphosphorylated tau; DAM, disease-associated microglia; MCI, mild cognitive impairment; UMAP, uniform manifold approximation and projection.

To determine if expression of the DAM-associated gene set was altered in our human microglia clusters, average expression of the DAM gene set was calculated per cell. Mean expression per cluster was compared to all other clusters. The mean expression level of the DAM gene set was significantly reduced in clusters 0 and 1 and significantly increased in cluster 2 (**Figure 3E**, **Supplementary Table S9**). To validate these observations, the same analysis was performed for two other gene sets. The first was obtained from gene expression modules in myeloid cells from a comparison between AD tissue and multiple neurodegeneration-related mouse models (Friedman et al., 2018) and the second from a study investigating single-nucleus transcriptomes in the prefrontal cortex of human AD donors (Mathys et al., 2019). Similar to the results of the DAM gene set, cells in cluster 1 showed a significant decrease in mean gene expression of the myeloid neurodegeneration-related and human AD-related single-nucleus gene sets (**Figure 3E**, **Supplementary Table S9**). Cluster 2 showed a significant increase in mean gene expression of the DAM gene set and the human AD-related single-nucleus gene set (**Figure 3E**, **Supplementary Table S9**). Although statistically significant, mean expression level changes are likely too small to be biologically relevant. Together with the identified cluster-enriched genes and associated GO terms, cluster 2 might have increased immune activated gene expression. However, cluster 2 was not enriched in AD-donor derived microglia (**Figure 3B**), indicating that the immune activated phenotype of this microglial subpopulation is not unique to AD pathology.

Taken together, scRNAseq analysis of approximately 10,000 microglia from 14 donors identified subtle microglial heterogeneity but no AD-specific microglia subpopulation.

Microglia Diversity but No DAM-Like Cluster in an Individual MCI and AD Donor With High Microglial Cell Numbers

The proportion of microglia associated with AD pathology in the human brain might be relatively low and could potentially be missed by the more limited cell numbers analyzed by bc-Smart-seq2 expression profiling. Therefore, ∼3,000 microglia per donor from two donors were analyzed using scRNAseq with the 10× Genomics platform, leading to a considerably higher cell number compared to the 714 microglia per donor analyzed with bc-Smart-seq2. We hypothesized that different microglial subpopulations, such as plaque-associated and homeostatic microglia populations, are present in the AD brain and that analysis of a higher number of microglia from the same donor would allow for the identification of relatively small subpopulations. To prevent donor-associated variables (sex, age, postmortem delay, tissue quality, etc.) affecting microglia clustering, each donor was analyzed individually: 2,881 cells were analyzed from donor 1: AD, female, 81 years, LPS tissue with high Aβ burden, and modest but visible PHF-tau protein (donor #2018-135, **Supplementary Table S2**), and 3,079 single cells were analyzed from donor 2: MCI donor, female, 77 years old, LPS tissue with moderate Aβ pathology, and high levels of PHF-tau deposits (donor #2019-010, **Supplementary Table S2**).

In both donors, three microglial clusters were identified (**Figures 4A,E**, **Supplementary Tables S10**, **S11**). To identify whether cells in any of these clusters were enriched in the expression of genes associated with neurodegenerative diseases, we averaged gene expression of the mouse DAM (Keren-Shaul et al., 2017), the myeloid neurodegeneration-related (Friedman et al., 2018), and the human AD-related single-nucleus (Mathys et al., 2019) gene sets per cell. Next, mean expression per cluster was compared to all other clusters (**Figures 4B–D,F–H**, **Supplementary Table S9**). A significant increase in mean gene expression of the human AD-associated single-nucleus gene set was observed in cluster 1 microglia of the AD (**Figure 4D**) but not the MCI donor (**Figure 4H**). To summarize, although a high number of microglia was analyzed per donor, none of the three clusters per donor could consistently be related to known microglia gene expression changes associated with AD.

DISCUSSION

In this study, we aimed to identify transcriptomic changes in human microglia at the end stage of AD by applying both bulk and scRNAseq of microglia isolated from acute postmortem CNS tissue. In parietal and frontal cortex, we analyzed microglia as bulk samples allowing the most sensitive detection of small gene expression changes. Here, transcriptomic differences between AD and CTR were not detected but were present between AD and CTR+. Possibly, the difference between CTR vs. AD could not be detected in our data set due to limited sample numbers and/or relatively small changes. Alternatively, CTR+ donors with amyloid-beta plaques and tau pathology have different transcriptomic changes in microglia than CTR donors with respect to AD. Disease-associated genes identified previously in AD mouse models were not enriched in bulk human AD microglia. Next, single-cell sequencing analysis was applied to detect microglial subtypes that possibly consist of low cell numbers and might be undetected in the average transcriptome obtained by bulk RNAseq. In single microglia transcriptomes, the relative contribution to microglia clusters did not differ between AD and control donors, when using the bc-Smart-seq2 protocol. In addition, expression of genes related to neurodegenerative disease from previous studies (Keren-Shaul et al., 2017; Friedman et al., 2018; Mathys et al., 2019) were not altered with meaningful effect sizes in any cluster.

The neurodegenerative disease-associated microglial subtype originally described by Krasemann et al. (2017) and similarly described by Keren-Shaul et al. (2017) represented a relatively small fraction of the total microglia population. To rule out that the lack of a cluster associated with AD pathology in our bc-Smart-seq2 data was due to the analysis of low cell numbers, a higher number of microglia from two donors were single-cell sequenced using the 10× Genomics platform. Clustering was performed per donor to avoid donor variation that might mask such a potential cluster. None of the clusters identified with 10× Genomics scRNAseq were consistently enriched in mean expression of gene sets related to neurodegenerative diseases. In

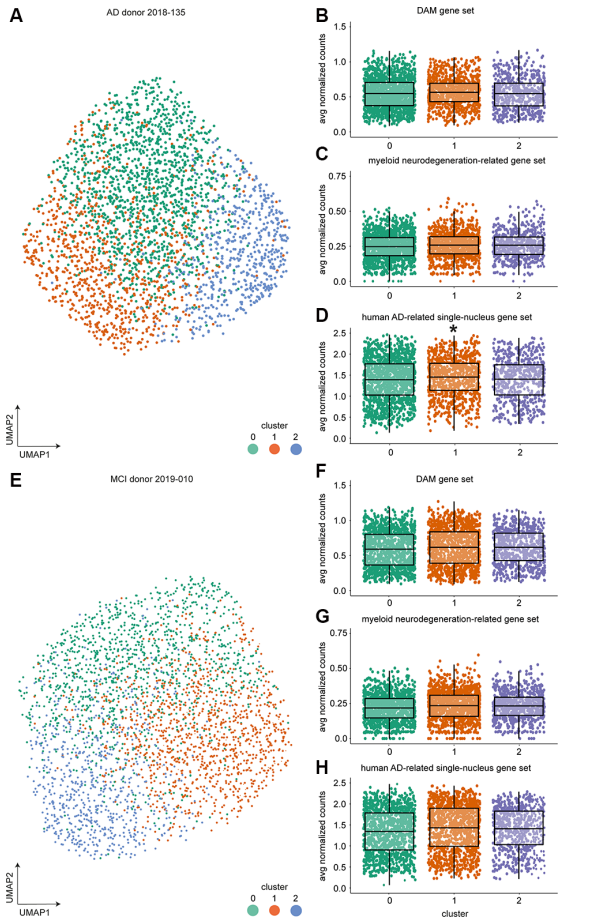

FIGURE 4 | Single-cell expression profiling of microglia from individual donors identified three clusters but no DAM-like cluster using 10× Genomics. **(A)** UMAP visualization and unsupervised clustering of microglia from AD donor 2018-135. **(B–D)** Average expression of the mouse DAM **(B)**, myeloid neurodegeneration-related **(C)**, and human AD-related single-nucleus **(D)** gene set expression per cell across clusters for AD donor 2018-135 (multiple linear regression with Bonferroni correction, *indicate p-value < 0.001). **(E)** UMAP visualization and unsupervised clustering of MCI donor 2019-010. **(F–H)** Average expression of the mouse DAM **(F)**, myeloid neurodegeneration-related **(G)** and human AD-related single-nucleus **(H)** gene set expression per cell across clusters for MCI donor 2019-010. Horizontal lines in the boxplots represent the mean; the lower and upper hinges represent the 25th and 75th percentiles. Abbreviations: AD, Alzheimer's Disease; avg, average; CPM, counts per million; CTR, Control; CTR+, Control with Aβ plaques and/or hyperphosphorylated tau; DAM, disease-associated microglia; MCI, mild cognitive impairment; UMAP, uniform manifold approximation and projection.

conclusion, a DAM-like microglial subtype was absent in AD donors profiling relatively high cell numbers.

When comparing the clustering results of the 10× Genomics and bc-Smart-seq2 scRNAseq techniques, differences were observed. Clusters 0–2 in the bc-Smart-seq2 data contain the vast majority of microglia and are most similar to the three clusters identified per donor in the 10× Genomics data set. The smaller clusters in the bc-Smart-seq2 data (4–8) were not identified in the microglia profiled by 10× Genomics and are possibly associated with the plate-based protocol as we observed similar small clusters in a different bc-Smart-seq2 data set from our group (unpublished results).

There are multiple possible explanations for the absence of AD-associated changes in bulk and single-cell microglia acutely isolated from postmortem human brain tissue. Limitations of this study are the relatively small sample sizes, especially in the CTR group. In addition, interindividual differences between donors might mask gene expression differences in the bc-Smart-seq2 study. The presence of comorbidity, medication, and varying postmortem delay (time from death to autopsies) might interfere with AD-specific effects on the microglial transcriptome. However, these factors are difficult to avoid in human postmortem data. Another explanation for the lack of AD-related transcripts in bulk and single-cell microglia could be that the relevant microglia associated with AD plaques are more vulnerable to the isolation procedure. This would imply that, using conventional isolation and sorting of microglia would enrich a population of cells that are not related to AD pathology. Streit and colleagues first introduced the concept of dystrophic microglia that occur around neuronal structures positive for hyperphosphorylated tau protein (Streit et al., 2004, 2009) and were later found to also occur around Aβ plaques (Streit et al., 2018). Possibly, dystrophic microglia and microglia embedded inside the Aβ plaque are more vulnerable and, therefore, preferentially lost during FACS gating of live, single cells from human brain tissue.

When comparing AD mouse models to human AD, the distinction between parenchymal and plaque-associated microglia might be more pronounced for amyloid mouse models than for human end-stage AD samples. In transgenic amyloid mouse models, especially 5xFAD mice, Aβ is overexpressed in a nonphysiological manner. This results in very fast Aβ plaque formation and, at end stages, a much higher plaque burden in AD mouse models than in the human AD brain (Drummond and Wisniewski, 2017; Liu et al., 2017). Transgenic mouse models lack regional brain atrophy and show less widespread neurodegeneration than human AD cases (Drummond and Wisniewski, 2017). Possibly, compared to plaque-associated microglia, parenchymal microglia are less affected in amyloid mouse models than in human AD brain tissue. Furthermore, single human microglia studies will most likely require much larger cell numbers to capture sufficient plaque-associated human microglia than studies using AD mouse models. Additionally, interindividual variation will influence human microglia transcriptomes more than mouse microglia transcriptomes. Together, these factors might lead to a more pronounced change between parenchymal and plaque-associated microglia in amyloid mouse models than in human AD samples.

DAMs were not only associated with neurodegenerative diseases, but also with natural aging (Keren-Shaul et al., 2017; Krasemann et al., 2017). This was confirmed in a study identifying an AppNL-G-F-associated microglia subpopulation, activated response microglia, which overlap with DAMs (Sala Frigerio et al., 2019). Activated response microglia already comprised a few percent of microglia in the brains of wild-type mice at a young age and evolve naturally with aging (Sala Frigerio et al., 2019). Furthermore, a consensus gene

expression network module co-occurring both during aging and neurodegeneration was previously described (Holtman et al., 2015). The described module included DAM signature genes, such as *Csf1*, *Spp1*, *Apoe*, *Axl*, *B2m*, *Ctsz*, *Cd9*, *Cstb*, and *Cst7*. Biological annotation of module-specific genes included phagosome and lysosomal pathways (Holtman et al., 2015), functions associated with DAMs (Keren-Shaul et al., 2017). Taken together, this suggests the presence of DAM-like microglia could be expected, albeit at low levels, in aged controls as well as AD donor-derived microglia.

It is still an unresolved question whether a subpopulation resembling DAMs exist among human microglia. Three other studies previously addressed this question. Olah et al. (2018) observed 23 clusters of human microglia, where five out of 23 clusters were enriched for DAM signature genes. Three of the 15 donors suffered from AD pathology, making it difficult to connect their microglia subpopulations with AD-induced gene expression changes. Srinivasan et al. (2019) investigated frozen myeloid cells from AD brain tissue and observed that, from the 100 DAM genes, only expression of *APOE* did change in myeloid cells from AD donors compared to controls. Mathys et al. (2019) used single-nuclei sequencing and subclustered ∼2,400 microglia of 48 donors into four subpopulations. They highlighted the *microglia1* cluster as AD-pathology-associated human microglia. From the 257 DAM genes investigated by Mathys et al. (2019), 28 were overlapping with marker genes for the *microglia1* cluster, and 16 of these 28 overlapping marker genes were ribosomal genes. Although this reveals a starting point, a larger-scale investigation of microglia nuclei is needed to identify AD-associated microglia subpopulations in humans.

Single nucleus gene expression faithfully recapitulates cellular gene expression profiles (Lake et al., 2017; Gerrits et al., 2020). Therefore, single-nucleus sequencing offers an alternative to scRNAseq that is especially useful in tissues from which recovering intact cells is difficult (Grindberg et al., 2013; Lake et al., 2017; Gerrits et al., 2020). An important advantage of single-nucleus sequencing is the possibility to use frozen samples from brain banks containing large, well-characterized donor cohorts. For example, a donor cohort to differentiate the effects of natural aging and AD pathology would be possible by comparing aged-matched (young) control donors to early-onset familial AD cases using frozen samples from brain banks. In the future, single-nucleus sequencing of microglia, including tissues of early, presymptomatic stages of AD will be most promising to potentially identify microglia biomarkers for AD.

DATA AVAILABILITY STATEMENT

The data sets generated for this study can be found in the Gene Expression Omnibus, GSE146639.

ETHICS STATEMENT

The studies involving human participants were reviewed and approved by Ethics committee of the VU University Medical Center (VUMC, Amsterdam, The Netherlands). The patients/participants provided their written informed consent to participate in this study.

AUTHOR CONTRIBUTIONS

EB, BE, EH, JM, and SK were responsible for the overall conception of the project and provided supervision. QJ, AA, and LK conducted the experimental work and/or analyzed the data, prepared the figures, and wrote the manuscript. EG and RD assisted with sample processing, data discussion, and performed the immunohistochemistry. NB, AM, MD, MW, AW, SX, KB, TM, JM, and RD assisted with maintenance of availability of reagents, sample processing, data discussion, optimization issues, and/or data analysis. All authors contributed to the article and approved the submitted version.

FUNDING

MW, SX, AW, TM, and KB are employed by AbbVie, Inc., which has subsidized the study. BE acquired funding from the foundation Alzheimer Nederland. EH, EB, and BE received funding from ZonMW-Memorabel. AA and EG are funded by Abbvie. AA was supported by the Jan Kornelis de Cock-Hadders foundation. QJ was funded by the Li Ka-shing Foundation at Shantou University Medical College, China, the Abel Tasman Talent Program, University Medical Center Groningen/University of Groningen, The Netherlands, and the Graduate School of Medical Sciences (GSMS), University of Groningen, The Netherlands. LK holds a scholarship from the GSMS, University of Groningen, The Netherlands.

ACKNOWLEDGMENTS

We thank the Netherlands Brain Bank and the NeuroBiobank of the Institute Born-Bunge, Belgium. We thank M. Borggrewe, J. Villamil Ortiz, T. Oshima, M. Wijering, S. Eskandar, R. van der Pijl, E. Wesseling, C. Grit, and C. B. Haas for assistance and/or maintenance of sample processing and bulk and/or single-cell isolations. We are grateful to W. Abdulahad, G. Mesander, T. Bijma, and J. Teunis from The Central Flowcytometry Unit of the University of Groningen, University Medical Center Groningen (UMCG), for technical assistance on FACS sorting. We thank P. van der Vlies, D. Brandenburg, N. Festen, and W. Uniken Venema for their assistance setting up the bc-SmartSeq2 protocol. We thank M. Meijer for ICT-related support. We appreciate sequencing-related advice provided by D. Spierings, K. Hoekstra-Wakker, J. Beenen, and N. Halsema.

SUPPLEMENTARY MATERIAL

The Supplementary Material for this article can be found online at: https://www.frontiersin.org/articles/10.3389/fnmol.2020.00134/full#supplementary-material.

FIGURE S1 | Donor classification based on immunohistochemistry. Representative immunohistochemical images of Aß, PHF-tau, and IBA1 staining of consecutive sections from the LPS of the three donor groups (CTR, CTR+, AD). Scale bar = 300 μm, scale bar inset = 50 μm. Abbreviations: AD, clinically

diagnosed Alzheimer's Disease with Aβ plaques and/or hyperphosphorylated tau; CTR, Control; CTR+, Control with Aβ plaques and/or hyperphosphorylated tau; LPS, superior parietal lobe.

FIGURE S2 | Quality metrics of bulk RNAseq data. **(A–D)** Total reads **(A)**, uniquely mapped reads **(B)**, exonic reads **(C)**, RNA Integrity (RIN) values **(D)** are depicted for all microglia samples (CTR, CTR+, AD) of both brain regions (GFS, LPS). Abbreviations: AD, clinically diagnosed Alzheimer's Disease with Aβ plaques and/or hyperphosphorylated tau; CTR, Control; CTR+, Control with Aβ plaques and/or hyperphosphorylated tau; GFS, superior frontal gyrus; LPS, superior parietal lobe; M, million; RIN, RNA integrity value.

FIGURE S3 | Differentially expressed genes between parietal (LPS) and frontal (GFS) brain regions. Selected examples of expression levels of genes differentially expressed between LPS and GFS shown in $\log_2$ CPM (likelihood ratio test; *JAML* ***FDR < 0.001, *CST7* ***FDR < 0.001 and *TREM1* ***FDR < 0.001, *AC011451.1* * FDR = 0.04). Abbreviations: CPM, counts per million; GFS, superior frontal gyrus; LPS, superior parietal lobe.

FIGURE S4 | Bc-Smart-seq2 single-cell RNA sequencing quality of donors and clusters. **(A–F)** Boxplots displaying the number of detected UMIs, unique genes and percentage of mitochondrial transcripts in single cells per donor **(A,B,D)** and per cluster **(D–F)**. Abbreviations: AD, clinically diagnosed Alzheimer's Disease with Aβ plaques and/or hyperphosphorylated tau; CTR, Control; CTR+, Control with Aβ plaques and/or hyperphosphorylated tau, UMI; unique molecular identifier.

FIGURE S5 | Biological annotation of marker genes for each cluster. Dot plots displaying the top 10 gene ontology terms per cluster identified in bc-Smart-seq2 single-cell data. Gene ontology terms were ordered on gene count. Color indicates the adjusted *p*-value. No GO terms were significantly associated with genes of clusters 5 and 6.

TABLE S1 | Detailed donor information of bulk sequenced samples.

TABLE S2 | Detailed donor information of single-cell sequenced samples.

TABLE S3 | Differential gene expression analysis of male vs. female bulk microglia samples.

TABLE S4 | Differential gene expression analysis of LPS vs. GFS bulk microglia samples (related to **Figure S3**).

TABLE S5 | Differential gene expression analysis of CTR+/CTR vs. AD bulk microglia samples (related to **Figure 2B**).

TABLE S6 | Cluster-enriched genes of the identified seven clusters with bc-Smart-seq2 single-cell RNA sequencing.

TABLE S7 | Average scaled expression for and percentage of cells expressing selected genes in clusters identified with bc-Smart-seq2 single-cell RNA sequencing (related to **Figure 3D**).

TABLE S8 | GO terms associated with the cluster-enriched genes of bc-Smart-seq2 single-cell RNA sequencing (related to **Supplementary Figure S5**).

TABLE S9 | Statistics of the average gene set expression changes in single-cell clusters (related to **Figures 3E**, **4B–D,F–H**).

TABLE S10 | Cluster-enriched genes of the identified three clusters of donor 2018-135 with 10× Genomics single-cell RNA sequencing.

TABLE S11 | Cluster-enriched genes of the identified three clusters of donor 2019-10 with 10× Genomics single-cell RNA sequencing.

REFERENCES

Bakshi, P., Margenthaler, E., Reed, J., Crawford, F., and Mullan, M. (2011). Depletion of CXCR2 inhibits γ-secretase activity and amyloid-β production in a murine model of Alzheimer's disease. *Cytokine* 53, 163–169. doi: 10.1016/j.cyto.2010.10.008

Beckers, L., Ory, D., Geric, I., Declercq, L., Koole, M., Kassiou, M., et al. (2018). Increased expression of translocator protein (TSPO) marks pro-inflammatory microglia but does not predict neurodegeneration. *Mol. Imaging Biol.* 20, 94–102. doi; 10.1007/s11307-017-1099-1

Beschorner, R., Nguyen, T. D., Gözalan, F., Pedal, I., Mattern, R., Schluesener, H. J., et al. (2002). CD14 expression by activated parenchymal microglia/macrophages and infiltrating monocytes following human traumatic brain injury. *Acta Neuropathol.* 103, 541–549. doi: 10.1007/s00401-001-0503-7

Bogie, J. F. J., Boelen, E., Louagie, E., Delputte, P., Elewaut, D., van Horssen, J., et al. (2018). CD169 is a marker for highly pathogenic phagocytes in multiple sclerosis. *Mult. Scler. J.* 24, 290–300. doi: 10.1177/1352458517698759

Bradburn, S., McPhee, J., Bagley, L., Carroll, M., Slevin, M., Al-Shanti, N., et al. (2018). Dysregulation of C-X-C motif ligand 10 during aging and association with cognitive performance. *Neurobiol. Aging* 63, 54–64. doi: 10.1016/j.neurobiolaging.2017.11.009

Butler, A., Hoffman, P., Smibert, P., Papalexi, E., and Satija, R. (2018). Integrating single-cell transcriptomic data across different conditions, technologies and species. *Nat. Biotechnol.* 36, 411–420. doi: 10.1038/nbt.4096

Cristóvaõ, J. S., and Gomes, C. M. (2019). S100 proteins in Alzheimer's disease. *Front. Neurosci.* 13:463. doi: 10.3389/fnins.2019.00463

Drummond, E., and Wisniewski, T. (2017). Alzheimer's disease: experimental models and reality. *Acta Neuropathol.* 133, 155–175. doi: 10.1007/s00401-016-1662-x

Friedman, B. A., Srinivasan, K., Ayalon, G., Meilandt, W. J., Lin, H., Huntley, M. A., et al. (2018). Diverse brain myeloid expression profiles reveal distinct microglial activation states and aspects of Alzheimer's disease not evident in mouse models. *Cell Rep.* 22, 832–847. doi: 10.1016/j.celrep.2017.12.066

Galatro, T. F., Holtman, I. R., Lerario, A. M., Vainchtein, I. D., Brouwer, N., Sola, P. R., et al. (2017a). Transcriptomic analysis of purified human cortical microglia reveals age-associated changes. *Nat. Neurosci.* 20, 1162–1171. doi: 10.1038/nn.4597

Galatro, T. F., Vainchtein, I. D., Brouwer, N., Boddeke, E. W. G. M., and Eggen, B. J. L. (2017b). Isolation of microglia and immune infiltrates from mouse and primate central nervous system. *Methods Mol. Biol.* 1559, 333–342. doi: 10.1007/978-1-4939-6786-5_23

Galimberti, D., Schoonenboom, N., Scheltens, P., Fenoglio, C., Bouwman, F., Venturelli, E., et al. (2006). Intrathecal chemokine synthesis in mild cognitive impairment and Alzheimer disease. *Arch Neurol.* 63, 538–543. doi: 10.1001/archneur.63.4.538

George, N. I., and Chang, C. W. (2014). DAFS: a data-adaptive flag method for RNA-sequencing data to differentiate genes with low and high expression. *BMC Bioinformatics* 15:92. doi: 10.1186/1471-2105-15-92

Gerrits, E., Heng, Y., Boddeke, H. W. G. M., and Eggen, B. J. L. (2020). Transcriptional profiling of microglia; current state of the art and future perspectives. *Glia* 68, 740–755. doi: 10.1002/glia.23767

Griffiths, J. A., Richard, A. C., Bach, K., Lun, A. T. L., and Marioni, J. C. (2018). Detection and removal of barcode swapping in single-cell RNA-seq data. *Nat. Commun.* 9:2667. doi: 10.1038/s41467-018-05083-x

Grindberg, R. V., Yee-Greenbaum, J. L., McConnell, M. J., Novotny, M., O'Shaughnessy, A. L., Lambert, G. M., et al. (2013). RNA-sequencing from single nuclei. *Proc. Natl. Acad. Sci. U S A* 110, 19802–19807. doi: 10.1073/pnas.1319700110

Holtman, I. R., Raj, D. D., Miller, J. A., Schaafsma, W., Yin, Z., Brouwer, N., et al. (2015). Induction of a common microglia gene expression signature by aging and neurodegenerative conditions: a co-expression meta-analysis. *Acta Neuropathol. Commun.* 3:31. doi: 10.1186/s40478-015-0203-5

Hyman, B. T., and Trojanowski, J. Q. (1997). Editorial on consensus recommendations for the postmortem diagnosis of Alzheimer disease from the National Institute on Aging and the Reagan Institute Working Group on diagnostic criteria for the neuropathological assessment of Alzheimer disease. *J. Neuropathol. Exp. Neurol.* 56, 1095–1097. doi: 10.1097/00005072-199710000-00002

Kamphuis, W., Kooijman, L., Schetters, S., Orre, M., and Hol, E. M. (2016). Transcriptional profiling of CD11c-positive microglia accumulating around

amyloid plaques in a mouse model for Alzheimer's disease. *Biochim. Biophys. Acta* 1862, 1847–1860. doi: 10.1016/j.bbadis.2016.07.007

Keren-Shaul, H., Spinrad, A., Weiner, A., Matcovitch-Natan, O., Dvir-Szternfeld, R., Ulland, T. K., et al. (2017). A unique microglia type associated with restricting development of Alzheimer's disease. *Cell* 169, 1276.e17–1290.e17. doi: 10.1016/j.cell.2017.05.018

Kim, D., Langmead, B., and Salzberg, S. L. (2015). HISAT: a fast spliced aligner with low memory requirements. *Nat. Methods* 12, 357–360. doi: 10.1038/nmeth.3317

Krasemann, S., Madore, C., Cialic, R., Baufeld, C., Calcagno, N., El Fatimy, R., et al. (2017). The TREM2-APOE pathway drives the transcriptional phenotype of dysfunctional microglia in neurodegenerative diseases. *Immunity* 47, 566.e9–581.e9. doi: 10.1016/j.immuni.2017.08.008

Lake, B. B., Codeluppi, S., Yung, Y. C., Gao, D., Chun, J., Kharchenko, P. V., et al. (2017). A comparative strategy for single-nucleus and single-cell transcriptomes confirms accuracy in predicted cell-type expression from nuclear RNA. *Sci. Rep.* 7:6031. doi: 10.1038/s41598-017-04426-w

Lake, B., Shen, R., Ronaghi, M., Fan, J., Wang, W., and Zhang, K. (2016). Neuronal subtypes and diverstiy revealed by single-nucleus RNA sequencing of human brain. *Science* 352, 1586–1590. doi: 10.1126/science.aaf1204

Liao, Y., Smyth, G. K., and Shi, W. (2014). FeatureCounts: an efficient general purpose program for assigning sequence reads to genomic features. *Bioinformatics* 30, 923–930. doi: 10.1093/bioinformatics/btt656

Liu, P., Reichl, J. H., Rao, E. R., McNellis, B. M., Huang, E. S., Hemmy, L. S., et al. (2017). Quantitative comparison of dense-core amyloid plaque accumulation in amyloid-β protein precursor transgenic mice. *J. Alzheimers Dis.* 56, 743–761. doi: 10.3233/JAD-161027

Mathys, H., Davila-Velderrain, J., Peng, Z., Gao, F., Mohammadi, S., Young, J. Z., et al. (2019). Single-cell transcriptomic analysis of Alzheimer's disease. *Nature* 570, 332–337. doi: 10.1101/164889

Mhatre, S. D., Tsai, C. A., Rubin, A. J., James, M. L., and Andreasson, K. I. (2015). Microglial malfunction: the third rail in the development of Alzheimer's disease. *Trends Neurosci.* 38, 621–636. doi: 10.1016/j.tins.2015.08.006

Nott, A., Holtman, I. R., Coufal, N. G., Schlachetzki, J. C. M., Yu, M., Hu, R., et al. (2019). Brain cell type-specific enhancer-promoter interactome maps and disease-risk association. *Science* 366, 1134–1139. doi: 10.1126/science.aay0793

Olah, M., Menon, V., Habib, N., Taga, M., Yung, C., Elyaman, W., et al. (2018). A single cell-based atlas of human microglial states reveals associations with neurological disorders and histopathological features of the aging brain. *bioRxiv* [Preprint]. 343780. doi: 10.1101/343780

Picelli, S., Faridani, O. R., Bjorklund, A. K., Winberg, G., Sagasser, S., and Sandberg, R. (2014). Full-length RNA-seq from single cells using Smart-seq2. *Nat. Protoc.* 9, 171–181. doi: 10.1038/nprot.2014.006

Robinson, M. D., Mccarthy, D. J., and Smyth, G. K. (2010). edgeR: a bioconductor package for differential expression analysis of digital gene expression data. *Bioinformatics* 26, 139–140. doi: 10.1093/bioinformatics/btp616

Rogers, J., and Lue, L.-F. (2001). Microglial chemotaxis, activation and phagocytosis of amyloid β-peptide as linked phenomena in Alzheimer's disease. *Neurochem. Int.* 39, 333–340. doi: 10.1016/s0197-0186(01)00040-7

Ryu, J. K., Cho, T., Choi, H. B., Jantaratnotai, N., and McLarnon, J. G. (2015). Pharmacological antagonism of interleukin-8 receptor CXCR2 inhibits inflammatory reactivity and is neuroprotective in an animal model of Alzheimer's disease. *J. Neuroinflammation* 12:144. doi: 10.1186/s12974-015-0339-z

Sala Frigerio, C., Wolfs, L., Fattorelli, N., Thrupp, N., Voytyuk, I., Schmidt, I., et al. (2019). The major risk factors for Alzheimer's disease: age, sex and genes modulate the microglia response to Aβ plaques. *Cell Rep.* 27, 1293.e6–1306.e6. doi: 10.1016/j.celrep.2019.03.099

Sarlus, H., and Heneka, M. T. (2017). Microglia in Alzheimer's disease. *J. Clin. Invest.* 127, 3240–3249. doi: 10.1172/JCI90606

Smith, T., Heger, A., and Sudbery, I. (2017). UMI-tools: modelling sequencing error in unique molecular identifiers to improve quantification. *Genome Res.* 27, 491–499. doi: 10.1101/gr.209601.116

Spangenberg, E., Severson, P. L., Hohsfield, L. A., Crapser, J., Zhang, J., Burton, E. A., et al. (2019). Sustained microglial depletion with CSF1R inhibitor impairs parenchymal plaque development in an Alzheimer's disease model. *Nat. Commun.* 10:3758. doi: 10.1038/s41467-019-11674-z

Srinivasan, K., Friedman, B. A., Etxeberria, A., Huntley, M. A., van der Brug, M. P., Foreman, O., et al. (2019). Alzheimer's patient brain myeloid cells exhibit enhanced aging and unique transcriptional activation. *bioRxiv* [Preprint]. 610345. doi: 10.1101/610345

Streit, W. J., Braak, H., Del Tredici, K., Leyh, J., Lier, J., Khoshbouei, H., et al. (2018). Microglial activation occurs late during preclinical Alzheimer's disease. *Glia* 66, 2550–2562. doi: 10.1002/glia.23510

Streit, W. J., Braak, H., Xue, Q.-S., and Bechmann, I. (2009). Dystrophic (senescent) rather than activated microglial cells are associated with tau pathology and likely precede neurodegeneration in Alzheimer's disease. *Acta Neuropathol.* 118, 475–485. doi: 10.1007/s00401-009-0556-6

Streit, W. J., Sammons, N. W., Kuhns, A. J., and Sparks, D. L. (2004). Dystrophic microglia in the aging human brain. *Glia* 45, 208–212. doi: 10.1002/glia.10319

The ENCODE Consortium. (2016). ENCODE guidelines and best practices for RNA-Seq: revised December 2016. Available online at: https://www.encodeproject.org/documents/cede0cbe-d324-4ce7-ace4-f0c3eddf5972/@@download/attachment/ENCODE%20Best%20Practices%20for%20RNA_v2.pdf. Accessed June 16, 2020.

Ulrich, J. D., Finn, M. B., Wang, Y., Shen, A., Mahan, T. E., Jiang, H., et al. (2014). Altered microglial response to Aβ plaques in APPPS1–21 mice heterozygous for TREM2. *Mol. Neurodegener.* 9:20. doi: 10.1186/1750-1326-9-20

Uniken Venema, W. T., Voskuil, M. D., Vila, A. V., van der Vries, G., Jansen, B. H., Jabri, B., et al. (2019). Single-cell RNA sequencing of blood and ileal T cells from patients with Crohn's disease reveals tissue-specific characteristics and drug targets. *Gastroenterology* 156, 812.e22–815.e22. doi: 10.1053/j.gastro.2018.10.046

Veenstra, M., and Ransohoff, R. M. (2012). Chemokine receptor CXCR2: physiology regulator and neuroinflammation controller? *J. Neuroimmunol.* 246, 1–9. doi: 10.1016/j.jneuroim.2012.02.016

Venegas, C., Kumar, S., Franklin, B. S., Dierkes, T., Brinkschulte, R., Tejera, D., et al. (2017). Microglia-derived ASC specks cross-seed amyloid-β in Alzheimer's disease. *Nature* 552, 355–361. doi: 10.1038/nature25158

Xia, M. Q., and Hyman, B. T. (2002). GROα/KC, a chemokine receptor CXCR2 ligand, can be a potent trigger for neuronal ERK1/2 and PI-3 kinase pathways and for tau hyperphosphorylation-a role in Alzheimer's disease? *J. Neuroimmunol.* 122, 55–64. doi: 10.1016/s0165-5728(01)00463-5

Yin, Z., Raj, D., Saiepour, N., Van Dam, D., Brouwer, N., Holtman, I. R., et al. (2017). Immune hyperreactivity of Aβ plaque-associated microglia in Alzheimer's disease. *Neurobiol. Aging* 55, 115–122. doi: 10.1016/j.neurobiolaging.2017.03.021

Yu, G., Wang, L.-G., Han, Y., and He, Q.-Y. (2012). clusterProfiler: an r package for comparing biological themes among gene clusters. *OMICS* 16, 284–287. doi: 10.1089/omi.2011.0118

Zhang, B., Gaiteri, C., Bodea, L.-G., Wang, Z., McElwee, J., Podtelezhnikov, A. A., et al. (2013). Integrated systems approach identifies genetic nodes and networks in late-onset Alzheimer's disease. *Cell* 153, 707–720. doi: 10.1016/j.cell.2013.03.030

Zhong, S., Zhang, S., Fan, X., Wu, Q., Yan, L., Dong, J., et al. (2018). A single-cell RNA-seq survey of the developmental landscape of the human prefrontal cortex. *Nature* 555, 524–528. doi: 10.1038/nature25980

Conflict of Interest: MW, AW, SX, TM and KB were full time employees of Abbvie during the time of the studies.

The remaining authors declare that the research was conducted in the absence of any commercial or financial relationships that could be construed as a potential conflict of interest.

frontiers in Neurology

SYSTEMATIC REVIEW
published: 19 November 2020
doi: 10.3389/fneur.2020.590480

RANK/RANKL/OPG Signaling in the Brain: A Systematic Review of the Literature

Anton Glasnović[1,2]*, *Niall O'Mara*[3], *Nataša Kovačić*[2,4], *Danka Grčević*[2,5] and *Srećko Gajović*[1,2]

[1] Department of Histology and Embryology, Zagreb University School of Medicine, Zagreb, Croatia, [2] Croatian Institute for Brain Research, Zagreb University School of Medicine, Zagreb, Croatia, [3] Department of Medicine, Cork University Hospital, Cork, Ireland, [4] Department of Anatomy, Zagreb University School of Medicine, Zagreb, Croatia, [5] Department of Physiology and Immunology, Zagreb University School of Medicine, Zagreb, Croatia

Together with its dominant immunological and bone remodeling involvement, RRO axis, comprising of receptor activator of nuclear factor-κB (RANK), RANK ligand (RANKL), and osteoprotegerin (OPG) signaling, is as well-implicated in CNS functioning and corresponding pathologies. The CNS aspects of RANKL/RANK/OPG (RRO) axis were systematically reviewed. With search 10 databases, and 7 additional resources from first article publication to July 2019, resulted in total 2,222 hits, from which 33 relevant articles were selected. The elements of RRO axis in CNS include cells involved in neuroinflammation, predominantly in microglia, but as well in resident macrophages and inflammatory cells migrating across the blood-brain barrier. The expression in neurons and oligodendrocytes is mainly confined to processes of differentiation and cell death. RRO axis tunes the neuroinflammatory response, depending on the molecular, cellular and pathological context. RANK/RANKL signaling is neuroprotective in TLR-mediated inflammation, while OPG seems detrimental in stroke, but beneficial in multiple sclerosis. The levels of RRO axis elements can serve as biomarkers in the blood and cerebrospinal fluid. They act as neuroprotectant after brain damage even being implicated in body weight- and thermo-regulation. As derivatives of RRO axis already exist as therapeutic agents in bone remodeling, it would be intriquing to see if these or new RRO-based pharmaceuticals would appear effective in CNS therapies.

Keywords: OPG - RANKL - RANK, BBB rupturing, neural mediators, stroke repair, multiple sclerosis - etiology, neuroinflammatory cytokines

OPEN ACCESS

Edited by:
Amanda Sierra, Achucarro Basque Center for Neuroscience, Spain

Reviewed by:
Eleonora Allocati, Mario Negri Pharmacological Research Institute (IRCCS), Italy
Jelena Milasin, University of Belgrade, Serbia
Ivica Bilic, University of Split, Croatia

***Correspondence:**
Anton Glasnović
anton.glasnovic@mef.hr

Specialty section:
This article was submitted to Multiple Sclerosis and Neuroimmunology, a section of the journal Frontiers in Neurology

Received: *01 August 2020*
Accepted: *22 October 2020*
Published: *19 November 2020*

Citation:
Glasnović A, O'Mara N, Kovačić N, Grčević D and Gajović S (2020) RANK/RANKL/OPG Signaling in the Brain: A Systematic Review of the Literature. Front. Neurol. 11:590480. doi: 10.3389/fneur.2020.590480

INTRODUCTION

The receptor activator of nuclear factor-κB (RANK)/RANK ligand (RANKL)/osteoprotegerin (OPG) (RRO axis) was originally discovered through parallel investigations in the late 1990's within the immune and bone systems (1–4). This signaling triad regulates a variety of metabolic and cellular processes, thus its disturbance contributes to the pathogenesis of bone and immune diseases, such as rheumatoid arthritis, osteoporosis, diabetes mellitus and certain types of cancer. Recent evidence suggests that the triad is also implicated in a number of neurological conditions, in particular in various aspects of neural tissue damage and subsequent reparative processes (5). Further elucidation of the functional relationship between certain neurological diseases and the disturbances in the RRO axis may provide potential diagnostic and therapeutic targets.

The RRO axis involves the interactions between three members of the tumor necrosis factor (TNF) superfamily (TNFSF), RANK (also known as TNFRSF11a), its cognate ligand RANKL (also known as TNFSF11) and a decoy receptor OPG (also known as TNFRSF11b). RANKL, a member of the TNF ligand superfamily binds to RANK and a decoy receptor OPG, both from the TNF receptor (TNFR) superfamily (6). RANKL, secreted by T cells, has been shown to enhance the immune response by promotion of dendritic cell survival and function mediated by RANK signaling (2, 7). Conversely, RANKL may induce immune tolerance by stimulating the regulatory T cell (Treg) differentiation in certain autoimmune diseases such as diabetes mellitus and chronic colitis (8, 9). Based on these results, it can be concluded that, depending on the other microenvironmental signals, the RRO system may either activate or suppress immune response.

In addition to the immune system, the RRO axis is well-characterized in the context of bone remodeling. RANKL, secreted by osteoblasts, osteocytes, hypertrophying chondrocytes, and bone marrow stromal cells, stimulates the responsive RANK-bearing osteoclast precursors, to differentiate into active bone-resorbing osteoclasts. This negative feedback-loop is important for physiological bone remodeling, and the equilibrium between bone formation and bone resorption. OPG is secreted by osteoblasts, bone marrow stromal cells, B cells, and dendritic cells. It acts as a decoy receptor for RANKL, preventing its interaction with RANK and, consequently, blocking osteoclast maturation Moreover, the imbalance in RANKL/RANK signaling may lead to a number of bone disorders, such as rheumatoid, arthritis and osteoporosis (10–13).

Members of the RRO axis are widely expressed in different embryonic and adult tissues (5, 14). RANK is mostly expressed by monocyte/macrophage lineage cells. Depending on the milieu created by the mediators in the residing tissue, these cells may be directed toward effector myeloid progenies or remain dormant until receiving maturation signals (15, 16). In addition to classical pro-inflammatory mediators, activated T and B cells produce RANKL during inflammatory and immune responses. It is important to acknowledge that there are two forms of RANKL, one membrane-bound, and the other one soluble, which is detached from the surface of the cell by proteases. Lymphocytes serve as a significant source of soluble (s)RANKL, which potentiates dendritic cell activation and osteoclast differentiation (17–19). In particular, helper T (Th) cells, Th1 and Th17, are the primary T cell subsets associated with immune activation and subsequent stimulation of osteoclastogenesis. Conversely, Tregs suppress immune response, and inhibit osteoclast differentiation (20, 21). In addition to the activation of myeloid cells, it is hypothesized that RANKL further potentiates inflammatory processes through the provision of bone-derived Ca^{2+} ions, which interact with the calcium sensing receptors and simulate proinflammatory mediators (20, 22). Such pathogenic roles of RRO axis have been observed in states of pathological or persistent inflammation where reduction in bone mass has been associated with immune cell activation (21, 23–25).

Together with the role in bone and immune system of RRO axis, the growing evidence implicates that it also has role in nervous system, therefore this review focuses to this particular aspect. The purpose of this article is to provide a systematic review on the current knowledge of the RRO axis in relation to the neurological diseases.

SEARCH METHODS FOR IDENTIFICATION OF STUDIES

We conducted a comprehensive search (from the first published article available online to July 2019) and developed detailed search strategies, based on the strategy for MEDLINE (using MeSH terms and text keywords) but revised appropriately for each resource, and used English language while searching the entire database.

We searched the following databases:

1. Cochrane Central Register of Controlled Trials (CENTRAL/Cochrane Library; via Ovid)
2. MEDLINE (via Ovid)
3. Scopus
4. Web of Science Core Collection (via Web of Science)
5. Current Contents (via Web of Science)
6. SciELO Citation Index (via Web of Science)
7. KCI-Korean Journal Database (via Web of Science)
8. Russian Science Citation Index (via Web of Science)
9. BIOSIS Citation Index (via Web of Science)
10. Data Citation Index (via Web of Science).

We searched additional resources including:

1. ProQuest Dissertations & Theses Global
2. OpenGrey
3. African Index Medicus
4. IndMED
5. ClinicalTrials.gov
6. WHO International Clinical Trials Registry Platform (WHO ICTRP)
7. CenterWatch.

Our search strategy is described in detail in **Supplemental Material 1**, resulting in 33 references for qualitative synthesis (**Figure 1**, **Supplemental Material 2**). All included references had to be relevant and eligible for the major topic of our research and that was RANKL/RANK/OPG axis in CNS. All studies, including research articles, case reports, experimental studies, conferrence abstracts and preliminary results were comprised in the review. Exclusion of studies was based upon non-relevance to any of the given major topic (not pertaining to central nervous system and RANKL/RANK/OPG axis). Namely, we excluded studies that used the same abbreviation for different categories (e.g., OPG being optical pathway glioma), assessed RRO axis in systemic vascular diseases, or included inflammatory/autoimmune diseases with minor reference to CNS tissues. Finally, 1,098 studies were excluded for consideration from our review. Critical appraisal of selected studies was done by all authors.

Relatively low number of references on this topic (33 in total), due to the risk of bias, may indicate an insufficient number of

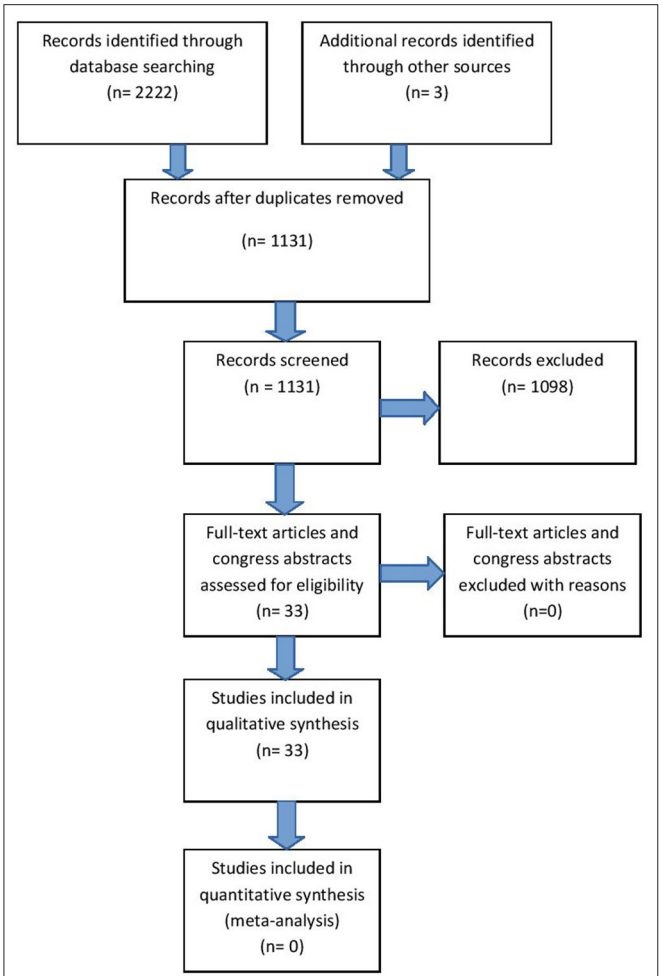

FIGURE 1 | Study flow diagram (From: The PRISMA Group 2009).

studies whose results could directly and undoubtedly be used for further research or some other application in practice.

CELLULAR AND SOLUBLE ELEMENTS OF RRO AXIS IN THE BRAIN

The RRO axis and osteoclast paradigm is applicable to microglial cells as both osteoclasts and microglia share some developmental and functional properties, including hematopoietic origin, phagocytosis, and immunomodulation (26). Moreover, this can be extended to all myeloid populations within the central nervous system (CNS), including parenchymal microglia in the nerve tissue, perivascular phagocytic cells, meningeal macrophages, and choroid plexus macrophages (27–30). In contrast to other tissue-resident macrophages which arise from the embryonic yolk sac and fetal liver, microglia originates exclusively from yolk sac-derived hematopoietic progenitors (27). These progenitors infiltrate the brain during early development, differentiate into microglia, and maintain their population by self-renewal (26).

Recent studies have demonstrated that members of the RRO axis are expressed by several types of cells within neural tissue; this includes microglia, other resident macrophages, neurons and oligodendrocyte precursor cells (28–30). It has also been noted that RANKL, alongside brain-derived neurotrophic factor (BDNF) could induce differentiation of human umbilical cord blood cells into neurons and glial cells, and that both have synergistic effect (31). Moreover, the expression pattern of RRO axis is tuned by neuro-inflammatory events associated with blood-brain barrier (BBB) disruption. Inflammatory monocytes cross the BBB by the stepwise process initiated by various stimuli, such as soluble mediators secreted by pro-inflammatory T cells and activated microglia, becoming infiltrating macrophages. In case of further BBB damage, additional cells passively enter and accumulate at the inflammatory site within CNS (32). In the early phase of the inflammation, RRO mediators are produced almost exclusively by microglia, whereas in the later phases of the inflammatory response they originate from mixed microglia/macrophage (M/M) cells (32–34).

In vitro studies showed that, in certain conditions of cellular stress, OPG can be expressed by neurons and oligodendrocyte progenitors, protecting the neurons from apoptosis caused by death receptor stimulation (35). However, this effect and its consequences *in vivo* are still to be confirmed.

RRO AXIS IN CONTEXT OF MICROGLIAL REGULATION

In the physiological conditions, microglial cells exert two main functions: 1. Immune surveillance, and 2. Synaptic pruning. They also maintain neuronal homeostasis through the release of BDNF and neuronal growth factor (NGF) (36, 37). Moreover, they act as an innate immunity sentinel in the brain and present the first line of defense upon activation by brain tissue injury and infection. In such conditions, microglia upregulates expression of major histocompatibility complex (MHC) and costimulatory molecules, and enhances chemotaxis and recruitment of immune cells (36, 38, 39). Depending on the nature of the neuroinflammatory event, microglia may translate from physiological (termed "resting") to pathological (termed "activated") state, and orchestrate subsequent cellular events in favor of either pro-inflammatory or anti-inflammatory effector arm (**Figure 2**).

In vitro activated microglia polarizes into either pro-inflammatory (producing inflammatory cytokines, chemokines, and other mediators) or anti-inflammatory (mediating phagocytosis of tissue debris and regeneration) subtype, a concept adapted from polarization of peripheral tissue macrophages (40). Interleukin (IL)-1β, tumor necrosis factor (TNF)-α and interferon (IFN)-γ secreted from activated Th1 cells may enhance the inflammatory neurotoxic response and activate microglia to secret IL-1β, TNF-α, IL-6, CC-chemokine ligand 2 (CCL2), nitric oxide, and IL-12p70 (41–44). This triggers immune cell infiltration across BBB and neuronal

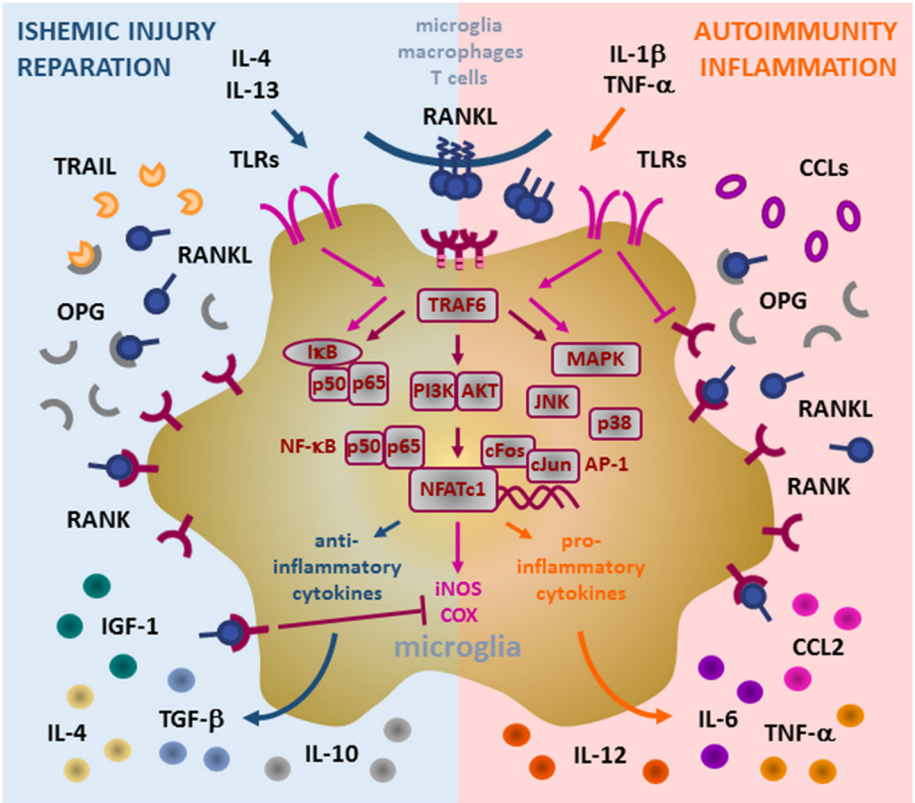

FIGURE 2 | Role of RANK/RANKL/OPG (RRO) axis in microglia. Binding of membrane or soluble RANKL induces trimerization of RANK expressed on the microglia and initiates signal transduction. RANK lacks the intrinsic enzymatic activity in its intracellular domain and transduces a signal by recruiting adaptor molecules from the TRAF family of proteins, mainly TRAF6 (via three TRAF6-binding sites in its C-terminal cytoplasmic tail). Upon formation of the RANK/TRAF6 complex, multiple signaling pathways are activated, including NF-κB (activation of p65:p50 subunits/IκB complex), PI3K/AKT, and MAPK (including p38 and JNK). These signaling cascades potently induce transcription factors NFATc1 and AP-1 (cFos and cJun) to initiate transcription of target genes. In pathological conditions, microglia acquire different context-dependent functions. Under ischemic conditions, induced by anti-inflammatory IL-4 and IL-13 cytokines, microglia may exhibit neuroprotective action by production of immunosuppressive and reparative cytokines and growth factors (IL-4, IL-10, TGF-β, and IGF-1). Under such response, induced RANKL production and overexpression of RANK contribute to transcription of anti-inflammatory mediators and suppress iNOS and COX induced by TLR (TLR3/TLR4) signaling, whereas upregulation of OPG blocks ligation of TRAIL and protects microglia from apoptosis. During inflammatory and autoimmune processes, pro-inflammatory IL-1beta and TNF-alpha cytokines drive microglia to support inflammatory reaction. Enhanced RANKL/RANK signaling in this context may promote up-regulation of pro-inflammatory cytokines and chemokines (including TNF-α, IL-6, CCL2, IL-1β), which in turn attract additional inflammatory and immune cells, induce Th1 polarization of infiltrating T cells by IL-12 and thus, neural tissue damage. TLR signaling interfere with RANK signaling in microglia, namely TLR4 suppress RANK expression but auto-amplify TLR3-initiated cascades (NK-κB and MAPK), thus perpetuating the microglia inflammatory response. However, the precise mechanisms of the signaling interplay between RANK and TLRs are still to be fully revealed. RANK, receptor activator of nuclear factor-κB; RANKL, RANK ligand; OPG, osteoprotegerin; TRAF, TNF receptor-associated factor; IL, interleukin; TNF, tumor necrosis factor; TGF, transforming growth factor; IGF, insulin-like growth factor; CCL, CC-chemokine ligand; TRAIL, TNF-related apoptosis-inducing ligand; TLR, Toll-like receptor; NF-κB, nuclear factor-κB; IκB, inhibitor of NF-κB; PI3K/AKT, phosphatidylinositol 3-kinase/protein kinase B; MAPK, mitogen-activated protein kinase; AP-1, activator protein 1; NFATc1, nuclear factor of activated T cells, cytoplasmic 1.

damage. In contrast, IL-4 and IL-13 secreted by Th2 and Tregs direct microglia toward production of IL-4, IL-10, transforming growth factor (TGF)-β and insulin-like growth factor (IGF)-1. These mediators polarize the immune response toward neuroprotection and reparation, initiating the resolution of inflammation and secretion of neurotrophic factors (45–47).

Under physiological conditions microglial morphology shows branched processes oriented radially to a small elliptical soma, facilitating important functions in the refinement of synaptic networks, production of neurothropic factors, and removal of cell debris. Although polarization has not been clearly confirmed in an *in vivo* context, evidence shows that microglia undergo dynamical and temporal phenotypical and functional changes in response to brain injury. In diseased tissue microglia have enlarged cell bodies with fewer and shorter processes, mainly serving as phagocytic and innate immune cells (26, 40, 44).

Microglia also expresses Toll-like receptors (TLRs) which serve as pathogen recognition receptors (48). RANK expressed by both microglia and monocytes/macrophages, counteract TLR3- and TLR4-mediated signals. It has been shown that RANKL pre-treatment of microglial cells decreased the ability of TLR3/TLR4 pathway to induce the expression of inflammatory markers,

such as inducible nitric oxide synthase (iNOS) and cyclo-oxygenase (COX) 2 (**Figure 2**). On the other hand, activated TLR4 suppresses the expression of RANK and potentiates the expression of TLR3, which in turn, amplifies pro-inflammatory signaling through a positive feedback loop. Since RANKL can decrease the pro-inflammatory effects of TLR agonists, RANKL/RANK signaling is thought to be neuroprotective in TLR-mediated neuroinflammation (28). However, the role of OPG remains controversial. It is possible that microglia and macrophages upregulate OPG production in order to neutralize the inhibitory effect of RANKL on overactive microglia. In parallel, increased secretion of OPG may have protective effect, by blocking the pro-apoptotic signaling of TNF-related apoptosis-inducing ligand (TRAIL) in microglia (28, 35, 49).

RRO AXIS IN DIFFERENT PATHOLOGICAL CONDITIONS

The RRO axis has been studied in both, a variety of experimental animal models, and humans with different pathological conditions. These studies suggest that RRO triad may be a novel target for diagnostic and therapeutic approaches. Some research groups have developed RRO axis modifiers applicable to neurological setting and are working toward their application in clinic, some of these will be discussed below.

RRO Axis and Brain Ischemia

Recent studies of the RANKL/RANK/OPG signaling pathway indicate its involvement in ischemic brain injury in particular in microglial activation. The relevance of microglia in ischemic injury is highlighted by its contribution to the reparative processes during the latter stages of CNS damage (50, 51).

In their resting state, microglial cells express negligible amounts of RRO mediators. In the active state and in the presence of TLR4 ligands, microglia up-regulate membrane expression of RANK and, simultaneously, enhance autocrine and paracrine secretion of sRANKL (48). Enhancement of RRO signaling decreases microglial activation by counteracting the TLR4 receptor pathway (48, 49, 52). Microglia at peri-infarction sites overexpress both, RANK and RANKL, which in turn, reduces ischaemic injury (49). *In vitro* studies using recombinant (r)RANKL confirmed this neuroprotective effect. However, it was seen only in mixed neuron/glia cell cultures, but not in cell cultures comprised only of cortical neurons. In peri-infarction areas, OPG is also overexpressed, but its exact cellular source is still under debate (35). Based on the data obtained through the *in vitro* studies, it is postulated that neurons and oligodendrocytes secrete OPG under ischaemic stress, and this secretion invokes damage to brain tissue due to its pro-inflammatory effect. OPG can even have the neurotoxic effect when overexpressed in hypoxic neurons, due to inhibition of RANK-signaling pathway in microglial cells (35).

In an experimental model of stroke (middle cerebral artery occlusion, MCAO), OPG deficient mice were found to have reduced infarction volume compared to wild-type (WT) controls. Administration of anti-RANKL neutralizing antibody increased the infarction volume in both OPG –/– and WT mice, although the effect was less pronounced in WT than in OPG –/– mice. These data imply that RANKL/RANK signaling has a protective role in ischaemic brain injury, whereas OPG exterts an opposite effect (49).

Based on the available data, it is proposed that blockade of TLR signal would reduce the extent of post-ischaemic brain injury. In such context, activation of the RANKL/RANK axis could be considered as an "anti-TLR" agent (**Figure 2**). However, systemic administration of rRANKL is limited in its clinical utility, as it would lead to clinically unacceptable osteoclast activation and osteoporosis in post-stroke patients (52). Recently, a recombinant anti-TLR agent, microglial-healing peptide (MHP)1, has been developed, and its structure is based upon the structure of the RANKL molecule. In the transient MCAO model, ischaemic injury was reduced by MHP1 injection either intra-cerebroventricularly at 4 h post-ischemia or intravenously 4/6 h post-ischaemia. Additionally, MHP1-AcN, a MHP1 derivative, can effectively attenuate tissue plasminogen activator-induced hemorrhage formation (53, 54). The only human study done on subject of brain ischemia and RRO axis showed that in Italian population, genetic variability of OPG gene (T245G, T950C, and G1181C polymorphisms) acts as an independent risk factor for ischemic stroke (55, 56). Some other studies that researched OPG levels in stroke patients were excluded from the review as they mainly focused on carotid calcifications and metabolism of calcium, which was not directly related to brain (stroke in these patients was rather the consequence of peripheral events).

These results collectively suggest that blockade of the RRO axis may lead to overstimulation of microglial cells, and in turn may exacerbate neural damage following tissue injury. In contrast, activation of RANK-signaling cascade ameliorates the unwanted inflammatory response, thus protecting the brain tissue from further damage.

RRO Axis and Multiple Sclerosis

Autoimmune-mediated neuroinflammatory processes damage the integrity of the BBB and this results in a loss of immune privilege (57, 58). Besides being the structural part of the vascular wall, BBB functionally includes the Virchow-Robin's space, where the perivascular macrophages, constantly replenished by blood-born monocytes, juxtapose tunica media and contribute to its impermeability. The BBB is absent at certain sites, including the choroid plexus, retina and circumventricular organs. Immune cells recruited by CCL20 produced within the choroid plexus enter CNS and act within an immune surveillance capacity (57–59). However, in the presence of CNS inflammation immune privilege is lost, the BBB is compromised, and circulating immune cells can enter the CNS in an unregulated manner (60, 61). Intrathecal T cells infiltrate the brain parenchyma following their activation by specific brain tissue-resident antigen-presenting cells, such as microglia, astrocytes and dendritic cells (59, 60, 62). Evidence from murine models and human diseases has shown that activated T cells produce RANKL, especially in chronic inflammatory conditions (20, 21, 63, 64). A number of studies have sought to elucidate the

underlying immunological mechanisms of RANKL expression and autoimmune inflammation in the brain.

Autoimmune disorders of the CNS, such as multiple sclerosis (MS), are associated with myelin sheath damage mainly caused by aberrant T cell response. The RRO axis has been found to potentially play a role in murine experimental autoimmune encephalomyelitis (EAE) as a model of human MS (59, 65, 66). In EAE, production of RANKL by T cells induces secretion of CCL20 in astrocytes. RANKL expression was found to be associated with trafficking of pathogenic T cells within brain parenchyma, particularly Th17 subset. RANKL inhibition exerted a reduction of T cell infiltration and a significant protective effect in murine EAE, and thus offers a potential therapeutic target (65, 67).

In relation to possible biomarkers, the concentrations of RANKL and OPG are found to be higher in the blood of MS patients. Primary progressive (PP)-MS is in particular associated with the highest levels of RANKL in parallel with other inflammatory makers (C-reactive protein [CRP], IL-1β, TNF-α) (68). Another study showed higher levels of RANKL in patients with relapsing-remitting (RR)-, PP- and secondary progressive (SP)- MS compared to healthy controls, and confirmed that RANKL levels were the highest in PP-MS (69). These studies focused only on the peripheral blood and did not examine the intrathecal expression of RRO mediators. Systemic higher levels of RANKL may reflect the disease pathogenesis, but as well induce additional effects including promotion of osteoclastogenesis, release of calcium from bone and peripheral activation of dendritic cells.

Through the parallel profiling of peripheral blood and cerebrospinal fluid (CSF), our group was the first to compare the levels of RANKL and OPG in control subjects and MS patients at clinical onset (70). It is important to stress that these naïve patients were excluded from the use of any immunomodulatory or immunosuppressive agents known to interfere with the RRO axis (71). CSF levels of OPG were decreased in patients with MS at clinical onset in comparison to healthy controls, together with higher sRANKL/OPG ratio, while there was no difference between groups in RANKL and OPG expression in peripheral blood. These data indicate the initial RRO dysregulation at intrathecal sites already at the outset of the disease. Additional analysis of plasma samples and peripheral blood mononuclear cells from patients with RR-MS revealed upregulation of chemokines CCL2 and CXCL12 as well as increase in sRANKL and sRANKL/OPG ratio with the disease progression (70). Another clinical study on MS patients found higher OPG and lower RANKL levels in serum of patients with RR-MS compared to those with SP-MS. However, chronic forms of MS are often associated with immunosuppressive treatment and immobility both of which affect the RRO axis, therefore it is difficult to exclude these as potential confounders (71, 72). Studies on MS patients during glatiramer-acetate (GA) or interferon (IFN)-β treatment showed, among other molecules, modulation of OPG levels (73, 74), supporting our claim about immunomodulatory treatment affecting RRO axis.

In conclusion, RRO axis has potential as both a disease biomarker and therapeutic target in certain autoimmune diseases of the CNS such as MS.

RRO Axis in Brain Tumors

Primary CNS tumors account for a significant proportion of morbidity and mortality up to 29.9 per 100,000 persons (75, 76). Several studies have dealt with the RRO axis role in the malignant processes of different types of brain tumors.

Glioma cell lines and murine glioblastoma multiforme (GBM) models have demonstrated that GBM has employed immune escape mechanism that involve secretion of CCL20 and OPG, which acts directly and indirectly on microglia cells triggering their production of CCL2. This chemokine gradient attracts CCR4-expressing Tregs and CCR2-expressing monocytic myeloid-derived suppressor cells to the site of GBM, which in turn reduces the inflammatory response to tumor cells (77–80). One *in vivo* xenograft study, in which human glioma cells were stereotactically injected into mouse brain, revealed that GBM cells expressing high level of endogenous RANKL resulted in a more invasive tumor form compared to GBM cells expressing relatively low endogenous RANKL. Furthermore, the number of activated astrocytes was markedly increased in the periphery of RANKL-abundant invasive tumors, suggesting that RANKL is able to activate astrocytes through NF-κB signaling. These astrocytes have been shown to secrete various factors that regulate glioma cell invasion (81).

RANKL expression has also been examined in pituitary adenoma cell lines, in the context of death receptor activation. The cytotoxic agent containing the fused tripeptide sequence Arg-Gly-Asp (RGD) (interacting with transmembrane integrins) and Fas ligand was used for targeted activation of receptor Fas in several adenoma cell lines. In parallel to the increase in caspase expression, administration of RGD-Fas ligand stimulated the expression of RANKL, indicating that the RRO axis and its mediators are functionally linked to pro-apoptotic members of the TNF superfamily (82, 83).

RRO Axis in Other Conditions Related to Brain

The RRO axis may be implicated in neurological conditions not directly related to ischaemic injury, neuroinflammation or tumorigenesis, indicating a general biological role within the CNS. A recent study of prednisolone-induced neurotoxicity in rat brain demonstrated that it is associated with the attenuation of RRO signaling through modulation of OPG and RANK expression (84). This study proposed that prednisolone-induced neurotoxicity is mediated by disturbances of the vitamin D3 endocrine signal. In contrast, vitamin D3 treatment mediates a critical neuroprotective role through reduced OPG expression and increased RANKL expression, resulting in enhanced RANK signaling (84, 85). It appears that activation of the RRO axis and greater bioavailability of vitamin D3 in the CNS decrease activation of pro-inflammatory microglia. Thus, the interplay of vitamin D3 and RRO signal may prevent autoimmune response as well as influence degenerative diseases such as Alzheimer's disease.

There is also evidence that RANKL reduces food intake and causes weight loss via modulating the hypothalamic neuropeptide Y(NPY)/cocaine- and amphetamine-regulated transcript (CART) peptide pathways (86, 87). RANK deletion

from NPY neurons may downregulate NPY mRNA expression in hypothalamus, indicating that RANK signaling regulates the balance between bone mass and body weight by modulating NPY levels (87).

Three studies suggest the involvement of RRO axis in thermoregulation. It seems that RANKL may activate brain regions involved in thermoregulation and induce fever via COX2-prostaglandin E2/EP3 receptor pathway in neurons and astrocytes. RANK mutation in both rodents and humans results in an abrogated fever response compared to controls (88–90).

CONCLUSION

The increasing evidence is accumulated that RRO axis has an important role in neural tissue pathophysiology and could be a common functional link between different inflammatory processes within the CNS.

The elements of RRO axis in CNS include immune cells, predominantly microglia, but also other resident and infiltrating macrophages, mediating homeostatic and neuroinflammatory mechanisms. The expression in neurons and oligodendrocytes is mainly confined to differentiation and apoptotic processes. RRO axis tunes the neuroinflammatory response, highly depending on the tissue context. Research into RRO signaling has demonstrated apparent contradictory effects and suggests that RRO signaling is beneficial in ischemic lesions and deleterious in autoimmune reactions. We propose that this paradox may be explained by the stimulation of different microglial subtypes and the induction of diverse downstream effector functions (**Figure 2**). However, precise regulation of microglia activity *in vivo* by RRO mediators and their functional interactions with other cytokines and growth factors still need to be fully elucidated.

To date most studies involving RRO mediators in human samples have focused on the peripheral blood biomarkers. Future research is needed to identify their specific effects within brain tissue and to develop novel agents that can modulate RRO signaling. Several such modulators are presently in clinical use for different conditions, including RANKL agonists as well as OPG-mediated axial antagonists. We believe that modulation of the RRO axis may complement current treatment strategies for certain neurological disorders providing novel therapeutic and diagnostic targets.

DATA AVAILABILITY STATEMENT

The original contributions presented in the study are included in the article/supplementary materials, further inquiries can be directed to the corresponding author/s.

AUTHOR CONTRIBUTIONS

AG, NO'M, DG, and SG: conception and design of the study. AG, NO'M, NK, DG, and SG: agreement to be accountable for all aspects of the work, final approval of the version to be submitted, critical revision of the manuscript for important intellectual content, drafting of the manuscript, analysis, and interpretation of the data. All authors contributed to the article and approved the submitted version.

FUNDING

This work was supported by EU European Regional Development Fund, Operational Programme Competitiveness and Cohesion, grant agreement No. KK.01.1.1.01.0007, CoRE – Neuro, and by Croatian Science Foundation projects IP-06-2016-1892 and IP-2018-01-2414.

ACKNOWLEDGMENTS

We would like to thank Mrs. Helena Markulin for her help with technical issues during our research.

SUPPLEMENTARY MATERIAL

The Supplementary Material for this article can be found online at: https://www.frontiersin.org/articles/10.3389/fneur.2020.590480/full#supplementary-material

REFERENCES

1. Anderson DM, Marasovsky E, Billingsley WL, Dougall WC, Tometsko ME, Roux ER, et al. A homologue of the TNF receptor and its ligand enhance T-cell growth and dendritic-cell function. *Nature.* (1997) 390:175–9. doi: 10.1038/36593
2. Wong BR, Josien R, Lee SY, Sauter B, Li HL, Steinman RM, et al. TRANCE (tumor necrosis factor [TNF]-related activation-induced cytokine), a new TNF family member predominantly expressed in T cells, is a dendritic cell-specific survival factor. *J Exp Med.* (1997) 186:2075–80. doi: 10.1084/jem.186.12.2075
3. Lacey DL, Timms E, Tan HL, Kelley MJ, Dunstan CR, Burgess T, et al. Osteoprotegerin ligand is a cytokine that regulates osteoclast differentiation and activation. *Cell.* (1998) 93:165–75. doi: 10.1016/S0092-8674(00)81569-X
4. Yasuda H, Shima N, Nakagawa N, Yamaguchi K, Kinosaki M, Mochizuki S, et al. Osteoclast differentiation factor is a ligand for osteoprotegerin/osteoclastogenesis-inhibitory factor and is identical to TRANCE/RANKL. *Proc Natl Acad Sci USA.* (1998) 95:3597–602. doi: 10.1073/pnas.95.7.3597
5. Walsh MC, Choi Y. Biology of the RANKL-RANK-OPG system in immunity, bone, beyond. *Front Immunol.* (2014) 5:511. doi: 10.3389/fimmu.2014.00511
6. Aggarval BB. Signalling pathways of the TNF superfamily: a double-edged sword. *Nat Rev Immunol.* (2003) 3:745–56. doi: 10.1038/nri1184
7. Josien R, Li HL, Ingulli E, Sarma S, Wong BR, Vologodaskaia M, et al. TRANCE, a tumor necrosis factor family member, enhances the longevity and adjuvant properties of dendritic cells in vivo. *J Exp Med.* (2000) 191:495–502. doi: 10.1084/jem.191.3.495
8. Green EA, Choi Y, Flavell RA. Pancreatic lymph node-derived CD4(+)CD25(+) Treg cells: highly potent regulators of diabetes that require TRANCE-RANK signals. *Immunity.* (2002) 16:183–91. doi: 10.1016/S1074-7613(02)00279-0
9. Totsuka T, Kanai T, Nemoto Y, Tomita T, Okamoto R, Tsuchiya K, et al. RANK-RANKL pathway is critically involved in the function of CD4+CD25+ regulatory T cells in chronic colitis. *J Immunol.* (2009) 182:6079–87. doi: 10.4049/jimmunol.0711823
10. Hofbauer LC, Heufelder AE. Role of receptor activator of nuclear factor-kappaB ligand and osteoprotegerin in bone cell biology. *J Mol Med.* (2001) 79:243–53. doi: 10.1007/s001090100226

11. Hofbauer LC, Khosla S, Dunstan CR, Lacey DL, Boyle WJ, Riggs L. The roles of osteoprotegerin and osteoprotegerin ligand in the paracrine regulation of bone resorption. *J Bone Miner Res.* (2000) 15:2–12. doi: 10.1359/jbmr.2000.15.1.2
12. Roodman GD. Role of cytokines in the regulation of bone resorption. *Calcif Tissue Int.* (1993) 53(Suppl. 1):S94–8. doi: 10.1007/BF01673412
13. Teitelbaum SL. Bone resorption by osteoclasts. *Science.* (2000) 289:1504–8. doi: 10.1126/science.289.5484.1504
14. Okamoto K, Nakashima T, Shinohara M, Negishi-Koga T, Komatsu N, Terashima A, et al. Osteoimmunology: the conceptual framework unifying the immune and skeletal systems. *Physiol Rev.* (2017) 97:1295–349. doi: 10.1152/physrev.00036.2016
15. Horowitz MC, Lorenzo JA. The origins of osteoclasts. *Curr Opin Rheumatol.* (2004) 16:464–8. doi: 10.1097/01.bor.0000127825.05580.eb
16. Xing L, Schwarz EM, Boyce BF. Osteoclast precursors, RANKL/RANK, and immunology. *Immunol Rev.* (2005) 208:19–29. doi: 10.1111/j.0105-2896.2005.00336.x
17. Lum L, Wong BR, Josien R, Becherer JD, Erdjument-Bromage H, Schlondorff J, et al. Evidence for a role of a tumor necrosis factor-α (TNF-α)-converting enzyme-like protease in shedding of TRANCE, a TNF family member involved in osteoclastogenesis and dendritic cell survival. *J Biol Chem.* (1999) 274:13613–8. doi: 10.1074/jbc.274.19.13613
18. Nakashima T, Kobayashi Y, Yamasaki S, Kawakami A, Eguchi K, Sasaki H, et al. Protein expression and functional difference of membrane-bound and soluble receptor activator of NF-κB ligand: modulation of the expression by osteotropic factors and cytokines. *Biochem Biophys Res Commun.* (2000) 275:768–75. doi: 10.1006/bbrc.2000.3379
19. Hikita A, Yana I, Wakeyama H, Nakamura M, Kadono Y, Oshima Y, et al. Negative regulation of osteoclastogenesis by ectodomain shedding of receptor activator of NF-κB ligand. *J Biol Chem.* (2006) 281:36846–55. doi: 10.1074/jbc.M606656200
20. Takayanagi H. Osteoimmunology: shared mechanisms and crosstalk between the immune and bone systems. *Nat Rev Immunol.* (2007) 7:292–304. doi: 10.1038/nri2062
21. Tsukasaki M, Takayanagi H. Osteoimmunology: evolving concepts in bone-immune interactions in health and disease. *Nat Rev Immunol.* (2019) 19:626–42. doi: 10.1038/s41577-019-0178-8
22. Negishi-Koga T, Takayanagi H. Ca2+-NFATc1 signalling is an essential axis of osteoclast differentiation. *Immunol Rev.* (2009) 231:241–56. doi: 10.1111/j.1600-065X.2009.00821.x
23. Schett G. Review: immune cells and mediators of inflammatory arthritis. *Autoimmunity.* (2008) 41:224–9. doi: 10.1080/08916930701694717
24. Chen B, Wu W, Sun W, Zhang Q, Yan F, Xiao Y. RANKL expression in periodontal disease: where does RANKL come from? *Biomed Res Int.* (2014) 2014:731039. doi: 10.1155/2014/731039
25. Figueredo CM, Lira-Junior R, Love RM. T and B cells in periodontal disease: new functions in a complex scenario. *Int J Mol Sci.* (2019) 20:3949. doi: 10.3390/ijms20163949
26. Holtman IR, Skola D, Glass CK. Transcriptional control of microglia phenotypes in health and disease. *J Clin Invest.* (2017) 127:3220–9. doi: 10.1172/JCI90604
27. Prinz M, Priller J, Sisodia SS, Ransohoff RM. Heterogeneity of CNS myeloid cells and their roles in neurodegeneration. *Nat Neurosci.* (2011) 14:1227–35. doi: 10.1038/nn.2923
28. Kichev A, Eede P, Gressens P, Thornton C, Hagberg H. Implicating receptor activator of NF-kB (RANK)/RANK ligand signalling in microglial responses to toll-like receptor stimuli. *Dev Neurosci.* (2017) 39:192–206. doi: 10.1159/000464244
29. Serrano EM, Ricofort RD, Zuo J, Ochotny N, Manolson MF, Holliday LS. Regulation of vacuolar H(+)-ATPase in microglia by RANKL. *Biochem Biophys Res Commun.* (2009) 389:193–7. doi: 10.1016/j.bbrc.2009.08.122
30. Hofbauer LC, Cepok S, Hemmer B. Osteoprotegerin is highly expressed in the spinal cord and cerebrospinal fluid. *ActaNeuropathol.* (2004) 107:575–7. doi: 10.1007/s00401-004-0854-y
31. Zhao ZM, Lu SH, Zhang QJ, Liu HY, Yang RC, Cai YL, et al. The preliminary study on in vitro differentiation of human umbilical cord blood cells into neural cells. *Chinese J Hematol.* (2003) 24:484–7.
32. Yin J, Valin KL, Dixon ML, Laevenworth JW. The role of microglia and macrophages in CNS homeostasis, autoimmunity, and cancer. *J Immunol Res.* (2017) 2017:5150678. doi: 10.1155/2017/5150678
33. Varol C, Mildner A, Jung S. Macrophages: development and tissue specialization. *Annu Rev Immunol.* (2015) 33:643–75. doi: 10.1146/annurev-immunol-032414-112220
34. Lambertsen KL, Biber K, Finsen B. Inflammatory cytokines in experiemental and human stroke. *J Cereb Blood Flow Metab.* (2012) 32:1677–98. doi: 10.1038/jcbfm.2012.88
35. Kichev A, Rousset CI, Baburamani AA; Levison SW, Wood TL, Gressens P, et al. Tumor Necrosis Factor-related Apoptosis-inducing Ligand (TRAIL) signaling and cell death in the immature central nervous system after hypoxia-ischemia and inflammation. *J Biol Chem.* (2014) 289:9430–9. doi: 10.1074/jbc.M113.512350
36. Lenz KM, Nelson LH. Microglia and beyond: innate immune cells as regulators of brain development and behavioural function. *Front Immunol.* (2018) 9:698. doi: 10.3389/fimmu.2018.00698
37. Augusto-Oliveira M, Arrifano GP, Lopes-Araujo A, Santos-Sacrament L, Takeda PY, Anthony DC. What do microglia really do in healthy adult brain? *Cells.* (2019) 8:1293. doi: 10.3390/cells8101293
38. Tang Y, Le W. Differential roles of M1 and M2 microglia in neurodegenerative diseases. *Mol Neurobiol.* (2016) 53:1181–94. doi: 10.1007/s12035-014-9070-5
39. Arcuri C, Mecca C, Bianchi R, Giambanco I, Donato R. The pathophysiological role of microglia in dynamic surveillance, phagocytosis and structural remodeling of the developing CNS. *Front Mol Neurosci.* (2017) 10:191. doi: 10.3389/fnmol.2017.00191
40. Ransohoff RM. A polarizing question: do M1 and M2 microglia exist? *Nat Neurosci.* (2016) 19:987–91. doi: 10.1038/nn.4338
41. Lively S, Schlichter LC. Microglia responses to pro-inflammatory stimuli (LPS, IFNγ+TNFα) and reprogramming by resolving cytokines (IL-4, IL-10). *Front Cell Neurosci.* (2018) 12:215. doi: 10.3389/fncel.2018.00215
42. Orihuela R, McPherson CA, Harry GJ. Microglial M1/M2 polarization and metabolic states. *Br J Pharmacol.* (2016) 173:649–65. doi: 10.1111/bph.13139
43. Khooroshi R, Dieu R, Arpe MLH, Cedile O, Morch MT, Lienenklaus S, et al. Type I interferon and receptor activator of nuclear factor Kappa B signaling within the central nervous system. *43rd Meeting of the Scandinavian-Society-for-Immunology*. Turku (2016).
44. Lan X, Han X, Li Q, Yang Q, Wang J. Modulators of microglial activation and polarization after intracerebral haemorrhage. *Nat Rev Neurol.* (2017) 13:420–33. doi: 10.1038/nrneurol.2017.69
45. Ley K. M1 means kill; M2 means heal. *J Immunol.* (2017) 199:2193. doi: 10.4049/jimmunol.1701135
46. Prajeeth CK, Lohr K, Floes S, Zimmerman J, Ulrich R, Gudi V, et al. Effector molecules released by Th1 but not Th17 cells drive an M1 response in microglia. *Brain Behav Immun.* (2014) 37:248–59. doi: 10.1016/j.bbi.2014.01.001
47. Prajeeth CK, Dittrich-Breiholz O, Talbot SR, Robert PA, Huehn J, Stangel M. IFN-γ producing Th1 cells induce different transcriptional profiles in microglia and astrocytes. *Front Cell Neurosci.* (2018) 12:352. doi: 10.3389/fncel.2018.00352
48. Iadecola C, Anrather J. The immunology of stroke: from mechanisms to translation. *Nat Med.* (2011) 17:796–808. doi: 10.1038/nm.2399
49. Shimamura M, Nakagami H, Osako MK, Kurinami H, Koriyama H, Zhengda P, et al. OPG/RANKL/RANK axis is a critical inflammatory signaling system in ischaemiac brain in mice. *Proc Natl Acad Sci USA.* (2014) 111:8191–6. doi: 10.1073/pnas.1400544111
50. Mantovani A, Sica A, Sozzani S, Allavena P, Vecchi A, Locati M. The chemokine system in diverse forms of macrophage activation and polarization. *Trends Immunol.* (2004) 25:677–86. doi: 10.1016/j.it.2004.09.015
51. Sakai S, Shichita T. Inflammation and neural repair after ischaemic brain injury. *Neurochem Int.* (2019) 130:104316. doi: 10.1016/j.neuint.2018.10.013
52. Ferrari-Lacraz S, Ferrari S. Do RANKL inhibitors (denosumab) affect inflammation and immunity? *Osteoporos Int.* (2011) 22:435–46. doi: 10.1007/s00198-010-1326-y
53. Kurinami H, Shimamura M, Nakagami H, Shimizu H, Koriyama H, Kawano T, et al. A novel therapeutic peptide as a partial agonist of RANKL in ischaemic stroke. *Sci Rep.* (2016) 6:38062. doi: 10.1038/srep38062
54. Shimamura M, Nakagami H, Shimizu H, Mukai H, Watanabe R, Okuzono T, et al. Development of novel RANKL-based peptide, microglial healing peptide1-AcN (MHP-AcN), for treatment of ischaemic stroke. *Sci Rep.* (2018) 8:17770. doi: 10.1038/s41598-018-35898-z
55. Biscetti F, Straface G, Giovannini S, Santoliquido A, Angelini F, Santoro L, et al. Association between TNFRSF11B gene polymorphisms and history of

ischaemic stroke in Italian diabetic patients. *Hum Genet.* (2013) 132:49–55. doi: 10.1007/s00439-012-1224-9
56. Biscetti F, Giovannini S, Straface G, Bertucci F, Angelini F, Porreca C, et al. RANKL/RANK/OPG pathway: genetic association with history of ischemic stroke in Italian population. *Eur Rev Med Pharmacol Sci.* (2016) 20:4574. Available online at: https://www.europeanreview.org/wp/wp-content/uploads/4574-4580-RANKRANKLOPG-pathway-genetic-association-with-history-of-ischemic-stroke-in-Italian-population.pdf
57. Hoftberger R. Neuroimmunology: an expanding frontier in autoimmunity. *Front Immunol.* (2015) 6:206. doi: 10.3389/fimmu.2015.00206
58. Dendrou CA, Fugger L, Friese MA. Immunopathology of multiple sclerosis. *Nat Rev Immunol.* (2015) 15:545–58. doi: 10.1038/nri3871
59. Pilli D, Zou A, Tea F, Dale RC, Brilot F. Expanding role of T cells in human autoimmune diseases of the central nervous system. *Front Immunol.* (2017) 8:652. doi: 10.3389/fimmu.2017.00652
60. Stephenson J, Nutma E, van der Valk P, Amor S. Inflammation in the CNS neurodegenerative diseases. *Immunology.* (2018) 154:204–19. doi: 10.1111/imm.12922
61. Owens T, Bechmann I, Engelhardt B. Perivascular spaces and the two steps to neuroinflammation. *J Neuropathol Exp Neurol.* (2008) 67:1113–21. doi: 10.1097/NEN.0b013e31818f9ca8
62. de Paula Alves Sousa A, Johnson KR, Nicholas R, Darko S, Price DA, Douek DC, et al. Intrathecal T-cell clonal expansions in patients with multiple sclerosis. *Ann ClinTransl Neurol.* (2016) 3:422–33. doi: 10.1002/acn3.310
63. Kuwabara T, Ishikawa F, Kondo M, Kakiuchi T. The role of IL-17 and related cytokines in inflammatory autoimmune diseases. *Mediators Inflamm.* (2017) 2017:3908061. doi: 10.1155/2017/3908061
64. Yue Y, Stone S, Lin W. Role of nuclear factor kb in multiple sclerosis and experimental autoimmune encephalomyelitis. *Neural Regen Res.* (2018) 13:1507–15. doi: 10.4103/1673-5374.237109
65. Guerrini MM, Okamoto K, Komatsu N, Sawa S, Danks L, Penninger JM, et al. Inhibition of the TNF family cytokine RANKL prevents autoimmune inflammation in the central nervous system. *Immunity.* (2015) 43:1174–85. doi: 10.1016/j.immuni.2015.10.017
66. Wagner CA, Roque PJ, Goverman JM. Pathogenic T cell cytokines in multiple sclerosis. *J Exp Med.* (2019) 217:e20190460. doi: 10.1084/jem.20190460
67. Yi H, Bai Y, Zhu X, Lin L, Zhao L, Wu X, et al. IL-17A induces MIP-1a expression in primary astrocytes via Src/MAPK/PI3K/NF-kB pathways: implication for multiple sclerosis. *J NeuroimmunePharmacol.* (2014) 9:629–41. doi: 10.1007/s11481-014-9553-1
68. Kurban S, Akpinar Z, Mehmetoglu I. Receptor activator of nuclear factor kappaB ligand (RANKL) and osteoprotegerin levels in multiple sclerosis. *Mult Scler.* (2008) 14:431–2. doi: 10.1177/1352458507084028
69. Alatab S, Maghbooli Z, Hossein-Nezhad A, Khosrofar M, Mokhtari F. Cytokine profile, Foxp3 and nuclear factor-kB ligand levels in multiple sclerosis subtypes. *Minerva Med.* (2011) 102:461–8.
70. Glasnović A, Stojić M, DeŽmalj L, Tudorić-Deno I, Romić D, Jeleč V, et al. RANKL/RANK/OPG axis is deregulated in the cerebrospinal fluid of multiple sclerosis patients at clinical onset. *Neuroimmunomodulation.* (2018) 25:23–33. doi: 10.1159/000488988
71. Weinstock-Guttman B, Hong J, Santos R, Tamano-Blanco M, Badgett D, Patrick K, et al. Interferon-beta modulates bone-associated cytokines and osteoclast precursor activity in multiple sclerosis patients. *MultScler.* (2006) 12:541–50. doi: 10.1177/1352458506070605
72. Mirzaei K, Ahmadi S, Hossein-Nezhad A, Mokhtari F. Potential role of OPG/RANKL system and FokI genotypes in pathogenesis and clinical manifestations in multiple sclerosis. *Minerva Med.* (2012) 103:313–21.
73. Holmoy T, Loken-Amsrud KI, Bakke SJ, Beiske AG, Bjerve KS, Hovdal H, et al. Inflammation markers in multiple sclerosis: CXCL 16 reflects and may also predict disease activity. *PLoS ONE.* (2013) 8:e75021. doi: 10.1371/journal.pone.0075021
74. Carrieri PB, Carbone F, Perna F, Bruzzese D, La Rocca C, Galgani M, et al. Longitudinal assesment of immuno-metabolic parameters in multiple sclerosis patients during treatment with glatiramer acetate. *Metabolism.* (2015) 64:1112–21. doi: 10.1016/j.metabol.2015.05.001
75. Kohler BA, Ward E, McCarthy BJ, Schymura MJ, Ries LA, Eheman C, et al. Annual report to the nation on the status of cancer, 1975-2007, featuring tumors of the brain and other nervous system. *J Natl Cancer Inst.* (2011) 103:714–36. doi: 10.1093/jnci/djr077
76. Ostrom QT, Gittleman H, Truitt G, Boscia A, Kruchko C, Barnholz-Sloan JS. CBTRUS statistical report: primary brain and other central nervous system tumors diagnosed in the United States in 2011-2015. *Neuro Oncol.* (2018) 20:iv1–86. doi: 10.1093/neuonc/noy131
77. Vladimirova V, Waha A, Luckerath K, Pesheva P, Probmeier R. Runx2 is expressed in human glioma cells and mediates the expression of galectin-3. *J Neurosci Res.* (2008) 86:2450–61. doi: 10.1002/jnr.21686
78. Naumann U, Wick W, Beschorner R, Meyermann R, Weller M. Expression and functional activity of osteoprotegerin in human malignant gliomas. *Acta Neuropathol.* (2004) 107:17–22. doi: 10.1007/s00401-003-0772-4
79. Chang AL, Miska K, Wainwright DA, Dey M, Rivetta CV, Yu D, et al. CCL2 Produced by the glioma microenvironment is essential for the recruitment of regulatory T cells and myeloid-derived suppressor cells. *Cancer Res.* (2016) 76:5671–82. doi: 10.1158/0008-5472.CAN-16-0144
80. Chang AL. The CCL2 chemokine axis recruits regulatory T cells and myeloid-derived suppressor cells in glioblastoma multiforme. Chicago, IL: The University of Chicago, ProQuest Dissertations Publishing (2017).
81. Kim JK, Jin X, Sohn YM, Jin X, Jeon HY, Kim EJ, et al. Tumoral RANKL activates astrocytes that promote glioma cell invasion through cytokine signaling. *Cancer Lett.* (2014) 353:194–200. doi: 10.1016/j.canlet.2014.07.034
82. Chen L, Zhuang G, Li W, Liu Y, Zhang J, Tian X. RGD-FasL induces apoptosis of pituitary adenoma cells. *Cell Mol Immunol.* (2008) 5:61–8. doi: 10.1038/cmi.2008.8
83. Chen L, Tian X, Li W, Agarwal A, Zhuang G. Expressions of Fas/DcR3 and RGD-FasL mediated apoptosis in pituitary adenomas. *Neurol India.* (2009) 57:28–30. doi: 10.4103/0028-3886.48808
84. Lisakovska O, Shymanskyy I, Mazanova A, Khomenko A, Veliky M. Vitamin D3 protects against prednisolone-induced liver injury associated with the impairment of the hepatic NF-kB/INOS/NO pathway. *Biochem Cell Biol.* (2017) 95:213–22. doi: 10.1139/bcb-2016-0070
85. Lisakovska O, Labudzynskyi D, Savosko S, Shymanskyy, Veliky M. Vitamin D3 exerts a protective effect on glucocorticoid-induced neurotoxicity in rats via modulation of signaling through receptor activator of NF-kappa B. *30th Congress of the European-College-of-Neuropsychopharmacology*. Paris (2017).
86. Zhu P, Zhang Z, Huang X, Liang S, Khandekar N, Song Z, et al. RANKL reduces body weight and food intake via the modulation of hypothalamic NPY/CART pathway expression. *Int J Med Sci.* (2018) 15:969–77. doi: 10.7150/ijms.24373
87. Lee NJ, Clarke IM, Enriquez RF, Nagy V, Penninger J, Baldock PA, et al. Central RANK signalling in NPY neurons alters bone mass in male mice. *Neuropeptides.* (2018) 68:75–83. doi: 10.1016/j.npep.2018.02.004
88. Hanada R, Penninger JM. Central regulation of body temperature by RANKL/RANK pathway. *Clinical Calcium.* (2011) 21:1201–8.
89. Hanada R, Leibbrandt A, Hanada T, Kitaoka S, Furuyashiki T, Fujihara H, et al. Central control of fever and female body temperature by RANKL/RANK. *Nature.* (2009) 462:505–9. doi: 10.1038/nature08596
90. Adler EM. RANKLed about fevers? *Sci Signal.* (2009) 2:ec389. doi: 10.1126/scisignal.2100ec389

Conflict of Interest: The authors declare that the research was conducted in the absence of any commercial or financial relationships that could be construed as a potential conflict of interest.

frontiers in Immunology

MINI REVIEW
published: 08 December 2020
doi: 10.3389/fimmu.2020.614972

Honing the Double-Edged Sword: Improving Human iPSC-Microglia Models

Anne Hedegaard[†], *Szymon Stodolak*[†], *William S. James and Sally A. Cowley*[*]

Sir William Dunn School of Pathology, University of Oxford, Oxford, United Kingdom

Human induced Pluripotent Stem Cell (hiPSC) models are a valuable new tool for research into neurodegenerative diseases. Neuroinflammation is now recognized as a key process in neurodegenerative disease and aging, and microglia are central players in this. A plethora of hiPSC-derived microglial models have been published recently to explore neuroinflammation, ranging from monoculture through to xenotransplantation. However, combining physiological relevance, reproducibility, and scalability into one model is still a challenge. We examine key features of the *in vitro* microglial environment, especially media composition, extracellular matrix, and co-culture, to identify areas for improvement in current hiPSC-microglia models.

Keywords: microglia, human, induced pluripotent stem cells, *in vitro* models, media composition, 3D scaffolds, co-culture, physiological relevance

OPEN ACCESS

Edited by:
Amanda Sierra, Achucarro Basque Center for Neuroscience, Spain

Reviewed by:
Mathew Blurton-Jones, University of California, Irvine, United States
Simona Lange, Roche, Switzerland

***Correspondence:**
Sally A. Cowley
sally.cowley@path.ox.ac.uk

[†]*These authors have contributed equally to this work*

Specialty section:
This article was submitted to Multiple Sclerosis and Neuroimmunology, a section of the journal Frontiers in Immunology

Received: *07 October 2020*
Accepted: *04 November 2020*
Published: *08 December 2020*

Citation:
Hedegaard A, Stodolak S, James WS and Cowley SA (2020) Honing the Double-Edged Sword: Improving Human iPSC-Microglia Models. Front. Immunol. 11:614972. doi: 10.3389/fimmu.2020.614972

INTRODUCTION

Microglia represent a branch of tissue-resident macrophages which originate primarily in the yolk sac (1) and finally mature in the central nervous system (CNS) (2, 3). Once within the CNS, microglia function as important homeostatic cells and innate immune sentinels, attracting the analogy of a double-edged sword through their contribution to both health and disease. They influence developing neural networks by regulating the rate of neurogenesis and pruning neuronal synapses [(4), reviewed by (5)]. As ramified cells, they aid brain homeostasis by surveying the brain parenchyma and clearing cellular debris. However, as amoeboid cells, they secrete cytokines in response to pathogens (e.g. viral infection), misfolded proteins (e.g. Alzheimer's disease), or cellular damage (e.g. brain injury). The cytokine response can exacerbate neuronal damage if prolonged, contributing to chronic neurodegenerative disease [(6), reviewed by (7)]. This key pathological process is still inadequately understood, hindered by the lack of good quality *in vitro* models.

WHY USE hiPSC-MICROGLIA TO MODEL MICROGLIA?

Human induced Pluripotent Stem Cells (hiPSC) offer unprecedented advantages over other commonly used primary and immortalized cell cultures, notably human genetic background, normal karyotype, limitless self-renewal, and suitability for gene editing [reviewed by (8)]. The human genetic background solves the poor representation of disease-relevant gene orthologs in

mouse models (9, 10) deemed partly responsible for the poor success-rate of translating therapeutic modalities from mouse studies into the clinic [reviewed by (11, 12)]. Many neurological diseases are multigenic, and therefore particularly difficult to model in mice, whereas hiPSC enable representation of extremes of polygenic risk score (13), and endogenous levels of protein expression.

Microglial identity is driven by both developmental origin and brain environment [reviewed by (14)]. They derive from early waves of primitive yolk sac macrophages, which migrate to the brain rudiment even before neural progenitors develop (1, 15), and are maintained by local self-renewal throughout life (16). Several strategies have been published recently to derive microglia from hiPSC, which generally mirror the main characteristics of primitive hematopoiesis, including dependence on PU.1 and IRF8 transcription factors and MYB independence [(15, 17) reviewed by (18)], though the *in vitro* developmental pathway does not necessarily conform exactly to *in vivo* primitive waves. While mesoderm/hemogenic endothelium/myeloid differentiation can be achieved using simple growth factor cocktails (minimally BMP4, VEGF, SCF, followed by IL-3, M-CSF), mature microglial identity subsequently relies on cues present in the CNS environment, and this is where protocols differ in terms of their final medium composition and use of monoculture *versus* co-culture to induce microglial maturation (19–28). Some protocols have been more widely adopted and implemented within independent labs and used at scale by companies, making them highly reproducible [see (19, 26, 29) and (25) adopted by (27, 30)].

Within hours of isolation from the brain, both human and rodent primary microglia downregulate several key mature microglial markers, particularly TMEM119, P2RY12, and SALL1 (2, 31), which can be restored upon re-transplantation into the brains of microglia-deficient mice (32). Likewise, hiPSC-microglia assume the closest identity to *in vivo* microglia when they are transplanted into rodent brains (9, 19, 33–35). However, this is clearly not practical for high-throughput experiments, and is still limited by the xenogenic environment. Therefore, further improving *in vitro* hiPSC-microglia models to better represent their *in vivo* counterparts remains paramount. The pros and cons of different hiPSC-microglia models, and their application for disease modeling, have been reviewed recently (18, 36–39), but how to improve the physiological relevance of these models is an under-covered area. In this mini review, we focus on how to better mimic the CNS habitat, with relevant media composition, extracellular matrix, and co-culture, which will further improve the physiological applications and reproducibility of existing *in vitro* hiPSC-microglia protocols.

IMPROVING hiPSC-MICROGLIA MEDIA COMPOSITION

To better understand, compare, and control hiPSC-microglia, we need fully defined, open-source media, which not only supply relevant survival/differentiation factors, but also reflect the composition of the brain interstitial fluid, mimicking ionic composition, energy-substrates, nutrients, minerals, vitamins, pH, and osmolarity. However, many conventional media compositions are not at all physiological, but rather a hangover from culturing cancer cell lines with high metabolic and proliferative rates. Firstly, media with high levels of glucose (up to 25 mM, *versus* physiological levels of 5 mM), can mask cellular phenotypes (40, 41), which is problematic, as microglial metabolic dysregulation is associated with disease phenotype (42). Secondly, while serum is a major source of nutrients, and its use made cell-culture of microglia possible in the first place (43), it is still often used for *in vitro* culture of glial cells, despite the fact that glia are not exposed to serum under normal conditions *in vivo*, as they are separated by the blood-brain barrier [reviewed by (44)]. Further, each serum batch is different, its composition is undefined, and it contains lipopolysaccharide (LPS)-binding proteins which aid binding to toll-like receptor 4 (TLR4), thereby enhancing microglial responses to LPS (45). Thirdly, a hangover from explant cultures are components which contain immunosuppressive molecules, notably B27 supplement, developed to prevent excessive cell death and reactivity, but which interfere with microglia responses (46).

Defined, more physiological media now exist [e.g. BrainPhys (47)], and serum-free conditions have been demonstrated to be viable for rodent microglia with the recently developed "TIC media." TIC supplements DMEM/F12 with astrocyte-derived factors TGF-β, IL-34, and cholesterol (32). TGF-β promotes maturation and specialization of microglia within the developing brain, helps maintain the identity of cultured microglia [both when isolated as primary cells (2, 31) or derived from human iPSCs (19)], and encourages an anti-inflammatory quiescent microglia phenotype (48). IL-34 is the main ligand in the brain for Colony Stimulating Factor 1 receptor (CSF-1R), signaling through which is essential for microglial survival (1, 49). Cholesterol further improved the benefit conveyed by IL-34/TGF-β, despite myeloid cells being capable of *de novo* cholesterol synthesis [(50) reviewed by (51)]. However, despite TIC factors enabling survival, serum was still required to initiate microglial phagocytic activity (32). Overall, whilst the field is clearly moving towards defined, physiological media for hiPSC-microglia, serum confounds this, and use of immunomodulatory additives needs to be noted when comparing inflammatory responses across studies.

IMPROVING hiPSC-MICROGLIA THROUGH SCAFFOLDED 3D EXTRACELLULAR ENVIRONMENT

Microglia *in vivo* are embedded in a three-dimensional network of macromolecules derived from both neuronal and glial cells, mainly glycosaminoglycans (e.g. hyaluronic acid), proteoglycans, glycoproteins, and low levels of fibrous proteins (including collagen, laminin, fibronectin, and vitronectin), creating a rather "soft," viscoelastic brain environment of ~3 kPa (52, 53).

Unfortunately, these basic features are mostly absent in conventional *in vitro* conditions. Mimicking this 3D extracellular environment should enable hiPSC-microglia to adopt a more authentic phenotype. This is particularly important as immune cells are especially prone to develop unwanted and inflammatory responses to a suboptimal environment, such as covalently cross-linked (purely elastic) synthetic matrices, which lack viscoelastic properties [(54), reviewed by (55)].

3D cell culture, both scaffolded and scaffold-free, is becoming more widely used, as it preserves natural cell shape, supports cell-to-cell and cell-to-matrix communication, enhances cell differentiation, and pushes gene and protein expression towards that found *in vivo* [reviewed by (56)]. Surprisingly, only a few groups have cultured microglial cells in a 3D scaffolded environment (**Table 1**), and several of them primarily focus on other cell types co-cultured with microglia, including neurons (70) and glioblastoma cells (71, 72). To properly distinguish the effects attributable to 3D conditions, systematic studies using relevant 2D controls are required for appropriate comparisons to be made.

Scaffolded 3D culture influences microglial morphology and attachment, but the outcome depends on the scaffold composition and structure. Choosing a material that optimizes microglial phenotype still remains a challenge. Hydrogels of synthetic peptide (68), collagen (61, 64), or PEG (66) enhanced ramification in both postnatal rat microglia and immortalized murine BV-2 cells. Likewise, primary rat microglia cultured within a 3D fibrous poly(trimethylene carbonate-co-ϵ-caprolactone) scaffold had smaller cells with elongated processes *versus* cells attached to flat solvent-cast films (69). However, this was not observed in 3D graphene scaffolds, where BV-2 cells remained mostly amoeboid (65). Some peptides, like neural cell adhesion molecule (NCAM)-derived KHIFSDDSSE, favor neuron and astrocyte attachment but not microglial attachment (73). Functionalizing hydrogels with extracellular matrix (ECM) components have provided mixed results; a basal lamina mixture prompted primary postnatal rat microglia within a glial co-culture to disperse throughout the hyaluronic acid-based scaffold (59), whereas coating a collagen hydrogel with fibronectin and laminin decreased ramification in BV-2 cells (64).

3D culture can also affect microglial behavior and interaction with other cell types. Neuronal survival in conditioned media from 3D-cultured BV-2 cells was higher than from 2D-cultured cells, and LPS-induced BV-2-mediated neuronal toxicity was also reduced as a result of 3D microglial culture (65). Meanwhile, more BV-2 cells upregulated CD40 (induced through NF-κB and STAT-1α) in response to LPS when in 3D collagen than in 2D (61), suggesting a more homogenous inflammatory response in 3D (74). Although BV-2 and other immortalized cell lines have been a valuable resource for studying microglia, it is likely that microglial responses to a 3D environment might be masked or even reversed by the aberrantly proliferative and primed state of such cells (75, 76). Nonetheless, 3D culture of microglia in specific scaffolds seems to promote a production of growth factors and an anti-inflammatory phenotype beneficial to other cell types.

IMPROVING hiPSC-MICROGLIA THROUGH CO-CULTURE

The simplest approach to study cross-talk between microglia and neurons or astrocytes, is by transferring medium conditioned by these cells cultured separately. This provides a high level of experimental control, as the conditioned media can be analyzed independently to identify cytokines produced by stimulated microglia (77), assess the impact of individual factors on survival (32), or interrogate the process studied using drugs. However, conditioned media only allows study of uni-directional signaling. Transwells or Boyden chambers allow different cell types to exchange secreted factors bi-directionally [reviewed by (78)]. This improves physiological relevance but offers less insight into which cell type the secreted signals originated from, or control over which cells are targeted with any manipulation or drug given. Furthermore, these culture methods are also limited by the effective concentration of secreted signals, being much lower compared to local concentrations if cells were in physical contact.

To fully capture the physiology of cellular interactions, physical contact-mediated cues, through receptor-ligand interactions, are required. Microglial quiescence is maintained through neuronal CD200 glycoprotein interaction with the microglial CD200 receptor [(79) reviewed by (80)], as well as neuronal transmembrane (but possibly also secreted) CD22 interaction with microglial CD45 receptors (81). The mainly neuronal chemokine CX3CL1 ("fractalkine") maintains microglia in a surveying state when the membrane-bound form makes contact with the microglial CX3CR1 receptors, whereas soluble CX3CL1 has a chemoattractant effect on microglia [(82), reviewed by (83)]. Furthermore, the idea that electrical activity from neurons might play a role in immune-response suppression has been around for two decades (84), but the nature of this interaction is not well understood. Generating physical-contact co-cultures would evidently enable microglia to experience all modes of interaction with other cell types, yet when increasing the physiological relevance of the culture model, the degree of control over the experimental system decreases, highlighting the importance of choosing the appropriate culture-model for each research question (**Figure 1**).

Most hiPSC-microglia studies have focused on characterizing the gene expression and functionality of the resulting microglia in monoculture [reviewed by (8, 36)], but a few have included co-cultures with neurons (19, 24, 27) in 2D (3D co-cultures will be discussed later). Physical contact with neurons increases the expression of mature microglial genes, enhances ramified morphology compared to conditioned media, as well as eliciting a dampened response to LPS + IFNγ, high microglial motility and extension of processes to sites of injury (19, 24, 27), reflecting the homeostatic surveillance and response to injury associated with microglia *in vivo* (85). The exact cues responsible for these phenotypes are yet to be elucidated. Our understanding of interactions between microglia and astrocytes is limited, these cells typically being examined in isolation, but interest in their complex relationship, in terms of maintaining homeostasis in

TABLE 1 | Key studies of microglial culture in 3D scaffolds.

	Material	Modifications	Serum	Microglia	Observations	Reference
NATURAL HYDROGEL AND DERIVATIVES	Alginate	RGD sequence	√	Fetal rat primary	1. Amoeboid morphologies over 2 weeks	Frampton et al. (57)
	Methacrylated hyaluronic acid	×	√	Postnatal rat primary	1. Heterogenous morphology (mostly amoeboid) 2. Microglia wrapped processes around other cells—perhaps phagocytosis or cell–cell interaction	Jeffery et al. (58)
	Hyaluronic acid	Combined with basal lamina mixture	√	Postnatal rat primary	1. Microglia in 3D hyaluronic acid hydrogel mostly small with few processes 2. Microglia in 3D hyaluronic acid lamina hydrogel more dispersed and more thin processes	Koss et al. (59)
	Hyaluronic acid-gelatin	Combined with Gelin-S and heparin	√	Human fetal immortalized CHME3	1. Protective effect of microglia on GBM greater in the 3D model when challenged with cytotoxics 2. Microglia promoted GBM proliferation more in 3D *vs* 2D	Leite et al. (60)
	Collagen I	×	√	Murine immortalized BV-2	1. 3D collagen promotes multiplanar projections 2. Increased inflammatory response following LPS stimulation *versus* 2D collagen coating	Haw et al. (61)
	Collagen I	×	√	Murine immortalized BV-2	3D collagen hydrogel *vs* 2D uncoated: 1. Smaller fold change in gene expression following LPS treatment 2. Smaller fold changes in ROS production following LPS treatment	Cho et al. (62)
	Matrigel	×	√	Human immortalized SV40	1. Microglia seeded in 3D Matrigel in an angular chamber presented protrusions 2. Microglia only migrated to the central chamber with neurons and astrocytes when neural cells were overexpressing Aβ 3. Once together with neurons and astrocytes, microglia were actively in contact with neurons and astrocytes by expanding and retracting their protrusions	Park et al. (63)
SYNTHETIC HYDROGEL & OTHERS	Synthetic peptide	Fibronectin or collagen I coating	√	Murine immortalized BV-2	1. Peptide hydrogel promoted ramification 2. Fibronectin or collagen addition promoted deramification	Pöttler et al. (64)
	Graphene foam	×	√	Murine immortalized BV-2	3D graphene *vs* 2D graphene: 1. did not induce further microglial ramification 2. decreased NO production following LPS stimulation 3. Conditioned medium (CM) promoted greater survival of mouse primary neural stem cells 5. CM rescued LPS-induced neuroinflammation	Song et al. (65)
	PEG	MMP-degradable peptide cross-links and CRGDS sequence peptide	×	Derived from human ESC line H1	1. Microglia adopted both ramified and ameboid morphologies in 3D co-culture with other brain cell types	Schwartz et al. (66)
	Graphene foam	×	√	Murine immortalized BV-2	1. CM from microglia in 3D graphene (*vs* 2D graphene) promoted neurosphere formation, facilitated mouse primary NSC migration from neurospheres, and increased single cell polarization by activating the SDF-1α/CXCR4 signaling pathway and enhanced cell adhesion on the substrate.	Jiang et al. (67)
	Fmoc–Phe3 peptide	×	√	Postnatal rat primary	1. Fmoc–Phe3 peptide hydrogel stimulated microglial proliferation and NGF secretion (due to the peptide, not 3D conditions)	Chronopoulou et al. (68)
	P(TMC-CL)	×	√	Postnatal rat primary	1. Cells cultured within a 3D P(TMC-CL) scaffold were smaller and with elongated processes compared to cells cultured on a P(TMC-CL) flat film. 2. Following exposure to myelin, only cells in 2D conditions presented abberant multinucleated phenotype	Pires et al. (69)

Aβ, amyloid beta; CM, conditioned media; CRGDS, peptide sequence of Cys-Arg-Gly-Asp-Ser present in fibronection; CXCR4, C-X-C chemokine receptor 4; ESC, embryonic stem cell; GBM, glioblastoma multiforme; LPS, lipopolysaccharide; MMP, matrix metalloproteinase; NGF, nerve growth factor; NO, nitric oxide; NSC, neural stem cell; PEG, polyethylene glycol; P(TMC-CL), poly(trimethylene carbonate-co-ϵ-caprolactone); RGD, tripeptide motif of Arg-Gly-Asp present in fibronectin; SDF-1α, stromal cell-derived factor 1 α.

health and reactive cross-talk in disease, is growing [reviewed by (86)]. Pandya et al. used astrocytes as a feeder layer for maturing their hiPSC-microglia for 1–2 weeks before isolating the $CD39^+$ microglia for monoculture (23), but interactions between mature hiPSC-microglia and astrocytes are otherwise currently under-explored.

The maturity and functionality of the non-microglial co-cultured cells is important to consider, as crucial microglial

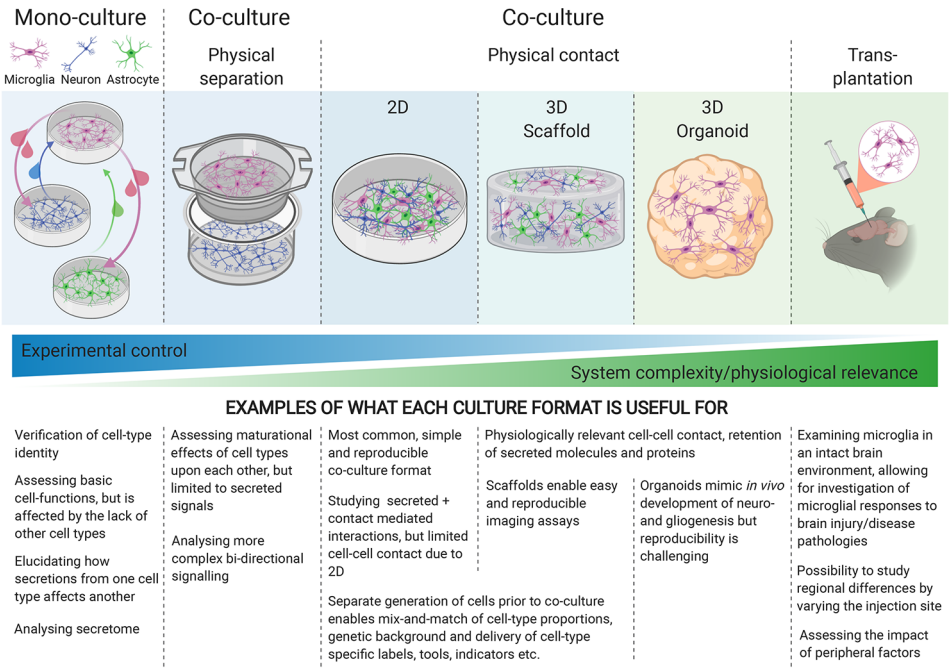

FIGURE 1 | Different culture environments convey different levels of experimental control and physiological relevance, with mono-cultures at one end of the spectrum, and transplantation into intact brains at the other. The experimental question being investigated should guide the choice of culture-system.

functions like synaptic pruning are likely only observable if the synaptic network is sufficiently mature, which may depend on more than bi-culture. Tri-culture of microglia with neurons and astrocytes will enable further maturation, more fully capture additional aspects of cross-talk and identify potential compensatory mechanisms between different brain cell types. Microglia and astrocytes operate in concert, both possessing that "double-edged sword" capacity to either support neuronal recovery (simplistically, "helpful" M2 and A2 phenotypes) or cause neuronal death ("harmful" M1 and A1 reactive phenotypes) [(77) reviewed by [87)]. A primary rodent tri-culture system of neurons, astrocytes and microglia in serum-free conditions (using TIC-supplemented media) shows promise in modeling different neuroinflammatory scenarios (88), in line with both *in vivo* and *in vitro* studies (77, 89, 90). However, TIC factors could not be omitted in the tri-cultures (88), indicating that endogenous secretion from the cultured astrocytes was not sufficient to retain a viable and physiologically active microglial phenotype. Interestingly, co-culture with hiPSC-neurons and astrocytes is capable of shifting the transcriptional profile of hiPSC-microglia further towards an *ex vivo* state than TIC media, although the gap between *in vitro* and *ex vivo* microglia is not fully closed (29).

Oligodendrocytes, endothelial cells, and/or vasculature are also likely to affect microglial function, yet they are rarely included in *in vitro* culture models, or assessment of their impact on microglia is lacking (66). Excitingly though, with the advent of single-cell RNAseq and single-cell proteomics, analyzing complex co-culture systems has become more straightforward and informative. These high-throughput methods allow for detection of overall cellular changes and activation/inactivation of biological pathways within each cell type, providing important clues to understand inter-cellular cross-talk. Using hiPSC, it is now possible to "mix and match" the genetic background of each cell type within the co-culture, such that the effect of a mutation can be studied in one cell type at a time. Strategies for co-culturing multiple hiPSC cell-types are increasingly popular and are beginning to move towards three dimensional environments as well.

COMBINING CO-CULTURE AND 3D ENVIRONMENT FOR hiSC-MICROGLIA

Providing microglia with a more physiologically relevant cellular environment relies on the principle of letting separately derived microglia populate pre-existing 3D neuronal cultures, brain organoids, or xenotransplantation into rodent brains [reviewed by (18)]. 3D scaffolded cultures confer a high degree of reproducibility and experimental flexibility, as individual cell types can be derived separately and added to the scaffold one at a time. This enables mix and match of co-cultures, i.e. cell types, ratios, genetic backgrounds, genetic tools, and fluorescent reporters. A 3D scaffold culture with microfluidic chambers has demonstrated that immortalized human SV40-derived microglia display ramified morphologies when seeded within Matrigel, migrate towards Amyloid-beta (Aβ)-expressing neurons, and cleave their axons while producing neurotoxic mediators (63). This encouraging study could be made more

physiologically relevant by replacing the genetically aberrant SV40-microglial cells with hiPSC-derived microglia, and mouse sarcoma-derived Matrigel with a defined hydrogel more reminiscent of brain ECM.

3D organoids preserve the human model context, yet high variability between organoid batches remains a technical challenge. Remarkably, cerebral organoids spontaneously containing microglia have been obtained (91), but this is only apparent when mesoderm is not sufficiently suppressed. More conventionally, organoids and microglia are derived separately, due to the differing ontogeny between ectodermally derived CNS cells and mesodermally derived microglia. Integrated microglia adopt ramified morphologies, display migration to the site of injury (19, 20, 28) and phagocytose Aβ (92).

Xenotransplantation offers the benefit of transplanting hiPSC-derived microglia into a more mature and structurally developed environment. However, immune-deficiency and expression of human CSF1 or IL34 are crucial for survival of the transplanted human microglia (33, 93), and ablation of host microglia is usually preferable. Excitingly, several recent xenotransplantation studies have detected improved hiPSC-microglial morphologies, with transcriptional profiles showing higher degrees of similarity between xenotransplanted microglia and freshly isolated human microglia than with cultured primary microglia (9, 33, 34). Meanwhile, the pattern of differentially expressed genes revealed a more muted response to LPS in transplanted cells than in *in vitro* cultured microglia (33). Engrafted microglia associate with Aβ plaques, appear to phagocytose them (19, 33), and upregulate disease-associated microglia markers, including CD9, MERTK, and TREM2 (33). Xenotransplantation is therefore a viable option for studying hiPSC-derived human microglia allowed to mature in an *in vivo* brain environment, where the issue of altered *in vitro* gene expression (31, 32) appears to have been resolved, but making this technique amenable to large scale-up will be extremely challenging.

DISCUSSION

Strides towards more physiological hiPSC-microglia culture conditions are being made apace, including the use of defined serum-free media in monoculture, the implementation of co-cultures, whether in 2D format, organoids, or xenotransplantation. One important underdeveloped gap in the repertoire is an *in vitro* model containing multiple hiPSC types embedded in a defined 3D scaffold, which would both enhance microglial identity and be amenable to advanced approaches, including arrayed drug screening, genome-wide CRISPR screens, high content imaging, cell multiplexing, and single cell transcriptomics. Further work is necessary to identify viscoelastic scaffold materials and ECM components that optimize microglial morphology, adhesion, and function. The process of neuroinflammation is arguably best modeled with all participating cell types present. Loss of function in astrocytes and/or microglia, impacting homeostatic support, or a toxic gain of function in the same cells, leading to the release of neurotoxic factors, would both probably have detrimental effects on neuronal health. Both scenarios are likely occurring in tandem in various neurodegenerative diseases, as well as in normal ageing, where defective phagocytosis as well as pro-inflammatory profiles have recently been reported (94, 95). Many links in the harmful inflammatory cascades that have been demonstrated to originate with microglia, propagate to astrocytes, and ultimately cause neurodegeneration, are not fully elucidated [(77), reviewed by (87)], and there is much more to learn about cross-talk and compensatory mechanisms between these cell types. Ultimately, the trade-off between the physiological relevance of a culture-system and experimental control over conditions must be decided based on the scientific question asked. Various hiPSC-microglia models will continue to be relevant, but the more defined and comparable we can make them, the better we will be able to understand and control the double-edged sword that is microglial function.

AUTHOR CONTRIBUTIONS

Conceptualization: SS, AH, and SC. Writing—Original Draft: SS and AH. Writing—Review and Editing: SS, AH, WJ, and SC. Funding Acquisition: WJ and SC. Supervision: WJ and SC. All authors contributed to the article and approved the submitted version.

FUNDING

We thank the following for financial support: The Oxford Martin School for core support to the James Martin Stem Cell Facility (LC0910-004; SC); BBSRC industrial CASE studentship (BB/M011224/1; SS); Eli Lilly and Company (AH, SS). The authors declare that this study received funding from Eli Lilly and Company. The funder was not involved in the study design, collection, analysis, interpretation of data, the writing of this article or the decision to submit it for publication.

ACKNOWLEDGMENTS

The figure was created with BioRender.com.

REFERENCES

1. Ginhoux F, Greter M, Leboeuf M, Nandi S, See P, Gokhan S, et al. Fate mapping analysis reveals that adult microglia derive from primitive macrophages. *Science (80)* (2010) 330:841–5. doi: 10.1126/science.1194637
2. Butovsky O, Jedrychowski MP, Moore CS, Cialic R, Lanser AJ, Gabriely G, et al. Identification of a unique TGF-β-dependent molecular and functional signature in microglia. *Nat Neurosci* (2014) 17:131–43. doi: 10.1038/nn.3599
3. Swinnen N, Smolders S, Avila A, Notelaers K, Paesen R, Ameloot M, et al. Complex invasion pattern of the cerebral cortex bymicroglial cells during development of the mouse embryo. *Glia* (2013) 61:150–63. doi: 10.1002/glia.22421

4. Paolicelli RC, Bolasco G, Pagani F, Maggi L, Scianni M, Panzanelli P, et al. Synaptic pruning by microglia is necessary for normal brain development. *Science (80)* (2011) 333:1456–8. doi: 10.1126/science.1202529
5. Sakai J. Core Concept: How synaptic pruning shapes neural wiring during development and, possibly, in disease. *Proc Natl Acad Sci USA* (2020) 117:16096–9. doi: 10.1073/pnas.2010281117
6. Matcovitch-Natan O, Winter DR, Giladi A, Aguilar SV, Spinrad A, Sarrazin S, et al. Microglia development follows a stepwise program to regulate brain homeostasis. *Science* (2016) 353(6301):aad8670. doi: 10.1126/science.aad8670
7. Li Q, Barres BA. Microglia and macrophages in brain homeostasis and disease. *Nat Rev Immunol* (2018) 18:225–42. doi: 10.1038/nri.2017.125
8. Sabogal-Guáqueta AM, Marmolejo-Garza A, de Pádua VP, Eggen B, Boddeke E, Dolga AM. Microglia alterations in neurodegenerative diseases and their modeling with human induced pluripotent stem cell and other platforms. *Prog Neurobiol* (2020) 190:101805. doi: 10.1016/j.pneurobio.2020.101805
9. Mancuso R, Van Den Daele J, Fattorelli N, Wolfs L, Balusu S, Burton O, et al. Stem-cell-derived human microglia transplanted in mouse brain to study human disease. *Nat Neurosci* (2019) 22:2111–6. doi: 10.1038/s41593-019-0525-x
10. Dubbelaar ML, Kracht L, Eggen BJL, Boddeke EWGM. The Kaleidoscope of Microglial Phenotypes. *Front Immunol* (2018) 9:1753. doi: 10.3389/fimmu.2018.01753
11. Sayed N, Liu C, Wu JC. Translation of Human-Induced Pluripotent Stem Cells from Clinical Trial in a Dish to Precision Medicine. *J Am Coll Cardiol* (2016) 67:2161–76. doi: 10.1016/j.jacc.2016.01.083
12. Dawson TM, Golde TE, Lagier-Tourenne C. Animal models of neurodegenerative diseases. *Nat Neurosci* (2018) 21:1370–9. doi: 10.1038/s41593-018-0236-8
13. Rehbach K, Zhang H, Das D, Abdollahi S, Prorok T, Ghosh S, et al. Publicly available hiPSC lines with extreme polygenic risk scores for modeling schizophrenia. *bioRxiv* (2020). doi: 10.1101/2020.07.04.185348
14. Bennett ML, Bennett FC. The influence of environment and origin on brain resident macrophages and implications for therapy. *Nat Neurosci* (2020) 23:157–66. doi: 10.1038/s41593-019-0545-6
15. Bian Z, Gong Y, Huang T, Lee CZW, Bian L, Bai Z, et al. Deciphering human macrophage development at single-cell resolution. *Nature* (2020) 582:571–6. doi: 10.1038/s41586-020-2316-7
16. Askew K, Li K, Olmos-Alonso A, Garcia-Moreno F, Liang Y, Richardson P, et al. Coupled Proliferation and Apoptosis Maintain the Rapid Turnover of Microglia in the Adult Brain. *Cell Rep* (2017) 18:391–405. doi: 10.1016/j.celrep.2016.12.041
17. Buchrieser J, James W, Moore MD. Human Induced Pluripotent Stem Cell-Derived Macrophages Share Ontogeny with MYB-Independent Tissue-Resident Macrophages. *Stem Cell Rep* (2017) 8:334–45. doi: 10.1016/j.stemcr.2016.12.020
18. Hasselmann J, Blurton-Jones M. Human iPSC-derived microglia: A growing toolset to study the brain's innate immune cells. *Glia* (2020) 68:721–39. doi: 10.1002/glia.23781
19. Abud EM, Ramirez RN, Martinez ES, Healy LM, Cecilia HH, Newman SA, et al. iPSC-derived human microglia-like cells to study neurological diseases. *Neuron* (2017) 94:278–93. doi: 10.1016/j.neuron.2017.03.042.iPSC-derived
20. Brownjohn PW, Smith J, Solanki R, Lohmann E, Houlden H, Hardy J, et al. Functional Studies of Missense TREM2 Mutations in Human Stem Cell-Derived Microglia. *Stem Cell Rep* (2018) 10:1294–307. doi: 10.1016/j.stemcr.2018.03.003
21. Claes C, Van Den Daele J, Boon R, Schouteden S, Colombo A, Monasor LS, et al. Human stem cell–derived monocytes and microglia-like cells reveal impaired amyloid plaque clearance upon heterozygous or homozygous loss of TREM2. *Alzheimer's Dement* (2019) 15:453–64. doi: 10.1016/j.jalz.2018.09.006
22. Douvaras P, Sun B, Wang M, Kruglikov I, Lallos G, Zimmer M, et al. Directed Differentiation of Human Pluripotent Stem Cells to Microglia. *Stem Cell Rep* (2017) 8:1516–24. doi: 10.1016/j.stemcr.2017.04.023
23. Pandya H, Shen MJ, Ichikawa DM, Sedlock AB, Choi Y, Johnson KR, et al. Differentiation of human and murine induced pluripotent stem cells to microglia-like cells. *Nat Neurosci* (2017) 20:753–9. doi: 10.1038/nn.4534
24. Takata K, Kozaki T, Lee CZW, Thion MS, Otsuka M, Lim S, et al. Induced-Pluripotent-Stem-Cell-Derived Primitive Macrophages Provide a Platform for Modeling Tissue-Resident Macrophage Differentiation and Function. *Immunity* (2017) 47:183–98.e6. doi: 10.1016/j.immuni.2017.06.017
25. Garcia-reitboeck P, Phillips A, Piers TM, Houlden H, Hardy J, Pocock JM, et al. Human Induced Pluripotent Stem Cell-Derived Mutations Show Specific Deficits in Phagocytosis Article Human Induced Pluripotent Stem Cell-Derived Microglia-Like Cells Harboring TREM2 Missense Mutations Show Specific Deficits in Phagocytosis. *CellReports* (2018) 24:2300–11. doi: 10.1016/j.celrep.2018.07.094
26. McQuade A, Coburn M, Tu CH, Hasselmann J, Davtyan H, Blurton-Jones M. Development and validation of a simplified method to generate human microglia from pluripotent stem cells. *Mol Neurodegener* (2018) 13:1–13. doi: 10.1186/s13024-018-0297-x
27. Haenseler W, Sansom SN, Buchrieser J, Newey SE, Moore CS, Nicholls FJ, et al. A Highly Efficient Human Pluripotent Stem Cell Microglia Model Displays a Neuronal-Co-culture-Specific Expression Profile and Inflammatory Response. *Stem Cell Rep* (2017) 8:1727–42. doi: 10.1016/j.stemcr.2017.05.017
28. Muffat J, Li Y, Yuan B, Mitalipova M, Omer A, Corcoran S, et al. Efficient derivation of microglia-like cells from human pluripotent stem cells. *Nat Med* (2016) 22:1358–67. doi: 10.1038/nm.4189
29. Grubman A, Vandekolk TH, Schröder J, Sun G, Hatwell-Humble J, Chan J, et al. A CX3CR1 Reporter hESC Line Facilitates Integrative Analysis of In-Vitro-Derived Microglia and Improved Microglia Identity upon Neuron-Glia Co-culture. *Stem Cell Rep* (2020) 14:1018–32. doi: 10.1016/j.stemcr.2020.04.007
30. Gutbier S, Wanke F, Dahm N, Rümmelin A, Zimmermann S, Christensen K, et al. Large-scale production of human IPSC-derived macrophages for drug screening. *Int J Mol Sci* (2020) 21:1–23. doi: 10.3390/ijms21134808
31. Gosselin D, Skola D, Coufal NG, Holtman IR, Schlachetzki JCM, Sajti E, et al. An environment-dependent transcriptional network specifies human microglia identity. *Science (80)* (2017) 356:1248–59. doi: 10.1126/science.aal3222
32. Bohlen CJ, Bennett FC, Tucker AF, Collins HY, Mulinyawe SB, Barres BA. Diverse requirements for microglial survival, specification, and function revealed by defined-medium cultures. *Neuron* (2017) 94:759–73. doi: 10.1016/j.neuron.2017.04.043
33. Hasselmann J, Coburn MA, England W, Figueroa Velez DX, Kiani Shabestari S, Tu CH, et al. Development of a Chimeric Model to Study and Manipulate Human Microglia In Vivo. *Neuron* (2019) 103:1016–33.e10. doi: 10.1016/j.neuron.2019.07.002
34. Svoboda DS, Barrasa MI, Shu J, Rietjens R, Zhang S, Mitalipova M, et al. Human iPSC-derived microglia assume a primary microglia-like state after transplantation into the neonatal mouse brain. *Proc Natl Acad Sci USA* (2019) 116:25293–303. doi: 10.1073/pnas.1913541116
35. Xu R, Li X, Boreland AJ, Posyton A, Kwan K, Hart RP, et al. Human iPSC-derived mature microglia retain their identity and functionally integrate in the chimeric mouse brain. *Nat Commun* (2020) 11:1–16. doi: 10.1038/s41467-020-15411-9
36. Haenseler W, Rajendran L. Concise Review: Modeling Neurodegenerative Diseases with Human Pluripotent Stem Cell-Derived Microglia. *Stem Cells* (2019) 37:724–30. doi: 10.1002/stem.2995
37. Miron VE, Priller J. Investigating Microglia in Health and Disease : Challenges and Opportunities. *Trends Immunol* (2020) 41(9):785–93. doi: 10.1016/j.it.2020.07.002
38. Speicher AM, Wiendl H, Meuth SG, Pawlowski M. Generating microglia from human pluripotent stem cells: Novel *in vitro* models for the study of neurodegeneration. *Mol Neurodegener* (2019) 14:1–16. doi: 10.1186/s13024-019-0347-z
39. Hanger B, Couch A, Rajendran L, Srivastava DP, Vernon AC. Emerging Developments in Human Induced Pluripotent Stem Cell-Derived Microglia: Implications for Modelling Psychiatric Disorders With a Neurodevelopmental Origin. *Front Psychiatry* (2020) 11:789. doi: 10.3389/fpsyt.2020.00789
40. Kleman AM, Yuan JY, Aja S, Ronnett GV, Landree LE. Physiological glucose is critical for optimized neuronal viability and AMPK responsiveness *in vitro*. *J Neurosci Methods* (2008) 167:292–301. doi: 10.1016/j.jneumeth.2007.08.028
41. Rocktäschel P, Sen A, Cader MZ. High glucose concentrations mask cellular phenotypes in a stem cell model of tuberous sclerosis complex. *Epilepsy Behav* (2019) 101:106581. doi: 10.1016/j.yebeh.2019.106581
42. Andreone BJ, Przybyla L, Llapashtica C, Rana A, Davis SS, van Lengerich B, et al. Alzheimer's-associated PLCγ2 is a signaling node required for both TREM2 function and the inflammatory response in human microglia. *Nat Neurosci* (2020) 23:927–38. doi: 10.1038/s41593-020-0650-6
43. Giulian D, Baker TJ. Characterization of ameboid microglia isolated from developing mammalian brain. *J Neurosci* (1986) 6:2163–78. doi: 10.1523/jneurosci.06-08-02163.1986
44. Witting A, Möller T. Microglia Cell Culture: A Primer for the Novice. In: *In Vitro Neurotoxicology*. Totowa, NJ: Springer Protocols by Humana Press (2011). p. 49–66. doi: 10.1007/978-1-61779-170-3

45. Schumann RR, Leong SR, Flaggs GW, Gray PW, Wright SD, Mathison JC, et al. Structure and Function of Lipopolysaccharide Binding Protein. *Science (80)* (1990) 249:1429–32. doi: 10.1126/science.2402637
46. Liu JJ, Mustafa S, Barratt DT, Hutchinson MR. Corticosterone preexposure increases NF-κB translocation and sensitizes IL-1β responses in BV2 microglia-like cells. *Front Immunol* (2018) 9:3. doi: 10.3389/fimmu.2018.00003
47. Bardy C, van den Hurk M, Eames T, Marchand C, Hernandez RV, Kellogg M, et al. Neuronal medium that supports basic synaptic functions and activity of human neurons *in vitro*. *Proc Natl Acad Sci USA* (2015) 112(25):2725–34. doi: 10.1073/pnas.1504393112
48. Abutbul S, Shapiro J, Szaingurten-Solodkin I, Levy N, Carmy Y, Baron R, et al. TGF-β signaling through SMAD2/3 induces the quiescent microglial phenotype within the CNS environment. *Glia* (2012) 60:1160–71. doi: 10.1002/glia.22343
49. Elmore MRP, Najafi AR, Koike MA, Nazih N, Spangenberg EE, Rice RA, et al. CSF1 receptor signaling is necessary for microglia viability, which unmasks a cell that rapidly repopulates the microglia- depleted adult brain. *Neuron* (2014) 82:380–97. doi: 10.1016/j.neuron.2014.02.040.CSF1
50. Nieweg K, Schaller H, Pfrieger FW. Marked differences in cholesterol synthesis between neurons and glial cells from postnatal rats. *J Neurochem* (2009) 109:125–34. doi: 10.1111/j.1471-4159.2009.05917.x
51. Loving BA, Bruce KD. Lipid and Lipoprotein Metabolism in Microglia. *Front Physiol* (2020) 11:393. doi: 10.3389/fphys.2020.00393
52. McIlvain G, Schwarb H, Cohen NJ, Telzer EH, Johnson CL. Mechanical properties of the *in vivo* adolescent human brain. *Dev Cognit Neurosci* (2018) 34:27–33. doi: 10.1016/j.dcn.2018.06.001
53. Lam D, Enright HA, Cadena J, Peters SKG, Sales AP, Osburn JJ, et al. Tissue-specific extracellular matrix accelerates the formation of neural networks and communities in a neuron-glia co-culture on a multi-electrode array. *Sci Rep* (2019) 9:1–15. doi: 10.1038/s41598-019-40128-1
54. Sadtler K, Wolf MT, Ganguly S, Moad CA, Chung L, Majumdar S, et al. Divergent immune responses to synthetic and biological scaffolds. *Biomaterials* (2019) 192:405–15. doi: 10.1016/j.biomaterials.2018.11.002
55. Chaudhuri O, Cooper-white J, Janmey PA, Mooney DJ, Shenoy VB. Effects of extracellular matrix viscoelasticity on cellular behaviour. *Nature* (2020) 584:535–46. doi: 10.1038/s41586-020-2612-2
56. Jensen C, Teng Y. Is It Time to Start Transitioning From 2D to 3D Cell Culture? *Front Mol Biosci* (2020) 7:33. doi: 10.3389/fmolb.2020.00033
57. Frampton JP, Hynd MR, Shuler ML, Shain W. Fabrication and optimization of alginate hydrogel constructs for use in 3D neural cell culture. *Biomed Mater* (2011) 6(1):015002. doi: 10.1088/1748-6041/6/1/015002
58. Jeffery AF, Churchward MA, Mushahwar VK, Todd KG, Elias AL. Hyaluronic acid-based 3D culture model for in vitro testing of electrode biocompatibility. *Biomacromolecules* (2014) 15(6):2157–65. doi: 10.1021/bm500318d
59. Koss KM, Churchward MA, Jeffery AF, Mushahwar VK, Elias AL, Todd KG. Improved 3D hydrogel cultures of primary glial cells for *in vitro* modelling of neuroinflammation. *J Vis Exp* (2017) 2017:e56615. doi: 10.3791/56615
60. Leite DM, Baskovic BZ, Civita P, Neto C, Gumbleton M, Pilkington GJ. A human co-culture cell model incorporating microglia supports glioblastoma growth and migration, and confers resistance to cytotoxics. *FASEB J* (2020) 34 (1):1710–27. doi: 10.1096/fj.201901858RR
61. Haw RTY, Tong CK, Yew A, Lee HC, Phillips JB, Vidyadaran S. A three-dimensional collagen construct to model lipopolysaccharide-induced activation of BV2 microglia. *J Neuroinflammation* (2014) 11:134. doi: 10.1186/1742-2094-11-134
62. Cho HJ, Verbridge SS, Davalos RV, Lee YW. Development of an in vitro 3D brain tissue model mimicking in vivo-like pro-inflammatory and pro-oxidative responses. *Ann Biomed Eng* (2017) 46:877–87. doi: 10.1007/s10439-018-2004-z
63. Park J, Wetzel I, Marriott I, Dréau D, D'Avanzo C, Kim DY, et al. Cho H. A 3D human triculture system modeling neurodegeneration and neuroinflammation in Alzheimer's disease. *Nat Neurosci* (2018) 21:941–51. doi: 10.1038/s41593-018-0175-4
64. Pöttler M, Zierler S, Kerschbaum HH. An artificial three-dimensional matrix promotes ramification in the microglial cell-line, BV-2. *Neurosci Lett* (2006) 410:137–40. doi: 10.1016/j.neulet.2006.09.082
65. Song Q, Jiang Z, Li N, Liu P, Liu L, Tang M, et al. Anti-inflammatory effects of three-dimensional graphene foams cultured with microglial cells. *Biomaterials* (2014) 35:6930–40. doi: 10.1016/j.biomaterials.2014.05.002
66. Schwartz MP, Hou Z, Propson NE, Zhang J, Engstrom CJ, Costa VS, et al. Human pluripotent stem cell-derived neural constructs for predicting neural toxicity. *Proc Natl Acad Sci USA* (2015) 112:12516–21. doi: 10.1073/pnas.1516645112
67. Jiang Z, Song Q, Tang M, Yang L, Cheng Y, Zhang M, et al. Enhanced migration of neural stem cells by microglia grown on a three- dimensional graphene scaffold ACS. *Appl. Mater. Interfaces* (2016) 8(38):25069–77. doi: 10.1021/acsami.6b06780
68. Chronopoulou L, Togna AR, Guarguaglini G, Masci G, Giammaruco F, Togna GI, et al. Self-assembling peptide hydrogels promote microglial cells proliferation and NGF production. *Soft Matter* (2012) 8:5784–90. doi: 10.1039/c2sm25528f
69. Pires LR, Rocha DN, Ambrosio L, Pêgo AP. The role of the surface on microglia function: Implications for central nervous system tissue engineering. *J R Soc Interface* (2015) 12:1–10. doi: 10.1098/rsif.2014.1224
70. Liu L, Koo Y, Akwitti C, Russell T, Gay E, Laskowitz DT, et al. Three-dimensional (3D) brain microphysiological system for organophosphates and neurochemical agent toxicity screening. *PLoS One* (2019) 14:e0224657. doi: 10.1371/journal.pone.0224657
71. Blazquez R, Pukrop T. 3D coculture model of the brain parenchyma–metastasis interface of brain metastasis. In: *Methods in Molecular Biology*. New York, NY: Springer Protocols by Humana Press Inc. (2017). p. 213–22. doi: 10.1007/978-1-4939-7021-6_16
72. Hermida MA, Kumar JD, Schwarz D, Laverty KG, Di Bartolo A, Ardron M, et al. Three dimensional *in vitro* models of cancer: Bioprinting multilineage glioblastoma models. *Adv Biol Regul* (2020) 75:100658. doi: 10.1016/j.jbior.2019.100658
73. Sridar S, Churchward MA, Mushahwar VK, Todd KG, Elias AL. Peptide modification of polyimide-insulated microwires: Towards improved biocompatibility through reduced glial scarring. *Acta Biomater* (2017) 60:154–66. doi: 10.1016/j.actbio.2017.07.026
74. Qin H, Wilson CA, Sun JL, Zhao X, Benveniste EN. LPS induces CD40 gene expression through the activation of NF-κB and STAT-1α in macrophages and microglia. *Blood* (2005) 106:3114–22. doi: 10.1182/blood-2005-02-0759
75. Blasi E, Barluzzi R, Bocchini V, Mazzolla R, Bistoni F. Immortalization of murine microglial cells by a v-raf/v-myc carrying retrovirus. *J Neuroimmunol* (1990) 27:229–37. doi: 10.1016/0165-5728(90)90073-V
76. Amadio S, De Ninno A, Montilli C, Businaro L, Gerardino A, Volonté C. Plasticity of primary microglia on micropatterned geometries and spontaneous long-distance migration in microfluidic channels. *BMC Neurosci* (2013) 14:1–12. doi: 10.1186/1471-2202-14-121
77. Liddelow SA, Guttenplan KA, Clarke LE, Bennett FC, Bohlen CJ, Schirmer L, et al. Neurotoxic reactive astrocytes are induced by activated microglia. *Nature* (2017) 541:481–7. doi: 10.1038/nature21029
78. Guttenplan KA, Liddelow SA. Astrocytes and microglia: Models and tools. *J Exp Med* (2019) 216:71–83. doi: 10.1084/jem.20180200
79. Wright GJ, Puklavec MJ, Willis AC, Hoek RM, Sedgwick JD, Brown MH, et al. Lymphoid/neuronal cell surface OX2 glycoprotein recognizes a novel receptor on macrophages implicated in the control of their function. *Immunity* (2000) 13:233–42. doi: 10.1016/S1074-7613(00)00023-6
80. Biber K, Neumann H, Inoue K, Boddeke HWGM. Neuronal "On" and "Off" signals control microglia. *Trends Neurosci* (2007) 30:596–602. doi: 10.1016/j.tins.2007.08.007
81. Mott RT, Ait-Ghezala G, Town T, Mori T, Vendrame M, Zeng J, et al. Neuronal expression of CD22: Novel mechanism for inhibiting microglial proinflammatory cytokine production. *Glia* (2004) 46:369–79. doi: 10.1002/glia.20009
82. Maciejewski-Lenoir D, Chen S, Feng L, Maki R, Bacon KB. Characterization of fractalkine in rat brain cells: migratory and activation signals for CX3CR-1-expressing microglia. *J Immunol* (1999) 163:1628–35.
83. Szepesi Z, Manouchehrian O, Bachiller S, Deierborg T. Bidirectional Microglia–Neuron Communication in Health and Disease. *Front Cell Neurosci* (2018) 12:323. doi: 10.3389/fncel.2018.00323
84. Neumann H, Wekerle H. Neuronal Control of the Immune Response in the Central Nervous System: Linking Brain Immunity to Neurodegeneration. *J Neuropathol Exp Neurol* (1998) 57:1–9. doi: 10.1097/00005072-199801000-00001
85. Nimmerjahn A, Kirchhoff F, Helmchen F. Neuroscience: Resting microglial cells are highly dynamic surveillants of brain parenchyma *in vivo*. *Science (80)* (2005) 308:1314–8. doi: 10.1126/science.1110647

86. Liddelow SA, Marsh SE, Stevens B. Microglia and astrocyte interactions in health and disease: Dynamic Duo or Partners in Crime? *Trends Immunol* (2020) 41:1–16. doi: 10.1016/j.it.2020.07.006
87. Liddelow SA, Barres BA. Reactive Astrocytes: Production, Function, and Therapeutic Potential. *Immunity* (2017) 46:957–67. doi: 10.1016/J.IMMUNI.2017.06.006
88. Goshi N, Morgan RK, Lein PJ, Seker E. A primary neural cell culture model to study neuron, astrocyte, and microglia interactions in neuroinflammation. *J Neuroinflammation* (2020) 17:155. doi: 10.1186/s12974-020-01819-z
89. Nimmervoll B, White R, Yang JW, An S, Henn C, Sun JJ, et al. LPS-induced microglial secretion of TNFα increases activity-dependent neuronal apoptosis in the neonatal cerebral cortex. *Cereb Cortex* (2013) 23:1742–55. doi: 10.1093/cercor/bhs156
90. Wang X, Chen S, Ma G, Ye M, Lu G. Involvement of proinflammatory factors, apoptosis, caspase-3 activation and Ca2+ disturbance in microglia activation-mediated dopaminergic cell degeneration. *Mech Ageing Dev* (2005) 126:1241–54. doi: 10.1016/j.mad.2005.06.012
91. Ormel PR, Vieira de Sá R, van Bodegraven EJ, Karst H, Harschnitz O, Sneeboer MAM, et al. Microglia innately develop within cerebral organoids. *Nat Commun* (2018) 9:1–14. doi: 10.1038/s41467-018-06684-2
92. Lin YT, Seo J, Gao F, Feldman HM, Wen HL, Penney J, et al. APOE4 Causes Widespread Molecular and Cellular Alterations Associated with Alzheimer's Disease Phenotypes in Human iPSC-Derived Brain Cell Types. *Neuron* (2018) 98:1141–54.e7. doi: 10.1016/j.neuron.2018.05.008
93. Mathews S, Branch Woods A, Katano I, Makarov E, Thomas MB, Gendelman HE, et al. Human Interleukin-34 facilitates microglia-like cell differentiation and persistent HIV-1 infection in humanized mice. *Mol Neurodegener* (2019) 14:12. doi: 10.1186/s13024-019-0311-y
94. Marschallinger J, Iram T, Zardeneta M, Lee SE, Lehallier B, Haney MS, et al. Lipid-droplet-accumulating microglia represent a dysfunctional and proinflammatory state in the aging brain. *Nat Neurosci* (2020) 23:194–208. doi: 10.1038/s41593-019-0566-1
95. Olah M, Patrick E, Villani AC, Xu J, White CC, Ryan KJ, et al. A transcriptomic atlas of aged human microglia. *Nat Commun* (2018) 9:1–8. doi: 10.1038/s41467-018-02926-5

Conflict of Interest: The authors declare that the research was conducted in the absence of any commercial or financial relationships that could be construed as a potential conflict of interest.

frontiers in Immunology

METHODS
published: 29 January 2021
doi: 10.3389/fimmu.2020.620602

Assessing Autophagy in Microglia: A Two-Step Model to Determine Autophagosome Formation, Degradation, and Net Turnover

Ainhoa Plaza-Zabala[1,2*], *Virginia Sierra-Torre*[2,3] *and Amanda Sierra*[2,3,4*]

[1] Department of Pharmacology, University of the Basque Country UPV/EHU, Leioa, Spain, [2] Glial Cell Biology Lab, Achucarro Basque Center for Neuroscience, Leioa, Spain, [3] Department of Neuroscience, University of the Basque Country UPV/EHU, Leioa, Spain, [4] Ikerbasque Foundation, Bilbao, Spain

OPEN ACCESS

Edited by:
Jorge Correale,
Fundación Para la Lucha Contra las Enfermedades Neurológicas de la Infancia (FLENI), Argentina

Reviewed by:
Daniela Bakula,
University of Copenhagen, Denmark
Xiaohong Zhuang,
The Chinese University of Hong Kong, China
Eisuke Itakura,
Chiba University, Japan

***Correspondence:**
Amanda Sierra
amanda.sierra@achucarro.org
Ainhoa Plaza-Zabala
ainhoa.plaza@achucarro.org

Specialty section:
This article was submitted to Multiple Sclerosis and Neuroimmunology, a section of the journal Frontiers in Immunology

Received: 23 October 2020
Accepted: 11 December 2020
Published: 29 January 2021

Citation:
Plaza-Zabala A, Sierra-Torre V and Sierra A (2021) Assessing Autophagy in Microglia: A Two-Step Model to Determine Autophagosome Formation, Degradation, and Net Turnover. Front. Immunol. 11:620602. doi: 10.3389/fimmu.2020.620602

Autophagy is a complex process that encompasses the enclosure of cytoplasmic debris or dysfunctional organelles in membranous vesicles, the autophagosomes, for their elimination in the lysosomes. Autophagy is increasingly recognized as a critical process in macrophages, including microglia, as it finely regulates innate immune functions such as inflammation. A gold-standard method to assess its induction is the analysis of the autophagic flux using as a surrogate the expression of the microtubule-associated light chain protein 3 conjugated to phosphatidylethanolamine (LC3-II) by Western blot, in the presence of lysosomal inhibitors. Therefore, the current definition of autophagy flux actually puts the focus on the degradation stage of autophagy. In contrast, the most important autophagy controlling genes that have been identified in the last few years in fact target early stages of autophagosome formation. From a biological standpoint is therefore conceivable that autophagosome formation and degradation are independently regulated and we argue that both stages need to be systematically analyzed. Here, we propose a simple two-step model to understand changes in autophagosome formation and degradation using data from conventional LC3-II Western blot, and test it using two models of autophagy modulation in cultured microglia: rapamycin and the ULK1/2 inhibitor, MRT68921. Our two-step model will help to unravel the effect of genetic, pharmacological, and environmental manipulations on both formation and degradation of autophagosomes, contributing to dissect out the role of autophagy in physiology and pathology in microglia as well as other cell types.

Keywords: autophagy, autophagosome, formation, degradation, LC3, microglia

INTRODUCTION

Autophagy is a complex phenomenon dedicated to eliminate intracellular debris, from protein aggregates to dysfunctional organelles, and is thus essential to maintain cell fitness (1, 2). In the brain, initial studies focused on its major role in neuronal survival (3, 4), but more recent evidence suggests that autophagy also controls health and function of other brain cell types, including microglia, the brain macrophages (1, 5). Autophagy controls several processes in microglia, including metabolic fitness (6), inflammation, phagocytosis of amyloid beta in rodent models of Alzheimer's disease (7), degradation of extracellular beta-amyloid fibrils (8) and synuclein (9), myelin phagocytosis in acute experimental encephalomyelitis (10), as well as synaptic pruning and social behavior in mice (11). Overall, autophagy is emerging as a major controller of immune cell function, regulating innate and adaptive immune responses (12).

Assessing autophagy is complicated and current guidelines recommend using several complementary methods (13). Nonetheless, the gold standard remains the analysis of the autophagic flux using LC3 (microtubule-associated light chain protein 3). During autophagy, cytosolic LC3 (LC3-I) is conjugated to phosphatidylethanolamine and recruited to the nascent phagophore membranes (LC3-II). The phagophore then encloses cytosolic material or organelles forming a double-membrane autophagosome, which is then redirected towards the lysosome for its enzymatic degradation. The autophagic flux is calculated as the differential amount of LC3-II in the presence/absence of lysosomal inhibitors, such as bafilomycin or chloroquine, among others. As lysosomal degradation is inhibited autophagosomes accumulate and, therefore, the change in LC3-II expression informs about the autophagosomes that would have been degraded, ergo, it is a measure of autophagosome degradation. However, LC3-II Western blot raw data contains information about both autophagosome formation and degradation (**Figure 1A**).

Importantly, formation and degradation are regulated by concerted but independent mechanisms: most autophagic-regulatory genes are involved in the early stages of autophagy, as is the case of the ATG family encoding proteins that are mainly involved in autophagosome formation and maturation (1, 14). In contrast, autophagosome degradation largely depends on lysosomal proteins and enzymes (**Figure 1B**). Therefore, both early and late stages of autophagy should be systematically analyzed to understand the autophagosome turnover in any given condition.

Abbreviations: APh, Autophagosome; ATG, Autophagy-related protein; BAF, Bafilomycin A1; BCA, Bicinchoninic Acid; DegR, Degradation ratio; DMEM, Dulbecco's Modified Eagle Medium; ECL, Enhanced Chemoluminescence; EXP^-, basal condition; EXP^+, experimental condition; FBS, Fetal Bovine Serum; FormR, Formation ratio; GM-CSF, Granulocyte-Macrophage Colony Stimulating Factor; LC3-II, microtubule-associated light chain protein 3 conjugated to phosphatidylethanolamine; mTORC1, Mechanistic Target of Rapamycin Complex 1; NetR, Net ratio; PD, Parkinson's disease; ss, steady-state; TBS-T, Tris Buffered Saline containing 0.1% Tween 20; TFEB, transcription factor-EB; ULK1/2, unc-51-like kinases 1/2.

METHODS

Cell Culture

The murine microglial BV2 cell line and primary microglia were used to test autophagy modulating compounds. BV2 microglia were grown and maintained in Dulbecco's Modified Eagle Medium (DMEM) (Gibco) supplemented with Fetal Bovine Serum 10% (FBS, Gibco) and a mixture of antibiotics/antimycotic (1%) including, penicillin, streptomycin, and amphotericin (all from Gibco). For experiments, $1x10^6$ cells adhered to uncoated plastic plates were used. Primary microglia cultures were performed as previously described (15, 16). Postnatal day 0–1 (P0-P1) fms-EGFP mice pup brains were extracted, and the meninges were peeled off. The olfactory bulb and cerebellum were discarded, and the rest of the brain was then mechanically homogenized by careful pipetting and enzymatically digested with papain (20 U/ml, Sigma), and deoxyribonuclease (DNAse; 150 U/µl, Invitrogen) for 15 min at 37°C. The resulting cell suspension was then filtered through a 40 µm nylon cell strainer (Fisher) and transferred to a 50 ml Falcon tube quenched by 5 ml of 20% FBS (Gibco) in HBSS. Afterwards, the cell suspension was centrifuged at 200 g for 5 min, the pellet was resuspended in 1 ml DMEM (Gibco) supplemented with 10% FBS and 1% Antibiotic/Antimycotic (Gibco), and seeded in T75 Poly L-lysine-coated (15 µl/ml, Sigma) culture flasks at a density of two brains per flask. Medium was changed the day after and then every 3–4 days, always enriched with Granulocyte Macrophage Colony Stimulating Factor (5 ng/ml GM-CSF, Sigma). After confluence (at 37°C, 5% CO_2 for approximately 14 d), microglia cells were harvested by shaking at 100–150 rpm, 37°C, 4 h. Isolated cells were counted and plated at a density of $2x10^6$ cells/well on poly-l-lysine-coated plastic plates. BV2 and primary microglia were allowed to settle for at least 24 h before experiments.

Drug Treatments

BV2 microglia were treated with rapamycin 100 nM (Fisher Scientific) for 6 h in the presence and absence of bafilomycin 100 nM (SelleckChem) for autophagy induction. Primary microglia were treated with the autophagy inhibitor MRT68921 1, 10, or 30 µM (Sigma) for 3 or 6 h with or without bafilomycin 100 nM (SelleckChem).

Protein Extraction and Western Blot

Microglia were directly lysed in plastic plates with RIPA buffer containing protease inhibitor cocktail (100x) (ThermoFisher). The cell suspension was then sonicated for 5s and centrifuged (10,000 g, 10 min) to obtain solubilized protein in the supernatant. Sample protein content was quantified in triplicates by BCA (Bicinchoninic Acid) assay kit (ThermoFisher) at 590 nm using a microplate reader (Synergy HT, BioTek). β-mercaptoethanol denatured proteins (15–20 ug) were loaded onto 14% Tris-glycine polyacrylamide gels (ThermoFisher) and run at 120V for 90min. Protein samples were then blotted to nitrocellulose membranes (0.45 µm pore size) (ThermoFisher) at 200 mA for 90 min or using the Trans-Blot Turbo Mini Nitrocellulose Transfer Pack (Bio-Rad).

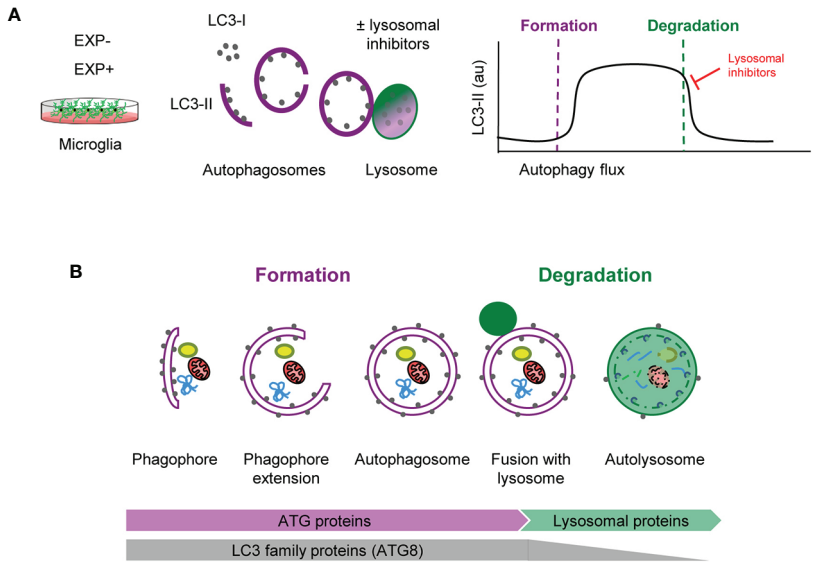

FIGURE 1 | Estimation of autophagy flux variations using LC3 turnover assay. **(A)** Total protein homogenates obtained from microglia under control (EXP^-) and experimental conditions (EXP^+) are analyzed by Western Blot to evaluate LC3 levels in the presence and absence of lysosomal inhibitors. When autophagy is activated, LC3-I (soluble form) is lipidated to the phophatidylethanolamine of the nascent phagophore forming LC3-II (membrane-bound form). LC3-II accumulates along the extension of the autophagic vacuoles as it closes and is used as an estimate of the number of autophagosomes. Upon fusion with lysosomes, LC3-II levels decrease due to the degradation of the inner autophagosomal membrane simultaneously with the luminal cargo. In the presence of lysosomal inhibitors, no degradation occurs and LC3-II levels are maintained. The subtraction of LC3-II quantities in the presence and absence of lysosomal inhibitors provides an estimate of the autophagosomes that have been degraded during the experimental period of time. **(B)** Early stages of autophagy, which lead to the *de novo* formation of autophagosomes, are mainly regulated by ATG proteins. The LC3 family of proteins (ATG8) participate in the formation of autophagosomes and progressively disappear after lysosomal fusion and cargo degradation in autolysosomes. Late stages of autophagy depend on the functionality of lysosomal proteins and enzymes.

Transfer efficiency was verified by Ponceau S (Sigma) staining. For immunoblotting, membranes were rinsed in Tris Buffered Saline containing 0.1% Tween 20 (Sigma) (TBS-T) and then blocked for 1 h in TBS-T containing 5% powder milk. Membranes were afterwards incubated with rabbit primary antibody to LC3 (1:3,000, NB100-2220, Novus Biologicals), and mouse primary antibody to β-actin (1:5,000, Sigma), in TBS-T containing 4% Bovine Serum Albumin (BSA) overnight (4°C, shaker). Next day, membranes were rinsed and incubated with Horseradish Peroxidase (HRP) conjugated anti-rabbit (1:5,000) and anti-mouse (1:5,000) secondary antibodies (Cell Signaling) for the rapamycin blot or with the fluorescent StarBright Blue 700 anti-mouse (1:5,000) and StarBright Blue 700 anti-rabbit (1:5,000) secondary antibodies (Bio-Rad) for the MRT68921 blots in TBS-T containing 5% powder milk. After rinsing membranes, protein was visualized by Enhanced ChemiLuminescence (ECL) using Supersignal West Femto Maximum Sensitivity Substrate (ThermoFisher) for the rapamycin blot or by immunofluorescence for the MRT68921 blots, in a ChemiDoc imaging system (BioRad). Band intensity was quantified using the Gel Analyzer method of Fiji software.

Statistics

Statistical analysis was performed with SigmaPlot. Normality and homoscedasticity were assessed prior to analysis. Raw LC3 data was initially analyzed by two-way ANOVA, but since an interaction between treatment (rapamycin, MRT68921) and bafilomycin was found, the global effect of the treatment was subsequently analyzed by one-way ANOVA. In addition, flux, and formation and degradation rates were analyzed by one-tail Student t-test (**Figures 5A, B**) or by one-way ANOVA followed by a Holm-Sidak posthoc test (**Figure 5C**). Formation and degradation rates were compared to one using a one-tail Student t-test. Data is shown as mean ± SEM. Only tests with $p < 0.05$ are considered significantly different; tests with $p < 0.1$ are reported to have a tendency.

MODELING AUTOPHAGOSOME FORMATION AND DEGRADATION

Here we propose a simple two-step model to analyze autophagy, in which the net number of autophagosomes (i.e., the autophagosome pool) at any given time is treated as a black box to which there is an input (formation) and an output (degradation) (**Figure 2A**). The formation phase encompasses phagophore formation, cargo sequestration, and autophagosome closure, and the degradation phase summarizes the lysosomal fusion and the enzymatic degradation of the autophagosome contents. Nonetheless, the precise definition of formation/degradation in each experimental setup depends on the physiological process blocked by the particular lysosomal inhibitor used: fusion inhibitors, such as vinblastine, which blocks transport of autophagosomes by microtubules; protease

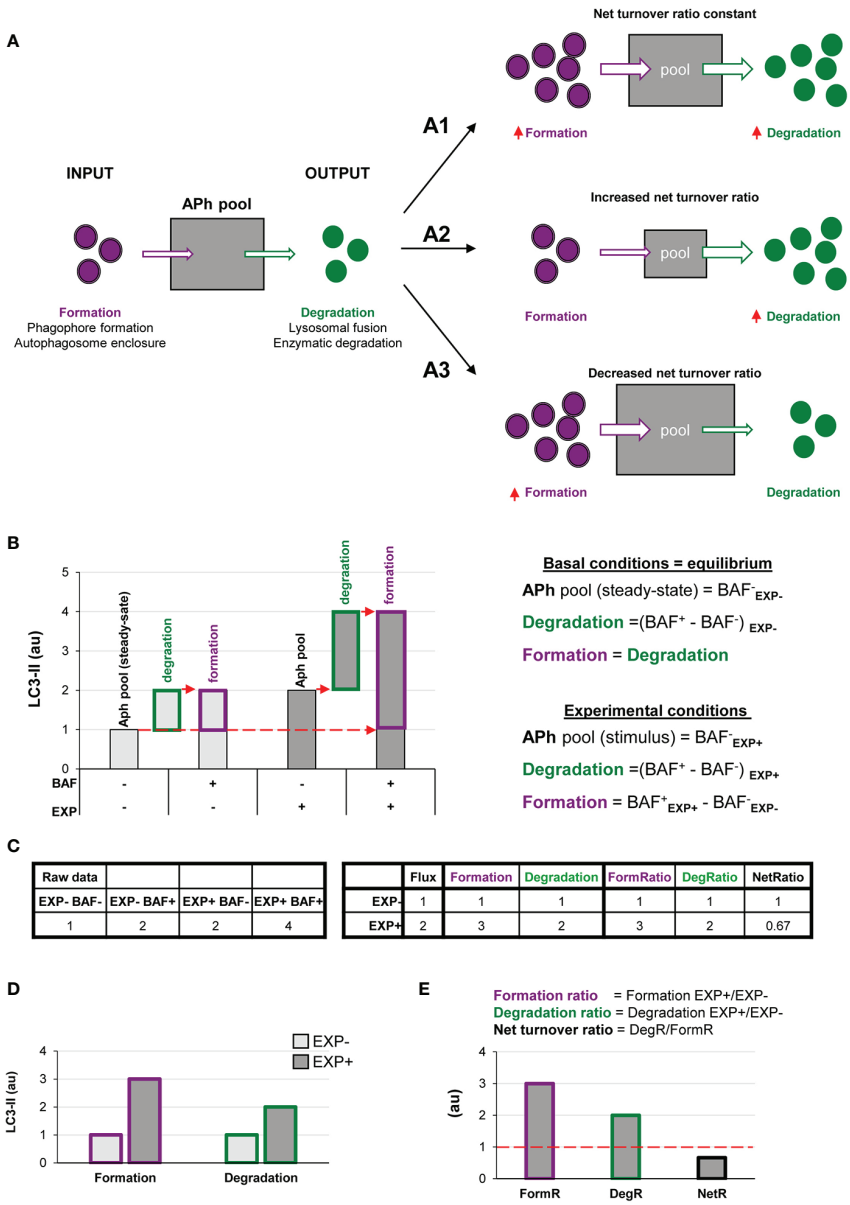

FIGURE 2 | A two-step model of autophagy to analyze formation and degradation of autophagosomes. **(A)** The model represents the autophagosomes as a box with an input (autophagosome formation, purple dots) and an output (autophagosome degradation, green dots) that determines the autophagosome net turnover. A1–A3 represent different possible scenarios with no changes (A1), an increase (A2) and a decrease (A3) in the autophagosome net turnover. **(B)** Graph representing the amount of LC3-II (au, arbitrary units) in two experimental conditions representing (EXP^- and EXP^+) in the presence or absence of the lysosomal inhibitor bafilomycin (BAF^- and BAF^+), and the formulas used to calculate formation, degradation, and net turnover. The dotted red arrows mark the LC3-II raw data values used to calculate the formation and degradation rates and ratios. **(C)** Simulated raw LC3-II data (au) (left) used to calculate the formation and degradation rates and ratios (right) used in the graphs shown in **(B, D, E)**. **(D, E)** Graphs representing the rate of change of formation, degradation and net turnover between the two experimental conditions.

inhibitors, such as E64d and leupeptin; or proton pump inhibitors, such as bafilomycin. This conceptual frame can be easily modeled by a simple equation in which the size of the autophagosome (APh) pool in a given time point depends on the number of autophagosomes in the steady-state (ss) plus the number of autophagosomes formed minus the autophagosomes degraded in a certain period of time:

$$APh_t = APH_{ss} + APh\ Formation - APh\ Degradation$$

The ratio between degradation and formation is the net autophagic turnover, which is a measure of the relative velocity of autophagosome formation versus degradation. A given

stimulus could act proportionally both on the formation and the degradation, maintaining the size of the APh pool and resulting in a constant net turnover ratio (**Figure 2A1**). However, under some conditions, the regulation of the formation and degradation of autophagosomes may be dissociated: an increased degradation would decrease the size of the APh pool and increase the net turnover (**Figure 2A2**); and an increased formation would increase the size of the APh pool and decrease the net turnover (**Figure 2A3**). Thus, we propose that to understand the complexity of the biology underneath the autophagosome turnover we need to analyze separately formation, degradation, and the net autophagic turnover.

This analysis can be performed using the data available in conventional LC3 assays by Western blot. In this type of analysis, cells or tissue from two experimental conditions (EXP^-: control and EXP^+: experimental stimulus) are incubated in the presence or absence of lysosomal inhibitors such as bafilomycin (BAF^- and BAF^+) for a certain period of time. Protein from these four conditions is extracted and the expression of LC3-II is analyzed by Western blot and, ideally, normalized to reference proteins such as actin (13). In addition, the complementary normalization of LC3-II to LC3-I may facilitate the understanding of the full picture of the autophagy response (13).

In the basal condition (EXP^-), the amount of LC3-II in the absence of lysosomal inhibitors (BAF^-) represents the APh pool in the steady state, analogous to taking a snapshot of the autophagic process (**Figure 2B**). The difference between the amount of LC3-II in cells incubated with and without lysosomal inhibitors (BAF^+ – BAF^-) in the basal condition represents the autophagosomes that have disappeared (i.e., the degradation phase), which is what is conventionally called autophagic flux. To calculate the autophagosomes that have formed, our model stems from the assumption that in the basal condition autophagy is at an equilibrium because formation and degradation occur at the same speed:

$$\text{Basal condition:}$$

$$\text{APh Formation} = \text{APh Degradation}$$

$$\text{APh}_{\text{equilibrium}} = \text{APh}_{\text{ss}}$$

Thus, in the basal condition (EXP^-) the autophagosomes that have formed are identical to the autophagosomes that have degraded, and thus are also represented by the amount of LC3-II with and without lysosomal inhibitors (BAF^+ – BAF^-) (**Figures 2B, C**).

In the experimental condition (EXP^+), the amount of LC3-II in the absence of lysosomal inhibitors (BAF^- in EXP^+) represents the size of the APh pool under the stimulus. Again, degradation can be calculated as the difference in LC3-II with and without lysosomal inhibitors [(BAF^+ in EXP^+) – (BAF^- in EXP^+)]. Formation can be calculated as the difference between the amount of LC3-II in the presence of lysosomal inhibitors minus the size of the initial APh pool in steady-state conditions [(BAF^+ in EXP^+) - (BAF^- in EXP^-)] (**Figures 2B, C**). This procedure allows us to calculate the formation and degradation of autophagosomes in control and experimental conditions (**Figure 2D**). To then compare whether the stimulus acts proportionally in both formation and degradation, we can calculate the ratio between experimental and basal conditions (EXP^+/EXP^-) for both formation and degradation (**Figure 2E**). Finally, to compare the relative magnitude of degradation compared to formation, we can calculate the ratio between both as the net turnover ratio (**Figure 2E**), which has a value of one in basal conditions, because autophagosome formation and degradation occur at the same rate (red dotted line in **Figure 2E**).

DISSECTING OUT AUTOPHAGOSOME FORMATION AND DEGRADATION

This model allows us to discriminate and quantify different potential biological scenarios that may affect autophagosome formation, degradation, or both. For instance, a typical autophagic stimulus would be expected to proportionally increase autophagosome formation and degradation, maintaining a balanced autophagy (**Figure 3A1**). Examples of this scenario are treatment with the well-known autophagy activator rapamycin, an inhibitor of the mTORC1 complex (Mechanistic Target Of Rapamycin Complex 1) (17); or activation of the transcription factor-EB (TFEB), which coordinately regulates the biogenesis of autophagosomes and lysosomes (18), maintaining the equilibrium between formation and degradation.

To exemplify this scenario, we simulated raw LC3-II Western blot data from a canonical autophagy stimulus (**Figure 3A2**), and from here we calculated the classic autophagy flux, showing the expected increase (**Figure 3A3**). We then applied our model to the raw data and observed that the canonical autophagic stimulus increased both formation and degradation (**Figure 3A4**). Importantly, both formation and degradation ratios were similar and, as a result, the net autophagy ratio was constant (**Figure 3A5**), implying a maintenance of the net autophagic turnover but at a higher rate/velocity, that could be possibly maintained in the long term.

In contrast, there are other biological scenarios that are not so easily discriminated using the conventional calculation of the autophagy flux (**Figures 3B, C**). Examples of these scenarios are situations in which autophagosome formation is increased (**Figure 3B**) or decreased (**Figure 3C**), without concomitantly affecting degradation. For instance, overexpression of ATG proteins or accumulation of intracellular debris would lead to increased autophagosome formation. But if lysosomal efficiency (i.e., degradation) is not proportionally increased, autophagosomes will stall in the lysosomes without degrading the autophagic cargo, leading to a decreased net turnover ratio and increased autophagosome pool. This effect has been for example observed in cells that overexpress Atg5 but whose lysosomal function is compromised (19). In this case, calculation of the autophagy flux would not reveal any changes (**Figures 3B1, C1**), although the raw LC3-II data is evidently different (**Figures 3B2, C2**). Our model would help to quantify

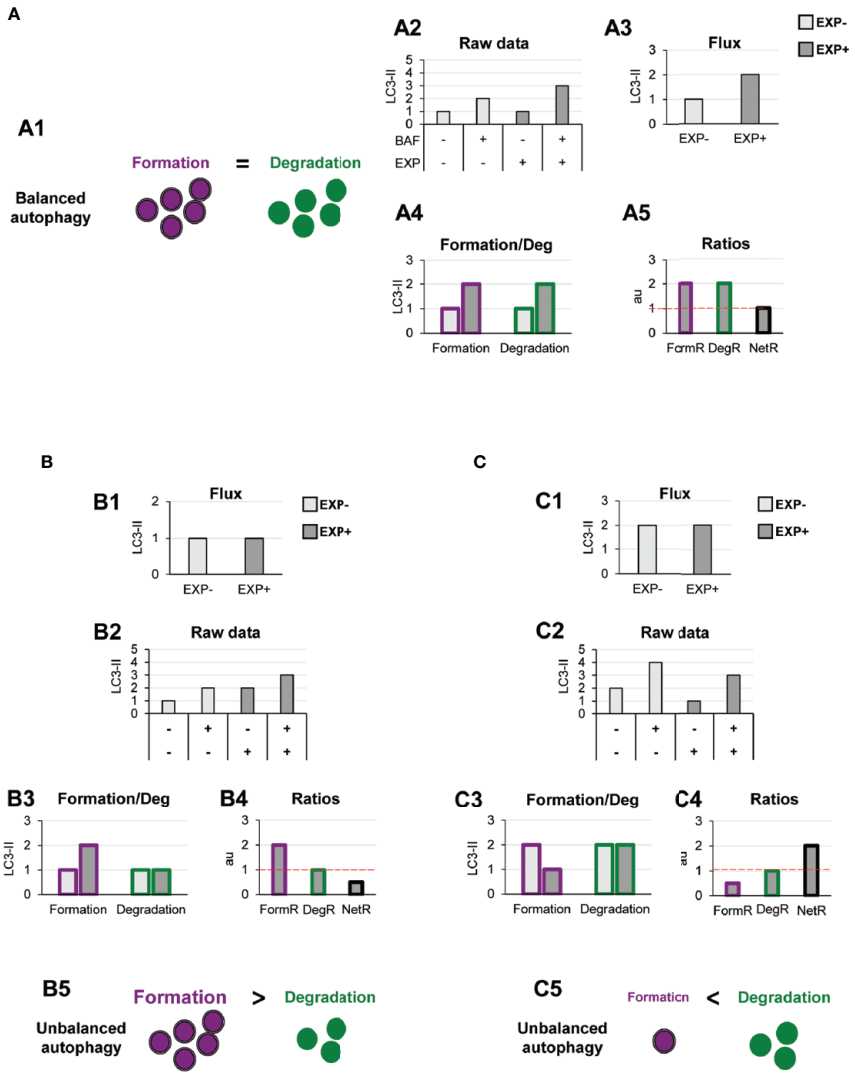

FIGURE 3 | Theoretical examples of variations in the formation of autophagosomes that lead to balanced or unbalanced autophagy. **(A)** Example of a balanced flux with proportional increase in autophagosome formation and degradation. The model of balanced flux with equal formation (purple dots) and degradation (green dots) (A1), the raw LC3-II/actin Western blot data (A2), the conventional autophagy flux (A3), the formation and degradation rates (A4), and the formation, degradation, and net ratios (A5) are shown. The red dotted line represents the threshold of one to determine a significant change (over 1, basal conditions) in the formation, degradation and net turnover ratios. **(B, C)** Show examples with similar conventional flux (B1, C1), which are in fact derived from dissimilar raw LC3-II/actin Western blot data (B2, C2). In **(B)** Our model would reveal increased autophagosome formation rate and no changes in degradation rate (B3), leading to an increased formation ratio and reduced net ratio (B4), and an unbalanced autophagy (B5). In contrast, in **(C)** our model would reveal decreased autophagosome formation rate and no changes in degradation rate (C3), leading to an increased formation ratio and reduced net ratio (C4), and an unbalanced autophagy (C5).

the specific effect on formation (**Figures 3B3, C3**), and the alteration of the net autophagy ratio (**Figures 3B4, C4**), revealing an unbalanced autophagy (**Figures 3B5, C5**), and a potentially catastrophic situation for the cell that could not possibly be maintained over time.

Other biological scenarios that cannot be discriminated using conventional analysis of the autophagy flux are shown in **Figures 4**, **5**. Some stimuli may selectively increase autophagosome degradation without affecting their formation coordinately (**Figure 4A**), or even reducing it (**Figure 4B**). For example, enhanced lysosomal biogenesis or lysosomal enzymes efficiency might lead to increased autophagosome degradation, resulting in an increased net turnover ratio and reduced autophagosome pool size. This imbalance has been reported in mice genetically deficient for the cathepsin inhibitor cystatin B, which exhibit enhanced lysosomal proteolysis (20). Whereas in this case the calculation of the autophagy flux would suggest an enhanced autophagy, our model would reveal the imbalance between formation and degradation, suggesting that in fact cellular debris would not be removed any faster from the cytoplasm.

Another scenario in which our model may prove useful is one where autophagosome degradation is reduced but formation is

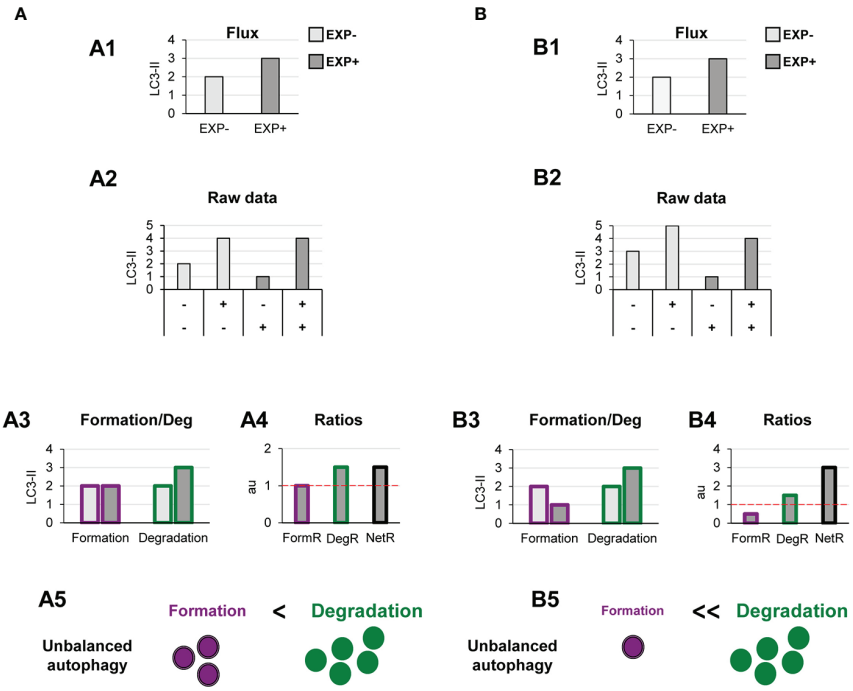

FIGURE 4 | Theoretical examples of increased autophagosome degradation that lead to unbalanced autophagy. **(A, B)** show examples with similar conventional flux (A1, B1), derived from apparently similar raw LC3-II/actin Western blot data (A2, B2). In **(A)** our model would reveal an increased autophagosome degradation rate and no changes in the formation rate (A3), leading to an increased degradation ratio and net ratio (A4), and an unbalanced autophagy (A5). In contrast, in **(B)** our model would reveal decreased autophagosome formation rate but increased degradation (B3), leading to decreased formation ratio, increased degradation ratio, and a strong increase in the net ratio (C4), ultimately resulting in a highly unbalanced autophagy (B5).

maintained (**Figure 5A**) or even increased (**Figure 5B**). An example of this scenario is a pathological condition where dysfunctional organelles accumulate and the cell tries to enclose them in autophagosomes but lysosomal functionality is compromised, for instance because lysosomes are defective or engaged in other degradation pathways such as phagocytosis or endocytosis. This effect could be observed in Parkinson's disease (PD) dopaminergic neurons, which contain LC3-positive Lewy bodies, and have stalled autophagosomes, and lysosomal depletion (21). This complex effect cannot be fully understood by simply analyzing the reduction in the autophagy flux but would be instead clearly described by our two-step model.

TESTING THE MODEL *IN VITRO*

We have directly tested our model with experimental data using two well-characterized autophagy modulators: the autophagy inducer rapamycin, which inhibits mTORC1 (22); and the autophagy inhibitor MRT68921, which blocks ULK1/2 (unc-51-like kinases 1/2) (22, 23). Both mTORC1 and ULK1/2 are early checkpoints of canonical autophagy: mTORC1 transduces signals from energy and damage sensors and is inhibited under stressful situations, releasing ULK1/2 (unc-51-like kinase 1/2) by a series of phosphorylation and dephosphorylation events to initiate the autophagy cascade (1, 14). As a cell model we used cultures of microglia (BV2 cells or primary cultures) and analyzed the amount of LC3-II by Western blot as a measurement of the size of the autophagosome pool.

In BV2 microglia rapamycin (6 h, 100 nM) showed the expected response and a tendency to increased LC3-II flux (**Figure 6A**). In addition, our model uncovered a parallel increase in formation and degradation of autophagosomes, resulting in a constant size of the APh pool and no changes in the net autophagosome turnover. Thus, rapamycin allowed the maintenance of the equilibrium between formation and degradation (**Figure 6A**), indicating a sustained autophagy that the cell can maintain over time.

On the other hand, MRT68921 (3 h, 30 μM) resulted in the expected decrease in the LC3-II flux in primary microglia (**Figure 6B**). However, analysis with our model revealed that only degradation was reduced whereas autophagosome formation remained constant (**Figure 6B**). This data is in apparent contradiction with the described role of MRT in blocking the autophagy pre-initiation complex (22, 23). To address this discrepancy, we used a second paradigm of MRT68921 with a longer treatment and lower dosage (6 h, 1–10 μM; **Figure 6C**), and observed that the upstream effect of inhibition of autophagosome formation with MRT 10μM translated into a similar decrease in degradation (**Figure 6C**). Therefore, our model proves useful to discriminate the effect of experimental manipulations on the formation and/or degradation of autophagosomes.

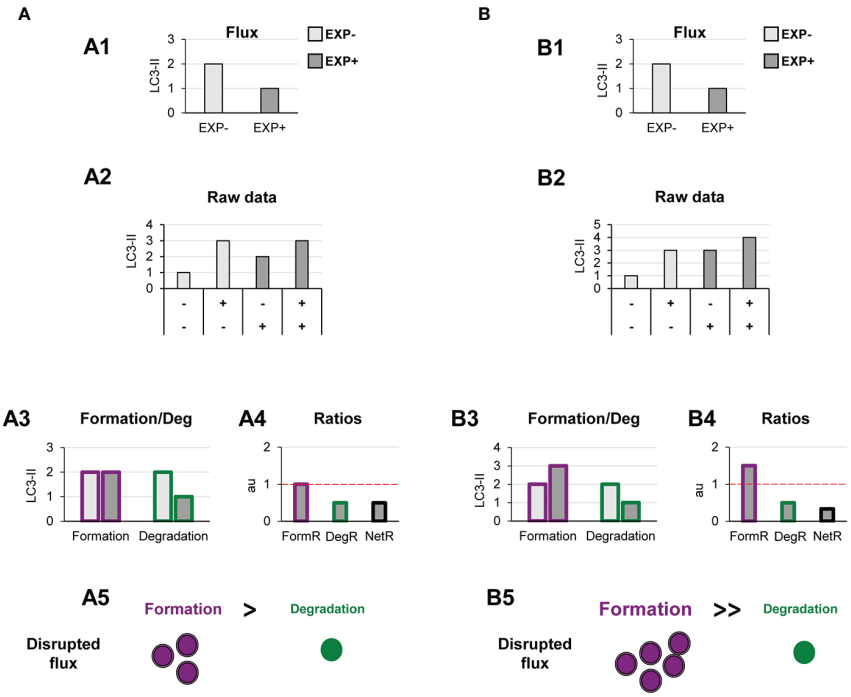

FIGURE 5 | Theoretical examples of decreased autophagosome degradation that lead to unbalanced autophagy. **(A, B)** show examples with similar conventional flux (A1, B1), derived from apparently similar raw LC3-II/actin Western blot data (A2, B2). In **(A)** our model would reveal a decreased autophagosome degradation rate and no changes in the formation rate (A3), leading to a reduced degradation ratio and net ratio (A4), and an unbalanced autophagy (A5). In contrast, in **(B)** our model would reveal increased autophagosome formation rate but decreased degradation (B3), leading to increased formation ratio, reduced degradation ratio, and a strong reduction in the net ratio (C4), ultimately resulting in a highly unbalanced autophagy (B5).

FUTURE DIRECTIONS

Autophagy is a complex multi-step phenomenon and its assessment is a complicated task that requires using complimentary methods, as most current guidelines recommend (13, 24). Visualization of double-membrane autophagosomes by transmission electron microscopy, live imaging of LC3 acidification using ratiometric analysis of fluorophores, or analysis of substrate degradation should corroborate the data obtained by analysis of LC3-II expression as a proxy for autophagosome formation and degradation. It is also important to note that autophagy is a time-dependent process and, as such, its dynamics should be assessed over time (25). In addition, LC3-II immunoblotting assays have several limitations, such as the reference protein used to normalize LC3-II values, the timing and concentration of the lysosomal inhibitor used, or the intrinsic nonlinear detection of proteins by enhanced chemoluminescence (ECL) (26). The most widely used method to asses autophagy is, nonetheless, the analysis of the LC3-II flux in the presence of lysosomal inhibitors. However, the complexities associated to interpreting LC3-II flux have been thoroughly pointed out before, in the quest for an optimal "autophagomometer" (26). One of the key points is that autophagosomes formation and degradation are spatially and temporally dissociated (27) and that therefore they need to be assessed independently.

To address this issue, we here propose a simple conceptual frame to help interpreting LC3-II flux experiments. Our two-step model conceives the steady-state levels of LC3-II as an indirect measure of the pool of autophagosomes present when the snapshot is taken. Assuming that in the basal condition the cells or tissue of interest are in some sort of equilibrium, the amount of autophagosomes formed and degraded should be roughly the same. Thus, the autophagosome pool can be treated as a black box to which the input (formation) and output (degradation) are identical, and can be estimated as the difference between LC3-II levels in the presence and absence of lysosomal inhibitors. In the experimental condition, degradation can be similarly calculated as the difference between LC3-II levels in the presence and absence of lysosomal inhibitors (i.e., the conventional LC3-II flux). In addition, we propose that the formation of autophagosomes in the experimental condition can be estimated by subtracting the steady-state autophagosome pool to the autophagosomes that have accumulated in the presence of lysosomal inhibitors. This model allows us to dissect out the effects of the experimental conditions to autophagosome formation and degradation. In addition, it also allows us to understand the net changes in the size of the autophagosomal pool that are the result of maintaining (or not) the net turnover ratio at equilibrium.

We have tested the two-step model using pharmacological autophagy modulators such as the autophagy inducer rapamycin and the autophagy inhibitor MRT68921 in microglia. As expected, rapamycin enhanced autophagy flux increasing both

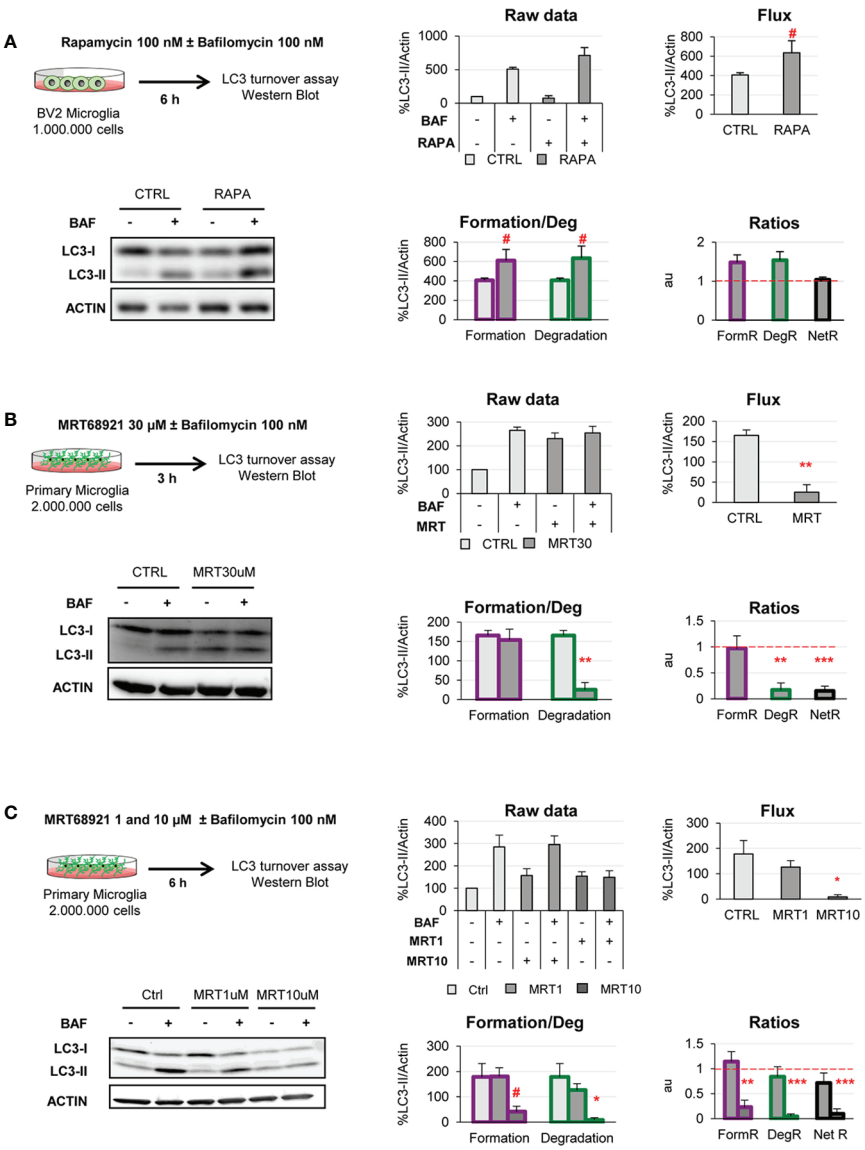

FIGURE 6 | Validation of the two-step model with autophagy modulating compounds. **(A)** Autophagy induction assessed after treatment with rapamycin (100 nM, 6 h) in the presence and absence of Bafilomycin (100 nM) in the BV2 microglia cell line. A representative blot, the raw data obtained, and the calculations of flux, autophagosome formation and degradation, and net turnover ratios are shown. Data is presented as % over control (LC3-II/actin). **(B, C)** Autophagy inhibition assessed after treatment with MRT68921 (30 µM, 3 h in **(B)**; 1 and 10 µM, 6 h in **(C)** in the presence and absence of Bafilomycin (100 nM) in mouse primary microglia. A representative blot, the raw data obtained, and the calculations of flux, autophagosome formation and degradation, and net turnover ratios are shown. Data is presented as % over control (LC3-II/actin). Data represent mean ± SEM of 3 independent experiments. #represents $p < 0.1$, *represents $p < 0.05$ and ** represents $p < 0.01$ by one tailed Student t-test **(A, B)**, or Holm-Sidak after a significant effect of the treatment was found with 1-way ANOVA **(C)**.

autophagosome formation and degradation at the concentration (100 nM) and time point (6 h) tested. However, the autophagy inhibitor MRT68921 exhibited concentration and time-dependent differential effects. At a medium concentration (10 µM) and long time-point (6 h), MRT68921 decreased both autophagosome formation and degradation, in line with the inhibitory effects described over ULK1/2 kinase activity, while no effect was observed at a lower concentration (1 µM). Nevertheless, at high concentration (30 µM) and short time-point (3h), MRT68921 selectively decreased autophagosome degradation while maintaining their formation. This was an unexpected result since MRT68921 inhibits ULK1/2 kinase, a protein mainly known for its role in autophagy initiation (28). However, ULK1/2 kinase also regulates the recruitment of other autophagy-related proteins for the productive formation of autophagosomes (23, 29). Thus, inhibition of ULK1/2 kinase activity at high concentrations and short time-points could preferentially affect autophagosome degradation activity,

maintaining residual autophagy initiation activities, leading to the formation of LC3-II positive stalled phagophores and LC3-II accumulation after inhibitor treatment (23). Overall, using pharmacological modulators of autophagy, we demonstrate that our two-step model is able to accurately measure the selective changes that may occur in autophagosome formation and/or degradation in microglia after exposure of autophagy modulating stimuli.

Nonetheless, our two-step model has several limitations that should be considered. The most important one is the assumption that autophagy (formation and degradation) are at equilibrium in the basal condition. This equilibrium implies coordinated control mechanisms that would be necessary to maintain autophagy in the long term (30), but each cell type may have different regulation mechanisms under different metabolic constraints (31), and would depend on experimental conditions such as cell density. Another important point is that autophagosome formation and degradation are not independent phenomena, as assumed in our model. For instance, it is obvious that if the lysosomal pool is not a limiting factor, the degradation will directly depend on the formation. In addition, feed-back mechanisms may link excessive lysosomal degradation with a subsequent reduction in autophagosome formation (32). In spite of these limitations, our model can provide a more expanded insight into the complexity of the autophagy process than simply analyzing the autophagic flux. In summary, we here show that using the LC3 turnover assay, our two-step model helps to systematically determine changes in autophagosome formation vs degradation, the net turnover and the size of the autophagosome pool to obtain a more comprehensive understanding of autophagy.

Due to the universal nature of LC3 turnover assays, our two-step model is useful to estimate changes in autophagosome formation and degradation in virtually all mammalian cell types, including microglia. As autophagy has emerged as a regulator of a plethora of microglial functions (1) related to regulation of metabolic status, inflammation, and phagocytosis (6, 7, 10), our two-step model may provide a simple framework to understand the basic dynamics of microglial autophagy in health and disease.

DATA AVAILABILITY STATEMENT

Requests to access the datasets should be directed to AS, amanda.sierra@achucarro.org.

ETHICS STATEMENT

The animal study was reviewed and approved by Comité de Ética en Experimentación Animal (CEEA), University of the Basque Country EHU/UPV.

AUTHOR CONTRIBUTIONS

AS and AP-Z conceived the idea and wrote the manuscript. VS-T performed experiments and wrote the manuscript. All authors contributed to the article and approved the submitted version.

FUNDING

This work was supported by grants from the Spanish Ministry of Science and Innovation (https://www.ciencia.gob.es/) with FEDER funds (RTI2018-099267-B-I00) and a Tatiana Foundation project (P-048-FTPGB 2018) to AS. VS-T holds a predoctoral fellowship from the Basque Government.

REFERENCES

1. Plaza-Zabala A, Sierra-Torre V, Sierra A. Autophagy and Microglia: Novel Partners in Neurodegeneration and Aging. *Int J Mol Sci* (2017) 18(3):598. doi: 10.3390/ijms18030598
2. Levine B, Kroemer G. Biological Functions of Autophagy Genes: A Disease Perspective. *Cell* (2019) 176(1):11–42. doi: 10.1016/j.cell.2018.09.048
3. Hara T, Nakamura K, Matsui M, Yamamoto A, Nakahara Y, Suzuki-Migishima R, et al. Suppression of basal autophagy in neural cells causes neurodegenerative disease in mice. *Nature* (2006) 441(7095):885–9. doi: 10.1038/nature04724
4. Komatsu M, Waguri S, Chiba T, Murata S, Iwata J-I, Tanida I, et al. Loss of autophagy in the central nervous system causes neurodegeneration in mice. *Nature* (2006) 441(7095):880–4. doi: 10.1038/nature04723
5. Sung K, Jimenez-Sanchez M. Autophagy in Astrocytes and its Implications in Neurodegeneration. *J Mol Biol* (2020) 432(8):2605–21. doi: 10.1016/j.jmb.2019.12.041
6. Ulland TK, Song WM, Huang SC-C, Ulrich JD, Sergushichev A, Beatty WL, et al. TREM2 Maintains Microglial Metabolic Fitness in Alzheimer's Disease. *Cell* (2017) 170(4):649–63.e13. doi: 10.1016/j.cell.2017.07.023
7. Heckmann BL, Teubner BJW, Tummers B, Boada-Romero E, Harris L, Yang M, et al. LC3-Associated Endocytosis Facilitates β-Amyloid Clearance and Mitigates Neurodegeneration in Murine Alzheimer's Disease. *Cell* (2019) 178(3):536–51.e14. doi: 10.1016/j.cell.2019.05.056
8. Cho M-H, Cho K, Kang H-J, Jeon E-Y, Kim H-S, Kwon H-J, et al. Autophagy in microglia degrades extracellular β-amyloid fibrils and regulates the NLRP3 inflammasome. *Autophagy* (2014) 10(10):1761–75. doi: 10.4161/auto.29647
9. Choi I, Zhang Y, Seegobin SP, Pruvost M, Wang Q, Purtell K, et al. Microglia clear neuron-released α-synuclein via selective autophagy and prevent neurodegeneration. *Nat Commun* (2020) 11(1):1386. doi: 10.1038/s41467-020-15119-w
10. Berglund R, Guerreiro-Cacais AO, Adzemovic MZ, Zeitelhofer M, Lund H, Ewing E, et al. Microglial autophagy–associated phagocytosis is essential for recovery from neuroinflammation. *Sci Immunol* (2020) 5(52):eabb5077. doi: 10.1126/sciimmunol.abb5077
11. Kim HJ, Cho MH, Shim WH, Kim JK, Jeon EY, Kim DH, et al. Deficient autophagy in microglia impairs synaptic pruning and causes social behavioral defects. *Mol Psychiatry* (2017) 22(11):1576–84. doi: 10.1038/mp.2016.103
12. Shibutani ST, Saitoh T, Nowag H, Münz C, Yoshimori T. Autophagy and autophagy-related proteins in the immune system. *Nat Immunol* (2015) 16(10):1014–24. doi: 10.1038/ni.3273
13. Klionsky DJ, Abdelmohsen K, Abe A, Abedin MJ, Abeliovich H, Acevedo Arozena A, et al. Guidelines for the use and interpretation of assays for monitoring autophagy (3rd edition). *Autophagy* (2016) 12(1):1–222. doi: 10.1080/15548627.2015.1100356
14. Mercer TJ, Gubas A, Tooze SA. A molecular perspective of mammalian autophagosome biogenesis. *J Biol Chem* (2018) 293(15):5386–95. doi: 10.1074/jbc.R117.810366
15. Abiega O, Beccari S, Diaz-Aparicio I, Nadjar A, Layé S, Leyrolle Q, et al. Neuronal Hyperactivity Disturbs ATP Microgradients, Impairs Microglial Motility, and Reduces Phagocytic Receptor Expression Triggering Apoptosis/Microglial

Phagocytosis Uncoupling. *PloS Biol* (2016) 14(5):e1002466. doi: 10.1371/journal.pbio.1002466
16. Beccari S, Diaz-Aparicio I, Sierra A. Quantifying Microglial Phagocytosis of Apoptotic Cells in the Brain in Health and Disease. *Curr Protoc Immunol* (2018) 122(1):e49. doi: 10.1002/cpim.49
17. Civiletto G, Dogan SA, Cerutti R, Fagiolari G, Moggio M, Lamperti C, et al. Rapamycin rescues mitochondrial myopathy via coordinated activation of autophagy and lysosomal biogenesis. *EMBO Mol Med* (2018) 10(11):e8799. doi: 10.15252/emmm.201708799
18. Settembre C, Di Malta C, Polito VA, Arencibia MG, Vetrini F, Erdin S, et al. TFEB Links Autophagy to Lysosomal Biogenesis. *Science* (2011) 332 (6036):1429. doi: 10.1126/science.1204592
19. Pyo J-O, Yoo S-M, Ahn H-H, Nah J, Hong S-H, Kam T-I, et al. Overexpression of Atg5 in mice activates autophagy and extends lifespan. *Nat Commun* (2013) 4(1):2300. doi: 10.1038/ncomms3300
20. Yang D-S, Stavrides P, Mohan PS, Kaushik S, Kumar A, Ohno M, et al. Reversal of autophagy dysfunction in the TgCRND8 mouse model of Alzheimer's disease ameliorates amyloid pathologies and memory deficits. *Brain* (2011) 134(1):258–77. doi: 10.1093/brain/awq341
21. Dehay B, Bové J, Rodríguez-Muela N, Perier C, Recasens A, Boya P, et al. Pathogenic Lysosomal Depletion in Parkinson's Disease. *J Neurosci* (2010) 30 (37):12535. doi: 10.1523/JNEUROSCI.1920-10.2010
22. Morel E, Mehrpour M, Botti J, Dupont N, Hamaï A, Nascimbeni AC, et al. Autophagy: A Druggable Process. *Annu Rev Pharmacol Toxicol* (2017) 57 (1):375–98. doi: 10.1146/annurev-pharmtox-010716-104936
23. Petherick KJ, Conway OJL, Mpamhanga C, Osborne SA, Kamal A, Saxty B, et al. Pharmacological Inhibition of ULK1 Kinase Blocks Mammalian Target of Rapamycin (mTOR)-dependent Autophagy. *J Biol Chem* (2015) 290 (18):11376–83. doi: 10.1074/jbc.C114.627778
24. Mizushima N, Yoshimori T, Levine B. Methods in mammalian autophagy research. *Cell* (2010) 140(3):313–26. doi: 10.1016/j.cell.2010.01.028
25. Martin KR, Barua D, Kauffman AL, Westrate LM, Posner RG, Hlavacek WS, et al. Computational model for autophagic vesicle dynamics in single cells. *Autophagy* (2013) 9(1):74–92. doi: 10.4161/auto.22532
26. Rubinsztein DC, Cuervo AM, Ravikumar B, Sarkar S, Korolchuk VI, Kaushik S, et al. In search of an "autophagomometer". *Autophagy* (2009) 5(5):585–9. doi: 10.4161/auto.5.5.8823
27. Börlin CS, Lang V, Hamacher-Brady A, Brady NR. Agent-based modeling of autophagy reveals emergent regulatory behavior of spatio-temporal autophagy dynamics. *Cell Commun Signal* (2014) 12:56. doi: 10.1186/s12964-014-0056-8
28. Wong P-M, Puente C, Ganley IG, Jiang X. The ULK1 complex. *Autophagy* (2013) 9(2):124–37. doi: 10.4161/auto.23323
29. Turco E, Fracchiolla D, Martens S. Recruitment and Activation of the ULK1/Atg1 Kinase Complex in Selective Autophagy. *J Mol Biol* (2020) 432(1):123–34. doi: 10.1016/j.jmb.2019.07.027
30. Shen H-M, Mizushima N. At the end of the autophagic road: an emerging understanding of lysosomal functions in autophagy. *Trends Biochem Sci* (2014) 39(2):61–71. doi: 10.1016/j.tibs.2013.12.001
31. Nwadike C, Williamson LE, Gallagher LE, Guan J-L, Chan EYW. AMPK Inhibits ULK1-Dependent Autophagosome Formation and Lysosomal Acidification via Distinct Mechanisms. *Mol Cell Biol* (2018) 38(10):e00023–18. doi: 10.1128/MCB.00023-18
32. Yu L, McPhee CK, Zheng L, Mardones GA, Rong Y, Peng J, et al. Termination of autophagy and reformation of lysosomes regulated by mTOR. *Nature* (2010) 465(7300):942–6. doi: 10.1038/nature09076

Conflict of Interest: The authors declare that the research was conducted in the absence of any commercial or financial relationships that could be construed as a potential conflict of interest.

frontiers in Immunology

ERRATUM
published: 25 June 2021
doi: 10.3389/fimmu.2021.724901

Erratum: Assessing Autophagy in Microglia: A Two-Step Model to Determine Autophagosome Formation, Degradation, and Net Turnover

*Frontiers Production Office**

Frontiers Media SA, Lausanne, Switzerland

OPEN ACCESS

Approved by:
Frontiers Editorial Office, Frontiers Media SA, Switzerland

***Correspondence:**
Frontiers Production Office
production.office@frontiersin.org

Specialty section:
This article was submitted to Multiple Sclerosis and Neuroimmunology, a section of the journal Frontiers in Immunology

Received: *14 June 2021*
Accepted: *14 June 2021*
Published: *25 June 2021*

Citation:
Frontiers Production Office (2021) Erratum: Assessing Autophagy in Microglia: A Two-Step Model to Determine Autophagosome Formation, Degradation, and Net Turnover. Front. Immunol. 12:724901. doi: 10.3389/fimmu.2021.724901

Keywords: autophagy, autophagosome, formation, degradation, LC3, microglia

An Erratum on

Assessing Autophagy in Microglia: A Two-Step Model to Determine Autophagosome Formation, Degradation, and Net Turnover
Plaza-Zabala A, Sierra-Torre V and Sierra A (2021). Front. Immunol. 11:620602. doi: 10.3389/fimmu.2020.620602

Due to a production error, there was an error in affiliations 1, 2 and 3. Instead of "[1]Department of Pharmacology, Achucarro Basque Center for Neuroscience, Leioa, Spain, [2]Glial Cell Biology Lab, Achucarro Basque Center for Neuroscience, University of the Basque Country UPV/EHU, Leioa, Spain, [3]Department of Neuroscience, Achucarro Basque Center for Neuroscience, Leioa, Spain," it should be "[1]Department of Pharmacology, University of the Basque Country UPV/EHU, Leioa, Spain, [2]Glial Cell Biology Lab, Achucarro Basque Center for Neuroscience, Leioa, Spain, [3]Department of Neuroscience, University of the Basque Country UPV/EHU, Leioa, Spain." The publisher apologizes for this mistake.

The original version of this article has been updated.

frontiers in Immunology

ORIGINAL RESEARCH
published: 03 February 2021
doi: 10.3389/fimmu.2020.617860

Alzheimer's Risk Gene TREM2 Determines Functional Properties of New Type of Human iPSC-Derived Microglia

Marvin Reich[1,2†‡], Iñaki Paris[1,3‡], Martin Ebeling[4], Nadine Dahm[5], Christophe Schweitzer[1], Dieter Reinhardt[1], Roland Schmucki[4], Megana Prasad[4], Fabian Köchl[4], Marcel Leist[2], Sally A. Cowley[6], Jitao David Zhang[4], Christoph Patsch[5†], Simon Gutbier[5] and Markus Britschgi[1*]*

[1] Roche Pharma Research and Early Development, Neuroscience and Rare Diseases Discovery and Translational Area, Roche Innovation Center Basel, F. Hoffmann-La Roche Ltd, Basel, Switzerland, [2] In Vitro Toxicology and Biomedicine, Department inaugurated by the Doerenkamp-Zbinden Foundation, University of Konstanz, Konstanz, Germany, [3] Achucarro Basque Center for Neuroscience, Science Park of the UPV/EHU, Leioa, Spain, [4] Roche Pharma Research and Early Development, Pharmaceutical Sciences, Roche Innovation Center Basel, F. Hoffmann-La Roche Ltd, Basel, Switzerland, [5] Roche Pharma Research and Early Development, Therapeutic Modalities, Roche Innovation Center Basel, F. Hoffmann-La Roche Ltd, Basel, Switzerland, [6] James Martin Stem Cell Facility, Sir William Dunn School of Pathology, University of Oxford, Oxford, United Kingdom

Microglia are key in the homeostatic well-being of the brain and microglial dysfunction has been implicated in neurodegenerative disorders such as Alzheimer's disease (AD). Due to the many limitations to study microglia *in situ* or isolated for large scale drug discovery applications, there is a high need to develop robust and scalable human cellular models of microglia with reliable translatability to the disease. Here, we describe the generation of microglia-like cells from human induced pluripotent stem cells (iPSC) with distinct phenotypes for mechanistic studies in AD. We started out from an established differentiation protocol to generate primitive macrophage precursors mimicking the yolk sac ontogeny of microglia. Subsequently, we tested 36 differentiation conditions for the cells in monoculture where we exposed them to various combinations of media, morphogens, and extracellular matrices. The optimized protocol generated robustly ramified cells expressing key microglial markers. Bulk mRNA sequencing expression profiles revealed that compared to cells obtained in co-culture with neurons, microglia-like cells derived from a monoculture condition upregulate mRNA levels for Triggering Receptor Expressed On Myeloid Cells 2 (TREM2), which is reminiscent to the previously described disease-associated microglia. TREM2 is a risk gene for AD and an important regulator of microglia. The regulatory function of TREM2 in these cells was confirmed by comparing wild type with isogenic TREM2 knock-out iPSC microglia. The TREM2-deficient cells presented with stronger increase in free cytosolic calcium upon stimulation with ATP and ADP, as well as stronger migration towards complement C5a, compared to TREM2 expressing cells. The functional differences were associated with

OPEN ACCESS

Edited by:
Rosa Chiara Paolicelli, University of Lausanne, Switzerland

Reviewed by:
Jessica Elaine Young, University of Washington, United States
Susanne Krasemann, University Medical Center Hamburg-Eppendorf, Germany

***Correspondence:**
Simon Gutbier
simon.gutbier@roche.com
Markus Britschgi
markus.britschgi@roche.com

†Present address:
Marvin Reich, Chair of Metabolic Biochemistry, Biomedical Center (BMC), Faculty of Medicine, Ludwig-Maximilians-Universität München, Munich, Germany
Christoph Patsch, BlueRock Therapeutics, New York, NY, United States

‡*These authors share first authorship*

Specialty section:
This article was submitted to Multiple Sclerosis and Neuroimmunology, a section of the journal Frontiers in Immunology

Received: *15 October 2020*
Accepted: *29 December 2020*
Published: *03 February 2021*

Citation:
Reich M, Paris I, Ebeling M, Dahm N, Schweitzer C, Reinhardt D, Schmucki R, Prasad M, Köchl F, Leist M, Cowley SA, Zhang JD, Patsch C, Gutbier S and Britschgi M (2021) Alzheimer's Risk Gene TREM2 Determines Functional Properties of New Type of Human iPSC-Derived Microglia. Front. Immunol. 11:617860. doi: 10.3389/fimmu.2020.617860

gene expression modulation of key regulators of microglia. In conclusion, we have established and validated a work stream to generate functional human iPSC-derived microglia-like cells by applying a directed and neuronal co-culture independent differentiation towards functional phenotypes in the context of AD. These cells can now be applied to study AD-related disease settings and to perform compound screening and testing for drug discovery.

Keywords: iPSC (induced pluripotent stem cell), microglia, cell culture protocols, drug development, TREM2 (triggering receptor expressed on myeloid cells), Alzheimer's disease (AD)

INTRODUCTION

Microglia play a key role in the well-being of the brain by fulfilling various functions in development, homeostasis and the first-line immune defense (1–7). Alzheimer's disease (AD) is a devastating age-related neurodegenerative disorder where microglia have been implicated for over a century in the pathogenesis based on neuropathological findings and by mimicking microglia dysfunction in preclinical models (8). More recently, genome wide association studies substantiated the long-time proposed active implication of microglia within initiation and progression of AD and other neurodegenerative diseases of the central nervous system (9, 10). Together, this strongly supports the rationale for developing therapies that pharmacologically modulate microglia.

In order to facilitate investigating the biology of microglia and to make them available for drug screening assays, cellular models had to be established. Until recently, *in vitro* studies with microglia have been limited to either employing primary rodent cells or cell lines (e.g. BV2) (11). Due to the stress implicated during their isolation process and the loss of tissue context, primary cells rapidly alter their previous *in situ* microglial properties (12, 13), and batch-to-batch variations as well as impurities are known hurdles of this approach. Moreover, generation of primary cells requires either euthanizing large numbers of animals or accessing difficult to obtain highly characterized human brain samples with short postmortem delay. Both approaches result in only a small number of cells, which in turn limits the throughput for compound screening campaigns or larger biological studies (14, 15). In contrast, due to their proliferative nature, cell lines do not have limitations in cell numbers, can be of human origin and are therefore often used in screening setups (16). However, due to their immortalization or neoplastic-origin, cell lines show strong discrepancies compared to the desired *in vivo* characteristics (17, 18).

With the arrival of human induced pluripotent stem cell (iPSC) technology (19, 20), and with the evolving understanding of microglial origin (21–23), several methods were reported for the generation of iPSC-derived microglia-like cells (24–26), hereafter called iPSC microglia. These protocols commonly aim to resemble the yolk sac ontogeny for the generation of primitive macrophage progenitors. Current reports indicate that iPSC microglia seem to be superior to primary cells or cell lines with regard to expressing key microglial marker genes (25). Importantly, unlike primary cells, iPSC microglia or their macrophage precursors can be generated robustly and in a controlled manner in scalable amounts (25, 27). This makes iPSC microglia ideal for drug screening and for extensively studying biological mechanisms under conditions resembling better the physiological state of microglia. Additionally, iPSC based models provide the opportunity to study the effect of disease associated genes with isogenic mutations or knockout pairs.

Despite the advances in developing cell culture models, *in vitro* microglia often lack important properties such as modulating the expression of a fully functional repertoire of various surface receptors, which microglia require to interact with their environment (28). For instance, microglia are the major cell type in the brain to express Triggering Receptor Expressed On Myeloid Cells 2 (TREM2). Signaling through this receptor modulates crucial microglia functions such as phagocytosis, proliferation, survival, and lipid metabolism in homeostatic, inflammatory or neurodegenerative conditions [extensively reviewed in (29, 30)]. Mutations in TREM2 are associated with an increased risk to develop various neurodegenerative disorders including AD (9, 10, 31–36). In the context of amyloid plaques, a neuropathological hallmark of AD, TREM2 was found in preclinical experiments to be essential for the metabolic fitness and transition of homeostatic to disease-associated microglia (DAM) (37, 38). Although the function and role of TREM2 in AD pathogenesis remains unclear, it became a key target for potential therapeutic intervention (39–41).

Some TREM2 loss-of-function-related phenotypes in the context of AD were recently described by others in iPSC-derived microglia (42–45). While the literature about iPSC microglia is growing, more descriptions are needed to compare different approaches that generate robust and scalable human cellular models of microglia. Such cellular models of microglia will hopefully become soon more translatable to microglia in the brain thereby establishing themselves as valuable tools to study disease mechanisms and to perform compound screens for drug development *in vitro*.

Here, we present the optimization of a protocol to generate iPSC microglia in a monoculture condition and explored whether these cells can serve as a model to study microglia function and gene expression in the context of TREM2 modulation. Building on our previously published large scale differentiation protocol of myeloid progenitors from iPSC (27), we have extended the differentiation of these myeloid progenitors for additional 14 days to microglia-like-cells. As a major distinction from previously published co-culture methods, we observed in iPSC microglia from monoculture an increased TREM2 mRNA expression. The regulatory function of

TREM2 in these cells was confirmed by comparing wild type with isogenic TREM2 knock-out iPSC microglia. The overall approach resulted in a work stream to generate human iPSC microglia by a directed and neuronal co-culture independent differentiation resulting in distinct phenotypes for mechanistic studies in AD. Our iPSC microglia protocol can now be applied to scale up the production of these cells, study certain AD-related disease settings, and perform compound screening and mechanistic experiments in drug development.

MATERIALS AND METHOD

iPSC Culture

All work with human iPSC and the derived cell types was performed under the respective Swiss legislation, ethical guidelines, and approval. All media compositions are summarized in **Table S1**. We recently reported an improved and highly scalable variant of the method published by van Wilgenburg et al. (27, 46) for the differentiation of iPSC to primitive macrophages. In brief, for iPSC maintenance culture dishes (Corning) were coated with 12.5 µg/ml rhLaminin-521 (BioLamina). Human iPSC were seeded and cultured in mTesR1 media (StemCell Technologies) at 37°C with 5% CO_2 and media was changed daily. Cells were passaged at 90% confluency, media was removed, cells were washed 1x with PBS and detached with Accutase™ (Innovative Cell Technologies) for 2 to 5 min at 37° C. After removal of Accutase™ by centrifugation cells were either used for maintenance or start of differentiation. The cell lines used in this study, Bioneer WT (BIONi010-C) and Bioneer C17 (BIONi010-C17/TREM2 KO) were obtained from Bioneer. Cells were quality controlled by STR profiling, SNP phenotyping and karyotyping after banking. To avoid genetic drift and variations sub-culturing was limited to an absolute minimum.

Differentiation of iPSC to Primitive Macrophages

Embryoid Body (EB) Generation

This step was performed as previously described (27). Briefly, to obtain uniform EBs, iPSCs were seeded into AggreWell 800 (StemCell Technologies) plates. Two ml mTesR1, supplemented with 10 µM ROCK inhibitor (Y27632, StemCell Technologies) and containing a single cell suspension of $4*10^6$ iPSCs were added to each AggreWell and centrifuged for 3 min at 100xg to assure an even and fast distribution of the iPSC into the AggreWells. The next day, mesoderm and subsequent hemogenic endothelium induction was started by exchange of 75% of the mTeSR1 media with mTeSR1 media supplemented with 50 ng/ml rhBMP4 (biotechne), 50 ng/ml rhVEGF (biotechne), and 20 ng/ml rhSCF (biotechne), and repeated the following 2 days.

Plating of EBs and Continued Maturation Along the Myeloid Lineage

On day 4 of differentiation, EBs were harvested and transferred to factory media, consisting of X-VIVO 15 media (Lonza) supplemented with 2 mM GlutaMAX (Thermo Fisher Scientific), 10 U/ml Penicillin/Streptomycin (Thermo Fisher Scientific), 50 µg/ml Mercaptoethanol (Thermo Fisher Scientific), 100 ng/ml rhM-CSF (Miltenyi Biotech), and 25 ng/ml rhIL3 (Miltenyi Biotech). EBs were plated at a density of 1 EB/cm^2 in growth factor reduced matrigel (Corning) precoated cell culture vessels and myeloid factories were matured as described previously (25).

Macrophage Progenitor Harvesting

Macrophage progenitors were collected from the supernatant by centrifugation (4 min, 300xg) and were either matured into co-culture or monoculture microglia-like cells (**Figure 1A**).

Differentiation of iPSC Into Microglia-Like Cells in Co-Culture

Induced pluripotent stem cells were differentiated to neurons using a protocol that was previously published (47). Neurons were quickly thawed at 37°C and seeded at a density of 200,000 cells/cm^2 in neuronal differentiation media [consisting of 1:1 Advanced DMEM/F12 media (with GlutaMAX I) (Thermo Fisher Scientific) and Neurobasal media (Thermo Fisher Scientific) + 1% B27 supplement without vitamin A (Thermo Fisher Scientific), 1% N2 supplement (Thermo Fisher Scientific), 50 µg/ml Beta-Mercaptoethanol (Thermo Fisher Scientific), 10 U/ml Penicillin-Streptomycin (Thermo Fisher Scientific), 20 ng/ml rhBDNF (PeproTech), 10 ng/ml rhGDNF (PeproTech), 100 µM Aa2-P (Sigma Aldrich), 500 µM cAMP (BIOLOG Life Science), and 1 µg/ml murine laminin (Roche), supplemented with 10 µM ROCKi (Y27632, StemCell Technologies) for seeding]. After a 100% media change one day after seeding, 50% of the media was changed twice a week. After 14 days, macrophage precursor cells were added at a density of 160,000 cells/cm^2. Therefore, the media was replaced with a macrophage precursor cell suspension in N2 media [Advanced DMEM/F12 + 1% N2 supplement, 10 U/ml Penicillin-Streptomycin, 2 mM Glutamax, 50 µg/ml β-ME, 100 ng/ml rhIL34 (Miltenyi Biotech), and 10 ng/ml rhGM-CSF (biotechne)]. Half of the media was changed twice a week for two additional weeks.

Differentiation of iPSC to Microglia-Like Cells in Monoculture

Initially, different variations of coating and media were tested (indicated in figure legends). For the final protocol flasks and plates were coated with fibronectin. Fibronectin (Corning, 10 µg/ml in $PBS^{-/-}$) was added and incubated for 3 h at RT, before washing three times with water. Macrophage precursors were seeded in RPMI media [RPMI 1640 media (Thermo Fisher Scientific) + 10 U/ml P/S supplemented with 100 ng/ml rhIL34, 25 ng/ml rhM-CSF, and 50 ng/ml rhTGF-β1 (PeproTech) at a density of 160,000 cells/cm^2]. Half the media was changed twice a week for 14 days. On day 14, cells were replated by collecting cells from the supernatant and detaching adherent cells with Accutase™. These cells were replated into fibronectin pre-coated assay plates and cultured for at least two additional days prior to the assays.

Magnetic-Activated Cell Sorting (MACS)

For the separation of co-cultured iPSC-derived microglia-like cells from neurons and astrocytes, immunomagnetic separation

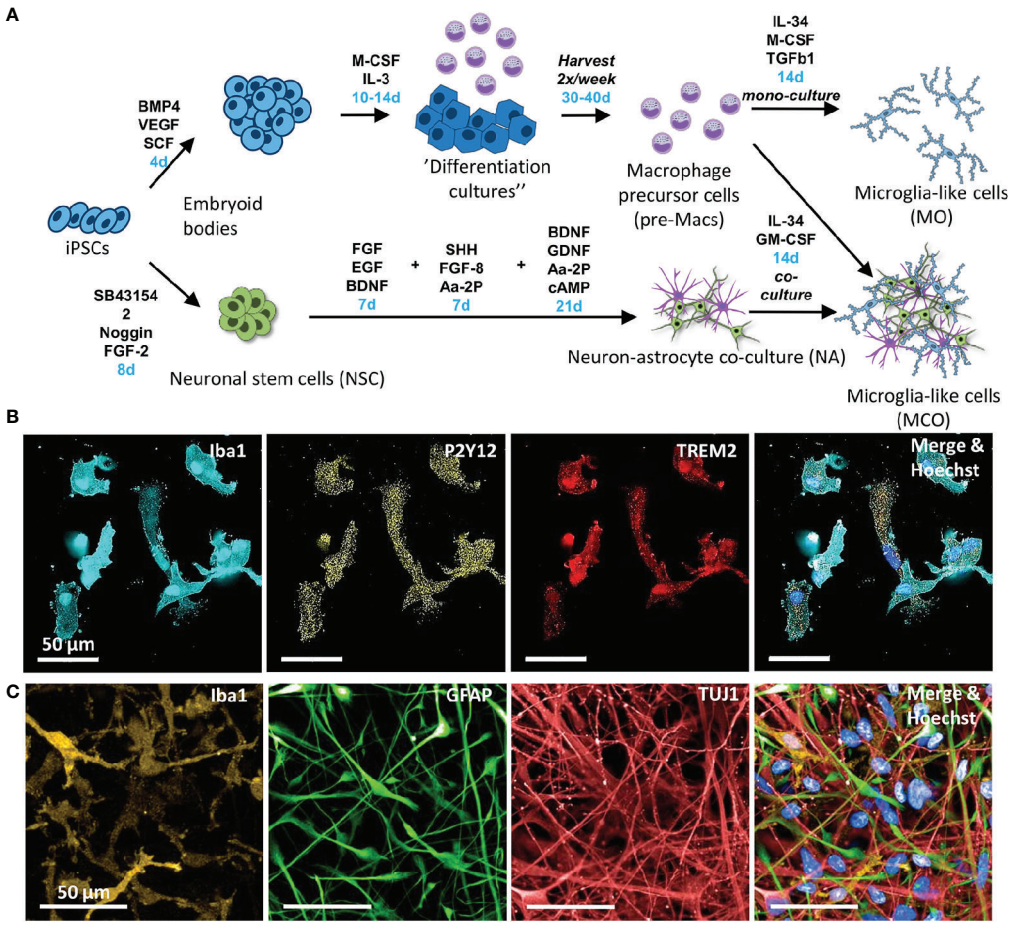

FIGURE 1 | Approaches employed to differentiate human iPSC towards microglia-like cells. **(A)** Schematic diagram of the protocols to generate different microglia-like cells from human iPSC. Relevant growth factors and durations (blue) of differentiation steps are indicated. The upper part depicts the differentiation of iPSCs into "myeloid factories" that produce macrophage precursor cells (pre-Macs) (27). For the generation of monocultured iPSC-derived microglia, pre-Macs were differentiated in the presence of IL-34, M-CSF, and TGF-β1. The lower part depicts the differentiation steps from iPSCs to neural stem cells and further to neurons. For the generation of neural co-culture-derived microglia, pre-Macs were seeded on top of the neuron/astrocyte cultures. **(B)** Representative images of immunostaining of iPSC microglia after 24 days differentiation in monoculture. Monoculture-derived microglia-like cells stain positive for Iba1 (cyan), P2Y12 (yellow), and TREM2 (red). Cellular nuclei were labeled with Hoechst 33342 (blue). **(C)** Immunostaining of microglia-like cells, neurons and astrocytes after 14 days differentiation in co-culture. Representative images are shown from three biological replicates. Microglia-like cells are detected by Iba1 (orange), astrocytes by GFAP (green), and neurons by TuJ1 (red), respectively. Cellular nuclei were labeled with Hoechst 33342 (blue).

was applied. Cells were detached after 14 days in co-culture by incubation with accutase at 37°C for 45 min. After centrifugation at 300xg for 5 min, the cells were resuspended in N2 media containing 100 U/ml DNaseI (Roche) and incubated at RT for 10 min to minimize the amount of free-floating DNA and cell aggregates. Then, the cell suspension was filtered through a 70 µm cell strainer (Greiner). Magnetic labeling and magnetic separation using the autoMACSpro (Miltenyi Biotec) was performed using anti-CD45 MicroBeads (Miltenyi Biotech), following the CD45 MicroBeads separation manual, provided by Miltenyi Biotech. Higher specificity of antigen-binding was achieved by the addition of 12.5 µg/ml Fc Block (BD Biosciences) during incubation with the MicroBeads. Microglia-like cells were obtained in the positive selection.

Quantitative Real-Time PCR

Cells were lysed and the RNA purified using the High Pure RNA Isolation Kit from Roche following the provided protocol. Macrophage precursor cell aggregates were lysed directly after the harvest, microglia-like cells, derived using the monoculture protocol were lysed directly in the cell culture plate. Co-cultured microglia-like cells were lysed directly after MACS.

For a one-step reverse transcription and PCR, the AgPath-ID One-Step RT-PCR kit (Thermo Fisher) was used. It contains an enzyme mix of reverse transcriptase and DNA polymerase. The reaction mixture was prepared according to the manufacturers descriptions and reverse transcription as well as PCR performed in LightCycler 480 384-well plates in a LightCycler 480 II (Roche) (reverse transcription for 10 min at 45°C, reverse

transcriptase inactivation and initial denaturation for 10 min at 95°C, 50 cycles of 15 s denaturation at 95°C and 60 s annealing at 60°C). PPIA was used as a housekeeping gene and was detected simultaneously with the gene of interest using two different dyes (VIC for PPIA, FAM for the gene of interest). Specificity of the readout was ensured using no-enzyme and no-primer controls. A detailed list of the primers used can be found in **Table S2**.

RNAseq and Data Analysis

Characterization by Bulk RNA Sequencing

Induced pluripotent stem cell derived macrophage progenitors, co- and monoculture microglia were generated as described above. Co-cultured microglia were purified as described above. All cultures were started at five different days to obtain five independent replicates for the RNAseq experiment. Cells were lysed and the RNA purified as described above. RNA purity was assessed using the Agilent 2100 Bioanalyzer. Strand-specific mRNA-seq libraries were generated from 1 μg total RNA using the TruSeq Stranded mRNA library prep kit (Illumina) according to manufacturer's instructions. Briefly, mRNA was purified from total RNA by polyA capture, fragmented and subjected to first-strand cDNA synthesis. The second-strand synthesis was performed incorporating dUTP instead of dTTP to ensure strand-specificity. Barcoded DNA adapters were ligated to both ends of the double-stranded cDNA and subjected to PCR amplification. The resulting libraries were checked on an AATI Fragment Analyzer, quantified with Qubit and pooled. The resulting library pool was diluted for cluster generation on the cBot2 and finally sequenced on the Illumina HiSeq 4000 platform.

RNAseq Analysis

Base calling was performed with BCL to FASTQ file converter bcl2fastq v2.17.1.14 from Illumina (https://support.illumina.com/downloads.html). In order to estimate gene expression levels, paired-end RNASeq reads were mapped to the human genome (build hg38) with STAR aligner version 2.5.2a using default mapping parameters (48). Aligned reads were quality checked with FastQC and MultiQC version 1.7 (49, 50). Numbers of mapped reads for all RefSeq transcript variants of a gene (counts) were combined into a single value by using SAMTOOLS software (51) and normalized as rpkms (number of mapped reads per kilobase transcript per million sequenced reads (52),. RNA-seq data have been deposited in Gene Expression Omnibus (GEO accession number GSE159108).

Principal Component Analysis and Heatmaps

Principal component analysis (PCA) of the gene expression profiles was generated using ClustVis (53). Each dot in the PCA plot is a biological replicate. Heatmaps were generated using ClustVis and default settings (53).

Generation of MA Plots

To visualize changes in gene expression between different conditions MA plots were generated. The MA plots are based on gene expression levels measured in $\log_2$(RPKM), the logarithm to the base of two of the reads per kilobase of transcript per million reads sequenced. The x axis shows, for every gene, the average expression value between the two conditions that were compared. On the y axis, the difference between the two expression levels for every gene is depicted. Each gene is represented by a single dot. Some strongly affected genes were highlighted in yellow, with gene names specified.

Microglia Expression Modules

Microglia expression modules were derived from the publication of Friedman et al. (54) and complemented by two modules (DAM signatures TREM2 dependent and TREM2 independent) derived from the publication of Keeren shaul et al. (38). Gene list for expression modules can be found in **Table S3**. Differences between two groups in these expression modules were visualized in a Radar plot using python.

Gene Ontology Analysis

A gene ontology analysis was performed that used the differentially expressed genes that showed at least four RPKM difference between WT and TREM2 KO. The GO terms were condensed using the GO slim immune response tool from dice tools (55).

Immunofluorescence Staining

Cells were fixed by replacing the medium with 4% PFA (Thermo Fisher Scientific, in PBS) followed by incubation at RT for 15 min. After washing three times using PBS, the cells were permeabilized by incubation in 0.1% PBS-T [0.1% Triton-X-100 (Sigma Aldrich) in PBS] for 15 min at RT. Following another washing step, non-specific binding sites were blocked by incubation in SuperBlock (Thermo Fisher Scientific) for 60 min at RT. The primary antibody was added in SuperBlock and incubated overnight at 4°C. Iba1, TREM2 and P2Y12 were added together, as well as Iba1, TuJ1, and GFAP. For the no-primary antibody controls, only SuperBlock was added. Following three washing steps, the cells were incubated with the three respective secondary antibodies (donkey anti-goat AF555, donkey anti-mouse AF647 and donkey anti-rabbit AF488, in SuperBlock) for 90 min at RT in the dark and unbound antibodies removed in two washing steps. Nuclei were counterstained with Hoechst33342 (Invitrogen, in SuperBlock) in the dark at RT, followed by two washing steps. The cells were kept in PBS and images acquired using the 63x objective of an OperaPhenix (Perkin Elmer). Images were processed and analyzed using the built-in Harmony software. The no-primary antibody control was used for background correction. A complete list of the antibodies used can be found in **Table S4**.

Mitochondrial Respiration Assay

The assay was performed using the Seahorse XF Cell Mito Stress Test kit (Agilent). Cells were differentiated as described above (14 days monoculture microglia like) and, in a Seahorse XF96

cell culture microplate, 50,000 cells (480,000 cells/cm^2) were seeded two days prior to the experiment. On the day of the experiment, the medium was replaced with 180 µl media for the mitochondrial respiration stress test (base medium + 2 mM L-glutamine (Thermo Fisher Scientific), 1 mM sodium pyruvate (Thermo Fisher Scientific), and 0.45% glucose (Sigma Aldrich), pH 7.4). Prior to the experiment, the cell culture microplate was incubated for 1 h at 37 °C in a non-CO_2 incubator. The assay was performed using a Seahorse XFe 96 Analyzer and compounds (prepared according to the assay manual) were injected sequentially (1 µM oligomycin, 2 µM FCCP, and 500 mM rotenone/antimycin A) and the oxygen consumption rate (OCR) measured three times before treatment and after every injection. Data was processed and analyzed using the Seahorse Wave software. For normalization, cells were fixed with 4% PFA at 37°C for 15 min and nuclei stained with Hoechst 33342 for 15 min, before washing twice with PBS. The Operetta CLS high-content screening system (Perkin Elmer) was used for imaging nuclei counted and the ratio between cell types calculated.

Transwell Migration Assay

Cells were differentiated as described above (14 days monoculture microglia like), detached from the dishes with accutase and plated at a density of 8,000 cells per well in a 96-well IncuCyte ClearView cell migration plate (Essen BioScience). In the lower compartment, either recombinant human complement C5a (biotechne, 1 ng/ml) or solvent control were added as chemoattractant, which generates by natural diffusion a gradient of the chemoattractant. Plates were incubated in an IncuCyte S3 (Essen BioScience) and images acquired using the 10x objective every 4 h for upper and lower well. Migration was assessed for 72 h and quantified using the Incucyte software Migration Analysis tool.

Determination of Free Intracellular Ca^{2+}

Cells were differentiated as described above (14 days monoculture microglia like) and 8,000 cells were plated per well of a 384 well plate. For calcium measurements, cells were incubated with the FLIPR calcium 6 imaging dye (Molecular Devices) following the manufacturer's instructions. Briefly, dye was dissolved in 10 ml of assay buffer 1 and 20 µl per well were added to the cells. Cells were incubated for 2 h with the dye. Increase in cytosolic calcium in response to ATP (Thermo Fisher Scientific), ADP (Sigma Aldrich), as well as C5a was assessed using the Hamamatsu FDSS7000 detection system. Background signal (average of 10 pictures prior to addition of stimuli) was subtracted from the measured maximum following stimulation. RFU values were assessed per well.

Phagocytosis Assay

Cells were differentiated as described above (14 days monoculture microglia like) and 40,000 cells were plated per well of a 96 well plate (Falcon 353219). For the phagocytosis assay, cells were incubated with Abeta coated, pHrodo labeled beads. To obtain these beads Amidine Latex Beads (A37322/ Thermo Fisher Scientific) were washed once with PBS, pelleted by centrifugation (16,000 g/5 min) and incubated at 37°C overnight in PBS containing 1 mg/ml Aβ42 (AnaSpec). After incubation with Aβ42 beads were pelleted, washed with PBS and re-suspended PBS containing 0.2 mg/ml pHrodo™ Red, succinimidyl ester (pHrodo™ Red, SE/Thermo Fisher Scientific). Beads and pHrodo were incubated for 1 h at room temperature. After the incubation, beads were washed with PBS and re-suspended in PBS. Phagocytosis of beads was monitored using Incucyte S3 acquiring brightfield and red fluorescence images. Cells were recognized using the Incucyte software adherent cell-by-cell classification tool.

Statistics

Unless otherwise mentioned, all data values are expressed as means ± standard deviation (SD). Unless otherwise indicated, experiments were performed at least three times (i.e., using three different cell preparations), with at least three technical replicates per condition. Statistical methods for analyzing the various data sets are indicated directly in the figure legends, data were analyzed using Graphpad Prism software.

RESULTS

For the generation of iPSC microglia many protocols still mostly rely on co-culturing microglia with neurons, astrocytes or neurons and astrocytes to mimic the brain environment (25, 26, 56). However, for drug screening purposes, e.g., with functional cellular assays, pure cultures of monolayer cells are highly desirable. One key aspect is to achieve proper microglia morphology *in vitro* in order to establish their functional phenotype as well (8).

In our hands, using the media condition that was closest to the previously published approach to generate iPSC microglia in monoculture (25), the cells showed only little ramifications (**Figure S1** N2, IL34, GM-CSF, Fibronectin). To increase ramification and marker gene expression of iPSC monoculture microglia, we began to screen existing protocols and tested six different media conditions (either N2 or RPMI media supplemented with either IL34+GM-CSF, IL34+M-CSF+TGF-β1 or IL34+M-CSF+TGF-β+CD200+CX3CL1) in combination with six different matrix coatings (Tissue culture treated only, Poly-D-lysine, CollagenI, Gelatin, Fibronectin, or Laminin) (**Figure S1A**). Conditions, where cells displayed ramifications, were chosen for follow up qPCR analysis (**Figure S1B**). Strongest differences between the different cultures were observed for key regulatory receptors of microglia such as fractalkine receptor CX3CR1, ADP chemoreceptor P2Y12, receptor tyrosine kinase AXL and lipoprotein lipase LPL mRNA expression. Based on the morphology and only minor differences upon CD200 and CX3CL1 addition for the last three days of differentiation, we chose for further analysis the condition of RPMI supplemented with IL-34, M-CSF and TGF-β1 on fibronectin coating (**Figure S1A** and **Figure 1A** for timeline). Under this condition, we confirmed the expression of P2Y12 on protein level by immunocytochemistry as well (**Figure 1B**). The iPSC microglia from monoculture displayed a similar morphology as the co-culture iPSC microglia (**Figure 1C**) suggesting that the fibronectin matrix resembles aspects of the matrix found in co-cultures.

To benchmark the microglia monoculture model towards iPSC microglia in co-culture with iPSC-derived neurons, we performed magnetic-activated cell sorting to remove the neurons and compared the microglia based on their bulk RNA-seq profile. A principal component analysis (PCA) demonstrated a sufficient cellular differentiation of the mono- and co-culture derived microglia with their common macrophage precursor (pre-Macs) (**Figure 2A**). Similarly, gene expression profiling between mono- versus co-cultured microglia revealed a higher expression of ENPP2, FOSB,CCL13, F13A1, IL1B, CD74 in microglia co-cultured with iPSC-derived neurons, whereas monocultured microglia expressed higher levels of ID1, LINC01235, MRC2, FABP4, TIMP3, APOE, and SPP1 (**Figure 2B**). Together, this confirms that the mono- and co-culture conditions induce two different microglia subsets.

Microglia are highly plastic cells that can change their morphological and functional phenotype as a reaction to different stimuli (8). Such stimuli can derive from environmental alterations in the brain due to aging and neurodegeneration. In support of this, comprehensive RNA-seq analyses of microglia isolated from human and mouse brain in an AD or other neurodegenerative disease context indicate an association between gene transcription pattern and a specific activation state of microglia. Recently, different transcription patterns were proposed to categorize microglia into different subsets (38, 54, 57, 58). In that context the

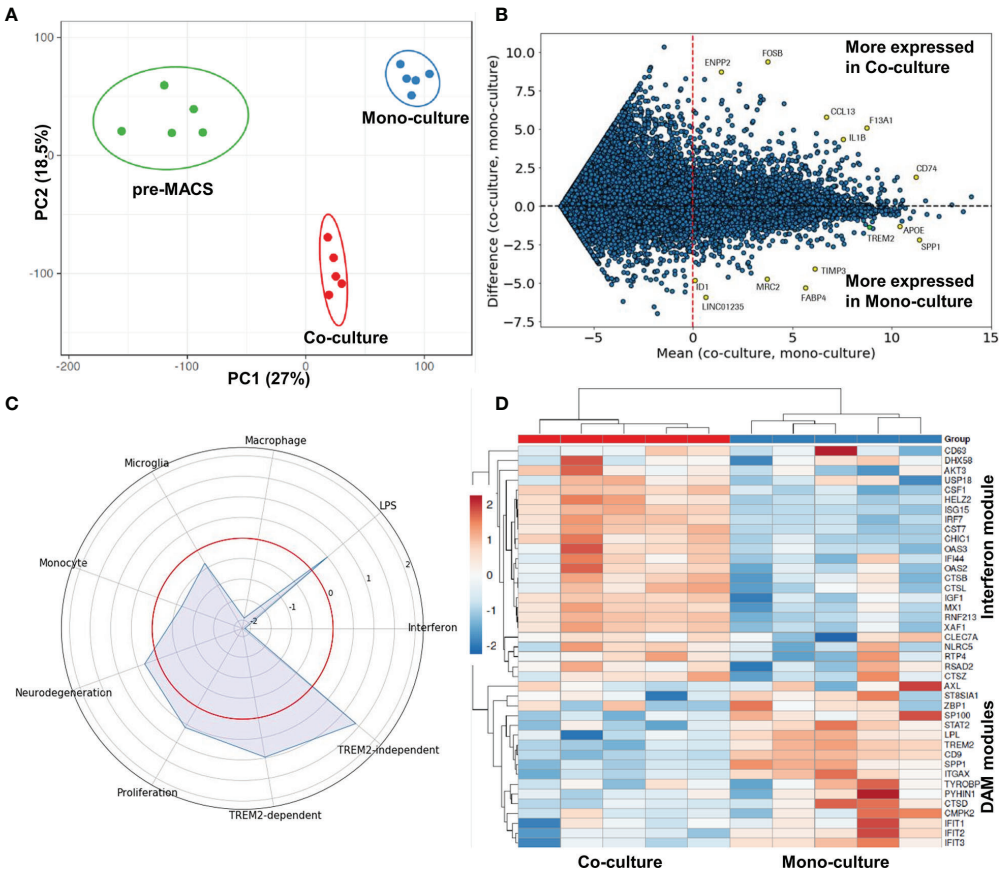

FIGURE 2 | Comparison of gene expression profiles in mono- and co-culture-derived microglia. **(A)** Principal component analysis of complete expression profiles of macrophage precursors (pre-MACS), mono- and co-cultured microglia-like cells. The lack of any intersection between the ellipses (95% confidence interval) indicates a clear statistically significant separation between the gene patterns of the different cell types. **(B)** MA plot to visualize gene expression differences between mono- and co-culture-derived microglia-like cells. The MA plot is based on gene expression levels measured in $\log_2$(rpkm), the logarithm to the base of two of the reads per kilobase of transcript per million reads sequenced. The x-axis shows, for every gene, the average expression value between the two conditions, on the y-axis is, for every gene, the difference between the two expression levels. Some strongly affected genes are highlighted in yellow, with gene names specified. **(C)** Radar plot to visualize changes in gene expression in microglial modules. The red circle indicates the reference level as detected in co-cultured microglia. Peaks outside the red circle indicate higher expression in monoculture microglia and modules closer to the center indicate higher expression in microglia generated in co-culture with neurons. **(D)** Heatmap of the genes belonging to the DAM or interferon module in co- and monoculture derived microglia. Expression values were standardized and depicted on a z-scale with red indicating high and blue low expression, respectively. The five red and five blue boxes on top of the heatmap indicate the two different culture conditions, respectively, and that each culture condition was performed in five independent experiments. The downregulation of the "interferon" module and the upregulation of "DAM" modules is consistent between different experiments as indicated by the similar gene expression patterns between different biological replicates. This confirms the robustness of our new protocol.

upregulation of APOE and SPP1 as observed in our monoculture condition is part of a DAM signature (38). This indicates that in contrast to the co-culture condition, our monoculture condition provides stimuli that drive iPSC microglia towards a more disease associated expression pattern.

In order to explore the transcriptional pattern of the monoculture microglia further and to gain more insight into the different stimuli that possibly induced the transcriptional phenotype, we defined nine different modules of microglia states based on published data sets (See **Table S3** for the names of the genes and of the different modules) (38, 54). We then mapped the differences in gene expression profiles of the two culture conditions towards these modules (**Figure 2C**). Our mono- and co-culture iPSC microglia were similar in the "microglia" module validating the chosen differentiation conditions to generate microglia. The most prominent differences were observed for "macrophage" and "interferon" modules, which were lower expressed in the monocultured iPSC microglia. The reduced "interferon" signature is most likely attributed to the change from GM-CSF supplementation in co-culture to M-CSF supplementation in monoculture (59). The lower "macrophage" signature combined with the also slightly reduced "monocyte" module indicates an even stronger differentiation away from the peripheral myeloid cells than the co-cultured microglia. Furthermore, we observed upregulation of "TREM2-dependent" and "TREM2-independent" modules suggesting a more DAM-like phenotype for iPSC microglia in monoculture compared with microglia from co-culture. The downregulation of the "interferon" module and the upregulation of "DAM" modules is consistent between different experiments as indicated by the similar gene expression patterns between different biological replicates (**Figure 2D**).

At this point, we wanted to complement the DAM-like gene expression pattern of our monoculture iPSC microglia with functional data. Given the implication of TREM2 in the DAM-like expression pattern and the association of TREM2 with AD we focused on modulating this gene. To that end, we employed the isogenic TREM2 knock-out (KO) of the same iPSC line and differentiated the two cell lines in parallel in the same monoculture condition. As before, we first made sure there is an effect of TREM2 KO on a gene expression level. The PCA revealed a minor but clear separation in RNAseq-based gene expression between iPSC-derived microglia and their isogenic KO form (**Figure 3A**). The majority of differentially regulated genes were downregulated in the KO compared to the cells having functional TREM2 (**Figure 3B**). This included DAM-signature associated genes and became evident in the module analysis as well (**Figure 3C**). The iPSC-derived microglia lacking TREM2 also displayed an upregulation of the interferon, proliferation and macrophage module, while the monocyte and neurodegeneration module were downregulated. Confirming the genotype, TREM2 independent DAM signature stayed unaffected by the loss of TREM2. The upregulation of the "interferon" module and the downregulation of "DAM" modules in the TREM2 KO microglia compared with wild type cells is consistent and robust between different experiments as indicated by the similar gene expression patterns between different biological replicates (**Figure 3D**). A gene ontology (GO) term analysis revealed that in iPSC-derived microglia lacking TREM2 "myeloid cell homeostasis", "myeloid cell development", and "myeloid progenitor cell differentiation", and GO terms related to cell adhesion, motility, and migration as well as lipid metabolism and mitochondrial organization were enriched (**Figure S2**, red boxes). Together, this indicates that the transcriptional phenotypes of the TREM2 KO and wild type iPSC microglia are sufficiently different from each other in order to expect functional differences as well.

To confirm some of the GO term associated functions and to explore feasibility of functional assays with microglia from our monoculture condition, we subsequently tested iPSC-derived microglia for their mitochondrial activity, cellular calcium responses and migratory capacity. First, we used Seahorse extracellular flux analysis to assess mitochondrial respiration. TREM2 KO microglia displayed a significantly lower basal mitochondrial respiration (**Figure 4A, B**), spare respiratory capacity (**Figure 4C**), and less ATP production (**Figure 4D**), while there was no significant difference detected in the proton leak (**Figure 4E**) when compared to isogenic wild type iPSC microglia, indicating reduced use of the respiratory chain for ATP production.

Microglia continuously monitor their environment and can react to damage signals (e.g., ADP/ATP released by dying neurons, local activation of complement pathways in the aging brain and in neurodegeneration), i.e., by directed migration to the damage site (60). Many of the microglial receptors rely on changes of free intracellular calcium levels to mediate the internal signal transmission and integration. For instance, chemoattractants and damage-associated molecules signal through GPCR receptors thereby increasing intracellular calcium levels. To check for this functionality, we stimulated the cells with different concentrations of the typical chemoattractants and damage signals ADP, ATP and complement factor C5a (**Figures 5A–C**) and monitored the related intracellular calcium changes. The anaphylatoxin C5a is a well-described chemoattractant for innate immune cells that can be employed in cell culture (27). In an *in vivo* setting light induced microglial migration in the retina has been reported to be C5aR dependent (61) and in context of AD recent reports suggest a role of C5a in the regulation of microglial inflammatory response (62). ATP and its metabolites are also well-described chemoattractants for microglia through their plethora of receptors (63–65) Confirming the GO term result, TREM2 KO cells reacted already at lower concentrations and with a higher maximum to all three stimuli than their isogenic wild type iPSC microglia. This indicates a potentially more rapid signal integration in the TREM2 KO versus the wild type microglia. This is supported by a slightly elevated baseline migratory phenotype, and much more by the robust almost doubling of the migration speed of TREM2 KO versus wild type microglia upon stimulation by C5a (**Figure 5D**).

Phagocytosis and in particular uptake of Aβ—a major component of senile plaques in the AD brain—is a prominent function of microglia, which according to preclinical *in vitro* and *in vivo* models is reduced by TREM2 loss of function (39, 66–68). In line with literature, we observed a strongly diminished uptake

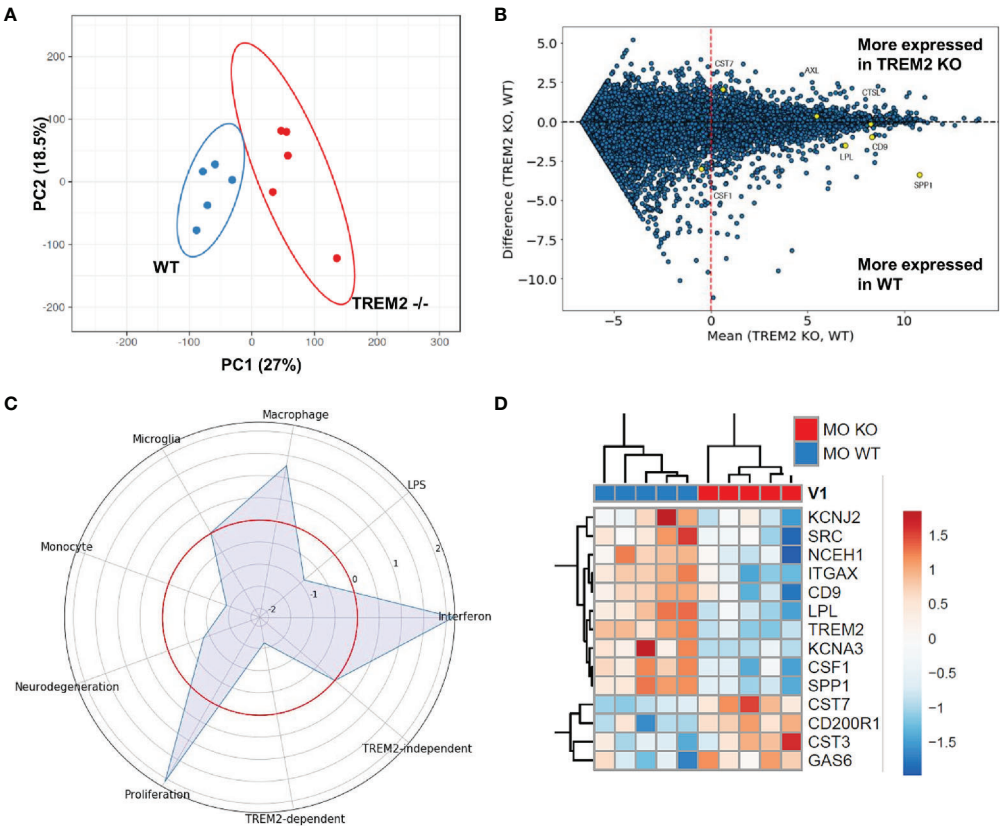

FIGURE 3 | Differences in gene expression in wild type and TREM2 KO monoculture-derived iPSC microglia. **(A)** Principal component analysis of complete expression profile of monoculture derived microglia-like cells generated from wild type (WT) and TREM2 knockout (KO) iPSC lines. The lack of intersection between the ellipses (95% confidence interval) indicate a statistically significant separation between the gene patterns of the two cell types while the fact that the ellipses seem to touch each other indicate only a minimal separation in the PCA. **(B)** MA plot to visualize gene expression differences between WT and TREM2 KO monoculture iPSC microglia. The MA plot is based on gene expression levels measured in $\log_2$(rpkm), the logarithm to the base of two of the reads per kilobase of transcript per million reads sequenced. The x-axis shows, for every gene, the average expression value between the two conditions, on the y-axis is, for every gene, the difference between the two expression levels. Genes highlighted in yellow are part of the TREM2-dependent DAM signature genes according to Keren-Shaul et al. (38). **(C)** Radar plot to visualize changes in gene expression in microglial modules. The red circle indicates the reference level as detected in WT iPSC microglia. Peaks outside the red circle indicate higher expression in TREM2 KO microglia and modules closer to the center indicate higher expression in microglia generated from the WT iPSC line. **(D)** Heatmap of the genes belonging to the DAM module in WT and KO monoculture microglia. Expression values were standardized and depicted as z-scores with red indicating high and blue low expression, respectively. The five red and five blue boxes on top of the heatmap indicate the two different cell types, respectively, and that each cell type was analyzed in five independent experiments. The gene expression patterns for each cell type appear consistent between different experiments. This confirms the robustness of our new protocol for WT and TREM2 KO iPSC microglia.

of Aβ-coated beads by the TREM2 KO compared with the wild type microglia (**Figures 5E, F**) confirming a critical role of TREM2 in regulation of microglial phagocytosis. Together, these functional data confirm the DAM-like phenotype of our iPSC microglia; a phenotype which can be reversed by knocking out TREM2.

In conclusion, the overall results of our different approaches to generate iPSC microglia combined with gene expression and functional phenotypes confirm the feasibility to employ monoculture conditions to generate microglia-like cells, which express relevant functional gene sets including the key surface receptor TREM2. The ability to ablate specific genes such as TREM2 to reverse their DAM-like phenotype make these iPSC microglia a valuable tool for studying biological mechanisms relevant for AD and to perform compound screening and testing for drug discovery.

DISCUSSION

Studying microglia in humans and ultimately finding and testing novel therapeutic approaches targeting these cells remains a huge challenge. This is attributed to the heterogeneity of phenotypes microglia can acquire. For instance, proliferation, migration, phagocytosis, neurotrophic signaling, factor release for the

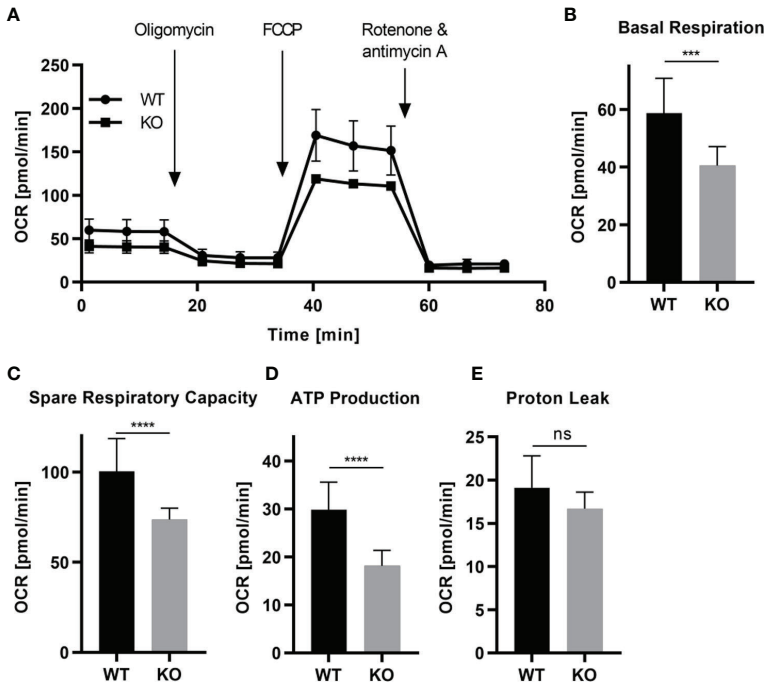

FIGURE 4 | Differential mitochondrial respiratory activity in TREM2 KO versus wild type iPSC microglia. WT and TREM2 KO monoculture iPSC microglia-like cells were re-plated after 14 days of differentiation into fibronectin pre-coated seahorse assay plates **(A–E)**. **(A)** The baseline oxygen consumption rate (OCR) of WT and TREM2 KO cells was assessed, followed by the sequential injection of different indicated mitochondrial electron transport chain complex inhibitors (oligomycin and a combination of rotenone and antimycin A) and the mitochondrial uncoupler carbonyl cyanide-4-(trifluoromethoxy)phenylhydrazone (FCCP). OCR was measured three times initially and after each injection. **(B)** The basal respiration was calculated by subtracting the OCR of non-mitochondrial respiration (OCR after rotenone/antimycin A injection) from the baseline OCR. **(C)** The spare respiratory capacity results from the subtraction of the basal respiration from the maximal respiration [(OCR after FCCP injection) – (non-mitochondrial respiration)]. **(D)** ATP production is the OCR of the basal respiration with the proton leak subtracted. **(E)** The proton leak is the remaining OCR after injection with oligomycin without non-mitochondrial respiration. n=3; Data shown as mean with standard deviation. Statistical analysis was performed using t-test. (ns, $p \geq 0.05$; ***$p \leq 0.001$; ****$p \leq 0.0001$).

modulation of immune function and blood-brain barrier integrity contribute to their high degree of plasticity (1–7, 69). This allows them to react to various cues and to switch between the phenotypes rapidly (8). Moreover, microglia are reported to have different regional abundance and activity states during aging, brain activity and neurodegenerative processes (58, 70–72). In addition, accessing microglia in the human brain is in the majority of cases only possible in postmortem tissue (73).

To overcome the need to study microglia in or isolated from humans, the field investigates rodent microglia *in situ* or as primary cells *in vitro* as a surrogate (38, 74, 75). Apart from the need to use large numbers of animals in order to isolate sufficient quantities of microglia, there are also many technical caveats when using rodent microglia; for instance batch-to-batch variations caused by the isolation process and a rapid switch of their previous gene expression pattern and phenotype (12, 13). Additionally, there are concerns about phenotypes induced by in-breeding, different mouse strains with different immune backgrounds and the often-limited translatability between mice and humans. This inter species translatability is of general concern for all animal models but especially for various receptors and ligands related to innate immunity and particularly microglia (74, 76).

Besides rodent models, microglia like cells have also been derived from human peripheral monocytes (77). These cells have been shown to resemble microglia specific gene signatures and functional properties. However, due to the difference in hematopoietic origin, these cells rather resemble infiltrating monocytes than brain resident microglia (77).

The iPSC technology together with the evolving understanding of microglial origin in mice and humans (21–23) allow now the robust generation of human iPSC-derived microglia-like cells (24–26, 78) in large amounts (25, 27).This provides the opportunity to employ human iPSC microglia for large-scale drug screening and for extensively studying biological mechanisms under more physiological and translational conditions. Additionally, iPSC based models provide the opportunity to study the effect of disease associated genes with isogenic mutation or knockout pairs (42, 43, 45). All of these protocols aim to follow the course of embryonic development and to recapitulate this *in vitro* as far as possible (24–27, 79). For the first part, the generation of myeloid progenitors *via*

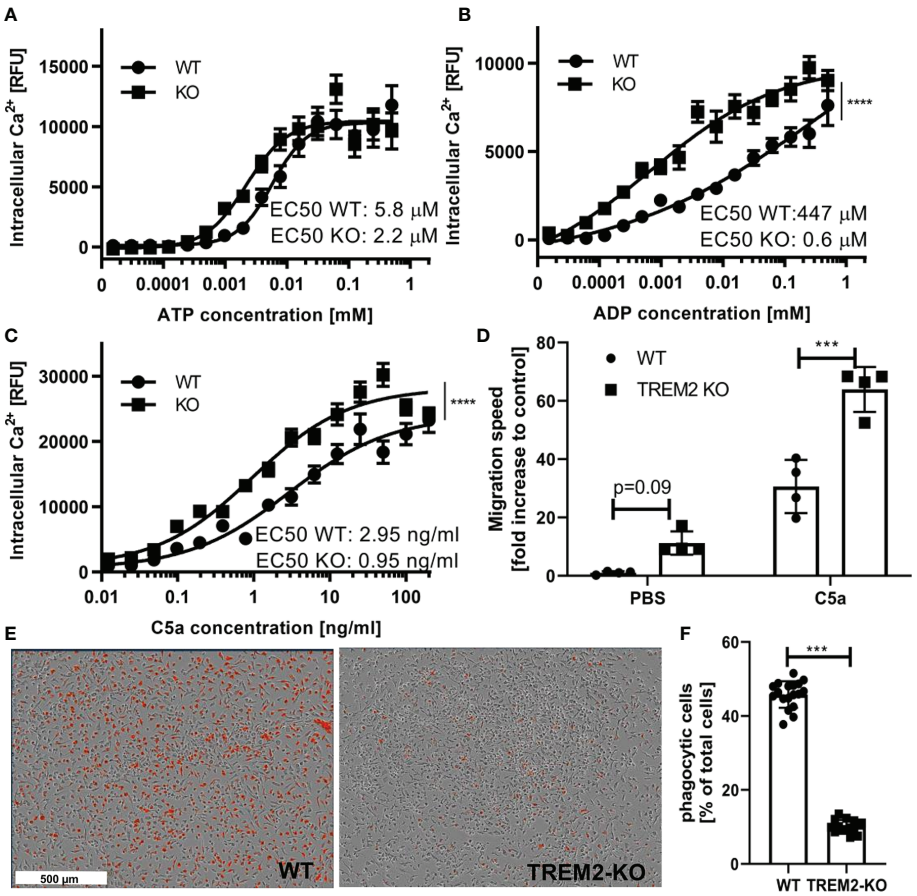

FIGURE 5 | Functional differences in TREM2 KO versus wild type iPSC microglia. **(A–C)** Intracellular calcium kinetics following different stimuli. **(A)** Intracellular calcium levels upon stimulation with different concentrations of ATP. Maximum measured fluorescence is indicated as relative fluorescence units (RFU), which are baseline corrected (n = 3). Data shown as mean with standard error of the mean. Statistical analysis of two data sets was performed using a two-way ANOVA. **(B)** Intracellular calcium levels upon treatment with different concentrations of ADP. Maximum measured fluorescence is indicated as relative fluorescence units (RFU), which are baseline corrected (n = 3). Data shown as mean with standard error of the mean Statistical analysis of two data sets was performed using a two-way ANOVA(****$p < 0.0001$). **(C)** Intracellular calcium levels upon treatment of different concentrations of complement component 5a (C5a). Maximum measured fluorescence is indicated as relative fluorescence units (RFU), which are baseline corrected (n = 3). Data shown as mean with standard error of the mean. Statistical analysis of two data sets was performed using a two-way ANOVA (****$p < 0.0001$). **(D)** Migration speed of WT and TREM2 KO monoculture microglia in presence or absence of 1 ng/ml C5a as chemoattractant in the bottom compartment. Migration speed was calculated from the increase in iPSC microglia occupied area over time in the bottom compartment of the transwell and expressed relative to untreated WT control. Statistical analysis was performed using t-test for PBS and complement C5a condition, respectively (***$p < 0.001$). **(E)** Representative images of WT and TREM2 KO iPSC microglia incubated for 2 h with pH-rodo labeled Aß-coated beads. **(F)** Quantification of pHrodo positive microglia after 2 h incubation with pHrodo labeled Aß-coated beads. n = 3; Data shown as mean with standard deviation. Statistical analysis was performed using t-test (***$p < 0.001$).

transcription factor MYB-independent primitive myelopoiesis, most protocols are broadly similar. However, the challenge for microglia generation as well as for the maintenance of primary microglia lies in the simulation of the correct neuronal microenvironment that determines the final differentiation and is essential for the maintenance of the phenotype (12). Several approaches exist for the *in vitro* simulation of this tissue niche, most of which are based on co-culture approaches with either neurons (25), astrocytes (42) or both. Other approaches use chemokines, morphogens and metabolites to differentiate the microglia-like cells in monoculture (17, 80)

Recently, we demonstrated the scalability of a protocol for the generation of myeloid precursors and primitive macrophages (27). The protocol is based on a publication by van Wilgenburg et al. (46) and cells generated with this differentiation protocol have already been used previously to obtain microglia like cells in co-cultures (2 and 3D) as well as in monoculture (25, 81). However, further optimization of the monoculture protocol seemed desirable. In our study, we aimed for such a reductionist approach of monoculture microglia and compared them on the morphological and gene expression level to the more elaborate co-culture model. Our observations on the

transcriptional as well as on the phenotypic level correlate with the results reported from others (24, 25, 78)and extend these. The constitution of growth factors in our finally chosen microglia differentiation media is similar to the one published by McQuade and colleagues (78). Even though the two protocols differ in mesoderm induction and pre-Mac generation, resulting cells showed similar transcriptional and morphological profiles. However, a key advantage of the protocol shown here is the long lifetime of the myeloid factories, which allows continuous pre-Mac supply over a production period of 60–80 days (27).

We observed on the transcriptional level that monoculture-derived iPSC microglia showed an increase in genes related to the so-called DAM signature compared with neuronal co-culture derived microglia (**Figure 2**). The cell surface receptor TREM2 is part of the DAM signature (37, 38). It is an important molecule for microglia to interact with their environment and mutations in the gene for TREM2 are associated with neurodegenerative disorders including AD (9, 10, 31–36). Due to the importance of TREM2 for microglia and in drug discovery attempts for AD in general, we focused the characterization of our human iPSC microglia on TREM2 related functions and chose a TREM2 KO isogenic pair to further challenge the suitability of our monoculture model in cellular assays. First, we compared the isogenic controls on the transcriptional level and identified differences in genes associated with mitochondrial organization, cell motility and migration. Indeed, we could confirm differences in mitochondrial respiration by the Seahorse assay. Furthermore, we observed different responses in free intracellular calcium following exposure to well-established microglia chemoattractants, and pronounced differences in the migration towards one of these attractants (complement C5a) (**Figures 5A–D**), which is in line with observations by others (82). Furthermore, we demonstrated that the monocultured iPSC microglia are also suitable for phagocytosis assays (**Figures 5E, F**) and confirmed here observations published by others (39, 66–68). TREM2 signals *via* DAP12 and phosphorylation of SYK resulting in phosphorylation of the downstream kinases PI3K, PLCy and ERK (42, 67). These pathways have already been linked to alterations in cell proliferation, survival, metabolism, motility, and phagocytosis (42, 82–84). TREM2 KO has been shown to restore a homeostatic phenotype in AD and SOD models *in vivo* (82, 84). However, our observation that TREM2 KO cells show an increase in proliferative signatures and in motility was rather unexpected. One possible explanation could be that DAP12 may be stronger involved in the integration of other signaling cascades upon TREM2 loss. For the complete understanding of the pathway, we plan to explore the effect of loss of downstream targets on the cellular phenotypes in future studies.

Overall, our monoculture microglia model performed robustly in the applied functional cellular assays, pointing to its suitability to study cellular effects of TREM2 modulation. In a next step, our iPSC microglia model could be applied for cellular screening and profiling of various microglia modulatory pathways in the context of AD or other neurological diseases. Additionally, the established protocol to generate iPSC microglia now forms the basis to expand the single cell type culture with other cell types in order to generate multicellular spheroids and organoids. However, such complex cell models also come with greatly increased cultivation time, limited throughput and reduced number of available readouts (85) and more optimization will be required.

In this study, we have not addressed the suitability of the monoculture microglia system to investigate the effects of other disease-associated mutations or to model aspects of other diseases. However, the transcriptional data set in combination with the microglial module analysis provides a good basis to judge suitability of this model for other purposes. Using this as a starting point, one could test a variety of stimuli and see how they affect the expression in the different modules. Once we know what drives the differentiation of iPSC microglia towards a desired phenotype could enable the development of a toolbox for modeling key aspects of different microglial subtypes in monoculture.

In conclusion, the combined results of our experiments demonstrate that human iPSC microglia can be produced robustly in monoculture and our data confirm that these cells can be used in various microglia-relevant functional assays. Additionally, genetic ablation of TREM2 leads to the expected phenotypes validating these cells as a valuable tool for studying microglia-related biological mechanisms and to perform compound screening and testing for drug discovery.

DATA AVAILABILITY STATEMENT

The datasets presented in this study can be found in online repositories. The names of the repository and accession number can be found here: https://www.ncbi.nlm.nih.gov/geo/, GSE159108.

AUTHOR CONTRIBUTIONS

MB and SG conceived, designed, and supervised the study and SC and ME provided critical scientific input. MR, IP, ND, DR, and CS performed the cellular experiments. FK, MP, RS, and ME did the RNAseq analysis and evaluated the data. SG drafted the article and co-wrote the paper with MB. CP, SC, ML, MR, ME, and JZ revised the article critically. ML academically supervised MR's master's thesis, which is part of this manuscript. All authors contributed to the article and approved the submitted version.

FUNDING

SG was supported by the Roche Postdoctoral Fellowship (RPF) program and IP by the Roche Internships for Scientific Exchange (RiSE) program.

ACKNOWLEDGMENTS

We thank Dr. A. Sierra for academic mentorship of IP and critical feedback on the manuscript. We thank K. Dernick for support with imaging.

SUPPLEMENTARY MATERIAL

The Supplementary Material for this article can be found online at: https://www.frontiersin.org/articles/10.3389/fimmu.2020.617860/full#supplementary-material

REFERENCES

1. Ousman SS, Kubes P. Immune surveillance in the central nervous system. *Nat Neurosci* (2012) 15:1096–101. doi: 10.1038/nn.3161
2. Paolicelli RC, Bolasco G, Pagani F, Maggi L, Scianni M, Panzanelli P, et al. Synaptic Pruning by Microglia Is Necessary for Normal Brain Development. *Science* (2011) 333:1456–8. doi: 10.1126/science.1202529
3. Parkhurst CN, Yang G, Ninan I, Savas JN, Yates JR,3, Lafaille JJ, et al. Microglia promote learning-dependent synapse formation through brain-derived neurotrophic factor. *Cell* (2013) 155(7):1596–609. doi: 10.1016/j.cell.2013.11.030
4. Schafer DP, Lehrman EK, Kautzman AG, Koyama R, Mardinly AR, Yamasaki R, et al. Microglia sculpt postnatal neural circuits in an activity and complement-dependent manner. *Neuron* (2012) 74:691–705. doi: 10.1016/j.neuron.2012.03.026
5. Shigemoto-Mogami Y, Hoshikawa K, Goldman JE, Sekino Y, Sato K. Microglia Enhance Neurogenesis and Oligodendrogenesis in the Early Postnatal Subventricular Zone. *J Neurosci* (2014) 34:2231–43. doi: 10.1523/JNEUROSCI.1619-13.2014
6. Sierra A, Encinas JM, Deudero JJ, Chancey JH, Enikolopov G, Overstreet-Wadiche LS, et al. Microglia shape adult hippocampal neurogenesis through apoptosis-coupled phagocytosis. *Cell Stem Cell* (2010) 7:483–95. doi: 10.1016/j.stem.2010.08.014
7. Zhou L-J, Peng J, Xu Y-N, Zeng W-J, Zhang J, Wei X, et al. Microglia Are Indispensable for Synaptic Plasticity in the Spinal Dorsal Horn and Chronic Pain. *Cell Rep* (2019) 27:3844–3859.e6. doi: 10.1016/j.celrep.2019.05.087
8. Sierra A, Paolicelli RC, Kettenmann H. Cien Anos de Microglia: Milestones in a Century of Microglial Research. *Trends Neurosci* (2019) 42:778–92. doi: 10.1016/j.tins.2019.09.004
9. Kunkle BW, Grenier-Boley B, Sims R, Bis JC, Damotte V, Naj AC, et al. Genetic meta-analysis of diagnosed Alzheimer's disease identifies new risk loci and implicates Aβ, tau, immunity and lipid processing. *Nat Genet* (2019) 51:414–30. doi: 10.1038/s41588-019-0358-2
10. Lambert J-C, Ibrahim-Verbaas CA, Harold D, Naj AC, Sims R, Bellenguez C, et al. Meta-analysis of 74,046 individuals identifies 11 new susceptibility loci for Alzheimer's disease. *Nat Genet* (2013) 45:1452–8. doi: 10.1038/ng.2802
11. Henn A, Lund S, Hedtjarn M, Schrattenholz A, Porzgen P, Leist M. The suitability of BV2 cells as alternative model system for primary microglia cultures or for animal experiments examining brain inflammation. *ALTEX* (2009) 26:83–94. doi: 10.14573/altex.2009.2.83
12. Bohlen CJ, Bennett FC, Tucker AF, Collins HY, Mulinyawe SB, Barres BA. Diverse Requirements for Microglial Survival, Specification, and Function Revealed by Defined-Medium Cultures. (2017) 94(4):759–73. doi: 10.1016/j.neuron.2017.04.043
13. Lund S, Christensen KV, Hedtjarn M, Mortensen AL, Hagberg H, Falsig J, et al. The dynamics of the LPS triggered inflammatory response of murine microglia under different culture and in vivo conditions. *J Neuroimmunol* (2006) 180:71–87. doi: 10.1016/j.jneuroim.2006.07.007
14. Mizee MR, Miedema SSM, van der Poel M, Schuurman AKG, van Strien ME, Melief J, et al. Isolation of primary microglia from the human post-mortem brain: effects of ante- and post-mortem variables. *Acta Neuropathologica Commun* (2017) 5:16. doi: 10.1186/s40478-017-0418-8
15. Olah M, Raj D, Brouwer N, De Haas AH, Eggen BJL, Den Dunnen WFA, et al. An optimized protocol for the acute isolation of human microglia from autopsy brain samples. *Glia* (2012) 60:96–111. doi: 10.1002/glia.21251
16. Timmerman R, Burm SM, Bajramovic JJ. An Overview of in vitro Methods to Study Microglia. *Front Cell Neurosci* (2018) 12:242. doi: 10.3389/fncel.2018.00242
17. Butovsky O, Jedrychowski MP, Moore CS, Cialic R, Lanser AJ, Gabriely G, et al. Identification of a unique TGF-β–dependent molecular and functional signature in microglia. *Nat Neurosci* (2014) 17:131–43. doi: 10.1038/nn.3599
18. Melief J, Sneeboer MAM, Litjens M, Ormel PR, Palmen SJMC, Huitinga I, et al. Characterizing primary human microglia: A comparative study with myeloid subsets and culture models. *Glia* (2016) 64:1857–68. doi: 10.1002/glia.23023
19. Takahashi K, Tanabe K, Ohnuki M, Narita M, Ichisaka T, Tomoda K, et al. Induction of Pluripotent Stem Cells from Adult Human Fibroblasts by Defined Factors. *Cell* (2007) 131:861–72. doi: 10.1016/j.cell.2007.11.019
20. Takahashi K, Yamanaka S. Induction of Pluripotent Stem Cells from Mouse Embryonic and Adult Fibroblast Cultures by Defined Factors. *Cell* (2006) 126:663–76. doi: 10.1016/j.cell.2006.07.024
21. Ginhoux F, Greter M, Leboeuf M, Nandi S, See P, Gokhan S, et al. Fate Mapping Analysis Reveals That Adult Microglia Derive from Primitive Macrophages. *Science* (2010) 330:841–5. doi: 10.1126/science.1194637
22. Gomez Perdiguero E, Klapproth K, Schulz C, Busch K, Azzoni E, Crozet L, et al. Tissue-resident macrophages originate from yolk-sac-derived erythro-myeloid progenitors. *Nature* (2015) 518:547–51. doi: 10.1038/nature13989
23. Kierdorf K, Erny D, Goldmann T, Sander V, Schulz C, Perdiguero EG, et al. Microglia emerge from erythromyeloid precursors via Pu.1- and Irf8-dependent pathways. *Nat Neurosci* (2013) 16:273–80. doi: 10.1038/nn.3318
24. Abud EM, Ramirez RN, Martinez ES, Healy LM, Nguyen CHH, Newman SA, et al. iPSC-Derived Human Microglia-like Cells to Study Neurological Diseases. *Neuron* (2017) 94:278–293.e9. doi: 10.1016/j.neuron.2017.03.042
25. Haenseler W, Sansom SN, Buchrieser J, Newey SE, Moore CS, Nicholls FJ, et al. A Highly Efficient Human Pluripotent Stem Cell Microglia Model Displays a Neuronal-Co-culture-Specific Expression Profile and Inflammatory Response. *Stem Cell Rep* (2017) 8:1727–42. doi: 10.1016/j.stemcr.2017.05.017
26. Pandya H, Shen MJ, Ichikawa DM, Sedlock AB, Choi Y, Johnson KR, et al. Differentiation of human and murine induced pluripotent stem cells to microglia-like cells. *Nat Neurosci* (2017) 20:753–9. doi: 10.1038/nn.4534
27. Gutbier S, Wanke F, Dahm N, Rummelin A, Zimmermann S, Christensen K, et al. Large-Scale Production of Human iPSC-Derived Macrophages for Drug Screening. *Int J Mol Sci* (2020) 21:4808. doi: 10.3390/ijms21134808
28. Lucin KM, Wyss-Coray T. Immune activation in brain aging and neurodegeneration: too much or too little? *Neuron* (2009) 64:110–22. doi: 10.1016/j.neuron.2009.08.039
29. Jay TR, von Saucken VE, Landreth GE. TREM2 in Neurodegenerative Diseases. *Mol Neurodegeneration* (2017) 12:56. doi: 10.1186/s13024-017-0197-5
30. Ulland TK, Colonna M. TREM2 - a key player in microglial biology and Alzheimer disease. *Nat Rev Neurol* (2018) 14:667–75. doi: 10.1038/s41582-018-0072-1
31. Colonna M, Wang Y. TREM2 variants: new keys to decipher Alzheimer disease pathogenesis. *Nat Rev Neurosci* (2016) 17:201–7. doi: 10.1038/nrn.2016.7
32. Guerreiro R, Wojtas A, Bras J, Carrasquillo M, Rogaeva E, Majounie E, et al. TREM2 variants in Alzheimer's disease. *New Engl J Med* (2013) 368:117–27. doi: 10.1056/NEJMoa1211851
33. Jonsson T, Stefansson H, Steinberg S, Jonsdottir I, Jonsson PV, Snaedal J, et al. Variant of TREM2 associated with the risk of Alzheimer's disease. *New Engl J Med* (2013) 368:107–16. doi: 10.1056/NEJMoa1211103
34. Kleinberger G, Brendel M, Mracsko E, Wefers B, Groeneweg L, Xiang X, et al. The FTD-like syndrome causing TREM2 T66M mutation impairs microglia function, brain perfusion, and glucose metabolism. *EMBO J* (2017) 36:1837–53. doi: 10.15252/embj.201796516
35. Korvatska O, Leverenz JB, Jayadev S, McMillan P, Kurtz I, Guo X, et al. R47H Variant of TREM2 Associated With Alzheimer Disease in a Large Late-Onset Family: Clinical, Genetic, and Neuropathological Study. *JAMA Neurol* (2015) 72:920–7. doi: 10.1001/jamaneurol.2015.0979

36. Sims R, van der Lee SJ, Naj AC, Bellenguez C, Badarinarayan N, Jakobsdottir J, et al. Rare coding variants in PLCG2, ABI3, and TREM2 implicate microglial-mediated innate immunity in Alzheimer's disease. *Nat Genet* (2017) 49:1373–84. doi: 10.1038/ng.3916
37. Deczkowska A, Keren-Shaul H, Weiner A, Colonna M, Schwartz M, Amit I. Disease-Associated Microglia: A Universal Immune Sensor of Neurodegeneration. *Cell* (2018) 173:1073–81. doi: 10.1016/j.cell.2018.05.003
38. Keren-Shaul H, Spinrad A, Weiner A, Matcovitch-Natan O, Dvir-Szternfeld R, Ulland TK, et al. A Unique Microglia Type Associated with Restricting Development of Alzheimer's Disease. *Cell* (2017) 169:1276–1290.e17. doi: 10.1016/j.cell.2017.05.018
39. Gratuze M, Leyns CE, Sauerbeck AD, St-Pierre MK, Xiong M, Kim N, et al. Impact of TREM2R47H variant on tau pathology-induced gliosis and neurodegeneration. *J Clin Invest* (2020) 130:4954–68. doi: 10.1172/JCI138179
40. Schlepckow K, Monroe KM, Kleinberger G, Cantuti-Castelvetri L, Parhizkar S, Xia D, et al. Enhancing protective microglial activities with a dual function TREM2 antibody to the stalk region. *EMBO Mol Med* (2020) 12:e11227. doi: 10.15252/emmm.201911227
41. Wang S, Mustafa M, Yuede CM, Salazar SV, Kong P, Long H, et al. Anti-human TREM2 induces microglia proliferation and reduces pathology in an Alzheimer's disease model. *J Exp Med* (2020) 217:9. doi: 10.1084/jem.20200785
42. Andreone BJ, Przybyla L, Llapashtica C, Rana A, Davis SS, van Lengerich B, et al. Alzheimer's-associated PLCγ2 is a signaling node required for both TREM2 function and the inflammatory response in human microglia. *Nat Neurosci* (2020) 23:927–38. doi: 10.1038/s41593-020-0650-6
43. Garcia-Reitboeck P, Phillips A, Piers TM, Villegas-Llerena C, Butler M, Mallach A, et al. Human Induced Pluripotent Stem Cell-Derived Microglia-Like Cells Harboring TREM2 Missense Mutations Show Specific Deficits in Phagocytosis. *Cell Rep* (2018) 24:2300–11. doi: 10.1016/j.celrep.2018.07.094
44. Nugent AA, Lin K, van Lengerich B, Lianoglou S, Przybyla L, Davis SS, et al. TREM2 Regulates Microglial Cholesterol Metabolism upon Chronic Phagocytic Challenge. *Neuron* (2020) 105:837–854.e9. doi: 10.1016/j.neuron.2019.12.007
45. Piers TM, Cosker K, Mallach A, Johnson GT, Guerreiro R, Hardy J, et al. A locked immunometabolic switch underlies TREM2 R47H loss of function in human iPSC-derived microglia. *FASEB J* (2020) 34:2436–50. doi: 10.1096/fj.201902447R
46. van Wilgenburg B, Browne C, Vowles J, Cowley SA. Efficient, long term production of monocyte-derived macrophages from human pluripotent stem cells under partly-defined and fully-defined conditions. *PloS One* (2013) 8: e71098. doi: 10.1371/journal.pone.0071098
47. Cusulin C, Wells I, Badillo S, Duran-Pacheco GC, Baumann K, Patsch C. Gamma secretase modulators and BACE inhibitors reduce Aβ production without altering gene expression in Alzheimer's disease iPSC-derived neurons and mice. *Mol Cell Neurosci* (2019) 100:103392. doi: 10.1016/j.mcn.2019.103392
48. Dobin A, Davis CA, Schlesinger F, Drenkow J, Zaleski C, Jha S, et al. STAR: ultrafast universal RNA-seq aligner. *Bioinf (Oxford England)* (2013) 29:15–21. doi: 10.1093/bioinformatics/bts635
49. Andrews S. FastQC: a quality control tool for high throughput sequence data. *Babraham Institute* (2010).
50. Ewels P, Magnusson M, Lundin S, Käller M. MultiQC: summarize analysis results for multiple tools and samples in a single report. *Bioinf (Oxford England)* (2016) 32:3047–8. doi: 10.1093/bioinformatics/btw354
51. Li H, Handsaker B, Wysoker A, Fennell T, Ruan J, Homer N, et al. The Sequence Alignment/Map format and SAMtools. Bioinformatics (Oxford. *England)* (2009) 25:2078–9. doi: 10.1093/bioinformatics/btp352
52. Mortazavi A, Williams BA, McCue K, Schaeffer L, Wold B. Mapping and quantifying mammalian transcriptomes by RNA-Seq. *Nat Methods* (2008) 5:621–8. doi: 10.1038/nmeth.1226
53. Metsalu T, Vilo J. ClustVis: a web tool for visualizing clustering of multivariate data using Principal Component Analysis and heatmap. *Nucleic Acids Res* (2015) 43:W566–70. doi: 10.1093/nar/gkv468
54. Friedman BA, Srinivasan K, Ayalon G, Meilandt WJ, Lin H, Huntley MA, et al. Diverse Brain Myeloid Expression Profiles Reveal Distinct Microglial Activation States and Aspects of Alzheimer's Disease Not Evident in Mouse Models. *Cell Rep* (2018) 22:832–47. doi: 10.1016/j.celrep.2017.12.066
55. Pomaznoy M, Ha B, Peters B. GOnet: a tool for interactive Gene Ontology analysis. *BMC Bioinf* (2018) 19:470. doi: 10.1186/s12859-018-2533-3
56. Muffat J, Li Y, Yuan B, Mitalipova M, Omer A, Corcoran S, et al. Efficient derivation of microglia-like cells from human pluripotent stem cells. *Nat Med* (2016) 22:1358–67. doi: 10.1038/nm.4189
57. Sala Frigerio C, Wolfs L, Fattorelli N, Thrupp N, Voytyuk I, Schmidt I, et al. The Major Risk Factors for Alzheimer's Disease: Age, Sex, and Genes Modulate the Microglia Response to Aβ Plaques. *Cell Rep* (2019) 27:1293–1306.e6. doi: 10.1016/j.celrep.2019.03.099
58. Srinivasan K, Friedman BA, Etxeberria A, Huntley MA, van der Brug MP, Foreman O, et al. Alzheimer's Patient Microglia Exhibit Enhanced Aging and Unique Transcriptional Activation. *Cell Rep* (2020) 31:107843. doi: 10.1016/j.celrep.2020.107843
59. Hamilton JA. GM-CSF-Dependent Inflammatory Pathways. *Front Immunol* (2019) 10:2055. doi: 10.3389/fimmu.2019.02055
60. Nimmerjahn A, Kirchhoff F, Helmchen F. Resting Microglial Cells Are Highly Dynamic Surveillants of Brain Parenchyma in Vivo. *Science* (2005) 308:1314–8. doi: 10.1126/science.1110647
61. Song D, Sulewski ME Jr., Wang C, Song J, Bhuyan R, Sterling J, et al. Complement C5a receptor knockout has diminished light-induced microglia/macrophage retinal migration. *Mol Vis* (2017) 23:210–8.
62. Gasque P, Singhrao SK, Neal JW, Gotze O, Morgan BP. Expression of the receptor for complement C5a (CD88) is up-regulated on reactive astrocytes, microglia, and endothelial cells in the inflamed human central nervous system. *Am J Pathol* (1997) 150:31–41.
63. Haynes SE, Hollopeter G, Yang D, Kurpius ME, Dailey W-B, Gan D, et al. The P2Y12 receptor regulates microglial activation by extracellular nucleotides. *Nat Neurosci* (2006) 9(12):1512–9. doi: 10.1038/nn1805
64. Honda S, Sasaki K, Ohsawa Y, Imai Y, Nakamura K, Inoue S, et al. Extracellular ATP or ADP induce chemotaxis of cultured microglia through Gi/o-coupled P2Y receptors. (2011). doi: 10.1523/JNEUROSCI.21-06-01975.2001
65. Light AR, Wu Y, Hughen RW, Guthrie PB. Purinergic receptors activating rapid intracellular Ca increases in microglia. *Neuron Glia Biol* (2006) 2 (2):125–38. doi: 10.1017/S1740925X05000323
66. Kleinberger G, Yamanishi Y, Suárez-Calvet M, Czirr E, Lohmann E, Cuyvers E, et al. TREM2 mutations implicated in neurodegeneration impair cell surface transport and phagocytosis. *Sci Trans Med* (2014) 6:243ra86. doi: 10.1126/scitranslmed.3009093
67. Yeh FL, Wang Y, Tom I, Gonzalez LC, Sheng M. TREM2 Binds to Apolipoproteins, Including APOE and CLU/APOJ, and Thereby Facilitates Uptake of Amyloid-Beta by Microglia. *Neuron* (2016) 91:328–40. doi: 10.1016/j.neuron.2016.06.015
68. Meilandt WJ, Ngu H, Gogineni A, Lalehzadeh G, Lee SH, Srinivasan K, et al. Trem2 Deletion Reduces Late-Stage Amyloid Plaque Accumulation, Elevates the Aβ42:Aβ40 Ratio, and Exacerbates Axonal Dystrophy and Dendritic Spine Loss in the PS2APP Alzheimer's Mouse Model. *J Neurosci Off J Soc Neurosci* (2020) 40:1956–74. doi: 10.1523/JNEUROSCI.1871-19.2019
69. Carrano A, Hoozemans JJ, van der Vies SM, van Horssen J, de Vries HE, Rozemuller AJ. Neuroinflammation and blood-brain barrier changes in capillary amyloid angiopathy. *Neurodegener Dis* (2012) 10:329–31. doi: 10.1159/000334916
70. Gosselin D, Skola D, Coufal NG, Holtman IR, Schlachetzki JCM, Sajti E, et al. An environment-dependent transcriptional network specifies human microglia identity. *Science* (2017) 356:6344. doi: 10.1126/science.aal3222
71. Haruwaka K, Ikegami A, Tachibana Y, Ohno N, Konishi H, Hashimoto A, et al. Dual microglia effects on blood brain barrier permeability induced by systemic inflammation. *Nat Commun* (2019) 10:5816. doi: 10.1038/s41467-019-13812-z
72. Marschallinger J, Iram T, Zardeneta M, Lee SE, Lehallier B, Haney MS, et al. Lipid-droplet-accumulating microglia represent a dysfunctional and proinflammatory state in the aging brain. *Nat Neurosci* (2020) 23:194–208. doi: 10.1038/s41593-019-0566-1
73. Zilkova M, Nolle A, Kovacech B, Kontsekova E, Weisova P, Filipcik P, et al. Humanized tau antibodies promote tau uptake by human microglia without any increase of inflammation. *Acta Neuropathol Commun* (2020) 8:74. doi: 10.1186/s40478-020-00948-z

74. Hammond TR, Dufort C, Dissing-Olesen L, Giera S, Young A, Wysoker A, et al. Single-Cell RNA Sequencing of Microglia throughout the Mouse Lifespan and in the Injured Brain Reveals Complex Cell-State Changes. *Immunity* (2019) 50:253–271.e6. doi: 10.1016/j.immuni.2018.11.004
75. Jung S, Aliberti J, Graemmel P, Sunshine MJ, Kreutzberg GW, Sher A, et al. Analysis of fractalkine receptor CX(3)CR1 function by targeted deletion and green fluorescent protein reporter gene insertion. *Mol Cell Biol* (2000) 20:4106–14. doi: 10.1128/MCB.20.11.4106-4114.2000
76. Jackson HM, Foley KE, O'Rourke R, Stearns TM, Fathalla D, Morgan BP, et al. A novel mouse model expressing human forms for complement receptors CR1 and CR2. *BMC Genet* (2020) 21:101. doi: 10.1186/s12863-020-00893-9
77. Ryan KJ, White CC, Patel K, Xu J, Olah M, Replogle JM, et al. A human microglia-like cellular model for assessing the effects of neurodegenerative disease gene variants. *Sci Trans Med* (2017) 9:421. doi: 10.1126/scitranslmed.aai7635
78. McQuade A, Coburn M, Tu CH, Hasselmann J, Davtyan H, Blurton-Jones M. Development and validation of a simplified method to generate human microglia from pluripotent stem cells. *Mol Neurodegeneration* (2018) 13:67. doi: 10.1186/s13024-018-0297-x
79. Douvaras P, Sun B, Wang M, Kruglikov I, Lallos G, Zimmer M, et al. Directed Differentiation of Human Pluripotent Stem Cells to Microglia. *Stem Cell Rep* (2017) 8:1516–24. doi: 10.1016/j.stemcr.2017.04.023
80. Xiang X, Piers TM, Wefers B, Zhu K, Mallach A, Brunner B, et al. The Trem2 R47H Alzheimer's risk variant impairs splicing and reduces Trem2 mRNA and protein in mice but not in humans. *Mol Neurodegeneration* (2018) 13:49. doi: 10.1186/s13024-018-0280-6
81. Brüll M, Spreng AS, Gutbier S, Loser D, Krebs A, Reich M, et al. Incorporation of stem cell-derived astrocytes into neuronal organoids to allow neuro-glial interactions in toxicological studies. *Altex* (2020) 37:409–28. doi: 10.14573/altex.1911111
82. Mazaheri F, Snaidero N, Kleinberger G, Madore C, Daria A, Werner G, et al. TREM2 deficiency impairs chemotaxis and microglial responses to neuronal injury. *EMBO Rep* (2017) 18:1186–98. doi: 10.15252/embr.201743922
83. Shi Y, Holtzman DM. Interplay between innate immunity and Alzheimer disease: APOE and TREM2 in the spotlight. *Nat Rev Immunol* (2018) 18:759–72. doi: 10.1038/s41577-018-0051-1
84. Krasemann S, Madore C, Cialic R, Baufeld C, Calcagno N, El Fatimy R, et al. The TREM2-APOE Pathway Drives the Transcriptional Phenotype of Dysfunctional Microglia in Neurodegenerative Diseases. *Immunity* (2017) 47:566–581 e9. doi: 10.1016/j.immuni.2017.08.008
85. Alepee N, Bahinski A, Daneshian M, De Wever B, Fritsche E, Goldberg A, et al. State-of-the-art of 3D cultures (organs-on-a-chip) in safety testing and pathophysiology. *ALTEX* (2014) 31:441–77. doi: 10.14573/altex.1406111

Conflict of Interest: During the course of this study, MR, IP, ND, CS, DR, RS, ME, JZ, CP, SG, and MB are or were full time employees or trainees at Roche and they may additionally hold Roche stock/stock options.

The remaining authors declare that the research was conducted in the absence of any commercial or financial relationships that could be construed as a potential conflict of interest.

frontiers in Immunology

REVIEW
published: 19 February 2021
doi: 10.3389/fimmu.2021.616301

The Emerging Role of Microglia in Neuromyelitis Optica

Tingjun Chen[1], *Dale B. Bosco*[1], *Yanlu Ying*[1], *Dai-Shi Tian*[2] *and Long-Jun Wu*[1,3,4*]

[1] Department of Neurology, Mayo Clinic, Rochester, MN, United States, [2] Department of Neurology, Tongji Medical College, Huazhong University of Science and Technology, Wuhan, China, [3] Department of Neuroscience, Mayo Clinic, Jacksonville, FL, United States, [4] Department of Immunology, Mayo Clinic, Rochester, MN, United States

Neuromyelitis optica (NMO) is an autoantibody-triggered neuro-inflammatory disease which preferentially attacks the spinal cord and optic nerve. Its defining autoantibody is specific for the water channel protein, aquaporin-4 (AQP4), which primarily is localized at the end-feet of astrocytes. Histopathology studies of early NMO lesions demonstrated prominent activation of microglia, the resident immune sentinels of the central nervous system (CNS). Significant microglial reactivity is also observed in NMO animal models induced by introducing AQP4-IgG into the CNS. Here we review the potential roles for microglial activation in human NMO patients as well as different animal models of NMO. We will focus primarily on the molecular mechanisms underlying microglial function and microglia-astrocyte interaction in NMO pathogenesis. Understanding the role of microglia in NMO pathology may yield novel therapeutic approaches for this disease.

Keywords: microglia, neuromyelitis optica, complement C3, aquaporin-4, astrocyte-microglia communication, autoimmune, C3a receptor

OPEN ACCESS

Edited by:
Amanda Sierra, Achucarro Basque Center for Neuroscience, Spain

Reviewed by:
José Luis Marín-Teva, University of Granada, Spain
Frederike Cosima Oertel, University of California, San Francisco, United States

***Correspondence:**
Long-Jun Wu
wu.longjun@mayo.edu

Specialty section:
This article was submitted to Multiple Sclerosis and Neuroimmunology, a section of the journal Frontiers in Immunology

Received: *11 October 2020*
Accepted: *04 January 2021*
Published: *19 February 2021*

Citation:
Chen T, Bosco DB, Ying Y, Tian D-S and Wu L-J (2021) The Emerging Role of Microglia in Neuromyelitis Optica. Front. Immunol. 12:616301. doi: 10.3389/fimmu.2021.616301

INTRODUCTION

Neuromyelitis optica (NMO) is an autoimmune inflammatory disorder of the central nervous system (CNS) which mainly affects optic nerves and the spinal cord (1). Attacks upon optic nerves can often lead to blindness, while the extensive transverse myelitis induced within the spinal cord can cause weakness or paralysis in the legs and arms, loss of sensation, bladder and bowel function issues, and respiratory failure (2). Additionally, NMO disproportionately affects women and non-Caucasian populations and is a relapsing-remitting disease. Repeated attacks can lead to severe cumulative damage to optic nerves and the spinal cord (3). Therefore, prevention of new attacks is critical to mitigating long-term effects.

NMO was largely considered a subtype of multiple sclerosis (MS), until 2004 when Lennon and colleagues identified that autoantibodies directed towards aquaporin-4 (AQP4-IgG, also called NMO-IgG) were a biomarker for NMO pathology (4). This key finding was used to distinguish NMO from MS and other inflammatory CNS demyelinating disorders. AQP4-IgG binds the ectodomain of AQP4 water channels that are located on the astrocytic end-feet embracing capillaries, ventricular walls, and pial-glial interfaces (4). AQP4-IgG can also sometimes be detected in a patient's cerebrospinal fluid (CSF) (5). AQP4-IgG concentrations in the blood and CSF have been reported to correlate with clinical outcome (6–10). It should also be noted that antibodies against myelin oligodendrocyte glycoprotein (MOG-IgG) have also been suggested to induce NMO pathology (11). The idea that NMO pathology is related to pathogenic autoantibodies

has lead plasma exchange and B cell depletion to be accepted as first line therapies for the acute phase of NMO (12).

The histopathology of NMO lesions also show prominent microglial reactivity in AQP4-rich CNS regions (13, 14). However, mechanisms underlying microglial activation in NMO remains largely unknown. It would be reasonable to believe that microglia are the first responders to signals emanating from astrocytes following their activation by AQP4-IgG. As such, this review focuses on the emerging evidence that microglia play an important role in AQP4-IgG related NMO pathogenesis.

HISTOPATHOLOGY AND MICROGLIAL REACTIVITY IN NMO PATIENTS

The key hallmark of NMO immunopathology is the striking focal loss of AQP4 protein from astrocytes. Changes to glial fibrillary acidic protein (GFAP) expression in astrocytes varies in different brain regions and disease stages (14). In early lesions, astrocytes are spared and exhibit an activated phenotype (15). In later stages, when deposits of the complement terminal membrane attack complex C5b-C9 are abundant, terminal deoxynucleotidyl transferase dUTP nick end labeling (TUNEL) staining indicates astrocyte apoptosis and GFAP immunoreactivity is reduced (13–16). In some of these later lesions, microglia/macrophages contain GFAP remnants, indicating phagocytosis of astrocytes (14). Demyelination in NMO pathology, as shown by fast blue staining (14), generally accompanies astrocytic pathology (17) and local inflammation (18).

In vitro studies of NMO pathogenesis found that the binding of AQP4-IgG to its antigen induces AQP4 internalization (19, 20), reducing water permeability and spurring astrocytes to release various cytokines and chemokines (21). Coincidently, when AQP4 is internalized, excitatory amino acid transporter 2 (EAAT2) also disappears from astrocyte surface membranes (20). In the presence of requisite complement components, astrocytes undergo cytolysis during an NMO attack (13, 19, 22). Additionally, myelin loss in both grey and white matter is an immunohistochemical characteristic of fully established NMO lesions (14). However, demyelination appears to be a secondary event following the interaction of AQP4-IgG with astrocytes (17) and promotion of local inflammation (18). Neuronal loss has also been reported in the cerebral cortex of NMO patients, possibly explaining the cognitive impairment that is sometimes observed (23). As for MOG-IgG positive NMO patients, myelin loss was significant but AQP4 was preserved and dystrophic astrocytes were absent (24). Although MOG-IgG frequently co-existed with anti-N-methyl-D-aspartate (NMDA) receptor IgG, the prognosis in these patients are usually better than AQP4-IgG positive patients, indicating differences in pathogenesis (25).

In NMO patients' CNS, perivascular regions contain accumulations of lymphocytes, neutrophils and eosinophils (14–16). The abundance of these cellular infiltrates suggests disruption of the neurovascular unit following interaction of NMO-IgG with AQP4 in the vicinity of the blood-brain-barrier (BBB) (13). This is not surprising, considering astrocyte end-feet are an integral part of the neurovasculature. Consistently, AQP4 loss in the choroid plexus coinciding with C9 neoantigen (C9neo) immunoreactivity on choroidal epithelial membranes is evidence of focal BBB pathology (13). C9neo deposition can also be detected in MOG-IgG positive patients, but on myelin sheaths (24). Although peripherally activated B cells can enter the parenchyma through intact BBB (26), loss of astrocytic end-feet may further facilitate entry of either AQP4-IgG or AQP4-IgG secreting B cells into the CNS (27).

In addition to loss of AQP4 and astrocytes, neuronal injury, demyelination, microglial activation, and macrophage infiltration are prominent in AQP4-IgG seropositive NMO pathology (14). Microglia and macrophage reactivity is indicated by both morphological criteria (*i.e.*, amoeboid morphology) and positivity for the lysosome marker CD68 (14, 16). However, conventional histopathology cannot distinguish macrophages (infiltrating monocytes) from resident microglia in the CNS. Although there are conflicting reports as to whether the number of monocytes within circulation changes (28, 29) in response to NMO-IgG, infiltration of monocytes into the CSF is believed to happen (30). Indeed, there is an increased number of microglia-like cells within human NMO pathology. However, it is difficult to determine whether this is due to local microglial proliferation or monocyte infiltration after NMO-IgG attacks.

It should also be noted that reported CNS tissue distribution of activated microglia/macrophages is different between NMO and MS. In MS, microglial activation is wide-spread in the meninges and subpial cortex (31), while in AQP4-IgG positive NMO it is largely confined to regions that normally are AQP4-rich, like the CSF–brain interface in the corpus callosum, hypothalamic, and periventricular areas (13, 14, 32). Conversely, in MOG-IgG positive NMO, microglia/macrophages also appear in subpial, which is similar to MS; but it is associated with CD4 inflammatory infiltration and not CD8 T cells, which are abundant in MS (24). Additionally, microglia/macrophage reactivity in NMO lesions are surrounded by evidence of complement activation, which is an infrequent finding in MS lesions (14). Consistent with the role of complement in microglial function, microglia are able to secret complement components to activate astrocytes and mediate neuronal injury in a variety of neurological disorders (33–35). These complement components can also further activate microglia (36–38). Therefore, the difference in complement-related microglia activation patterns between MS and NMO indicate divergent molecular mechanisms. Nevertheless, clinical histopathology results strongly suggest the involvement of microglia in NMO pathogenesis. As such, NMO animal models are needed to investigate the precise function and mechanism of microglia in NMO.

RODENT MODELS OF NMO

To understand the cellular and molecular mechanisms underlying the pathogenesis of NMO, several rodent models of

NMO have been developed. Since AQP4-IgG was the original pathological cause of NMO, animal models that employed AQP4-IgG to develop pathology are the most common. As such, we will focus predominantly on AQP4-IgG related animal models.

Initial animal models were derived from experimental autoimmune encephalomyelitis (EAE) where pathology was induced *via* adoptive transfer of AQP4-IgG into animals with preexisting myelin targeted encephalitogenic T cells (5, 39–43). However, these models did not display any of the immunology characteristics of NMO. In particular, there were no AQP4 specific immune reactions (44–47). Another early model involved transplantation of AQP4-specific T cells into naïve animals (48–53). However, this model also did not induce the characteristic AQP4 loss unless AQP4-IgG were co-injected (48, 49). More recently, new models that more closely mimic the clinical features of AQP4-IgG related NMO have been developed (**Table 1**).

AQP4-IgG Seropositive Models

Some recent rodent models of NMO have utilized passive transfer of AQP4-IgG into animals to induce clinically relevant pathology and provide early evidence of microglial activation in NMO pathology (58, 61, 71). However, one complication in using passive transfer is that acute intravenous injection of AQP4-IgG has difficulty producing neurology dysfunction or NMO pathology (54, 55), as AQP4-IgGs cannot pass through an undamaged BBB. When the BBB is physically disrupted by needle puncture or ultrasound, NMO-liked pathology can be induced near leakage sites (54, 56). Repeated intraperitoneal AQP4-IgG injections has also been used to successfully induce wild-spread NMO-liked pathology in rats (57). The neurological abnormalities displayed in this model included neuropathic pain, salivation (correlates to nausea/vomiting behavior in rats/mice) (72), problems with balance, and motor impairment (57).

AQP4-IgG in seropositive models entered the CNS *via* three routes: (1) Circumventricular organs, which are highly vascularized structures surrounding the third and fourth ventricles and characterized by a lack of BBB (73). Using this route AQP4-IgG induces a lesion with AQP4 loss but intact GFAP staining. However, in circumventricular organs, microglia were not activated after repeated intraperitoneal AQP4-IgG injection. (2) Meningeal vessels and veins of the Virchow Robin spaces. Using this route AQP4-IgG induces meningitis 120 h after the initial intraperitoneal injection of AQP4-IgG. T cell, neutrophil and microglia activity were found in subpial lesions. Notably, microglial activity was accompanied with astrocyte damage in these areas. (3) Finally, parenchymal vessel unrelated to the meninges. Perivascular lesion deep within the parenchyma showed significant AQP4 loss and large number of activated microglia. In some lesions, strong complement deposition coincided with the loss of astrocytes and activation of microglia, which is similar with lesions of NMO medullas in patients (15).

Direct AQP4-IgG Injection Together With Human Complement

In these animal models, either AQP4-IgG derived from NMO patients or recombinant monoclonal AQP4-IgG is administered directly into the rodent CNS together with human complement (59, 60, 62). In wild type mice, when patient-derived AQP4-IgGs were intracerebrally injected acutely with human complement, matured NMO pathology including AQP4 and GFAP loss, myelin damage, complement deposition, and axon injury was observed (59). $CD45^+$ microglia/macrophages were also widely observed in the ipsilateral brain. Moreover, animals were more likely to turn to the injection side during Y maze test, indicating neurological dysfunction in injected hemisphere of brain. In contrast, mice treated with human control IgGs and complement exhibit no behavior abnormalities, AQP4 loss, astrocyte injury, axon loss, or microglia/macrophages activation, suggesting that APQ4-IgG is the main trigger for pathology (59).

Chronic infusion of recombined AQP4-IgG with human complement was also shown to induced astrocyte damage,

TABLE 1 | AQP4-IgG related NMO animal models.

NMO model	Animals	Site of pathology	AQP4 loss	GFAP loss	Complement activity	Microglia activity	Demyelination	Functional impairment	Reference
AQP4-IgG seropositive	mouse	Peripheral Organs	No	No	No	No	No	No	(54)
	rat	Brain (needle)	Yes	Yes	Yes	Yes	Yes	Yes	(55)
		Brain (Ultrasound)	Yes	Yes	Yes	Yes	Yes	Unclear	(56)
		Brain/Spinal cord/ Optic nerve							(57)
AQP4-IgG with human complement	mouse	Brain/Spinal cord	Yes	Yes	Yes	Yes	Yes	Unclear	(58)
		Brain						Yes	(59, 60)
		Optic nerve						Unclear	(55)
		Spinal cord						Yes	(61)
AQP4-IgG without human complement	rat	Brain	Yes	Yes	Yes	Yes	Yes	Unclear	(62)
		Brain			Yes	Yes	Yes	Yes	(63)
		Brain			No	No	No	Yes	(64)
		Optic nerve/retina			Yes	Yes	Yes	Yes	(65, 66)
		Spinal cord							(67, 68)
	mouse	Spinal cord	Yes	Yes	No	Yes	Yes	Yes	(69)
				No	C1q and C3				(70)

neutrophil infiltration, eosinophil infiltration, and microglia/macrophage activity in mice (58, 60). Additionally, deficiencies in complement regulator CD59 expression significantly increased the pathology induced by AQP4-IgG, including AQP4 loss, complement deposition, and $CD45^+$ cell activity (55, 61, 64). These results are quite surprising, as complement proteins themselves are known to induce microglial activity (74–76) followed by neuronal damage (77) and demyelination (78). Therefore, further studies are needed to clearly delineate the respective contribution of AQP4-IgG and complement to the outcomes of NMO-like phenotypes in these models.

Direct AQP4-IgG Injection Without Human Complement

Co-injection of complement, however, may not be necessary to induce pathology. In rodents, AQP4-IgG injection without human complement was able to induce neurological dysfunction and NMO pathology within the brain, retina, and optic nerves (62, 63, 65–68, 70). Microglial reactivity was observed within areas of AQP4 loss (64, 68–70). Administration of clodronate liposomes, which efficiently depletes microglia/macrophages, significantly reduced lesion size, suggesting that microglia/macrophages contributed to NMO pathology (62).

Nevertheless, there is still debate as to whether complement has a role in these types of models. For example, in CD59 deficient mice, AQP4-IgG induced worse functional impairment, more NMO-like pathology, and stronger microglial activity (67). These results indicate that AQP4-IgG could induce endogenous complement expression, which in turn facilitates the toxicity of AQP4-IgG. However, in other reports, no complement terminal protein was detected (64, 68, 70). Additionally, pretreatment with cobra venom factor, which inhibits complement activity (79), did not rescue functional impairment and pathology in the retina (65). Therefore, it is unclear whether the pathology and neuronal dysfunction induced in these models truly involved complement related mechanisms.

MICROGLIAL ACTIVATION IN ESTABLISHED ANIMAL MODELS OF NMO

As mentioned above, microglial activation has been observed in most animal models of NMO. However, it is unknown whether microglial activation is the cause or consequence of NMO pathogenesis. Moreover, it is unclear as to whether complement is involved in microglial activation, considering microglia reactivity has been observed in both complement dependent (59, 61, 67) and independent models (65, 69, 80). Serum concentrations of complement have also varied across different NMO cases, making it difficult to ascertain whether complement toxicity is initiated by AQP4-IgG (81–84). Nevertheless, the clear early events in NMO are astrocytic reactivity after AQP4-IgG binding (20) and AQP4 loss (22). AQP4-IgG activated astrocytes may then produce cytokines, which induce local inflammation and microglial activation (19–21, 70). Microglia, as the resident CNS immune cell, should typically be the first responders to reactive astrocytes following initiation of NMO pathology. However, limited direct evidence exists that illustrates microglial function and activation mechanisms in NMO. As such, a new murine model of NMO has recently been developed to determine where microglia fit into NMO pathology (70).

A NEW MURINE MODEL OF NMO THAT EMPLOYS CHRONIC AQP4-IGG INTRATHECAL INFUSION REVEALS THE IMPORTANT ROLE OF MICROGLIA

A new mouse model of NMO has been established that utilizes continuous infusing of AQP4-specific IgG into the spinal subarachnoid space, without exogenous complement (70). Recipients of monoclonal AQP4-IgG or NMO-patient-derived IgG displayed progressive motor impairment and immunohistopathology compatible to early clinical NMO pathology. The pathology showed that AQP4 levels in spinal cord tissue were decreased after AQP4-IgG infusion, but GFAP immunoreactivity was increased. Therefore, AQP4 is likely internalized but astrocytes are not undergoing apoptosis, mimicking the early stages of NMO. In AQP4 null mice, AQP4-IgG did not induce motor impairment, confirming that autoantibodies targeting AQP4 are responsible for triggering the pathology. Additionally, complement terminal proteins were not detected in this model. Instead, it was demonstrates that microglia play a central role in the observed pathology (70).

Microglia Are Required for NMO Pathogenesis

Activation of microglia/macrophages as determined by Iba1, CD11b, CD68, and C1q staining was significantly increased within the AQP4 loss lesion (70). These results are consistent with microglial/macrophages activation in human NMO patients (13, 14, 16). Interestingly, in $AQP4^{-/-}$ mice, AQP4-IgG did not activate microglia/macrophages, indicating that AQP4-IgG activated microglia *via* astrocyte signaling. Recent studies have proposed that microglia induce reactive astrocytes in many disease contexts, such as Alzheimer's disease, Huntington's disease, Parkinson's disease, amyotrophic lateral sclerosis, and MS (35, 85). The results in the mouse model of NMO demonstrated that astrocytes can induce the activation of microglial/macrophages. Astrocytic modulation of microglia is also observed in development and diseases (86, 87). For example, astrocytes release transforming growth factor (TGF)-β (88, 89) or interleukin 33 (IL-33) (86, 90) to promote microglial pruning of synapses in development. Under disease conditions, astrocyte up-regulate lipocalin-2 (LCN-2) (91) or orosomucoid (ORM) (92) to activate microglia, which leads to neuro-inflammation and degeneration.

To further investigate this proposed relationship between astrocyte-microglia communication and NMO pathology, microglia ablation approaches were employed (70). When microglia were depleted, AQP4-IgG infusion did not induce motor impairment. More strikingly, when microglial

replenishment started around day 5 after ablation, motor dysfunction appeared (70), suggesting that microglia are critical mediators of the behavioral impairment. It is important to point out that microglia ablation did not prevent AQP4 internalization or astrocytic activation induced by AQP-IgG infusion. This is consistent with a previous *in vitro* study, which demonstrated that autoantibody-induced AQP4 internalization was microglia independent (20). Among rodent models with clinical comparable NMO pathology (40, 55, 61, 69, 70), this new study provides the direct evidence of microglia in motor dysfunction. The microgliogenic pathology separates NMO from other neuro-inflammatory diseases like MS. For example, in MOG induced experimental autoimmune encephalomyelitis (EAE) models, during disease onset, infiltrated macrophages induce inflammation (45), while microglia clear debris and limit inflammation (46). Additionally, in demyelinating diseases, microglia trigger remyelination and promote recovery (46, 93–95). Therefore, although the study suggests a damaging role for microglia in the early phases of NMO pathogenesis, microglia function could be more diverse at later phases of NMO.

Astrocyte-Microglia Interaction Is Mediated by C3-C3aR Signaling

After AQP4-IgG infusion, microglia and astrocyte cell somas were found to overlap after AQP4-IgG infusion (70). This observation suggests astrocyte-microglia physical interaction in this animal model of NMO. While microglial process convergence towards neurons has been previously reported (96, 97) this is the first time that similar events have been observed with astrocytes after AQP4-IgG infusion. Complement C3 is typically absent in astrocytes under physiological conditions, but strongly expressed under pathological conditions (35). Consistently, AQP4-IgG infusion was found to upregulate astrocytic C3. AQP4-IgG infusion also did not induce motor impairment in $C3^{-/-}$ animals. Similar to ATP (98, 99), the cleavage produce of C3, C3a, can act as a chemoattractant, possibly inducing the observed microglial processes convergence through C3a receptor (C3aR) expressed in microglia (100). In $C3^{-/-}$ and $C3aR^{-/-}$ mice after chronic infusion of AQP4-IgG, even though AQP4 loss still occurred, astrocyte-microglia interaction and motor deficits were largely abolished (70). Therefore, astrocyte-microglia interaction is likely mediated by C3-C3aR signaling and this interaction is a driver of this model's NMO pathogenesis (**Figure 1**).

Complement C3 shapes brain function in healthy and diseased conditions (34, 101–103). Recent experimental evidence indicates that microglia are critical for C3-C3aR signaling in neurodegenerative diseases (104, 105). In addition, C3 signaling can also participate in neurodegeneration by activating microglial complement receptor 3 (CR3) (34, 103, 106, 107). Indeed, exogenous human complement C3 can activate murine microglia (105). Administration of AQP4-IgG

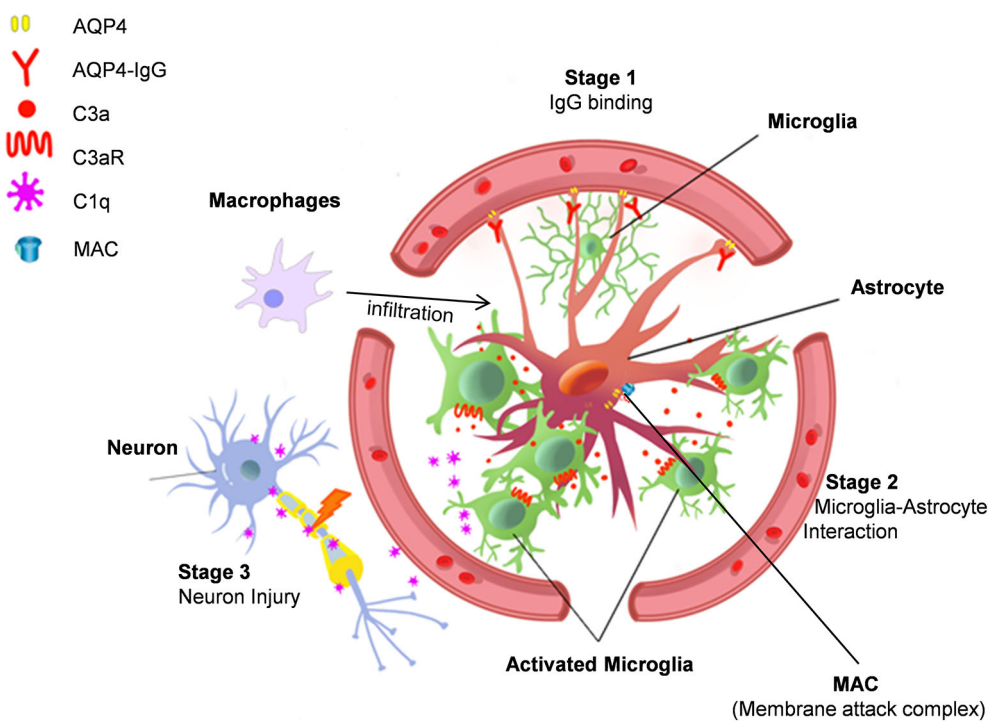

FIGURE 1 | Astrocyte-microglia interaction drives NMO pathology. Stage 1. AQP4-IgG binds to AQP4 water channel protein in astrocyte end-feet and induces AQP4 protein internalization. Stage 2. AQP4 internalization activates astrocytes, which then increases complement C3 expression to induce microglia chemotaxis. Stage 3. Activated microglia interact with astrocytes and release C1q, which may cause neuronal injury. Additional mechanisms in NMO pathogenesis include complement dependent cytotoxicity mediated by membrane attack complexes (MAC) and focal inflammation induced by macrophage infiltration.

with complement induces astrocytes depletion in hours (108), which skipped the initial stage of astrocytic reactions in NMO pathology (15, 19, 20). Astrocyte acute ablation likely results in neuronal damage (109), but the question is whether such models really reflect the unique pathology of NMO. In animal models with AQP4-IgG chronic infusion without complement, activation of astrocytes, microglia, and neuronal damage happen in a temporally and spatially dependent manner (68, 70). The downstream cascade might also involve microglial phagocytosis of C3 labeled neurons/synapse, which is observed during neuronal development, neuro-inflammation, and neurodegeneration diseases (35, 103, 106).

Neuronal Damage Is Possibly Mediated by Microglia-Derived C1q

After AQP4-IgG chronic infusion, microglial C3aR induces the expression of complement C1q in microglia (70), the complement cascade initiator (110). However, functional impairment does not seem related to complement induced toxicity for two reasons. First, there was no evidence of terminal complement complexes in this model. Second, astrocytes were activated but not injured. Therefore, it is possible that microglial C1q induces cell stress *via* different mechanisms other than classical complement cascades. Notably, C1q is able to inhibit mitochondrial function (111), which can lead to myelin and neuronal injury (107, 111, 112). Additionally, C1q can directly bind synapses and induce neuronal damage in a microglial phagocytosis dependent manner (106, 113). However, further study is needed to test whether there is complement-dependent microglial "phagoptosis" of neurons in NMO. Regardless, this model of NMO demonstrates a clear role for microglia in which microglial C1q may induce neuronal dysfunction in a complement cascade independent manner (**Figure 1**).

TARGETING MICROGLIA FOR NMO TREATMENT

Based on our recent understanding of critical microglial function in NMO, we propose that microglia may represent a novel therapeutic target for NMO treatment. Typically, acute NMO attacks are first treated with intravenous methylprednisolone for 3~5 days (11), combined with plasma exchange (PLEX) or immunoabsorption (114) to help reduce AQP4-IgG concentrations (115). Subsequently, low doses of prednisone/prednisolone are used for preventative immunosuppressive therapy, however this can induce serious side effects (116). Additional therapeutic treatments for NMO include Azathioprine and Rituximab, which inhibit lymphocyte and $CD19^+$ B cell activity (117). Mycophenolate mofetil has also been useful to inhibit B cells and T cells, but patients will have elevated risk of leucopenia when combined with other immunosuppress therapies (118). It remains to be determined whether these immunosuppressive therapies reduce microglial activation when they exert their therapeutic effects.

The most exciting breakthrough in NMO therapy is eculizumab, which greatly reduces the risk of relapse in AQP4-IgG seropositive patients (3). Eculizumab neutralizes complement C5, which is mainly expressed by microglia in the CNS (74). Interestingly, C5a receptors are highly and exclusively expressed by microglia (119). Clinical evidence indicates NMO pathology is mediated by immunoglobulin and terminal complement complex (C5b-9; C9neo) (16), highlighted the importance of complement dependent cytotoxicity (CDC) in NMO. Besides immunoglobulin mediated astrocyte CDC, the demyelination in NMO lesions can be induced by production of anaphylatoxins (C3a, C4a and C5a) and opsonins (C3b and C1q) that recruit inflammatory cells (120), enhance antibody-dependent cell-mediated cytotoxicity (ADCC) (121), and facilitate phagocytosis (120). Although microglia reactivity has not been examined in eculizumab treated patients yet, early studies already implied how complement C5 inhibition modulate microglia function in CNS disease. First, inhibition of C5a receptors reduced microglia activity and provided strong benefit in mouse models of Alzheimer's disease (112). Moreover, microglial C5a is a strong chemoattractant for polymorph nuclear cells (122), mediates eosinophil and neutrophil degranulation (123, 124). Therefore, future studies are needed to investigate whether eculizumab can reduce the relapsing risk of NMO *via* inhibition of microglial C5 receptor signaling.

Lastly, other microglia-targeting therapeutic approaches could be considered for NMO treatment. First, microglial inhibitor minocycline has been shown to reduce microglial activation in many CNS disorders (125–127). Clinical trials of minocycline are currently in progress for schizophrenia, autism, anxiety, and bipolar disorders (128, 129). Second, colony stimulating factor 1 (CSF1) receptor antagonists, such as PLX3397 or PLX5562, can deplete microglia *via* oral administration (130). PLX3397 (pexidartinib) was approved by FDA for treatment of giant-cell tumor of the tendon sheath in 2019 (131). Whether PLX compounds can be used for NMO therapy still need further investigation. However, microglia depletion/inhibition *via* CSF1 receptor antagonists may also result in side effects including affecting hematopoiesis and the function of macrophages in mice (132). Last but not least, C3 signaling such as C3 and C3a receptor, is critical for microglial activation and motor impairment in NMO (70). Inhibition of C3aR or neutralization of C3a may provide therapeutic effects. The C3a receptor is an especially attractive target as it is highly expressed in activated microglia (78, 104, 105).

FUTURE DIRECTIONS AND CONCLUSION

Recent studies have demonstrated the emerging role of microglia in NMO (70). Targeting microglia for NMO treatment is promising but still challenging, considering that microglia share many common molecules with peripheral immune systems (133, 134). To develop microglia specific treatments, future studies are needed to further our understanding of the molecular mechanisms underlying the role of microglia in NMO. Additional considerations include accounting sex differences in

NMO, where the female to male ratio in NMO patients is above 8:2 (135). Coincidently, microglial function show clear sex differences evidenced by studies in chronic pain (136, 137), depression (138), stroke (139), and aging (140). It would be interesting to test whether female microglia may have stronger complement or proinflammatory activation in response to AQP4-IgG. In addition, the regional heterogeneity of microglia function is emerging. Whether microglial heterogeneity contributes to preferential development of lesions in optic nerves and the spinal cord warrants further investigations. Finally, it is unknown what the role of microglia is during the remission phase of NMO. Current animal models demonstrate that motor dysfunction can partially recover after AQP4-IgG infusion stopped (68, 70). Thus, the question remains as to whether microglia initiates NMO remission due to microglial reparative function or releasing trophic factors.

In a variety of neurological disorders (*e.g.*, stroke, chronic pain, epilepsy, and neurodegenerative diseases), microglia play beneficial or detrimental function depending on the context and timing of their activation (141–145). The novel mouse model of NMO presented in this review demonstrates a critical role for microglia in the evolution of motor impairment and the neuropathology progression initiated by AQP4-IgG activated astrocytes (70). With the emergence of new genetic tools for microglial research (146, 147), the function and mechanisms of microglia in NMO will be revealed. These will corroborate the idea that microglia may represent a novel therapeutic target in NMO treatment.

AUTHOR CONTRIBUTIONS

TC and L-JW conceived the study and wrote the manuscript. DB, YY, D-ST, and L-JW edited the manuscript. All authors contributed to the article and approved the submitted version.

FUNDING

The work is supported by the National Institutes of Health (R01NS110949, R01NS088627, R01NS112144, R01NS110825, R21AG064159) to L-JW.

ACKNOWLEDGMENTS

We thank members of Wu lab at Mayo for the discussion, and Dr. Vanda Lennon, Dr. Linda Wu, Ms. Jiaying Zheng, and Mr. Lingxiao Wang, for editing the manuscript.

REFERENCES

1. Jarius S, Wildemann B. AQP4 antibodies in neuromyelitis optica: diagnostic and pathogenetic relevance. *Nat Rev Neurol* (2010) 6:383–92. doi: 10.1038/nrneurol.2010.72
2. Zekeridou A, Lennon VA. Aquaporin-4 autoimmunity. *Neurol Neuroimmunol Neuroinflamm* (2015) 2:e110. doi: 10.1212/NXI.0000000000000110
3. Pittock SJ, Berthele A, Fujihara K, Kim HJ, Levy M, Palace J, et al. Eculizumab in Aquaporin-4-Positive Neuromyelitis Optica Spectrum Disorder. *N Engl J Med* (2019) 381:614–25. doi: 10.1056/NEJMoa1900866
4. Lennon VA, Wingerchuk DM, Kryzer TJ, Pittock SJ, Lucchinetti CF, Fujihara K, et al. A serum autoantibody marker of neuromyelitis optica: distinction from multiple sclerosis. *Lancet* (2004) 364:2106–12. doi: 10.1016/S0140-6736(04)17551-X
5. Bennett JL, Lam C, Kalluri SR, Saikali P, Bautista K, Dupree C, et al. Intrathecal pathogenic anti-aquaporin-4 antibodies in early neuromyelitis optica. *Ann Neurol* (2009) 66:617–29. doi: 10.1002/ana.21802
6. Bergamaschi R, Pichiecchio A, Persico A, Bastianello S. Relevance of clinical findings for diagnosis of neuromyelitis optica in MRI and NMO-IgG era. *Eur J Neurol* (2009) 16:e76–7. doi: 10.1111/j.1468-1331.2009.02561.x
7. Jarius S, Franciotta D, Bergamaschi R, Wright H, Littleton E, Palace J, et al. NMO-IgG in the diagnosis of neuromyelitis optica. *Neurology* (2007) 68:1076–7. doi: 10.1212/01.wnl.0000256822.01222.bd
8. Matiello M, Lennon VA, Jacob A, Pittock SJ, Lucchinetti CF, Wingerchuk DM, et al. NMO-IgG predicts the outcome of recurrent optic neuritis. *Neurology* (2008) 70:2197–200. doi: 10.1212/01.wnl.0000303817.82134.da
9. Klawiter EC, Alvarez E3rd, Xu J, Paciorkowski AR, Zhu L, Parks BJ, et al. NMO-IgG detected in CSF in seronegative neuromyelitis optica. *Neurology* (2009) 72:1101–3. doi: 10.1212/01.wnl.0000345066.57745.50
10. Weinshenker BG, Wingerchuk DM, Vukusic S, Linbo L, Pittock SJ, Lucchinetti CF, et al. Neuromyelitis optica IgG predicts relapse after longitudinally extensive transverse myelitis. *Ann Neurol* (2006) 59:566–9. doi: 10.1002/ana.20770
11. Jarius S, Ruprecht K, Kleiter I, Borisow N, Asgari N, Pitarokoili K, et al. MOG-IgG in NMO and related disorders: a multicenter study of 50 patients. Part 2: Epidemiology, clinical presentation, radiological and laboratory features, treatment responses, and long-term outcome. *J Neuroinflamm* (2016) 13:280. doi: 10.1186/s12974-016-0718-0
12. Kim SH, Jeong IH, Hyun JW, Joung A, Jo HJ, Hwang SH, et al. Treatment Outcomes With Rituximab in 100 Patients With Neuromyelitis Optica: Influence of FCGR3A Polymorphisms on the Therapeutic Response to Rituximab. *JAMA Neurol* (2015) 72:989–95. doi: 10.1001/jamaneurol.2015.1276
13. Guo Y, Weigand SD, Popescu BF, Lennon VA, Parisi JE, Pittock SJ, et al. Pathogenic implications of cerebrospinal fluid barrier pathology in neuromyelitis optica. *Acta Neuropathol* (2017) 133:597–612. doi: 10.1007/s00401-017-1682-1
14. Lucchinetti CF, Guo Y, Popescu BF, Fujihara K, Itoyama Y, Misu T. The pathology of an autoimmune astrocytopathy: lessons learned from neuromyelitis optica. *Brain Pathol* (2014) 24:83–97. doi: 10.1111/bpa.12099
15. Roemer SF, Parisi JE, Lennon VA, Benarroch EE, Lassmann H, Bruck W, et al. Pattern-specific loss of aquaporin-4 immunoreactivity distinguishes neuromyelitis optica from multiple sclerosis. *Brain* (2007) 130:1194–205. doi: 10.1093/brain/awl371
16. Lucchinetti CF, Mandler RN, McGavern D, Bruck W, Gleich G, Ransohoff RM, et al. A role for humoral mechanisms in the pathogenesis of Devic's neuromyelitis optica. *Brain* (2002) 125:1450–61. doi: 10.1093/brain/awf151
17. Bukhari W, Barnett MH, Prain K, Broadley SA. Molecular pathogenesis of neuromyelitis optica. *Int J Mol Sci* (2012) 13:12970–93. doi: 10.3390/ijms131012970
18. Hoftberger R, Lassmann H. Inflammatory demyelinating diseases of the central nervous system. *Handb Clin Neurol* (2017) 145:263–83. doi: 10.1016/B978-0-12-802395-2.00019-5
19. Hinson SR, Romero MF, Popescu BF, Lucchinetti CF, Fryer JP, Wolburg H, et al. Molecular outcomes of neuromyelitis optica (NMO)-IgG binding to aquaporin-4 in astrocytes. *Proc Natl Acad Sci USA* (2012) 109:1245–50. doi: 10.1073/pnas.1109980108
20. Hinson SR, Clift IC, Luo N, Kryzer TJ, Lennon VA. Autoantibody-induced internalization of CNS AQP4 water channel and EAAT2 glutamate transporter requires astrocytic Fc receptor. *Proc Natl Acad Sci USA* (2017) 114:5491–6. doi: 10.1073/pnas.1701960114

21. Howe CL, Kaptzan T, Magana SM, Ayers-Ringler JR, LaFrance-Corey RG, Lucchinetti CF. Neuromyelitis optica IgG stimulates an immunological response in rat astrocyte cultures. *Glia* (2014) 62:692–708. doi: 10.1002/glia.22635
22. Hinson SR, Pittock SJ, Lucchinetti CF, Roemer SF, Fryer JP, Kryzer TJ, et al. Pathogenic potential of IgG binding to water channel extracellular domain in neuromyelitis optica. *Neurology* (2007) 69:2221–31. doi: 10.1212/01.WNL.0000289761.64862.ce
23. Saji E, Arakawa M, Yanagawa K, Toyoshima Y, Yokoseki A, Okamoto K, et al. Cognitive impairment and cortical degeneration in neuromyelitis optica. *Ann Neurol* (2013) 73:65–76. doi: 10.1002/ana.23721
24. Hoftberger R, Guo Y, Flanagan EP, Lopez-Chiriboga AS, Endmayr V, Hochmeister S, et al. The pathology of central nervous system inflammatory demyelinating disease accompanying myelin oligodendrocyte glycoprotein autoantibody. *Acta Neuropathol* (2020) 139:875–92. doi: 10.1007/s00401-020-02132-y
25. Fan S, Xu Y, Ren H, Guan H, Feng F, Gao X, et al. Comparison of myelin oligodendrocyte glycoprotein (MOG)-antibody disease and AQP4-IgG-positive neuromyelitis optica spectrum disorder (NMOSD) when they co-exist with anti-NMDA (N-methyl-D-aspartate) receptor encephalitis. *Mult Scler Relat Disord* (2018) 20:144–52. doi: 10.1016/j.msard.2018.01.007
26. Alter A, Duddy M, Hebert S, Biernacki K, Prat A, Antel JP, et al. Determinants of human B cell migration across brain endothelial cells. *J Immunol* (2003) 170:4497–505. doi: 10.4049/jimmunol.170.9.4497
27. Ikeshima-Kataoka H. Neuroimmunological Implications of AQP4 in Astrocytes. *Int J Mol Sci* (2016) 17:1306–23. doi: 10.3390/ijms17081306
28. Zeng Q, Dong X, Ruan C, Hu B, Luo Y, Luo Z, et al. CD14(+)CD16(++) monocytes are increased in patients with NMO and are selectively suppressed by glucocorticoids therapy. *J Neuroimmunol* (2016) 300:1–8. doi: 10.1016/j.jneuroim.2016.09.011
29. Yandamuri SS, Jiang R, Sharma A, Cotzomi E, Zografou C, Ma AK, et al. Charitable Foundation, High-throughput investigation of molecular and cellular biomarkers in NMOSD. *Neurol Neuroimmunol Neuroinflamm* (2020) 7(5):e852. doi: 10.1212/NXI.0000000000000852
30. Shimizu M, Okuno T, Kinoshita M, Sumi H, Fujimura H, Yamashita K, et al. Mitochondrial DNA enhance innate immune responses in neuromyelitis optica by monocyte recruitment and activation. *Sci Rep* (2020) 10:13274. doi: 10.1038/s41598-020-70203-x
31. Moll NM, Rietsch AM, Ransohoff AJ, Cossoy MB, Huang D, Eichler FS, et al. Cortical demyelination in PML and MS: Similarities and differences. *Neurology* (2008) 70:336–43. doi: 10.1212/01.wnl.0000284601.54436.e4
32. Pittock SJ, Weinshenker BG, Lucchinetti CF, Wingerchuk DM, Corboy JR, Lennon VA. Neuromyelitis optica brain lesions localized at sites of high aquaporin 4 expression. *Arch Neurol* (2006) 63:964–8. doi: 10.1001/archneur.63.7.964
33. Fonseca MI, Chu SH, Hernandez MX, Fang MJ, Modarresi L, Selvan P, et al. Cell-specific deletion of C1qa identifies microglia as the dominant source of C1q in mouse brain. *J Neuroinflamm* (2017) 14:48. doi: 10.1186/s12974-017-0814-9
34. Hong S, Beja-Glasser VF, Nfonoyim BM, Frouin A, Li S, Ramakrishnan S, et al. Complement and microglia mediate early synapse loss in Alzheimer mouse models. *Science* (2016) 352:712–6. doi: 10.1126/science.aad8373
35. Liddelow SA, Guttenplan KA, Clarke LE, Bennett FC, Bohlen CJ, Schirmer L, et al. Neurotoxic reactive astrocytes are induced by activated microglia. *Nature* (2017) 541:481–7. doi: 10.1038/nature21029
36. Moller T, Nolte C, Burger R, Verkhratsky A, Kettenmann H. Mechanisms of C5a and C3a complement fragment-induced [Ca2+]i signaling in mouse microglia. *J Neurosci* (1997) 17:615–24. doi: 10.1523/JNEUROSCI.17-02-00615.1997
37. Song D, Sulewski MEJr., Wang C, Song J, Bhuyan R, Sterling J, et al. Complement C5a receptor knockout has diminished light-induced microglia/macrophage retinal migration. *Mol Vis* (2017) 23:210–8.
38. Wing MG, Seilly DJ, Nicholas RS, Rahman S, Zajicek J, Lachmann PJ, et al. Comparison of C1q-receptors on rat microglia and peritoneal macrophages. *J Neuroimmunol* (1999) 94:74–81. doi: 10.1016/S0165-5728(98)00227-6
39. Kinoshita M, Nakatsuji Y, Kimura T, Moriya M, Takata K, Okuno T, et al. Neuromyelitis optica: Passive transfer to rats by human immunoglobulin. *Biochem Biophys Res Commun* (2009) 386:623–7. doi: 10.1016/j.bbrc.2009.06.085
40. Bradl M, Misu T, Takahashi T, Watanabe M, Mader S, Reindl M, et al. Neuromyelitis optica: pathogenicity of patient immunoglobulin in vivo. *Ann Neurol* (2009) 66:630–43. doi: 10.1002/ana.21837
41. Saini H, Rifkin R, Gorelik M, Huang H, Ferguson Z, Jones MV, et al. Passively transferred human NMO-IgG exacerbates demyelination in mouse experimental autoimmune encephalomyelitis. *BMC Neurol* (2013) 13:104. doi: 10.1186/1471-2377-13-104
42. Lee CL, Wang KC, Chen SJ, Chen CM, Tsai CP, Chen SY. Repetitive intrathecal injection of human NMO-IgG with complement exacerbates disease severity with NMO pathology in experimental allergic encephalomyelitis mice. *Mult Scler Relat Disord* (2019) 30:225–30. doi: 10.1016/j.msard.2019.02.025
43. Kurosawa K, Misu T, Takai Y, Sato DK, Takahashi T, Abe Y, et al. Severely exacerbated neuromyelitis optica rat model with extensive astrocytopathy by high affinity anti-aquaporin-4 monoclonal antibody. *Acta Neuropathol Commun* (2015) 3:82. doi: 10.1186/s40478-015-0259-2
44. Saligrama N, Zhao F, Sikora MJ, Serratelli WS, Fernandes RA, Louis DM, et al. Opposing T cell responses in experimental autoimmune encephalomyelitis. *Nature* (2019) 572:481–7. doi: 10.1038/s41586-019-1467-x
45. Ajami B, Bennett JL, Krieger C, McNagny KM, Rossi FM. Infiltrating monocytes trigger EAE progression, but do not contribute to the resident microglia pool. *Nat Neurosci* (2011) 14:1142–9. doi: 10.1038/nn.2887
46. Yamasaki R, Lu H, Butovsky O, Ohno N, Rietsch AM, Cialic R, et al. Differential roles of microglia and monocytes in the inflamed central nervous system. *J Exp Med* (2014) 211:1533–49. doi: 10.1084/jem.20132477
47. Monaghan KL, Zheng W, Hu G, Wan ECK. Monocytes and Monocyte-Derived Antigen-Presenting Cells Have Distinct Gene Signatures in Experimental Model of Multiple Sclerosis. *Front Immunol* (2019) 10:2779. doi: 10.3389/fimmu.2019.02779
48. Zeka B, Hastermann M, Hochmeister S, Kogl N, Kaufmann N, Schanda K, et al. Highly encephalitogenic aquaporin 4-specific T cells and NMO-IgG jointly orchestrate lesion location and tissue damage in the CNS. *Acta Neuropathol* (2015) 130:783–98. doi: 10.1007/s00401-015-1501-5
49. Zeka B, Hastermann M, Kaufmann N, Schanda K, Pende M, Misu T, et al. Aquaporin 4-specific T cells and NMO-IgG cause primary retinal damage in experimental NMO/SD. *Acta Neuropathol Commun* (2016) 4:82. doi: 10.1186/s40478-016-0355-y
50. Sagan SA, Winger RC, Cruz-Herranz A, Nelson PA, Hagberg S, Miller CN, et al. Tolerance checkpoint bypass permits emergence of pathogenic T cells to neuromyelitis optica autoantigen aquaporin-4. *Proc Natl Acad Sci USA* (2016) 113:14781–6. doi: 10.1073/pnas.1617859114
51. Jones MV, Huang H, Calabresi PA, Levy M. Pathogenic aquaporin-4 reactive T cells are sufficient to induce mouse model of neuromyelitis optica. *Acta Neuropathol Commun* (2015) 3:28. doi: 10.1186/s40478-015-0207-1
52. Pohl M, Kawakami N, Kitic M, Bauer J, Martins R, Fischer MT, et al. T cell-activation in neuromyelitis optica lesions plays a role in their formation. *Acta Neuropathol Commun* (2013) 1:85. doi: 10.1186/2051-5960-1-85
53. Cruz-Herranz A, Sagan SA, Sobel RA, Green AJ, Zamvil SS. T cells targeting neuromyelitis optica autoantigen aquaporin-4 cause paralysis and visual system injury. *J Nat Sci* (2017) 3(5):e358.
54. Ratelade J, Bennett JL, Verkman AS. Intravenous neuromyelitis optica autoantibody in mice targets aquaporin-4 in peripheral organs and area postrema. *PLoS One* (2011) 6:e27412. doi: 10.1371/journal.pone.0027412
55. Asavapanumas N, Verkman AS. Neuromyelitis optica pathology in rats following intraperitoneal injection of NMO-IgG and intracerebral needle injury. *Acta Neuropathol Commun* (2014) 2:48. doi: 10.1186/2051-5960-2-48
56. Yao X, Adams MS, Jones PD, Diederich CJ, Verkman AS. Noninvasive, Targeted Creation of Neuromyelitis Optica Pathology in AQP4-IgG Seropositive Rats by Pulsed Focused Ultrasound. *J Neuropathol Exp Neurol* (2019) 78:47–56. doi: 10.1093/jnen/nly107
57. Hillebrand S, Schanda K, Nigritinou M, Tsymala I, Bohm D, Peschl P, et al. Circulating AQP4-specific auto-antibodies alone can induce neuromyelitis optica spectrum disorder in the rat. *Acta Neuropathol* (2019) 137:467–85. doi: 10.1007/s00401-018-1950-8

58. Zhang H, Verkman AS. Eosinophil pathogenicity mechanisms and therapeutics in neuromyelitis optica. *J Clin Invest* (2013) 123:2306–16. doi: 10.1172/JCI67554
59. Saadoun S, Waters P, Bell BA, Vincent A, Verkman AS, Papadopoulos MC. Intra-cerebral injection of neuromyelitis optica immunoglobulin G and human complement produces neuromyelitis optica lesions in mice. *Brain* (2010) 133:349–61. doi: 10.1093/brain/awp309
60. Saadoun S, Waters P, Owens GP, Bennett JL, Vincent A, Papadopoulos MC. Neuromyelitis optica MOG-IgG causes reversible lesions in mouse brain. *Acta Neuropathol Commun* (2014) 2:35. doi: 10.1186/2051-5960-2-35
61. Zhang H, Verkman AS. Longitudinally extensive NMO spinal cord pathology produced by passive transfer of NMO-IgG in mice lacking complement inhibitor CD59. *J Autoimmun* (2014) 53:67–77. doi: 10.1016/j.jaut.2014.02.011
62. Asavapanumas N, Ratelade J, Verkman AS. Unique neuromyelitis optica pathology produced in naive rats by intracerebral administration of NMO-IgG. *Acta Neuropathol* (2014) 127:539–51. doi: 10.1007/s00401-013-1204-8
63. Matsumoto Y, Kanamori A, Nakamura M, Takahashi T, Nakashima I, Negi A. Sera from patients with seropositive neuromyelitis optica spectral disorders caused the degeneration of rodent optic nerve. *Exp Eye Res* (2014) 119:61–9. doi: 10.1016/j.exer.2013.12.010
64. Marignier R, Ruiz A, Cavagna S, Nicole A, Watrin C, Touret M, et al. Neuromyelitis optica study model based on chronic infusion of autoantibodies in rat cerebrospinal fluid. *J Neuroinflamm* (2016) 13:111. doi: 10.1186/s12974-016-0577-8
65. Felix CM, Levin MH, Verkman AS. Complement-independent retinal pathology produced by intravitreal injection of neuromyelitis optica immunoglobulin G. *J Neuroinflamm* (2016) 13:275. doi: 10.1186/s12974-016-0746-9
66. Zhang Y, Bao Y, Qiu W, Peng L, Fang L, Xu Y, et al. Structural and visual functional deficits in a rat model of neuromyelitis optica spectrum disorders related optic neuritis. *Exp Eye Res* (2018) 175:124–32. doi: 10.1016/j.exer.2018.06.011
67. Yao X, Verkman AS. Marked central nervous system pathology in CD59 knockout rats following passive transfer of Neuromyelitis optica immunoglobulin G. *Acta Neuropathol Commun* (2017) 5:15. doi: 10.1186/s40478-017-0417-9
68. Geis C, Ritter C, Ruschil C, Weishaupt A, Grunewald B, Stoll G, et al. The intrinsic pathogenic role of autoantibodies to aquaporin 4 mediating spinal cord disease in a rat passive-transfer model. *Exp Neurol* (2015) 265:8–21. doi: 10.1016/j.expneurol.2014.12.015
69. Yick LW, Ma OK, Ng RC, Kwan JS, Chan KH. Aquaporin-4 Autoantibodies From Neuromyelitis Optica Spectrum Disorder Patients Induce Complement-Independent Immunopathologies in Mice. *Front Immunol* (2018) 9:1438. doi: 10.3389/fimmu.2018.01438
70. Chen T, Lennon VA, Liu YU, Bosco DB, Li Y, Yi MH, et al. Astrocyte-microglia interaction drives evolving neuromyelitis optica lesion. *J Clin Invest* (2020) 130:4025–38. doi: 10.1172/JCI134816
71. Ratelade J, Zhang H, Saadoun S, Bennett JL, Papadopoulos MC, Verkman AS. Neuromyelitis optica IgG and natural killer cells produce NMO lesions in mice without myelin loss. *Acta Neuropathol* (2012) 123:861–72. doi: 10.1007/s00401-012-0986-4
72. Piddlesden SJ, Lassmann H, Zimprich F, Morgan BP, Linington C. The demyelinating potential of antibodies to myelin oligodendrocyte glycoprotein is related to their ability to fix complement. *Am J Pathol* (1993) 143:555–64.
73. Czosnyka M, Czosnyka Z, Momjian S, Pickard JD. Cerebrospinal fluid dynamics. *Physiol Meas* (2004) 25:R51–76. doi: 10.1088/0967-3334/25/5/R01
74. Griffin RS, Costigan M, Brenner GJ, Ma CH, Scholz J, Moss A, et al. Complement induction in spinal cord microglia results in anaphylatoxin C5a-mediated pain hypersensitivity. *J Neurosci* (2007) 27:8699–708. doi: 10.1523/JNEUROSCI.2018-07.2007
75. Mestas J, Hughes CC. Of mice and not men: differences between mouse and human immunology. *J Immunol* (2004) 172:2731–8. doi: 10.4049/jimmunol.172.5.2731
76. Holers VM, Kinoshita T, Molina H. The evolution of mouse and human complement C3-binding proteins: divergence of form but conservation of function. *Immunol Today* (1992) 13:231–6. doi: 10.1016/0167-5699(92)90160-9
77. Simonetti M, Hagenston AM, Vardeh D, Freitag HE, Mauceri D, Lu J, et al. Nuclear calcium signaling in spinal neurons drives a genomic program required for persistent inflammatory pain. *Neuron* (2013) 77:43–57. doi: 10.1016/j.neuron.2012.10.037
78. Zhang LY, Pan J, Mamtilahun M, Zhu Y, Wang L, Venkatesh A, et al. Microglia exacerbate white matter injury via complement C3/C3aR pathway after hypoperfusion. *Theranostics* (2020) 10:74–90. doi: 10.7150/thno.35841
79. Kock MA, Hew BE, Bammert H, Fritzinger DC, Vogel CW. Structure and function of recombinant cobra venom factor. *J Biol Chem* (2004) 279:30836–43. doi: 10.1074/jbc.M403196200
80. Duan T, Smith AJ, Verkman AS. Complement-independent bystander injury in AQP4-IgG seropositive neuromyelitis optica produced by antibody-dependent cellular cytotoxicity. *Acta Neuropathol Commun* (2019) 7:112. doi: 10.1186/s40478-019-0766-7
81. Nytrova P, Potlukova E, Kemlink D, Woodhall M, Horakova D, Waters P, et al. Complement activation in patients with neuromyelitis optica. *J Neuroimmunol* (2014) 274:185–91. doi: 10.1016/j.jneuroim.2014.07.001
82. Veszeli N, Fust G, Csuka D, Trauninger A, Bors L, Rozsa C, et al. A systematic analysis of the complement pathways in patients with neuromyelitis optica indicates alteration but no activation during remission. *Mol Immunol* (2014) 57:200–9. doi: 10.1016/j.molimm.2013.09.010
83. Chen Y, Li R, Wu AM, Shu YQ, Lu ZQ, Hu XQ. The complement and immunoglobulin levels in NMO patients. *Neurol Sci* (2014) 35:215–20. doi: 10.1007/s10072-013-1481-y
84. Jitprapaikulsan J, Fryer JP, Majed M, Smith CY, Jenkins SM, Cabre P, et al. Clinical utility of AQP4-IgG titers and measures of complement-mediated cell killing in NMOSD. *Neurol - Neuroimmunol Neuroinflamm* (2020) 7:e727. doi: 10.1212/NXI.0000000000000727
85. Yun SP, Kam TI, Panicker N, Kim S, Oh Y, Park JS, et al. Block of A1 astrocyte conversion by microglia is neuroprotective in models of Parkinson's disease. *Nat Med* (2018) 24:931–8. doi: 10.1038/s41591-018-0051-5
86. Vainchtein ID, Molofsky AV. Astrocytes and Microglia: In Sickness and in Health. *Trends Neurosci* (2020) 43:144–54. doi: 10.1016/j.tins.2020.01.003
87. Jha MK, Jo M, Kim JH, Suk K. Microglia-Astrocyte Crosstalk: An Intimate Molecular Conversation. *Neuroscientist* (2019) 25:227–40. doi: 10.1177/1073858418783959
88. Bialas AR, Stevens B. TGF-beta signaling regulates neuronal C1q expression and developmental synaptic refinement. *Nat Neurosci* (2013) 16:1773–82. doi: 10.1038/nn.3560
89. Norden DM, Fenn AM, Dugan A, Godbout JP. TGFbeta produced by IL-10 redirected astrocytes attenuates microglial activation. *Glia* (2014) 62:881–95. doi: 10.1002/glia.22647
90. Vainchtein ID, Chin G, Cho FS, Kelley KW, Miller JG, Chien EC, et al. Astrocyte-derived interleukin-33 promotes microglial synapse engulfment and neural circuit development. *Science* (2018) 359:1269–73. doi: 10.1126/science.aal3589
91. Kim JH, Ko PW, Lee HW, Jeong JY, Lee MG, Kim JH, et al. Astrocyte-derived lipocalin-2 mediates hippocampal damage and cognitive deficits in experimental models of vascular dementia. *Glia* (2017) 65:1471–90. doi: 10.1002/glia.23174
92. Jo M, Kim JH, Song GJ, Seo M, Hwang EM, Suk K. Astrocytic Orosomucoid-2 Modulates Microglial Activation and Neuroinflammation. *J Neurosci* (2017) 37:2878–94. doi: 10.1523/JNEUROSCI.2534-16.2017
93. Lampron A, Larochelle A, Laflamme N, Prefontaine P, Plante MM, Sanchez MG, et al. Inefficient clearance of myelin debris by microglia impairs remyelinating processes. *J Exp Med* (2015) 212:481–95. doi: 10.1084/jem.20141656
94. Sariol A, Mackin S, Allred MG, Ma C, Zhou Y, Zhang Q, et al. Microglia depletion exacerbates demyelination and impairs remyelination in a neurotropic coronavirus infection. *Proc Natl Acad Sci USA* (2020) 117:24464–74. doi: 10.1073/pnas.2007814117
95. Miron VE, Boyd A, Zhao JW, Yuen TJ, Ruckh JM, Shadrach JL, et al. M2 microglia and macrophages drive oligodendrocyte differentiation during CNS remyelination. *Nat Neurosci* (2013) 16:1211–8. doi: 10.1038/nn.3469

96. Eyo UB, Gu N, De S, Dong H, Richardson JR, Wu LJ. Modulation of microglial process convergence toward neuronal dendrites by extracellular calcium. *J Neurosci* (2015) 35:2417–22. doi: 10.1523/JNEUROSCI.3279-14.2015
97. Eyo UB, Peng J, Murugan M, Mo M, Lalani A, Xie P, et al. Regulation of Physical Microglia-Neuron Interactions by Fractalkine Signaling after Status Epilepticus. *eNeuro* (2016) 3:0209-16. doi: 10.1523/ENEURO.0209-16.2016
98. Davalos D, Grutzendler J, Yang G, Kim JV, Zuo Y, Jung S, et al. ATP mediates rapid microglial response to local brain injury in vivo. *Nat Neurosci* (2005) 8:752–8. doi: 10.1038/nn1472
99. Eyo UB, Peng J, Swiatkowski P, Mukherjee A, Bispo A, Wu LJ. Neuronal hyperactivity recruits microglial processes via neuronal NMDA receptors and microglial P2Y12 receptors after status epilepticus. *J Neurosci* (2014) 34:10528–40. doi: 10.1523/JNEUROSCI.0416-14.2014
100. Zhang Y, Chen K, Sloan SA, Bennett ML, Scholze AR, O'Keeffe S, et al. An RNA-sequencing transcriptome and splicing database of glia, neurons, and vascular cells of the cerebral cortex. *J Neurosci* (2014) 34:11929–47. doi: 10.1523/JNEUROSCI.1860-14.2014
101. Vasek MJ, Garber C, Dorsey D, Durrant DM, Bollman B, Soung A, et al. A complement-microglial axis drives synapse loss during virus-induced memory impairment. *Nature* (2016) 534:538–43. doi: 10.1038/nature18283
102. Schafer DP, Lehrman EK, Kautzman AG, Koyama R, Mardinly AR, Yamasaki R, et al. Microglia sculpt postnatal neural circuits in an activity and complement-dependent manner. *Neuron* (2012) 74:691–705. doi: 10.1016/j.neuron.2012.03.026
103. Werneburg S, Jung J, Kunjamma RB, Ha SK, Luciano NJ, Willis CM, et al. Targeted Complement Inhibition at Synapses Prevents Microglial Synaptic Engulfment and Synapse Loss in Demyelinating Disease. *Immunity* (2020) 52:167–182 e7. doi: 10.1016/j.immuni.2019.12.004
104. Lian H, Litvinchuk A, Chiang AC, Aithmitti N, Jankowsky JL, Zheng H. Astrocyte-Microglia Cross Talk through Complement Activation Modulates Amyloid Pathology in Mouse Models of Alzheimer's Disease. *J Neurosci* (2016) 36:577–89. doi: 10.1523/JNEUROSCI.2117-15.2016
105. Litvinchuk A, Wan YW, Swartzlander DB, Chen F, Cole A, Propson NE, et al. Complement C3aR Inactivation Attenuates Tau Pathology and Reverses an Immune Network Deregulated in Tauopathy Models and Alzheimer's Disease. *Neuron* (2018) 100:1337–53.e5. doi: 10.1016/j.neuron.2018.10.031
106. Anderson SR, Zhang J, Steele MR, Romero CO, Kautzman AG, Schafer DP, et al. Complement Targets Newborn Retinal Ganglion Cells for Phagocytic Elimination by Microglia. *J Neurosci* (2019) 39:2025–40. doi: 10.1523/JNEUROSCI.1854-18.2018
107. Dejanovic B, Huntley MA, De Maziere A, Meilandt WJ, Wu T, Srinivasan K, et al. Changes in the Synaptic Proteome in Tauopathy and Rescue of Tau-Induced Synapse Loss by C1q Antibodies. *Neuron* (2018) 100:1322–1336 e7. doi: 10.1016/j.neuron.2018.10.014
108. Herwerth M, Kalluri SR, Srivastava R, Kleele T, Kenet S, Illes Z, et al. In vivo imaging reveals rapid astrocyte depletion and axon damage in a model of neuromyelitis optica-related pathology. *Ann Neurol* (2016) 79:794–805. doi: 10.1002/ana.24630
109. Schreiner B, Romanelli E, Liberski P, Ingold-Heppner B, Sobottka-Brillout B, Hartwig T, et al. Astrocyte Depletion Impairs Redox Homeostasis and Triggers Neuronal Loss in the Adult CNS. *Cell Rep* (2015) 12:1377–84. doi: 10.1016/j.celrep.2015.07.051
110. Nesargikar PN, Spiller B, Chavez R. The complement system: history, pathways, cascade and inhibitors. *Eur J Microbiol Immunol (Bp)* (2012) 2:103–11. doi: 10.1556/EuJMI.2.2012.2.2
111. Ten VS, Yao J, Ratner V, Sosunov S, Fraser DA, Botto M, et al. Complement component c1q mediates mitochondria-driven oxidative stress in neonatal hypoxic-ischemic brain injury. *J Neurosci* (2010) 30:2077–87. doi: 10.1523/JNEUROSCI.5249-09.2010
112. Fonseca MI, Ager RR, Chu SH, Yazan O, Sanderson SD, LaFerla FM, et al. Treatment with a C5aR antagonist decreases pathology and enhances behavioral performance in murine models of Alzheimer's disease. *J Immunol* (2009) 183:1375–83. doi: 10.4049/jimmunol.0901005
113. Bie B, Wu J, Foss JF, Naguib M. Activation of mGluR1 Mediates C1q-Dependent Microglial Phagocytosis of Glutamatergic Synapses in Alzheimer's Rodent Models. *Mol Neurobiol* (2019) 56:5568–85. doi: 10.1007/s12035-019-1467-8
114. Faissner S, Nikolayczik J, Chan A, Gold R, Yoon MS, Haghikia A. Immunoadsorption in patients with neuromyelitis optica spectrum disorder. *Ther Adv Neurol Disord* (2016) 9:281–6. doi: 10.1177/1756285616646332
115. Kleiter I, Gahlen A, Borisow N, Fischer K, Wernecke KD, Wegner B, et al. Neuromyelitis optica: Evaluation of 871 attacks and 1,153 treatment courses. *Ann Neurol* (2016) 79:206–16. doi: 10.1002/ana.24554
116. Patt H, Bandgar T, Lila A, Shah N. Management issues with exogenous steroid therapy. *Indian J Endocrinol Metab* (2013) 17:S612–7. doi: 10.4103/2230-8210.123548
117. Nikoo Z, Badihian S, Shaygannejad V, Asgari N, Ashtari F. Comparison of the efficacy of azathioprine and rituximab in neuromyelitis optica spectrum disorder: a randomized clinical trial. *J Neurol* (2017) 264:2003–9. doi: 10.1007/s00415-017-8590-0
118. Jacob A, Matiello M, Weinshenker BG, Wingerchuk DM, Lucchinetti C, Shuster E, et al. Treatment of neuromyelitis optica with mycophenolate mofetil: retrospective analysis of 24 patients. *Arch Neurol* (2009) 66:1128–33. doi: 10.1001/archneurol.2009.175
119. Martin CB, Ingersoll SA, Martin BK. Regulation of the C5a receptor promoter in glial cells: Minimal dependence upon the CCAAT element in astrocytes. *Mol Immunol* (2007) 44:713–21. doi: 10.1016/j.molimm.2006.04.016
120. Stephan AH, Barres BA, Stevens B. The complement system: an unexpected role in synaptic pruning during development and disease. *Annu Rev Neurosci* (2012) 35:369–89. doi: 10.1146/annurev-neuro-061010-113810
121. Derer S, Cossham M, Rosner T, Kellner C, Beurskens FJ, Schwanbeck R, et al. A Complement-Optimized EGFR Antibody Improves Cytotoxic Functions of Polymorphonuclear Cells against Tumor Cells. *J Immunol* (2015) 195:5077–87. doi: 10.4049/jimmunol.1501458
122. Sewell DL, Nacewicz B, Liu F, Macvilay S, Erdei A, Lambris JD, et al. Complement C3 and C5 play critical roles in traumatic brain cryoinjury: blocking effects on neutrophil extravasation by C5a receptor antagonist. *J Neuroimmunol* (2004) 155:55–63. doi: 10.1016/j.jneuroim.2004.06.003
123. Giembycz MA, Lindsay MA. Pharmacology of the eosinophil. *Pharmacol Rev* (1999) 51:213–340.
124. Saadoun S, Waters P, MacDonald C, Bell BA, Vincent A, Verkman AS, et al. Neutrophil protease inhibition reduces neuromyelitis optica-immunoglobulin G-induced damage in mouse brain. *Ann Neurol* (2012) 71:323–33. doi: 10.1002/ana.22686
125. Chini M, Popplau JA, Lindemann C, Carol-Perdiguer L, Hnida M, Oberlander V, et al. Resolving and Rescuing Developmental Miswiring in a Mouse Model of Cognitive Impairment. *Neuron* (2020) 105:60–74 e7. doi: 10.1016/j.neuron.2019.09.042
126. Manso Y, Holland PR, Kitamura A, Szymkowiak S, Duncombe J, Hennessy E, et al. Minocycline reduces microgliosis and improves subcortical white matter function in a model of cerebral vascular disease. *Glia* (2018) 66:34–46. doi: 10.1002/glia.23190
127. Park D, Kim S, Kim H, Shin J, Jung H, Um JW. Seizure progression triggered by IQSEC3 loss is mitigated by reducing activated microglia in mice. *Glia* (2020) 68:2661–73. doi: 10.1002/glia.23876
128. Delorme R, Ey E, Toro R, Leboyer M, Gillberg C, Bourgeron T. Progress toward treatments for synaptic defects in autism. *Nat Med* (2013) 19:685–94. doi: 10.1038/nm.3193
129. Chaudhry IB, Hallak J, Husain N, Minhas F, Stirling J, Richardson P, et al. Minocycline benefits negative symptoms in early schizophrenia: a randomised double-blind placebo-controlled clinical trial in patients on standard treatment. *J Psychopharmacol* (2012) 26:1185–93. doi: 10.1177/0269881112444941
130. Elmore MR, Najafi AR, Koike MA, Dagher NN, Spangenberg EE, Rice RA, et al. Colony-stimulating factor 1 receptor signaling is necessary for microglia viability, unmasking a microglia progenitor cell in the adult brain. *Neuron* (2014) 82:380–97. doi: 10.1016/j.neuron.2014.02.040
131. Denny WA, Flanagan JU. Small-molecule CSF1R kinase inhibitors; review of patents 2015-present. *Expert Opin Ther Pat* (2020) 30:3510–27. doi: 10.1080/13543776.2021.1839414
132. Lei F, Cui N, Zhou C, Chodosh J, Vavvas DG, Paschalis EI. CSF1R inhibition by a small-molecule inhibitor is not microglia specific; affecting

hematopoiesis and the function of macrophages. *Proc Natl Acad Sci USA* (2020) 117:23336–8. doi: 10.1073/pnas.1922788117
133. Butovsky O, Jedrychowski MP, Moore CS, Cialic R, Lanser AJ, Gabriely G, et al. Identification of a unique TGF-beta-dependent molecular and functional signature in microglia. *Nat Neurosci* (2014) 17:131–43. doi: 10.1038/nn.3599
134. Ajami B, Samusik N, Wieghofer P, Ho PP, Crotti A, Bjornson Z, et al. Single-cell mass cytometry reveals distinct populations of brain myeloid cells in mouse neuroinflammation and neurodegeneration models. *Nat Neurosci* (2018) 21:541–51. doi: 10.1038/s41593-018-0100-x
135. Borisow N, Kleiter I, Gahlen A, Fischer K, Wernecke KD, Pache F, et al. Influence of female sex and fertile age on neuromyelitis optica spectrum disorders. *Mult Scler* (2017) 23:1092–103. doi: 10.1177/1352458516671203
136. Sorge RE, Mapplebeck JC, Rosen S, Beggs S, Taves S, Alexander JK, et al. Different immune cells mediate mechanical pain hypersensitivity in male and female mice. *Nat Neurosci* (2015) 18:1081–3. doi: 10.1038/nn.4053
137. Chen G, Luo X, Qadri MY, Berta T, Ji RR. Sex-Dependent Glial Signaling in Pathological Pain: Distinct Roles of Spinal Microglia and Astrocytes. *Neurosci Bull* (2018) 34:98–108. doi: 10.1007/s12264-017-0145-y
138. Liu LL, Li JM, Su WJ, Wang B, Jiang CL. Sex differences in depressive-like behaviour may relate to imbalance of microglia activation in the hippocampus. *Brain Behav Immun* (2019) 81:188–97. doi: 10.1016/j.bbi.2019.06.012
139. Villa A, Gelosa P, Castiglioni L, Cimino M, Rizzi N, Pepe G, et al. Sex-Specific Features of Microglia from Adult Mice. *Cell Rep* (2018) 23:3501–11. doi: 10.1016/j.celrep.2018.05.048
140. Olmedillas Del Moral M, Frohlich N, Figarella K, Mojtahedi N, Garaschuk O. Effect of Caloric Restriction on the in vivo Functional Properties of Aging Microglia. *Front Immunol* (2020) 11:750. doi: 10.3389/fimmu.2020.00750
141. Salter MW, Stevens B. Microglia emerge as central players in brain disease. *Nat Med* (2017) 23:1018–27. doi: 10.1038/nm.4397
142. Qin C, Zhou LQ, Ma XT, Hu ZW, Yang S, Chen M, et al. Dual Functions of Microglia in Ischemic Stroke. *Neurosci Bull* (2019) 35:921–33. doi: 10.1007/s12264-019-00388-3
143. Ransohoff RM, Brown MA. Innate immunity in the central nervous system. *J Clin Invest* (2012) 122:1164–71. doi: 10.1172/JCI58644
144. Eyo UB, Wu LJ. Microglia: Lifelong patrolling immune cells of the brain. *Prog Neurobiol* (2019) 179:101614. doi: 10.1016/j.pneurobio.2019.04.003
145. Peng J, Gu N, Zhou L, U BE, Murugan M, Gan WB, et al. Microglia and monocytes synergistically promote the transition from acute to chronic pain after nerve injury. *Nat Commun* (2016) 7:12029. doi: 10.1038/ncomms12029
146. Umpierre AD, Wu LJ. Microglia Research in the 100th Year Since Its Discovery. *Neurosci Bull* (2020) 36:303–6. doi: 10.1007/s12264-020-00477-8
147. Sierra A, Paolicelli RC, Kettenmann H. Cien Anos de Microglia: Milestones in a Century of Microglial Research. *Trends Neurosci* (2019) 42:778–92. doi: 10.1016/j.tins.2019.09.004

Conflict of Interest: The authors declare that the research was conducted in the absence of any commercial or financial relationships that could be construed as a potential conflict of interest.

frontiers in Immunology

REVIEW
published: 23 February 2021
doi: 10.3389/fimmu.2021.640937

Strategies and Tools for Studying Microglial-Mediated Synapse Elimination and Refinement

Raffaella Morini[1], *Matteo Bizzotto*[1,2], *Fabio Perrucci*[1,2], *Fabia Filipello*[1,2,3]* and *Michela Matteoli*[1,4]*

[1] Laboratory of Pharmacology and Brain Pathology, Neurocenter, Humanitas Clinical and Research Center - IRCCS, Rozzano, Italy, [2] Department of Biomedical Sciences, Humanitas University, Pieve Emanuele, Italy, [3] Department of Psychiatry, Washington University School of Medicine, St. Louis, MO, United States, [4] Consiglio Nazionale Delle Ricerche (CNR), Institute of Neuroscience – URT Humanitas, Rozzano, Italy

The role of microglia in controlling synapse homeostasis is becoming increasingly recognized by the scientific community. In particular, the microglia-mediated elimination of supernumerary synapses during development lays the basis for the correct formation of neuronal circuits in adulthood, while the possible reactivation of this process in pathological conditions, such as schizophrenia or Alzheimer's Disease, provides a promising target for future therapeutic strategies. The methodological approaches to investigate microglial synaptic engulfment include different *in vitro* and *in vivo* settings. Basic *in vitro* assays, employing isolated microglia and microbeads, apoptotic membranes, liposomes or synaptosomes allow the quantification of the microglia phagocytic abilities, while co-cultures of microglia and neurons, deriving from either WT or genetically modified mice models, provide a relatively manageable setting to investigate the involvement of specific molecular pathways. Further detailed analysis in mice brain is then mandatory to validate the *in vitro* assays as representative for the *in vivo* situation. The present review aims to dissect the main technical approaches to investigate microglia-mediated phagocytosis of neuronal and synaptic substrates in critical developmental time windows.

Keywords: microglia, synaptic pruning, phagocytosis, confocal microscopy, flow cytometry

OPEN ACCESS

Edited by:
Rosa Chiara Paolicelli, University of Lausanne, Switzerland

Reviewed by:
Ryuta Koyama, The University of Tokyo, Japan
Urte Neniskyte, Vilnius University, Lithuania

***Correspondence:**
Fabia Filipello
filipellof@wustl.edu
Michela Matteoli
michela.matteoli@hunimed.eu

Specialty section:
This article was submitted to Multiple Sclerosis and Neuroimmunology, a section of the journal Frontiers in Immunology

Received: *12 December 2020*
Accepted: *01 February 2021*
Published: *23 February 2021*

Citation:
Morini R, Bizzotto M, Perrucci F, Filipello F and Matteoli M (2021) Strategies and Tools for Studying Microglial-Mediated Synapse Elimination and Refinement. Front. Immunol. 12:640937. doi: 10.3389/fimmu.2021.640937

INTRODUCTION

Synapse formation is a critical step in the assembly of neuronal circuits. Both secreted and membrane-associated proteins contribute to the formation and maturation of synapses. The process of synaptogenesis is started when initial contacts between synaptic partners are established through filopodia, which lose their motility and become stabilized, to transform into synaptic structures. Synaptic contacts are generated in excess during the early phases of development and therefore, at subsequent stages, the redundant, weak synapses are eliminated, while the more active are strengthened. This selective loss of synapses during a critical period is responsible for structuring neuronal circuits for the remainder of life. In the last years, microglia have emerged as a key player in the process of synapse formation as well as in synapse elimination (1, 2).

Microglia, which derive from myeloid progenitors in the yolk sac, invade the brain around embryonic day 9 in mice (3). As development proceeds, microglia acquire a highly ramified morphology with multiple, motile processes that continuously monitor the brain

microenvironment and supervise the neuronal health state. The functional interactions of microglia with neurons are spatially and temporally controlled and comprise several processes including phagocytosis of apoptotic cells, modulation of neurogenesis and regulation of myelin formation (4). Furthermore, microglia have a key role in synapse surveillance, which occurs through the frequent, transient physical interactions between these cells and synapses (5, 6). Short contacts of dendrites by microglia in the somatosensory cortex during the synaptogenesis period were shown to induce filopodia and dendritic spines, via calcium-, actin- and neurotrophin-mediated mechanisms (7, 8), while microglia–spine contacts were associated to the ability of microglia to phagocytose and eliminate synaptic material. To carry out these critical, diverse tasks, microglia assume distinctive states that change over time and which are defined by unique molecular signatures over the course of development (9).

Since the 1970s, neuroscientists have known that synaptic density in the brain changes with age. In 1983, the psychiatrist Irwin Feinberg, at the University of California in San Francisco, described the reduction in spine density as synaptic "pruning" (10, 11). In this process, the removal of weaker structures reallocates resources to those remaining, allowing them to grow stronger and more stable (12, 13). With the clear evidence that synaptic activity guides proper pruning (14, 15), researchers' attention turned to uncovering the cellular mechanisms that might regulate the remodeling. In 2007, Stevens et al. identified an unexpected role for the classical complement cascade in CNS synapses elimination. In particular, they showed that complement proteins opsonize or "tag" synapses in the brain during a discrete window of postnatal development and that the complement proteins C1q and C3 were required for synapse elimination in the developing retinogeniculate pathway (16). These data, combined with the already described phagocytic capacity of myeloid cells, led to the hypothesis that microglia may have a role in phagocytic elimination of synapses as part of the widespread pruning of supernumerary synaptic connections during development.

Consistent with their selective elimination, synaptic components were detected inside microglial phagocytic compartments. However, whether significant portions of synapses are engulfed or small (<1 um) synaptic membrane components are rapidly captured through a process named trogocytosis, is still debated (17). As expected, an excess of immature synapses was detected in mice lacking either the fractalkine receptor Cx3cr1, a chemokine receptor expressed by microglia in the brain (18), or complement components (15). The occurrence of supernumerary synapses was also detected recently in mice genetically lacking TREM2, an innate immune receptor of the immunoglobulin superfamily, expressed by microglia in the central nervous system (CNS), and playing a pivotal role in microglial cell activation, phagocytosis, survival, clustering to amyloid beta (Aβ) plaques [reviewed in (19)]. These recent findings, therefore unveiled TREM2 as a key microglial phagocytic receptor mediating the process of synapse elimination during neurodevelopment (20, 21). The presence of multiple tags seems therefore to be required in order to univocally mark the synapse to be eliminated, while additional protective molecules avoid the inappropriate synapse removal. Among the latter, the "don't eat me" signal CD47 and its receptor, signal regulatory protein α (SIRPα), were found to represent molecular brakes for excessive pruning in the developing retinogeniculate system (22).

In the last years, evidence emerged that the mechanisms of synapse elimination, operating during development, can become aberrantly "reactivated," and may possibly contribute to pathological synapse loss occurring in neurodegenerative diseases (23). Consistent with this view, both the complement cascade and TREM2 were found as implicated in Alzheimer Disease, with synaptic C1q being aberrantly elevated and contributing to synapse loss (24, 25) and several TREM2 variants being associated to the disease [reviewed in (26)]. Also, a reduction in the synapse-protecting molecule CD47 has been reported in patients with multiple sclerosis (27). Furthermore, several studies described an altered phagocytic function of microglia in Parkinson's Disease [reviewed in (28)]. The occurrence of a concomitant increase of "eat me" signals and decrease of "don't eat me" signals in these diseases, leading to an aberrant microglial phagocytosis and producing synaptic alterations, is becoming therefore a realistic possibility.

Based on these considerations and on the emerging role of abnormal synapse elimination in neurodegenerative processes, we expect that this process will be an increasingly important area of future investigation, also as a potential therapeutic target for reducing excessive phagocytosis in pathological conditions. In this review, we intend to provide a survey of the different technical approaches for studying, both *in vitro* and *in vivo*, the phagocytosis of neuronal and synaptic substrates by microglia. For each of these strategies, strengths and weaknesses will be evidenced, and possible resolution approaches will be proposed.

Abbreviations: Atg7, Autophagy Related 7; C1q, Complement Component 1q; C3, Complement Component 3; CD11b, Cluster of Differentiation 11b; CD200, Cluster of Differentiation 200; CD206, Cluster of Differentiation 206; CD45, Cluster of Differentiation 45; CD47, Cluster of Differentiation 47; CD68, Cluster of Differentiation 68; CD86, Cluster of Differentiation 86; CSF-1, macrophage colony-stimulating factor 1; CX3CL1, CX3C- chemokine ligand 1; Cx3CR1, C-X3-C Motif Chemokine Receptor 1; EZH2, Enhancer of Zeste Homolog 2; FBS, Fetal Bovine Serum; GM-CSF, macrophage colony-stimulating factor 1; GRN, Granulin; IBA1, Ionized Calcium-Binding Adapter 1; IFNγ, Interferon γ; IGF-1, Insulin Like Growth Factor 1; IL- 10, Interleukin 10; IL-1β, Interleukin 1 β; IL-34, Interleukin-34; IL-4, Interleukin 4; iNOS, Cytokine-inducible Nitric Oxidase Synthase; LPS, Lipopolysaccharide; PPARγ, Peroxisome Proliferator-activated receptor γ; PRC2, Polycomb Repressive Complex 2; PSD-95, Post synaptic Density Protein 95; PTEN, Phosphatase and Tensin Homolog; SIRPα, Signal Regulatory Protein α; SNAP25, Synaptosomal Associated Protein; SZ, Schizophrenia; TDP-43, TAR DNA-binding Protein; Tgfbr1, Transforming Growth Factor β receptor 1; Tgfbr2, Transforming Growth Factor β receptor 2; TNFα, Tumor Necrosis Factor α; TREM2, Triggering Receptor Expressed on Myeloid Cells 2; TTX, Tetrodotoxin; vGLUT1, Vescicular Glutamate Transporter 1; SR-A, Scavenger Receptor A.

MICROGLIA SOURCES

Microglial Cell Lines

Despite *in vitro* conditions clearly represent an over-simplified scenario, microglial cultures are doubtless a very useful tool to study phagocytosis, thanks to the possibility to control almost all the experimental settings. Immortalized cell lines are often

chosen, due to their ability to proliferate and provide abundant material when the use of animal models is not possible. One of the most frequently adopted cell line are BV2 cells, an immortalized murine cell line obtained by infecting primary microglia with J2 retrovirus carrying v-raf/v-myc oncogene (29). Transformed cells express several macrophage markers, as MAC-1, MAC-2 and IBA1 (30), and are able to develop an adequate response to classical stimuli. For example, LPS stimulates the release of IL1β in BV2 cells (29) and Aβ fibrils promote phagocytosis (31–34). In addition to BV2, the most implemented mouse cell line is N9, which was developed by immortalizing mouse primary microglia with the v-myc or v-mil oncogenes of the avian retrovirus MH2. N9 cells share many phenotypical features with primary microglia cultures. Indeed, N9 cells express the microglial markers FcR, Mac-1, and F4/80 (35) and two purinergic receptor subtypes, metabotropic (P2Y) and ionotropic (P2Z) (36). As for primary microglial cultures, they respond to TNFα stimulation with a reduction of the expression of the SR-A and CD36 and also in Aβ uptake (37). Moreover, LPS stimulation induces the release of IL-6, TNFα, and IL-1β in N9 cell line (35). Further additional cell lines include the colony stimulating factor-1 dependent EOC cells (38), C8-B4 and RA2 cell line which are not genetically modified (39–42). Although these cells have been widely adopted in several studies, related in particular to inflammation (43), it is increasingly clear that data obtained from cell lines need to be compared to results from primary microglia and *in vivo* models, to be considered as reliable (44). Indeed, prolonged culturing of cell lines can negatively influence their characteristics. After many generations, immortalized cell lines can suffer of duplications or chromosomes rearrangement, therefore, mutations and epigenetic changes risk to accumulate over time (45, 46). Das et al. adopted an RNA-seq approach to finely distinguish the differences in gene expression between primary cultured microglia cells and BV2 after LPS treatment (47). Primary microglia had a stronger response to the stimulus and the expression of numerous cytokines, chemokines and interferon regulated genes was uniquely affected, for example IL12 and CCL5, whose increased levels have been associated to neuroinflammation [(48, 49) for a more detailed list, see (47)]. A few years later, Butovsky et al., showed that the microglial cell lines N9 and BV2 do not express any of the genes characteristic of the TGF-β–dependent adult microglia signature (50).

Primary Newborn Microglia

Relative to cell lines, more advisable is the use of primary microglia, that can be isolated from embryos and newborn mouse pups in the P0–P4 time window (51, 52) (**Figure 1**). Dissociated cells are collected through enzymatic digestion of mouse brains and seeded as mixed glial culture. Microglia growing on top of a confluent astrocyte layer, generally in 2 weeks, are next purified through mechanical tapping of mixed glial culture [for a protocol see (53)]. After 2 h, microglia attach to the bottom and, after replacement with fresh culture medium, are ready to be used, starting from the next day. The use of primary microglia allows to perform *in vitro* assays in controlled conditions, with a relatively short time interval from the cultured cell collection to their employment (39). Although representing an advancement toward the use of immortalized cell lines, the use of cultured primary microglia suffers of important limitations. First, local environment is known to exert a profound influence on microglia, and indeed it is widely recognized that microglia quickly lose their transcriptional phenotype after niche removal (54, 55). In addition, the use of media containing serum, which are usually adopted to ensure vitality and proliferation of freshly isolated microglia, results in a low reproducibility of data, due to batch-to-batch heterogeneity (39). Since factors required for microglia survival can be found in media conditioned by astrocytes (56), a number of protocols for culturing primary microglia from newborn mice use mixed cultures composed by a confluent layer of astrocytes on which microglia grow in semi-suspension (21, 53). Although listing the different methods for isolating and culturing primary microglia is not the purpose of this review, possible hints to at least partially overcome these issues are discussed in the relative chapter.

Primary Adult Microglia

Because of the clear evidence of the central role played by microglia during physiological and in pathological context, the possibility to isolate intact microglia from the adult brain has become very appealing through the years and has been pursued by many groups. Microglia isolation from the adult brain presents some challenges, and several protocols have been published and optimized along the way (**Figure 2**). One of the first studies describing a successful method for isolating microglia from human and rat brain homogenates, was carried out by M. L. Cuzner's group in 1988 (57), followed by another work from Volker Ter Meulen's group a few years later (58). These protocols are based on an initial enzymatic digestion followed by separation steps using a Percoll gradient of various densities that allows separating myelin debris from nervous cells. Over the years, this procedure has been improved and optimized. Indeed, while until 2015, homogenization of the whole brain or of specific brain areas was mostly performed by enzymatic digestion (by using enzyme like Collagenase D, Dispase, Trypsin, and or Papain) carried at 37° or at room temperature (RT) (51, 59–66), more recently Ben A. Barres' group modified the existing microglia isolation protocols in order to minimize microglia activation during the isolation procedure. The whole procedure is now carried out under consistently cold conditions (on ice or at 4°C) and the brains are mechanically homogenized using a dounce homogenizer instead of undergoing to enzymatic digestion. Flow cytometry and RNAseq expression of cell-type–specific markers showed that avoiding enzymes and maintaining cold temperatures throughout the whole isolation process prevented transcriptional phenotypic changes and hyper activation of isolated microglia (9, 67). Furthermore, a reliable cell separation is now successfully obtained through the following three approaches: (1) Fluorescence activated cell sorting (FACS), (2) Magnetic-activated cell sorting (MACS), and (3) Immunopanning (**Figure 2**).

Fluorescence Activated Cell Sorting (FACS)

This is the most widely used approach where microglia are sorted with a high cell purity from other major CNS cell types through immune cell markers. CD45 and CD11b, which are

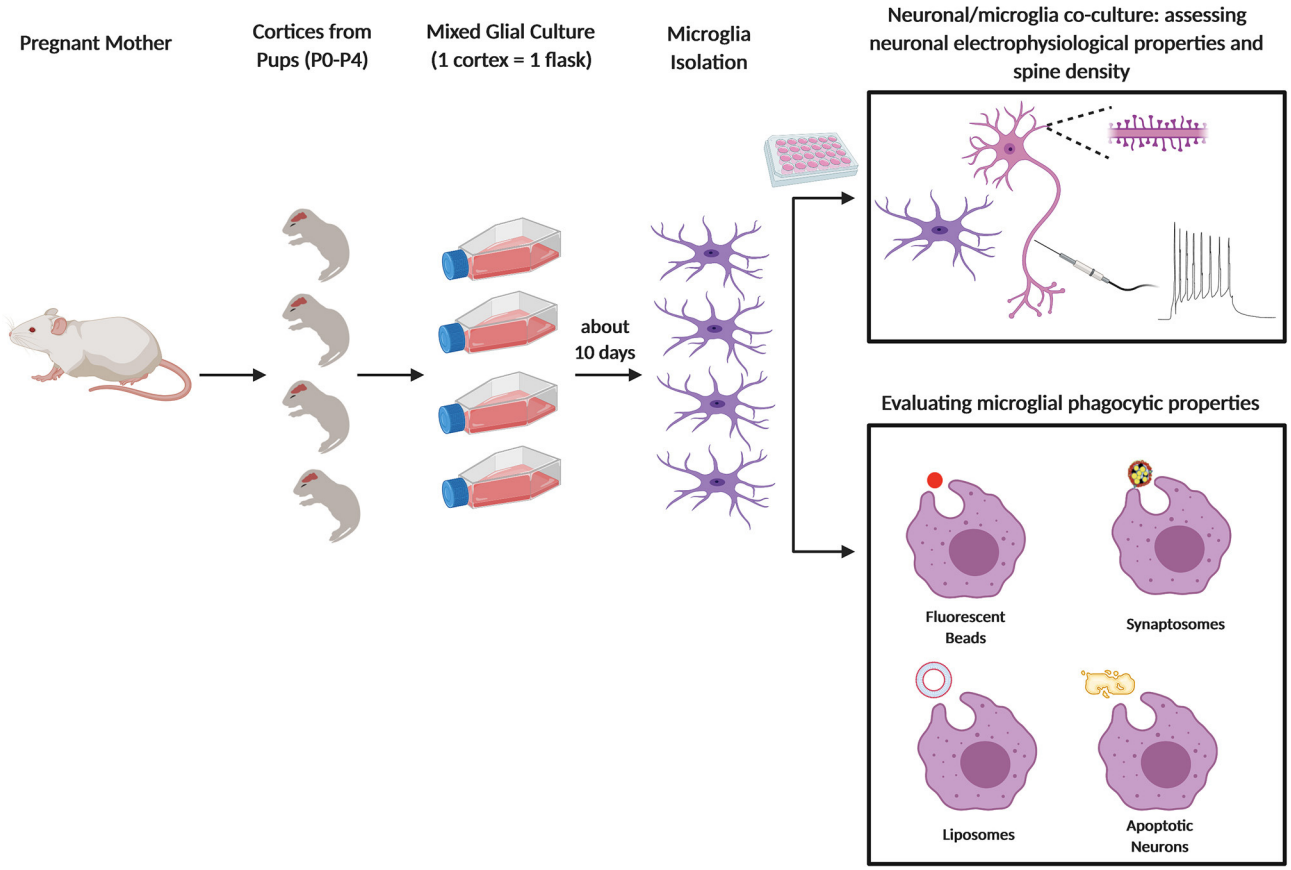

FIGURE 1 | Primary microglia culture and main usages to assess the phagocytic process. Schematic figure depicting newborn mice (P0–P4) from pregnant female used to obtain primary microglia culture. After dissection and enzymatic digestion of cortices and hippocampi, cells are resuspended in growth medium (usually composed by either DMEM or EMEM with 10 to 20% of FBS), to sustain microglial growth. Cells are plated in T75 flasks and cultured for at least 10 days at 37°C. Microglia are subsequently collected either by vigorously tapping the flasks, by agitation at 230–245 rpm for 45 min or through mild trypsinization. In some assays, microglia are cultured alone or co-cultured with neurons and the cells are analyzed by fluorescent microscopy (e.g. to quantify neuronal spine number) or by electrophysiology (top panel); in other assays, microglia phagocytic properties are assessed by feeding the cells with specific substrates: fluorescent beads, synaptosomes, liposomes, or apoptotic neurons (bottom panel).

not present on the surface of other glial cells or neurons, are commonly used to identify microglia (20, 59, 60, 68–70). Microglia are $CD45^{low}CD11b^{+}$ and can be therefore distinguished from monocyte and macrophage populations ($CD45^{high}CD11b^{+}$) (58). However, since the separation based on CD45 expression levels is not sufficient to cleanly separate microglia from all the other myeloid populations, such as neutrophils or choroid plexus macrophages, many groups recently invested increasing efforts in order to identify unique and highly specific markers to selectively distinguish microglia. The Transmembrane Protein 119 (tmem119) and the Purinergic Receptor P2y12 have been shown to be exclusively expressed by microglia and have been added to the sorting procedure (50, 67, 71). More recently, the hexosaminidase subunit beta (Hexb) has been described as a stably expressed microglia core gene, with a rather stable expression also during inflammation and neurodegeneration (72).

Magnetic-Activated Cell Sorting (MACS)

This approach is based on the use of anti-CD11b immunomagnetic beads. The anti-CD11b antibodies recognize CD11b surface antigens on microglia by positive selection. Since these antibodies are conjugated to magnetic beads, they allow the retention of labeled cells in a magnetic field. Therefore, this strategy efficiently selects $CD11b^{+}$ cells over other major CNS cell types, and the large majority of $CD11b^{+}$ cells from the uninjured CNS are in fact microglia (63, 73). Myelin debris can also be removed using the same immunomagnetic beads approach, instead of using Percoll gradient.

Immunopanning

In this strategy, antibodies recognizing CD11b surface antigens are immobilized on a Petri dish and used to retain microglia from brain single-cell suspensions. Panning is trivial, involving only three steps: (1) enzymatic preparation of a cell suspension, (2)

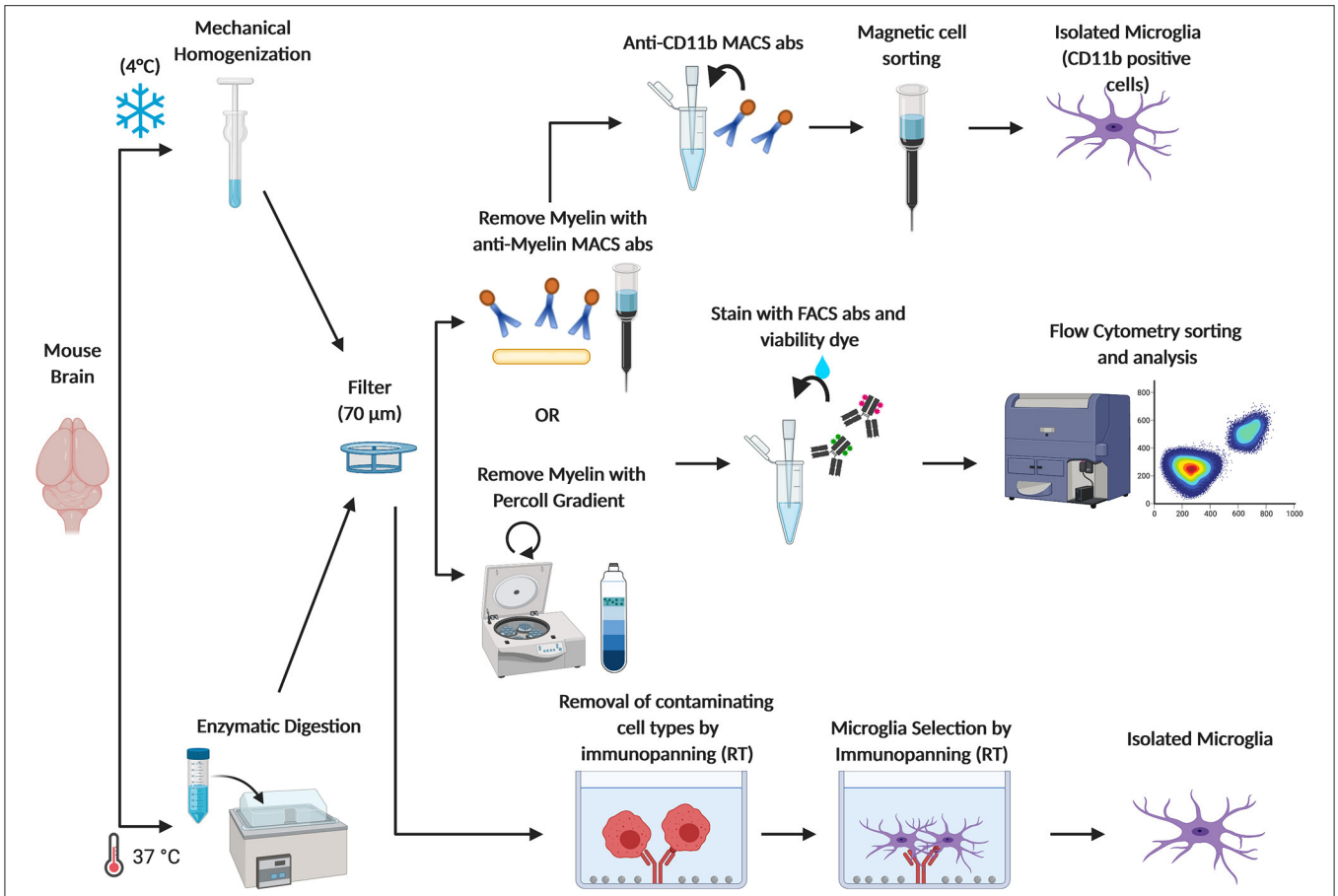

FIGURE 2 | Schematic figure depicting current methods adopted to obtain freshly isolated microglia. Brains from adult mice are (1) homogenized with a dounce homogenizer at 4°C to avoid microglia activation or (2) enzymatically digested at 37°C in the water bath, and filtered through a 70 µm cell strainer. Myelin is removed either by centrifugation with a Percoll gradient or by using anti-myelin magnetic cell sorting (MACS) antibodies. Then, microglia are sorted from other CNS cell types by FACS through specific cell markers. Otherwise, microglia are isolated by MACS anti-CD11b antibodies. Microglia can also be isolated by immunopanning. In this approach, the cells suspension is passed over a series of antibody coated dishes in order to remove contaminating cell types. Then, microglia are positively isolated in the last coated dish.

passing this suspension over a series of antibody-coated dishes, and (3) removing the purified cells from the final dish. This protocol has been less commonly used (74–76).

After isolation, fresh microglia from adult mice can be cultured *in vitro* or directly assayed for their functional and phagocytic properties. Many protocols have been developed to maintain adult microglia in culture for several days. Some groups showed the generation of pure microglia from adult mice and their maintenance in culture for more than 60 days starting from a mixed glial population treated with GM-CSF (77). Yet, these cultures maintain a high proliferative capacity, which might be due to an immature phenotype of these cells, since adult microglia is not mitotically active nor proliferate in response to GM-CSF or M-CSF (50, 59, 78).

More recently, Bohlen et al., shed a clearer light on previous procedures and proposed a new method to maintain adult microglia in culture. They were able to successfully culture microglia from juvenile or adult rat brains, but they observed that microglia cultures from old mice (>P14) were not viable. Cultures from mice younger than <P14 were viable, although the yields and survival rates were lower if compared to rat tissue. So, the authors concluded that microglia cultures from rat and mice should be performed starting from young animals since cell yield and viability drop with increasing animal age. Once isolated, microglia were maintained in culture in the presence of TGF-β2 and IL-34 or M-CSF of absence of FBS (75). Due to the challenges of maintaining adult microglia *in vitro* and after the discovery that microglia lose many of the core signature genes such as Tmem119 and P2ry12 only after a few days *in vitro* (50, 56, 79), a limited number of studies have performed phagocytic assays on adult microglia cultures. Indeed, most of the phagocytic assays currently described in literature are performed using microglia prepared from newborn mice as we described in the first section. This is still a reliable and useful system, in which the cells are easier to obtain and can be cultured for a longer period of time (20, 21).

Human Microglia-Like Cells

Recently, different groups demonstrated the existence of significant differences between murine and human microglia (79–81). This further highlighted the importance of finding new models to better understand the genetics and function of human microglia. With this purpose, a large effort has been done by the scientific community to generate human microglia-like cells (iMGLs) from human embryonic stem cells (ESCs) or by the reprogramming of adult cells (i.e., fibroblast or blood cells) into induced pluripotent stem cells (iPSCs) via the overexpression of specific transcription factors.

Several detailed methods for the generation of iMGLs have been published in the past 4–5 years (82–87). The common thread of these new generation protocols is that the specific steps through which iPSCs are differentiated into microglia-like cells, seek to mimic microglia ontogeny.

Indeed, developmental ontogeny studies showed that microglia are of mesodermal origin, deriving from erythromyeloid progenitor (EMP), that arise from the yolk-sac (3, 88, 89). Therefore, the new methods generate cells that transition from iPSCs to primitive hematopoietic precursor cells (HPCs), EMPs, and, ultimately, microglia.

iMGLs phenotype has been shown to be induced by incubation of human iPSC-derived microglial and/or macrophage progenitors with various combinations of cytokines, including high levels of CSF-1 and IL-34 (85); IL-34 and GM-CSF (83); and IL-3, IL-34 and GM- CSF (86). In order to recreate the brain environment, and to push iMGLs maturation further, some of these protocols also proposed to co-culture iMGLs with neurons (84, 87) or to add further cytokines such as TGF-β1, CX3CL1 (also known as fractalkine), and CD200 which are critical for microglia homeostasis and to mimic neuronal proximity (82) [reviewed in (90)].

Moreover, microglia-like cells from iPSCs allows the comparison between healthy donors and patients with neurological disorders. This aspect is of primary interest and, together with further recent improvements, such as the addition of iMGLs to iPSC-derived brain organoids or the xenotransplantation of HPCs/ iMGLs into mouse brain, makes iMGLs a powerful system to study properties and dysfunctions of human microglia [reviewed in (91)].

Pitfalls and Hints

Although primary microglia isolated from embryonic (92) or neonatal mice and rats are widely used as *in vitro* models, recently it has become evident that the tissue environment has a major impact on microglia transcriptome (50, 56, 79). Despite the important advances that have been made to improve culture conditions of microglia and iPSCs-derived microglial cells (39), *in vitro* microglia, although being informative and providing a useful setting to dissect basic mechanisms and possible dysfunctions of phagocytic microglia (20, 21, 50), is far from recapitulating the profile and function of microglia in their physiological environment.

As mentioned, the main limit of microglial culturing is the wide adoption of medium containing serum for their maintenance. Fetal bovine serum is usually added to medium to a final concentration of 10–20% in order to promote microglia proliferation and survival (20, 21, 53). However, microglia are not exposed to serum proteins in the brain and FBS perturbs microglia phenotype *in vitro* (39, 56), thus increasing the risks of *in vitro* artefacts. A solution to this problem has been provided by Bohlen et al., who identified in CSF-1, TGF-β and cholesterol the minimum supplement requirement for microglia culturing, a condition which allows obtaining an *in vitro* model with a significantly higher reproducibility (56).

The authors purified microglial cells from postnatal rat brain by immunopanning, and quantified their viability 5 days after plating. As expected, microglia showed a high mortality when serum was removed from the medium, but a robust pro-survival rate was reached by culturing microglial cell in a medium preconditioned by astrocytes. As CSF-1 and TGF-β were not sufficient to promote microglia viability, they cleverly dissected the conditioned medium and added cholesterol as the third key element, obtaining the so-called TIC medium (TGF-β2 2 ng/mL, IL-34 100 ng/mL, and cholesterol 1.5 mg/mL) (56). More recently, the Seker's group established an innovative tri-culture of neurons, astrocytes and microglia adopting the same cocktail used in TIC medium. Under these conditions, microglia showed a neuroprotective role when neurons were exposed to excitotoxic events, and the response to external stimuli mimicked neuroinflammatory responses better than classical co-cultures (93). Nevertheless, in contrast with Bohlen's results, cytokines detected in unstimulated TIC medium reflected slightly inflamed state and microglia exhibited an amoeboid morphology. As suggested by the authors, it should be considered that the two systems differ in the age of mice from which cultures were obtained. Moreover, the tri-culture medium includes also B27 supplement, whose elements could influence microglial cell phenotype (56, 93).

Another critical issue in microglia culturing resides in the process of cells collection after *in vitro* maintenance. Microglia proliferate in semi-suspension, above a layer of astrocyte and shaking of the culture support (flask or petri-dish) for a defined time and speed is sufficient to detach microglia from the astrocytes layer, re-suspending them in the medium (20, 21, 53). After 10–15 days, the shaken culture will be re-populated by new microglia that could in principle be employed for a new cell collection, the so-called "second-shaking." A main pitfall in this process is the clonal-selection of a sub-population from the original culture, that makes it only partially comparable to a fresh culture (94). Moreover, the shaking process can stress the cells, inducing phenotypic variations in primary microglia. For these reasons, a mild trypsinization protocol has been adopted as an alternative. Lin et al., compared shaking vs. mild trypsinization (95), demonstrating that microglial morphology and cytokine expression vary depending on the methodology of isolation. Indeed, the shaking protocol induced a higher expression of microglia activation markers, iNOS, CD86, CD206, and arginase 1, together with pro-inflammatory cytokines, TNFα, IL-1β, IL-10, and IGF-1 (95), although both conditions fully maintained microglia ability to respond to classic stimuli, such as IL-4, LPS, and IFNγ (95). Interestingly, by analyzing a panel of genes commonly upregulated during

aging or after LPS or Aβ stimulation, it was found that CD11b magnetic-associated cell sorting (MACS) guarantees the highest expression of *Tgfbr1* and *Tgfbr2* genes, and results in a "more quiescent" microglia phenotype, as compared to cells obtained by mild trypsinization and shaking (96). Thus, cell manipulation can heavily influence the microglia condition. Caution should therefore be applied when performing experiments and well-defined control conditions are mandatory to be applied.

Moreover, as already mentioned, the microenvironment exerts a strong effect on the microglia transcriptome (50, 56, 79). In particular, human and mouse microglia *in vitro* cultures exhibit down-regulation of genes characteristic of the core transcriptome signature of microglia and, on the other side, upregulate genes typically only observed *in vivo* in the context of disease or injury (56, 70, 79).

Microglia isolation from the adult brain also presents several challenges. This is primarily due to the fact that microglia are highly responsive to CNS tissue damage, which is inevitable during their isolation, and easily undergo hyper-activation and gene transcription changes after manipulation (9, 67). Another reason is that the final yield obtained after isolation is very low since microglia only account for 5–12% of the total cells in the brain (97–99) [the total yield per brain expected after isolation ranges between 5 and 10×10^4 cell from mice between postnatal (P) days 10 to P21] (75).

Furthermore, the procedures used to isolate and select microglia from adult brain have some disadvantages that need to be considered, especially depending on the use to be done with microglia after their sorting. FACS, the first-choice procedure, allows to obtain a very high cell purity and it is widely and successfully used. Yet, it requires specific and very well-organized FACS facilities, instrumentations that need to be always up to date, and specialized technicians able to manage and use sorters optimally. Another caveat of cell sorting is that the detection antibodies remain bound to the cells at the end of the process, blocking the epitopes and potentially impacting cell function. Also, sorting procedures cause hydrodynamic stress to the cells, even though it has been demonstrated that this does not affect cell structure or function. The second method, based on positive selection of $CD11b^+$ cells through magnetic beads, is in fact highly effective but requires significant upfront investment in reagents and equipment that are particularly expensive. A disadvantage of this approach is that positive selection utilizes cell receptor antibodies to target the specific cell type of interest and may potentially turn on activation cascades through these receptors or cause receptor blockade and inhibit the downstream functions of the isolated cells. Moreover, these protocols do not separate microglia from barrier-associated macrophages, monocytes, neutrophils, or certain B cells also present in the tissue. The third strategy, immunopanning, requires minimal reagent investment or specialized equipment but does not provide a high specificity. Indeed, separation of different myeloid populations is unlikely to be achievable using immunopanning due to the propensity of various myeloid cell populations to adhere to the panning dish, even dishes not coated with antibodies. Moreover, this protocol requires cells trypsinization but on the other side, avoids introduction of magnetic particles in downstream applications. Therefore, this approach is not preferable if the final goal is to isolate a pure and homogeneous microglia population.

IN VITRO AND *EX VIVO* ENGULFMENT ASSAYS

Once microglia are isolated from brain and deposited in culture, their phagocytic properties can be evaluated using several different substrates (**Figure 1**). Below we describe some of the assays which can be used to test microglia phagocytosis. Although the focus of this review is on microglial synapse elimination, in this chapter the strategies and the tools that can be used to analyze the basic phagocytic activity by microglia will be described (see **Table 1**). These assays may provide suitable control conditions, needed to complement the study of synapse elimination by microglia. It is to be considered that the receptors and molecular machineries that coordinate phagocytosis and digestion are likely to differ depending on the specific substrate. Importantly, the substrates and phagocytic events described in this section

TABLE 1 | *In vitro* engulfment assays.

Samples	Type of cells	Engulfed substrates	Techniques adopted	References
Cell lines	Microglia cell line BV-2	Fluorescent beads	Fluorescent microscopy, Flow cytometry	(100)
	Microglial cell line MMGT12	Fluorescent beads	Flow cytometry	(101)
	Microglial cell line BV-2	Synaptosomes	Fluorescent microscopy	(102)
iPC-derived microglia	Induced Microglia Like Cells (iMGL)	Synaptosomes	Fluorescent microscopy	(103, 104)
Primary cultures	Newborn microglia	Fluorescent beads and liposomes (DiO Labeled)	Fluorescent microscopy	(21)
		fluorescent beads	Fluorescent microscopy, Flow cytometry	(20)
		Fluorescent bioparticles	Fluorescent microscopy	(105)
	Adult microglia	Ultraviolet-irradiated (UV-irr) dead neurons	Fluorescent microscopy	(78)
		Fluorescent microspheres	Fluorescent microscopy	(62)
	Macrophages	Bacteria and cancer cells	CyTOF	(106)

The table reports some commonly used experimental approaches to study microglial phagocytosis in vitro.

can only partially model the process of synapses and neurites phagocytosis *in vivo*.

Fluorescent Beads

Latex beads have been widely used to analyze the basic phagocytic process by microglia. This type of assay is advantageously used to demonstrate that the phagocytic machinery of microglia is properly functional, even when synapse elimination may be defective. Further, purification of phagosomes containing engulfed latex beads has allowed to understand the phagosome biology on a biochemical and functional standpoint and to dissect the sequential steps at the basis of this process (107–109).

The use of Fluorescent Latex Beads (FLB) has allowed a fast and quantitative analysis of phagocytosis in different cell populations either by FACS (101, 110, 111) or by a simple count of FLB internalization by fluorescence or confocal microscopy (112, 113). FLB, which are routinely used to calibrate flow cytometers, may be excited by a specific wavelength or, alternatively, contain a mixture of fluorophores that enable them to be excited at any wavelength of UV and visible light. FLB have a wide range of sizes (the most commonly used range from 0.5 to 6.0 μm) and are inert, so they are not toxic and do not interfere with cell viability (100, 101). FLB may be either used without any modifications (20, 21, 100, 114, 115) or pre-opsonized with FBS or BSA to improve phagocytosis by microglia (101, 116), since it has been shown that the engulfment of synapses is strictly dependent on complement proteins deposition, such as C1q and C3, and their interaction with microglial cells (24, 103). Moreover, beads can be also carboxylated so to add a negative charge, a model that can be used to mimic negative surface charge of phosphatidylserine-exposing cells (117). The engulfment rate is dependent on FLB concentration and incubation time (115). To precisely evaluate microglia phagocytic capacity, FLB amount and time of incubation need to be precisely set.

Pathogen-associated molecular patterns (PAMPs), such as LPS, significantly increase FLB internalization by microglia (101, 115). Also, in line with the observation that FLB internalization by microglia is accompanied by an increase in TNF-α and TGF-β production (69), MDG548, a neuroprotective PPARγ agonist used for experimental Parkinson's Disease treatment was found to increase FLB engulfment, while decreasing TNFα levels, thus providing a possible basis for PPARγ agonists protective role (101).

Besides PAMPs, basic phagocytic activity by microglia is also enhanced by neurodegeneration-associated molecular patterns (NAMPs), which include the Aβ and neurofibrillary tangles (118, 119). This activation modifies microglial phenotype, turning them into disease associated microglia (DAM) (120). In this framework, Nagano et al., showed, by both confocal microscopy and flow cytometry analysis, that the presence of Aβ deposits is able to increase the engulfment rate of FLB in primary rat microglia. This effect is reversed after the treatment with Prostaglandin E2 (PGE2), through the involvement of microglial E-prostanoid receptor 2 (EP2) (121). Allendorf et al., confirmed that treatment of primary rat microglia with pro-inflammatory stimuli such as LPS, Aβ or Tau induces an increase of FLB phagocytic activity (100). Finally, Yin et al. (111) have shown that the inhibition of EZH2, the catalytic subunit core PRC2, a gene involved in silencing a number of tumor suppressor genes, is able to increase the levels of pro-inflammatory cytokines and the FLB phagocytic capacity of microglia, which are abundant in the tumor environment (111, 122).

Of note, the engulfment of FLB can be also assessed *in vivo*. Hughes et al. (114) injected FLB [6 μm] intrahippocampally in ME7 mice, a model of prion disease, in order to study their engulfment capacity. They discovered that microglia in the degenerating brain, internalize FLB and apoptotic cells, demonstrating that the phagocytic machinery of the microglia in ME7 mice is properly functional.

Liposomes

An additional substrate that can be successfully exploited for phagocytosis assays are liposomes, or unilamellar vesicles (UVs) (123), a useful tool to specifically investigate the nature of "eat-me" signals which need to be exposed by the target membrane to allow microglial phagocytosis (21).

UVs can be distinguished in three categories depending on their size: small UVs (SUV), large UVs (LUV) and giant UVs (GUV), having a diameter of 20–100, 100–1,000 nm, and 1–200 μm, respectively. UVs stability depends on the experimental conditions; indeed, oxygen reactive species react with unsaturated fatty acid chains, thus altering lipid properties and liposomes structures (124). This responsiveness to the environmental conditions has been exploited for improving drug delivery, through the generation of smart vesicles able to deliver drugs to the target and release them only after a local stimulus-response (124). One of the biggest advantages of this tool is that UVs with virtually any composition can be prepared, enriching them with specific membrane proteins or different lipids (125, 126). For example, in a recent paper, a convenient protocol was published for the preparation of proteo-GUVs containing functionally active neuronal SNARE (soluble N-ethylmaleimide-sensitive factor activating protein receptor) proteins for the study of membrane fusion *in vitro* (125). More recently, the Matteoli's group took advantage of DiO labeled liposomes composed of variable amounts of phosphatidylserine (PS) and cardiolipin (CL) to investigate whether exposed PS impacts microglia ability to engulf lipidic membranes (21). Specifically, the researchers incubated for 1 h liposomes endowed with different lipidic composition with microglial cells isolated from mice either WT or genetically lacking TREM2, a receptor which shows high affinity for phospholipids as phosphatidylcholine and PS (127). Confocal analysis of liposome engulfment inside CD68-positive phagolysosomal organelles in Iba1-positive microglia (15, 21) exploiting the Bitplane Imaris software to generate a 3D reconstruction of the fluorescent signal, allowed to demonstrate that the extent of PS positively correlates with microglia phagocytosis (127). For this kind of experiments, attention should be paid to the type of solvents used for permeabilization before the staining (128). Specifically, the use of saponin allowed to selectively create pores the cholesterol shaft of the plasma membrane (129) but not in liposomes, thus avoiding loss of DiO signal from liposomes (21).

Liposomes with similar composition have been used not only to characterize the phagocytic properties of microglial cells but also to assess their responsiveness to stimuli. In particular, Hashioka et al. reported that pretreatment of microglia with PS/PC (phosphatidylcholine) liposomes considerably inhibited the TNF-α, NO, and radical O_2- production induced by Aβ/IFN-γ, suggesting that PS and PC-containing liposomes -after being phagocytosed by microglia- inhibit Aβ and interferon-γ-induced microglial activation (130). Of note, phagocytosis of PS-containing liposome has been shown to induce the secretion of anti-inflammatory mediators including prostaglandin E(2) PGE(2) (131, 132).

Thanks to their high versatility, the use of liposomes can be a very useful tool to assess microglial phagocytic functions.

Apoptotic Neurons

Apoptotic membranes are another commonly used substrate in microglial phagocytic assays. Like in the case of beads, this type of assay can be used to investigate whether and at which extent the phagocytic machinery of microglia is functional even when synapse elimination is not properly working.

Apoptotic cells exhibit specific find-me and eat-me signals that are rapidly recognized and engulfed by phagocytes, which may or may not overlap with signals exposed at synaptic sites. Notably, phosphatidylserine externalization has been established as one of the first detectable events to occur in cells undergoing apoptosis. Clearance of apoptotic cells by phagocytes actively suppresses the initiation of inflammatory and immune responses and it is therefore fundamental for brain homeostasis (133). Moreover, apoptosis-like phenomena including caspase activation has been found locally in synapses in a process designated as "synaptic apoptosis" (134, 135).

Several protocols have been developed to study apoptotic membranes phagocytosis by microglia, describing the cellular types employed, the specific stimuli used to induce cell apoptosis and analyzing the receptors and molecular mechanisms involved. In the work by Nolte's group, cerebellar granule neurons were treated with 100 μM *S*-nitrosocysteine to induce apoptosis, event that was confirmed by nuclear condensation and PS exposure. Primary microglial cells then were added to neurons 2 h after apoptosis induction and co-cultured for 6 h. Cultures were stained with propidium iodide (PI) (to detect apoptotic/necrotic neurons) and lectin to visualize microglia and analyzed by fluorescence microscopy (136). Zhao et al. cultured rat cortical neurons and used irradiation to induce neuronal apoptosis. Again, after propidium iodide (PI) staining, dead neurons (DNs) were exposed to microglia cultures. By fluorescence microscopy, they counted the number of DNs engulfed by each microglia, and calculated the phagocytic index, that consists in the average number of phagocytosed dead neurons (PI-DNs) within each microglia and gives a quantification of microglia phagocytic efficacy (137, 138).

Using adult microglia cultures, Butovsky et al., measured the amount of ultraviolet-irradiated (UV-irr) dead neurons engulfed by adult microglia isolated from spinal cord and cultured *in vitro*. Through IF staining they were able to quantify fluorescent dead neurons engulfed by iba1 positive cells (78). Apoptotic cellular debris can be also detected by using AnnexinV (ANXV), an innate molecule that binds with high affinity to PS-bearing membranes. As shown in a recent work performed in Drosophila, apoptotic membranes were labeled with an ANXV-conjugated fluorophore and apoptosis was induced using 10 mM cycloheximide (139).

From the point of view of the receptors or mechanisms involved in the phagocytosis of apoptotic membranes, Takahashi et al., analyzed phagocytosis of apoptotic neurons by microglia after TREM2 knockdown or overexpression. In their experimental setting, neurons were labeled by a red fluorescent membrane dye and pretreated with okaidic acid to induce apoptosis. After incubating apoptotic neurons with microglia for 1 or 24 h, phagocytosis of apoptotic membrane fragments was detected by fluorescence microscopy and flow cytometry (20, 140, 141)). Beccari et al., provided an exhaustive protocol (142) in which the authors describe a series of parameters to directly quantify in more accurate and complete way than conventionally used indirect methods, microglial apoptotic membrane phagocytosis *in vivo* and *in vitro*. In a recent work (143), the authors applied a xenogenic *in vitro* model of apoptotic cells phagocytosis to study the mechanism by which microglial phagocytosis regulates neurogenesis. Phagocytosis experiments were performed in DMEM 10% FBS to ensure the presence of complement molecules, which are related to microglial phagocytosis *in vivo* (143). Primary microglia cells were fed for different time points with SH-SY5Y cells, a human neuroblastoma cell line derived from the bone marrow, previously labeled with the membrane marker CM-DiI and treated with staurosporine to induce apoptosis. Only floating dead-cells fraction was collected from the supernatant and added to primary microglia cultures in a proportion of 1:1. Apoptotic cells were visualized and quantified by trypan blue in a Neubauer chamber. By confocal analysis, the percentage of microglia containing CM-DiI and/or DAPI inclusions along a time course was identified as actively engulfed.

Synaptosomes

The process of synapse engulfment by microglia can be more specifically investigated using synaptosomes (SYNs), biochemically isolated structures consisting of pinched-off nerve terminals and juxtaposed postsynaptic densities. Since they maintain the molecular and biochemical features of a functioning synapse (144, 145), SYNs have been widely used by the neuroscientific community to study the synaptic structure and the functional properties of neurotransmitter release (146). In the recent years, the use of SYNs has been extended to simulate the interactions between synapses and microglia/astrocytes and test the phagocytic capacity of glial cells. To this aim, they may be used indifferently either freshly prepared or maintained as frozen (103).

To visualize their engulfment by microglia or astrocytes, SYNs can be stained with dyes sensitive to acidic pH (102–104, 147). These dyes (one of the most widely employed is pHrodo) show little or no fluorescent signal at neutral pH, while they fluoresce brightly when in acidic environments, thus allowing SYN visualization only when engulfed by acidic phagosomes.

Sellgren et al. analyzed the engulfment of patient-derived SYNs by iMGLs to investigate the features of synaptic pruning in schizophrenia (SZ) patients. Phagocytosis was analyzed by both real-time imaging upon SYN labeling with a pH sensitive fluorescent dye (pHrodo) and confocal microscopy, combining the staining for pH sensitive cyanine dye and the post-synaptic marker PSD-95. Through this assay, the authors showed an increased phagocytic capacity of iMGL cells from SZ patients compared to healthy controls (103, 104).

Using a similar approach, Keaney et al. showed that the blockade of Bruton's Tyrosine Kinase (BTK), a protein involved in different processes such as B cell receptor signaling, pro-inflammatory cytokine release and phagocytosis, reduces the uptake of pHrodo-labeled SYNs by microglia (102). PHrodo labeled SYNs were also used by Madore et al., to show the relevance of poly-unsaturated omega-3 fatty acids (n-3 PUFAs) in controlling microglial phagocytosis in the developing brain. In particular, exposing microglia deriving from either n-3 deficient or n-3 sufficient mice to pHrodo labeled SYN, the authors showed that the lack of n-3 from microglia increases the phagocytic capacity of microglial cells, inducing an excessive synaptic loss (148). Recently, Evans et al., exploited pHrodo labeled SYNs in order to show that beta-adrenergic antagonists, such as metropolol, are able to significantly increase phagocytosis of primary microglia from rats, whereas beta-adrenergic agonists, such as xamoterol and isoproterenol, attenuate SYNs engulfment (149). SYNs labeled with pH sensitive dyes have been also exploited to investigate the engulfment capacity of astrocytes (147), which supported astrocyte critical role not only in trophic functions and neurotransmitters recycling, but also in synapse elimination pruning (150).

SYNs can also be stained by fluorescent dyes lacking pH sensitivity. Among these, the FM Lipophilic Styril dyes, which are able to emit fluorescence only when inserted in the outer leaflet of the plasma membrane, and are mainly used to study synaptic vesicles trafficking (103, 151). Filipello et al., exposed *Trem2* knockout (*Trem2*$^{-/-}$) and WT primary microglia to SYNs labeled with FM1-43 dye, demonstrating a key role of TREM2 in the microglia phagocytic process. Flow cytometric analysis of CD11b^{+} microglia also positive for FM1-43 dye was successfully used to quantify SYNs engulfment (20).

Finally, SYNs can be isolated from mice expressing fluorescent markers in neuronal cells. As an example, in a recent work, researchers used SYNs derived from the brain of mice expressing red fluorescent protein (RFP)-to investigate whether microglia autophagy might be involved in synaptic pruning and be responsible for an impaired behavior (152). Using this approach, the authors showed that primary microglia lacking Atg7, which is vital for autophagy, displayed impaired degradation of (RFP)-expressing SYNs.

Pitfalls and Hints

The exploitation of assays employing LTBs, liposomes, apoptotic membranes or synaptosomes are relatively user-friendly, yet, some specific problems can be encountered using some of these substrates. Technical details are reported in the papers specifically quoted in the chapter above. Regarding the analysis of FLB phagocytosis by microglia, it is important to precisely set both the amount of FLB used and the incubation time. Moreover, even though FLB are effectively employed without any modification (20, 21, 100, 114, 115), they cannot be considered specific phagocytic targets unless properly opsonized. Opsonization can be carried out using FBS or BSA (101, 116). However, since the amount of complement proteins like C1q and C3 in FBS and BSA is not specified, it is not possible to infer the contribution of serum to beads phagocytosis (24, 103).

Although liposomes represent a useful tool for studying targeted phagocytosis (124), an intrinsic pitfall of their preparation is the variability in their size, that is a striking characteristic to consider in the context of phagocytosis. Given UVs dimensions also influence their stability, small UVs are a good choice (124, 153). However, SUVs are not bigger than 100 nM and this could enhance the non-specific phagocytic process called macropinocytosis, or fluid phase uptake (154), which is actin-dependent and, in macrophages, it is activated by the CSF-1 (155). A basal amount of engulfed material could be thus explained by the occurrence of this process.

A more specific substrate used to analyze microglia phagocytosis is represented by synaptosomes. However, it was shown that synaptosomes expose phosphatidylserine (PS) and show caspase activation rapidly after preparation, causing alterations in assessing the phagocytic process (156).

EXPERIMENTAL SETTINGS FOR INVESTIGATING SYNAPSE ELIMINATION BY MICROGLIA

This section describes the main technical approaches which allow to directly assess the microglia ability to eliminate synaptic contacts. The chapter analyzes both *in vitro* and *in vivo* experimental settings (see **Tables 1**, **2**).

Synapse Elimination by Microglia *in vitro*

In order to directly analyze the process of synapse elimination, multicellular culture models provide several advantages (93, 161). The generation of microglial-neuron co-cultures offers flexibility in experimental design and, when exploited in concomitance with the use of cell types deriving from genetically modified mice, allows to address a variety of mechanistic questions (162–165). Furthermore, since neurons are grown separately from microglia prior the co-culture, the two cell types can be subjected to specific treatments thus allowing to test drug effects in a selected cell populations before co-culturing. In general, *in vitro* experimental systems are not able to mimic developmental stages as it occurs *in vivo*. Yet they are useful tools and, in the last years, these experimental settings have been exploited to investigate the process of synapse elimination and its molecular underpinning.

In a recent study, Lui et al., (166) focused on Progranulin (PGRN), the product of the *Grn* gene, implicated in the regulation of phagocytosis and release of pro-inflammatory cytokines from microglia and macrophages (167, 168). The authors designed a co-culture system in which wild type cortical neurons were plated at low density to allow uniform

TABLE 2 | *In vivo* and *ex vivo* engulfment assays.

Models	Brain areas	Engulfed substrates	Techniques adopted	References
Cx3xr1-/- mouse	Hippocampus	SNAP25+, PSD95+ synaptic materials	Confocal microscopy; immune-gold electron microscopy	(18)
Itgam-/-; *C3-/-* mouse	Visual System	RGC inputs	Confocal microscopy dimensional (3D) surface volume rendering	(15)
Trem2-/- mouse	Hippocampus	PSD95+ synaptic materials	Fluorescent microscopy	(20)
Zebrafish	Spinal cord	Apoptotic neuron	Fluorescent microscopy, 3D rendering	(157)
Mertk-/- Mouse	Cortex	Apoptotic neuron	Time-lapse two-photon imaging	(158)
Adult microglia *ex vivo*	Cortex	Alexa-488 labeled apoptotic (dNs) or live neurons	Flow cytometry	(70)
		Amyloid beta (through the fluorescent marker Methoxy-XO4)		(159)
		Synaptic markers VGLUT1 and synaptophysin		(160)

The table reports some of the experimental approaches used to study microglia engulfment in vivo and ex vivo in different animal models.

synapse development for 14 days *in vitro* (DIV14). Concurrently, microglia isolated from $Grn^{+}/^{+}$ or $Grn^{-}/^{-}$ neonatal brains were added to cortical neurons at a 1:3 microglia/neuron ratio and co-cultured for 72 h. Using a modified Sholl analysis to measure the density of synapses in the vicinity of microglia cell bodies and Imaris software to perform 3D reconstructions of confocal images, the authors quantified the amount of synaptic material within microglial phagolysosomes and demonstrated a significant increase in synaptic pruning when neurons were co-cultured with microglia isolated from mice genetically lacking *Grn*. A similar approach was used by Filipello et al., to study the role of microglial TREM2 in synapse elimination. By co-culturing microglia with hippocampal neurons at a microglia to neuron ratio of 1.5:1 for 24 h, and through the analysis of miniature excitatory post-synaptic currents (mEPSC) and dendritic spines density, the authors demonstrated that microglia are able to reduce the density of excitatory synaptic contacts *in vitro* and that microglial TREM2 is required for this process to occur (20). To better visualize neurons and spines, WT neurons were GFP-transfected at DIV 11–12 before adding microglia to the co-culture. The use of transwell inserts between the two cell types allowed to discriminate the effects of microglia that require the direct contacts with neurons.

An additional study where microglia and neurons derived from mutant or knock out mice were combined in mixed culture to investigate synapse elimination, focused on the role of PTEN, a well-recognized syndromic risk allele for autism spectrum disorder (169). Using co-cultures of primary neurons and microglia from $Pten^{WT/WT}$, $Pten^{WT/m3m4}$, or $Pten^{m3m4/m3m4}$ mice in different combinations, followed by co-localization of pre- and post-synaptic markers, the authors demonstrated that $Pten^{m3m4/m3m4}$ mutation results in increased microglia-dependent synaptic pruning *in vitro*. Interestingly, the largest decrease in synaptic contact density was observed when $Pten^{m3m4/m3m4}$ neurons were cultured with $Pten^{m3m4/m3m4}$ microglia indicating an additive effect when the mutation occurs in both cell types. A relevant technological addition of this study is the setting of a protocol which allows co-culturing microglia and neurons for a week in a microglia/neuron ratio 1:1 (i.e., a longer time compared to the generally used general protocols).

The co-culture setting allows to test pharmacological or experimental treatments which reduce microglial phagocytic ability. Inhibition of synapse phagocytosis *in vitro* was recently demonstrated upon the exposure of hippocampal neurons to ANXV, an innate molecule that binds phosphatidylserine-bearing membranes with high affinity, 15 min before co-culturing them with microglia. ANXV, by cloaking externalized PS, prevents its recognition by microglial TREM2 and prevents synapse elimination, as demonstrated by the lack of dendritic spine density and mEPSC frequency reduction. A similar approach was taken in another recent work, where microglial cells were exposed to different treatments before being added to neuronal cultures (100). Specifically, Allendorf et al., demonstrated that LPS, fibrillar Aβ, phorbol 12-myristate 13-acetate (PMA) or rTAU protein induced removal of sialic acid residues in microglial cells. This resulted in an enhanced microglia ability to phagocytose neuronal components. Of note neuronal phagocytosis was inhibited by a blocking antibody against CD11b/CR3 (100).

Besides co-cultures of murine microglia and neurons, recent studies took advantage of the use of human cells. In a very interesting paper, Sellgren et al. developed and validated a high-throughput method for modeling synaptic pruning *in vitro*, using cells derived from SZ patients or healthy subjects (103). Specifically, the authors employed iPSC-derived-microglia like cells and iPSC-derived neurons, the latter generated from an inducible neurogenin 2 (NGN2) expressing stable NPC lines. After 21 days of neural differentiation, mature iMGLs derived from monocytes were added to neurons for 48 h. iMGLs, maintained under serum-free *in vitro* conditions, were found to engulf synapses from iPSC-derived neural cultures, as assessed by live imaging of iPSC-derived neurons stained for Alexa Fluor 488-phalloidin and by measuring PSD-95 engulfment. Using this asset, the authors demonstrated a significantly higher, complement-dependent,

uptake of synaptic structures when cells from SZ patients were employed (103).

Synapse Elimination by Microglia *in vivo*

Since Ito et al. in 1998 isolated and identified a novel gene "the *iba1* gene" specifically expressed in microglia, traditionally, Iba-1 antibodies have been used to label/stain microglia using immunohistochemistry (170). Confocal laser scanning microscopy is frequently used to image fluorescently labeled microglia in tissue sections (fixed), retinal whole mounts (fixed or fresh) and organotypic brain slices (fresh) to investigate microglial density, morphology, distribution, and dynamic interactions with different cell types (171, 172).

In the last decades, thanks to the advancement of high resolution live microscopy techniques, Iba1-positive microglia have been characterized as highly motile cells, extending and retracting their processes as they survey the microenvironment in the healthy brain (173). Both pre-synaptic boutons and postsynaptic spines have been shown to be contacted by microglial processes (6, 174). In the visual cortex, the microglia-synapse contacts were examined in closer resolution using 3D reconstruction serial electron microscopy (6). This study revealed that, in addition to pre- and postsynaptic specializations, microglial processes also contacted peri-synaptic astrocytes and the synaptic cleft.

Subsequently, the close microglia-synapse contacts appeared to result in the shaping, or re-wiring, of neuronal circuits by phagocytosis of synaptic materials. The phagocytic properties of microglia have been extensively analyzed through different microscopy-based approaches: confocal imaging, electron microscopy, two-photon microscopy and lightsheet microscopy (15, 173, 175–177). These techniques allow to visualize and quantify, in a very reliable manner, the material engulfed by microglia in the brain, generating a clear picture of the phagocytic process in specific time windows. 3D reconstruction of the phagocyte and its intracellular structures (e.g., phagolysosomes and other intracellular organelles) by softwares like Imaris, ilastik [(178); 1.3.2] and CellProfiler [(179); v3.0] has been successfully used to generate very detailed images of phagocytic microglia and to quantify the material internalized.

Two milestones articles first demonstrated, by electron microscopy and super-resolution confocal microscopy, the presence of pre- and post-synaptic structures inside microglial phagolysosomes in different brain regions (mouse visual system and hippocampus) during critical periods of synaptic refinement. In particular, in 2011, Paolicelli et al. spotted synaptic material inside microglia, providing the demonstration that these cells play an active role in pruning synapses. Specific presynaptic (SNAP25) and postsynaptic (PSD95) proteins were identified inside microglial processes following synaptic contacts, by confocal or immune-gold electron microscopy, respectively (18). Furthermore, disrupting the fractalkine (Cx3cl1/Cx3cr1)-mediated communication between microglia and neurons in an otherwise healthy mouse, resulted in brain circuits persisting as immature into adulthood (18, 180, 181). In 2012, the Stevens' lab at Boston Children's Hospital, found that, in the newborn mouse visual system, microglia can engulf synapses in the lateral geniculate nucleus (LGN) through a process mediated by both complement and neuronal activity. Using Cholera Toxin B Subunit (CTB) injections in *Cx3cr1* $^{gfp/+}$ mice, in which microglia express GFP, the authors elegantly showed for the first time, by 3D reconstructions that microglia contain engulfed RGC inputs. By either silencing or promoting neuronal activity in one eye using TTX or forskolin, respectively, they further showed that microglia selectively prune the weaker inputs. Notably, by examining microglial engulfment in C3 mutants and C3-receptor mutants, Schafer et al. showed that this process critically relies on the complement cascade. Of note, impaired microglial engulfment in both these mutants correlated with long-lasting defects in the segregation of ipsi- and contralateral RGC inputs in the dLGN, with an increase in synaptic densities (15). To confirm that inputs are in fact phagocytosed by microglia, Schafer et al. introduced a staining of *in situ* microglia for the phagolysosomal marker CD68, performing the subsequent colocalization with synaptic materials. Only the synaptic material internalized in CD68-positive phagolysosomal structures was considered for the analysis. A few years later, the same group published a detailed methodology for imaging and quantitatively measuring engulfment using confocal microscopy combined with 3D surface volume rendering, a method which is widely used by the scientific community (182).

Still today these two papers represent the landmark for researchers interested in studying microglia-mediated synapse elimination *in vivo*. Indeed, most if not all the subsequent studies heavily relied on the methods introduced by these pioneering works. Filipello et al. (20), used the same protocol of engulfment analysis and quantification proposed by Schafer et al. to describe the role of TREM2 in regulating synapse phagocytosis during hippocampal development. The same approaches were used to demonstrate the role of CD47, a transmembrane immunoglobulin superfamily protein that directly inhibits phagocytosis by binding to its receptor, SIRPα, thus behaving as a "don't eat me" signal during postnatal development (22). With the aim to detect the phagocytosis of a different substrate, a similar approach was also taken by Cignarella et al. who analyzed myelin engulfment and degradation by microglia in the cuprizone model of brain demyelination. By confocal analysis and subsequent 3D reconstruction, the authors showed that a TREM2 agonistic antibody enhanced myelin uptake and degradation, resulting in accelerated myelin debris removal by microglia. Again, 3D reconstruction by the Imaris software of CD68 structures inside Iba1-positive microglia containing dMBP-positive myelin debris, was used as a consolidated method of analysis (183).

Using time-lapse imaging, Weinhard et al., recently reported that, rather than removing the whole synaptic structure, microglia prune presynaptic structures through a selective partial phagocytic process termed trogocytosis, or "nibbling." The authors studied microglia "nibbling" on presynaptic structures of neurons in organotypic tissue culture, an *ex vivo* model that preserves tissue architecture important for microglia physiology and offers the advantages of a tissue-relevant context effective in studying the synaptic elimination processes. Subsequent analysis of fixed hippocampal tissue from postnatal day 15 (P15) mice

using quantitative confocal microscopy as well as correlative light and electron microscopy, revealed that microglia only capture small (<1 um) presynaptic components though a process which involves the "sinking" of presynaptic structures into the microglial cytoplasm prior to membrane closure. Conversely, pseudopodia, a hallmark of phagocytosis, were not observed (17). Further lines of investigation are expected to provide additional insights into the precise mechanisms by which microglia remove and digest synaptic contacts.

Facs-Based Microglia Phagocyitc Assays *ex vivo*

The analyses described in the previous paragraphs rely on the use of *in vitro* microglia, prepared as described in Microglia Cell Lines, Primary Newborn Microglia, and Human Microglia-Like Cells sections. However, similar assays can also be performed taking advantage of microglia freshly isolated from the adult or juvenile brain and analyzed right away (see Primary Adult Microglia chapter). The latter setting maintains closer features to those of the same cells when present in brain environment, despite of the isolation process and the consequent manipulation. In 2007, Biber's group showed the possibility to isolate microglia from specific brain regions (optic nerve, striatum, hippocampus, cerebellum, spinal cord, cortex) and to quantify the amount of fluorescent microspheres phagocytosis by confocal microscopy (62).

In the recent years, the use of flow cytometry has implemented microscopy techniques thus becoming a very useful approach to dissect the phagocytic properties of microglia not only in *in vitro* assays but also using freshly isolated microglia *ex vivo*. This strategy was successfully used by Krasemann et al., who identified a role for apolipoprotein E (APOE) in regulating a subset of microglia, exhibiting a common neurodegenerative-associated phenotype (MGnD). To determine the mechanisms through which MGnD were induced during neurodegeneration, they injected Alexa-488 labeled apoptotic (dead, dNs) or live neurons (Ns) into the cortex and hippocampus of naïve mice. In parallel, they also injected fluorescent E. coli or zymosan as a control. By gating the $CD11b^+$ $CD45^{low}$ population they were able to distinguish the phagocytic cells that internalized 488-labeled apoptotic neurons ($CD11b^+$ $CD45^{low}$ dNs-Alexa 488^+) vs. non-phagocytic microglia ($CD11b^+$ $CD45^{low}$ dNs-Alexa 488^-) (70).

A similar approach was used by Tejera and Heneka who showed in detail how to analyze Aβ phagocytosis by flow cytometry using microglia freshly isolated from adult mice. Mice were intraperitoneally injected with the Aβ fluorescent marker Methoxy-XO4, and microglia were isolated through a Percoll gradient and directly analyzed by FACS. The $CD11b^+CD45^{low}$ population, also positive for Methoxy-XO4, represented microglia phagocytosing Aβ (159). Using a different strategy, Levey's group validated a rapid flow cytometric assays to test phagocytic capacity of acutely isolated CNS mononuclear phagocytes (MPs). MPs were isolated through a Percoll gradient and subsequently incubated with macroparticle and fibrillar Aβ42 (fAβ42). Flow cytometric analysis revealed distinct phagocytic capacities of $CD11b^+CD45^{low}$ and $CD11b^+CD45^{high}$ cells both in physiological condition and in disease models (184).

The use of mass cytometry (CyTOF), a technique that combines flow cytometry with mass spectrometry, has enabled a high-dimensional analysis of cell surface markers, signaling molecules and cytokines in brain myeloid cells at the single-cell level (185–187). Because the method is largely unhampered by interference from spectral overlap, it allows for the detection of considerably more simultaneous parameters than does traditional flow cytometry. This has facilitated the understanding of phenotypic diversity of mouse and human macrophages *in vitro* and *in vivo* (188, 189). Interestingly, different macrophage phenotypes were found to have different phagocytic activities. In 2019, Schulz et al., created a functional assay to assess phagocytic activity of macrophages by mass cytometry. This method combines an in-depth phenotypic characterization of macrophages based on the expression of 36 protein markers with an analysis of biological function. The authors assessed the abilities of macrophages activated *in vitro* under different conditions to phagocytose bacteria and cancer cells. By correlating the phagocytic activity with markers expression of single cells, they defined characteristic signatures preferentially associated with phagocytosis of specific targets. This strategy can be also applied to better understand and link cell phenotype to phagocytic function in microglia in health and disease (106).

Pitfalls and Hints

The study of synapse elimination using co-cultures of neurons and microglia requires specific attention especially in relation to the establishment of the adequate co-culture conditions. In particular, defining the optimal density of microglial cells and the neuron/microglia ratio represents the most critical issue. The optimal ratio may vary depending on the experimental design and should be established accordingly. Another limitation to be considered is the limited time window (24–72 h) during which the microglia-neuron model can be maintained in co-culture. This limitation, which results from the fact that the two different cell types prefer different culture conditions (56), discourage the setting of experiments addressing processes which develop in the long term. The limited time-scale of this model is due to the negative effect of the continuous presence of microglia on the overall health of the neurons and to the fact that the culture media contains a high concentration of serum used to support the microglia, likely causing the microglia to be in an already activated state.

To overcome this issue, recently, it has been developed a tri-culture system consisting of neurons, astrocytes, and microglia. Primary rat cortical cells were maintained in a serum-free culture media developed to support all three cell types. It has been demonstrated that adding astrocytes in the culture system ameliorates neurons conditions. This "tri-culture" system can be maintained for at least 14 days *in vitro* (DIV), without any negative effect of the continuous presence of microglia on the overall health of the neurons (93).

Regarding the *in vivo* studies, one of the major risks associated with the study of microglia *in vivo*, is that manipulation of the

CNS tissues (as an example, during brain slices preparation) can lead to tissue injury and subsequent microglia activation. To solve this issue, tissue clearing techniques coupled with light sheet microscopy can be used to visualize microglia within intact transparent CNS tissues. Although, so far, this technique has not been used to study synaptic pruning, it could be relevant in the future. Indeed, besides allowing an unbiased global investigation, the method will eliminate the need to perform histological sectioning [methods and applications reviewed in (190)].

Moreover, it needs to be considered that iba1 antibodies which have been traditionally used to label microglia *in situ*, also recognize border-associated macrophages (BAMs) as well as subsets of peripheral myeloid cells. The possibility to differentiate microglia from BAMs, which reside within the meninges, choroid plexus and brain perivascular spaces as well as from circulating myeloid cells that infiltrate the CNS during neuroinflammation, is therefore mandatory. More recent studies have focused on identifying microglia-specific markers that can reliably distinguish microglia from other leukocytes, both in healthy conditions and disease. Given the range of markers and antibodies that can be used to identify microglia, the choice of targets needs to be carefully considered for each scientific question. Under this respect, recently described reporter mice have taken advantage of microglia-specific signature genes, including Tmem119eGFP (140), Tmem119TdTomato (141), Sall1GFP (142), and HexbTdTomato (159) mice are knock-in strains in which the expression of fluorescent reporter proteins is largely restricted to microglia. Another critical point when studying microglia *in vivo* is most of the confocals microscopes have limited imaging depth and require therefore the specimens to be sectioned (brain) or microdissected (retina). Also, image acquisition can be slow and Photobleaching of tissue can occur, while fixation may affect MG morphology. Finally, although modern microscopy provides a qualitative appraisal of synaptic proteins inside microglia, yet they have some drawbacks for a fast and unbiased quantification. In particular, the spatial resolution of confocal microscopy may be insufficient to resolve microglial and synaptic structures when they are less than few hundreds of nanometers apart from each other (17) [see (184) for an exhaustive review of several confocal, multiscale imaging methods for brain research]. Further, although limitations due to the fact that penetration of infrared light is limited to 1,000 μm in depth from the surface (191), *in vivo* two-photon excitation microscopy enabled direct measurement of synapse turnover in mice at postnatal 2 and 3 weeks and obtained the reliable data of spine turnover in neocortical areas (192). Synapse turnover in the hippocampus and other subcortical areas can be measured by endoscope technology, although this technique is less reliable than the two-photon imaging, mainly due to the lower resolution (192).

Given the technical limitations, the development of alternative approaches is currently in high demand (133). New technologies that could provide important advantages are holographic microscopy which brings the resolution of electron microscopy to the order of the Armstrong, and multi-isotope imaging mass spectrometry. The latter technique also allows to image and quantify molecules and presents a great potential for identifying new molecular targets in neuroimmunological field (145).

The analysis of freshly isolated microglia by FACS-based phagocytic assays *ex vivo* may pose a few specific problems. As already mentioned, it is critical to choose protocols generating freshly isolated microglia from the adult brain that avoid hyper-activation and stress of this type of cells. Again, flow cytometers need to be up to date, and FACS lasers should be often calibrated and constantly maintained by specialists at the FACS facilities. The combination of antibodies used to stain microglia and to detect the phagocytic material need to be chosen taking into account fluorophore emission/excitation spectra overlapping and the subsequent compensation. It is always necessary to add the proper isotype controls to the staining panel to discriminate unspecific signal. Negative and positive controls and cells deriving from mice knockout for the specific gene of interest should be run in parallel when analyzing signal/proteins that have not been described before. Importantly, the gating strategy used to select $CD11b^{+}$ $CD45^{low}$ microglia should be carefully chosen taking into account that other immune cells also positive for those markers are present in the brain parenchima and meninges. Finally, when choosing antibodies to specifically target microglia (i.e., Tmem119, P2ry12) it is important to consider that during pathological /inflammatory conditions these molecules can change being down or upregulated, therefore making it necessary to revise the gating strategy and the antibodies panel.

CONCLUSIONS

In the last years, several novel techniques and approaches have been introduced which have significantly advanced the study of how microglia cells, at specific stages of brain development, perform engulfment and elimination of neuronal and synaptic components. Phagocytic assays employing liposomes, synaptosomes or apoptotic membranes allow the dissection of the molecular and lipidic components that direct the engulfment process. Co-cultures of neurons and microglia derived from WT or genetically modified mouse models provide the possibility to successfully assess, by different methods, the molecular requirements and the functional consequences of the synapse elimination process. While these methods provide settings suited to easily investigate the mechanistic aspects of the process of microglia-mediated phagocytosis, they suffer from the major problem that isolated microglia do not maintain the phenotypic and functional features they have in the brain. The *in vitro* assays need therefore to be combined with analysis in brain sections or using microglia freshly isolated from the adult or juvenile brain and immediately analyzed, which allows to maintain closer features to those of the same cells present in brain environment. The use of flow cytometry has implemented confocal and electron microscopy techniques, revealing as a very useful approach.

Finally, the possibility to generate microglia-like cells from human embryonic stem cells or by the reprogramming of adult cells into induced pluripotent stem cells is providing new,

important possibilities to investigate the process of neuronal and synaptic phagocytosis employing material derived from human patients. It is expected that these methods will be soon implemented by the possibility of incorporating the appropriate number of microglia-like cells derived from human embryonic stem cells into brain organoids, in order to obtain a cell type ratio comparable to that of the human brain and allowing at the same time the microglia differentiation in a 3-dimensional structure. Together with the combined use of high resolution microscopy, FACS and mass cytometry analysis, we can expect that these approaches will represent a further step toward a deeper comprehension of the process of synapse elimination in healthy or diseased contexts.

AUTHOR CONTRIBUTIONS

RM, FF, and MM designed the review outline. All the authors contributed to writing and designing the scheme.

FUNDING

The work in our laboratory was supported by PRIN (Ministero dell'Istruzione dell'Università e della Ricerca, #2017A9MK4R); MinSal FR 2016 (Ministero della Salute #RF-201602361571) and CARIPLO grant 2018 (#2018-0364) to FF. FP was supported by Fondazione Umberto Veronesi 2017 grant. Images created with BioRender.com.

REFERENCES

1. Allen NJ, Lyons DA. Glia as architects of central nervous system formation and function. *Science.* (2018) 362:181–5. doi: 10.1126/science.aat0473
2. Reemst K, Noctor SC, Lucassen PJ, Hol EM. The indispensable roles of microglia and astrocytes during brain development. *Front Hum Neurosci.* (2016) 10:1–28. doi: 10.3389/fnhum.2016.00566
3. Ginhoux F, Greter M, Leboeuf M, Nandi S, See P, Gokhan S, et al. Fate mapping analysis reveals that adult microglia derive from primitive macrophages. *Science.* (2010) 330:841–5. doi: 10.1126/science.1194637
4. Schafer DP, Stevens B. Microglia function in central nervous system development and plasticity. *Cold Spring Harb Perspect Biol.* (2015) 7:1–8. doi: 10.1101/cshperspect.a020545
5. Wake H, Moorhouse AJ, Jinno S, Kohsaka S, Nabekura J. Resting microglia directly monitor the functional state of synapses *in vivo* and determine the fate of ischemic terminals. *J Neurosci.* (2009) 29:3974–80. doi: 10.1523/JNEUROSCI.4363-08.2009
6. Tremblay ME, Lowery RL, Majewska AK. Microglial interactions with synapses are modulated by visual experience. *PLoS Biol.* (2010) 8:e1000527. doi: 10.1371/journal.pbio.1000527
7. Miyamoto A, Wake H, Ishikawa AW, Eto K, Shibata K, Murakoshi H, et al. Microglia contact induces synapse formation in developing somatosensory cortex. *Nat Commun.* (2016) 7:12540. doi: 10.1038/ncomms12540
8. Parkhurst CN, Yang G, Ninan I, Savas JN, Yates JR III, Lafaille JJ, et al. Microglia promote learning-dependent synapse formation through brain-derived neurotrophic factor. *Cell.* (2013) 155:1596–609. doi: 10.1016/j.cell.2013.11.030
9. Hammond TR, Dufort C, Dissing-Olesen L, Giera S, Young A, Wysoker A, et al. Single-Cell RNA sequencing of microglia throughout the mouse lifespan and in the injured brain reveals complex cell-state changes. *Immunity.* (2019) 50:253–71.e6. doi: 10.1016/j.immuni.2018.11.004
10. Feinberg I. Schizophrenia: caused by a fault in programmed synaptic elimination during adolescence? *J Psychiatr Res.* (1982) 17:319–34. doi: 10.1016/0022-3956(82)90038-3
11. Huttenlocher PR. Synaptic density in human frontal cortex - developmental changes and effects of aging. *Brain Res.* (1979) 163:195–205. doi: 10.1016/0006-8993(79)90349-4
12. Shatz CJ. The prenatal development of the cat's retinogeniculate pathway. *J Neurosci.* (1983) 3:482–99. doi: 10.1523/JNEUROSCI.03-03-00482.1983
13. Sretavan D, Shatz CJ. Prenatal development of individual retinogeniculate axons during the period of segregation. *Nature.* (1984) 308:845–8. doi: 10.1038/308845a0
14. Li Y, Du X-F, Liu C-S, Wen Z-L, Du J-L. Reciprocal regulation between resting microglial dynamics and neuronal activity *in vivo*. *Dev Cell.* (2012) 23:1189–202. doi: 10.1016/j.devcel.2012.10.027
15. Schafer DP, Lehrman EK, Kautzman AG, Koyama R, Mardinly AR, Yamasaki R, et al. Microglia sculpt postnatal neural circuits in an activity and complement-dependent manner. *Neuron.* (2012) 74:691–705. doi: 10.1016/j.neuron.2012.03.026
16. Stevens B, Allen NJ, Vazquez LE, Howell GR, Christopherson KS, Nouri N, et al. The classical complement cascade mediates CNS synapse elimination. *Cell.* (2007) 131:1164–78. doi: 10.1016/j.cell.2007.10.036
17. Weinhard L, Di Bartolomei G, Bolasco G, Machado P, Schieber NL, Neniskyte U, et al. Microglia remodel synapses by presynaptic trogocytosis and spine head filopodia induction. *Nat Commun.* (2018) 9:1228. doi: 10.1038/s41467-018-03566-5
18. Paolicelli RC, Bolasco G, Pagani F, Maggi L, Scianni M, Panzanelli P, et al. Synaptic pruning by microglia is necessary for normal brain development. *Science.* (2011) 333:1456–8. doi: 10.1126/science.1202529
19. Ulland TK, Colonna M. TREM2 - a key player in microglial biology and Alzheimer disease. *Nat Rev Neurol.* (2018) 14:667–75. doi: 10.1038/s41582-018-0072-1
20. Filipello F, Morini R, Corradini I, Zerbi V, Canzi A, Michalski B, et al. The microglial innate immune receptor TREM2 is required for synapse elimination and normal brain connectivity. *Immunity.* (2018) 48:979–91.e8. doi: 10.1016/j.immuni.2018.04.016
21. Scott-Hewitt N, Perrucci F, Morini R, Erreni M, Mahoney M, Witkowska A, et al. Local externalization of phosphatidylserine mediates developmental synaptic pruning by microglia. *EMBO J.* (2020) 39:e105380. doi: 10.15252/embj.2020105380
22. Lehrman EK, Wilton DK, Litvina EY, Welsh CA, Chang ST, Frouin A, et al. CD47 protects synapses from excess microglia-mediated pruning during development. *Neuron.* (2018) 100:120–34.e6. doi: 10.1016/j.neuron.2018.09.017
23. Salter MW, Stevens B. Microglia emerge as central players in brain disease. *Nat Med.* (2017) 23:1018–27. doi: 10.1038/nm.4397
24. Hong S, Beja-Glasser VF, Nfonoyim BM, Frouin A, Li S, Ramakrishnan S, et al. Complement and microglia mediate early synapse loss in Alzheimer mouse models. *Science.* (2016) 352:712–6. doi: 10.1126/science.aad8373
25. Dejanovic B, Huntley MA, De Mazière A, Meilandt WJ, Wu T, Srinivasan K, et al. Changes in the synaptic proteome in tauopathy and rescue of tau-induced synapse loss by C1q antibodies. *Neuron.* (2018) 100:1322–36.e7. doi: 10.1016/j.neuron.2018.10.014
26. Ulrich JD, Ulland TK, Colonna M, Holtzman DM. Elucidating the role of TREM2 in Alzheimer's disease. *Neuron.* (2017) 94:237–48. doi: 10.1016/j.neuron.2017.02.042
27. Han MH, Lundgren DH, Jaiswa S, Chao M, Graham KL, Garris CS, et al. Janus-like opposing roles of CD47 in autoimmune brain inflammation in humans and mice. *J Exp Med.* (2012) 209:1325–34. doi: 10.1084/jem.20101974
28. Janda E, Boi L, Carta AR. Microglial phagocytosis and its regulation: a therapeutic target in parkinson's disease? *Front Mol Neurosci.* (2018) 11:144. doi: 10.3389/fnmol.2018.00144
29. Blasi E, Barluzzi R, Bocchini V, Mazzolla R, Bistoni F. Immortalization of murine microglial cells by a v-raf/v-myc carrying retrovirus. *J Neuroimmunol.* (1990) 27:229–37. doi: 10.1016/0165-5728(90)90073-V

30. Bignami A, Eng LF, Dahl D, Uyeda CT. Localization of the glial fibrillary acidic protein in astrocytes by immunofluorescence. *Brain Res.* (1972) 43:429–35. doi: 10.1016/0006-8993(72)90398-8
31. Mazaheri F, Snaidero N, Kleinberger G, Madore C, Daria A, Werner G, et al. TREM2 deficiency impairs chemotaxis and microglial responses to neuronal injury. *EMBO Rep.* (2017) 18:1186–98. doi: 10.15252/embr.201743922
32. Stansley B, Post J, Hensley K. A comparative review of cell culture systems for the study of microglial biology in Alzheimer's disease. *J Neuroinflamm.* (2012) 9:115. doi: 10.1186/1742-2094-9-115
33. Boza-Serrano A, Reyes JF, Rey NL, Leffler H, Bousset L, Nilsson U, et al. The role of Galectin-3 in α-synuclein-induced microglial activation. *Acta Neuropathol Commun.* (2014) 2:156. doi: 10.1186/PREACCEPT-1285543917141325
34. Kopec KK, Carroll RT. Alzheimer's beta-amyloid peptide 1-42 induces a phagocytic response in murine microglia. *J Neurochem.* (1998) 71:2123–31. doi: 10.1046/j.1471-4159.1998.71052123.x
35. Righi M, Mori L, De Libero G, Sironi M, Biondi A, Mantovani A, et al. Monokine production by microglial cell clones. *Eur J Immunol.* (1989) 19:1443–8. doi: 10.1002/eji.1830190815
36. Ferrari D, Villalba M, Chiozzi P, Falzoni S, Ricciardi-Castagnoli P, Di Virgilio F. Mouse microglial cells express a plasma membrane pore gated by extracellular ATP. *J Immunol.* (1996) 156:1531–9.
37. Hickman SE, Allison EK, El Khoury J. Microglial dysfunction and defective beta-amyloid clearance pathways in aging Alzheimer's disease mice. *J Neurosci.* (2008) 28:8354–60. doi: 10.1523/JNEUROSCI.0616-08.2008
38. Walker WS, Gatewood J, Olivas E, Askew D, Havenith CE. Mouse microglial cell lines differing in constitutive and interferon-gamma-inducible antigen-presenting activities for naive and memory CD4+ and CD8+ T cells. *J Neuroimmunol.* (1995) 63:163–74. doi: 10.1016/0165-5728(95)00146-8
39. Timmerman R, Burm SM, Bajramovic JJ. An overview of *in vitro* methods to study microglia. *Front Cell Neurosci.* (2018) 12:242. doi: 10.3389/fncel.2018.00242
40. Alliot F, Marty M-C, Cambier D, Pessac B. A spontaneously immortalized mouse microglial cell line expressing CD4. *Dev Brain Res.* (1996) 95:140–3. doi: 10.1016/0165-3806(96)00101-0
41. Takenouchi T, Ogihara K, Sato M, Kitani H. Inhibitory effects of U73122 and U73343 on Ca2+ influx and pore formation induced by the activation of P2X7 nucleotide receptors in mouse microglial cell line. *Biochim Biophys Acta.* (2005) 1726:177–86. doi: 10.1016/j.bbagen.2005.08.001
42. Sousa C, Biber K, Michelucci A. Cellular and molecular characterization of microglia: a unique immune cell population. *Front Immunol.* (2017) 8:198. doi: 10.3389/fimmu.2017.00198
43. Tao X, Li N, Liu F, Hu Y, Liu J, Zhang Y-M. *In vitro* examination of microglia-neuron crosstalk with BV2 cells, and primary cultures of glia and hypothalamic neurons. *Heliyon.* (2018) 4:e00730. doi: 10.1016/j.heliyon.2018.e00730
44. Henn A, Lund S, Hedtjärn M, Schrattenholz A, Pörzgen P, Leist M. The suitability of BV2 cells as alternative model system for primary microglia cultures or for animal experiments examining brain inflammation. *ALTEX.* (2009) 25:83–94. doi: 10.14573/altex.2009.2.83
45. Lorsch JR, Collins FS, Lippincott-Schwartz J. Cell biology. Fixing problems with cell lines. *Science.* (2014) 346:1452–53. doi: 10.1126/science.1259110
46. Das A, Chai JC, Kim SH, Park KS, Lee YS, Jung KH, et al. Dual RNA sequencing reveals the expression of unique transcriptomic signatures in lipopolysaccharide-induced BV-2 microglial cells. *PLoS ONE.* (2015) 10:e0121117. doi: 10.1371/journal.pone.0121117
47. Das A, Kim SH, Arifuzzaman S, Yoon T, Chai JC, Lee YS, et al. Transcriptome sequencing reveals that LPS-triggered transcriptional responses in established microglia BV2 cell lines are poorly representative of primary microglia. *J Neuroinflamm.* (2016) 13:182. doi: 10.1186/s12974-016-0644-1
48. Constantinescu CS, Goodman DB, Hilliard B, Wysocka M, Cohen JA. Murine macrophages stimulated with central and peripheral nervous system myelin or purified myelin proteins release inflammatory products. *Neurosci Lett.* (2000) 287:171–4. doi: 10.1016/S0304-3940(00)01184-8
49. Proudfoot AEI, de Souza ALS, Muzio V. The use of chemokine antagonists in EAE models. *J Neuroimmunol.* (2008) 198:27–30. doi: 10.1016/j.jneuroim.2008.04.007
50. Butovsky O, Jedrychowski MP, Moore CS, Cialic R, Lanser AJ, Gabriely G, et al. Identification of a unique TGF-β-dependent molecular and functional signature in microglia. *Nat Neurosci.* (2014) 17:131–43. doi: 10.1038/nn.3599
51. Lee J-K, Tansey MG. Microglia isolation from adult mouse brain. *Methods Mol Biol.* (2013) 1041:17–23. doi: 10.1007/978-1-62703-520-0_3
52. Harms AS, Tansey MG. Isolation of murine postnatal brain microglia for phenotypic characterization using magnetic cell separation technology. *Methods Mol Biol.* (2013) 1041:33–9. doi: 10.1007/978-1-62703-520-0_5
53. Lian H, Roy E, Zheng H. Protocol for primary microglial culture preparation. *Bio Protocol.* (2016) 6:e1989. doi: 10.21769/BioProtoc.1989
54. Holtman IR, Skola D, Glass CK. Transcriptional control of microglia phenotypes in health and disease. *J Clin Invest.* (2017) 127:3220–9. doi: 10.1172/JCI90604
55. Amit I, Winter DR, Jung S. The role of the local environment and epigenetics in shaping macrophage identity and their effect on tissue homeostasis. *Nat Immunol.* (2016) 17:18–25. doi: 10.1038/ni.3325
56. Bohlen CJ, Bennett FC, Tucker AF, Collins HY, Mulinyawe SB, Barres BA. Diverse requirements for microglial survival, specification, and function revealed by defined-medium cultures. *Neuron.* (2017) 94:759–73.e8. doi: 10.1016/j.neuron.2017.04.043
57. Hayes GM, Woodroofe MN, Cuzner ML. Characterisation of microglia isolated from adult human and rat brain. *J Neuroimmunol.* (1988) 19:177–89. doi: 10.1016/0165-5728(88)90001-X
58. Sedgwick JD, Schwender S, Imrich H, Dörries R, Butcher GW, ter Meulen V. Isolation and direct characterization of resident microglial cells from the normal and inflamed central nervous system. *Proc Natl Acad Sci USA.* (1991) 88:7438–42. doi: 10.1073/pnas.88.16.7438
59. Ford AL, Goodsall AL, Hickey WF, Sedgwick JD. Normal adult ramified microglia separated from other central nervous system macrophages by flow cytometric sorting. Phenotypic differences defined and direct *ex vivo* antigen presentation to myelin basic protein-reactive CD4+ T cells compared. *J Immunol.* (1995) 154:4309–21.
60. De Groot CJ, Montagne L, Janssen I, Ravid R, Van Der Valk P, Veerhuis R. Isolation and characterization of adult microglial cells and oligodendrocytes derived from postmortem human brain tissue. *Brain Res Brain Res Protoc.* (2000) 5:85–94. doi: 10.1016/S1385-299X(99)00059-8
61. Cardona AE, Huang D, Sasse ME, Ransohoff RM. Isolation of murine microglial cells for RNA analysis or flow cytometry. *Nat Protoc.* (2006) 1:1947–51. doi: 10.1038/nprot.2006.327
62. de Haas AH, Boddeke HWGM, Brouwer N, Biber K. Optimized isolation enables *ex vivo* analysis of microglia from various central nervous system regions. *Glia.* (2007) 55:1374–84. doi: 10.1002/glia.20554
63. Nikodemova M, Watters JJ. Efficient isolation of live microglia with preserved phenotypes from adult mouse brain. *J Neuroinflamm.* (2012) 9:147. doi: 10.1186/1742-2094-9-147
64. Yip PK, Kaan TKY, Fenesan D, Malcangio M. Rapid isolation and culture of primary microglia from adult mouse spinal cord. *J Neurosci Methods.* (2009) 183:223–37. doi: 10.1016/j.jneumeth.2009.07.002
65. Garcia JA, Cardona SM, Cardona AE. Isolation and analysis of mouse microglial cells. *Curr Protoc Immunol.* (2014) 104:14.35.1–15. doi: 10.1002/0471142735.im1435s104
66. Joseph B, Venero JL. A brief overview of multitalented microglia. *Methods Mol Biol.* (2013) 1041:3–8. doi: 10.1007/978-1-62703-520-0_1
67. Bennett ML, Bennett FC, Liddelow SA, Ajami B, Zamanian JL, Fernhoff NB, et al. New tools for studying microglia in the mouse and human CNS. *Proc Natl Acad Sci USA.* (2016) 113:E1738–46. doi: 10.1073/pnas.1525528113
68. Olah M, Raj D, Brouwer N, De Haas AH, Eggen BJL, Den Dunnen WFA, et al. An optimized protocol for the acute isolation of human microglia from autopsy brain samples. *Glia.* (2012) 60:96–111. doi: 10.1002/glia.21251
69. Sierra A, Gottfried-Blackmore AC, McEwen BS, Bulloch K. Microglia derived from aging mice exhibit an altered inflammatory profile. *Glia.* (2007) 55:412–24. doi: 10.1002/glia.20468
70. Krasemann S, Madore C, Cialic R, Baufeld C, Calcagno N, El Fatimy R, et al. The TREM2-APOE pathway drives the transcriptional phenotype of dysfunctional microglia in neurodegenerative diseases. *Immunity.* (2017) 47:566–81.e9. doi: 10.1016/j.immuni.2017.08.008

71. Haynes SE, Hollopeter G, Yang G, Kurpius D, Dailey ME, Gan W-B, et al. The P2Y12 receptor regulates microglial activation by extracellular nucleotides. *Nat Neurosci.* (2006) 9:1512–9. doi: 10.1038/nn1805
72. Masuda T, Amann L, Sankowski R, Staszewski O, Lenz M, D Errico P, et al. Author correction: novel Hexb-based tools for studying microglia in the CNS. *Nat Immunol.* (2020) 21:1302. doi: 10.1038/s41590-020-0774-6
73. Grabert K, McColl BW. Isolation and phenotyping of adult mouse microglial cells. *Methods Mol Biol.* (2018) 1784:77–86. doi: 10.1007/978-1-4939-7837-3_7
74. Barres BA. Designing and troubleshooting immunopanning protocols for purifying neural cells. *Cold Spring Harb Protoc.* (2014) 2014:1342–47. doi: 10.1101/pdb.ip073999
75. Bohlen CJ, Friedman BA, Dejanovic B, Sheng M. Microglia in brain development, homeostasis, and neurodegeneration. *Annu Rev Genet.* (2019) 53:263–88. doi: 10.1146/annurev-genet-112618-043515
76. Tsatas O, Ghasemlou N. Isolation and RNA purification of macrophages/microglia from the adult mouse spinal cord. *J Immunol Methods.* (2020) 477:112678. doi: 10.1016/j.jim.2019.112678
77. Moussaud S, Draheim HJ. A new method to isolate microglia from adult mice and culture them for an extended period of time. *J Neurosci Methods.* (2010) 187:243–53. doi: 10.1016/j.jneumeth.2010.01.017
78. Butovsky O, Jedrychowski MP, Cialic R, Krasemann S, Murugaiyan G, Fanek Z, et al. Targeting miR-155 restores abnormal microglia and attenuates disease in SOD1 mice. *Ann Neurol.* (2015) 77:75–99. doi: 10.1002/ana.24304
79. Gosselin D, Skola D, Coufal NG, Holtman IR, Schlachetzki JCM, Sajti E, et al. An environment-dependent transcriptional network specifies human microglia identity. *Science.* (2017) 356:eaal3222–13. doi: 10.1126/science.aal3222
80. Galatro TF, Holtman IR, Lerario AM, Vainchtein ID, Brouwer N, Sola PR, et al. Transcriptomic analysis of purified human cortical microglia reveals age-associated changes. *Nat Neurosci.* (2017) 20:1162–71. doi: 10.1038/nn.4597
81. Smith AM, Dragunow M. The human side of microglia. *Trends Neurosci.* (2014) 37:125–35. doi: 10.1016/j.tins.2013.12.001
82. Abud EM, Ramirez RN, Martinez ES, Healy LM, Nguyen CHH, Newman SA, et al. iPSC-derived human microglia-like cells to study neurological diseases. *Neuron.* (2017) 94:278–93.e9. doi: 10.1016/j.neuron.2017.03.042
83. Douvaras P, Sun B, Wang M, Kruglikov I, Lallos G, Zimmer M, et al. Directed differentiation of human pluripotent stem cells to microglia. *Stem Cell Rep.* (2017) 8:1516–24. doi: 10.1016/j.stemcr.2017.04.023
84. Haenseler W, Sansom SN, Buchrieser J, Newey SE, Moore CS, Nicholls FJ, et al. A highly efficient human pluripotent stem cell microglia model displays a neuronal-co-culture-specific expression profile and inflammatory response. *Stem Cell Rep.* (2017) 8:1727–42. doi: 10.1016/j.stemcr.2017.05.017
85. Muffat J, Li Y, Yuan B, Mitalipova M, Omer A, Corcoran S, et al. Efficient derivation of microglia-like cells from human pluripotent stem cells. *Nat Med.* (2016) 22:1358–67. doi: 10.1038/nm.4189
86. Pandya H, Shen MJ, Ichikawa DM, Sedlock AB, Choi Y, Johnson KR, et al. Differentiation of human and murine induced pluripotent stem cells to microglia-like cells. *Nat Neurosci.* (2017) 20:753–9. doi: 10.1038/nn.4534
87. Takata K, Kozaki T, Lee CZW, Thion MS, Otsuka M, Lim S, et al. Induced-pluripotent-stem-cell-derived primitive macrophages provide a platform for modeling tissue-resident macrophage differentiation and function. *Immunity.* (2017) 47:183–98.e6. doi: 10.1016/j.immuni.2017.06.017
88. Kierdorf K, Erny D, Goldmann T, Sander V, Schulz C, Perdiguero EG, et al. Microglia emerge from erythromyeloid precursors via Pu.1- and Irf8-dependent pathways. *Nat Neurosci.* (2013) 16:273–80. doi: 10.1038/nn.3318
89. Schulz C, Gomez Perdiguero E, Chorro L, Szabo-Rogers H, Cagnard N, Kierdorf K, et al. A lineage of myeloid cells independent of Myb and hematopoietic stem cells. *Science.* (2012) 336:86–90. doi: 10.1126/science.1219179
90. Pocock JM, Piers TM. Modelling microglial function with induced pluripotent stem cells: an update. *Nat Rev Neurosci.* (2018) 19:445–52. doi: 10.1038/s41583-018-0030-3
91. Hasselmann J, Blurton-Jones M. Human iPSC-derived microglia: a growing toolset to study the brain's innate immune cells. *Glia.* (2020) 68:721–39. doi: 10.1002/glia.23781
92. Gingras M, Gagnon V, Minotti S, Durham HD, Berthod F. Optimized protocols for isolation of primary motor neurons, astrocytes and microglia from embryonic mouse spinal cord. *J Neurosci Methods.* (2007) 163:111–8. doi: 10.1016/j.jneumeth.2007.02.024
93. Goshi N, Morgan RK, Lein PJ, Seker E. A primary neural cell culture model to study neuron, astrocyte, and microglia interactions in neuroinflammation. *J Neuroinflamm.* (2020) 17:155. doi: 10.1186/s12974-020-01819-z
94. Saura J, Tusell JM, Serratosa J. High-yield isolation of murine microglia by mild trypsinization. *Glia.* (2003) 44:183–89. doi: 10.1002/glia.10274
95. Lin L, Desai R, Wang X, Lo EH, Xing C. Characteristics of primary rat microglia isolated from mixed cultures using two different methods. *J Neuroinflamm.* (2017) 14:1–0. doi: 10.1186/s12974-017-0877-7
96. He Y, Yao X, Taylor N, Bai Y, Lovenberg T, Bhattacharya A. RNA sequencing analysis reveals quiescent microglia isolation methods from postnatal mouse brains and limitations of BV2 cells. *J Neuroinflamm.* (2018) 15:153. doi: 10.1186/s12974-018-1195-4
97. Lawson LJ, Perry VH, Dri P, Gordon S. Heterogeneity in the distribution and morphology of microglia in the normal adult mouse brain. *Neuroscience.* (1990) 39:151–70. doi: 10.1016/0306-4522(90)90229-W
98. Cuadros MA, Martin C, Coltey P, Almendros A, Navascués J. First appearance, distribution, and origin of macrophages in the early development of the avian central nervous system. *J Comp Neurol.* (1993) 330:113–29. doi: 10.1002/cne.903300110
99. Pan J, Ma N, Yu B, Zhang W, Wan J. Transcriptomic profiling of microglia and astrocytes throughout aging. *J Neuroinflamm.* (2020) 17:97. doi: 10.1186/s12974-020-01774-9
100. Allendorf DH, Puigdellívol M, Brown GC. Activated microglia desialylate their surface, stimulating complement receptor 3-mediated phagocytosis of neurons. *Glia.* (2020) 68:989–98. doi: 10.1002/glia.23757
101. Lecca D, Janda E, Mulas G, Diana A, Martino C, Angius F, et al. Boosting phagocytosis and anti-inflammatory phenotype in microglia mediates neuroprotection by PPARγ agonist MDG548 in Parkinson's disease models. *Br J Pharmacol.* (2018) 175:3298–314. doi: 10.1111/bph.14214
102. Keaney J, Gasser J, Gillet G, Scholz D, Kadiu I. Inhibition of Bruton's tyrosine kinase modulates microglial phagocytosis: therapeutic implications for Alzheimer's disease. *J Neuroimmune Pharmacol.* (2019) 14:448–61. doi: 10.1007/s11481-019-09839-0
103. Sellgren CM, Gracias J, Watmuff B, Biag JD, Thanos JM, Whittredge PB, et al. Increased synapse elimination by microglia in schizophrenia patient-derived models of synaptic pruning. *Nat Neurosci.* (2019) 22:374–85. doi: 10.1038/s41593-018-0334-7
104. Sellgren CM, Sheridan SD, Gracias J, Xuan D, Fu T, Perlis RH. Patient-specific models of microglia-mediated engulfment of synapses and neural progenitors. *Mol Psychiatry.* (2017) 22:170–7. doi: 10.1038/mp.2016.220
105. Zabel MK, Zhao L, Zhang Y, Gonzalez SR, Ma W, Wang X, et al. Microglial phagocytosis and activation underlying photoreceptor degeneration is regulated by CX3CL1-CX3CR1 signaling in a mouse model of retinitis pigmentosa. *Glia.* (2016) 64:1479–91. doi: 10.1002/glia.23016
106. Schulz D, Severin Y, Zanotelli VRT, Bodenmiller B. In-depth characterization of monocyte-derived macrophages using a mass cytometry-based phagocytosis assay. *Sci Rep.* (2019) 9:1925. doi: 10.1038/s41598-018-38127-9
107. Korn ED, Weisman RA. Phagocytosis of latex beads by *Acanthamoeba.* II. Electron microscopic study of the initial events. *J Cell Biol.* (1967) 34:219–27. doi: 10.1083/jcb.34.1.219
108. Desjardins M, Huber LA, Parton RG, Griffiths G. Biogenesis of phagolysosomes proceeds through a sequential series of interactions with the endocytic apparatus. *J Cell Biol.* (1994) 124:677–88. doi: 10.1083/jcb.124.5.677
109. Desjardins M, Griffiths G. Phagocytosis: latex leads the way. *Curr Opin Cell Biol.* (2003) 15:498–503. doi: 10.1016/S0955-0674(03)00083-8
110. Pul R, Chittappen KP, Stangel M. Quantification of microglial phagocytosis by a flow cytometer-based assay. *Methods Mol Biol.* (2013) 1041:121–7. doi: 10.1007/978-1-62703-520-0_14
111. Yin Y, Qiu S, Li X, Huang B, Xu Y, Peng Y. EZH2 suppression in glioblastoma shifts microglia toward M1 phenotype in tumor microenvironment. *J Neuroinflamm.* (2017) 14:1–1. doi: 10.1186/s12974-017-0993-4
112. Dunn PA, Eaton WR, Lopatin ED, McEntire JE, Papermaster BW. Lymphokine-stimulated macrophage phagocytosis of fluorescent

microspheres: a rapid new assay. *J Immunol Methods.* (1983) 64:71–83. doi: 10.1016/0022-1759(83)90385-X
113. Burleson GR, Fuller LB, Ménache MG, Graham JA. Poly(I):poly(C)-enhanced alveolar and peritoneal macrophage phagocytosis: quantification by a new method utilizing fluorescent beads. *Proc Soc Exp Biol Med Soc Exp Biol Med.* (1987) 184:468–76. doi: 10.3181/00379727-184-42501
114. Hughes MM, Field RH, Perry VH, Murray CL, Cunningham C. Microglia in the degenerating brain are capable of phagocytosis of beads and of apoptotic cells, but do not efficiently remove PrPSc, even upon LPS stimulation. *Glia.* (2010) 58:2017–30. doi: 10.1002/glia.21070
115. Kobayashi Y, Inagawa H, Kohchi C, Okazaki K, Zhang R, Kobara H, et al. Lipopolysaccharides derived from pantoea agglomerans can promote the phagocytic activity of amyloid in mouse microglial cells. *Anticancer Res.* (2017) 37:3917–20. doi: 10.21873/anticanres.11774
116. Ryu K-Y, Cho G-S, Piao HZ, Kim W-K. Role of TGF-β in survival of phagocytizing microglia: autocrine suppression of TNF-α production and oxidative stress. *Exp Neurobiol.* (2012) 21:151–7. doi: 10.5607/en.2012.21.4.151
117. Crespo-Castrillo A, Garcia-Segura L-M, Arevalo M-A. The synthetic steroid tibolone exerts sex-specific regulation of astrocyte phagocytosis under basal conditions and after an inflammatory challenge. *J Neuroinflamm.* (2020) 17:37. doi: 10.1186/s12974-020-1719-6
118. Huang Y, Mucke L. Alzheimer mechanisms and therapeutic strategies. *Cell.* (2012) 148:1204–22. doi: 10.1016/j.cell.2012.02.040
119. Tanzi RE. A brief history of Alzheimer's disease gene discovery. *J Alzheimers Dis.* (2013) 33(Suppl. 1):S5–13. doi: 10.3233/JAD-2012-129044
120. Deczkowska A, Keren-Shaul H, Weiner A, Colonna M, Schwartz M, Amit I. Disease-associated microglia: a universal immune sensor of neurodegeneration. *Cell.* (2018) 173:1073–81. doi: 10.1016/j.cell.2018.05.003
121. Nagano T, Kimura SH, Takemura M. Prostaglandin E2 reduces amyloid β-induced phagocytosis in cultured rat microglia. *Brain Res.* (2010) 1323:11–7. doi: 10.1016/j.brainres.2010.01.086
122. Hambardzumyan D, Gutmann DH, Kettenmann H. The role of microglia and macrophages in glioma maintenance and progression. *Nat Neurosci.* (2016) 19:20–7. doi: 10.1038/nn.4185
123. Witkowska A, Jahn R. Rapid SNARE-mediated fusion of liposomes and chromaffin granules with giant unilamellar vesicles. *Biophys J.* (2017) 113:1251–9. doi: 10.1016/j.bpj.2017.03.010
124. Rideau E, Dimova R, Schwille P, Wurm FR, Landfester K. Liposomes and polymersomes: a comparative review towards cell mimicking. *Chem Soc Rev.* (2018) 47:8572–610. doi: 10.1039/C8CS00162F
125. Witkowska A, Jablonski L, Jahn R. A convenient protocol for generating giant unilamellar vesicles containing SNARE proteins using electroformation. *Sci Rep.* (2018) 8:1–8. doi: 10.1038/s41598-018-27456-4
126. Roerdink F, Wassef NM, Richardson EC, Alving CR. Effects of negatively charged lipids on phagocytosis of liposomes opsonized by complement. *Biochim Biophys Acta.* (1983) 734:33–9. doi: 10.1016/0005-2736(83)90071-8
127. Wang Y, Cella M, Mallinson K, Ulrich JD, Young KL, Robinette ML, et al. TREM2 lipid sensing sustains the microglial response in an Alzheimer's disease model. *Cell.* (2015) 160:1061–71. doi: 10.1016/j.cell.2015.01.049
128. Urbaneja MA, Goñi FM, Alonso A. Structural changes induced by Triton X-100 on sonicated phosphatidylcholine liposomes. *Eur J Biochem.* (1988) 173:585–8. doi: 10.1111/j.1432-1033.1988.tb14039.x
129. Bangham AD. Physical structure and behavior of lipids and lipid enzymes. *Adv Lipid Res.* (1963) 1:65–104. doi: 10.1016/B978-1-4831-9937-5.50008-9
130. Hashioka S, Han Y-H, Fujii S, Kato T, Monji A, Utsumi H, et al. Phosphatidylserine and phosphatidylcholine-containing liposomes inhibit amyloid beta and interferon-gamma-induced microglial activation. *Free Radic Biol Med.* (2007) 42:945–54. doi: 10.1016/j.freeradbiomed.2006.12.003
131. Wu Z, Nakanishi H. Phosphatidylserine-containing liposomes: potential pharmacological interventions against inflammatory and immune diseases through the production of prostaglandin E(2) after uptake by myeloid derived phagocytes. *Arch Immunol Ther Exp.* (2011) 59:195–201. doi: 10.1007/s00005-011-0123-4
132. Takayama F, Wu Z, Ma HM, Okada R, Hayashi Y, Nakanishi H. Possible involvement of aiPLA2 in the phosphatidylserine-containing liposomes induced production of PGE2 and PGD2 in microglia. *J Neuroimmunol.* (2013) 262:121–4. doi: 10.1016/j.jneuroim.2013.06.011
133. Sierra A, Abiega O, Shahraz A, Neumann H. Janus-faced microglia: beneficial and detrimental consequences of microglial phagocytosis. *Front Cell Neurosci.* (2013) 7:6. doi: 10.3389/fncel.2013.00006
134. Mattson MP, Keller JN, Begley JG. Evidence for synaptic apoptosis. *Exp Neurol.* (1998) 153:35–48. doi: 10.1006/exnr.1998.6863
135. Nonaka S, Nakanishi H. Microglial clearance of focal apoptotic synapses. *Neurosci Lett.* (2019) 707:134317. doi: 10.1016/j.neulet.2019.134317
136. Witting A, Müller P, Herrmann A, Kettenmann H, Nolte C. Phagocytic clearance of apoptotic neurons by microglia/brain macrophages *in vitro*: involvement of lectin-, integrin-, and phosphatidylserine-mediated recognition. *J Neurochem.* (2000) 75:1060–70. doi: 10.1046/j.1471-4159.2000.0751060.x
137. Zhao X, Zhang L, Ting S-M, Aronowski J. Phagocytosis assay of microglia for dead neurons in primary rat brain cell cultures. *Bio-protocol.* (2016) 6:e1795. doi: 10.21769/BioProtoc.1795
138. Zhao X, Wang H, Sun G, Zhang J, Edwards NJ, Aronowski J. Neuronal interleukin-4 as a modulator of microglial pathways and ischemic brain damage. *J Neurosci.* (2015) 35:11281–91. doi: 10.1523/JNEUROSCI.1685-15.2015
139. McLaughlin CN, Perry-Richardson JJ, Coutinho-Budd JC, Broihier HT. Dying neurons utilize innate immune signaling to prime glia for phagocytosis during development. *Dev Cell.* (2019) 48:506–22.e6. doi: 10.1016/j.devcel.2018.12.019
140. Takahashi K, Rochford CDPP, Neumann H. Clearance of apoptotic neurons without inflammation by microglial triggering receptor expressed on myeloid cells-2. *J Exp Med.* (2005) 201:647–57. doi: 10.1084/jem.20041611
141. Neumann H, Takahashi K. Essential role of the microglial triggering receptor expressed on myeloid cells-2 (TREM2) for central nervous tissue immune homeostasis. *J Neuroimmunol.* (2007) 184:92–9. doi: 10.1016/j.jneuroim.2006.11.032
142. Beccari S, Diaz-Aparicio I, Sierra A. Quantifying microglial phagocytosis of apoptotic cells in the brain in health and disease. *Curr Protoc Immunol.* (2018) 122:e49. doi: 10.1002/cpim.49
143. Diaz-Aparicio I, Paris I, Sierra-Torre V, Plaza-Zabala A, Rodríguez-Iglesias N, Márquez-Ropero M, et al. Microglia actively remodel adult hippocampal neurogenesis through the phagocytosis secretome. *J Neurosci.* (2020) 40:1453–82. doi: 10.1523/JNEUROSCI.0993-19.2019
144. Ahmad F, Liu P. Synaptosome as a tool in Alzheimer's disease research. *Brain Res.* (2020) 1746:147009. doi: 10.1016/j.brainres.2020.147009
145. Evans GJO. The synaptosome as a model system for studying synaptic physiology. *Cold Spring Harb Protoc.* (2015) 2015:421–4. doi: 10.1101/pdb.top074450
146. Nicholls DG, Sihra TS. Synaptosomes possess an exocytotic pool of glutamate. *Nature.* (1986) 321:772–3. doi: 10.1038/321772a0
147. Byun YG, Chung WS. A novel *in vitro* live-imaging assay of astrocyte-mediated phagocytosis using pH indicator-conjugated synaptosomes. *J Vis Exp.* (2018) 2018:56647. doi: 10.3791/56647
148. Madore C, Leyrolle Q, Morel L, Rossitto M, Greenhalgh AD, Delpech JC, et al. Essential omega-3 fatty acids tune microglial phagocytosis of synaptic elements in the mouse developing brain. *Nat Commun.* (2020) 11:6133. doi: 10.1038/s41467-020-19861-z
149. Evans AK, Ardestani PM, Yi B, Park HH, Lam RK, Shamloo M. Beta-adrenergic receptor antagonism is proinflammatory and exacerbates neuroinflammation in a mouse model of Alzheimer's Disease. *Neurobiol Dis.* (2020) 146:105089. doi: 10.1016/j.nbd.2020.105089
150. Chung WS, Clarke LE, Wang GX, Stafford BK, Sher A, Chakraborty C, et al. Astrocytes mediate synapse elimination through MEGF10 and MERTK pathways. *Nature.* (2013) 504:394–400. doi: 10.1038/nature12776
151. Ivannikov M V, Sugimori M, Llinás RR. Synaptic vesicle exocytosis in hippocampal synaptosomes correlates directly with total mitochondrial volume. *J Mol Neurosci.* (2013) 49:223–30. doi: 10.1007/s12031-012-9848-8
152. Kim H-J, Cho M-H, Shim WH, Kim JK, Jeon E-Y, Kim D-H, et al. Deficient autophagy in microglia impairs synaptic pruning and causes social behavioral defects. *Mol Psychiatry.* (2017) 22:1576–84. doi: 10.1038/mp.2016.103
153. Jahn A, Vreeland WN, DeVoe DL, Locascio LE, Gaitan M. Microfluidic directed formation of liposomes of controlled size. *Langmuir.* (2007) 23:6289–93. doi: 10.1021/la070051a
154. Lim JP, Gleeson PA. Macropinocytosis: an endocytic pathway for internalising large gulps. *Immunol Cell Biol.* (2011) 89:836–43. doi: 10.1038/icb.2011.20

155. Lim JP, Gosavi P, Mintern JD, Ross EM, Gleeson PA. Sorting nexin 5 selectively regulates dorsal-ruffle-mediated macropinocytosis in primary macrophages. *J Cell Sci.* (2015) 128:4407–19. doi: 10.1242/jcs.174359
156. Gylys KH, Fein JA, Wiley DJ, Cole GM. Rapid annexin-V labeling in synaptosomes. *Neurochem Int.* (2004) 44:125–31. doi: 10.1016/S0197-0186(03)00146-3
157. Morsch M, Radford R, Lee A, Don EK, Badrock AP, Hall TE, et al. *In vivo* characterization of microglial engulfment of dying neurons in the zebrafish spinal cord. *Front Cell Neurosci.* (2015) 9:321. doi: 10.3389/fncel.2015.00321
158. Damisah EC, Hill RA, Rai A, Chen F, Rothlin C V, Ghosh S, et al. Astrocytes and microglia play orchestrated roles and respect phagocytic territories during neuronal corpse removal *in vivo*. *Sci Adv.* (2020) 6:eaba3239. doi: 10.1126/sciadv.aba3239
159. Tejera D, Heneka MT. *In vivo* phagocytosis analysis of amyloid beta. *Methods Mol Biol.* (2019) 2034:287–92. doi: 10.1007/978-1-4939-9658-2_21
160. Brioschi S, Zhou Y, Colonna M. Brain parenchymal and extraparenchymal macrophages in development, homeostasis, and disease. *J Immunol.* (2020) 204:294–305. doi: 10.4049/jimmunol.1900821
161. Roqué PJ, Costa LG. Co-culture of neurons and microglia. *Curr Protoc Toxicol.* (2017) 74:11.24.1–17. doi: 10.1002/cptx.32
162. Harry GJ, Kraft AD. Neuroinflammation and microglia: considerations and approaches for neurotoxicity assessment. *Expert Opin Drug Metab Toxicol.* (2008) 4:1265–277. doi: 10.1517/17425255.4.10.1265
163. Neher JJ, Neniskyte U, Zhao J-W, Bal-Price A, Tolkovsky AM, Brown GC. Inhibition of microglial phagocytosis is sufficient to prevent inflammatory neuronal death. *J Immunol.* (2011) 186:4973–83. doi: 10.4049/jimmunol.1003600
164. Fricker M, Oliva-Martín MJ, Brown GC. Primary phagocytosis of viable neurons by microglia activated with LPS or Aβ is dependent on calreticulin/LRP phagocytic signalling. *J Neuroinflamm.* (2012) 9:196. doi: 10.1186/1742-2094-9-196
165. Manelli AM, Bulfinch LC, Sullivan PM, LaDu MJ. Abeta42 neurotoxicity in primary co-cultures: effect of apoE isoform and Abeta conformation. *Neurobiol Aging.* (2007) 28:1139–147. doi: 10.1016/j.neurobiolaging.2006.05.024
166. Lui H, Zhang J, Makinson SR, Cahill MK, Kelley KW, Huang H-Y, et al. Progranulin deficiency promotes circuit-specific synaptic pruning by microglia via complement activation. *Cell.* (2016) 165:921–35. doi: 10.1016/j.cell.2016.04.001
167. Kao AW, Eisenhut RJ, Martens LH, Nakamura A, Huang A, Bagley JA, et al. A neurodegenerative disease mutation that accelerates the clearance of apoptotic cells. *Proc Natl Acad Sci USA.* (2011) 108:4441–6. doi: 10.1073/pnas.1100650108
168. Martens LH, Zhang J, Barmada SJ, Zhou P, Kamiya S, Sun B, et al. Progranulin deficiency promotes neuroinflammation and neuron loss following toxin-induced injury. *J Clin Invest.* (2012) 122:3955–9. doi: 10.1172/JCI63113
169. Sarn N, Jaini R, Thacker S, Lee H, Dutta R, Eng C. Cytoplasmic-predominant Pten increases microglial activation and synaptic pruning in a murine model with autism-like phenotype. *Mol Psychiatry.* (2020). doi: 10.1038/s41380-020-0681-0. [Epub ahead of print].
170. Ito D, Imai Y, Ohsawa K, Nakajima K, Fukuuchi Y, Kohsaka S. Microglia-specific localisation of a novel calcium binding protein, Iba1. *Mol Brain Res.* (1998) 57:1–9. doi: 10.1016/S0169-328X(98)00040-0
171. Lee JE, Liang KJ, Fariss RN, Wong WT. *Ex vivo* dynamic imaging of retinal microglia using time-lapse confocal microscopy. *Invest Ophthalmol Vis Sci.* (2008) 49:4169–76. doi: 10.1167/iovs.08-2076
172. Dailey ME, Eyo U, Fuller L, Hass J, Kurpius D. Imaging microglia in brain slices and slice cultures. *Cold Spring Harb Protoc.* (2013) 2013:1142–8. doi: 10.1101/pdb.prot079483
173. Nimmerjahn A, Kirchhoff F, Helmchen F. Neuroscience: resting microglial cells are highly dynamic surveillants of brain parenchyma *in vivo*. *Science.* (2005) 308:1314–8. doi: 10.1126/science.1110647
174. Stence N, Waite M, Dailey ME. Dynamics of microglial activation: a confocal time-lapse analysis in hippocampal slices. *Glia.* (2001) 33:256–66. doi: 10.1002/1098-1136(200103)33:3<256::AID-GLIA1024>3.0.CO;2-J
175. Bisht K, Sharma KP, Lecours C, Gabriela Sánchez M, El Hajj H, Milior G, et al. Dark microglia: a new phenotype predominantly associated with pathological states. *Glia.* (2016) 64:826–39. doi: 10.1002/glia.22966
176. Sipe GO, Lowery RL, Tremblay M, Kelly EA, Lamantia CE, Majewska AK. Microglial P2Y12 is necessary for synaptic plasticity in mouse visual cortex. *Nat Commun.* (2016) 7:10905. doi: 10.1038/ncomms10905
177. Villani A, Benjaminsen J, Moritz C, Henke K, Hartmann J, Norlin N, et al. Clearance by microglia depends on packaging of phagosomes into a unique cellular compartment. *Dev Cell.* (2019) 49:77–88.e7. doi: 10.1016/j.devcel.2019.02.014
178. Berg S, Kutra D, Kroeger T, Straehle CN, Kausler BX, Haubold C, et al. ilastik: interactive machine learning for (bio)image analysis. *Nat Methods.* (2019) 16:1226–32. doi: 10.1038/s41592-019-0582-9
179. McQuin C, Goodman A, Chernyshev V, Kamentsky L, Cimini BA, Karhohs KW, et al. CellProfiler 3.0: next-generation image processing for biology. *PLoS Biol.* (2018) 16:1–7. doi: 10.1371/journal.pbio.2005970
180. Lauro C, Catalano M, Trettel F, Limatola C. Fractalkine in the nervous system: neuroprotective or neurotoxic molecule? *Ann N Y Acad Sci.* (2015) 1351:141–8. doi: 10.1111/nyas.12805
181. Pawelec P, Ziemka-Nalecz M, Sypecka J, Zalewska T. The impact of the CX3CL1/CX3CR1 axis in neurological disorders. *Cells.* (2020) 9:2277. doi: 10.3390/cells9102277
182. Schafer DP, Lehrman EK, Heller CT, Stevens B. An engulfment assay: a protocol to assess interactions between CNS phagocytes and neurons. *J Vis Exp.* (2014) 88:51482. doi: 10.3791/51482
183. Cignarella F, Filipello F, Bollman B, Cantoni C, Locca A, Mikesell R, et al. TREM2 activation on microglia promotes myelin debris clearance and remyelination in a model of multiple sclerosis. *Acta Neuropathol.* (2020) 140:513–34. doi: 10.1007/s00401-020-02193-z
184. Rangaraju S, Raza SA, Li NX, Betarbet R, Dammer EB, Duong D, et al. Differential phagocytic properties of CD45(low) microglia and CD45(high) brain mononuclear phagocytes-activation and age-related effects. *Front Immunol.* (2018) 9:405. doi: 10.3389/fimmu.2018.00405
185. Bandura DR, Baranov VI, Ornatsky OI, Antonov A, Kinach R, Lou X, et al. Mass cytometry: technique for real time single cell multitarget immunoassay based on inductively coupled plasma time-of-flight mass spectrometry. *Anal Chem.* (2009) 81:6813–22. doi: 10.1021/ac901049w
186. Ornatsky O, Bandura D, Baranov V, Nitz M, Winnik MA, Tanner S. Highly multiparametric analysis by mass cytometry. *J Immunol Methods.* (2010) 361:1–20. doi: 10.1016/j.jim.2010.07.002
187. Bendall SC, Simonds EF, Qiu P, Amir ED, Krutzik PO, Finck R, et al. Single-cell mass cytometry of differential immune and drug responses across a human hematopoietic continuum. *Science.* (2011) 332:687–96. doi: 10.1126/science.1198704
188. Guilliams M, Dutertre C-A, Scott CL, McGovern N, Sichien D, Chakarov S, et al. Unsupervised high-dimensional analysis aligns dendritic cells across tissues and species. *Immunity.* (2016) 45:669–84. doi: 10.1016/j.immuni.2016.08.015
189. Becher B, Schlitzer A, Chen J, Mair F, Sumatoh HR, Teng KWW, et al. High-dimensional analysis of the murine myeloid cell system. *Nat Immunol.* (2014) 15:1181–9. doi: 10.1038/ni.3006
190. Ueda HR, Ertürk A, Chung K, Gradinaru V, Chédotal A, Tomancak P, et al. Publisher correction: tissue clearing and its applications in neuroscience. *Nat Rev Neurosci.* (2020) 21:298. doi: 10.1038/s41583-020-0291-5
191. Helmchen F, Denk W. Deep tissue two-photon microscopy. *Nat Methods.* (2005) 2:932–40. doi: 10.1038/nmeth818
192. Attardo A, Fitzgerald JE, Schnitzer MJ. Impermanence of dendritic spines in live adult CA1 hippocampus. *Nature.* (2015) 523:592–6. doi: 10.1038/nature14467

Conflict of Interest: The authors declare that the research was conducted in the absence of any commercial or financial relationships that could be construed as a potential conflict of interest.

frontiers in Immunology

REVIEW
published: 08 March 2021
doi: 10.3389/fimmu.2021.617564

Assessing Microglial Dynamics by Live Imaging

*Megumi Andoh and Ryuta Koyama**

Laboratory of Chemical Pharmacology, Graduate School of Pharmaceutical Sciences, The University of Tokyo, Tokyo, Japan

Microglia are highly dynamic in the brain in terms of their ability to migrate, proliferate, and phagocytose over the course of an individual's life. Real-time imaging is a useful tool to examine how microglial behavior is regulated and how it affects the surrounding environment. However, microglia are sensitive to environmental stimuli, so they possibly change their state during live imaging *in vivo*, mainly due to surgical damage, and *in vitro* due to various effects associated with culture conditions. Therefore, it is difficult to perform live imaging without compromising the properties of the microglia under physiological conditions. To overcome this barrier, various experimental conditions have been developed; recently, it has become possible to perform live imaging of so-called surveillant microglia *in vivo*, *ex vivo*, and *in vitro*, although there are various limitations. Now, we can choose *in vivo*, *ex vivo*, or *in vitro* live imaging systems according to the research objective. In this review, we discuss the advantages and disadvantages of each experimental system and outline the physiological significance and molecular mechanisms of microglial behavior that have been elucidated by live imaging.

Keywords: microglia, synapse, slice culture, acute slice, multiphoton/two-photon imaging, quadripartite synapse, microglial process, microglial motility

OPEN ACCESS

Edited by:
Amanda Sierra, Achucarro Basque Center for Neuroscience, Spain

Reviewed by:
Ukpong Bassey Eyo, University of Virginia, United States
Marie-Ève Tremblay, University of Victoria, Canada

***Correspondence:**
Ryuta Koyama
rkoyama@mol.f.u-tokyo.ac.jp

Specialty section:
This article was submitted to Multiple Sclerosis and Neuroimmunology, a section of the journal Frontiers in Immunology

Received: *15 October 2020*
Accepted: *16 February 2021*
Published: *08 March 2021*

Citation:
Andoh M and Koyama R (2021) Assessing Microglial Dynamics by Live Imaging. Front. Immunol. 12:617564. doi: 10.3389/fimmu.2021.617564

INTRODUCTION

Under physiological conditions, microglia have multiple finely branched protrusions, i.e., ramified processes, that constantly extend, and retract to monitor the extracellular environment (1–3). This dynamic process extension and retraction is characteristic of microglia, as neurons and astrocytes do not show significant morphological changes of their primary processes. These properties of microglia cannot be overlooked because they modulate microglial functions: production and directed release of inflammatory mediators, phagocytosis of pathogens and aggregate proteins, and cell–cell contacts (4). However, without a live imaging system, it is difficult to verify these phenomena; for example, if microglial density increases in a region as a result of observing fixed specimens, it is unclear whether this is due to microglial proliferation or migration. Additionally, it is difficult to discriminate whether increased cytokine expression or increased phagocytosis is the cause or effect of changes in the surrounding environment. Thus, understanding the molecular mechanisms and physiological significance of microglial motility requires direct live imaging of microglia while performing genetic and pharmacological manipulations.

Real-time imaging of microglia is essential; however, it is extremely difficult to observe microglia in their endogenous state in the brain. This is because microglia are sensitive to changes in the extracellular environment and can easily change their state during preparatory steps in experimental procedures, such as craniotomy (removal of the skull and replacement with a glass coverslip to allow transcranial viewing) for *in vivo* imaging, brain slice preparation for *ex vivo* imaging, and brain isolation for preparing cultures for *in vitro* imaging. More specifically, this

may occur by surgical damage when performing live imaging *in vivo* and by various influences associated with culture conditions when performing live imaging *in vitro*, such as the presence or absence of other types of cells, the contents, serum, pH, and osmolality of the medium (5–8). Thus, if the microglia have already responded to the process of preparation in experiments, there is a possibility that further response of microglia by stimuli, including physical or pharmacological stimulation, may be underestimated, masked, or altered.

The spatiotemporal resolution of real-time imaging of microglia has improved considerably in recent years due to a variety of conditional investigations of observational techniques to overcome problems mentioned above. In this review, we highlight studies that performed live imaging of microglia *in vivo*, *ex vivo* (acutely prepared brain slices and organotypic brain slice cultures), and *in vitro* (dispersed culture of primary microglia). We further review the results of these studies, which are important for improving our understanding of microglial function and identity. In particular, it has been reported that the basic morphology and motility of microglial processes seen *in vivo* can be to some extent reproduced in acute slice and slice cultures (**Figure 1**). Therefore, in the following sections, observed phenomena (i.e., migration and phagocytosis), animal types (mouse, rat, and zebrafish), sample preparation methods (i.e., craniotomy, preparation of brain slices, and isolation of microglia from the brain), imaging conditions, and quantifiable parameters are compared to help microglial researchers interpret findings from live imaging studies and select appropriate methods for observing microglial dynamics.

IN VIVO LIVE IMAGING

Essential Methods for *in vivo* Live Imaging

Preparation of Imaging Window

Mice and zebrafish have been often used for *in vivo* live imaging of microglia (**Table 1**). As the whole body including the brain of zebrafish is transparent, high-resolution imaging can be expected in any region if the sample is properly embedded and fixed in a gel. On the other hand, in case of mice, it is necessary to surgically create an imaging window because the skin and skull are not transparent enough for live imaging of the brain.

Since 2005, there has been increasing research on *in vivo* live imaging of microglia, and now thinned skull and open skull are recognized as the two major methods for preparing imaging window. The pros and cons of each method are well-summarized in the review article by Dorand et al. (48). Removing skull could stimulate microglia and change their state, and it requires several weeks for microglia to return to the physiological state (5, 16). The open skull method, on the other hand, has the advantage of a wider imaging depth and higher resolution than the thinned skull method (46, 49). Abnormal changes in microglial state induced by removing skull are critical not only because it affects the morphology and motility of microglia themselves, but also because cytokines released by microglia could affect the properties of surrounding cells. Although Isshiki and Okabe reported that they could not observe synaptic structures clearly using through the thinned skull (31), several studies have reported successful observation of synaptic structures such as dendritic spines *in vivo* through a thin-skull window (24, 44, 46, 47).

It is important to consider whether to use an open skull method or a thinned skull method, depending on the brain region or phenomenon being targeted. It should also be noted that both methods require technical proficiency of the experimenter to increase the success rate, and that there are difficulties in *in vivo* live imaging to achieve a high level of imaging between specimens.

Anesthesia

Proper anesthesia of animals is essential for *in vivo* live imaging. Live imaging with awake animals using head fixation is possible, and although many papers have been published on awake imaging, there is no doubt that anesthesia is useful for reducing motion artifacts, which may affect live imaging of microstructures such as synapses and microglial filopodia, and achieving more stable imaging. However, there is still the problem that the activity of each brain cell (including neuronal firing and microglial motility) is affected by anesthesia. For example, anesthesia suppresses neuronal firing activity (50) and alters the turnover rate of dendritic spines (40, 51). In recent years, it has been reported that anesthesia affects not only neuronal activity but also microglial motility, and the way in which this is affected depends on the type of anesthesia. For example, isoflurane, one of the most commonly used anesthetics, reduces the motility of microglial processes by inhibiting the potassium channel THIK-1 in acutely sectioned brain slices, whereas urethane has no such effect (52). On the other hand, live-imaging studies have also suggested that isoflurane enhanced microglial surveillance by increasing the length and velocity of surveilling processes as well as the frequency of extension and retraction of processes during both physiological and pathological conditions (33, 41, 42). It has also recently been shown that ketamine/xylazine, which is as frequently used as isoflurane, reduces the morphological complexity and process motility of microglia under physiological conditions (29). Morphological changes in microglia are likely to result in functional changes, and it is almost certain that anesthesia will influence experimental results and their interpretation. It is hoped that further research will reveal which anesthetics are able to preserve microglial properties in the awake state.

Phenomena Verified by *in vivo* Live Imaging

Colonization of Microglia

During the embryonic period, microglia migrate from the yolk sac to the brain parenchyma. In 2016, Xu et al. observed the migration of microglia in zebrafish larvae using live imaging (53). The advantage of using zebrafish larvae is their small size and high transparency. This makes it possible to obtain high-resolution images of cell motility *in vivo*. Another attraction is the wide range of transgenic lines available, allowing live imaging of cells without viral infection or injection of fluorescent reagents. In addition, molecules involved in the detection and phagocytosis of dead cells by microglia are conserved in vertebrates, and if the observed phenomenon is carefully interpreted, it may

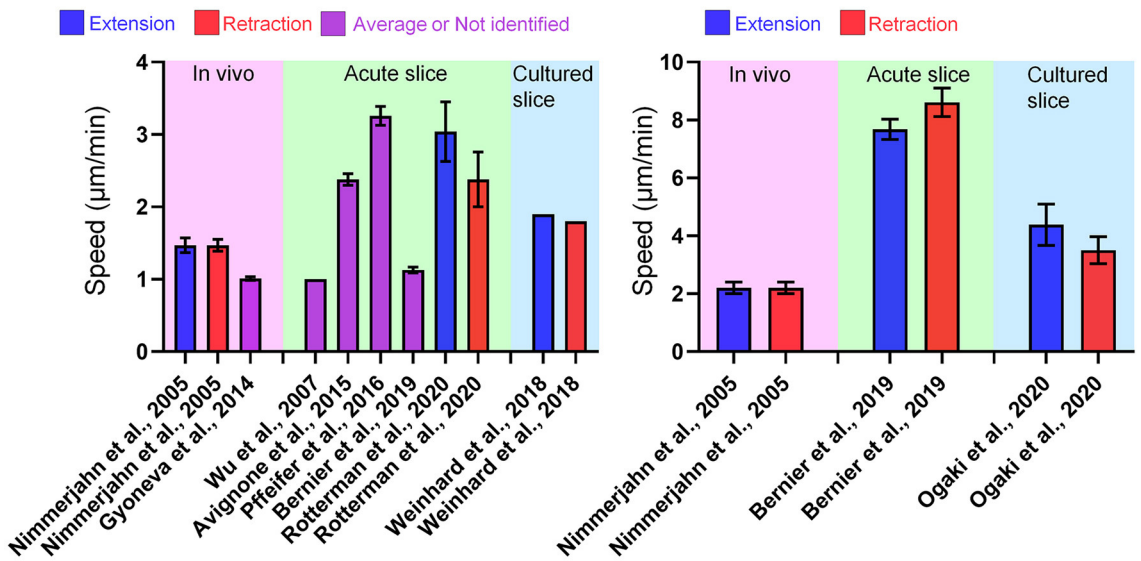

FIGURE 1 | Microglial process motility in each live-imaging condition. **(A)** Speed of large process motility of microglia reported in papers referred in this review. In some cases, the speed of process motility was not specified as "extraction" or "retraction." **(B)** Speed of filopodia motility of microglia reported in papers referred in this review. In Bernier et al. (9), the authors defined tiny protrusions near the tip of large process as filopodia, and provided the quantitative data of filopodia and large process. In Nimmerjahn et al. (1) and Ogaki et al. (10), short branches that emanated from the primary process of microglia were regarded as filopodia.

be possible to extrapolate and validate findings acquired from studies using zebrafish to mammals. Xu et al. found that microglial progenitor cells infiltrate the optic tectum through a circulation-independent pathway. In addition, based on the fact that neuronal death occurs in the optic tectum during microglial migration, the authors investigated the possibility that apoptotic cells are involved in microglial migration. Suppression of neuronal cell death by overexpression of the anti-apoptotic protein bcl-2 significantly suppressed microglial infiltration into the optic tectum. Furthermore, ATP and lysophosphatidylcholine (LPC) released from apoptotic cells were identified as molecules that promote infiltration.

Casano et al. published a paper around the same time as Xu et al. in which they also examined the relationship between developmental microglial colonization and apoptotic cells (15). Suppression of neuronal cell death by administration of the caspase inhibitor Z-VAD-fmk or promotion of neuronal cell death by UV irradiation inhibited or promoted microglial infiltration to the brain parenchyma, respectively. Next, they showed that inhibition of nucleic acid release by pannexin-1a knockdown or inhibition of purinergic receptors by suramin suppressed microglial infiltration. A study using live imaging of acute slices of mouse embryonic cerebral cortex (54) reported that the migration rate of microglia is higher in the earlier embryonic period, which may be due to differential concentrations of apoptotic cell-derived molecules.

Contrary to the findings by Xu et al. (53), there are reports suggesting that the infiltration of microglia into the parenchyma is circulation-dependent in the fetal mouse brain (55). Furthermore, in live imaging of acute hippocampal slices prepared from 1-week-old mice, Eyo et al. showed that knockout of the apoptotic protein BAX did not affect microglial morphology or motility, and concluded that apoptotic cells do not regulate microglial dynamics (56). Thus, it is quite possible that the same phenomenon has different underlying mechanisms in different species.

Askew et al. examined the mechanism of microglial population maintenance by live imaging over 22 days (12). Interestingly, immediately after division, newborn microglia exhibited a 2-fold higher mortality rate than resident microglia. Furthermore, the authors found that microglial division is spatiotemporally coupled with microglial mortality. The molecular mechanism of this coupling has not been clarified, but CSF1R, which is essential for microglial survival, and IL-1R, which promotes microglial repopulation, have been considered as candidates.

Microglial proliferation is known to be enhanced in the brain following neurodegeneration and injury. Füger et al. developed an impressive method to examine the rate of microglial proliferation and turnover (22). The authors successfully fluorescently labeled single microglia within the field of view by using CD11b-CreERT2;R26-tdTomato mice with modified tamoxifen administration. They followed the same microglial fate with biweekly imaging for 6 months and with monthly imaging afterwards (starting at 4 months of age). It was reported that both the proliferation and disappearance rates of microglia were 13%. The median survival time was 15 months, which means that approximately half of all microglia in mice are present for

TABLE 1 | Experimental conditions of live imaging of microglia *in vivo*.

Animal	Age	Skull	Anesthesia	Region (depth from the surface)	Cellular visualization	Microscopy	Objective lens	Resolution (x, y) z stack	Interval time Total time	References
CX3CR1-GFP$^{+/-}$ mice	2 mo	Thinned	Isoflurane	Cortex	GFP (microglia)	Two-photon	25x (NA = 1.05)	– 1 μm step	1.5 min 13.5 min	Abiega et al. (11)
CX3CR1-GFP$^{+/-}$ mice	8–12 mo	Open	Isoflurane	Cortex	GFP (microglia)	Two-photon	20x (NA = 1.0)	317 × 317 μm 50–80 μm with 1 μm step	– 22 days	Askew et al. (12)
CX3CR1-GFP$^{+/-}$ mice	8–10 wo	Thinned	–	Cortex (100–150 μm)	GFP (microglia) mCherry (axonal bouton)	Two-photon	25x (NA = 1.10)	1,024 × 1,024 pixel (0.1269 μm/pixel) 1 μm step	1 min 3 h	Badimon et al. (13)
C57BL/6 mice	2–6 mo	Thinned	Isoflurane	Somatosensory cortex (∼330 μm)	Twitch-2B (microglia)	Confocal	20x (NA = 1.0), 40x (NA = 0.8)	0.15–0.31 μm/pixel	1 frame/s, 10 min or 0.13 frame/s, 30–120 s	Brawek et al. (14)
pU.1::Gal4-UAS::TagRFP, mpeg1::Gal4-UAS::Kaede, nbt::DlexPR::NTR-mCherry, and slc7a7::Kaede (zebrafish)	2–3 dpf	–	0.01% tricaine		RFP, Kaede (microglia) mCherry (neuron)	Confocal	20x (NA = 0.4), 10x (NA = 0.25)	– 30–40 planes with 1.5–2 μm step	–	Casano et al. (15)
C57BL/6 mice	P4-19	Open	Isoflurane	Cortex (300–450 μm)	EGFP (neuron)	Two-photon	40×	78 × 79 μm 20 sections with 1 μm step	– ∼2 h	Cruz-Martin et al. (16)
CX3CR1-GFP$^{+/-}$;Thy1-YFP$^{+/-}$ mice	–	Thinned	Ketamine and xylazine	Cortex (∼300 μm)	GFP (microglia) YFP (neuron) SR101 (astrocyte) Hoechst (nuclei)	Two-photon	20x (NA = 1.0)	1,024 × 1,024 pixel (0.204 μm/pixel) 34 planes with 3 μm step	2–3 h –	Damisah et al. (17)
CX3CR1-GFP$^{+/-}$ mice	–	Thinned	Ketamine and xylazine	Cortex (∼200 μm)	GFP (microglia)	Two-photon	40x (NA = 0.8), 60x (NA = 0.9 or 1.0)	– 0.75–2 μm step	–	Davalos et al. (2)
CX3CR1-GFP$^{+/-}$;Thy1-YFP$^{+/-}$ mice	–	Thinned	–	Cortex	GFP (microglia) YFP (neuron) Alexa594 (fibrinogen)	Multi-photon	10x (NA = 0.4), 40x (NA = 0.8)	– 1.0–1.5 or 3–4 μm step	120–240 s 30–90 min	Davalos et al. (18)
CX3CR1-GFP$^{+/-}$ mice	–	Open	Mixture of ketamine, xylazine and acepromazine	Spinal cord	GFP (microglia) rhodamine dextran (vessel)	Two-photon	–	–	–	Davalos et al. (19)
CX3CR1-GFP$^{+/-}$ mice	P40-130	Open	Pentobarbital sodium and methohexital sodium	Spinal cord	GFP (microglia)	Two-photon	40x (NA = 0.75), 20x (NA = 1.0)	256 × 256 or 1,024 × 1,024 pixel (0.24–0.72 μm/pixel) 16–24 planes with 1.5–2.0 μm step	1–2 min –	Dibaj et al. (20)
WT mice CX3CR1-GFP$^{+/-}$ mice	2–4 mo	Thinned	Isoflurane	Cortex	GFP, OGB-1, Fluo-4, Isolectin B4 conjugated to Alexa Fluor 594 (microglia)	Two-photon	40x (NA = 0.8), 60x (NA = 1.0)	– 10 μm with 1 μm step	–	Eichhoff et al. (21)

(Continued)

TABLE 1 | Continued

Animal	Age	Skull	Anesthesia	Region (depth from the surface)	Cellular visualization	Microscopy	Objective lens	Resolution (x, y) z stack	Interval time Total time	References
CD11b-CreERT2;R26-tdTomato;APPPS1 mice	4, 10 mo	Open	Isoflurane	Cortex (200–250 μm)	tdTomato (microglia)	Two-photon	25x (NA = 0.95)	0.27 μm/pixel or 1.49 μm/pixel –	Biweekly or monthly 1.5 years	Füger et al. (22)
TH-tdTomato$^{+/-}$; CX3CR1-GFP$^{+/-}$ mice	P56	Thinned	Isoflurane	Olfactory bulb	GFP (microglia) TH neuron (mCherry)	Two-photon	20x (NA = 1.0)	0.09 μm/pixel or 0.99 μm/pixel –	30 s 10 min	Grier et al. (23)
Thy1-YFP$^{+/-}$ mice CX3CR1-EGFP$^{+/-}$ mice	–	Thinned	Ketamine and xylazine	Cortex (∼100 μm for neuron and ∼200 μm for microglia)	YFP (neuron) EGFP (microglia)	Two-photon	60x (NA = 1.1)	512 × 512 pixel (66.7 × 66.7 μm) 0.75 μm step	– ∼2 h	Grutzendler et al. (24)
Thy1-YFP$^{+/-}$ mice (H-line)	6–7 mo	Open	Ketamine and xylazine	Hippocampus (50 μm below the pyramidal cell layer)	YFP (neuron)	Two-photon	16x (NA = 0.8)	100 × 100 μm (0.09 μm/pixel) 60 μm with 1 μm step	4 d interval –	Gu et al. (25)
CX3CR1-GFP$^{+/-}$ mice	–	Thinned	–	Cortex	GFP (microglia)	Two-photon	-	– 15 planes with 2 μm step	4 min 40 min	Haynes et al. (26)
mpeg1:GFP (zebrafish)	4 dpf	–	0.01% MS-222	Brain (100–150 μm) trunk(80–120 μm)	GFP (microglia) PI (dead cell)	Confocal	-	– 3.6–6 μm step	6 min –	Herzog et al. (27)
CX3CR1-GFP$^{+/-}$;Cnp-mEGFP$^{+/-}$;Plp-DsRed$^{+/-}$ mice	P30-1,100	Thinned or open	–	Somatosensory cortex (∼75 μm)	GFP (microglia) mEGFP (myelin) DsRed (oligodendrocyte)	Confocal or two-photon	20x (NA = 1.0)	–	–	Hill et al. (28)
CX3CR1-GFP$^{+/-}$ mice	6–10 wo	Thinned	Awake or mixture of ketamine and xylazine or pentobarbital	Somatosensory cortex (50–150 μm)	GFP (microglia)	Two-photon	20x (NA = 0.95)	521 × 521 pixel (0.38 μm/pixel) 26–37 planes with 1 μm step	30 s 15–20 min	Hristovska et al. (29)
NSG-CCR2-RFP$^{+/-}$;CX3CR1-GFP$^{+/-}$ mice	8–12 wo	–	Isoflurane	Frontal cortex	GFP (microglia) RFP (macrophage) BFP (tumor)	Two-photon	20x (NA = 0.95)	1,024 × 1,024 pixel (0.584 μm/pixel) 7 planes with 1 μm step	–	Hutter et al. (30)
Thy1-GFP$^{+/-}$ mice (M-line)	–	Open or thinned	Ketamine and xylazine	Somatosensory cortex (∼100 μm)	GFP (neuron)	Two-photon	25x (NA = 1.05)	78 × 78 μm (0.15 μm/pixel) 0.75 or 0.5 μm step	90 min –	Isshiki and Okabe (31)
Tg(Apo-E:eGFP) (zebrafish)	5–8 dpf	–	Awake	–	GFP (microglia) OGB-AM (Ca^{2+})	Confocal or two-photon	40x (NA = 0.80)	– 1 μm step	2–4 s or 1.5–5 min	Li et al. (32)

(Continued)

TABLE 1 | Continued

Animal	Age	Skull	Anesthesia	Region (depth from the surface)	Cellular visualization	Microscopy	Objective lens	Resolution (x, y) z stack	Interval time Total time	References
CX3CR1-GFP$^{+/-}$ mice	2–3 mo	Open	Awake or isoflurane or ketamine and xylazine	Cortex	GFP (microglia)	Two-photon	40x	512 × 512 pixel (0.35 μm/pixel) 8 planes with 2 μm step	1 min –	Liu et al. (33)
Iba1-EGFP$^{+/-}$ mice	P8-10	Open	Urethane and atropine or awake	Cortex (45–250 μm)	GFP (microglia) tdTomato (neuron) GCaMP6m (Ca^{2+})	Two-photon	25x (NA = 1.05)	512 × 512 pixel (0.099 μm/pixel) 0.5 μm step	5 min, 30 min-2 h or 1.6 s-1 min, 27 min or 8 Hz, 30 min	Miyamoto et al. (34)
Tg(mpeg1:GAL4, UAS:mCherry); rwTg(isl1:GFP); Tg(-3.5ubb:secAnnexin V-mVenus) (zebrafish)	2–5 dpf	–	0.01% tricaine	Spinal cord	mCherry (microglia) GFP (neuron) mVenus (AnnexinV)	Confocal	10x (NA = 0.3), 40x (NA = 0.8), 63x (NA = 0.9)	– 10–15 planes with 1–2 μm step	3–8 min	Morsch et al. (35)
CX3CR1-GFP$^{+/-}$ mice	1.5–15 mo	Thinned	Isoflurane	Cortex (75 μm)	GFP (microglia)	Two-photon	–	– 15–25 planes with 1–2 μm step	20–45 s Several hours	Nimmerjahn et al. (1)
CX3CR1-GFP$^{+/-}$ mice	2–4, 9–11, 18–21 mo	Thinned	Isoflurane	Cortex (80–100 μm)	GFP (microglia) Oregon Green 488 (Ca^{2+})	Two-photon	40x (NA = 0.80)	–	4 frames/s or 10 frames/s or 30 s, 20 min	Olmedillas Del Moral et al. (36)
CX3CR1$^{CreER/+}$: Thy1 YFP-H mice	P19-34	Thinned	Ketamine and xylazine	Motor cortex (∼100 μm)	YFP (neuron)	Two-photon	60x (NA = 1.1)	–	4 d –	Parkhurst et al. (37)
ApoE-GFP;NBT-DsRed (zebrafish)	3 dpf	–	0.01% tricaine	–	GFP (microglia) DsRed (neuron) LysoTracker DND-9 (lysosome)	Confocal	40x (NA = 1.2)	– 4 stacks spanning 10 μm	–	Peri et al. (38)
PC::G5-tdTomato mice	2–4 mo	Thinned	Isoflurane	Visual or somatosensory cortex (∼100 μm)	tdTomato (microglia) GCaMP5G (Ca^{2+})	Two-photon	16x (NA = 0.8)	512 × 512 or 1,024 × 1,024 pixel	0.125 frames/s or 0.5 Hz –	Pozner et al. (39)
B6.Cg-Tg(Thy1-YFP)HJrs/J mice (#003782, JaxLab)	4–10 wo	Open	Isoflurane and ketamine	Somatosensory cortex	YFP (neuron)	Two-photon	25x (NA = 1.05)	166.7 × 166.7 μm (512 × 512 or 800 × 800 pixel) 30–70 μm with 1 μm step	24 h –	Pryazhnikov et al. (40)
CX3CR1-GFP$^{+/-}$;Thy1-YFP$^{+/-}$ mice	3–17 wo	Open	Awake or dexmedetomidine and midazolam	Cortex	GFP (microglia) YFP (neuron)	Two-photon	20x (NA = 0.95)	– 1 μm step	5 min 1 h	Stowell et al. (41)
CX3CR1-GFP$^{+/-}$ mice	3–4 mo	Open	Awake or isoflurane or ketamine	Cortex (100–150 μm)	GFP (microglia)	Two-photon	20x (NA = 1.00)	512 × 512 pixel (0.77 μm/pixel) 6 planes with 2 μm step	20 s 33 min	Sun et al. (42)

(Continued)

TABLE 1 | Continued

Animal	Age	Skull	Anesthesia	Region (depth from the surface)	Cellular visualization	Microscopy	Objective lens	Resolution (x, y) z stack	Interval time Total time	References
CX3CR1-GFP$^{+/-}$ mice, CX3CR1CreER-eYFP mice, and Rosa-CAG-LSL-eYFP-WPRE mice	2–5 mo	Open	Isoflurane	Somatosensory cortex (50–100 μm)	GFP, YFP (microglia) Evans lue,Rhodamine-dextran (vessel)	Multi-photon	40x (NA = 0.8)	800 × 800 pixel (0.18 μm/pixel) –	4 min 40–60 min	Taylor et al. (43)
CX3CR1-GFP$^{+/-}$;Thy1-YFP$^{+/-}$ mice	P28-39	Thinned	–	Primary visual cortex (50 μm)	GFP (microglia) YFP (neuron)	Two-photon	20x (NA = 0.95)	– 1 μm step	5 min 30 min-2 h	Tremblay et al. (44)
Rosa26-CAG-LSL-GCaMP6s mice, Rosa26-CAG-LSL-Lck-GCaMP6f mice, and CX3CR1$^{CreER-eYFP}$ mice	3–5 mo	Open	Awake	Somatosensory cortex (55–80 μm)	GCaMP6s, GCaMP6f (Ca^{2+}) GFP (microglia)	Two-photon	16x (NA = 0.8)	512 × 512 pixel (300 × 300 μm)	1 s –	Umpierre et al. (45)
Iba1-EGFP$^{+/-}$;Thy1-GFP$^{+/-}$ mice	6–10 wo	Thinned	Ketamine and xylazine	Cortex (100–250 μm)	GFP (microglia) YFP (neuron)	Two-photon	60x (NA = 1.1)	– 40–50 planes with 0.5 μm step	0.3–1.0 s –	Wake et al. (3)
Thy1-YFP$^{+/-}$ mice (H-line)	2–7 mo	Open or thinned	–	Barrel cortex (0–100 μm)	YFP (neuron)	Two-photon	60x (NA = 0.9)	–	–	Xu et al. (5)
Tg(-2.8elavl3:eGFP; coro1a:DsRedx) (zebrafish)	1–5 dpf	–	Awake or 0.01% tricaine	–	DsRed-Express (microglia) GFP (neuron)	Confocal	20x	– 40–50 planes with 3 μm step	3–5 min –	Xu et al. (53)
Thy1-YFP$^{+/-}$ mice (H-line) CX3CR1-EGFP$^{+/-}$ mice	–	Thinned	Ketamine and xylazine	Cortex (∼100 μm for neuron and ∼200 μm for microglia)	YFP (neuron) EGFP (microglia)	Two-photon	60x (NA = 1.1)	512 × 512 pixel (66.7 × 66.7 μm) 0.75 μm step	– ∼2 h	Yang et al. (46)
Thy1-YFP$^{+/-}$ mice Thy1-GFP$^{+/-}$ mice	1 mo	Thinned	Ketamine and xylazine	Motor cortex (100–200 μm)	YFP or GFP (neuron)	Two-photon	60x (NA = 1.1)	70 × 70 μm (512 × 512 pixels) 9 planes with 0.7 μm step	–	Yu et al. (47)

mo, month-old; dpf, days post-fertilization; wo, week-old; P, post-natal day; –, not available.

life. The authors also crossed CD11b-CreERT2;R26-tdTomato mice with APP/PS1 mice and examined microglia around the Aβ plaques (between 4 and 6 months of age). The rate of proliferation and disappearance of microglia around Aβ plaques approximately doubled (20%).

Microglial Contact to Other Type of Cells

One of the most important things that cannot be revealed without live imaging is how microglia interact with other cell types. By observing this interaction, we can discover new phenomena and get ideas for examining cell-cell signaling. In a report by Nimmerjahn et al. (1), the authors provided quantitative data on the process dynamics of microglia and even mentioned their interactions with other cell types. First, the authors labeled astrocytes, one of the major glial cells, with the red fluorescent dye sulforhodamine 101 (SR101) and showed that astrocytes, in contrast to microglia, showed virtually no change in morphology of their soma and primary processes. However, it should be noted that SR101 does not label the fine, distal astrocytic processes which are motile and only the proximal branches are labeled. They also captured the microglia coming into contact with the area where the SR101 signal was missing, presumably the cell bodies of the neurons, and with the area surrounding the astrocytes, presumably the blood vessels, which are surrounded by processes of the astrocytes. When the blood-brain barrier was disrupted by laser irradiation, microglial processes accumulated in the irradiated area, suggesting that microglia may also interact with blood vessels.

The improved imaging resolution has enabled real-time observation of microstructures such as microglial filopodia and synapses. Wake et al. performed *in vivo* two-photon imaging of the sensory or visual cortex in mice (3). They found that microglia make contact with axonal boutons and dendritic spines. It was shown that microglial contact with synapses increased with elevated neural activity by manipulating neural activity through visual stimulation and thermoregulation in mice. Furthermore, the duration of microglial contact with boutons was prolonged after the induction of ischemia, and more than half of the contacted boutons were lost. These results indicate that microglia may monitor synapses by contact and remove abnormal synapses. These results suggest that the ramified form of microglia is suitable for monitoring synapses.

Tremblay et al. also focused on the synaptic monitoring by microglia and performed *in vivo* two-photon imaging of microglia and dendrites in the visual cortex (44). When mice were transferred from dark to light environments to increase neural activity, microglial motility increased. Electron microscopy revealed that microglial contact with synapses was increased in mice transferred from dark to light environments. Furthermore, live imaging confirmed that the size of the spine increased during microglial contact and decreased after contact. Spines with microglial contact had a higher rate of subsequent disappearance than spines without contact, suggesting that microglia are responsible for synaptic removal. The involvement of microglia in synapse elimination predicted from the work of Wake et al. (3) and Tremblay et al. (44) using *in vivo* live imaging was later proved histochemically by the work of Paolicelli et al. (57) and Schafer et al. (58) who found phagocytic inclusions containing synaptic elements in microglia.

It had also been suggested that microglia modulate synapse formation through the release of BDNF (37), but it remained unclear whether microglial contact with synapses is important for synapse formation. To test that point, Miyamoto et al. performed *in vivo* multiphoton imaging of layers II and III of the sensory cortex of post-natal (P) 8 to 10-day-old mice, where synaptogenesis is active (34). The formation rate of filopodia was significantly higher in dendritic shafts contacting microglia than in areas without microglia. On the other hand, administration of minocycline, a derivative tetracycline that inhibits pro-inflammatory response of microglia, did not change the frequency of microglial contact with the dendrites but decreased the probability of filopodia formation. The filopodia formation rate was higher when the microglial contact with dendrites was accompanied by a local increase in Ca^{2+} concentration on the dendrites. Furthermore, removal of microglia by the Dox system during P5-11 reduced the number of functional synapses, indicating the need for microglia in synapse formation. The authors suggested that microglial state is important for the increase in Ca^{2+} concentration and subsequent spine formation in dendrites on contact because minocycline reduced the expression of the Ca^{2+}-binding protein Iba1 mRNA in microglia.

Together, *in vivo* live imaging studies of microglia-synapse interactions have provided direct evidence that microglia regulate not only synapse removal, but also synapse formation.

Stowell et al. examined the effect of one of the major neurotransmitters, norepinephrine, on microglia-synapse interaction (41). Pharmacological experiments showed that norepinephrine caused microglial process retraction and inhibition of bulbous tip formation by activating β2-adrenoceptors expressed in microglia. Furthermore, activation of β2-adrenoceptors inhibited ocular dominance in the visual cortex due to monocular shielding and reduced the number of microglial contacts with dendritic spines. These results indicate that β2-adrenergic receptor-dependent microglial contact with the spine may modulate synaptic plasticity.

There are numerous reports of microglia interacting with neurons in response to neural activity, and live imaging studies have been useful in targeting this relationship. Performing *in vivo* imaging of zebrafish, Li et al. presented an important finding that microglia can both monitor and manipulate neural activity (32). When glutamate uncaging increased the neural activity, microglial processes were attracted toward the active neurons. In doing so, bulbous tips were formed at the tips of microglial processes. Furthermore, in combination with Ca^{2+} imaging, it was shown that neural activity was reduced following microglial contact. Visualization of microglial Rac using the FRET system further revealed that Rac activity was increased at the microglial process tip as neural activity increased, indicating that this is required for microglial contact to neurons and the formation of a bulbous tip.

Badimon et al. showed that microglia reduce neural activity via the release of adenosine (13). Live imaging of microglia, neuronal axons, and bouton-like structures revealed that

increased neural activity via the DREADD system promotes microglial process extension via activation of P2Y12.

Phagocytosis

Since the persistence of dead cells in the brain parenchyma threatens the homeostasis of brain functions, it is important to elucidate the mechanism of dead cell removal by microglia. Peri et al. performed *in vivo* live imaging of zebrafish larvae and observed microglial motility (38) to examine the involvement of microglia in the removal of dead cells. Animals knocked out for v0-ATPase a1, which encodes a component of the vacuolar ATPase (V-ATPase), a multisubunit enzyme that mediates the acidification of eukaryotic intracellular organelles, showed reduced digestion of dead cells incorporated into microglia. In addition, phagosomes incorporating dead cells fused with each other during the digestion process. Furthermore, knocking out v0-ATPase a1 also inhibited the fusion of phagosomes and lysosomes, i.e., the formation of phagolysosomes. This study is impactful in that it unveils the process of digestion of dead cells by microglia and shows that microglia have the ability to not only take in dead cells but also digest them.

Morsch et al. conducted live imaging of spinal cord of zebrafish and showed microglial migration toward and uptake of irradiated neurons upon induction of neuronal cell death by UV irradiation (35). In combination with AnnexinV-mVenus, it was revealed that irradiated neurons underwent apoptosis after being taken up by microglia. Furthermore, the morphology of the microglia changed to an amoeboid shape during neuronal phagocytosis and returned to a stellate morphology after the digestion of neurons. The authors also compared other parameters, such as migration speed and microglial size.

Traumatic brain injury (TBI) also causes pronounced neuronal cell death. Microglia remove dead cells through phagocytosis, but it is not clear whether this phenomenon is protective or damaging to the brain. Herzog et al. performed live imaging of juvenile zebrafish and confirmed that microglia migrate to the injury site within minutes after TBI and phagocytose dead cells (27). In addition, the KO of P2Y12, which is necessary for microglial migration to the injury site, and inhibition of the phosphatidylserine (PS) receptor BAI1 reduced microglial phagocytosis of dead cells and accelerated subsequent secondary cell death in the injury site. These results suggest that the removal of dead cells by microglia is neuroprotective.

Damisah et al. observed the response of microglia and astrocytes to dead neurons in live imaging using photochemical techniques to induce apoptosis in single cell (17). Microglia and astrocytes were observed in separate mice; while microglia phagocytosed cell bodies and proximal dendrites, astrocytes phagocytosed distal dendrites and debris. The authors showed that knocking out the receptor tyrosine kinase Mertk delayed the recognition of dead cells by microglia. In microglia-removed mice, multiple astrocytes around dead cells cooperated in the phagocytosis of cell bodies. This suggests that astrocytes function in a supportive manner for microglia in the phagocytosis of dead cells. Further simultaneous live imaging of microglia and astrocytes is needed to understand the interaction of the two major phagocytes in the brain.

Abiega et al. examined the effect of neuronal hyperexcitability on the clearance of apoptotic cells by microglia (11). Twenty-four hours after KA administration to the hippocampus, process motility (velocity) of cortical microglia decreased. In addition, using immunostaining, FACS and live imaging of acute slices, the authors found that ATP released from hyperexcitable neurons masked the eat-me signal from apoptotic cells, which inhibited phagocytosis of apoptotic cells by microglia. Furthermore, the delayed clearance of apoptotic cells exacerbated the inflammatory response, suggesting that microglial clearance of apoptotic cells is important for maintaining brain homeostasis in the epileptic brain. However, even though neuronal death and microglial phagocytosis of dead cells were prominent in the dentate gyrus and hippocampus, the *in vivo* live imaging in this study was performed in the cortex, not the hippocampus, highlighting the technical difficulty of imaging deep brain regions.

Grier et al. investigated the possibility that neural activity mediates phagocytosis by microglia in the mammalian olfactory bulb where the lifelong activity-dependent plasticity occurs (23). Dopaminergic neurons in the glomerular layer are particularly plastic, with a sharp decrease in tyrosine hydroxylase expression levels and dopamine production, followed by a decrease in the number of dopaminergic neurons upon blockade of sensory input (59, 60). The authors performed *in vivo* live imaging and found that the blockade of sensory input after nasal obstruction resulted in morphological change of microglia (increased perimeter length) and an increased change rate of perimeter length (23). These results suggest that the reduced neural activity caused by the blockade of sensory input increases the frequency of microglial process extension and retraction. Although not through live imaging, in the nasal obstruction group, the microglia appeared to cover the cell bodies of the dopaminergic neurons, some of which were completely incorporated into the microglia. It was also shown that the synapses of dopaminergic neurons were incorporated into the microglia. These results indicate that the activity-dependent plasticity of the olfactory bulb may be regulated by microglia.

Myelin, which covers axons and controls the velocity of nerve conduction, is also a highly plastic structure that should be studied to further elucidate the interaction between axons and microglia. Although there have been few reports of *in vivo* live imaging of myelin at present, Hill et al. successfully observed stable myelin in label-free, *in vivo* live imaging in genetically engineered mice with fluorescently labeled myelin (28). The authors found that the production of oligodendrocytes and the structural plasticity of myelin occur throughout life. They also showed that cell death of oligodendrocytes and myelin degradation occur in old mice. Furthermore, live imaging of mice in which myelin, oligodendrocytes, and microglia were fluorescently labeled revealed that myelin debris produced in old mice is removed by microglia via phagocytosis.

Recently, it has been suggested that microglia also phagocytose tumor cells. Glioblastoma multiforme is a malignant brain tumor and is considered incurable. Tumor-associated macrophages and microglia (TAMs) are major cell types in tumorigenesis and have been shown to promote tumor growth. Therefore, it has been hypothesized that regulating TAM function might conversely

inhibit tumor growth. Hutter et al. previously suggested that suppressing SIRPα-CD47 signaling, a "don't eat me" signal, and promoting tumor phagocytosis by TAM could treat a variety of tumors (61). However, this antitumor effect has been thought to be largely due to macrophages infiltrating from the periphery, and the contribution of brain-resident microglia has not been clarified. In 2019, Hutter et al. attempted to clarify this point by using mice that can distinguish between microglia and macrophages (30). The authors found that CD47 inhibition also promoted tumor phagocytosis by microglia, and *in vivo* live imaging showed that CD47 inhibition reduced the number of microglial processes, increased process straightness, and reduced the speed of process extension and retraction. These changes in microglial morphology and motility indicated increased microglial contact with tumor cells.

Second Messenger Signaling in Microglia

The ability to observe second messenger signaling within microglia in real time would reveal what molecules are involved in microglial surveillance and directed movement. Such studies would be a first step toward modulating brain function through microglial regulation. Intracellular Ca^{2+} dynamics in microglia had been difficult to observe because of the difficulty in efficiently introducing Ca^{2+} indicator and adeno-associated viruses into microglia, but Eichhoff et al. succeeded in visualizing microglial Ca^{2+} dynamics for the first time (21). The authors loaded microglia with a calcium indicator, Oregon green BAPTA 1 (OGB-1). In microglia, almost no spontaneous Ca^{2+} fluctuations or Ca^{2+} response to increased activity of adjacent neurons, which was induced by bicuculline, was observed. On the other hand, physical damage by electrodes to neurons increased the Ca^{2+} concentration in nearby microglia. It was also suggested that the increase in Ca^{2+} in microglia was due to the activation of the ATP receptor P2Y. Furthermore, the latency from neuronal damage to Ca^{2+} elevation was significantly shorter in microglia than that in astrocytes, suggesting that fluctuations in intracellular Ca^{2+} concentration underlie the agile response of microglia to tissue damage.

Pozner et al. monitored the intracellular Ca^{2+} concentration by GCaMP5G while observing microglial morphology with tdTomato using the PC::G5-tdT mouse line (39). Spontaneous increases in Ca^{2+} concentrations were almost non-existent, but the frequency of elevated Ca^{2+} concentrations increased ∼8-fold when the microglia were stimulated by LPS. This increase in Ca^{2+} concentration was observed simultaneously in several microglia. Furthermore, the rates of process extension and retraction of microglia with elevated Ca^{2+} concentrations were reduced compared to those of microglia without Ca^{2+} concentration fluctuations.

As mentioned earlier, observing intracellular Ca^{2+} concentrations in microglia has been technically challenging. Brawek et al. successfully visualized microglial Ca^{2+} concentrations (14) using a different method than Eichhoff et al. (21) and Pozner et al. (39). Brawek et al. took advantage of the lack of microRNA-9 expression in microglia to create and apply a lentivirus that expresses the Ca^{2+}-indicator protein Twitch-2B in a microRNA-9-dependent manner. They found that the *in vivo* quiescent microglia showed stable and low Ca^{2+} concentrations. Since similar results were obtained in the study by Pozner et al. using different tools, it is likely that there is almost no Ca^{2+} fluctuation in microglia (at least under physiological conditions). In addition, Ca^{2+} concentrations were elevated in acute slices and dispersed cultures immediately after excision from the brain. This was accompanied by increased expression levels of CD68 and IL-1β, suggesting that intracellular Ca^{2+} concentration is an indicator of microglial proinflammatory response. The authors also confirmed that *in vivo* laser-induced tissue damage and ATP injection increased microglial Ca^{2+} concentrations in microglia, suggesting an association between directed process extension to injured areas and intracellular Ca^{2+} concentrations.

Olmedillas Del Moral et al. applied single-cell electroporation of the Ca^{2+} indicator Oregon Green 488 to microglia and observed intracellular Ca^{2+} concentrations in microglia (36). In 2 to 4-month-old ("young adult"), 9 to 11-month-old ("middle-aged"), and 18 to 21-month-old ("old") mice, the frequency and amplitude of spontaneous Ca^{2+} concentration increases were found to be highest in middle-aged adults. In addition, the speed of process extension toward ATP increased the most in the old group, but the correlation between distance from the ATP injection site and the process speed was lowest in the old group, indicating that the ATP responsiveness varied. These results indicate that the effect of aging may be different between individual microglia.

Umpierre et al. observed Ca^{2+} dynamics in microglia of awake mice in 2020 (45). The authors achieved microglia-specific expression of GCaMP using CX3CR1-CreER mice. Awake mice also showed no spontaneous increase in Ca^{2+} concentration. Interestingly, an increase in Ca^{2+} with process elongation was confirmed in response to both an increased and decreased neuronal activity. Although the dynamics of Ca^{2+} in microglia has been observed by various methods, no study has yet addressed the molecular mechanism that control Ca^{2+} dynamics in microglia.

Response of Microglia to Damage

Brain injury is often accompanied by inflammation. As immune cells in the brain, microglia may both exacerbate and suppress inflammation. *In vivo* imaging of microglial dynamics in and around injured sites will highlight the study of microglia as a potential therapeutic target for brain injury and the subsequent brain diseases. Davalos et al. is the first report that succeeded in capturing live ramified microglia *in vivo* (2). In addition to this observation, the authors examined the changes in microglial dynamics caused by tissue damage using laser irradiation and glass electrodes. Furthermore, through a combination of pharmacological treatments, it was shown that ATP released from the site of injury causes microglial process extension via activation of purinergic G protein-coupled receptors in microglia.

Haynes et al. examined the molecular mechanism of directed movement of microglial processes to the site of injury (26). Using KO mice, they demonstrated that P2Y12, which is unique in that it is a Gi-type receptor among mostly Gq-type P2Y

receptors, is required for process extension toward the site of injury. Interestingly, knocking out P2Y12 did not affect the basic surveillance by microglia. Therefore, this study is significant in that it shows that directed process extension to the injury site and surveillance may be regulated by different molecular mechanisms. In the same paper, the authors also performed live imaging of acute slices and showed that P2Y12 expression levels were reduced in correlation with microglial state change.

In the white mater of the spinal cord, the induction of microglial processes at the site of injury was also tested (20). The results showed that elevated ATP and NO levels at the site of injury promoted the extension of microglial processes. Stable live imaging of spinal cord was considered to be difficult due to motion artifacts; Davalos et al. established a spinal cord live imaging system that overcame the above problems by increasing the depth of anesthesia and improving the fixation device (18). However, it should be noted that ketamine and xylazine used as anesthesia could affect the motility of microglia.

Davalos et al. investigated the functional changes in microglia that occur in the diseased brain by *in vivo* live imaging (19). The authors examined the causes of blood-brain barrier (BBB) damage, microglial state change and neurodegeneration in multiple sclerotic brains and the mechanisms by which they cause axonal damage. In addition, *in vivo* live imaging revealed that microglial accumulation and myelin shedding occurred before the manifestation of paralysis, a symptom of multiple sclerosis. Furthermore, inhibition of fibrinogen formation by the anticoagulant lepirudin, genetic removal of fibrinogen, and removal of the binding site of fibrinogen to CD11b/CD18 (Fib–/–, Fibγ390-396A mice) inhibited the perivascular accumulation of microglia and axonal damage. This study reaffirms the importance of live imaging because this technique unveiled the temporal relationship between microglial accumulation and state change, both of which are causes of multiple sclerosis.

Taylor et al. examined the effect of type I diabetes on the repair of damaged blood vessels by microglia (43). In a mouse model of diabetes, laser irradiation did not cause migration of microglia to the damaged vessels. And the loss of vascular repair by microglia exacerbated secondary vascular leakage, suggesting that microglia are important for the suppression of vascular damage. Furthermore, they found that an increase in IFN-γ levels in the blood of a mouse model of obese reduced the expression level of P2Y12 in microglia and suppressed the migration of microglia to damaged blood vessels. Since live imaging of intact blood vessels can only be performed *in vivo*, *in vivo* live imaging may be the most suitable method to verify the relationship between vascular injury and microglia.

Achievement and Limitation of *in vivo* Live Imaging

In summary, *in vivo* imaging studies have revealed the dynamics of ramified microglia and contributed to our understanding of the dynamics and significance of microglial motility. For example, it was revealed that microglia could migrate long distance and intracellular Ca^{2+} activity of microglia was clarified. Also, it was shown that microglia change their dynamics in response to various transmitters, neural activity, injury, and interaction between other cell types.

It is expected that advances in genetic modification and imaging technology will further refine *in vivo* live imaging methods for observing intact microglial dynamics, but various technical limitations should not be overlooked at this point. First, most of the live imaging in the studies described in section *In vivo* Live Imaging (see **Table 1** for Experimental Conditions) was performed in the vicinity of the brain surface, which highlights the difficulty of deep brain imaging. The cortical area is a good place to test the relationship between neural activity and microglial dynamics, as well as the relationship between animal behavior and microglial dynamics, since neural activity can be altered by the introduction of sensory stimuli such as visual and auditory stimuli. Live imaging of microglia in deeper brain regions such as the hippocampus and amygdala, which control learning, memory, and emotions, may lead to the discovery of region-specificity of microglial motility and new significance of microglial surveillance in brain functions. Gu et al. showed that *in vivo* live imaging of the hippocampus is possible by aspiration of the cortex (25). Microglia in the hippocampus have been shown by immunostaining to exhibit morphology such as reduced process length and hypertrophy of the cell body after surgery, but to return to the surveillant state after 10 days. Badimon et al. performed *in vivo* neuronal calcium imaging in the dorsal striatum using the gradient-index (GRIN) lens (13). Thus, it is expected that live imaging studies of microglia in deep brain regions will be further advanced by using techniques such as the GRIN optics and cortical aspiration, and that details of microglial dynamics related to brain structure and function will be revealed.

Furthermore, it seems difficult to combine *in vivo* live imaging with the cell function manipulation by pharmacological and optogenetic methods, because the presence of bones in the thinned skull or the presence of glass coverslips in the open skull will limit what can be done from the brain surface.

Problems of *in vivo* imaging such as limited observation regions, low resolution, and difficulty in stimulation have been improved. Thus, complementary understanding of the data obtained by *in vivo* imaging and *in vitro* imaging, which has advantages such as observation at super-resolution level and manipulation at high spatiotemporal resolution, will help us to understand the mechanism underlying microglia-neuron interaction such as synapse elimination (**Figure 2**).

EX VIVO LIVE IMAGING

Live imaging of microglia *ex vivo* has been attempted as a way to overcome technical difficulties *in vivo*. In section *Ex vivo* Live Imaging, we will present studies using live imaging of brain slices. Perhaps the most significant advantage of slice imaging is that the structures in the brain (cell layers and projection pathways) are preserved. This is important for validating the direction of microglial migration and helps facilitate the extrapolation of results obtained with slice imaging to *in vivo*. In the following

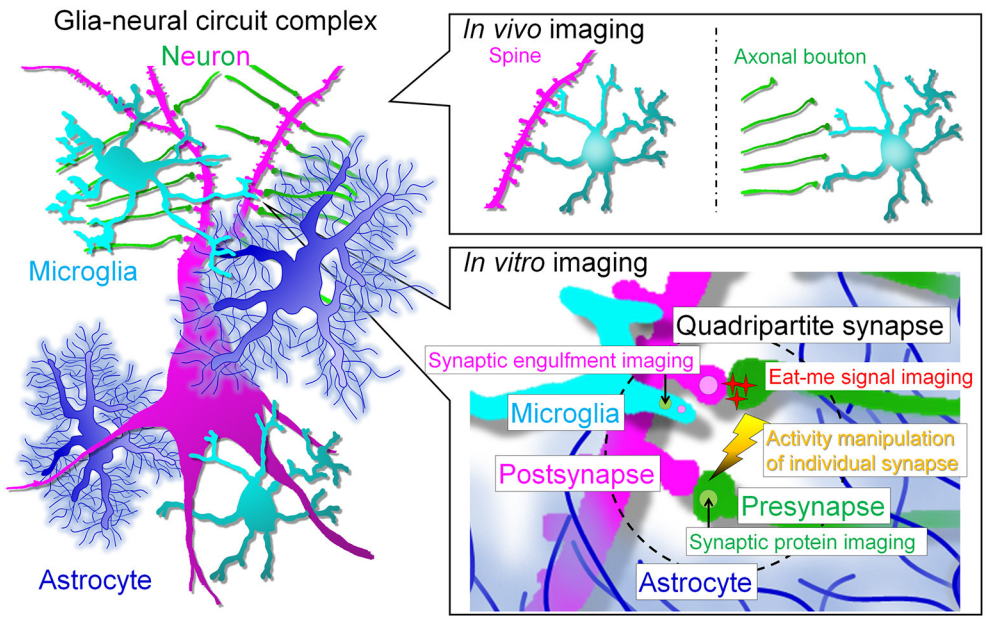

FIGURE 2 | Prospects for live imaging of glial cell-neural circuit complexes. *In vivo* multiphoton imaging studies have revealed that microglia interact with spines and axonal boutons. *In vivo* live imaging has greatly advanced the field by revealing the correlation between interactions and neural activity and has enhanced research interest in microglia. However, the next step will be to assess the interaction of each cell type at the synaptic site and the molecular mechanism of the interaction. For this purpose, we need to perform simultaneous high-resolution imaging of the quadripartite synapse, which consists of microglia, astrocytes and pre- and post-synapses. The simultaneous imaging of synapses, neuronal membranes, and microglia will help to answer the remaining major question of whether neurites are snipped off during synaptic phagocytosis. In addition, to understand the molecular mechanism of synaptic competition, it is necessary to control activity at the level of individual synapses. *In vitro* systems will facilitate live imaging with multiple colors, high resolution, and local stimulation, but a major barrier must be crossed: the establishment of glial cell culture systems that maintain *in vivo* morphology and gene expression. The realization of such systems is eagerly awaited to clarify the relationship between glia and neurons, especially synapses.

sections, we introduce acute slice imaging, in which sections cut out from the brain are observed immediately after preparation, and cultured slice imaging, in which sections are cultured and observed at any given time.

Acute Slice

Alterations of Microglial Process Dynamics by ATP and Neurotransmitters

Wu et al. examined the molecular mechanisms regulating microglial process motility by the ATP-P2Y receptor signaling pathway (76) (**Table 2**). Simultaneously, observing microglial motility by confocal microscopy and performing whole-cell patch-clamp recordings of microglia, the authors found that process extension to ATP correlated with the outward potassium current associated with P2Y receptor activation. It was also shown that both P2Y receptor activation and outward potassium currents are required for process extension to ATP and basal surveillance. Furthermore, it was shown that the PI3K signaling pathway is important for ATP-induced chemotaxis. Swiatkowski et al. showed that the regulation of process extension by outward potassium currents functions similarly in the microglial response to neuronal damage (75).

Molecules that act in the opposite way to ATP have also been studied. Gyoneva et al. tested the effect of norepinephrine on the motility of microglial processes: bath application of ATP induced microglial process elongation, whereas norepinephrine treatment retracted them (69). Microglia extend their processes to the site of injury in an ATP-P2Y12 signaling-dependent manner. In 2014, Gyoneva et al. tested this by preparing acute slices of mice that had been subjected to inflammatory conditions and performing live imaging (70). In the control group, microglial processes extended to the injured site, but this phenomenon was inhibited when inflammation was induced by prior LPS administration. In addition, MPTP treatment, which induced dopaminergic neuronal death and microglial state change, also inhibited process extension to the injured site. Furthermore, LPS and MPTP treatment increased adenosine A2A receptor expression in microglia and suppressed process extension to the injured site. Because adenosine retracts microglial processes via A2A receptors, treatment with preladenant, an antagonist of the A2A receptor, along with MPTP treatment, rescued the inhibition of process extension to the injury site.

Dissing-Olesen et al. showed that ATP released from neurons upon NMDAR activation attracts microglial processes (64). Pharmacological experiments showed that the induction of the microglial process was independent of ATP and NO release from Pannexin1 and astrocytic connexins associated with NMDAR activation. The formation of a bulbous tip-like structure at the tip of the microglial process upon ATP treatment indicates that the microglial processes may contact activated neurons

TABLE 2 | Experimental conditions of live imaging of microglia *ex vivo* (acute slice).

Animal	Age	Anesthesia	Region	Thickness Depth from the surface	Cellular visualization	Microscopy	Objective lens	Resolution (x, y) z stack	Interval time Total time	References
CX3CR1-GFP$^{+/-}$ mice	P30-40	–	Hippocampus	350 μm –	GFP (microglia)	Two-photon	40x (NA = 1.0)	– 11–25 μm thick	25 or 60 s ∼1 h	Avignone et al. (62)
CX3CR1-GFP$^{+/-}$ mice	P45-180	Isoflurane	Hippocampus	300 μm 150 ± 25 μm	GFP (microglia)	Two-photon	20x (NA = 1.0)	512 × 512 or 1,024 × 1,024 pixel 1–2 μm step	–	Bernier et al. (9)
C57BL/6 mice	6–8 wo	–	Coronal section	300 μm –	Alexa 488, 568 isolectin B4 (microglia)	Confocal	20x 40x	175 × 175 μm or 350 × 350 μm 40 μm	1.5 min –	Carbonell et al. (63)
CX3CR1-GFP$^{+/-}$ mice	P40-120	Halothane	Hippocampus	300 μm 150 ± 25 μm	GFP (microglia)	Two-photon	40x (NA = 1.0)	512 × 512 pixel 15 planes with 2 μm step	1 min –	Dissing-Olesen et al. (64)
CX3CR1-GFP$^{+/-}$ mice	P5-7	–	Hippocampus	400 μm 45–60 μm	GFP (microglia)	Confocal and multi-photon	20x (NA = 0.7)	775 × 775 μm 15 planes with 3 μm step	3–10 min –	Eyo et al. (65)
CX3CR1-GFP$^{+/-}$;Thy1-YFP$^{+/-}$ mice	4 wo	–	Hippocampus	300 μm 50–100 μm	GFP (microglia) YFP (neuron)	Two-photon	40x (NA = 0.8)	–	–	Eyo et al. (66)
CX3CR1-GFP$^{+/-}$ mice	P2-6	–	Hippocampus	400 μm 45–60 μm	GFP (microglia)	Confocal	20x (NA = 0.7)	775 × 775 μm 15 planes with 3 μm step	10 min –	Eyo et al. (56)
CX3CR1-GFP$^{+/-}$;Thy1-YFP$^{+/-}$ mice	3–5 wo	–	Cortex	300 μm 50–120 μm	GFP (microglia) YFP (neuron)	Two-photon	40x (NA = 0.8)	– 15 planes with 3 μm step or 10 planes with 2 μm step	30 s –	Eyo et al. (67)
CX3CR1-GFP$^{+/-}$ mice	3–8 mo	–	Retina	–	GFP (microglia)	Confocal	40x (NA = 0.8)	512 × 512 pixel –	10 s –	Fontainhas et al. (68)
CX3CR1-GFP$^{+/-}$ mice	1–4 mo	–	Cortex	200 μm	GFP (microglia)	Confocal	60x	– 30–50 planes with 1 μm step	1 min –	Gyoneva et al. (69)
CX3CR1-GFP$^{+/-}$ mice	–	–	Substantia nigra	200 μm	GFP (microglia)	Confocal	20x (NA = 0.50)	– 31 planes with 1 μm step	30–60 s 20 min	Gyoneva et al. (70)
SD rats Iba1-GFP$^{+/-}$ mice	P12 P15-27	–	Hippocampus	300 μm ∼50–100 μm	Isolectin B4-Alexa 594 or GFP (microglia)	Two-photon	20x (NA = 1.0)	512 × 512 pixel (0.49–0.39 μm/pixel) 21–31 planes with 2 μm step	60 s	Madry et al. (52)
MacGreen/cd39$^{-/-}$ mice	–	–	Somatosensory cortex	300 μm –	MacGreen (microglia)	Two-photon	40x (NA = 0.8)	307 × 307 μm 21 planes with 3 μm step		Matyash et al. (71)
SD rats Iba1-GFP$^{+/-}$ mice	P12 P15-27	–	Hippocampus	300 μm ∼50–100 μm	Isolectin B4-Alexa 594 or GFP (microglia)	Two-photon	20x (NA = 1.0)	512 × 512 pixel (0.49–0.39 μm/pixel) 21–31 planes with 2 μm step	60 s	Zhao et al. (72)

(Continued)

TABLE 2 | Continued

Animal	Age	Anesthesia	Region	Thickness Depth from the surface	Cellular visualization	Microscopy	Objective lens	Resolution (x, y) z stack	Interval time Total time	References
CX3CR1-GFP$^{+/-}$;Thy1-YFP$^{+/-}$ mice	P28-40	Isoflurane	Hippocampus	– –	GFP (microglia) YFP (neuron)	Confocal	40x (NA = 1.0)	512 × 512 pixel (0.39 μm/pixel) 11 planes with 1 μm step	30 s 80 min	Pfeiffer et al. (73)
CX3CR1-GFP$^{+/-}$ mice	3 mo∼	Euthasol	Spinal cord	350 μm –	GFP (microglia) Alexa Fluor 555 (neuron)	Two-photon	25x (NA = 0.95)	512 × 512 pixel 31 planes with 1.5 μm step	30–60 s 30–60 min	Rotterman and Alvarez (74)
Rats	P3-14	–	Hippocampus	400 μm –	FITC-IB 4 FITC-IB 4 FITC-IB 4 FITC-IB$_4$ (microglia)	Confocal	63x (NA = 1.2)	512 × 512 or 1,024 × 1,024 pixel 8–18 planes (∼60 μm)	2–5 min 30–90 min	Stence et al. (6)
CX3CR1-GFP$^{+/-}$ mice	3–6 wo	–	Coronal section	300 μm 50–100 μm	GFP (microglia)	Two-photon	40x (NA = 0.8)	1,024 × 1,024 pixel (0.16 μm/pixel) 15 planes with 3 μm step	1 min –	Swiatkowski et al. (75)
CX3CR1-GFP$^{+/-}$ mice	E12.5, 14.5, 17.5	–	Coronal section	300 μm 50 μm	GFP (microglia)	Confocal	20x (NA = 0.5)	1,024 × 1,024 pixel 72 μm with 8 μm step	2 min 1 h	Swinnen et al. (54)
CX3CR1-GFP$^{+/-}$ mice	8–10 wo	Halothane	Cortex	300 μm –	GFP (microglia)	Confocal	40x (NA = 0.8)	– 8–10 planes with 2 μm step	1 min –	Wu et al. (76)
rd10;CX3CR1-GFP$^{+/-}$ mice	P21-24	–	Eyecup	–	GFP (microglia) PI (dead cell) Hoechst (nuclei)	Confocal	40x or 60x	1,024 × 1,024 pixel –	1 min 2 h	Zhao et al. (77)

wo, week-old; mo, month-old; P, post-natal day; –, not available.

via the bulbous tips, and *in vivo* live imaging showed similar results. Eyo et al. showed that microglial process induction was also enhanced when neural activity was enhanced by kainic acid (66). Furthermore, they found that inhibiting microglial process number increases and process attraction by P2Y12 KO worsened kainic acid-induced seizures. These results suggest that microglial-neuronal contact in the epileptic brain has a neuroprotective effect.

Pfeiffer et al. examined the effect of increased neural activity associated with long-term potentiation (LTP) induction on the dynamics of microglia. After LTP induction, the number of microglial process branches increased, but the speed of extension and retraction was unchanged (73). Furthermore, live imaging of microglia and dendritic spines revealed an increase in the duration of microglial contact with spines after LTP induction, resulting in a decrease in the number of contacts. Furthermore, these changes were abolished by treatment with NMDA receptor antagonists. Taken together, these findings and the report by Dissing-Olesen et al. (64) suggest that neuron-derived ATP released in an NMDA receptor-dependent manner may regulate microglial-synaptic interactions.

While many studies have focused on microglial responses to excitatory neuron-derived neurotransmitters, Fontainhas et al. also focused on the inhibitory neurotransmitter GABA (68). Bath application of bicuculline, an inhibitor of ionic GABAA receptors, increased the length, extension and retraction rate and number of microglial processes and branches. On the other hand, a bath application of GABA reduced all these parameters. These results indicated that GABA decreases the motility of microglia.

Exploring the Regulatory Molecules of Microglial Dynamics Using Brain Injury Models

Zhao et al. tested the involvement of microglia in rod photoreceptor cell death in retinal degeneration (77). Live imaging of retinal explants in the rd10 mouse model of retinal degeneration showed that microglia phagocytose propidium iodide (PI)-positive and PI-negative rod photoreceptor cells. Microglial morphology and the way of phagocytosing rod photoreceptor cell varied, with amoeboid microglia forming a phagocytic cup near the cell body, and microglia with processes forming a phagocytic cup at the tip of the process or using lamellipodia.

Avignone et al. used a mouse model of kainic acid-induced status epilepticus and performed live imaging of microglia in hippocampal acute slices (62). Forty-eight hours after status epilepticus, microglia showed morphological changes such as enlarged soma and shorter process, but there was no change in surveillance or the extension speed of microglial processes to the site of injury. However, there was an increase in the extent to which a single process was explored and an increase in the speed of process extension to 2 Me-ADP. Eyo et al. also utilized a seizure model to examine the molecular mechanisms that regulate microglial contact with neurons and their relationship (67). Microglial process convergence (MPC), which is seen when microglia contact neurons, was used as an indicator of contact events. MPCs were increased when seizures were induced by kainic acid and pilocarpine. In addition, knocking out the CX3CR1 receptor, a fractalkine receptor, decreased MPCs, while treatment with its ligand CX3CL1 increased MPCs, indicating that the CX3CL1-CX3CR1 signaling pathway regulates microglial-neuron interactions. In addition, activation of CX3CR1 promoted IL-1β release from microglia. Furthermore, IL-1β promoted ATP release associated with increased neural activity and microglial process elongation via P2Y12 receptors. The aggravation of kainic acid- or pilocarpine-induced seizures in CX3CR1-KO mice suggests that microglia inhibit excessive neural activity by contacting neurons with elevated activity.

Carbonell et al. examined the response of mature microglia to thalamic damage (63). Acute slices were prepared 2, 3, 4, 6, and 8 days after the stab lesion and the thalamus was observed. The mobility of microglia around the injured site was highest after 3 days, but the direction of migration was random. As intracellular signaling, the authors focused on cysteine-cysteine (CC) chemokines involved in homing to the site of injury by leukocytes. They also showed that inhibition of CCR5 reduced migration speed and distance of microglia.

Eyo et al. focused on perinatal stroke and examined the effects of stroke-related deficiencies of oxygen and glucose on microglial motility (65). To model stroke, they treated acute hippocampal slices with hypoxia or oxygen-glucose deprivation (OGD). Both treatments reduced microglial motility and caused microglial death. Next, they compared the dynamics of microglia after OGD in slices of P2-3 and P6-7 and found that the former showed a lower cell death rate, a longer latency to death, and higher motility of microglia. These results suggest that the sensitivity of microglia to OGD increases with development.

Exploring the Molecules That Control the Morphology of Microglial Processes

The acute slice experimental system, which allows for more detailed pharmacological and genetic interventions than *in vivo* systems, including gene transfer, may contribute to the elucidation of mechanisms and molecules that could not be discovered *in vivo*. Matyash et al. found that knocking out of CD39 and CD73, which mediate the degradation of extracellular ATP to adenosine, reduced the length of microglial processes as well as the branching number (71). In acute slices of CD39-KO mice, the extension of microglial processes to ATP and the site of injury was suppressed. Microglial ramification was rescued by inhibition of the adenosine transporter and increased extracellular adenosine. A similar trend was observed in primary cultures of microglia. These results suggest that adenosine is important for the maintenance of the ramified morphology of microglia.

Madry et al. tested the possibility that the two-pore domain channel (THIK-1) regulates microglial process motility (52). THIK-1 is constitutively activated and is further activated upon activation of the P2Y12 receptor. Inhibition of THIK-1 activation reduced the ramification and surveillance of microglia but did not affect the extension of processes to ATP. In contrast, inhibition of P2Y12 receptors had no effect on the ramification or surveillance. Importantly, this research provided an interesting insight that directed extension and surveillance are distinct

modes of microglial process dynamics and may be regulated by different molecular mechanisms.

Bernier et al. focused on the kinetics of filopodia growing from the main processes of microglia and observed that inhibition of actin polymerization by cytochalasin treatment stopped the extension and retraction of filopodia (9). Increasing intracellular cAMP concentrations by treatment with IBMX and norepinephrine reduced the number of large processes but increased the number of filopodia. Furthermore, activation of P2Y12 by ATP treatment abolished filopodia and promoted the elongation of large processes and the formation of bulbous tips. These results suggest that fluctuations in intracellular cAMP concentrations in the quiescent state lead to the formation of filopodia and random surveillance, whereas elevated extracellular ATP concentrations cause filopodia to retract, promoting unidirectional process extension and the formation of bulbous tips.

Cultured Slice

When using acute slices, the effects of factors released due to the damage associated with section preparation need to be recognized. Cultured slices may partly overcome this point by recovering during the incubation period. In contrast to acute slices which require the experiment to be completed within 4 h of brain sectioning to observe ramified microglia (52), a major advantage of using cultured slices is the ability to image a relatively long time after manipulation, as it allows us to elucidate microglial changes in response to temporal changes (e.g., neurite outgrowth and transformation of the injured area). In addition, it is also possible to develop systems that recapitulate the synaptic connections between pre- and post-neurons by coculturing distant but neural-connected brain regions (e.g., retinal ganglion cells in retina and dorsal LGN neurons). However, one must be cautious of the unique reorganization of nerve fibers and glial proliferation in cultured slices and the different characteristics of microglia in the superficial and lower layers of slices (86). Additionally, as is often the case in culture systems, minute differences in techniques between experimenters of culture specimens may lead to significant differences in the morphology of microglia that are sensitive to environmental changes. The membrane used for culture sections is also important.

Recently, Ogaki et al. focused on the fact that PTEE membranes, which are frequently used to place slices in culture, make live imaging using inverted microscopy difficult due to the low light transmission of PTFE membranes (10) (**Table 3**). The authors evaluated the performance of the collagen membrane by placing sections on the light-permeable collagen membrane instead of the PTFE membrane and culturing the slices. The results showed that there was no significant difference in the number and viability of neurons and microglia between slices cultured on the PTFE membrane and slices cultured on the collagen membrane. In addition, the microglial processes, filopodia as well as cell contours were more clearly observed on the collagen membrane during live imaging. These innovations will broaden the use of slice culture for live imaging of microglia.

Studies on Microglial Dynamics That Require Long-Term Observation

Ohsawa et al. examined the effect of ADP on microglial process extension; treatment with RGD, an integrin inhibitor, together with ADP bath application, inhibited process extension to ADP (82). In conjunction with other experiments, the authors indicated that activation of microglial P2Y12 by ATP, which increases the expression level of integrin β1 and promotes adhesion to the extracellular matrix, is important for microglial process extension.

Although microglia are known to repopulate once removed, the function and motility of repopulated microglia have not been well-elucidated. Zhang et al. performed live imaging of retinal explant cultures to examine the response to ATP of repopulated microglia (87). After 60 days of repopulation, there was no change in basal process motility or the degree of process elongation during ATP treatment between repopulated and endogenous microglia.

In the cortical plate (CP), microglia are temporarily absent from E15 to E16 and instead are abundant in the ventricular zone (VZ), subventricular zone (SVZ), and intermediate zone (IZ) (88). However, it is not clear why or how microglia are absent from the CP during this period: neurons arising in the VZ/SVZ migrate to the CP and divide into various subtypes corresponding to the cortical layer structure. Changes in the expression of transcription factors that control differentiation lead to abnormal layer structure and the emergence of ectopic neurons. Hattori et al. proposed and tested the hypothesis that microglia may be temporarily absent from the CP to prevent interference with the functional differentiation of CP neurons (79). Live imaging of slices prepared from E14 mice showed that microglia migrate from the CP to the meninges and that removal of the meninges reduced the amount of migration. A similar trend was observed using *in vivo* imaging *in utero*: contrary to the microglia in the CP, microglia in the VZ/SVZ/IZ were observed to migrate in the apical direction. In addition, microglial migration was inhibited in slices prepared from CXCR4-KO mice, indicating that the CXCL12-CXCR4 signaling pathway may regulate microglial migration. At present, verification of cell migration along the dorsoventral axis can only be performed by live *ex vivo* imaging, and this study demonstrates the utility of slice culture imaging.

Interactions Between Microglia and Other Cells

Multinucleated neutrophils (PMNs), which invade the brain parenchyma during ischemia, injure neurons by eliciting inflammation. Neumann et al. tested the possibility that microglia may play a role in protecting neurons by removing neutrophils by phagocytosis (81). Oxygen glucose deprivation (OGD) treatment of cultured slices increased neuronal death, which was further accelerated by the addition of PMNs. On the other hand, the addition of microglia at the same time as PMN reduced some of the neuronal death. Next, to test the possibility of microglial phagocytosis of PMNs, the authors added fluorescently labeled PMNs and microglia to cultured slices and performed live imaging. Both endogenous and added microglia phagocytosed PMNs. It was also shown that the microglia phagocytosed both dead and live PMNs. Furthermore, treatment

TABLE 3 | Experimental conditions of live imaging of microglia *ex vivo* (slice culture).

Animal	Age	Imaging timing	Region	Thickness Depth from the surface	Cellular visualization	Microscopy	Objective lens	Resolution (x, y) z stack	Interval time Total time	References
CX3CR1-GFP$^{+/-}$ mice	P6-7	10–12 DIV	Hippocampus	300 μm	GFP (microglia)	Multi-photon	25x	– 21 planes with 1.5 μm step	1 min 15 min	Greenhalgh et al. (78)
CX3CR1-GFP$^{+/-}$ mice	E14	–	Cortex	350 μm	GFP (microglia)	Confocal	–	–	30 min 8 h	Hattori et al. (79)
Iba1-EGFP$^{+/-}$ mice	P6-7	13–14 DIV	Hippocampus	300 μm	GFP (microglia)	Fluorescence	20x (NA = 0.45)	–	20 min –	Katayama et al. (80)
Wistar rats	P7-9	10 DIV	Hippocampus	350 μm	CMTMR (microglia) CMAC (PMN)	Confocal	–	–	–	Neumann et al. (81)
CX3CR1-GFP$^{+/-}$ mice	P6	7–9 DIV	Entorhinal-hippocampus	400 μm	GFP (microglia)	Confocal	30x (NA = 1.05)	– 21 planes with 1 μm step	30 s –	Ogaki et al. (10)
Iba1-EGFP$^{+/-}$ mice	P4-7	–	Hippocampus	400 μm	GFP (microglia)	Confocal	20x	– 20 planes with 2 μm step	5 min 1 h	Ohsawa et al. (82)
SD rats	P4-6	1–8 DIV	Hippocampus	400 μm	IsolectinB4-FITC (microglia) Sytox Orange or To-Pro-3 (dead cell)	Confocal	20x (NA = 0.7)	512 × 512 pixel 5–10 planes with 5–8 μm step	2-4 min 2–11 h	Petersen et al. (83)
Cx3cr1::CreER; RC::LSL-tdTomato mice	P4	10–19 DIV	Hippocampus	300 μm 30 μm	tdTomato (microglia) neuron (iRFP)	Light sheet	60x (NA = 1)	0.13 × 0.13 μm 0.48 μm step	45–60 s 2–3 h	Weinhard et al. (84)
Rabbits	–	–	–	350 μm	Tomato Lectin 594 (microglia)	Confocal	20x	– 50–80 μm thick with 2–5 μm step	15 min 5.5–6 h	Zhang et al. (85)

E, embryonic day; P, post-natal day; DIV, day in vitro; –, not available.

with RGD and GluNAc (an inhibitor of lectins) reduced PMN phagocytosis and accelerated OGD treatment-induced neuronal death. These results suggest that phagocytosis of PMNs by microglia is neuroprotective.

Using live imaging of hippocampal culture slices, Weinhard et al. were able to capture the series of process in which microglia phagocytose the presynaptic structures (boutons) formed by dentate gyrus granule cells (84). They did not identify any instances of microglia phagocytosis of dendritic spines and argued that, at least under physiological conditions, microglia may preferentially phagocytose presynaptic components.

Studies on Brain Injury and Brain Diseases

In Petersen et al., the response of microglia to damaged neurons was observed at 1∼7 DIV (83). When adjacent cells died, microglia extended their own processes and phagocytosed the dead cells. The motility of microglial processes changed after contact with other microglia and dead cells, suggesting that contact determines the target for phagocytosis.

Katayama et al. subjected neurons to excitotoxicity by NMDA and observed the response of microglia to injured neurons (80). Microglia accumulated in the pyramidal cell layer after injury, indicating that this was independent of microglial proliferation. In addition, PI-positive neurons disappeared after being surrounded by microglia, and this was inhibited by removal of the microglia by clodronate treatment, suggesting that microglia phagocytose the injured neurons. Furthermore, the authors showed that phagocytosis of PI-positive neurons was promoted by p38 MAP kinase.

Anti-inflammatory therapy that targets microglia to block the microglial inflammatory response in cerebral palsy and autism is currently being explored. Zhang et al. used *E. coli*-induced maternal immune activations (MIAs) in rabbit fetuses and prepared hemispheric slice cultures to examine microglial migration and the interaction between microglia and dendrimers (85). Microglia in the MIA group exhibited an amoeboid shape, and their migration speed and distance were reduced. Since the microglia in the MIA group took up more dendrimers at a faster time, the authors claimed that the change in microglial motility was due to an interaction with dendrimers and proposed that assays using culture slices could be useful for drug discovery.

Greenhalgh et al. examined the effect of bone marrow-derived macrophages on the responsiveness of microglia during tissue injury (78). Cultured slices were laser-irradiated, and the induction of microglial processes to the irradiated area was quantified. There was no change in each parameter of process extension in the presence or absence of macrophages.

IN VITRO (DISPERSED CELL CULTURE)

In section *Ex vivo* Live Imaging, live imaging of microglia using acute or cultured slices was introduced. Slice imaging has clearly broadened the scope of microglial studies, as it allows live imaging of the brain in its layered structure without area limitations. However, the heterogeneity of microglia depends on the position of the slice, which must be noted in slice imaging (86). Thus, most papers specify in the materials and methods section how much depth (Z-axis distance) the imaging was performed from the surface of the slice. It is important to have some degree of homogeneity in microglial conditions before treatment, especially when comparing microglial morphology and function between the control and treated groups. To overcome the heterogeneity of microglia, dispersed cultures would be useful. The greatest advantage of using dispersed cultures is that the cell types present in the observation system can be regulated according to the purpose of the experiment, which is naturally different from the *in vivo* conditions though. These features make it possible to clarify which cell type a particular phenomenon strongly depends on, and may facilitate the screening of the molecular mechanisms involved. Taking advantage of this, cell culture systems have been widely used for disease research, pharmacological screening, and, more recently, iPS microglia research. In the future, more sophisticated cell culture systems, especially in terms of reproducing *in vivo* microglial morphology, will be needed to validate cell-cell interactions that underlie neural circuitry and brain function.

The medium and presence of heterogeneous cells may have a significant impact on the morphology and functions of microglia. For example, Montilla et al. examined the effect of medium composition on microglial properties (93). Compared to DMEM+10% FBS, the use of TIC medium which contains TGF-β, IL-34, and cholesterol (8) resulted in an increase in microglial process number, changes in purine receptor expression levels, reduced phagocytic ability, and increased motility (movement speed and distance traveled), which indicated that serum significantly influences microglial conditions. There is also a significant influence of serum; Rizzi et al. examined the effect of NGF on the behavior of microglia (94), finding that microglial motility, which was defined as the degree of change in the ratio of cell area/cell perimeter length, was increased by NGF, although the cell body migration speed did not change.

Disease Research

As mentioned above, the contribution of cell culture to disease research and drug screening systems is significant. Therefore, we present here a chronological list of some of the most important disease studies using live imaging of cell cultures. To mimic Huntington disease, microglia were cocultured with striatal and cortical neurons expressing Htt mutants (91) (**Table 4**). Live imaging showed that microglia moved into the vicinity of neuronal projections, which were then torn off. These results suggest that microglia cause neuronal degeneration.

To establish an *in vitro* model of amyotrophic lateral sclerosis (ALS), Frakes et al. cultured motor neurons from wild-type mice with microglia isolated by density gradient centrifugation from adult wild-type or SOD1-G93 mice (ALS model) (89). Seventy-two hours after the start of coculture, the number of motor neurons cocultured with microglia from the ALS model mice was reduced to ∼50% of the number when cocultured with microglia from wild-type mice. When shRNA against the SOD1 mutant was expressed by lentiviruses to reduce SOD1 expression in microglia to ∼25%, the reduction in motor neuron numbers was rescued. The authors also showed that the SOD1 mutant

TABLE 4 | Experimental conditions of live imaging of microglia *in vitro*.

Animal	Age	Isolation method	Region	Other cell type in the culture	Cellular visualization	Microscopy	Objective lens	Resolution (x, y) z stack	Interval time Total time	References
SOD1-G93A mice (animal model of myotrophic lateral sclerosis)	4 mo	Density gradient centrifugation	Whole brain	Motor neuron	Red (microglia) GFP (motor neuron)	Confocal	–	–	–	Frakes et al. (89)
C57BL/6 mice	P3	Mild trypsinization of mix glial coculture	Cortex	Bacteria	DIC	Epifluorescence	10x or 20x	–	–	Hupp et al. (90)
mice or rats	P1-2	Shaking of mix glial coculture	Cortex	Neuron	IsolectinB4-594 (microglia) YFP (neuron)	–	–	–	–	Kraft et al. (91)
iPSCs	–	Differentiation	–	Synaptosome	DIC (microglia) pHrodo (synapptosome)	Confocal	–	0.61 × 0.61 μm –	–	Sellgren et al. (92)

iPSCs, induced Pluripotent Stem Cells; P, post-natal day; mo, month-old; –, not available.

caused microglial inflammatory responses (increased expression of CD68, iNOS, and ROS) and motor neuron death via activation of NFκB. It should be noted that coculture with microglia did not affect neuronal death when microglia were isolated from neonatal microglia, suggesting that even isolated microglia may be able to reflect the condition of the derived individual to some extent.

In Hupp et al., the effect of *Streptococcus pneumoniae* on the function of microglia was examined (90). In both isolated cultures of microglia and cocultures with astrocytes, exposure to *Streptococcus pneumoniae* resulted in reduced chemotaxis to the bacteria and motility of microglia. This could be a strategy by which *Streptococcus pneumoniae* escapes phagocytosis by microglia.

Sellgren et al. developed an *in vitro* model of microglia-dependent synaptic removal to test the possibility that excessive synaptic removal may contribute to schizophrenia (92). The authors showed that synaptosomes derived from schizophrenia patients were more likely to be phagocytosed and that patient-derived microglia-like cells (iMGs) had a higher phagocytosis capacity. Furthermore, they found that C4, a schizophrenia risk gene, was involved in complement tagging to neurons and synaptic removal by microglia. Additionally, minocycline inhibited synaptic removal and reduced the risk of developing schizophrenia. Although representative images of differentiated iMGs showed a morphology relatively close to that *in vivo*, no image was presented to show the morphology of iMGs during synaptosome phagocytosis.

As reported by Hupp and Sellgren (see above), another advantage of the cell culture system is that the process of phagocytosis is easier to observe than other experimental systems. Taking advantage of this, Zhao et al. examined the effect of activation of mTOR signaling on phagocytosis in microglia (72). They added pHrodo to primary cultures of microglia and measured its uptake, finding that phagocytosis was enhanced in TSC1Cx3cr1CKO mice compared with microglia derived from wild-type mice. It should be noted that there are still no studies which succeeded in reproducing ramified morphology of microglia in the co-culture of microglia and neurons, and that *in vitro* system probably failed to reflect how microglia phagocyte neurons and synapses *in vivo*.

Sophistication of Culture Systems

One of the most challenging aspects of microglial isolation and culture is recreating microglial morphology *in vivo*, and there have been many attempts to improve the morphology of microglia in culture. For example, it has been shown that ATP, which promotes microglial process extension, increases the number of microglial primary processes (95). Thus, it would be useful to target molecules that have already been shown to regulate microglial ramification *in vivo* and *ex vivo*.

It has also been shown that the method of coating the surface of the culture dish may affect microglial morphology (96, 97). A strong candidate for factors that promote microglial ramification are astrocyte-derived molecules; since the 1990s, coculturing microglia with astrocytes and adding astrocyte culture supernatants (ACMs) to isolated cultures of microglial

conditions have been used to improve microglia *in vitro* (6, 98, 99). Recently, among astrocyte-derived factors, CSF-1, TGF-β, and cholesterol were found to be required for microglial ramification (8). This work was a breakthrough in microglial culture, as it allowed for studies to use *in vivo*-like microglia without coculturing with other cell types.

Because microglial functions, such as exploration of the brain environment and phagocytosis, are strongly dependent on the morphology of the process, recreating the ramified process is particularly important. Hyperramified microglia have been reported in the diseased brains of chronic despair models and alcoholism models (100, 101). Using electron microscopy, Bisht et al. also reported the existence of microglia with highly ramified processes, called dark microglia, in pathological conditions such as stress and Alzheimer's disease (102). A group of microglial genes whose expression levels are altered in each animal model is also being elucidated by RNA sequencing. Using this information, methods to promote microglial ramification *in vitro* may be discovered.

However, it should be noted that the ramified morphology of microglia *in vitro* does not necessarily reflect the characteristics of transcriptome under physiological conditions *in vivo*. Indeed, Bohlen et al. mentioned this limitation by comparing the RNA-sequence data between cultured microglia with ramified morphology and freshly isolated microglia (8).

CONCLUSION AND PERSPECTIVE

In section Achievement and Limitation of *in vivo* Live Imaging, we described studies that have performed live imaging of microglia *in vivo*, *ex vivo* (acute slice and cultured slice), and *in vitro* (primary culture). Although we have not been able to cover all of the published papers, the number of papers is roughly in the order of *in vivo*, *ex vivo*, and *in vitro*. *In vitro* systems are easier than other experimental systems to perform pharmacological and genetic manipulations (e.g., induction of synaptic competition, which is important in neuron-microglial interactions). In addition, multicolor live imaging is essential to investigate the relationship between microglia and synapses. Since a synaptic site contains at least four components, i.e., microglia, astrocytes, pre-synapses, and post-synapses, all of these components should be imaged as simultaneously as possible at high resolution to assess the function and identity of "quadripartite synapses" (103–105). The pros of *in vitro* system is that multicolor live imaging can be accomplished without the need of complicated breeding schemes and crossings of transgenic animals to label multiple cellular elements.

However, live imaging systems using *in vitro* tools still have limitations that need to be solved. The most critical point is that *in vitro* microglia differ from *in vivo* and *ex vivo* microglia in that they exhibit an abnormal form (hypertrophy of the cell body and loss of fine processes). This microglial morphological abnormality is unsuitable for examining microglial-synaptic interactions, which have recently received considerable attention among microglial functions. Conversely, if we can establish an *in vitro* experimental system that overcomes the abnormal morphology, it would be a breakthrough that could greatly advance microglial research. In particular, in the case of microglial-synaptic interactions, the detailed molecular mechanisms cannot be explored without observing and manipulating cell-cell interactions in the glia-neural circuit complex. For example, other than microglia, the involvement of astrocytes cannot be disregarded. Astrocyte micro-processes surround pre-synapses and post-synapses, forming a tripartite synapse structure (106). The formation of tripartite synapses is then promoted by increased neural activity (107). Therefore, to elucidate the activity-dependent microglial-synaptic interaction, a four-party structure that adds microglia to the conventional tripartite synapse, or quadripartite synapse, should be studied. To do so, it is necessary to solve the difficult problem of morphological abnormalities in cultured microglia. If we can induce synaptic competition at the individual synapse level and subsequently detect changes in glial intracellular signaling and glial gene expression, we will obtain many novel insights into the synaptic plasticity that underlies brain function (**Figure 2**). In addition to morphological abnormalities, discrepancies of gene expression characteristics with *in vivo* microglia are also issues to be solved in *in vitro* experimental systems. In the future, it is expected to develop *in vitro* experimental systems that mimic the gene expression characteristics of microglia *in vivo*.

Another significant limitation of using *in vitro* systems may be the inability to fully reproduce the brain environment. There are many components of the brain that are lacking in cell culture and may affect microglial morphology and function, such as the blood brain barrier (BBB), blood vessels, extracellular matrix (ECM), and other cell types. In recent years, many attempts have been made to reconstitute BBB, blood vessels, and ECM *in vitro* (108, 109) and to culture ramified microglia with other cell types (110).

In conclusion, in order to understand the role of microglial dynamics in brain function and the underlying cellular and molecular mechanisms, it is important to develop appropriate *in vitro* live imaging systems that reflect the findings of *in vivo* live imaging and fully exploit the convenience of genetic and pharmacological manipulation of brain cells *in vitro*.

AUTHOR CONTRIBUTIONS

MA and RK wrote the manuscript. Both authors contributed to the article and approved the submitted version.

FUNDING

This research was funded by [JSPS] grant number [20H05897] and by [JST] grant number [JPMJPR18H4].

REFERENCES

1. Nimmerjahn A, Kirchhoff F, Helmchen F. Resting microglial cells are highly dynamic surveillants of brain parenchyma *in vivo*. *Science.* (2005) 308:1314–8. doi: 10.1126/science.1110647
2. Davalos D, Grutzendler J, Yang G, Kim JV, Zuo Y, Jung S, et al. ATP mediates rapid microglial response to local brain injury *in vivo*. *Nat Neurosci.* (2005) 8:752–8. doi: 10.1038/nn1472
3. Wake H, Moorhouse AJ, Jinno S, Kohsaka S, Nabekura J. Resting microglia directly monitor the functional state of synapses *in vivo* and determine the fate of ischemic terminals. *J Neurosci.* (2009) 29:3974–80. doi: 10.1523/JNEUROSCI.4363-08.2009
4. Colonna M, Butovsky O. Microglia function in the central nervous system during health and neurodegeneration. *Annu Rev Immunol.* (2017) 35:441–68. doi: 10.1146/annurev-immunol-051116-052358
5. Xu HT, Pan F, Yang G, Gan WB. Choice of cranial window type for *in vivo* imaging affects dendritic spine turnover in the cortex. *Nat Neurosci.* (2007) 10:549–51. doi: 10.1038/nn1883
6. Stence N, Waite M, Dailey ME. Dynamics of microglial activation: a confocal time-lapse analysis in hippocampal slices. *Glia.* (2001) 33:256–66. doi: 10.1002/1098-1136(200103)33:3<256::AID-GLIA1024>3.0.CO;2-J
7. Tanaka J, Maeda N. Microglial ramification requires nondiffusible factors derived from astrocytes. *Exp Neurol.* (1996) 137:367–75. doi: 10.1006/exnr.1996.0038
8. Bohlen CJ, Bennett FC, Tucker AF, Collins HY, Mulinyawe SB, Barres BA. Diverse requirements for microglial survival, specification, and function revealed by defined-medium cultures. *Neuron.* (2017) 94:759–73.e8. doi: 10.1016/j.neuron.2017.04.043
9. Bernier LP, Bohlen CJ, York EM, Choi HB, Kamyabi A, Dissing-Olesen L, et al. Nanoscale surveillance of the brain by microglia via cAMP-Regulated filopodia. *Cell Rep.* (2019) 27:2895–908.e4. doi: 10.1016/j.celrep.2019.05.010
10. Ogaki A, Araki T, Ishikawa M, Ikegaya Y, Koyama R. A live imaging-friendly slice culture method using collagen membranes. *Neuropsychopharmacol Rep.* (2020) 40:307–13. doi: 10.1002/npr2.12128
11. Abiega O, Beccari S, Diaz-Aparicio I, Nadjar A, Layé S, Leyrolle Q, et al. Neuronal hyperactivity disturbs ATP microgradients, impairs microglial motility, and reduces phagocytic receptor expression triggering apoptosis/microglial phagocytosis uncoupling. *PLoS Biol.* (2016) 14:e1002466. doi: 10.1371/journal.pbio.1002466
12. Askew K, Li K, Olmos-Alonso A, Garcia-Moreno F, Liang Y, Richardson P, et al. Coupled proliferation and apoptosis maintain the rapid turnover of microglia in the adult brain. *Cell Rep.* (2017) 18:391–405. doi: 10.1016/j.celrep.2016.12.041
13. Badimon A, Strasburger HJ, Ayata P, Chen X, Nair A, Ikegami A, et al. Negative feedback control of neuronal activity by microglia. *Nature.* (2020) 586:417–23. doi: 10.1038/s41586-020-2777-8
14. Brawek B, Liang Y, Savitska D, Li K, Fomin-Thunemann N, Kovalchuk Y, et al. A new approach for ratiometric *in vivo* calcium imaging of microglia. *Sci Rep.* (2017) 7:6030. doi: 10.1038/s41598-017-05952-3
15. Casano AM, Albert M, Peri F. Developmental apoptosis mediates entry and positioning of microglia in the zebrafish brain. *Cell Rep.* (2016) 16:897–906. doi: 10.1016/j.celrep.2016.06.033
16. Cruz-Martin A, Portera-Cailliau C. *In vivo* imaging of axonal and dendritic structures in neonatal mouse cortex. *Cold Spring Harb Protoc.* (2014) 2014:57–64. doi: 10.1101/pdb.prot080150
17. Damisah EC, Hill RA, Rai A, Chen F, Rothlin CV, Ghosh S, et al. Astrocytes and microglia play orchestrated roles and respect phagocytic territories during neuronal corpse removal *in vivo*. *Sci Adv.* (2020) 6:eaba3239. doi: 10.1126/sciadv.aba3239
18. Davalos D, Akassoglou K. *In vivo* imaging of the mouse spinal cord using two-photon microscopy. *J Vis Exp.* (2012) e2760. doi: 10.3791/2760
19. Davalos D, Ryu JK, Merlini M, Baeten KM, Le Moan N, Petersen MA, et al. Fibrinogen-induced perivascular microglial clustering is required for the development of axonal damage in neuroinflammation. *Nat Commun.* (2012) 3:1227. doi: 10.1038/ncomms2230
20. Dibaj P, Nadrigny F, Steffens H, Scheller A, Hirrlinger J, Schomburg ED, et al. NO mediates microglial response to acute spinal cord injury under ATP control *in vivo*. *Glia.* (2010) 58:1133–44. doi: 10.1002/glia.20993
21. Eichhoff G, Brawek B, Garaschuk O. Microglial calcium signal acts as a rapid sensor of single neuron damage *in vivo*. *Biochim Biophys Acta.* (2011) 1813:1014–24. doi: 10.1016/j.bbamcr.2010.10.018
22. Füger P, Hefendehl JK, Veeraraghavalu K, Wendeln AC, Schlosser C, Obermüller U, et al. Microglia turnover with aging and in an Alzheimer's model via long-term *in vivo* single-cell imaging. *Nat Neurosci.* (2017) 20:1371–6. doi: 10.1038/nn.4631
23. Grier BD, Belluscio L, Cheetham CE. Olfactory sensory activity modulates microglial-neuronal interactions during dopaminergic cell loss in the olfactory bulb. *Front Cell Neurosci.* (2016) 10:178. doi: 10.3389/fncel.2016.00178
24. Grutzendler J, Yang G, Pan F, Parkhurst CN, Gan WB. Transcranial two-photon imaging of the living mouse brain. *Cold Spring Harb Protoc.* (2011) 2011:1080–8. doi: 10.1101/pdb.prot065474
25. Gu L, Kleiber S, Schmid L, Nebeling F, Chamoun M, Steffen J, et al. Long-term *in vivo* imaging of dendritic spines in the hippocampus reveals structural plasticity. *J Neurosci.* (2014) 34:13948–53. doi: 10.1523/JNEUROSCI.1464-14.2014
26. Haynes SE, Hollopeter G, Yang G, Kurpius D, Dailey ME, Gan WB, et al. The P2Y12 receptor regulates microglial activation by extracellular nucleotides. *Nat Neurosci.* (2006) 9:1512–9. doi: 10.1038/nn1805
27. Herzog C, Pons Garcia L, Keatinge M, Greenald D, Moritz C, Peri F, et al. Rapid clearance of cellular debris by microglia limits secondary neuronal cell death after brain injury. *Development.* (2019) 146:dev174698. doi: 10.1242/dev.174698
28. Hill RA, Li AM, Grutzendler J. Lifelong cortical myelin plasticity and age-related degeneration in the live mammalian brain. *Nat Neurosci.* (2018) 21:683–95. doi: 10.1038/s41593-018-0120-6
29. Hristovska I, Verdonk F, Comte JC, Tsai ES, Desestret V, Honnorat J, et al. Ketamine/xylazine and barbiturates modulate microglial morphology and motility differently in a mouse model. *PLoS ONE.* (2020) 15:e0236594. doi: 10.1371/journal.pone.0236594
30. Hutter G, Theruvath J, Graef CM, Zhang M, Schoen MK, Manz EM, et al. Microglia are effector cells of CD47-SIRPα antiphagocytic axis disruption against glioblastoma. *Proc Natl Acad Sci USA.* (2019) 116:997–1006. doi: 10.1073/pnas.1721434116
31. Isshiki M, Okabe S. Evaluation of cranial window types for *in vivo* two-photon imaging of brain microstructures. *Microscopy.* (2014) 63:53–63. doi: 10.1093/jmicro/dft043
32. Li Y, Du XF, Liu CS, Wen ZL, Du JL. Reciprocal regulation between resting microglial dynamics and neuronal activity *in vivo*. *Dev Cell.* (2012) 23:1189–202. doi: 10.1016/j.devcel.2012.10.027
33. Liu YU, Ying Y, Li Y, Eyo UB, Chen T, Zheng J, et al. Neuronal network activity controls microglial process surveillance in awake mice via norepinephrine signaling. *Nat Neurosci.* (2019) 22:1771–81. doi: 10.1038/s41593-019-0511-3
34. Miyamoto A, Wake H, Ishikawa AW, Eto K, Shibata K, Murakoshi H, et al. Microglia contact induces synapse formation in developing somatosensory cortex. *Nat Commun.* (2016) 7:12540. doi: 10.1038/ncomms12540
35. Morsch M, Radford R, Lee A, Don EK, Badrock AP, Hall TE, et al. *In vivo* characterization of microglial engulfment of dying neurons in the zebrafish spinal cord. *Front Cell Neurosci.* (2015) 9:321. doi: 10.3389/fncel.2015.00321
36. Olmedillas Del Moral M, Asavapanumas N, Uzcátegui NL, Garaschuk O. Healthy brain aging modifies microglial calcium signaling *in vivo*. *Int J Mol Sci.* (2019) 20:589. doi: 10.3390/ijms20030589
37. Parkhurst CN, Yang G, Ninan I, Savas JN, Yates JR, Lafaille JJ, et al. Microglia promote learning-dependent synapse formation through brain-derived neurotrophic factor. *Cell.* (2013) 155:1596–609. doi: 10.1016/j.cell.2013.11.030
38. Peri F, Nüsslein-Volhard C. Live imaging of neuronal degradation by microglia reveals a role for v0-ATPase a1 in phagosomal fusion *in vivo*. *Cell.* (2008) 133:916–27. doi: 10.1016/j.cell.2008.04.037
39. Pozner A, Xu B, Palumbos S, Gee JM, Tvrdik P, Capecchi MR. Intracellular calcium dynamics in cortical microglia responding to focal laser injury in the PC::G5-tdT reporter mouse. *Front Mol Neurosci.* (2015) 8:12. doi: 10.3389/fnmol.2015.00012
40. Pryazhnikov E, Mugantseva E, Casarotto P, Kolikova J, Fred SM, Toptunov D, et al. Longitudinal two-photon imaging in somatosensory

cortex of behaving mice reveals dendritic spine formation enhancement by subchronic administration of low-dose ketamine. *Sci Rep.* (2018) 8:6464. doi: 10.1038/s41598-018-24933-8
41. Stowell RD, Sipe GO, Dawes RP, Batchelor HN, Lordy KA, Whitelaw BS, et al. Noradrenergic signaling in the wakeful state inhibits microglial surveillance and synaptic plasticity in the mouse visual cortex. *Nat Neurosci.* (2019) 22:1782–92. doi: 10.1038/s41593-019-0514-0
42. Sun W, Suzuki K, Toptunov D, Stoyanov S, Yuzaki M, Khiroug L, et al. Two-photon imaging of anesthesia-specific alterations in microglial surveillance and photodamage-directed motility in mouse cortex. *Front Neurosci.* (2019) 13:421. doi: 10.3389/fnins.2019.00421
43. Taylor S, Mehina E, White E, Reeson P, Yongblah K, Doyle KP, et al. Suppressing interferon-γ stimulates microglial responses and repair of microbleeds in the diabetic brain. *J Neurosci.* (2018) 38:8707–22. doi: 10.1523/JNEUROSCI.0734-18.2018
44. Tremblay M, Lowery RL, Majewska AK. Microglial interactions with synapses are modulated by visual experience. *PLoS Biol.* (2010) 8:e1000527. doi: 10.1371/journal.pbio.1000527
45. Umpierre AD, Bystrom LL, Ying Y, Liu YU, Worrell G, Wu LJ. Microglial calcium signaling is attuned to neuronal activity in awake mice. *Elife.* (2020) 9:e56502. doi: 10.7554/eLife.56502
46. Yang G, Pan F, Parkhurst CN, Grutzendler J, Gan WB. Thinned-skull cranial window technique for long-term imaging of the cortex in live mice. *Nat Protoc.* (2010) 5:201–8. doi: 10.1038/nprot.2009.222
47. Yu X, Zuo Y. Two-photon *in vivo* imaging of dendritic spines in the mouse cortex using a thinned-skull preparation. *J Vis Exp.* (2014) 87:51520. doi: 10.3791/51520
48. Dorand RD, Barkauskas DS, Evans TA, Petrosiute A, Huang AY. Comparison of intravital thinned skull and cranial window approaches to study CNS immunobiology in the mouse cortex. *Intravital.* (2014) 3:e29728. doi: 10.4161/intv.29728
49. Shih AY, Driscoll JD, Drew PJ, Nishimura N, Schaffer CB, Kleinfeld D. Two-photon microscopy as a tool to study blood flow and neurovascular coupling in the rodent brain. *J Cereb Blood Flow Metab.* (2012) 32:1277–309. doi: 10.1038/jcbfm.2011.196
50. Huh Y, Cho J. Urethane anesthesia depresses activities of thalamocortical neurons and alters its response to nociception in terms of dual firing modes. *Front Behav Neurosci.* (2013) 7:141. doi: 10.3389/fnbeh.2013.00141
51. Li N, Lee B, Liu RJ, Banasr M, Dwyer JM, Iwata M, et al. mTOR-dependent synapse formation underlies the rapid antidepressant effects of NMDA antagonists. *Science.* (2010) 329:959–64. doi: 10.1126/science.1190287
52. Madry C, Kyrargyri V, Arancibia-Cárcamo IL, Jolivet R, Kohsaka S, Bryan RM, et al. Microglial ramification, surveillance, and interleukin-1β release are regulated by the two-pore domain K. *Neuron.* (2018) 97:299–312.e6. doi: 10.1016/j.neuron.2017.12.002
53. Xu J, Wang T, Wu Y, Jin W, Wen Z. Microglia colonization of developing zebrafish midbrain is promoted by apoptotic neuron and lysophosphatidylcholine. *Dev Cell.* (2016) 38:214–22. doi: 10.1016/j.devcel.2016.06.018
54. Swinnen N, Smolders S, Avila A, Notelaers K, Paesen R, Ameloot M, et al. Complex invasion pattern of the cerebral cortex by microglial cells during development of the mouse embryo. *Glia.* (2013) 61:150–63. doi: 10.1002/glia.22421
55. Ginhoux F, Greter M, Leboeuf M, Nandi S, See P, Gokhan S, et al. Fate mapping analysis reveals that adult microglia derive from primitive macrophages. *Science.* (2010) 330:841–5. doi: 10.1126/science.1194637
56. Eyo UB, Miner SA, Weiner JA, Dailey ME. Developmental changes in microglial mobilization are independent of apoptosis in the neonatal mouse hippocampus. *Brain Behav Immun.* (2016) 55:49–59. doi: 10.1016/j.bbi.2015.11.009
57. Paolicelli RC, Bolasco G, Pagani F, Maggi L, Scianni M, Panzanelli P, et al. Synaptic pruning by microglia is necessary for normal brain development. *Science.* (2011) 333:1456–8. doi: 10.1126/science.1202529
58. Schafer DP, Lehrman EK, Kautzman AG, Koyama R, Mardinly AR, Yamasaki R, et al. Microglia sculpt postnatal neural circuits in an activity and complement-dependent manner. *Neuron.* (2012) 74:691–705. doi: 10.1016/j.neuron.2012.03.026
59. Baker H, Morel K, Stone DM, Maruniak JA. Adult naris closure profoundly reduces tyrosine hydroxylase expression in mouse olfactory bulb. *Brain Res.* (1993) 614:109–16. doi: 10.1016/0006-8993(93)91023-l
60. Sawada M, Kaneko N, Inada H, Wake H, Kato Y, Yanagawa Y, et al. Sensory input regulates spatial and subtype-specific patterns of neuronal turnover in the adult olfactory bulb. *J Neurosci.* (2011) 31:11587–96. doi: 10.1523/JNEUROSCI.0614-11.2011
61. Gholamin S, Mitra SS, Feroze AH, Liu J, Kahn SA, Zhang M, et al. Disrupting the CD47-SIRPα anti-phagocytic axis by a humanized anti-CD47 antibody is an efficacious treatment for malignant pediatric brain tumors. *Sci Transl Med.* (2017) 9:eaaf2968. doi: 10.1126/scitranslmed.aaf2968
62. Avignone E, Lepleux M, Angibaud J, Nägerl UV. Altered morphological dynamics of activated microglia after induction of status epilepticus. *J Neuroinflammation.* (2015) 12:202. doi: 10.1186/s12974-015-0421-6
63. Carbonell WS, Murase S, Horwitz AF, Mandell JW. Migration of perilesional microglia after focal brain injury and modulation by CC chemokine receptor 5: an in situ time-lapse confocal imaging study. *J Neurosci.* (2005) 25:7040–7. doi: 10.1523/JNEUROSCI.5171-04.2005
64. Dissing-Olesen L, LeDue JM, Rungta RL, Hefendehl JK, Choi HB, MacVicar BA. Activation of neuronal NMDA receptors triggers transient ATP-mediated microglial process outgrowth. *J Neurosci.* (2014) 34:10511–27. doi: 10.1523/JNEUROSCI.0405-14.2014
65. Eyo U, Dailey ME. Effects of oxygen-glucose deprivation on microglial mobility and viability in developing mouse hippocampal tissues. *Glia.* (2012) 60:1747–60. doi: 10.1002/glia.22394
66. Eyo UB, Peng J, Swiatkowski P, Mukherjee A, Bispo A, Wu LJ. Neuronal hyperactivity recruits microglial processes via neuronal NMDA receptors and microglial P2Y12 receptors after status epilepticus. *J Neurosci.* (2014) 34:10528–40. doi: 10.1523/JNEUROSCI.0416-14.2014
67. Eyo UB, Peng J, Murugan M, Mo M, Lalani A, Xie P, et al. Regulation of physical microglia-neuron interactions by fractalkine signaling after status epilepticus. *eNeuro.* (2016) 3:ENEURO.0209-16.2016. doi: 10.1523/ENEURO.0209-16.2016
68. Fontainhas AM, Wang M, Liang KJ, Chen S, Mettu P, Damani M, et al. Microglial morphology and dynamic behavior is regulated by ionotropic glutamatergic and GABAergic neurotransmission. *PLoS ONE.* (2011) 6:e15973. doi: 10.1371/journal.pone.0015973
69. Gyoneva S, Traynelis SF. Norepinephrine modulates the motility of resting and activated microglia via different adrenergic receptors. *J Biol Chem.* (2013) 288:15291–302. doi: 10.1074/jbc.M113.458901
70. Gyoneva S, Davalos D, Biswas D, Swanger SA, Garnier-Amblard E, Loth F, et al. Systemic inflammation regulates microglial responses to tissue damage *in vivo*. *Glia.* (2014) 62:1345–60. doi: 10.1002/glia.22686
71. Matyash M, Zabiegalov O, Wendt S, Matyash V, Kettenmann H. The adenosine generating enzymes CD39/CD73 control microglial processes ramification in the mouse brain. *PLoS ONE.* (2017) 12:e0175012. doi: 10.1371/journal.pone.0175012
72. Zhao X, Liao Y, Morgan S, Mathur R, Feustel P, Mazurkiewicz J, et al. Noninflammatory changes of microglia are sufficient to cause epilepsy. *Cell Rep.* (2018) 22:2080–93. doi: 10.1016/j.celrep.2018.02.004
73. Pfeiffer T, Avignone E, Nägerl UV. Induction of hippocampal long-term potentiation increases the morphological dynamics of microglial processes and prolongs their contacts with dendritic spines. *Sci Rep.* (2016) 6:32422. doi: 10.1038/srep32422
74. Rotterman TM, Alvarez FJ. Microglia dynamics and interactions with motoneurons axotomized after nerve injuries revealed by two-photon imaging. *Sci Rep*. (2020) 10:8648. doi: 10.1038/s41598-020-65363-9
75. Swiatkowski P, Murugan M, Eyo UB, Wang Y, Rangaraju S, Oh SB, et al. Activation of microglial P2Y12 receptor is required for outward potassium currents in response to neuronal injury. *Neuroscience.* (2016) 318:22–33. doi: 10.1016/j.neuroscience.2016.01.008
76. Wu LJ, Vadakkan KI, Zhuo M. ATP-induced chemotaxis of microglial processes requires P2Y receptor-activated initiation of outward potassium currents. *Glia.* (2007) 55:810–21. doi: 10.1002/glia.20500
77. Zhao L, Zabel MK, Wang X, Ma W, Shah P, Fariss RN, et al. Microglial phagocytosis of living photoreceptors contributes to inherited retinal degeneration. *EMBO Mol Med.* (2015) 7:1179–97. doi: 10.15252/emmm.201505298

78. Greenhalgh AD, Zarruk JG, Healy LM, Baskar Jesudasan SJ, Jhelum P, Salmon CK, et al. Peripherally derived macrophages modulate microglial function to reduce inflammation after CNS injury. *PLoS Biol.* (2018) 16:e2005264. doi: 10.1371/journal.pbio.2005264
79. Hattori Y, Naito Y, Tsugawa Y, Nonaka S, Wake H, Nagasawa T, et al. Transient microglial absence assists postmigratory cortical neurons in proper differentiation. *Nat Commun.* (2020) 11:1631. doi: 10.1038/s41467-020-15409-3
80. Katayama T, Kobayashi H, Okamura T, Yamasaki-Katayama Y, Kibayashi T, Kimura H, et al. Accumulating microglia phagocytose injured neurons in hippocampal slice cultures: involvement of p38 MAP kinase. *PLoS ONE.* (2012) 7:e40813. doi: 10.1371/journal.pone.0040813
81. Neumann J, Sauerzweig S, Rönicke R, Gunzer F, Dinkel K, Ullrich O, et al. Microglia cells protect neurons by direct engulfment of invading neutrophil granulocytes: a new mechanism of CNS immune privilege. *J Neurosci.* (2008) 28:5965–75. doi: 10.1523/JNEUROSCI.0060-08.2008
82. Ohsawa K, Irino Y, Sanagi T, Nakamura Y, Suzuki E, Inoue K, et al. P2Y12 receptor-mediated integrin-beta1 activation regulates microglial process extension induced by ATP. *Glia.* (2010) 58:790–801. doi: 10.1002/glia.20963
83. Petersen MA, Dailey ME. Diverse microglial motility behaviors during clearance of dead cells in hippocampal slices. *Glia.* (2004) 46:195–206. doi: 10.1002/glia.10362
84. Weinhard L, di Bartolomei G, Bolasco G, Machado P, Schieber NL, Neniskyte U, et al. Microglia remodel synapses by presynaptic trogocytosis and spine head filopodia induction. *Nat Commun.* (2018) 9:1228. doi: 10.1038/s41467-018-03566-5
85. Zhang F, Nance E, Alnasser Y, Kannan R, Kannan S. Microglial migration and interactions with dendrimer nanoparticles are altered in the presence of neuroinflammation. *J Neuroinflammation.* (2016) 13:65. doi: 10.1186/s12974-016-0529-3
86. Kasahara Y, Koyama R, Ikegaya Y. Depth and time-dependent heterogeneity of microglia in mouse hippocampal slice cultures. *Neurosci Res.* (2016) 111:64–9. doi: 10.1016/j.neures.2016.05.001
87. Zhang Y, Zhao L, Wang X, Ma W, Lazere A, Qian HH, et al. Repopulating retinal microglia restore endogenous organization and function under CX3CL1-CX3CR1 regulation. *Sci Adv.* (2018) 4:eaap8492. doi: 10.1126/sciadv.aap8492
88. Cunningham CL, Martínez-Cerdeño V, Noctor SC. Microglia regulate the number of neural precursor cells in the developing cerebral cortex. *J Neurosci.* (2013) 33:4216–33. doi: 10.1523/JNEUROSCI.3441-12.2013
89. Frakes AE, Ferraiuolo L, Haidet-Phillips AM, Schmelzer L, Braun L, Miranda CJ, et al. Microglia induce motor neuron death via the classical NF-κB pathway in amyotrophic lateral sclerosis. *Neuron.* (2014) 81:1009–23. doi: 10.1016/j.neuron.2014.01.013
90. Hupp S, Grandgirard D, Mitchell TJ, Leib SL, Hathaway LJ, Iliev AI. Pneumolysin and the bacterial capsule of *Streptococcus pneumoniae* cooperatively inhibit taxis and motility of microglia. *J Neuroinflammation.* (2019) 16:105. doi: 10.1186/s12974-019-1491-7
91. Kraft AD, Kaltenbach LS, Lo DC, Harry GJ. Activated microglia proliferate at neurites of mutant huntingtin-expressing neurons. *Neurobiol Aging.* (2012) 33:621.e617-633. doi: 10.1016/j.neurobiolaging.2011.02.015
92. Sellgren CM, Gracias J, Watmuff B, Biag JD, Thanos JM, Whittredge PB, et al. Increased synapse elimination by microglia in schizophrenia patient-derived models of synaptic pruning. *Nat Neurosci.* (2019) 22:374–85. doi: 10.1038/s41593-018-0334-7
93. Montilla A, Zabala A, Matute C, Domercq M. Functional and metabolic characterization of microglia culture in a defined medium. *Front Cell Neurosci.* (2020) 14:22. doi: 10.3389/fncel.2020.00022
94. Rizzi C, Tiberi A, Giustizieri M, Marrone MC, Gobbo F, Carucci NM, et al. NGF steers microglia toward a neuroprotective phenotype. *Glia.* (2018) 66:1395–1416. doi: 10.1002/glia.23312
95. Wollmer MA, Lucius R, Wilms H, Held-Feindt J, Sievers J, Mentlein R. ATP and adenosine induce ramification of microglia *in vitro*. *J Neuroimmunol.* (2001) 115:19–27. doi: 10.1016/s0165-5728(01)00257-0
96. Tam WY, Au NP, Ma CH. The association between laminin and microglial morphology *in vitro*. *Sci Rep.* (2016) 6:28580. doi: 10.1038/srep28580
97. Collins HY, Bohlen CJ. Isolation and culture of rodent microglia to promote a dynamic ramified morphology in serum-free medium. *J Vis Exp.* (2018) 57122. doi: 10.3791/57122
98. Suzumura A, Sawada M, Yamamoto H, Marunouchi T. Effects of colony stimulating factors on isolated microglia *in vitro*. *J Neuroimmunol.* (1990) 30:111–20. doi: 10.1016/0165-5728(90)90094-4
99. Eder C, Klee R, Heinemann U. Involvement of stretch-activated Cl^- channels in ramification of murine microglia. *J Neurosci.* (1998) 18:7127–37.
100. Hellwig S, Brioschi S, Dieni S, Frings L, Masuch A, Blank T, et al. Altered microglia morphology and higher resilience to stress-induced depression-like behavior in CX3CR1-deficient mice. *Brain Behav Immun.* (2016) 55:126–37. doi: 10.1016/j.bbi.2015.11.008
101. Socodato R, Henriques JF, Portugal CC, Almeida TO, Tedim-Moreira J, Alves RL, et al. Daily alcohol intake triggers aberrant synaptic pruning leading to synapse loss and anxiety-like behavior. *Sci Signal.* (2020) 13:eaba5754. doi: 10.1126/scisignal.aba5754
102. Bisht K, Sharma KP, Lecours C, Sánchez MG, El Hajj H, Milior G, et al. Dark microglia: a new phenotype predominantly associated with pathological states. *Glia.* (2016) 64:826–39. doi: 10.1002/glia.22966
103. Bennett MR. Synaptic P2X7 receptor regenerative-loop hypothesis for depression. *Aust N Z J Psychiatry.* (2007) 41:563–71. doi: 10.1080/00048670701399994
104. Tremblay M, Stevens B, Sierra A, Wake H, Bessis A, Nimmerjahn A. The role of microglia in the healthy brain. *J Neurosci.* (2011) 31:16064–9. doi: 10.1523/JNEUROSCI.4158-11.2011
105. Schafer DP, Lehrman EK, Stevens B. The "quad-partite" synapse: microglia-synapse interactions in the developing and mature CNS. *Glia.* (2013) 61:24–36. doi: 10.1002/glia.22389
106. Ventura R, Harris KM. Three-dimensional relationships between hippocampal synapses and astrocytes. *J Neurosci.* (1999) 19:6897–906.
107. Genoud C, Quairiaux C, Steiner P, Hirling H, Welker E, Knott GW. Plasticity of astrocytic coverage and glutamate transporter expression in adult mouse cortex. *PLoS Biol.* (2006) 4:e343. doi: 10.1371/journal.pbio.0040343
108. Shin Y, Choi SH, Kim E, Bylykbashi E, Kim JA, Chung S, et al. Blood-brain barrier dysfunction in a 3D *in vitro* model of Alzheimer's disease. *Adv Sci.* (2019) 6:1900962. doi: 10.1002/advs.201900962
109. Shimizu A, Goh WH, Itai S, Hashimoto M, Miura S, Onoe H. ECM-based microchannel for culturing *in vitro* vascular tissues with simultaneous perfusion and stretch. *Lab Chip.* (2020) 20:1917–27. doi: 10.1039/d0lc00254b
110. Goshi N, Morgan RK, Lein PJ, Seker E. A primary neural cell culture model to study neuron, astrocyte, and microglia interactions in neuroinflammation. *J Neuroinflammation.* (2020) 17:155. doi: 10.1186/s12974-020-01819-z

Conflict of Interest: The authors declare that the research was conducted in the absence of any commercial or financial relationships that could be construed as a potential conflict of interest.

frontiers in Immunology

REVIEW
published: 06 May 2021
doi: 10.3389/fimmu.2021.675660

Microglia: A Double-Edged Sword in Intracerebral Hemorrhage From Basic Mechanisms to Clinical Research

Jiachen Liu[1†], Lirong Liu[2†], Xiaoyu Wang[1], Rundong Jiang[1], Qinqin Bai[2] and Gaiqing Wang[3]*

[1] Xiangya Medical College of Central South University, Changsha, China, [2] Department of Neurology, Shanxi Medical University, Taiyuan, China, [3] Department of Neurology, Sanya Central Hospital (Hainan Third People's Hospital), Sanya, China

OPEN ACCESS

Edited by:
Amanda Sierra, Achucarro Basque Center for Neuroscience, Spain

Reviewed by:
Adam Denes, Institute of Experimental Medicine (MTA), Hungary
Susanne Kooistra, University Medical Center Groningen, Netherlands

***Correspondence:**
Gaiqing Wang
wanggq08@126.com;
wanggq08@163.com
orcid.org/0000-0002-8977-1383

[†]These authors have contributed equally to this work

Specialty section:
This article was submitted to Multiple Sclerosis and Neuroimmunology, a section of the journal Frontiers in Immunology

Received: *03 March 2021*
Accepted: *19 April 2021*
Published: *06 May 2021*

Citation:
Liu J, Liu L, Wang X, Jiang R, Bai Q and Wang G (2021) Microglia: A Double-Edged Sword in Intracerebral Hemorrhage From Basic Mechanisms to Clinical Research. Front. Immunol. 12:675660. doi: 10.3389/fimmu.2021.675660

Microglia are the resident immune cells of the central nervous system (CNS). It is well established that microglia are activated and polarized to acquire different inflammatory phenotypes, either pro-inflammatory or anti-inflammatory phenotypes, which act as a critical component in the neuroinflammation following intracerebral hemorrhage (ICH). Microglia produce pro-inflammatory mediators at the early stages after ICH onset, anti-inflammatory microglia with neuroprotective effects appear to be suppressed. Previous research found that driving microglia towards an anti-inflammatory phenotype could restrict inflammation and engulf cellular debris. The principal objective of this review is to analyze the phenotypes and dynamic profiles of microglia as well as their shift in functional response following ICH. The results may further the understanding of the body's self-regulatory functions involving microglia following ICH. On this basis, suggestions for future clinical development and research are provided.

Keywords: intracerebral hemorrhage, microglia, phenotype switch, neuroimmunology, neuroinflammation

INTRODUCTION

Microglia constitute 5% to 10% of adult brain cells and form the largest group of immune cells in the CNS (1). The primary source of microglia is yolk sac erythromyeloid precursors (EMPs) that migrate into the brain rudiment during embryo development (2). Under physiological conditions, microglia self-renew for the entire lifespan of the organism and interact with numerous other cells in the brain, such as astrocytes, neurons, and oligodendrocytes (3). Mounting evidence suggests that microglia, as brain resident immune cells, play an essential role in maintaining normal brain function. When pathologic changes disrupt homeostasis in the brain, microglia are activated to exert regulatory effects (4). Microglia are highly diverse, and their phenotype depends on the context and type of stressor or pathology (5). Specifically, during the different periods after intracerebral hemorrhage (ICH), microglia may polarize to produce pro-inflammatory mediators or acquire a more anti-inflammatory phenotype, which has a decisive influence on ICH progression (**Figure 1**) (6).

Pathological analysis of microglial activity during ICH has revealed that microglia induce potent immune responses after extravasation of blood into the brain (7). The strong inflammatory response in microglia is caused by the rapid accumulation of blood-derived products (e.g., hemoglobin, heme,

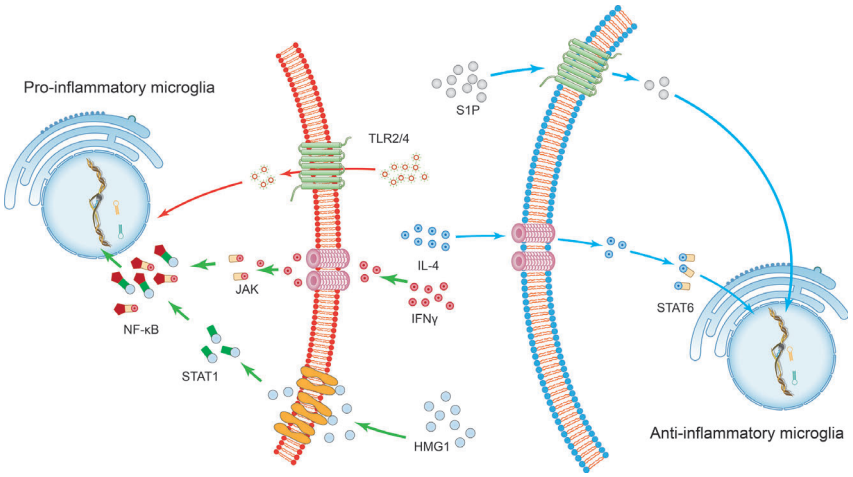

FIGURE 1 | The induction of microglial polarization by several transcription factors. Activation of high mobility histone 1 (HMG1) and Toll-like receptor (TLR) 2 or TLR4 promotes the pro-inflammatory phenotypic polarization of microglia. Interferon-gamma (IFN-γ) promotes the pro-inflammatory phenotypic polarization of microglia through the signaling sensors signal transducer and activator of transcription (STAT) 1 and Janus kinase (JAK). This series of processes involves the nuclear factor kappa B (NF-κB) signaling pathway. On the other hand, STAT6 accumulates under the action of IL-4 and is responsible for the transcription of M2 phenotype-related genes. The sphingosine-1-phosphate (S1P) receptor signaling pathway downregulates the expression of pro-inflammatory cytokines and enhances anti-inflammatory responses following intracerebral hemorrhage.

and iron) after ICH (8), which can directly damage the brain parenchyma, and a sustained microglia-mediated inflammatory response results in neurologic deterioration (9). Interestingly, Chang et al. (10) have experimentally proven that as early as 1 to 1.5 h after ICH, microglia respond to hemorrhagic injury and exhibit a protective alternative activation phenotype.

The role of microglia following ICH is complex, and the entirely different action of different phenotypes of microglia plays an essential role in the development of cerebral inflammatory injury and recovery of the brain after ICH (**Figure 2**). Besides, the neuroprotective effect of microglia may serve as promising targets for ICH treatment. For example, the primary role of activated microglia is to phagocytose the hematoma, thereby reducing ICH-induced brain swelling and neuronal loss and improving neurological deficits (11). Microglial depletion can lead to more severe brain swelling, neuronal loss, and functional defects following ICH (12).

The dual role of reactive microglia in inflammation processes has a biphasic influence on the brain, which acts as a double-edged offensive and defensive sword in brain injury. This paper reviews recent empirical studies on microglial activity following ICH to identify the most critical factors that influence this process, offering a fresh perspective for developing novel therapeutic strategies.

THE DUAL ROLE OF MICROGLIA AFTER ICH

The Effects of Microglia on the Blood-Brain Barrier Following ICH

Destruction of the blood-brain barrier (BBB) and consequent brain edema is the most common secondary causes of life-threatening events after ICH (13). One recent study by Chen et al. showed that microglia-derived TNF-α mediates endothelial necroptosis contributing to blood-brain-barrier disruption (14). Besides, activated microglia cause an imbalance between endogenous vasodilators and vasoconstrictors, further leading to edema formation after ICH (15).

Anti-inflammatory actions of microglia may mediate BBB protection and neural repair by producing anti-inflammatory cytokines, extracellular matrix proteins, glucocorticoids, and other substances (16). As signaling *via* IL-4 and IL-10 can induce an anti-inflammatory phenotype of microglia, it can be targeted for ICH treatment through modulating BBB physiology (17).

The Functions of Microglia in Secondary Brain Damage Following ICH

Intracranial hematoma is a crucial factor contributing to brain injury after ICH. Mechanical damage is induced in adjacent tissues due to compression and dissection. Simultaneously, iron, heme, and cytotoxic hemoglobin can be passively released due to the lysis of erythrocytes adjacent to the hematoma (18). Microglial phagocytosis of hematoma occurs before erythrocytes lysis to protect the brain (19, 20). This process can be regulated by alternative activation of microglia *via* activating the CCR4/ERK/Nrf2 pathway and peroxisome proliferator-activated receptor γ (PPAR-γ) (21–23) (**Figure 3**).

There is ample evidence that microglial activation is essential for secondary damage to the brain after ICH (24). For example, microglia also produce pro-inflammatory factors (TNF-α, IL-1β, IL-6) and chemokines (CXCL2), which promote neuroinflammation (25, 26). Besides, the absorption of hematoma may also trigger a series of inflammatory reactions leading to primary and secondary brain damage (27).

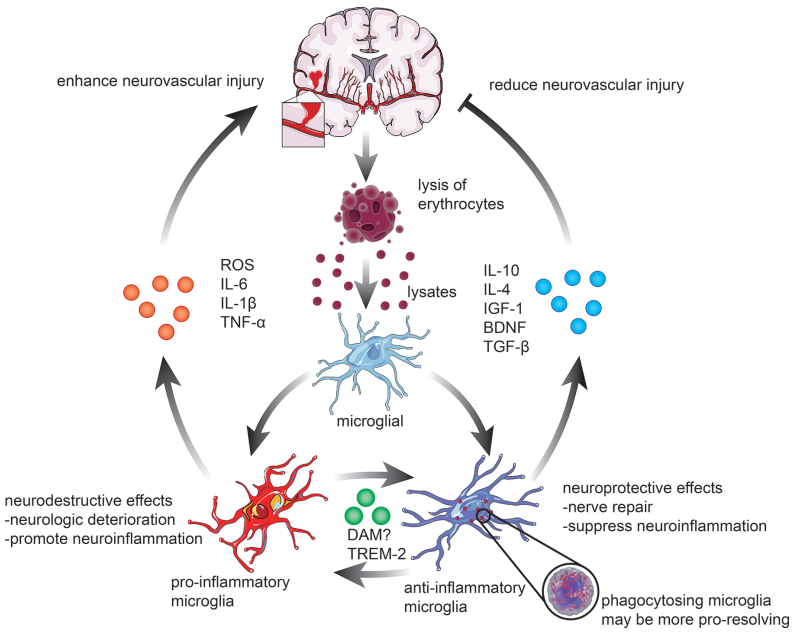

FIGURE 2 | Microglial activation and polarization following ICH. The polarization of microglia in response to stimulation with erythrocyte lysates after ICH can be broadly classified into two categories. 1) pro-inflammatory microglia elevate the levels of ROS, interleukin-6 (IL-6), interleukin-1β (IL-1β), and tumor necrosis factor-α (TNF-α), hence enhancing the pro-inflammatory and destructive effects of ICH on the brain. 2) anti-inflammatory microglia, on the contrary, mainly exert neuroprotective effects, including actions related to nerve repair and anti-inflammatory effects, through phagocytosis of lysates, which are always associated with higher expression of IL-10, IL-4, insulin-like growth factor-1 (IGF-1), brain-derived neurotrophic factor (BDNF), and transforming growth factor-β (TGF-β). In recent years, an increasing number of studies have revealed that microglia can also be polarized into neuroprotective and neurodestructive phenotypes, such as disease-associated microglia (DAM) and triggering receptor expressed on myeloid cells 2 (TREM2) phenotypes, which remain to be further investigated.

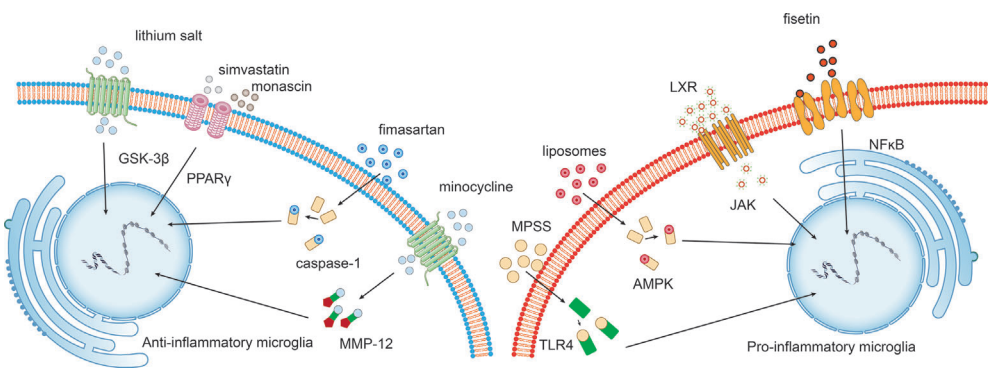

FIGURE 3 | Potential intervention strategies targeting the microglial phenotypic shift following ICH. Interventions that induce the polarization of pro-inflammatory microglia towards the anti-inflammatory phenotype exert beneficial effects following ICH. For example, fisetin mediates the NFκB pathway, and liver X receptor (LXR)-mediated JAK, liposome-mediated adenosine monophosphate-activated protein kinase (AMPK), and methylprednisolone sodium succinate (MPSS)-mediated TLR4 inhibit M1 microglia. While lithium salt mediates glycogen synthase kinase-3beta (GSK-3β) expression, simvastatin and monascin mediate peroxisome proliferator-activated receptor gamma (PPARγ) levels, fimasartan mediates caspase-1 levels, and minocycline upregulates matrix metalloproteinase 12 (MMP-12) expression.

MICROGLIAL POLARIZATION FOLLOWING ICH

Although the terminology of "microglia polarization" is still widely used in the literature, most commonly in the M1 and M2 phenotypes. Complex high-content experiment and multi-omics technologies, including transcriptomic, epigenomic, and proteomics, have found novel microglia polarization states beyond the standard M1/M2 dichotomy, which leads to a fierce debate in microglial M1/M2 polarization in recent years (28).

As early as 2013, Chiu and colleagues utilized flow cytometry and deep RNA sequencing of acutely isolated spinal cord microglia. The study aimed to prove that microglial reactions must be interpreted in light of the tissue in which the activating stimulus is present (29). However, the M1/M2 model is not a pure phenomenon *in vivo*, as previously proven by Butovsky, by profiling CNS cells with an MG400 microglial chip (30), which ignores the crucial concept demonstrated by Chiu et al. (30). Besides, transcriptionally distinguishable subpopulations of microglia that appear to be a transcriptional continuum of the local population of microglia can be detected during homeostasis (31, 32), representing a transcriptional basis for the microglia phenotype diversity (33).

Single-cell RNA-sequence analysis of microglia suggested converged expression of M1 and M2 markers due to the influence of disease-related inflammatory processes (34). Furthermore, precise categorization of different microglia or monocyte subtypes based on specific types and stages of pathology or their relation to specific tissue injury types is also possible (35). In conclusion, a precise definition of microglial polarization has proven elusive, and the description of M1 or M2 phenotypes is an oversimplification of the complex biology of microglia.

In a recent transcriptional single-cell study, Keren-Shaul et al. found that microglial phenotypes other than the M1/M2 phenotypes exist. For example, a new subpopulation named disease-associated microglia (DAM) has been discovered through genome-wide transcriptomic analyses of microglia under different disease conditions. Although the gene profile of DAM and M1 microglia partially overlapped, the molecular signatures have shown apparent differences (36). Interestingly, DAM also exhibits anti-inflammatory/phagocytic and pro-inflammatory profiles (37). Activation of DAM depends on triggering receptors expressed on myeloid cells 2 (TREM2), a receptor located mainly on the surface of microglia. TREM2 promotes the phagocytosis of apoptotic neurons producing tiny quantities of pro-inflammatory cytokines (38). Research has also shown that TREM2 is activated in perihematomal areas, which improved attenuated neuroinflammation and neuronal apoptosis after ICH (39). Besides, according to a study done by Gao et al. in 2019, CEBPα, IRF1, and LXRβ are likely regulators of pro-inflammatory and anti-inflammatory DAM states. Based on emerging findings, it is possible to conclude that DAM represents a switch that substantially alters microglial function (40). While the DAM concept has been widely used in neurodegenerative diseases such as Alzheimer's disease rather than ICH, it is clear that microglia is in a constant flux state and exquisitely sensitive to their environment.

Many studies have investigated the spatially and temporally restricted subsets of microglia during development and disease, further identifying the distinct molecular hallmarks and diverse cellular kinetics using massively parallel single-cell analysis and computational modeling (32, 41). For example, using single-cell RNA sequencing from human cerebral cortex samples, Olah et al. confirm the presence of four microglial subsets and elucidate the significance of subsets, such as the association with Alzheimer's disease (AD) (42). More recently, Ochocka et al. demonstrate cellular and functional heterogeneity of microglia using flow cytometry and scRNAseq. In this experiment, multiple microglial clusters were obtained, and gene expression profiles underlying a specific cluster could reflect different functions. Hom-MG and activated microglia (Act-MG) were identified, which shows the distinct spatial distribution in experimental gliomas (43). Furthermore, an environment-dependent transcriptional network specifying microglia-specific programs have been developed, which identified substantial subsets of microglia associate with neurodegenerative and behavioral diseases (44).

In summary, microglia are activated by various pathologic events or changes in brain homeostasis, which are highly diverse and depend on the context and type of stressor or pathology. The complicated functional roles of microglia support the existence of distinct pro-inflammatory and anti-inflammatory functional states following ICH. The significance of defining microglial subtypes is to identify novel microglial functional conditions; determine the impact of molecules on microglia types, and discover ways to mediate functions in healthy physiology or disease (45). During the ICH progress, most investigators continue to use the expression of M1/M2 markers and microglia polarization as a surrogate for a genuine mechanistic understanding of how microglial function changes (46). Therefore, it would be interesting to identify the regulators and influencing factors that contribute to the polarization of microglia towards a neuroprotective or neurodestructive phenotype, which may shed new light on the pathogenetic role of microglia following ICH.

Endogenous Mechanisms of Microglia

Much of the literature has emphasized the autoregulation of microglia during ICH progress. For example, studies by Wu et al. showed that soluble epoxide hydrolase expression is upregulated in microglia after ICH, which causes neuroinflammatory responses by degrading anti-inflammatory epoxyeicosatrienoic acid (47). Other studies have provided further evidence that microglial recruitment is associated with TWIK-related K+ channel 1 (TREK-1), which also triggers the secretion of pro-inflammatory factors such as IL-1β and TNF-α as well as cell adhesion molecules following ICH (48). Besides, low-density LRP1 in the neurovascular unit interacts with Mac-1 expressed by microglia to promote tPA-mediated activation of platelet-derived growth factor-cc (PDGF-cc). Activation of potential PDGF-cc and PDGF receptor-α signals can increase the permeability of the blood-brain barrier and deterioration following ICH (13).

Microglia have similarly been shown to be involved in anti-inflammatory and phagocytic effects on the hematoma, contributing to neurologic recovery after ICH. The correlation between regulatory T lymphocytes (Tregs) and neuroinflammatory response after ICH has been defined. In vitro experiments have demonstrated that Tregs modulate microglia polarization toward the anti-inflammation phenotype through the IL-10/GSK3β/PTEN axis in this regulatory process (49, 50).

The Regulatory Effect of miRNAs

As gene expression is regulated through genetic and epigenetic regulatory networks, there is growing evidence that miRNAs play essential roles in the microglial effects after ICH (51). For example, miRNA-7 (miR-7) can inhibit the expression of Toll-like receptor 4 (TLR4) and provoke a secondary microglia-mediated inflammatory response after ICH (52). Further studies have confirmed that agents that target TLR4 and miR-7, such as ligustilide (LIG) and senkyunolide H (SH), can exert neuroprotective effects against ICH by inhibiting Prx1/TLR4/NF-κB signaling *via* activation of microglia and astrocytes (53).

Recent studies have found that inhibition of miRNA-222 suppresses microglia-mediated inflammatory responses and improves neurological functions in a preclinical mouse model of ICH. Integrin subunit β8 (ITGB8) was identified as a directly negatively regulated target of miR−222 in microglial cells, leading to the attenuation of inflammation and apoptosis (54). Besides, miR-132 enhances the cholinergic blockade of the inflammatory response by targeting acetylcholinesterase (AChE), which also inhibits the activation of pro-inflammatory microglia and provides protection against neuronal death caused by ischemia (55).

Furthermore, as the critical factors in autophagy, miRNAs negatively regulate gene expression and autophagic activity of microglia. For example, miRNA-144 targets mTOR by directly interacting with 3′ untranslated regions (UTRs), which are involved in hemoglobin-mediated activation of microglial autophagy and inflammatory responses (56). The specific function of autophagy is dualistic and has been difficult to assess whether it has harmful or beneficial effects following ICH thus far. Despite many studies demonstrated that autophagy could enhance the protection of endoplasmic reticulum stress and reducing oxidative damage after ICH *via* clearing up the cell rubbish and oxidative-stress products (57, 58), recent studies showed autophagy positively regulates inflammation following ICH (59, 60).

Regulation of Microglia Function by Intracellular Signaling Following ICH

Anti-inflammatory microglia functions are accomplished by combining various signaling pathways that compose a complex network involved in multiple biological processes. Exploring the network of biological signaling pathways and its molecular basis contributes to novel interventions targeting signaling pathways that block the pathological progression of ICH (**Figure 3**).

The Roles of the AMPK Pathway and AdipoR1 in Microglia Function Following ICH

It has been demonstrated that adenosine monophosphate-activated protein kinase (AMPK) can drive the phenotypic shift from a pro-inflammatory state to an anti-inflammatory state (61). The expression of endogenous C1q/TNF-related protein 9 (CTRP9), an upstream trigger of the AMPK signaling pathway and an agonist of AdipoR1, is increased after ICH in animal models of long-term neurobehavior, peaking at 24 h after ICH. Further experiments have confirmed that the expression of AdipoR1 and p-AMPK can reduce the expression of inflammatory cytokines after ICH (62). Besides, the activation of MC4R also alleviates neurological deficits through the AMPK pathway following ICH, and interventions targeting MC4R, such as RO27-3225 administration, have been proven to be effective in animal experiments (63).

The Roles of the JNK Pathway in Microglia Function Following ICH

As mentioned above, Treg cells inhibit microglia-mediated inflammatory responses and improve neurological function *in vivo*, mainly by activate NF-κB through the JNK pathway (49, 64). There are controversies regarding the role of the JNK signaling pathway following ICH, which has received increased attention in the clinic in recent years. For example, the synthesis of the liver X receptor (LXR) agonist TO901317 was shown to exert specific effects in an ICH model by inhibiting JNK signaling. The hyperbaric oxygen preconditioning (HBOP) model of ICH has demonstrated the potential relevance between JNK phosphorylation and the immunological activity of anti-inflammatory microglia (65). As current practical limitations include drug side effects, uncertainties regarding efficacy, surgical injuries, and complications, there are no standardized clinical interventions for ICH except intracranial pressure-lowering therapies. Therefore, hyperbaric oxygen therapy provides a feasible alternative intervention with mild adverse effects against ICH, and the mechanism of HBOP in ICH needs further exploration and verification.

The Impact of the Toll-like Receptor 4 (TLR-4) Pathway on Microglia Function

Toll-like receptor 4 (TLR4) plays a crucial role in the innate immune response. It can be concluded that loss of TLR4 reduces the recruitment of pro-inflammatory microglia and markedly alleviates inflammation around the hematoma in the animal model (66). Further studies have shown that TLR4 also inhibits the phagocytosis of microglia on the surface of red blood cells, resulting in hematoma absorption delay and severe neurological deficits in ICH patients (67). TLR4-mediated autophagy of microglial activation contributes to secondary brain injury and brain recovery and inflammatory damage following ICH (68).

The role of TLR4 in secondary brain damage following ICH has been elaborated in detail, and therapeutic strategies targeting TLR4 are relatively well-developed. Therefore, TLR4 remains a promising target for inhibiting undesired microglial responses, and interventions targeting TLR4-related pathways may represent future candidates for ICH therapy.

Regulation of Microglia Function by Extracellular Signals Following ICH

As the regulatory effects of intracellular signaling pathways on microglia after ICH have been discussed, the final section of this paper addresses how extracellular signaling regulators influence microglial morphology and function. Compared with intracellular signals, extracellular signals are more complicated and vulnerable to disruption, which means they have the

potential to be translated into clinically effective targeted therapies for ICH.

Interventions Targeting Microglia Functions for ICH

Interleukins

The interleukins (ILs) level is intimately associated with the development and progression of ICH, which may be achieved by modulation of microglia functions. For example, activation of the IL-4/transcription 6 (STAT6) axis improved long-term functional recovery in a mouse model of ICH (69). Conversely, expression of IL-15 exacerbates brain injury following ICH by mediate the crosstalk between microglia and astrocytes (70).

Besides, antibodies against IL-17A can prevent ICH-induced expression of TNF-α, IL-1β, and IL-6 and inhibit microglial activation (71). Further examination revealed that IL-17A promotes autophagy in pro-inflammatory microglia, thus maintaining the body's normal immune response and alleviating brain edema after ICH (60). Notably, recent studies have found that intraventricular infusion of IL-33 can alleviate neurological deficits following ICH by promoting the transformation of pro-inflammatory microglia (72). Deferroxamine (DFA) can also inhibit the activation of pro-inflammatory microglia by downregulating IL-1β and TNF expression, reducing secondary brain insult following ICH.

Nuclear Factor-κB

Evidence has suggested that NF-κB translocates to the nucleus, and pro-inflammatory mediators (NO, TNF-a, and IL-6) are produced following inflammatory response after ICH. These results suggest that combined targeting of NF-κB signaling pathway inhibition may be a more effective anti-neuroinflammatory strategy following ICH (53).

Regulation of NF-κB activity may also have promising clinical benefits following ICH. Analysis of thrombin toxicity *in vitro* shows that has thrombin release after ICH led to the increased expression of NF-κB in microglia (73, 74). Treatment modalities disrupting this harmful process, such as miR-181c mimic therapy, are expected to regulate thrombin-driven inflammation after cerebral hemorrhage (75).

Glycogen Synthase Kinase-3β

It is widely acknowledged that glycogen synthase kinase-3beta (GSK-3β) exerts a potent pro-inflammatory effect following ICH (76). Studies have shown that the hematoma volume is significantly decreased by GSK-3β inhibition after ICH due to enhanced microglia-mediated phagocytosis (77). Consistently, the GSK-3β inhibitor 6-bromoindirubin-3′-oxime (BIO) has been shown to relieve inflammation by blocking GSK-3β Tyr216 phosphorylation/activation following ICH. BIO may exert a protective effect against ICH by increasing the number of anti-inflammatory microglia through inactivating GSK-3β (78).

It is interesting to note that the molecular mechanism by which lithium salt can treat ICH in clinical practice has already been elucidated. Recently, it has been shown that LiCl treatment decreased the death of mature oligodendrocytes (OLGs) in ICH mice, which may be regulated by the LiCl-induced inhibition of glycogen synthase kinase-3β (GSK-3β) (79).

Peroxisome Proliferator-Activated Receptor Gamma (PPAR-γ)

The phagocytic activity of microglia is required to remove the hematoma after ICH; however, the pro-inflammatory mediators and free radicals released as a result of microglial activation and phagocytosis are toxic to neighboring cells and lead to secondary brain damage following ICH (80). ICH mouse model demonstrated that peroxisome proliferator-activated receptor gamma (PPAR-γ) prevents LPS-induced pro-inflammatory microglial activation while facilitating microglial polarization towards the anti-inflammatory phenotype (81). Besides, PPAR-γ promotes phagocytosis in a timely and effective manner, limiting the toxic effects of hemolysis by facilitating hematoma clearance following ICH (82).

Studies have demonstrated that PPAR-γ activation is imperative for enhancing the phagocytic ability of anti-inflammatory microglia by CD36 (18). Furthermore, 15(S)-hydroxyeicosatetraenoic acid, an exogenous PPAR-γ agonist, improves functional recovery following ICH and exerts neuroprotective effects (83).

Based on in-depth basic research, PPAR-γ agonists have been widely used in clinical treatment. For example, the neuroprotective effects of statins following ICH through PPAR-γ activation and enhancement of microglia-induced erythrocyte phagocytosis have been established (84). Besides, monascin, as a novel dual agonist of PPAR-γ and Nrf2, facilitates microglial phagocytosis of the hematoma and exerts neuroprotective effects following ICH (85, 86).

Caspase Family

Caspase-mediated cascades play an essential role in mediating anti-inflammatory microglial death (87). For example, AC-YVAD-CMK can alleviate brain edema by inhibiting the activation of pro-caspase-1 and downregulating the expression of inflammation-related factors, which is accompanied by decreasing activated microglia at 24 h post-ICH (88).

Clinical studies have found that fimasartan (an angiotensin II receptor blocker) significantly reduces the activation of the caspase-1 pathway after ICH (89), suggesting that it is effective in ICH by regulating caspase-1–mediated microglial autophagy.

Matrix Metalloproteinases (MMPs)

The first serious discussions of MMP-12, which is harmful and contributes to secondary damage after ICH, emerged in 2005 (90). Subsequent studies found that MMP-9 binds to injured neurons in culture, activates pro-inflammatory microglia, and exerts neurotoxic effects after ICH (91). Based on this, further research proposed that inhibition of MMP-9 improves prognosis following ICH (92).

MMP-mediated microglial activation has become a potential therapeutic target for ICH. For example, minocycline, a widely available drug that alleviates brain damage, effectively reduces early upregulation of MMP-12 expression (93, 94)and induces anti-inflammation microglial polarization, which reduces the levels of inflammatory cytokines and the number of microglia surrounding the hematoma after ICH (86). It should be noted that although the molecular mechanism is unclear, MMP-12 expression and microglial infiltration around the hematoma are

significantly reduced after stem cell transplantation following ICH (95, 96).

Iron Chelators

Iron overload is a significant cause of brain damage because iron toxicity contributes to pro-inflammatory microglial activation following collagenase-induced ICH. Therefore, reducing the accumulation of iron can moderately improve the outcomes after ICH (97). As an iron chelator, minocycline can reduce free iron and iron handling protein levels, thus prevent neuronal death (98). Besides, VK-28, a brain-permeable iron chelator, is superior to and less toxic than DFA following ICH (99, 100).

The evidence from observational studies shows that microglia function is controlled by complex regulatory networks (**Table 1**), an understanding of which is critical for elucidating phenotypic and genotypic variations in microglia and developing therapeutic interventions for ICH (**Figure 4**).

POTENTIAL THERAPEUTIC STRATEGIES TARGETING MICROGLIA FUNCTION AFTER ICH

Exploring the regulatory mechanism of microglial immunophenotype changes may help identify the hematoma scavenging mechanism and a precise therapeutic target for ICH. The multi-omics technologies have made significant achievements in the research of microglial activation (101). The application of systematic multi-omics approaches to precision medicine and systems biology has great potential to improve the care of patients with ICH. Notably, the target gene identified by multi-omics studies can potentially be used for drug repositioning in ICH, which is approved to be cheaper, quicker, and effective (102).

CONCLUSION

This review aimed to objectively discuss and assess the role of microglia in regulating neuronal injury after ICH. The findings indicate that pro-inflammatory or anti-inflammatory microglia have divergent effects, which have significant implications for understanding microglia function *via* intracellular and extracellular signal-regulated pathways. Besides, this review provides the first comprehensive assessment of cellular and molecular mechanisms and pathways responsible for regulating microglia, including an in-depth analysis of signaling pathways strongly associated with microglia following ICH. Notwithstanding the relatively limited number of reliable clinical trials and the lack of molecular genetic studies on the phenotypic change of microglia, this work offers valuable insights into a novel

TABLE 1 | Potential interventions for microglia polarization after intracerebral hemorrhage.

Phenotype	Activating signals (events)	Markers (events)	Result	Purpose
Pro-inflammatory microglia	JNK (TO901317, HBOP -)GSK-3β (Lithium, BIO -) miR-222 (Fisetin -) TLR4 (Ligustilide, Senkyunolide H, MPSS, Eupatilin -)miR-124 TREK-1	MMP (Minocycline, sinomenine -) Caspase-1 (AC-YVAD-CMK, Fimasartan -) TNF-αIL-1βNF-κB (ITGB8, Andrographolide -) IL-6 IL-1	Pro-inflammation	Neurological deficit
Anti-inflammatory microglia	TregsAMPK (CTRP9, AdipoR1 +)IL-33	TGF-βIL-10 (Atorvastatin +)Tregs MC4R (RO27-3225 +)	Phagocytosis Anti-inflammation	Neurological recovery

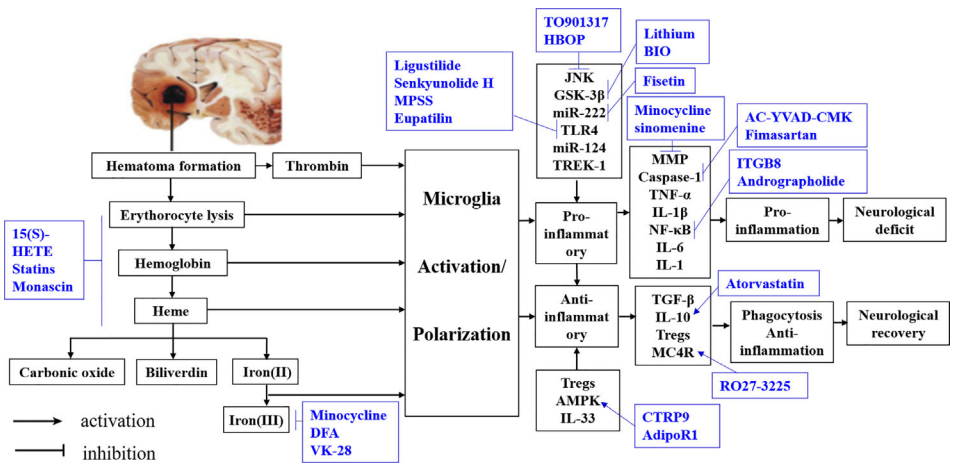

FIGURE 4 | Summary of interventions for ICH targeting microglial polarization. Available intervention strategies are labeled blue.

therapeutic strategy for ICH that targets microglia. Further research on interventions associated with microglial physiology is an essential next step in confirming a framework for assessing the feasibility of the novel therapy mentioned above.

DATA AVAILABILITY STATEMENT

The data that support the findings of this study are openly available in pubmed at https://pubmed.ncbi.nlm.nih.gov/. Data sharing is not applicable to this article as no new data were created or analyzed in this study.

AUTHOR CONTRIBUTIONS

All authors listed have made a substantial, direct and intellectual contribution to the work, and approved it for publication. All authors contributed to the article and approved the submitted version.

FUNDING

This work was supported by a grant from National Natural Science Foundation of China (81771294) and the National undergraduate innovation training project (2020105330289).

REFERENCES

1. Eldahshan W, Fagan SC, Ergul A. Inflammation Within the Neurovascular Unit: Focus on Microglia for Stroke Injury and Recovery. *Pharmacol Res* (2019) 147:104349. doi: 10.1016/j.phrs.2019.104349
2. Bian Z, Gong Y, Huang T, Lee CZW, Bian L, Bai Z, et al. Deciphering Human Macrophage Development At Single-Cell Resolution. *Nature* (2020) 582(7813):571–6. doi: 10.1038/s41586-020-2316-7
3. Prinz M, Jung S, Priller J. Microglia Biology: One Century of Evolving Concepts. *Cell* (2019) 179(2):292–311. doi: 10.1016/j.cell.2019.08.053
4. Wan S, Cheng Y, Jin H, Guo D, Hua Y, Keep RF, et al. Microglia Activation and Polarization After Intracerebral Hemorrhage in Mice: The Role of Protease-Activated Receptor-1. *Transl Stroke Res* (2016) 7(6):478–87. doi: 10.1007/s12975-016-0472-8
5. Wolf SA, Boddeke HW, Kettenmann H. Microglia in Physiology and Disease. *Annu Rev Physiol* (2017) 79:619–43. doi: 10.1146/annurev-physiol-022516-034406
6. Friedman BA, Srinivasan K, Ayalon G, Meilandt WJ, Lin H, Huntley MA, et al. Diverse Brain Myeloid Expression Profiles Reveal Distinct Microglial Activation States and Aspects of Alzheimer's Disease Not Evident in Mouse Models. *Cell Rep* (2018) 22(3):832–47. doi: 10.1016/j.celrep.2017.12.066
7. Yang Z, Zhao T, Zou Y, Zhang JH, Feng H. Curcumin Inhibits Microglia Inflammation and Confers Neuroprotection in Intracerebral Hemorrhage. *Immunol Lett* (2014) 160(1):89–95. doi: 10.1016/j.imlet.2014.03.005
8. Wang M, Hua Y, Keep RF, Wan S, Novakovic N, Xi G. Complement Inhibition Attenuates Early Erythrolysis in the Hematoma and Brain Injury in Aged Rats. *Stroke* (2019) 50(7):1859–68. doi: 10.1161/strokeaha.119.025170
9. Vinukonda G, Liao Y, Hu F, Ivanova L, Purohit D, Finkel DA, et al. Human Cord Blood-Derived Unrestricted Somatic Stem Cell Infusion Improves Neurobehavioral Outcome in a Rabbit Model of Intraventricular Hemorrhage. *Stem Cells Transl Med* (2019) 8(11):1157–69. doi: 10.1002/sctm.19-0082
10. Chang CF, Wan J, Li Q, Renfroe SC, Heller NM, Wang J. Alternative Activation-Skewed Microglia/Macrophages Promote Hematoma Resolution in Experimental Intracerebral Hemorrhage. *Neurobiol Dis* (2017) 103:54–69. doi: 10.1016/j.nbd.2017.03.016
11. Jing C, Bian L, Wang M, Keep RF, Xi G, Hua Y. Enhancement of Hematoma Clearance With Cd47 Blocking Antibody in Experimental Intracerebral Hemorrhage. *Stroke* (2019) 50(6):1539–47. doi: 10.1161/STROKEAHA.118.024578
12. Sekerdag E, Solaroglu I, Gursoy-Ozdemir Y. Cell Death Mechanisms in Stroke and Novel Molecular and Cellular Treatment Options. *Curr Neuropharmacol* (2018) 16(9):1396–415. doi: 10.2174/1570159x16666180302115544
13. Su EJ, Cao C, Fredriksson L, Nilsson I, Stefanitsch C, Stevenson TK, et al. Microglial-Mediated PDGF-CC Activation Increases Cerebrovascular Permeability During Ischemic Stroke. *Acta Neuropathol* (2017) 134(4):585–604. doi: 10.1007/s00401-017-1749-z
14. Chen AQ, Fang Z, Chen XL, Yang S, Zhou YF, Mao L, et al. Microglia-Derived TNF-alpha Mediates Endothelial Necroptosis Aggravating Blood Brain-Barrier Disruption After Ischemic Stroke. *Cell Death Dis* (2019) 10(7):487. doi: 10.1038/s41419-019-1716-9
15. Geraghty JR, Davis JL, Testai FD. Neuroinflammation and Microvascular Dysfunction After Experimental Subarachnoid Hemorrhage: Emerging Components of Early Brain Injury Related to Outcome. *Neurocrit Care* (2019) 31(2):373–89. doi: 10.1007/s12028-019-00710-x
16. Zlokovic BV. The Blood-Brain Barrier in Health and Chronic Neurodegenerative Disorders. *Neuron* (2008) 57(2):178–201. doi: 10.1016/j.neuron.2008.01.003
17. Ronaldson PT, Davis TP. Regulation of Blood-Brain Barrier Integrity by Microglia in Health and Disease: A Therapeutic Opportunity. *J Cereb Blood Flow Metab* (2020) 40(1_suppl):S6–s24. doi: 10.1177/0271678x20951995
18. Zhao X, Grotta J, Gonzales N, Aronowski J. Hematoma Resolution as a Therapeutic Target: The Role of Microglia/Macrophages. *Stroke* (2009) 40(3 Suppl):S92–4. doi: 10.1161/strokeaha.108.533158
19. Chang CF, Goods BA, Askenase MH, Hammond MD, Renfroe SC, Steinschneider AF, et al. Erythrocyte Efferocytosis Modulates Macrophages Towards Recovery After Intracerebral Hemorrhage. *J Clin Invest* (2018) 128(2):607–24. doi: 10.1172/jci95612
20. Wang G, Wang L, Sun XG, Tang J. Haematoma Scavenging in Intracerebral Haemorrhage: From Mechanisms to the Clinic. *J Cell Mol Med* (2018) 22(2):768–77. doi: 10.1111/jcmm.13441
21. Deng S, Sherchan P, Jin P, Huang L, Travis Z, Zhang JH, et al. Recombinant CCL17 Enhances Hematoma Resolution and Activation of CCR4/ERK/Nrf2/CD163 Signaling Pathway After Intracerebral Hemorrhage in Mice. *Neurotherapeutics* (2020) 17(4):1940–53. doi: 10.1007/s13311-020-00908-4
22. Zhuang J, Peng Y, Gu C, Chen H, Lin Z, Zhou H, et al. Wogonin Accelerates Hematoma Clearance and Improves Neurological Outcome Via the PPAR-γ Pathway After Intracerebral Hemorrhage. *Transl Stroke Res* (2020) 16. doi: 10.1007/s12975-020-00842-9
23. Tschoe C, Bushnell CD, Duncan PW, Alexander-Miller MA, Wolfe SQ. Neuroinflammation After Intracerebral Hemorrhage and Potential Therapeutic Targets. *J Stroke* (2020) 22(1):29–46. doi: 10.5853/jos.2019.02236
24. Carson MJ, Doose JM, Melchior B, Schmid CD, Ploix CC. CNS Immune Privilege: Hiding in Plain Sight. *Immunol Rev* (2006) 213:48–65. doi: 10.1111/j.1600-065X.2006.00441.x
25. Wang J. Preclinical and Clinical Research on Inflammation After Intracerebral Hemorrhage. *Prog Neurobiol* (2010) 92(4):463–77. doi: 10.1016/j.pneurobio.2010.08.001
26. Zhou Y, Wang Y, Wang J, Anne Stetler R, Yang QW. Inflammation in Intracerebral Hemorrhage: From Mechanisms to Clinical Translation. *Prog Neurobiol* (2014) 115:25–44. doi: 10.1016/j.pneurobio.2013.11.003
27. Zhang Z, Zhang Z, Lu H, Yang Q, Wu H, Wang J. Microglial Polarization and Inflammatory Mediators After Intracerebral Hemorrhage. *Mol Neurobiol* (2017) 54(3):1874–86. doi: 10.1007/s12035-016-9785-6
28. Ransohoff RM. A Polarizing Question: do M1 and M2 Microglia Exist? *Nat Neurosci* (2016) 19(8):987–91. doi: 10.1038/nn.4338
29. Chiu IM, Morimoto ET, Goodarzi H, Liao JT, O'Keeffe S, Phatnani HP, et al. A Neurodegeneration-Specific Gene-Expression Signature of Acutely Isolated Microglia From an Amyotrophic Lateral Sclerosis Mouse Model. *Cell Rep* (2013) 4(2):385–401. doi: 10.1016/j.celrep.2013.06.018

30. Martinez FO, Gordon S. The M1 and M2 Paradigm of Macrophage Activation: Time for Reassessment. *F1000Prime Rep* (2014) 6:13. doi: 10.12703/p6-13
31. Ajami B, Samusik N, Wieghofer P, Ho PP, Crotti A, Bjornson Z, et al. Single-Cell Mass Cytometry Reveals Distinct Populations of Brain Myeloid Cells in Mouse Neuroinflammation and Neurodegeneration Models. *Nat Neurosci* (2018) 21(4):541–51. doi: 10.1038/s41593-018-0100-x
32. Masuda T, Sankowski R, Staszewski O, Böttcher C, Amann L, Sagar, et al. Spatial and Temporal Heterogeneity of Mouse and Human Microglia At Single-Cell Resolution. *Nature* (2019) 566(7744):388–92. doi: 10.1038/s41586-019-0924-x
33. Davis MJ, Tsang TM, Qiu Y, Dayrit JK, Freij JB, Huffnagle GB, et al. Macrophage M1/M2 Polarization Dynamically Adapts to Changes in Cytokine Microenvironments in Cryptococcus Neoformans Infection. *mBio* (2013) 4(3):e00264–13. doi: 10.1128/mBio.00264-13
34. Desale SE, Chinnathambi S. Role of Dietary Fatty Acids in Microglial Polarization in Alzheimer's Disease. *J Neuroinflamm* (2020) 17(1):93. doi: 10.1186/s12974-020-01742-3
35. Lassmann H. Pathology of Inflammatory Diseases of the Nervous System: Human Disease Versus Animal Models. *Glia* (2020) 68(4):830–44. doi: 10.1002/glia.23726
36. García-Revilla J, Alonso-Bellido IM, Burguillos MA, Herrera AJ, Espinosa-Oliva AM, Ruiz R, et al. Reformulating Pro-Oxidant Microglia in Neurodegeneration. *J Clin Med* (2019) 8(10):32. doi: 10.3390/jcm8101719
37. Rangaraju S, Dammer EB, Raza SA, Rathakrishnan P, Xiao H, Gao T, et al. Identification and Therapeutic Modulation of a Pro-Inflammatory Subset of Disease-Associated-Microglia in Alzheimer's Disease. *Mol Neurodegener* (2018) 13(1):24. doi: 10.1186/s13024-018-0254-8
38. Arcuri C, Mecca C, Bianchi R, Giambanco I, Donato R. The Pathophysiological Role of Microglia in Dynamic Surveillance, Phagocytosis and Structural Remodeling of the Developing Cns. *Front Mol Neurosci* (2017) 10:191. doi: 10.3389/fnmol.2017.00191
39. Chen S, Peng J, Sherchan P, Ma Y, Xiang S, Yan F, et al. TREM2 Activation Attenuates Neuroinflammation and Neuronal Apoptosis Via PI3K/Akt Pathway After Intracerebral Hemorrhage in Mice. *J Neuroinflamm* (2020) 17(1):168. doi: 10.1186/s12974-020-01853-x
40. Brown GC, St George-Hyslop PH. Deciphering Microglial Diversity in Alzheimer's Disease. *Science* (2017) 356(6343):1123–4. doi: 10.1126/science.aan7893
41. Prinz M, Erny D, Hagemeyer N. Ontogeny and Homeostasis of CNS Myeloid Cells. *Nat Immunol* (2017) 18(4):385–92. doi: 10.1038/ni.3703
42. Olah M, Menon V, Habib N, Taga MF, Ma Y, Yung CJ, et al. Single Cell RNA Sequencing of Human Microglia Uncovers a Subset Associated With Alzheimer's Disease. *Nat Commun* (2020) 11(1):6129. doi: 10.1038/s41467-020-19737-2
43. Ochocka N, Segit P, Walentynowicz KA, Wojnicki K, Cyranowski S, Swatler J, et al. Single-Cell RNA Sequencing Reveals Functional Heterogeneity of Glioma-Associated Brain Macrophages. *Nat Commun* (2021) 12(1):1151. doi: 10.1038/s41467-021-21407-w
44. Gosselin D, Skola D, Coufal NG, Holtman IR, Schlachetzki JCM, Sajti E, et al. An Environment-Dependent Transcriptional Network Specifies Human Microglia Identity. *Science* (2017) 356(6344):11. doi: 10.1126/science.aal3222
45. Vainchtein ID, Molofsky AV. Astrocytes and Microglia: in Sickness and in Health. *Trends Neurosci* (2020) 43(3):144–54. doi: 10.1016/j.tins.2020.01.003
46. Lan X, Han X, Li Q, Yang QW, Wang J. Modulators of Microglial Activation and Polarization After Intracerebral Haemorrhage. *Nat Rev Neurol* (2017) 13(7):420–33. doi: 10.1038/nrneurol.2017.69
47. Wu CH, Shyue SK, Hung TH, Wen S, Lin CC, Chang CF, et al. Genetic Deletion or Pharmacological Inhibition of Soluble Epoxide Hydrolase Reduces Brain Damage and Attenuates Neuroinflammation After Intracerebral Hemorrhage. *J Neuroinflamm* (2017) 14(1):230. doi: 10.1186/s12974-017-1005-4
48. Fang Y, Tian Y, Huang Q, Wan Y, Xu L, Wang W, et al. Deficiency of TREK-1 Potassium Channel Exacerbates Blood-Brain Barrier Damage and Neuroinflammation After Intracerebral Hemorrhage in Mice. *J Neuroinflamm* (2019) 16(1):96. doi: 10.1186/s12974-019-1485-5
49. Zhou K, Zhong Q, Wang YC, Xiong XY, Meng ZY, Zhao T, et al. Regulatory T Cells Ameliorate Intracerebral Hemorrhage-Induced Inflammatory Injury by Modulating Microglia/Macrophage Polarization Through the IL-10/GSK3beta/PTEN Axis. *J Cereb Blood Flow Metab* (2017) 37(3):967–79. doi: 10.1177/0271678x16648712
50. Taylor RA, Chang CF, Goods BA, Hammond MD, Mac Grory B, Ai Y, et al. TGF-Beta1 Modulates Microglial Phenotype and Promotes Recovery After Intracerebral Hemorrhage. *J Clin Invest* (2017) 127(1):280–92. doi: 10.1172/jci88647
51. Yang Z, Jiang X, Zhang J, Huang X, Zhang X, Wang J, et al. Let-7a Promotes Microglia M2 Polarization by Targeting CKIP-1 Following ICH. *Immunol Lett* (2018) 202:1–7. doi: 10.1016/j.imlet.2018.07.007
52. Zhang XD, Fan QY, Qiu Z, Chen S. MiR-7 Alleviates Secondary Inflammatory Response of Microglia Caused by Cerebral Hemorrhage Through Inhibiting TLR4 Expression. *Eur Rev Med Pharmacol Sci* (2018) 22(17):5597–604. doi: 10.26355/eurrev_201809_15824
53. Liu DL, Zhao LX, Zhang S, Du JR. Peroxiredoxin 1-Mediated Activation of TLR4/NF-kappaB Pathway Contributes to Neuroinflammatory Injury in Intracerebral Hemorrhage. *Int Immunopharmacol* (2016) 41:82–9. doi: 10.1016/j.intimp.2016.10.025
54. Bai YY, Niu JZ. miR222 Regulates Brain Injury and Inflammation Following Intracerebral Hemorrhage by Targeting ITGB8. *Mol Med Rep* (2020) 21(3):1145–53. doi: 10.3892/mmr.2019.10903
55. Zhang Y, Han B, He Y, Li D, Ma X, Liu Q, et al. MicroRNA-132 Attenuates Neurobehavioral and Neuropathological Changes Associated With Intracerebral Hemorrhage in Mice. *Neurochem Int* (2017) 107:182–90. doi: 10.1016/j.neuint.2016.11.011
56. Wang Z, Yuan B, Fu F, Huang S, Yang Z. Hemoglobin Enhances miRNA-144 Expression and Autophagic Activation Mediated Inflammation of Microglia Via mTOR Pathway. *Sci Rep* (2017) 7(1):11861. doi: 10.1038/s41598-017-12067-2
57. Tan X, Yang Y, Xu J, Zhang P, Deng R, Mao Y, et al. Luteolin Exerts Neuroprotection Via Modulation of the P62/Keap1/Nrf2 Pathway in Intracerebral Hemorrhage. *Front Pharmacol* (2019) 10:1551. doi: 10.3389/fphar.2019.01551
58. Duan XC, Wang W, Feng DX, Yin J, Zuo G, Chen DD, et al. Roles of Autophagy and Endoplasmic Reticulum Stress in Intracerebral Hemorrhage-Induced Secondary Brain Injury In Rats. *CNS Neurosci Ther* (2017) 23(7):554–66. doi: 10.1111/cns.12703
59. Xiao H, Chen H, Jiang R, Zhang L, Wang L, Gan H, et al. NLRP6 Contributes to Inflammation and Brain Injury Following Intracerebral Haemorrhage by Activating Autophagy. *J Mol Med (Berl)* (2020) 98(9):1319–31. doi: 10.1007/s00109-020-01962-3
60. Shi H, Wang J, Wang J, Huang Z, Yang Z. Il-17A Induces Autophagy and Promotes Microglial Neuroinflammation Through ATG5 and ATG7 in Intracerebral Hemorrhage. *J Neuroimmunol* (2018) 323:143–51. doi: 10.1016/j.jneuroim.2017.07.015
61. Ohnishi M, Katsuki H, Fujimoto S, Takagi M, Kume T, Akaike A. Involvement of Thrombin and Mitogen-Activated Protein Kinase Pathways in Hemorrhagic Brain Injury. *Exp Neurol* (2007) 206(1):43–52. doi: 10.1016/j.expneurol.2007.03.030
62. Zhao L, Chen S, Sherchan P, Ding Y, Zhao W, Guo Z, et al. Recombinant CTRP9 Administration Attenuates Neuroinflammation Via Activating Adiponectin Receptor 1 After Intracerebral Hemorrhage in Mice. *J Neuroinflamm* (2018) 15(1):215. doi: 10.1186/s12974-018-1256-8
63. Chen S, Zhao L, Sherchan P, Ding Y, Yu J, Nowrangi D, et al. Activation of Melanocortin Receptor 4 With RO27-3225 Attenuates Neuroinflammation Through AMPK/JNK/p38 MAPK Pathway After Intracerebral Hemorrhage in Mice. *J Neuroinflamm* (2018) 15(1):106. doi: 10.1186/s12974-018-1140-6
64. Yang Z, Yu A, Liu Y, Shen H, Lin C, Lin L, et al. Regulatory T Cells Inhibit Microglia Activation and Protect Against Inflammatory Injury in Intracerebral Hemorrhage. *Int Immunopharmacol* (2014) 22(2):522–5. doi: 10.1016/j.intimp.2014.06.037
65. Wang M, Cheng L, Chen ZL, Mungur R, Xu SH, Wu J, et al. Hyperbaric Oxygen Preconditioning Attenuates Brain Injury After Intracerebral Hemorrhage by Regulating Microglia Polarization in Rats. *CNS Neurosci Ther* (2019) 25(10):1126–33. doi: 10.1111/cns.13208

66. Sansing LH, Harris TH, Welsh FA, Kasner SE, Hunter CA, Kariko K. Toll-Like Receptor 4 Contributes to Poor Outcome After Intracerebral Hemorrhage. *Ann Neurol* (2011) 70(4):646–56. doi: 10.1002/ana.22528
67. Fang H, Chen J, Lin S, Wang P, Wang Y, Xiong X, et al. CD36-Mediated Hematoma Absorption Following Intracerebral Hemorrhage: Negative Regulation by TLR4 Signaling. *J Immunol* (2014) 192(12):5984–92. doi: 10.4049/jimmunol.1400054
68. Yang Z, Liu B, Zhong L, Shen H, Lin C, Lin L, et al. Toll-Like receptor-4-mediated Autophagy Contributes to Microglial Activation and Inflammatory Injury in Mouse Models of Intracerebral Haemorrhage. *Neuropathol Appl Neurobiol* (2015) 41(4):e95–106. doi: 10.1111/nan.12177
69. Xu J, Chen Z, Yu F, Liu H, Ma C, Xie D, et al. Il-4/STAT6 Signaling Facilitates Innate Hematoma Resolution and Neurological Recovery After Hemorrhagic Stroke in Mice. *Proc Natl Acad Sci U S A* (2020) 117 (51):32679–90. doi: 10.1073/pnas.2018497117
70. Shi SX, Li YJ, Shi K, Wood K, Ducruet AF, Liu Q. Il (Interleukin)-15 Bridges Astrocyte-Microglia Crosstalk and Exacerbates Brain Injury Following Intracerebral Hemorrhage. *Stroke* (2020) 51(3):967–74. doi: 10.1161/strokeaha.119.028638
71. Yu A, Duan H, Zhang T, Pan Y, Kou Z, Zhang X, et al. Il-17A Promotes Microglial Activation and Neuroinflammation in Mouse Models of Intracerebral Haemorrhage. *Mol Immunol* (2016) 73:151–7. doi: 10.1016/j.molimm.2016.04.003
72. Chen Z, Xu N, Dai X, Zhao C, Wu X, Shankar S, et al. Interleukin-33 Reduces Neuronal Damage and White Matter Injury Via Selective Microglia M2 Polarization After Intracerebral Hemorrhage in Rats. *Brain Res Bull* (2019) 150:127–35. doi: 10.1016/j.brainresbull.2019.05.016
73. Yin M, Chen Z, Ouyang Y, Zhang H, Wan Z, Wang H, et al. Thrombin-Induced, TNFR-dependent miR-181c Downregulation Promotes MLL1 and NF-κb Target Gene Expression in Human Microglia. *J Neuroinflamm* (2017) 14(1):132. doi: 10.1186/s12974-017-0887-5
74. Ryu J, Pyo H, Jou I, Joe E. Thrombin Induces NO Release From Cultured Rat Microglia Via Protein Kinase C, Mitogen-Activated Protein Kinase, and NF-kappa B. *J Biol Chem* (2000) 275(39):29955–9. doi: 10.1074/jbc.M001220200
75. Yin M, Chen Z, Ouyang Y, Zhang H, Wan Z, Wang H, et al. Thrombin-Induced, TNFR-dependent miR-181c Downregulation Promotes MLL1 and NF-kappaB Target Gene Expression in Human Microglia. *J Neuroinflamm* (2017) 14(1):132. doi: 10.1186/s12974-017-0887-5
76. Zheng J, Liu Z, Li W, Tang J, Zhang D, Tang X. Lithium Posttreatment Confers Neuroprotection Through Glycogen Synthase kinase-3beta Inhibition in Intracerebral Hemorrhage Rats. *J Neurosurg* (2017) 127 (4):716–24. doi: 10.3171/2016.7.Jns152995
77. Li R, Liu Z, Wu X, Yu Z, Zhao S, Tang X. Lithium Chloride Promoted Hematoma Resolution After Intracerebral Hemorrhage Through GSK-3beta-mediated Pathways-Dependent Microglia Phagocytosis and M2-phenotype Differentiation, Angiogenesis and Neurogenesis in a Rat Model. *Brain Res Bull* (2019) 152:117–27. doi: 10.1016/j.brainresbull.2019.07.019
78. Zhao S, Liu Z, Yu Z, Wu X, Li R, Tang X. BIO Alleviates Inflammation Through Inhibition of GSK-3beta in a Rat Model of Intracerebral Hemorrhage. *J Neurosurg* (2020) 133(2):383–402. doi: 10.3171/2019.4.Jns183501
79. Li M, Xia M, Chen W, Wang J, Yin Y, Guo C, et al. Lithium Treatment Mitigates White Matter Injury After Intracerebral Hemorrhage Through Brain-Derived Neurotrophic Factor Signaling in Mice. *Transl Res* (2020) 217:61–74. doi: 10.1016/j.trsl.2019.12.006
80. Jung KH, Chu K, Lee ST, Kim SJ, Song EC, Kim EH, et al. Blockade of AT1 Receptor Reduces Apoptosis, Inflammation, and Oxidative Stress in Normotensive Rats With Intracerebral Hemorrhage. *J Pharmacol Exp Ther* (2007) 322(3):1051–8. doi: 10.1124/jpet.107.120097
81. Li Y, Zhu ZY, Lu BW, Huang TT, Zhang YM, Zhou NY, et al. Rosiglitazone Ameliorates Tissue Plasminogen Activator-Induced Brain Hemorrhage After Stroke. *CNS Neurosci Ther* (2019) 25(12):1343–52. doi: 10.1111/cns.13260
82. Zhao X, Sun G, Zhang J, Strong R, Song W, Gonzales N, et al. Hematoma Resolution as a Target for Intracerebral Hemorrhage Treatment: Role for Peroxisome Proliferator-Activated Receptor Gamma in Microglia/Macrophages. *Ann Neurol* (2007) 61(4):352–62. doi: 10.1002/ana.21097
83. Xu R, Wang S, Li W, Liu Z, Tang J, Tang X. Activation of Peroxisome Proliferator-Activated Receptor-Gamma by a 12/15-Lipoxygenase Product of Arachidonic Acid: A Possible Neuroprotective Effect in the Brain After Experimental Intracerebral Hemorrhage. *J Neurosurg* (2017) 127(3):522–31. doi: 10.3171/2016.7.Jns1668
84. Wang Y, Chen Q, Tan Q, Feng Z, He Z, Tang J, et al. Simvastatin Accelerates Hematoma Resolution After Intracerebral Hemorrhage in a PPARgamma-dependent Manner. *Neuropharmacology* (2018) 128:244–54. doi: 10.1016/j.neuropharm.2017.10.021
85. Wang G, Li T, Duan SN, Dong L, Sun XG, Xue F. PPAR-Gamma Promotes Hematoma Clearance Through Haptoglobin-Hemoglobin-CD163 in a Rat Model of Intracerebral Hemorrhage. *Behav Neurol* (2018) 2018:7646104. doi: 10.1155/2018/7646104
86. Miao H, Li R, Han C, Lu X, Zhang H. Minocycline Promotes Posthemorrhagic Neurogenesis Via M2 Microglia Polarization Via Upregulation of the TrkB/BDNF Pathway in Rats. *J Neurophysiol* (2018) 120(3):1307–17. doi: 10.1152/jn.00234.2018
87. Yao ST, Cao F, Chen JL, Chen W, Fan RM, Li G, et al. NLRP3 is Required for Complement-Mediated Caspase-1 and IL-1beta Activation in ICH. *J Mol Neurosci* (2017) 61(3):385–95. doi: 10.1007/s12031-016-0874-9
88. Liang H, Sun Y, Gao A, Zhang N, Jia Y, Yang S, et al. Ac-YVAD-cmk Improves Neurological Function by Inhibiting caspase-1-mediated Inflammatory Response in the Intracerebral Hemorrhage of Rats. *Int Immunopharmacol* (2019) 75:105771. doi: 10.1016/j.intimp.2019.105771
89. Yang X, Sun J, Kim TJ, Kim YJ, Ko SB, Kim CK, et al. Pretreatment With Low-Dose Fimasartan Ameliorates NLRP3 Inflammasome-Mediated Neuroinflammation and Brain Injury After Intracerebral Hemorrhage. *Exp Neurol* (2018) 310:22–32. doi: 10.1016/j.expneurol.2018.08.013
90. Wells JE, Biernaskie J, Szymanska A, Larsen PH, Yong VW, Corbett D. Matrix Metalloproteinase (MMP)-12 Expression has a Negative Impact on Sensorimotor Function Following Intracerebral Haemorrhage in Mice. *Eur J Neurosci* (2005) 21(1):187–96. doi: 10.1111/j.1460-9568.2004.03829.x
91. Wasserman JK, Schlichter LC. Minocycline Protects the Blood-Brain Barrier and Reduces Edema Following Intracerebral Hemorrhage in the Rat. *Exp Neurol* (2007) 207(2):227–37. doi: 10.1016/j.expneurol.2007.06.025
92. Xue M, Hollenberg MD, Yong VW. Combination of Thrombin and Matrix Metalloproteinase-9 Exacerbates Neurotoxicity in Cell Culture and Intracerebral Hemorrhage in Mice. *J Neurosci* (2006) 26(40):10281–91. doi: 10.1523/jneurosci.2806-06.2006
93. Wasserman JK, Zhu X, Schlichter LC. Evolution of the Inflammatory Response in the Brain Following Intracerebral Hemorrhage and Effects of Delayed Minocycline Treatment. *Brain Res* (2007) 1180:140–54. doi: 10.1016/j.brainres.2007.08.058
94. Wang G, Li Z, Li S, Ren J, Suresh V, Xu D, et al. Minocycline Preserves the Integrity and Permeability of BBB by Altering the Activity of DKK1-Wnt Signaling in ICH Model. *Neuroscience* (2019) 415:135–46. doi: 10.1016/j.neuroscience.2019.06.038
95. Liang H, Guan D, Gao A, Yin Y, Jing M, Yang L, et al. Human Amniotic Epithelial Stem Cells Inhibit Microglia Activation Through Downregulation of Tumor Necrosis Factor-Alpha, interleukin-1beta and Matrix metalloproteinase-12 In Vitro and in a Rat Model of Intracerebral Hemorrhage. *Cytotherapy* (2014) 16(4):523–34. doi: 10.1016/j.jcyt.2013.11.007
96. Chen M, Li X, Zhang X, He X, Lai L, Liu Y, et al. The Inhibitory Effect of Mesenchymal Stem Cell on Blood-Brain Barrier Disruption Following Intracerebral Hemorrhage in Rats: Contribution of TSG-6. *J Neuroinflamm* (2015) 12:61. doi: 10.1186/s12974-015-0284-x
97. Wu H, Wu T, Xu X, Wang J, Wang J. Iron Toxicity in Mice With Collagenase-Induced Intracerebral Hemorrhage. *J Cereb Blood Flow Metab* (2011) 31(5):1243–50. doi: 10.1038/jcbfm.2010.209
98. Zhao F, Hua Y, He Y, Keep RF, Xi G. Minocycline-Induced Attenuation of Iron Overload and Brain Injury After Experimental Intracerebral Hemorrhage. *Stroke* (2011) 42(12):3587–93. doi: 10.1161/strokeaha.111.623926
99. Li Q, Wan J, Lan X, Han X, Wang Z, Wang J. Neuroprotection of Brain-Permeable Iron Chelator VK-28 Against Intracerebral Hemorrhage in Mice. *J Cereb Blood Flow Metab* (2017) 37(9):3110–23. doi: 10.1177/0271678x17709186

100. Dai S, Hua Y, Keep RF, Novakovic N, Fei Z, Xi G. Minocycline Attenuates Brain Injury and Iron Overload After Intracerebral Hemorrhage in Aged Female Rats. *Neurobiol Dis* (2019) 126:76–84. doi: 10.1016/j.nbd.2018.06.001
101. Apolloni S, Amadio S, Fabbrizio P, Morello G, Spampinato AG, Latagliata EC, et al. Histaminergic Transmission Slows Progression of Amyotrophic Lateral Sclerosis. *J Cachexia Sarcopenia Muscle* (2019) 10(4):872–93. doi: 10.1002/jcsm.12422
102. Armando RG, Mengual Gómez DL, Gomez DE. New Drugs are Not Enough –Drug Repositioning in Oncology: *Int J Oncol* (2020) 56(3):651-84. doi: 10.3892/ijo.2020.4966

Conflict of Interest: The authors declare that the research was conducted in the absence of any commercial or financial relationships that could be construed as a potential conflict of interest.

frontiers in Immunology

ORIGINAL RESEARCH
published: 14 May 2021
doi: 10.3389/fimmu.2021.674189

GPCRomics of Homeostatic and Disease-Associated Human Microglia

Cheng-Chih Hsiao[1,2*], *Roman Sankowski*[3], *Marco Prinz*[3,4,5], *Joost Smolders*[2,6], *Inge Huitinga*[2,7] *and Jörg Hamann*[1,2*]

[1] Department of Experimental Immunology, Amsterdam institute for Infection and Immunity, Amsterdam University Medical Centers, Amsterdam, Netherlands, [2] Neuroimmunology Research Group, Netherlands Institute for Neuroscience, Amsterdam, Netherlands, [3] Institute of Neuropathology, Faculty of Medicine, University of Freiburg, Freiburg, Germany, [4] Signalling Research Centres BIOSS and CIBSS, University of Freiburg, Freiburg, Germany, [5] Center for Basics in NeuroModulation (NeuroModulBasics), Faculty of Medicine, University of Freiburg, Freiburg, Germany, [6] MS Center ErasMS, Departments of Neurology and Immunology, Erasmus Medical Center, Rotterdam, Netherlands, [7] Swammerdam Institute for Life Sciences, Center for Neuroscience, University of Amsterdam, Amsterdam, Netherlands

OPEN ACCESS

Edited by:
Amanda Sierra, Achucarro Basque Center for Neuroscience, Spain

Reviewed by:
Angela Schulz, Leipzig University, Germany
Marta Olah, Columbia University Irving Medical Center, United States

***Correspondence:**
Cheng-Chih Hsiao
c.hsiao@amsterdamumc.nl
Jörg Hamann
j.hamann@amsterdamumc.nl

Specialty section:
This article was submitted to Multiple Sclerosis and Neuroimmunology, a section of the journal Frontiers in Immunology

Received: *28 February 2021*
Accepted: *22 April 2021*
Published: *14 May 2021*

Citation:
Hsiao C-C, Sankowski R, Prinz M, Smolders J, Huitinga I and Hamann J (2021) GPCRomics of Homeostatic and Disease-Associated Human Microglia. Front. Immunol. 12:674189. doi: 10.3389/fimmu.2021.674189

G-protein-coupled receptors (GPCRs) are critical sensors affecting the state of eukaryotic cells. To get systematic insight into the GPCRome of microglia, we analyzed publicly available RNA-sequencing data of bulk and single cells obtained from human and mouse brains. We identified 17 rhodopsin and adhesion family GPCRs robustly expressed in microglia from human brains, including the homeostasis-associated genes *CX3CR1*, *GPR34*, *GPR183*, *P2RY12*, *P2RY13*, and *ADGRG1*. Expression of these microglial core genes was lost upon culture of isolated cells *ex vivo* but could be acquired by human induced pluripotent stem cell (iPSC)-derived microglial precursors transplanted into mouse brains. *CXCR4* and *PTGER4* were higher expressed in subcortical white matter compared to cortical grey matter microglia, and *ADGRG1* was downregulated in microglia obtained from normal-appearing white and grey matter tissue of multiple sclerosis (MS) brains. Single-cell RNA sequencing of microglia from active lesions, obtained early during MS, revealed downregulation of homeostasis-associated GPCR genes and upregulation of *CXCR4* expression in a small subset of MS-associated lesional microglia. Functional presence of low levels of CXCR4 on human microglia was confirmed using flow cytometry and transwell migration towards SDF-1. Microglia abundantly expressed the GPCR down-stream signaling mediator genes *GNAI2* (α_{i2}), *GNAS* (α_s), and *GNA13* (α_{13}), the latter particularly in white matter. Drugs against several microglia GPCRs are available to target microglia in brain diseases. In conclusion, transcriptome profiling allowed us to identify expression of GPCRs that may contribute to brain (patho)physiology and have diagnostic and therapeutic potential in human microglia.

Keywords: brain, microglia, GPCRs, G proteins, system biology, multiple sclerosis, CXCR4

INTRODUCTION

Microglia are brain-resident phagocytic cells that contribute to brain homeostasis as well as disease (1, 2). Populating the central nervous system (CNS) during embryonic development, microglia persist for the rest of life through local self-renewal. As a consequence, they possess a unique transcriptional signature that emerged only recently from RNA sequencing (RNAseq) of purified primary cells (3). Notably, G protein-coupled receptors (GPCRs) figure prominently in the microglia transcriptome, as exemplified by the characteristic surface expression of CX3CR1, GPR34, GPR183, $P2Y_{12}$, $P2Y_{13}$, and GPR56 (3, 4). GPCRs are the senses of our cells, comprising the largest and most diverse superfamily of membrane proteins in eukaryotic cells. Of particular interest is their widespread cellular distribution and the fact that ∼30% of all currently approved pharmaceuticals target them (5). GPCRs control cell and tissue physiology by regulating signaling pathways *via* heterotrimeric G proteins, which modulate cellular levels of second messengers and, in turn, a wide array of functional activities in all types of cells (6). Microglial GPCRs have been implicated in control of axon outgrowth and cortical laminar positioning during development as well as in support of survival of neurons (CX3CR1), in plasticity ($P2Y_{12}$) and complement-mediated pruning (C3AR1 and C5AR1) of synapses, in microglial brain colonization (CXCR4) and chemotaxis of microglia to injury ($P2Y_{12}$), and in neuropathic pain response ($P2Y_{12}$) (7). Exploring bulk and single cell RNAseq studies of microglia from mice and human, we here describe the expression of GPCR and G protein genes in relation to microglia homeostasis, location, health, and disease.

METHODS

RNAseq and Microarray Datasets

Genome-wide gene expression data of microglia, macrophages, and non-phagocytic cells were derived from various publicly available RNAseq data sets (**Table 1**). Numbers indicating gene expression are provided either as absolute counts, presenting fragments per kilobase of transcript per million mapped reads (FPKM) or transcripts per kilobase million (TPM), or as relative counts, related to arbitrary chosen, fixed thresholds of all genes in the gene set (e.g., the top 50% = 0.50 percentile). Heatmaps show gene expression intensity, based on the average of all genes, with white indicating low expression and red indicating high expression. *t*-distributed stochastic neighbor embedding (*t-SNE*) plots of the clusters of microglia were generated as described (15). Relative RNA expression levels for *CXCR4* and *CXCL12* from laser-dissected tissue from mixed active/inactive and inactive demyelinated lesions were obtained from a microarray dataset (18).

Flow Cytometry

Isolated human microglia from corpus callosum and subcortical white matter and occipital cortex grey matter were isolated and stained as described (4) with APC-conjugated anti-CD11b (clone ICRF44; eBioscience, San Diego, CA, USA), Alexa 700-conjugated anti-CD14 (clone MφP9; BD Biosciences, San Diego, CA, USA), PerCP-Cy5.5-conjugated anti-CD15 (clone HI98; BioLegend, San Diego, CA, USA), BB515-conjugated anti-CD45 (clone HI30; BioLegend), PE-Cy7-conjugated anti-CXCR4 (clone 12G5; BioLegend), and PE-conjugated anti-$P2Y_{12}$ (clone S16007D; BioLegend). Dead cells were visualized by fixable viability dye eFluor 780 (eBioscience). Background staining was determined using fluorescence minus one control. Membrane protein expression was measured on a FACSCanto II (BD Biosciences), and median fluorescence intensity was determined with FlowJo software version 10.1 (Ashland, OR, USA).

Transwell Migration

Human brain microglia and paired peripheral blood monocytes were separately isolated by CD11b and CD14 microbeads (Miltenyi Biotec, Bergisch Gladbach, Germany) as described (19). 2 x 10^5 cells were loaded in a volume of 100 µl RPMI1640 medium containing 0.3% bovine serum albumin on transwell filters with a pore size of 5 µm (Corning, Corning, NY, USA).

TABLE 1 | RNAseq datasets analyzed in this study.

Species	Cells	Dataset	Reference
various	microglia	bulk RNAseq of isolated cells from cortex (GM) (human) or whole brains (mouse)	Geirsdottir et al. (8)
human	brain lysate, microglia	bulk RNAseq of isolated cells from cortex (GM)	Galatro et al. (9)
human	microglia	bulk RNAseq of isolated cells from cortex (GM)	Gosselin et al. (10)
human	microglia	bulk RNAseq of isolated cells from corpus callosum (WM) and occipital cortex (GM) of control and MS donors	Van der Poel et al. (4)
human	microglia	bulk RNAseq of isolated cells from corpus callosum (WM) and occipital cortex (GM) of control donors	Mizee et al. (unpublished data)
mouse	various	bulk RNAseq of (isolated cells from) whole brains (neurons, oligodendrocytes, astrocytes, and microglia)	Zhang et al. (11)
mouse	microglia, macrophages	bulk RNAseq of isolated cells from whole organs	Van Hove et al. (12)
human	iPSC-derived iMPs	bulk RNAseq of isolated cells transplanted into the brain of neonatal mice in vivo or cultured in vitro	Svoboda et al. (13)
mouse	microglia	single cell RNAseq of cells from brains of 5XFAD mice	Keren-Shaul et al. (14)
human	microglia	single cell RNAseq of cells from cortical (GM) biopsies of active MS lesions	Masuda et al. (15)
human	microglia	single cell RNAseq of cells from cortical (GM) surgically resected brain tissue	Olah et al. (16)
human	microglia	bulk RNAseq of isolated cells from cerebral cortex (GM)	Olah et al. (17)

WM, white matter; GM, grey matter.

100 ng/ml SDF-1 (stromal cell-derived factor-1, CXCL12) was added as chemoattractant to the lower compartment. After 4 h incubation at 37°C, cells in the lower compartment were harvested and quantified by flow cytometry at a fixed high speed for 120 sec.

Statistics

All analyses were performed in GraphPad Prism 7 (GraphPad Software, San Diego, CA, USA). When data were not normally distributed, non-parametric tests, either Wilcoxon or Mann-Whitney U, were performed.

RESULTS

Species and Cell Type Specificity of GPCR and GPCR Signaling Molecule Expression in Microglia

To explore the presence of GPCRs in microglia, we utilized the list of GPCRs not involved in olfaction, taste, light perception, and pheromone signaling as provided by the International Union of Basic and Clinical Pharmacology (IUPHAR)/British Pharmacological Society (BPS) Guide to Pharmacology (https://www.guidetopharmacology.org) (20). According to the GRAFS classification (21), the 384 receptors comprise 303 rhodopsin, 33 adhesion, 22 glutamate, 15 secretin, and 11 frizzled family members.

To identify GPCR genes that are reliably expressed in human microglia, we first tested bulk RNAseq expression data of homeostatic microglia from different vertebrate species we recently published (8). We found 83 GPCR genes in the top 50% (0.5 percentile) of all genes in the human and/or mouse gene sets (**Figure 1A**). 42 of these genes were lowly expressed (0.5–0.67 percentile), 12 genes were medium expressed (0.68–0.85 percentile), and 29 genes belonged to the highly expressed genes (0.86–1.0 percentile). While the homeostatic microglia marker genes *CX3CR1*, *GPR34*, *GPR183*, *P2RY12*, *P2RY13*, and *ADGRG1* (encoding GPR56) were highly expressed in both species, expression of other GPCR genes was medium, low, or even absent in either human or mouse. For example, transcription of *ADGRE1*, encoding F4/80 in mouse, was lacking in human microglia, in line with its exclusive expression in human eosinophils (22). Other genes with a restricted, high expression in either mouse or human microglia were *CCR6*, *GPR84*, *GPR146*, and *FPR1*, respectively. Notably, *ADGRE5* (encoding CD97), which is abundantly expressed by all types of bone marrow-derived leukocytes (23) was lowly expressed in mouse and human microglia, in line with previous findings (24). The previously disputed gene *ADGRB1* (encoding BAI1) (25) was undetectable in mouse and human microglia.

We confirmed the list of well-expressed human microglia GPCR genes in four other bulk RNAseq studies of primary human microglia [(4, 9, 10) and Mizee et al, unpublished data]. We found 15 genes abundantly expressed across the different data sets, which formed, together with two genes with a medium expression in grey matter microglia but high expression in white matter microglia (see below), the core microglia GPCR gene set for our further analyses (for all other genes, see the supplementary information). This gene set comprises rhodopsin (e.g., adenosine, chemokine, complement peptide, lysophospholipid, purinergic, and orphan receptors) as well as adhesion, but not secretin, glutamate, or frizzled family members. Among the 17 selected genes were the homeostatic microglia marker genes *CX3CR1*, *GPR34*, *GPR183*, *P2RY12*, *P2RY13*, and *ADGRG1*.

We next tested the expression of microglial GPCRs in other cell types of the CNS. The three most highly expressed genes, *ADGRG1*, *P2RY12*, and *CX3CR1*, also appeared top-abundant in whole brain tissue (10) (**Figure 1B**). All selected genes were more abundantly expressed in pure microglia as compared to the whole human cortex, which was further corroborated by data on gene expression in the major cell types of the mouse CNS (11) (**Figure 1C** and **Supplementary Table 1**). Except for *Cxcr4*, expression in microglia was higher as compared to neurons, astrocytes, and oligodendrocytes. Interestingly, high expression in microglia regularly correlated with gene activity in oligodendrocytes, albeit at a lower level.

Next to parenchymal microglia, the CNS harbors border-associated macrophages with distinct transcriptional signatures, residing in the dura mater, subdural meninges, and choroid plexus (12). Most microglia GPCRs were expressed also in non-parenchymal macrophages of the CNS, at comparable, higher, or lower level (**Figure 1C** and **Supplementary Table 1**). Inclusion of tissue-resident macrophages from peritoneum, lung, and liver unveiled similar patterns (12). The signature genes *Cx3cr1*, *Gpr34*, *P2ry12*, *P2ry13*, and *Adgrg1* were particularly expressed in microglia.

Upon ligation, GPCRs diversify downstream signaling through four main classes of Gα subunit – $G\alpha_s$, $G\alpha_{i/o}$, $G\alpha_{q/11}$, and $G\alpha_{12/13}$ (6). Moreover, G protein-coupled receptor kinases (GRKs) phosphorylate intracellular domains of GPCRs and function together with β-arrestin to regulate the GPCR desensitization (6). Human and mouse microglia expressed *GNAI2* ($G\alpha_{i2}$), *GNAS* ($G\alpha_s$), *GNA13* ($G\alpha_{13}$), *GRK2*, and *ARRB2*. In addition, mouse microglia also expressed *Gna15* ($G\alpha_{15}$) (**Figure 1C** and **Supplementary Table 1**). *Gnai2*, *Gna15*, *Grk2*, and *Arrb2* were higher expressed in microglia as compared to neurons, astrocytes, and oligodendrocytes, while *Gnas* and *Gna12* were expressed in different cell types. G protein, GRK, and β-arrestin gene expression levels in macrophages in- and out-side the CNS were mostly comparable.

Regional and Disease Specificity of GPCR and GPCR Signaling Molecule Expression in Human Microglia

Dissected from their natural microenvironment, microglia change their transcriptional program and alter morphological and functional characteristics (10, 19). Indeed, expression of *ADORA3*, *ADRB2*, *CXCR4*, *CX3CR1*, *GPR34*, *LPAR5*, *LPAR6*, *P2RY12*, *P2RY13*, and *ADGRG1* was strongly downregulated or even lost in microglia cultured *ex vivo* for 1 or 7 days (**Figure 2** and **Supplementary Table 2**).

Human induced pluripotent stem cells (iPSCs) can be differentiated into induced microglial precursors cells (iMPs)

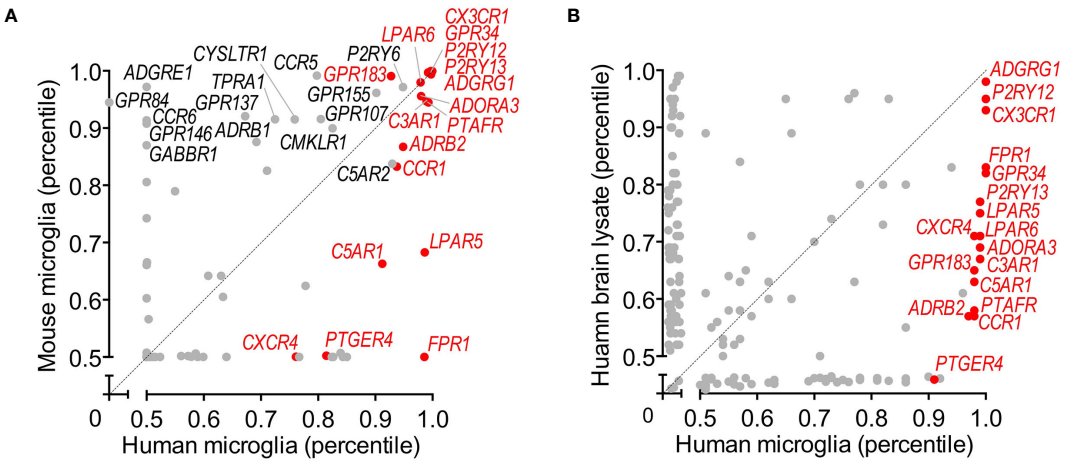

C

			Zhang et al, 2014					Van Hove et al, 2019						
					Glial cells			Brain mac				Peripheral mac		
Family	Subfamily	Gene	Whole cortex	Neuron	Astrocyte	Oligodentrocyte	Microglia	Microglia	MHCII^{high} dural mac	MHCII^{low} dural mac	Choroid plexus mac	Peritoneal mac	Lung mac	Liver mac
Rhodopsin	Adenosine receptor	*Adora3*	0	0	0	1	47	611	22	25	6	10	28	4
	Adrenoceptor	*Adrb2*	4	0	0	1	103	2568	8318	13501	6524	920	3847	2164
	Chemokine receptor	*Ccr1*	3	0	0	1	60	351	4349	6842	4333	14289	4427	37
		Cxcr4	8	35	0	2	8	9	615	344	492	10	915	22
		Cx3cr1	15	1	0	13	490	93867	31545	27598	41414	17	8	124
	Class A Orphan	*Gpr34*	13	1	0	10	157	35152	10342	12402	6735	15	281	23
		Gpr183	3	0	0	2	190	4390	5363	7206	6691	468	16	30
	Complement peptide receptor	*C3ar1*	8	0	0	2	108	8111	27479	25932	19051	10112	19	8427
		C5ar1	7	0	0	1	98	3965	16696	21873	11177	9108	21700	4935
	Formylpeptide receptor	*Fpr1*	0	0	0	0	1	1	378	1561	288	1063	14012	12786
	Lysophospholipid receptor	*Lpar5*	0	0	0	0	9	746	379	301	320	1718	175	282
		Lpar6	5	1	4	1	8	493	3395	3460	2698	387	35	1287
	P2Y receptor	*P2ry12*	26	1	1	25	330	93304	5264	9613	3827	396	325	4412
		P2ry13	8	0	1	7	267	35751	5401	10289	4917	65	2835	8736
	Platelet-activating factor receptor	*Ptafr*	2	0	0	1	96	700	1449	1809	578	524	55	42
	Prostanoid receptor	*Ptger4*	1	0	1	0	6	371	7999	5741	4149	3235	2993	473
Adhesion	G	*Adgrg1*	76	33	27	55	447	23317	48	685	50	0	970	361
Gα protein	alpha i	*Gnai2*	150	66	20	133	458	14834	25493	24947	19921	22665	24465	24241
		Gnai3	33	25	10	21	9	2158	4512	4469	2360	12449	6625	3438
	alpha q	*Gnaq*	34	42	10	16	9	932	1872	2126	1068	1775	1356	916
		Gna11	28	25	5	28	6	441	557	795	533	701	259	447
		Gna15	1	0	0	1	101	7242	2990	4390	2709	2784	1986	826
	alpha s	*Gnas*	477	494	97	364	341	12636	15085	15113	10936	22753	13594	21053
	alpha 12/13	*Gna12*	30	20	10	108	104	6018	11209	12568	6614	1297	2070	3055
		Gna13	24	16	37	12	56	3262	3998	4152	1932	2391	2352	2758
GRKs		*Grk2*	33	26	2	18	109	4605	8692	9972	4415	6702	5269	11039
Arrestin	β-arrestin	*Arrb2*	19	26	3	14	199	4274	8086	8073	5143	8830	2408	6376

FIGURE 1 | Identification of GPCR and GPCR signaling molecule genes expressed in microglia. **(A)** Scatter plot providing GPCR gene expression in microglia isolated from human and mice as percentile of all human/mouse genes (8). **(B)** Scatter plot providing GPCR gene expression in brain and microglia of human as percentile of all genes (10). **(C)** Expression of GPCR and GPCR signaling molecule genes in mouse cortical tissue, neurons, astrocytes, oligodendrocytes, and microglia (11), and in mouse microglia, non-parenchymal brain and peripheral tissue macrophages (12). Expression is provided as FPKM (11) and gene count (12), respectively. mac, macrophages.

showing the characteristic morphology and gene expression of primary human microglia (13). Notably, iMPs expressed the GPCRs typically found in microglia. When transplanted into the brains of NOD scid gamma (NSG) mice, carrying the human transgenes encoding IL-3, SCF, GM-CSF, and CSF1, expression of *ADRB2*, *CX3CR1*, *GPR183*, *FPR1*, *LPAR5*, *LPAR6*, *P2RY12*, *P2RY13*, and *ADGRG1* was further enhanced at day 10 and/or 60 (**Figure 2** and **Supplementary Table 2**). This induction was not seen in iMPs cultured for the same period *in vitro*, which rather resulted in a downregulation of the expression of several GPCRs.

Various studies have established regional differences in microglia gene expression (2). Using data from our laboratory, we compared GPCR expression between human microglia obtained from subcortical white and cortical grey matter (4) (**Figure 2** and **Supplementary Table 2**). We found seven genes ≥2-fold higher expressed in either white or grey matter, respectively. In a second, independent dataset, we could confirm a higher gene expression in white matter microglia for *CXCR4* and *PTGER4* (Mizee et al, unpublished data). Single cell RNAseq has facilitated the investigation of microglial heterogeneity within brain regions. A study addressing this question showed, with the exception of *C3AR1*, a similar activity of GPCR genes in cortical microglia subsets (16) (**Supplementary Figure 1**).

Changes in gene expression in mouse models for Alzheimer's disease and amyotrophic lateral sclerosis (ALS) have led to the description of a phenotype referred to as disease-associated microglia, associated with significantly reduced expression of several signature GPCR genes (14). When comparing gene expression in pure microglia from normal-appearing, non-lesional tissue of deceased multiple sclerosis (MS) autopsy cases and tissue of non-pathological brains (**Figure 2** and **Supplementary Table 2**), we found downregulation of *ADGRG1* in both, white and grey matter, while expression of other GPCR genes was not changed.

Single cell RNAseq data of (models of) Alzheimer's disease, ALS, and MS revealed that pathological reprogramming only occurs in small subsets of disease-associated microglia that coexist with large subsets of homeostatic microglia and small subsets of infiltrating monocytes (14–16). Notably, disease-associated microglia in lesion biopsies of patients with histologically confirmed early active MS pathology showed reduced expression of the core signature genes *CX3CR1*, *GPR34*, *GPR183*, *P2RY12*, *P2RY13*, and *ADGRG1* (15, 26) (**Figures 3A, B**).

			Gosselin et al, 2017			Svoboda et al, 2019					Van der Poel et al, 2019			
			Microglia			iMPs	in vivo		in vitro		WM		GM	
Family	Subfamily	Gene	0 d	1 d	7 d		10 d	60 d	10 d	60 d	CON	MS	CON	MS
Rhodopsin	Adenosine receptor	*ADORA3*	162	11	46	22265	4864	23998	30578	20433	4359	3640	4780	4124
	Adrenoceptor	*ADRB2*	86	2	2	2274	1381	8628	1495	673	5246	4813	2837	2975
	Chemokine receptor	*CCR1*	125	92	188	11746	4952	14665	14118	7546	2840	2712	5234	3877
		CXCR4	111	21	8	2141	90	293	8542	1841	15831	17984	1449	5984
		CX3CR1	920	4	2	5008	74358	346492	146	2243	9175	12011	19974	22293
	Class A Orphan	*GPR34*	542	26	57	44970	32383	106441	47660	37619	5318	5089	6863	6563
		GPR183	139	44	84	3199	5383	19006	1018	1841	14883	13521	2913	4397
	Complement peptide receptor	*C3AR1*	222	86	242	15484	9734	18585	24888	25134	6653	5580	6517	6158
		C5AR1	108	346	360	3273	483	1840	5131	7335	7527	8141	2089	2427
	Formylpeptide receptor	*FPR1*	394	65	323	8478	2127	27248	7967	2325	3730	2117	8204	2937
	Lysophospholipid receptor	*LPAR5*	202	21	42	5096	5311	21826	4454	3400	2662	2591	4430	3798
		LPAR6	232	38	66	11368	9222	19940	3599	3276	9451	8748	15106	18231
	P2Y receptor	*P2RY12*	1050	1	3	4949	22464	219754	704	184	8274	9272	23102	20329
		P2RY13	253	1	5	2487	8282	40696	735	756	5488	4518	5786	6253
	Platelet-activating factor receptor	*PTAFR*	116	116	37	14233	11427	49899	20366	11692	4132	4410	4404	4745
	Prostanoid receptor	*PTGER4*	34	39	37	311	121	276	1583	1144	6769	7984	783	1628
Adhesion	G	*ADGRG1*	477	7	10	9485	11692	43760	4	17	12277	5267	20512	10089
Gα protein	alpha i	*GNAI2*	285	410	423	39251	23304	29388	31371	18922	7050	7402	6785	7064
		GNAI3	21	22	25	8743	5210	5650	6868	6046	1969	2081	1419	1404
	alpha q	*GNAQ*	32	21	18	1142	253	599	573	452	2680	2808	2937	2992
		GNA11	7	7	13	126	47	90	137	117	479	407	381	615
		GNA15	36	63	52	3761	2210	3504	3203	3741	1385	1691	915	776
	alpha s	*GNAS*	426	413	472	6137	2921	5578	6861	5762	13587	15412	11851	14254
	alpha 12/13	*GNA12*	18	81	97	248	114	193	638	1062	1494	2388	751	1124
		GNA13	64	41	37	3689	1738	3542	3777	2180	12252	20970	3007	3684
GRKs		*GRK2*	183	88	61	1020	464	981	549	522	6982	6244	7575	7469
Arrestin	β-arrestin	*ARRB2*	324	255	197	7238	2364	4697	5784	4465	4696	5024	5987	5873

FIGURE 2 | Gene expression of selected GPCRs and GPCR signaling molecules in human microglia. Expression of GPCR and GPCR signaling molecule genes in microglia cultured *ex vivo* for 1 and 7 days (10), in iPSC-derived iMPs transplanted neonatal mouse brains or cultured *in vitro* for 10 and 60 days (13), and in white matter and grey matter microglia from control and MS brains (4). Expression is provided as TPM (10) and gene count (4, 13), respectively. CON, control; WM, white matter; GM, grey matter.

In contrast, both disease-associated microglia and infiltrating monocytes had upregulated expression of *CXCR4*. In disease-associated microglia in surgically resected material of Alzheimer's disease patients, GPCR expression was not altered (16).

The late onset of neurodegenerative diseases, such as Alzheimer's disease, Parkinson's disease, and ALS, has triggered interest in the effect of aging on microglia gene expression. A study of aged microglia found a lower expression of the microglia signature genes *GPR183*, *P2RY12*, and *P2RY13* (17).

Expression of GPCR signaling molecule genes in the data sets studied here was quite stable. Separation of microglia from their CNS microenvironment or transfer of iMPs into NSG mouse brains only moderately affected signaling molecule gene expression (**Figure 2**). However, white matter microglia more abundantly expressed *GNA13* as compared to grey mater microglia. GPCR signaling molecule genes expression was not altered in normal-appearing or lesional MS microglia from either white or grey matter (**Figure 3C**).

Expression and MS-Associated Upregulation of CXCR4 by Human White Matter Microglia

The presence and MS-associated upregulation of *CXCR4* expression in microglia is of particular interest since Werner et al. recently showed that CXCR4 distinguishes monocytes from microglia in mice (27). To test whether human microglia express CXCR4, we analyzed freshly isolated cells by flow cytometry, shown here for three donors with MS (**Figure 4A**). Expression was detectable, albeit levels were moderate on white matter microglia and low on grey matter microglia (**Figures 4A, B**). On lesional microglia, we noticed a slightly higher expression of CXCR4 as well as lower expression of $P2Y_{12}$ compared to

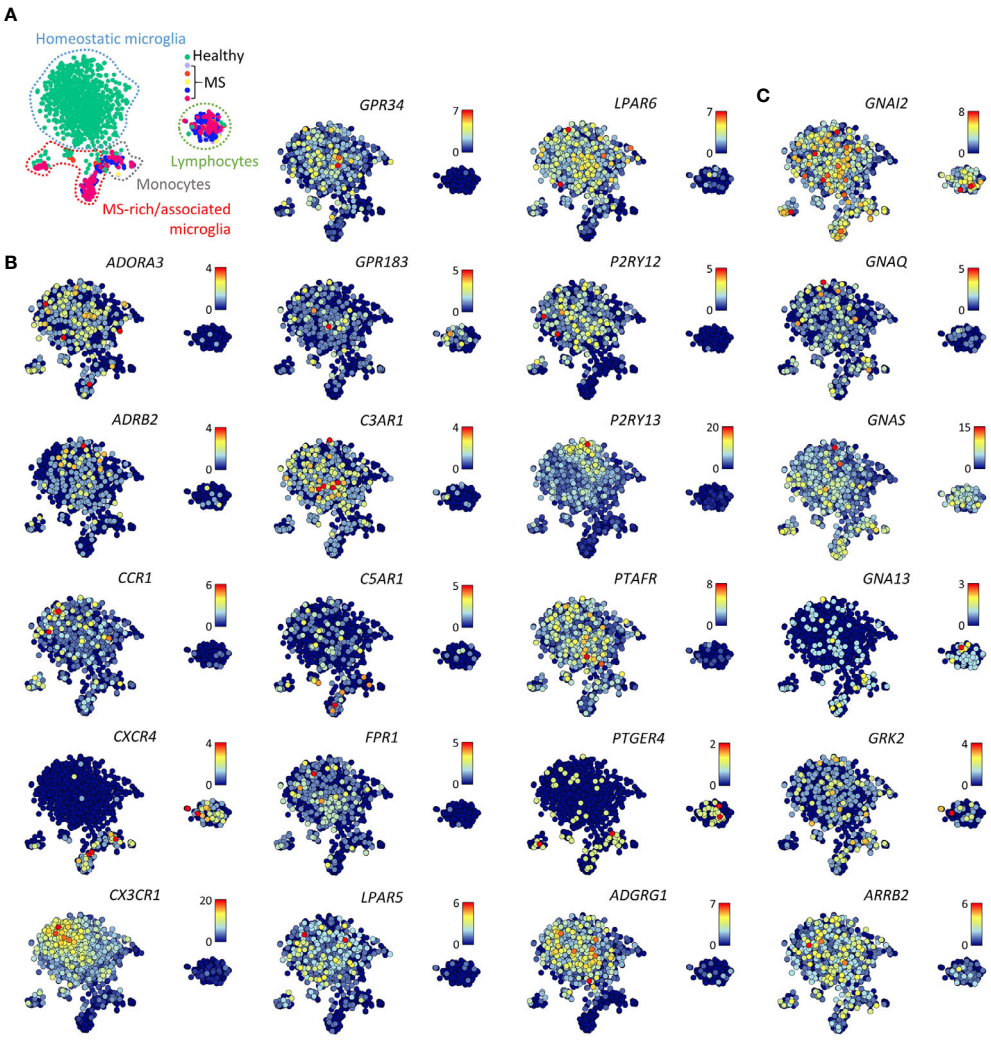

FIGURE 3 | Gene expression of selected GPCRs and GPCR signaling molecules in MS lesions. **(A)** *t*-SNE plot of 1,602 individual cells isolated from five non-pathological brains (healthy) and five brains of patients with early active MS representing with indicated homeostatic microglia, MS- enriched/associated microglia, monocytes, and lymphocytes. **(B, C)** *t*-SNE plots of GPCR **(B)** and GPCR signaling molecule **(C)** genes (15). Color codes represent expression levels.

microglia from subcortical normal-appearing white matter, the latter in line with Zrzavy et al. (26) (**Figures 4A, C**). Whole tissue gene expression microarray analysis of laser-dissected control white matter and white matter MS lesions (18) further confirmed increased expression of *CXCR4* in the rim of mixed active/inactive but not inactive lesions (**Figure 4D**).

To test whether expression of CXCR4 on microglia is functional, we studied transwell migration in response to SDF-1 (CXCL12) (14). SDF-1 binds to CXCR4 and CXCR7, the latter however is not expressed by microglia (**Supplementary Table 2**). Of note SDF-1 stimulated chemotaxis of monocytes, white matter and grey matter microglia at levels corresponding with the presence of CXCR4 (**Figure 4E**). We conclude that CXCR4 expression on human microglia is functional.

DISCUSSION

GPCRs constitute an important share of the sensome of eukaryotic cells. By analyzing various RNAseq datasets, we here provide a comprehensive overview of their presence in microglia. We identified 17 GPCR genes that are robustly transcribed in adult human microglia, including the homeostatic core genes *CX3CR1*, *GPR34*, *GPR183*, *P2RY12*, *P2RY13*, and *ADGRG1*, but also *ADORA3*, *ADRB2*, *CCR1*, *C3AR1*, *C5AR1*, *LPAR5*, *LPAR6*, and *PTAFR*. GPCRs genes well expressed in human microglia but hardly found in mouse microglia were *CXCR4*, *FPR1*, and *PTGER4*.

Figure 5 summarizes the findings of this study. As expected, isolated microglia rapidly lost expression of several GPCRs when

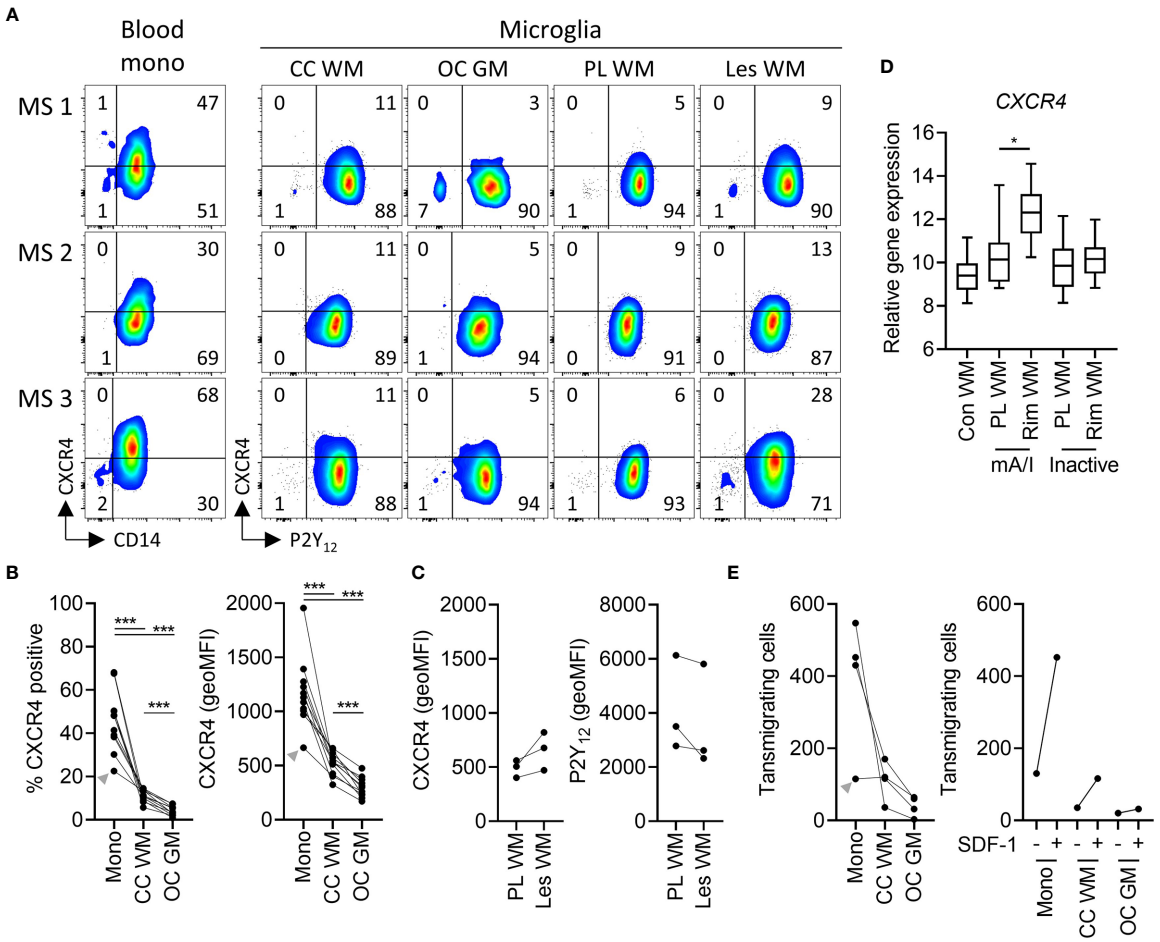

FIGURE 4 | Expression of functional CXCR4 in white and grey matter microglia in health and MS. **(A)** Representative dot plots of CXCR4 expression on paired peripheral CD14$^+$ blood monocytes and P2Y$_{12}^+$ microglia from corpus callosum white matter and occipital cortex grey matter, as well as P2Y$_{12}^+$ microglia from peri-lesional and lesional subcortical WM of three MS brain donors measured by flow cytometry. **(B)** Quantification of CXCR4 expression (percentage of positive cells and geoMFI) on monocytes, WM microglia, and GM microglia of n=11 brain donors (3 MS, 8 non-MS; Wilcoxon-signed rank test; ***p < 0.0005). **(C)** Quantification of CXCR4 and P2Y$_{12}$ expression on microglia from peri-lesional and lesional WM of three MS brain donors. **(D)** Quantification of tissue gene expression of *CXCR4* in control as well as peri-lesional and lesional WM from mixed active/inactive and inactive MS lesions (18) (Wilcoxon-signed rank test; *p < 0.05). **(E)** Quantification of transwell migration of monocytes, white matter microglia, and grey matter microglia in response to the CXCR4 ligand SDF-1 of n=4 brain donors (left panel). Of note, SDF-1-stimulated transwell migration was higher as compared to spontaneous transwell migration in all three cell types (n=1 brain donor; right panel). A donor with a relatively low expression of CXCR4 on monocytes also showed low monocyte transmigration towards SDF-1 (grey arrowhead). mono, monocytes; CC, corpus callosum; WM, white matter; OC, occipital cortex; GM, grey matter; PL, peri-lesional; Les, lesional; mA/I, mixed active/inactive; geoMFI, geometric mean fluorescence intensity.

cultured *ex vivo*, which limits the value of *in vitro*-expanded primary cells for functional studies. In contrast, iPSC-derived iMPs had a GPCR expression remarkably similar to primary microglia, which further equalized upon transfer into NSG mouse brains, ectopically providing critical human growth factors building the microglia phenotype. Regional diversity of microglia has been suggested (2), and we indeed found more abundant expression of *CXCR4* and *PTGER4* in white matter as compared to grey matter microglia in two independent studies [(4) and Mizee et al., unpublished data].

Disease-associated microglia in mouse models of AD and ALS downregulate expression of various GPCR genes, including *Cx3cr1*, *P2ry12*, *P2ry13*, and *Adgrg1* (14). The data presented here refer to MS, an inflammatory demyelinating and neurodegenerative disease. Bulk primary microglia collected post-mortem from normal-appearing tissue of MS donors showed downregulation of *ADGRG1* (4) in grey and white matter. *ADGRG1* encodes the adhesion family GPCR GPR56 (28), which is more widely expressed in the CNS and has been linked in neuronal precursors with cortical lamination and in oligodendrocyte precursors with proliferation (29). Abundant presence of GPR56 on human microglia (4) and regulation of synaptic refinement through a mouse GPR56 splicing isoform (30) have been reported only recently. Obviously, *ADGRG1* expression not only distinguishes microglia from other macrophages but also fades out in response to minor changes in the microenvironment, stressing its value as indicator of microglia homeostasis. In biopsies of active lesions in early cases of MS, diseases-associated microglia subsets showed the expected general downregulation of GPCR genes associated with microglia homeostasis. Single-cell mass cytometry indeed confirmed the appearance of active MS lesion-enriched clusters with a down-regulated surface expression of $P2Y_{12}$, CX3CR1, and GPR56 (31).

The distribution of the chemokine receptor CXCR4 is of particular interest. CXCR4 binds CXCL12 (SDF-1), which is expressed by the brain vasculature and upregulated in MS lesions (32). Werner et al. recently reported that CXCR4 distinguishes brain-infiltrating monocytes from resident microglia in mice (27). We here demonstrate that human microglia from white and – to a lesser extent – grey matter express CXCR4. Transmigration towards SDF-1 confirmed the relevance of the presence of CXCR4 on microglia. Expression of CXCR4 by both microglia and infiltrating monocytes and upregulation by small subset of MS-associated lesional microglia (15) makes this chemokine receptor, involved in immune cell homeostasis and margination (33), a potentially interesting target for therapeutic intervention. Indeed, *Cxcr4* gene ablation reduced monocyte infiltration and response gene expression in experimental stroke in mice (27).

When testing the expression of genes encoding signaling molecules downstream of GPCRs, in particular Gα proteins, GRKs, and β-arrestin (6), we found robust expression of *GNAI2*, *GNAS*, *GNA13*, *GRK2*, and *ARRB2*. Further, mice, but not human, abundantly expressed *Gna15*. Expression of these genes did not depend on the specific microenvironment of

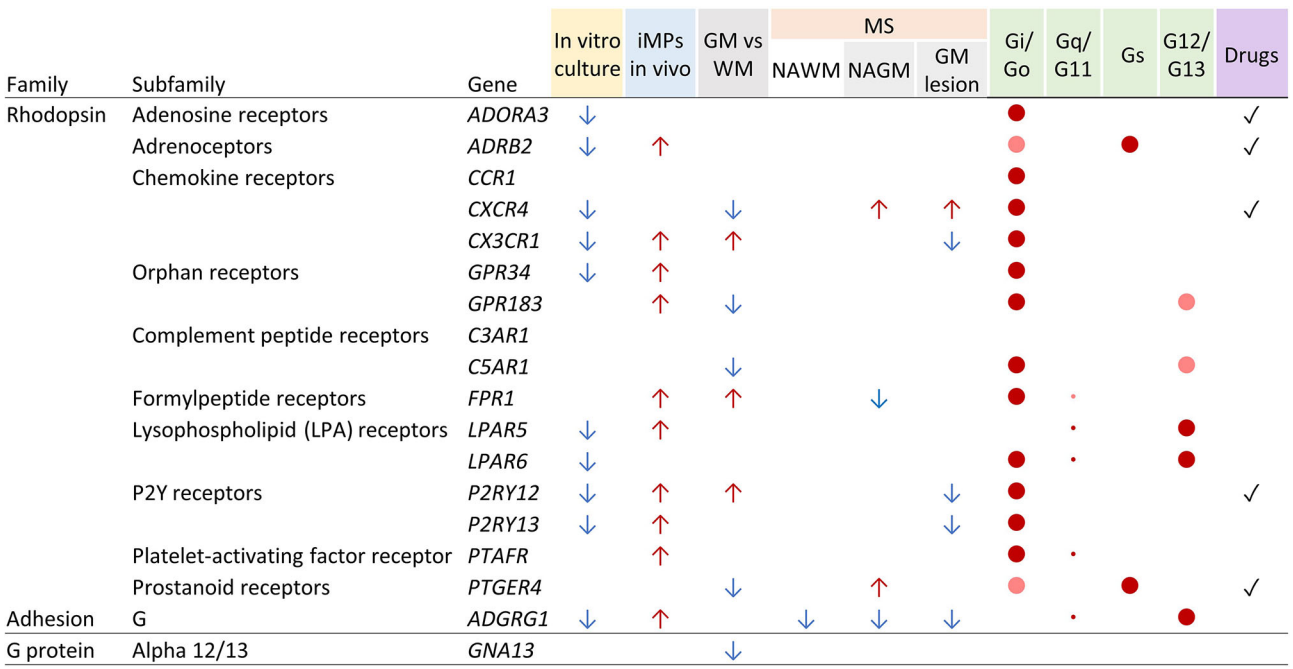

FIGURE 5 | Tabular summary of human microglia GPCR gene regulation, signaling, and drug availability. See Discussion for details. Arrows indicate the direction of regulation. Colored dots indicate prevalence of signaling of GPCRs through the respective G proteins (red = high; light red = medium) and abundance of gene expression of the G proteins in microglia (large dots = high; small dots = low). WM, white matter; GM, grey matter; NAGM, normal-appearing grey matter; NAWM, normal-appearing white matter.

microglia and was found at similar levels in other macrophages. $G\alpha_s$-coupled receptors activate adenylate cyclase, leading to cAMP accumulation. While *GNAS* transcripts were abundant in microglia, only two highly expressed GPCRs primarily couple to this Gα subunit (*ADRB2*, *PTGER4*) suggesting rather limited augmentation of cAMP levels in microglia through GPCR signaling. $G\alpha_i$-coupled receptors inhibit the cAMP-dependent pathway by inhibiting adenylyl cyclase activity. Our data indicate that $G\alpha_i$, the preferred Gα subunit of 12 of the 17 abundant microglia GPCRs, is well expressed in microglia, implying inhibition of cAMP-dependent protein kinase (PKA). $G\alpha_{12/13}$-coupled receptors activate the small GTPase RhoA. We found *GNA13* abundantly transcribed in white but not grey matter, which explains why initial studies of cortical microglia reported dim expression (10). Finally, $G\alpha_q$-coupled receptors activate phospholipase C to increase intracellular calcium concentration as well as activate protein kinase C, which results in Raf kinase activation of the MAPK pathway. *GNAQ* transcript levels were generally low, suggesting that LPAR5, LPAR6, and GPR56, which can engage $G\alpha_{12/13}$ as well as $G\alpha_q$, may rather control cell cytoskeleton remodeling and thus regulate microglia migration. Yet, in particular for GPR56, molecular mechanisms additional to G protein signaling may apply (28, 34).

GPCRs are known for their excellent drugability. A survey at DrugBank (https://www.drugbank.ca/) revealed approved drugs against at least five highly expressed microglia GPCRs with indications covering, amongst others, conditions of the lungs (ADORA3, ADRB2), eye (ADRB2), blood (CXCR4, $P2Y_{12}$), heart ($P2Y_{12}$), and uterus (PTGER4). Moreover, rodent models suggest efficacy of CXCR4 targeting in the treatment of stroke and glioma (35). Studying the effects of small molecules, penetrating the blood–brain barrier, on microglia *in vitro* and *in vivo* may disclose novel opportunities for the treatment of brain diseases in which microglia emerge as central players, including neurodevelopmental disorders (e.g., autism), neurodegenerative and -inflammatory conditions (e.g., Alzheimer's disease and MS), and chronic pain (1).

In summary, we here describe the GPCR repertoire of human microglia based on publicly available bulk and single-cell RNAseq data. GPCRs that belong to the core signature of microglia are abundantly expressed under homeostatic and rapidly downregulated under non-homeostatic conditions, making them interesting models for studying microenvironmental factors that shape microglia identity during brain development and disease. Datasets of microglia from brain donors with neurological diseases only lately became available and require further investigation. This in particular holds true as drugs targeting different highly expressed microglia GPCRs have been developed, implying their potential application for CNS diseases in which microglia figurate.

DATA AVAILABILITY STATEMENT

The datasets presented in this study can be found in online repositories. The names of the repository/repositories and accession number(s) can be found below: https://www.ncbi.nlm.nih.gov/ (accessible under accession code GEO: GSE52564, GSE98969, GSE99074, GSE108000, GSE111972, GSE124335, GSE128855, GSE134707, GSE139194), https://www.synapse.org/#!Synapse:syn21438358 and http://shiny.maths.usyd.edu.au/Ellis/MicrogliaPlots/.

ETHICS STATEMENT

Written informed consent was obtained from the individual(s) for the publication of any potentially identifiable images or data included in this article.

AUTHOR CONTRIBUTIONS

C-CH and RS extracted and analyzed data. C-CH, RS, MP, JS, IH, and JH designed research and interpreted results. C-CH and JH wrote the paper. All authors contributed to the article and approved the submitted version.

FUNDING

The German Research Foundation (FOR 2149 – JH), the Berta-Ottenstein-Programme for Clinical Scientists (RS), the MS Research Foundation (MS 13-830 – IH/JH), and the Nationaal MS Fonds (OZ2018-003 – JS) funded this research.

SUPPLEMENTARY MATERIAL

The Supplementary Material for this article can be found online at: https://www.frontiersin.org/articles/10.3389/fimmu.2021.674189/full#supplementary-material

REFERENCES

1. Salter MW, Stevens B. Microglia Emerge as Central Players in Brain Disease. *Nat Med* (2017) 23:1018–27. doi: 10.1038/nm.4397
2. Prinz M, Jung S, Priller J. Microglia Biology: One Century of Evolving Concepts. *Cell* (2019) 179:292–311. doi: 10.1016/j.cell.2019.08.053
3. Crotti A, Ransohoff RM. Microglial Physiology and Pathophysiology: Insights From Genome-wide Transcriptional Profiling. *Immunity* (2016) 44:505–15. doi: 10.1016/j.immuni.2016.02.013
4. van der Poel M, Ulas T, Mizee MR, Hsiao CC, Miedema SSM, Adelia, et al. Transcriptional Profiling of Human Microglia Reveals Grey–White Matter Heterogeneity and Multiple Sclerosis-Associated Changes. *Nat Commun* (2019) 10:1139. doi: 10.1038/s41467-019-08976-7
5. Hauser AS, Attwood MM, Rask-Andersen M, Schiöth HB, Gloriam DE. Trends in GPCR Drug Discovery: New Agents, Targets and Indications. *Nat Rev Drug Discov* (2017) 16:829–42. doi: 10.1038/nrd.2017.178
6. Pierce KL, Premont RT, Lefkowitz RJ. Seven-Transmembrane Receptors. *Nat Rev Mol Cell Biol* (2002) 3:639–50. doi: 10.1038/nrm908
7. Li Q, Barres BA. Microglia and Macrophages in Brain Homeostasis and Disease. *Nat Rev Immunol* (2018) 18:225–42. doi: 10.1038/nri.2017.125
8. Geirsdottir L, David E, Keren-Shaul H, Weiner A, Bohlen SC, Neuber J, et al. Cross-Species Single-Cell Analysis Reveals Divergence of the Primate

Microglia Program. *Cell* (2019) 179:1609–22.e16. doi: 10.1016/j.cell.2019.11.010
9. Galatro TF, Holtman IR, Lerario AM, Vainchtein ID, Brouwer N, Sola PR, et al. Transcriptomic Analysis of Purified Human Cortical Microglia Reveals Age-Associated Changes. *Nat Neurosci* (2017) 20:1162–71. doi: 10.1038/nn.4597
10. Gosselin D, Skola D, Coufal NG, Holtman IR, Schlachetzki JCM, Sajti E, et al. An Environment-Dependent Transcriptional Network Specifies Human Microglia Identity. *Science* (2017) 356:1248–59. doi: 10.1126/science.aal3222
11. Zhang Y, Chen K, Sloan SA, Bennett ML, Scholze AR, O'Keeffe S, et al. An RNA-sequencing Transcriptome and Splicing Database of Glia, Neurons, and Vascular Cells of the Cerebral Cortex. *J Neurosci* (2014) 34:11929–47. doi: 10.1523/JNEUROSCI.1860-14.2014
12. Van Hove H, Martens L, Scheyltjens I, De Vlaminck K, Pombo Antunes AR, De Prijck S, et al. A Single-Cell Atlas of Mouse Brain Macrophages Reveals Unique Transcriptional Identities Shaped by Ontogeny and Tissue Environment. *Nat Neurosci* (2019) 22:1021–35. doi: 10.1038/s41593-019-0393-4
13. Svoboda DS, Barrasa MI, Shu J, Rietjens R, Zhang S, Mitalipova M, et al. Human iPSC-derived Microglia Assume a Primary Microglia-Like State After Transplantation Into the Neonatal Mouse Brain. *Proc Natl Acad Sci USA* (2019) 116:25293–303. doi: 10.1073/pnas.1913541116
14. Keren-Shaul H, Spinrad A, Weiner A, Matcovitch-Natan O, Dvir-Szternfeld R, Ulland TK, et al. A Unique Microglia Type Associated With Restricting Development of Alzheimer's Disease. *Cell* (2017) 169:1276–1290.e17. doi: 10.1016/j.cell.2017.05.018
15. Masuda T, Sankowski R, Staszewski O, Böttcher C, Amann L, Sagar, et al. Spatial and Temporal Heterogeneity of Mouse and Human Microglia At Single-Cell Resolution. *Nature* (2019) 566:388–92. doi: 10.1038/s41586-019-0924-x
16. Olah M, Menon V, Habib N, Taga MF, Ma Y, Yung CJ, et al. Single Cell RNA Sequencing of Human Microglia Uncovers a Subset Associated With Alzheimer's Disease. *Nat Commun* (2020) 11:6129. doi: 10.1038/s41467-020-19737-2
17. Olah M, Patrick E, Villani AC, Xu J, White CC, Ryan KJ, et al. A Transcriptomic Atlas of Aged Human Microglia. *Nat Commun* (2018) 9:539. doi: 10.1038/s41467-018-02926-5
18. Hendrickx DAE, van Scheppingen J, van der Poel M, Bossers K, Schuurman KG, van Eden CG, et al. Gene Expression Profiling of Multiple Sclerosis Pathology Identifies Early Patterns of Demyelination Surrounding Chronic Active Lesions. *Front Immunol* (2017) 8:1810. doi: 10.3389/fimmu.2017.01810
19. Mizee MR, Miedema SSM, van der Poel M, Adelia, Schuurman KG, van Strien ME, et al. Isolation of Primary Microglia From the Human Post-Mortem Brain: Effects of Ante- and Post-Mortem Variables. *Acta Neuropathol Commun* (2017) 5:16. doi: 10.1186/s40478-017-0418-8
20. Alexander SPH, Christopoulos A, Davenport AP, Kelly E, Mathie A, Peters JA, et al. The CONCISE Guide TO Pharmacology 2019/20: G Protein-Coupled Receptors. *Br J Pharmacol* (2019) 176:S21–141. doi: 10.1111/bph.14748
21. Schiöth HB, Lagerström MC. Structural Diversity of G Proteincoupled Receptors and Significance for Drug Discovery. *Nat Rev Drug Discov* (2008) 7:339–57. doi: 10.1038/nrd2518
22. Hamann J, Koning N, Pouwels W, Ulfman LH, van Eijk M, Stacey M, et al. EMR1, the Human Homolog of F4/80, is an Eosinophil-Specific Receptor. *Eur J Immunol* (2007) 37:2797–802. doi: 10.1002/eji.200737553
23. Lin HH, Hsiao CC, Pabst C, Hébert J, Schöneberg T, Hamann J. Adhesion GPCRs in Regulating Immune Responses and Inflammation. *Adv Immunol* (2017) 136:163–201. doi: 10.1016/bs.ai.2017.05.005
24. Visser L, De Vos AF, Hamann J, Melief MJ, Van Meurs M, Van Lier RAW, et al. Expression of the EGF-TM7 Receptor CD97 and its Ligand CD55 (DAF) in Multiple Sclerosis. *J Neuroimmunol* (2002) 132:156–63. doi: 10.1016/S0165-5728(02)00306-5
25. Hsiao CC, Van Der Poel M, Van Ham TJ, Hamann J. Macrophages do Not Express the Phagocytic Receptor BAI1/ADGRB1. *Front Immunol* (2019) 10:962. doi: 10.3389/fimmu.2019.00962
26. Zrzavy T, Hametner S, Wimmer I, Butovsky O, Weiner HL, Lassmann H. Loss of "Homeostatic" Microglia and Patterns of Their Activation in Active Multiple Sclerosis. *Brain* (2017) 140:1900–13. doi: 10.1093/brain/awx113
27. Werner Y, Mass E, Ashok Kumar P, Ulas T, Händler K, Horne A, et al. Cxcr4 Distinguishes HSC-derived Monocytes From Microglia and Reveals Monocyte Immune Responses to Experimental Stroke. *Nat Neurosci* (2020) 23:351–62. doi: 10.1038/s41593-020-0585-y
28. Hamann J, Aust G, Araç D, Engel FB, Formstone C, Fredriksson R, et al. International Union of Basic and Clinical Pharmacology. XCIV. Adhesion G Protein-Coupled Receptors. *Pharmacol Rev* (2015) 67:338–67. doi: 10.1124/pr.114.009647
29. Langenhan T, Piao X, Monk KR. Adhesion G Protein-Coupled Receptors in Nervous System Development and Disease. *Nat Rev Neurosci* (2016) 17:550–61. doi: 10.1038/nrn.2016.86
30. Li T, Chiou B, Gilman CK, Luo R, Koshi T, Yu D, et al. A Splicing Isoform of GPR56 Mediates Microglial Synaptic Refinement Via Phosphatidylserine Binding. *EMBO J* (2020) 39:e104136. doi: 10.15252/embj.2019104136
31. Böttcher C, Van Der Poel M, Fernández-Zapata C, Schlickeiser S, Leman JKH, Hsiao CC, et al. Single-Cell Mass Cytometry Reveals Complex Myeloid Cell Composition in Active Lesions of Progressive Multiple Sclerosis. *Acta Neuropathol Commun* (2020) 8:136. doi: 10.1186/s40478-020-01010-8
32. Krumbholz M, Theil D, Cepok S, Hemmer B, Kivisäkk P, Ransohoff RM, et al. Chemokines in Multiple Sclerosis: CXCL12 and CXCL13 Up-Regulation is Differentially Linked to CNS Immune Cell Recruitment. *Brain* (2006) 129:200–11. doi: 10.1093/brain/awh680
33. Nagasawa T. CXC Chemokine Ligand 12 (CXCL12) and its Receptor CXCR4. *J Mol Med* (2014) 92:433–9. doi: 10.1007/s00109-014-1123-8
34. Langenhan T, Aust G, Hamann J. Sticky Signaling - Adhesion Class G Protein-Coupled Receptors Take the Stage. *Sci Signal* (2013) 6:re3. doi: 10.1126/scisignal.2003825
35. Tahirovic YA, Pelly S, Jecs E, Miller EJ, Sharma SK, Liotta DC, et al. Small Molecule and Peptide-Based CXCR4 Modulators as Therapeutic Agents. A Patent Review for the Period From 2010 to 2018. *Expert Opin Ther Pat* (2020) 30:87–101. doi: 10.1080/13543776.2020.1707186

Conflict of Interest: The authors declare that the research was conducted in the absence of any commercial or financial relationships that could be construed as a potential conflict of interest.

frontiers in Molecular Neuroscience

ORIGINAL RESEARCH
published: 20 May 2021
doi: 10.3389/fnmol.2021.582497

Microglia Stimulation by Protein Extract of Injured Rat Spinal Cord. A Novel *In vitro* Model for Studying Activated Microglia

*Joaquim Hernández, Isaac Francos-Quijorna, Elena Redondo-Castro, Rubén López-Vales and Xavier Navarro**

Group of Neuroplasticity and Regeneration, Department of Cell Biology, Physiology and Immunology, Institute of Neurosciences, Centro de Investigación Biomédica en Red sobre Enfermedades Neurodegenerativas (CIBERNED), Universitat Autònoma de Barcelona, Red de Terapia Celular (TerCel), Bellaterra, Spain

Research on microglia has established the differentiation between the so-called M1 and M2 phenotypes. However, new frameworks have been proposed attempting to discern between meaningful microglia profiles. We have set up an *in vitro* microglial activation model by adding an injured spinal cord (SCI) lysate to microglial cultures, obtained from postnatal rats, in order to mimic the environment of the spinal cord after injury. We found that under the presence of the SCI lysate microglial cells changed their phenotype, developing less ramified but longer processes, and proliferated. The SCI lysate also led to upregulation of pro-inflammatory cytokines, such as IL-1β, IL-6, and TNF-α, downregulation of the anti-inflammatory cytokines IL-10 and IL-4, and a biphasic profile of iNOS. In addition, a latex beads phagocytosis assay revealed the SCI lysate stimulated the phagocytic capacity of microglia. Flow cytometry analysis indicated that microglial cells showed a pro-inflammatory profile in the presence of SCI lysate. Finally, characterization of the microglial activation in the spinal cord on day 7 after contusion injury, we showed that these cells have a pro-inflammatory phenotype. Overall, these results indicate that the use of SCI lysates could be a useful tool to skew microglia towards a closer phenotype to that observed after the spinal cord contusion injury than the use of LPS or IFNγ.

Keywords: microglia, spinal cord injury, microglia culture, lysate, phagocytosis, mRNA expression, rat

OPEN ACCESS

Edited by:
Amanda Sierra, Achucarro Basque Center for Neuroscience, Spain

Reviewed by:
Daniel Garcia-Ovejero, National Paraplegic Hospital, Spain
Bente Finsen, University of Southern Denmark, Denmark

****Correspondence:***
Xavier Navarro
xavier.navarro@uab.cat

Specialty section:
This article was submitted to Molecular Signalling and Pathways, a section of the journal Frontiers in Molecular Neuroscience

Received: *12 July 2020*
Accepted: *14 April 2021*
Published: *20 May 2021*

Citation:
Hernández J, Francos-Quijorna I, Redondo-Castro E, López-Vales R and Navarro X (2021) Microglia Stimulation by Protein Extract of Injured Rat Spinal Cord. A Novel In vitro Model for Studying Activated Microglia. Front. Mol. Neurosci. 14:582497. doi: 10.3389/fnmol.2021.582497

INTRODUCTION

Spinal cord injury (SCI) leads to partial or complete loss of motor, sensory and autonomic functions below the injury level, due to damage to the local circuitry of the spinal cord and interruption of ascending and descending neural pathways (Ahuja et al., 2017). Traumatic SCI causes direct tissue damage that initiates a cascade of secondary events resulting in expanded tissue loss. There is a coordinated change in gene and protein expression profile associated with physiopathological events, including hemorrhage, excitotoxicity, oxidative stress, neuronal activity imbalance, and inflammation (Tator and Fehlings, 1991; Popovich, 2014; Siddiqui et al., 2015; Silver et al., 2015; Greenhalgh et al., 2020).

Microglia are one of the most important cells that participate in the inflammatory response that occurs after SCI. Although they are often considered to be macrophages of the CNS, recent studies documented microglia as a unique cell population, with distinct lineage and molecular signature than macrophages (Salter and Beggs, 2014). Microglia play many physiological functions in the CNS. For instance, they track tissue environment from insults or pathogens (Nimmerjahn, 2005), maintain tissue homeostasis and play a key role in the development of CNS (Prinz et al., 2019), control neuronal activity, synaptic maturation and plasticity, drive programmed cell death in CNS development, undergo central players in the innate immune response following injury (David and Kroner, 2011; Salter and Beggs, 2014).

Microglia rapidly change their phenotype in response to any disturbance of tissue homeostasis towards a commonly referred to as activated phenotype on the basis of changes in morphology or expression of cell surface antigens (Ransohoff and Perry, 2009; David and Kroner, 2011; Franco and Fernández-Suárez, 2015; Gensel and Zhang, 2015; Prinz et al., 2019). The specific activity of microglia after injury includes a wide range of functions, performed through specific roles of polarized microglia at different stages of the injury (Kigerl et al., 2009). It is usually considered as the concept of two different forms of microglia/macrophage polarization induced by either Th1 (IFNγ, LPS) or Th2 (IL-4 and IL-13) mediators. IFNγ/LPS-polarized microglia/macrophages are called M1 or "classically" activated microglia and macrophages and are characterized by expressing high levels of iNOS, TNF-α, or IL-1β, and the surface markers CD16/32. On the other hand, IL-4 or IL-13 promotes M2 or "alternatively activated" microglia and macrophage. M2 microglia/macrophages are characterized by expressing Arg1, CD206 and anti-inflammatory cytokines, such as IL-10 or TGF-β (Gordon and Taylor, 2005; David and Kroner, 2011; Francos-Quijorna et al., 2016). The current view of M1/M2 polarization is a simplified model that only represents two extremes of activation states (Ransohoff, 2016). However, after CNS injury, microglia are not stimulated by a single factor, such as IFNγ or IL-4, but by multiple mediators that lead microglia to adopt different activation states and functions to those observed in cell culture conditions. For this reason, there is a need to develop novel *in vitro* approaches that could drive microglia to a closer activation state to that observed *in vivo* after a CNS challenge. For this purpose, here we studied the effects of a spinal cord injury lysate on microglia activation as a more physiopathological approach than classical addition of IFNγ/LPS or IL-4. By studying microglia polarization *in vitro* under the effect of an SCI lysate, we aim to gain knowledge about microglia phenotype changes and to have a screening assay for comparison with the *in vivo* microglia reactivity after SCI.

MATERIALS AND METHODS

Spinal Cord Injury

Adult female Sprague–Dawley rats (9 weeks old; 250–300 g) were used. The animals were housed with free access to food and water at a room temperature (RT) of 22 ± 2°C under a 12:12 light-dark cycle. The experimental procedures were approved by the ethical committee of the Universitat Autònoma de Barcelona in accordance with the European Directive 86/609/EEC. Under anesthesia with ketamine (90 mg/kg; Imalgene^R 1000; Boehringer Ingelheim, Germany) and xylazine (10 mg/kg; Rompun^R; Bayer, Germany) and aseptic conditions, a longitudinal dorsal incision was made to expose the T6-T10 spinous processes. A laminectomy of T8-T9 vertebra was made and a cord contusion of 100 Kdynes was induced using an Infinite Horizon Impactor device (Precision System and Instrumentation, Fairfax Station, VA, USA). The wound was sutured by planes and the animals allowed to recover in a warm environment. An intraperitoneal (i.p.) bolus of saline solution (B.Braun Vetcare, UK) was administered immediately after surgery. To prevent infection, amoxicillin (500 mg/L; Normon, Spain) was given in the drinking water for 1 week. Postoperative analgesia was provided with buprenorphine (0.05 mg/kg; B.Braun Vetcare, UK) for 48 h. Bladders were expressed twice a day until reflex voiding was re-established.

Extracts were obtained from the intact spinal cord or from the injured spinal cord harvested at 7 days after the contusion. Fresh tissue was removed from the lesion site (around 1 cm), and an ultrasonic probe applied to disaggregate it in HBSS buffer (Gibco, USA). The extract was spun down (10,000 g) and filtered. Quantification of the protein content from the supernatant was made by the BCA method (Thermo Fisher Scientific, Germany), and a range of 15–20 μg protein/μl was obtained by colorimetry (Bio-Tek Instruments Inc., Germany). Extracts were water-soluble and were solubilized in HBSS buffer.

Microglial Cultures

Glial cell cultures were prepared from 1-day-old Sprague–Dawley rats, as previously described (Redondo-Castro et al., 2013). Briefly, following the removal of meninges, brain tissue was minced and incubated for 10 min at 37°C in Ca^{2+}-free Krebs-Ringer buffer containing 0.0025% trypsin (Sigma–Aldrich, St. Louis, MO, USA). Enzyme dissociated cells were mechanically triturated through a glass pipette and filtered through a 40-μm nylon mesh (Corning, USA) in the presence of 0.52 mg/ml soybean trypsin inhibitor (Gibco, USA) and 170 IU/ml DNAse (Roche, Switzerland). After centrifugation (500 g), the cells were stained with Trypan Blue exclusion dye (Sigma–Aldrich, St. Louis, MO, USA), counted in a Neubauer chamber, and then resuspended in 90% Dulbecco's modified Eagle medium (DMEM; Gibco, USA), 10% foetal bovine serum (FBS; Sigma–Aldrich, St. Louis, MO, USA), 20 U/ml penicillin and 20 mg/ml streptomycin (Sigma–Aldrich, St. Louis, MO, USA) at 3×10^5 cells/ml.

Cells were plated and incubated at 37°C in a humidified atmosphere of 5% CO_2 and 95% air (Heracell^{TM} 150i CO_2 incubator; Thermo Fisher Scientific); medium was replaced every 3 days. After 14–15 days *in vitro*, the culture became confluent and microglial cells were obtained by shaking the flasks for 2 h at 200 rpm. Floating cells were spun down to obtain the dislodged cells and cultured at 150,000 cells/ml. This enriched fraction (around 95–97%) of microglia was seeded on poly-D-lysine-treated well or glass cover-slips in 24-well plates (PDL from Sigma–Aldrich,

St. Louis, MO, USA), and maintained in DMEM medium supplemented with 10% FBS, 20 U/ml penicillin and 20 μg/ml streptomycin. After 3 days, microglial cells were ready to be treated.

Agents used for microglia activation were lipopolysaccharide at 10 ng/ml (LPS; *Escherichia coli* 0127:B Sigma–Aldrich, St. Louis, MO, USA), IL-4 at 10 ng/ml (Affymetrix eBioscience, USA), IFNγ at 10 ng/ml (Affymetrix eBioscience, USA) or an extract lysate obtained from the intact and 7 days injured spinal cords (SC lysate and SCI lysate). Different concentrations of the lysate were tested depending on the experiment (10, 25, 50 or 100 μg/ml).

Immunocytochemistry

After treatments, coverslips were fixed in 4% paraformaldehyde for 20 min at RT and washed in PBS. Blockade of nonspecific binding was performed with 5% foetal calf serum (FCS) in 0.1% Triton X-100/PBS. Then, coverslips were incubated in the same solution at 4°C overnight with primary antibodies: anti-rabbit iba1 (1:500; Wako, Japan) or anti-goat iba1 (1:200; Abcam, Cambridge, MA, USA), used to detect macrophage/microglial cells; anti-mouse GFAP (1:200; Sigma–Aldrich, St. Louis, MO, USA), used to detect astrocytes; anti-rabbit Tubulin β-3 (1:200; Biolegend, USA), used to detect neurons; anti-mouse O4 (1:200; Sigma–Aldrich, St. Louis, MO, USA), used to detect oligodendrocytes; or anti-rabbit Ki67 (1:200; Abcam, Cambridge, MA, USA), used to detect proliferation. After several washes in 0.1% Triton X-100/PBS, samples were incubated for 2 h at RT with donkey anti-rabbit Alexa Fluor 488-conjugated antibody (1:200; Invitrogen, USA), donkey anti-mouse Alexa Fluor 488-conjugated antibody (1:200; Invitrogen, USA), donkey anti-goat Alexa 488-conjugated antibody (1:200; Invitrogen, USA), donkey anti-rabbit Cy3-conjugated antibody (1:200; Jackson IR, USA) or donkey anti-mouse Cy3-conjugated antibody (1:200; Jackson IR, USA), in 0.1% Triton X-100/PBS with 1.5% FCS at RT. In the last wash, cells were incubated with DAPI (5 μg/ml; Sigma–Aldrich, St. Louis, MO, USA) to perform nuclear staining.

Morphological Analysis of Microglia

Microglia morphology was quantified in fluorescent images from Iba1-immunostained cultures by using ImageJ software (NIH, USA) and skeleton analysis plugin [Analyze Skeleton (2D/3D) from http://imageJ.net/AnalyzeSkeleton]. Analysis was performed according to a previously described procedure (Young and Morrison, 2018; Blasco et al., 2020). For this purpose, digital photomicrographs were transformed to 8-bit grayscale and then binarised to obtain a black and white image by means of a formerly established threshold. Every image was manually edited to obtain an image with a continuous set of pixels and gaps between processes belonging to neighboring cells. The image was then saved, and the plugin Skeleton (2D/3D) was run. This step results in a tagged skeleton image from which the number of endpoints and branch length can be summarized from the resulting output files. Endpoints and process length data are then used to estimate the range of microglia extensions in the photomicrograph. Four images per condition, from three biological replicates, were used to perform these analyses (ranging between 600 and 800 total cells per replicate).

Proliferation Assay

At 24 h upon microglia stimulation, cells were fixed with 4% paraformaldehyde (PFA) for 15 min and immunohistochemistry against Iba1 (1:500; Wako, Japan) and Ki67 (1:200; Abcam, Cambridge, MA, USA) was performed as indicated above. Several images were randomly taken and total cells and labeled Ki67 cells were counted. Microphotographs were analyzed using ImageJ software (NIH, USA); Ki67 was represented as percentage vs. total cells. Three biological replicates per condition were used for these analyses.

Survival Assay

Propidium iodide (PI) is a standard red-fluorescent probe enabling distinguishing viable cells from the dead ones. Cells were trypsinized and resuspended in 100 μl staining buffer containing PI (50 μg/ml; Sigma–Aldrich, St. Louis, MO, USA), and incubated for 15 min at RT in the dark (Calderwood and Prince, 2018). Once setting conditions were defined, samples were analyzed by flow cytometry (BD Bioscience, USA). There 10,000 events from each sample were analyzed. Dead cells were defined as PI+ cells. Percentages of PI+ cells were calculated from three biological replicates.

Metabolic Activity

MTT, 3-(4,5-dimethylthiazol-2-yl)-2,5-diphenyltetrazolium bromide (Sigma–Aldrich, St. Louis, MO, USA), was used to evaluate mitochondrial activity as an indirect measure of cell metabolic activity, as previously described (Redondo-Castro et al., 2013; Alé et al., 2015). Microglial cells were incubated with LPS, extract lysate or extract lysate with ibuprofen (Sigma–Aldrich, St. Louis, MO, USA). After 24 h incubation, 0.15 mg/ml of MTT was added and the cells were incubated for 3 h at 37°C. The formazan crystals were dissolved in 200 μl of dimethyl sulfoxide (DMSO; Sigma–Aldrich, St. Louis, MO, USA) and 150 μl were passed to 96-well plates. The optimal density was determined with a microculture plate reader (Bio-Tek Instruments Inc., Germany) at 570 and 620 nm (to counteract the noise of the plastic) and analyzed with KCjunior™ software (Bio-Tek Instruments Inc., Germany). Three biological replicates were done.

RNA Isolation, Reverse Transcription, and Real-Time PCR

Cells were collected in RTL buffer reagent (Qiagen, Germany) and RNA extracted using the RNeasy Mini kit (Qiagen, Germany), according to the protocol of the manufacturer. RNA was treated with DNase I (Qiagen, Germany) to eliminate genomic DNA contamination. One microgram of RNA obtained from microglia was primed with random hexamers (Promega, USA) and reverse transcribed using the Omniscript RT kit (Qiagen, Germany). RNase inhibitor (Roche, Switzerland) was added (1 U/μl final concentration) to avoid RNA degradation. Primer sequences for real-time PCR are specified in **Table 1**. Glyceraldehyde-3-phosphate dehydrogenase (GAPDH) was used

TABLE 1 | Primer sequences for real-time PCR analysis.

Gene (*Rattus norgevicus*)	Accession number	Primer sequence 5′-3′	Size	Product size (bp)
GAPDH	XM_573304.3	Forward: AATTCAACGGCACAGTCAAGGC	22	116
		Reverse: TACTCAGCACCGGCCTCACC	20	
Interleukin-1β	NM_031512.2	Forward: TCCCAAACAATACCCAAAGAAG	22	162
		Reverse: CCGACCATTGCTGTTTCC	18	
Interleukin-6	NM_012589.1	Forward: ATCTGCCCTTCAGGAACAGCTATG	24	110
		Reverse: ACTTGTGAAGTAGGGAAGGCAGTG	24	
Interleukin-10	X60675.1	Forward: TCCTTTCACTTGCCCTCATC	20	159
		Reverse: CGAGACTGGAAGTGGTTGC	19	
TGF-β1	NM_021578.2	Forward: AGGACCTGGGTTGGAAGTG	19	127
		Reverse: GTGTTGGTTGTAGAGGGCAAG	21	
TNF-α	NM_012675.3	Forward: GCGTGTTCATCCGTTCTC	18	190
		Reverse: CAGCGTCTCGTGTGTTTC	18	
Arginase 1	BC091158.1	Forward: TGGAACGAAACGGGAAGG	18	118
		Reverse: CTGGTTCTGTTCGGTTTGC	19	
iNOS	NM_012611.3	Forward: GAGTGAGGAGCAGGTTGAG	19	158
		Reverse: TGCTGTAACTCTTCTGGGTG	20	
IL-4	NM_201270.1	Forward: AACAAGGAACACCACGGAG	19	200
		Reverse: TTCAGTGTTGTGAGCGTGG	19	

as a housekeeping gene. Gene-specific mRNA analysis was performed by SYBR-green real-time PCR using the MyiQ5 real-time PCR detection system (Bio-Rad Laboratories, Spain). Previously, we had determined the optimal concentration of the cDNA to be used as a template for each gene analysis to obtain reliable CT (threshold cycle) values for quantification (between 800 ng and 1 μg/μl). The thermal cycling conditions comprised 3 min polymerase activation at 95°C, 40 cycles of 10 s at 95°C for denaturation and 30 s at 60°C for annealing and extension (62°C in the case of IL-6), followed by a DNA melting curve for determination of amplicon specificity. CT values were obtained and analyzed with BioRad Software. Fold change in gene expression was estimated using the CT comparative method ($2^{-\Delta\Delta CT}$; Livak and Schmittgen, 2001) normalizing to GADPH CT values and relative to control samples. Three samples were used per condition from three to five biological replicates.

Phagocytosis Assay

One day after the treatments, cells were incubated with latex microbeads (1 μm, 0.0025%, Sigma–Aldrich, St. Louis, MO, USA) for 30 or 120 min at 37°C. After this, the medium was removed, and the cells rinsed twice with glucose-phosphate-buffered saline (PBS) to wash out the free beads. Then cells were fixed with 4% paraformaldehyde (PFA) for 15 min. After rinsing, labeling against Iba1 (1:500; Wako, Japan) was used. Several images were randomly taken and the number of cells with beads inside as well as the number of beads in each cell were counted. A minimum of 300 cells were measured for each condition, from three independent biological replicates, using ImageJ software (NIH, USA); the number of beads per cell and percentage of cells with beads were calculated (based on Silva et al., 2011).

Fluorescent Activated Cell Sorting (FACS) Analysis

The cultured cell suspension was centrifuged twice at 300 g for 10 min at 4°C with DMEM containing 10% Foetal Bovine Serum (FBS). Primary antibody labeling was performed for 1 h at 4°C. Cells were labeled with mouse anti-rat conjugated antibody CD45-FITC (1:250; BD Bioscience, USA). For intracellular analysis of iNOS and ArgI, cells were fixed, washed, permeabilized and incubated with rabbit antibodies against iNOS (1:250; Abcam, Cambridge, MA, USA) and goat antibodies against ArgI (1:200 Santa Cruz, CA, USA). After 30 min of incubation, cells were washed and stained with PE (1:500; Affymetrix eBioscience, USA) or Alexa647 (1:500; Abcam, Cambridge, MA, USA) conjugated donkey secondary antibodies against goat or rabbit respectively for 30 min. Finally, the samples were washed and fixed in 1% PFA.

Immune cells from the injured spinal cord were analyzed by flow cytometry. Rats were terminally anaesthetized with an overdose of sodium pentobarbital and intracardially perfused with PBS. The spinal cord thoracic segment was harvested, mechanically triturated and then passed through a cell strainer of 70 μm (BD Bioscience, USA), with DMEM containing 10% of FBS. The cell suspension was centrifuged at 300 g for 10 min at 4°C. Samples were split into several tubes and immunostained. Primary antibody labeling was performed for 1 h at 4°C, using DMEM+10% FBS as a buffer. Cells were labeled with the following mouse anti-rat conjugated antibodies: CD45-PE-Cy7 (1:250; BD Bioscience, USA) and CD11b-FITC (1:250; BD Bioscience, USA). For intracellular staining, cells were fixed with 4% PFA and permeabilized with Permeabilization Wash Buffer (Invitrogen, USA), followed by staining with unconjugated rabbit antibodies against iNOS (1:200; Abcam, Cambridge, MA, USA) and goat antibodies against Arg1 (1:150; Santa Cruz, CA, USA), and rabbit (1:1,000 Wako, USA) or goat (1:500 Abcam, Cambridge, MA, USA) antibodies for Iba1 for 45 min. After that, we stained with PE (1:500; Affymetrix eBioscience, San Diego, USA) or Alexa 647 (1:500; Abcam, Cambridge, MA, USA) conjugated donkey secondary antibodies against goat or rabbit respectively for 30 min. The following combination of markers was used to identify microglia (CD45low, CD11b+), peripheral myeloid

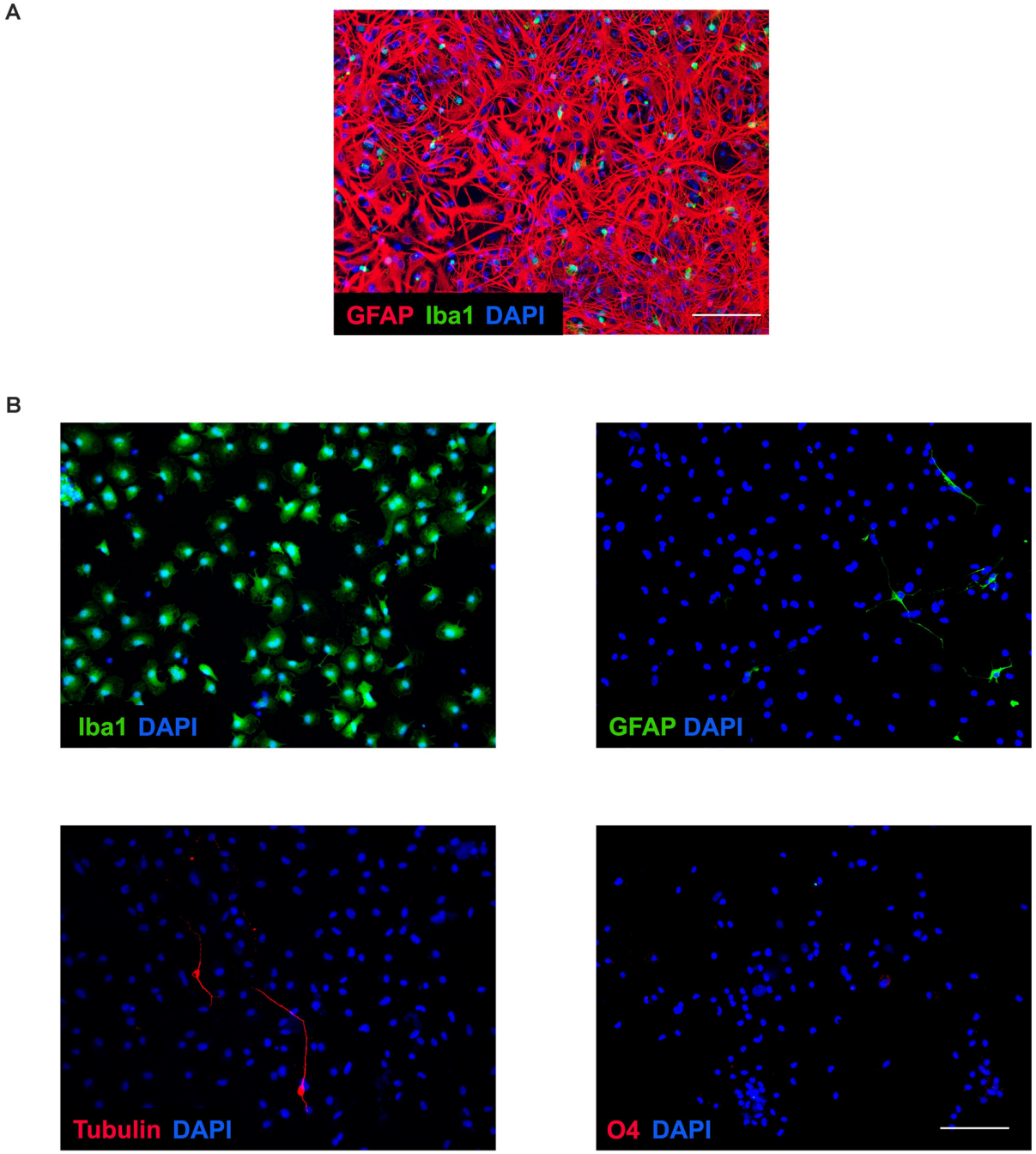

FIGURE 1 | Microglia purity. **(A)** Representative image of confluent and mixed culture after 14 days *in vitro*. Immunochemical image outlining labeling of GFAP (red), Iba1 (green), and DAPI (blue). Microglial cells were obtained by shaking of mixed culture. Scale bar: 100 μm. **(B)** Representative images of enriched microglial culture showing labeling of Iba1 (green), GFAP (green), tubulin β-3 (red), O4 (red), and DAPI (blue). Scale bar: 100 μm.

cells (CD45high, CD11b+), as previously described (Francos-Quijorna et al., 2016). Peripheral myeloid cells were further gated for Iba-1 to distinguish macrophages (CD45high, CD11b+, Iba-1+) from neutrophils since Iba-1 is not expressed in granulocytes. Cells were analyzed on a fluorescent activated cell sorting (FACS) Canto flow cytometer (BD Bioscience, USA) and the results analyzed using FlowJo® software version 10.0.7 (BD Bioscience, USA).

Statistical Analysis

Data are shown as the mean ± SEM. Statistical comparisons between groups were made using two-way ANOVA with

Bonferroni *post hoc* test in mRNA studies. One-way ANOVA with Tukey *post hoc* test was used for the assessment of cell counts, MTT assay, proliferation assay, survival assay, phagocytosis studies and microglial phenotype *in vitro*. Finally, *t*-test analyses were used in microglia morphology analysis and phenotype studies *in vivo* (IBM SPSS Statistics software, USA). Differences between groups were considered statistically significant at $p < 0.05$.

RESULTS

Purity of Cultured Cells

Mixed cell culture exhibits a network of cells, mainly astrocytes, with microglia around not firmly attached to the plate at 14 days *in vitro* (**Figure 1A**). However, once microglia were purified by shaking the mixed culture, this was highly enriched in microglial cells and we only observed occasional negligible cell contamination, mainly by astrocytes and neurons (**Figure 1B**).

Effect of SCI Lysate on Microglial Morphology, Metabolic Activity, Proliferation and Survival

Resting microglial cells in culture displayed a small round morphology with some short processes (**Figures 2A–C**). Activation with IFNγ induced many ramified extensions compared with the processes appearing with IL-4 activation (**Figure 2A**). The addition of lysates from the injured spinal cord produced qualitatively greater cell counts and morphological changes (**Figure 2**).

We therefore, assess the effects of the SCI lysates in cell counts, metabolic activity, and morphological changes. These experiments revealed that microglial cell counts increased after the stimulation with the SCI lysates in a concentration-dependent manner (**Figures 2B–D**), reaching a plateau at 50μg/ml concentration (**Figures 2B,D**). The effect of the SCI lysate on microglia metabolic activity was examined by MTT. When analyzing MTT activity in microglial we found that the addition of SCI lysate produced a significant increase in MTT activity (**Figure 2D**). Interestingly, ibuprofen, which is an anti-inflammatory drug (Redondo-Castro and Navarro, 2014), reduced the effects of the SCI lysates on microglial cell counts and MTT activity (**Figure 2D**). No changes in cell counts and MTT activity were observed in microglia upon LPS stimulation (**Figure 2D**).

Since microglia counts and MTT activity reached maximum levels at 50 μg/ml concentration of the SCI lysate, this concentration was used for the following studies.

We assessed whether the effect of the SCI lysates on microglia counts was due to the ability of the lysate to induce cell proliferation (**Figures 3A,B**). Immunostaining against Ki67 revealed that the SCI lysate triggered a significant proliferation of microglia (**Figure 3B**). However, the lysate did not lead to microglial cell death (**Figures 4A–C**).

We then assessed the morphological changes induced by the SCI lysate in microglia. These analyses revealed that microglia became less ramified by the SCI lysate as revealed by the number of endpoints per cell (**Figure 5A**). However, the length of these processes was markedly increased by the lysate (**Figure 5B**).

mRNA Expression in Microglial Cultures Treated With SC and SCI Lysates

In order to study the influence of SC and SCI lysate (50 μg/ml) on the expression of inflammatory mediators in microglial cells, we analyzed the transcript levels of IL-1β, IL-4, IL-6, IL-10, TNF-α, TGF-β1, and iNOS and Arginase 1 at different time points (0, 2, 4, 8, 12 and 24 h) as shown in **Figure 4**.

The transcripts of the pro-inflammatory cytokines IL-1β, IL-6, and TNF-α reached peak expression at 2 h upon stimulation and then decreased with time. The addition of the non-injured SC lysate produced a significant increase of the same pro-inflammatory cytokines, but to a much lower extent as compared to SCI lysate (**Figure 6**). Oppositely, the anti-inflammatory cytokines IL-10 and IL-4 were downregulated significantly by the addition of SCI lysate, whereas TGF-β1 showed a slight, but significant, upregulation at 2 h, and then a downregulation at 12 h (**Figure 6**). The reduced expression of IL-4 and IL-10 in microglial cells was also observed by the addition of the SC lysate, however, this was observed at later time points as compared to the SCI lysate.

Interestingly, inducible nitric oxide synthase (iNOS), a marker of pro-inflammatory microglia, showed a biphasic expression after the addition of the SCI, showing a significant increase in mRNA expression at 4 h and a later significant decrease from 8 h to 24 h. This early up-regulation in iNOS expression mediated by the SCI lysate was not observed by the addition of the SC lysate. Finally, the transcripts of Arginase 1 in microglia did not change upon SCI or SC lysate stimulation. These data provide clear evidence indicating that the SCI lysate drives microglia to adopt a pro-inflammatory phenotype.

Microglial Phagocytosis

A latex bead phagocytosis assay was performed in microglial cultures in the presence of SC and SCI lysates. Between 300 and 900 cells were analyzed from three independent experiments to avoid variability in the number of engulfed beads. Both lysates produced an increase in the number of beads detected inside the microglial cells. Representative images are shown in **Figure 7A**. Whilst in the control conditions, we observed that microglia engulfed approximately two beads per cell, either at 30 or 120 min after adding beads in the culture medium, microglia phagocytosed an average of four and five beads per cells after the addition of the SC and SCI lysate, respectively (**Figure 7B**). No significant changes were found in the number of engulfed beads per microglia after the addition of SC or SCI lysates. However, the SCI lysate significantly increased the percentage of microglia that phagocytosed beads as compared to the SC lysate (**Figure 7B**).

Activated Microglial Pattern *In vitro*

We analyzed the effects of microglial activation by IFNγ, IL-4 or SCI lysate *in vitro* using flow cytometry. IFNγ was used as a positive control for the pro-inflammatory phenotype, while IL-4 was used as positive control for the anti-inflammatory profile. At 24 h after the treatment, the

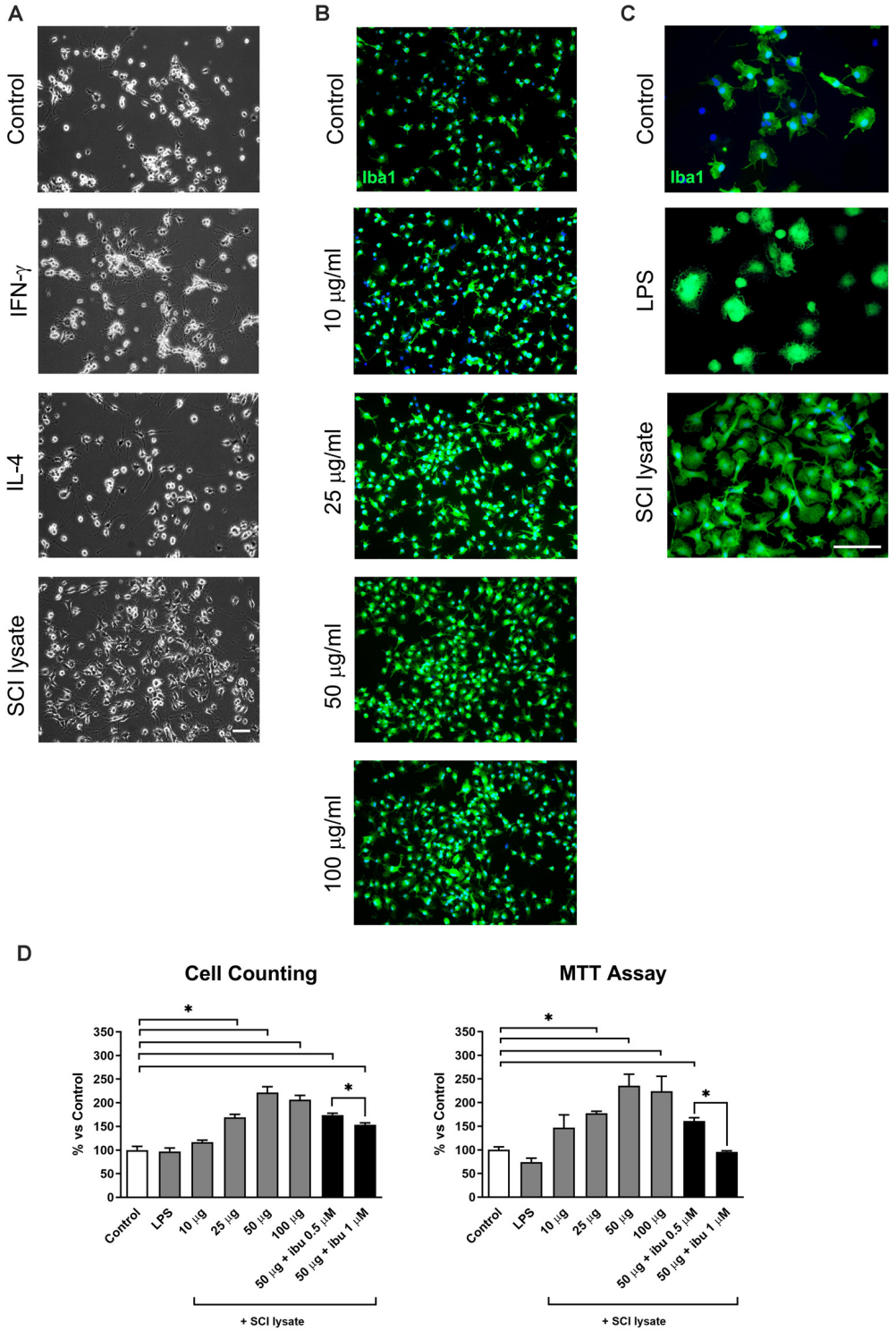

FIGURE 2 | Effects of lipopolysaccharide (LPS) and spinal cord injury (SCI) lysates in microglial cell count and metabolic activity. **(A)** Representative images of microglial cells activated by IFN-γ at 10 ng/ml, IL-4 at 10 ng/ml and SCI lysate at 50 μg/ml, 24 h after treatment. Scale bar: 50 μm. **(B)** Immunochemical images depicting labeling of Iba1 (green) and DAPI (blue) with increasing concentration of SCI lysate in the medium at 10, 25 and 50 μg/ml. Scale bar: 100 μm. **(C)** Higher magnification images of control microglia, and microglia activated by LPS or SCI lysate (50 μg/ml), labeled with anti-Iba1 (green) and DAPI (blue). Scale bar: 100 μm. **(D)** Graph showing microglia cell counts and MTT activity at 24 h upon being exposed to LPS (10 ng/ml), different concentrations of SCI lysate (10, 25, 50 and 100 μg/ml), and a combination of SCI lysate (50 μg/ml) with ibuprofen at 0.5 and 1 μM. Values are expressed as mean and SEM (*$P < 0.05$). $n = 3$ biological replicates per condition.

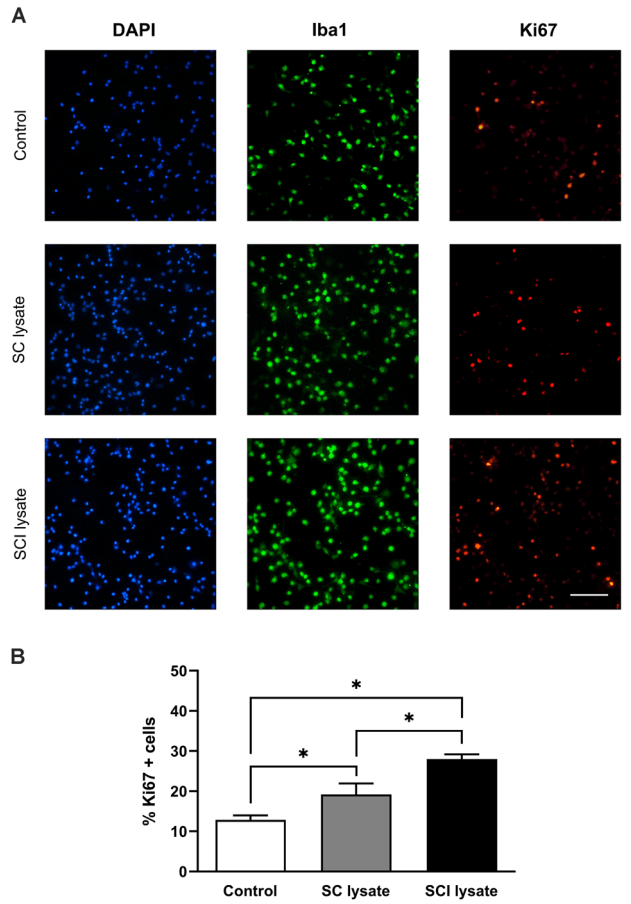

FIGURE 3 | Effects of injured spinal cord (SCI) lysates in microglial proliferation. **(A)** Representatives immunocytochemical images of microglial cells activated by SC and SCI lysate at 50 μg/ml, 24 h after treatment. Images depicting labeling of Iba1 (green), DAPI (blue), and Ki67 (red). Scale bar: 100 μm. **(B)** Results from counting Ki67 + cells after treatments. Values are expressed as mean and SEM (*$P < 0.05$). $n = 3$ biological replicates per condition.

expression of Arg1 was barely detectable in microglial cells stimulated with IFNγ or the SCI lysate, whereas ∼20% of the cells expressed Arg1 upon IL-4 treatment (**Figures 8A–C**). In contrast, ∼90% of microglia expressed iNOS upon IFNγ or SCI lysate stimulation, whereas this enzyme was observed in ∼75% of microglia after IL-4 (**Figures 8B,C**). Therefore these data indicate that phenotypically, microglial cells exposed to the SCI lysate were more similar to microglia stimulated with IFN-γ, and thus, further support the microglia adopt a pro-inflammatory phenotype after the addition of the SCI lysate.

Microglial Phenotype After Spinal Cord Injury Analyzed by Flow Cytometry

By using FACS, we assessed the changes in expression of iNOS and Arg1 markers in microglia and macrophages 7 days after spinal cord contusion injury in the rat. We found that microglia and macrophages expressed mainly the pro-inflammatory marker iNOS after SCI, whereas the expression of anti-inflammatory marker (Arg1) was restricted to a very small population of microglia and macrophages (**Figure 9**). The expression of iNOS was detected in a low proportion of microglial cells in the uninjured and injured spinal cords (∼27%). However, the proportion of iNOS+ macrophages increased significantly at 7 days post-injury as compared to those found in physiological conditions at very low numbers. These results, together with previous reports in the literature, indicate that microglia and macrophage are skewed towards a more pro-inflammatory phenotype.

DISCUSSION

Spinal cord injury produces an inflammatory response that includes the rapid activation of microglia and their release of pro-inflammatory mediators (Alexander and Popovich, 2009; David et al., 2015). Events that occur after spinal cord injury are characterized by hemorrhage, apoptosis, inflammation, and changes in the blood-spinal cord barrier and the extracellular matrix. All these processes produce a harmful and inhibitory environment that impairs endogenous regeneration and remyelination (Siddiqui et al., 2015). In addition, the balance of inflammatory and intrinsic repair processes influences the resolution of the neuroinflammatory reaction (DiSabato et al., 2016). The immune cell subsets, as major players involved in the immune response, play a key role in the pathological events after SCI (Plemel et al., 2014; David et al., 2015).

The microenvironment of the injured spinal cord in the acute phase contains many mediators, such as cytokines, chemokines, reactive oxygen species and secondary messengers (DiSabato et al., 2016). The SCI lysate obtained 7 days after lesion contains a profile of cytokines, pro-inflammatory mediators and other factors that come from the extracellular matrix and cellular contents of the lesion site and surrounding. We used this cocktail to study the response of microglia in culture. Microglia responded rapidly to the addition of the SCI lysate, showing marked changes in morphology, activity, and proliferation. Changes in microglia under the presence of SCI lysate in the medium were compared with classical administration of LPS, or the addition of IL-4 and IFNγ. In summary, SCI lysate induces changes in cell morphology (less ramified but longer processes), increases proliferation but does not affect survival. In a previous study, we studied the phenotype of neural stem cells (NSCs) derived from human induced pluripotent stem cells (iPSCs) under the presence of an SCI lysate (Lopez-Serrano et al., 2016), showing increased proliferation of iPSC-derived NSCs without changes in their immature stage, due to unknown factors present in the SCI lysate. It is well known that ischemia and immune infiltration can lead to oxidative stress and free radical production in the lesion area (Donnelly and Popovich, 2008). Ionic dysregulation following SCI contributes to cell damage and loss (Vosler et al., 2009). Furthermore, increasing glutamate levels, upregulating production of cytokines, matrix metalloproteinases (MMPs) or superoxide dismutase result ultimately in excitotoxic cell death (Donnelly and Popovich, 2008; Siddiqui et al., 2015; DiSabato et al., 2016).

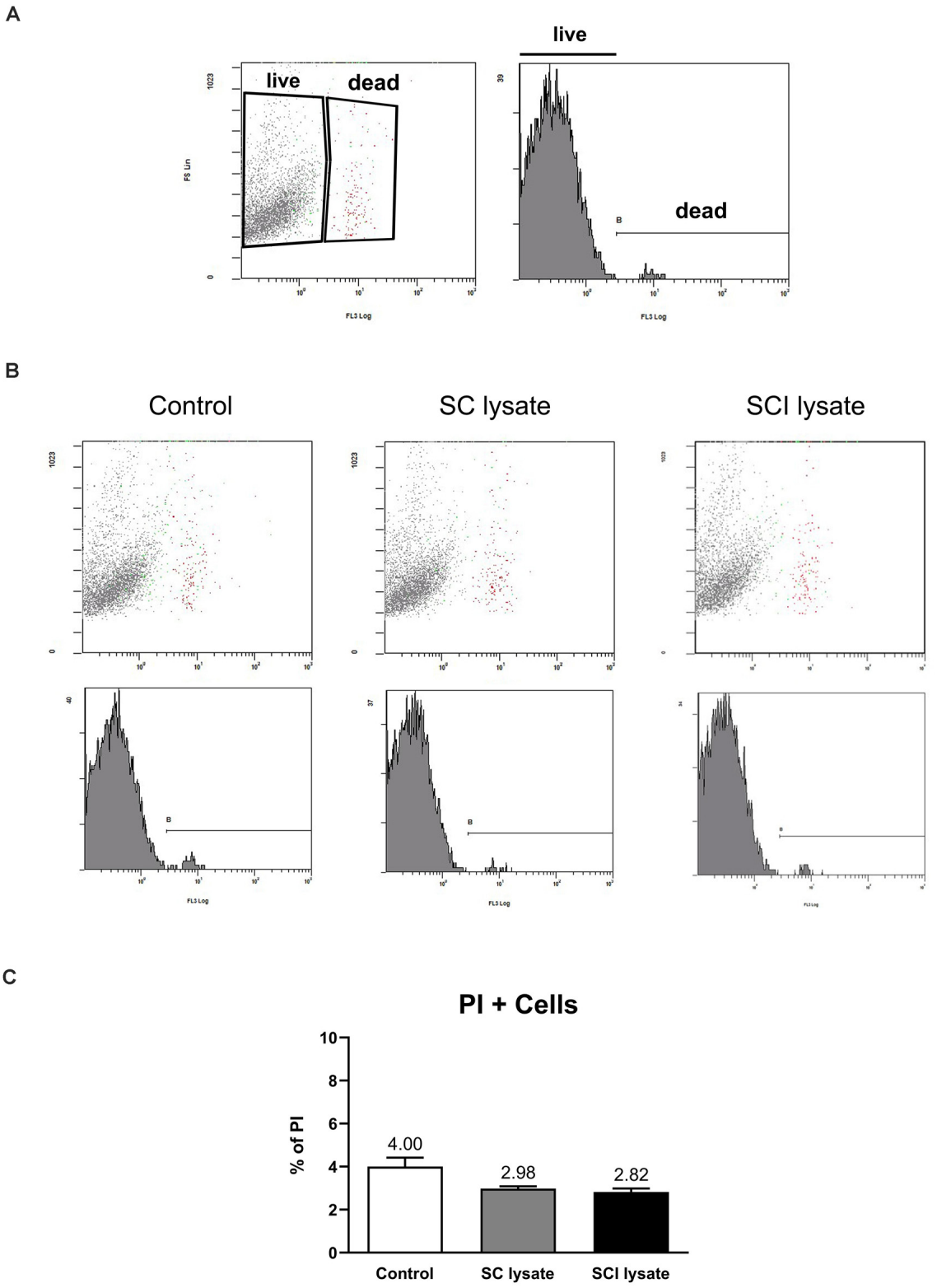

FIGURE 4 | Effects of SCI lysates in microglial cell death. **(A)** Representative setting from propidium iodide (PI) in fluorescent activated cell sorting (FACS) density plot and histogram, showing how live and dead microglia were gated. **(B)** Representative plots from control and microglial cells activated by SC and SCI lysate at 50 μg/ml, 24 h after treatment. **(C)** Graphs showing the quantification of **(B)** expressed as PI+ cells (dead cells in each condition). Values are expressed as mean and SEM. *n* = 3 biological replicates per condition.

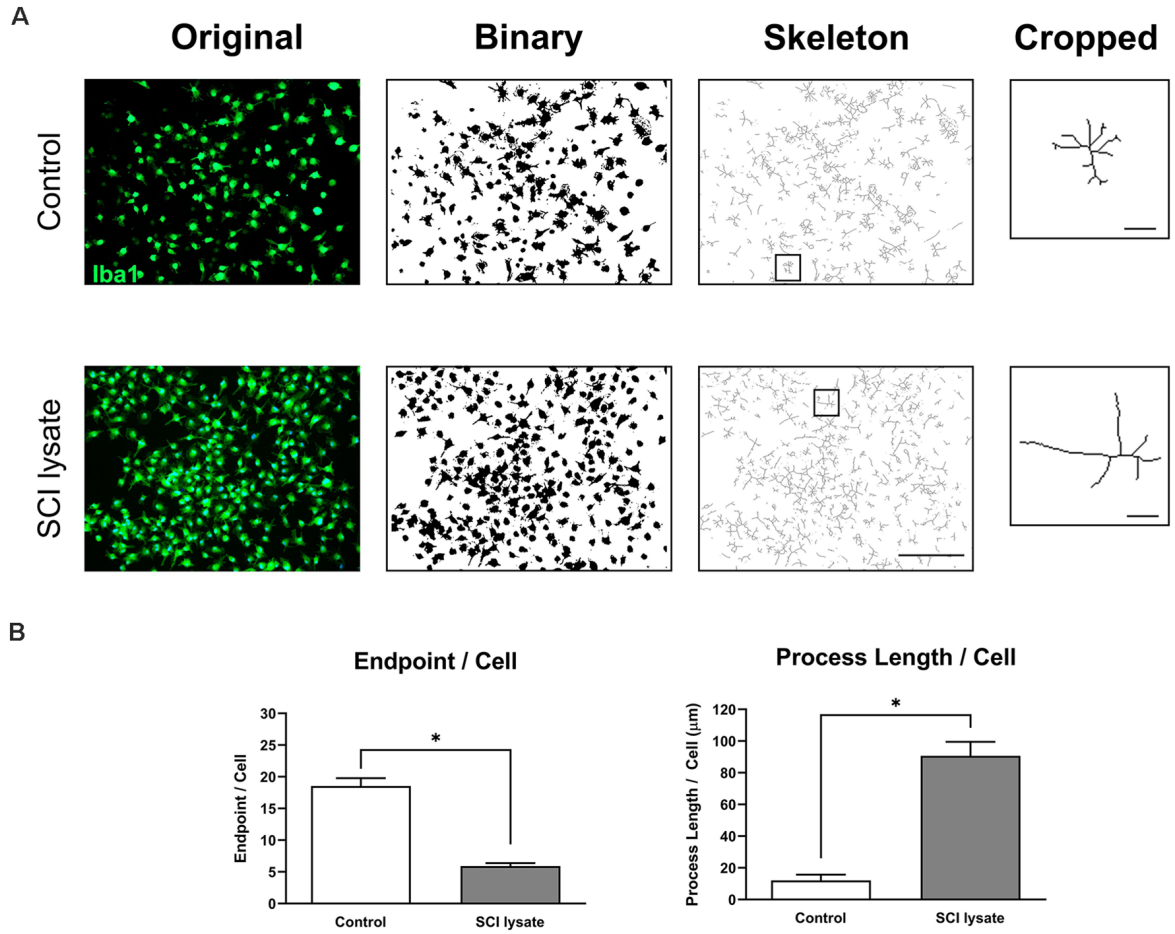

FIGURE 5 | Effects of SCI lysates in microglia morphology. **(A)** Example of original photomicrograph from control and cells treated with SCI lysate (50 µg/ml), and conversion to binary and skeletonized image. Cropped cell corresponds to the box in the skeleton image. Scale bar: 100 µm. Scale bar: 20 µm in cropped images. **(B)** Summary data of microglia endpoints/cell and process length/cell in control and after SCI lysate treatment. Values are expressed as mean and SEM (*$P < 0.05$). $n = 3$ biological replicates per condition.

The addition of a SCI lysate was a strategy to mimic the *in vivo* environment under controlled culture conditions. While microglia have been classically classified as either resting or activated (Streit et al., 1988), recently, some reports have used transcriptome profiles to identify genes selectively expressed in microglia. This microglial signature revealed a unique combination of genes, distinct from other immune cells (Wes et al., 2016). Our results revealed the response of microglial cells to an SCI lysate *in vitro*, showing a specific mRNA expression pattern, with a rapid and significant increase of IL-1β, IL-6, and TNF-α expression, downregulation of IL-10 and IL-4, and no changes in Arginase 1. iNOS showed a biphasic response with an early upregulation and a late downregulation. This cytokine profile is dynamic in time, between 2 and 24 h, indicating a phenotypic adjustment to the environment. The whole expression profile clearly indicates a proinflammatory phenotype, in agreement with other studies (David and Kroner, 2011). Microglia exposed to a non-injured SC lysate showed also a specific mRNA pattern profile. In this case, the increase in pro-inflammatory cytokines was transient and restricted in time, due to the SC lysate content, without free radicals and oxidative stress compounds. The *in vitro* phagocytosis assay (Redondo-Castro et al., 2013) revealed in our study that the SCI lysate induced a phagocytic phenotype in the microglia, indicated by the high number of cells with engulfed beads, compared with control cells or microglia with the SC lysate.

We also analyzed the microglial profile *in vitro* by flow cytometry. iNOS and Arg1 intracellular markers were used to characterize the microglia phenotype after $CD11b^+$ $CD45^+$ gating. In the presence of SCI lysate microglial cells showed an increased iNOS expression, and a slight decrease in Arg I expression, results that were similar to those found with IFN-γ treatment and in agreement with previous studies in macrophages and microglia (Mantovani et al., 2004; Franco and Fernández-Suárez, 2015). Thus, the SCI lysate promotes the microglia to adopt a proinflammatory phenotype as similar to what takes place *in vivo* after injury or *in vitro* after IFN-γ exposure.

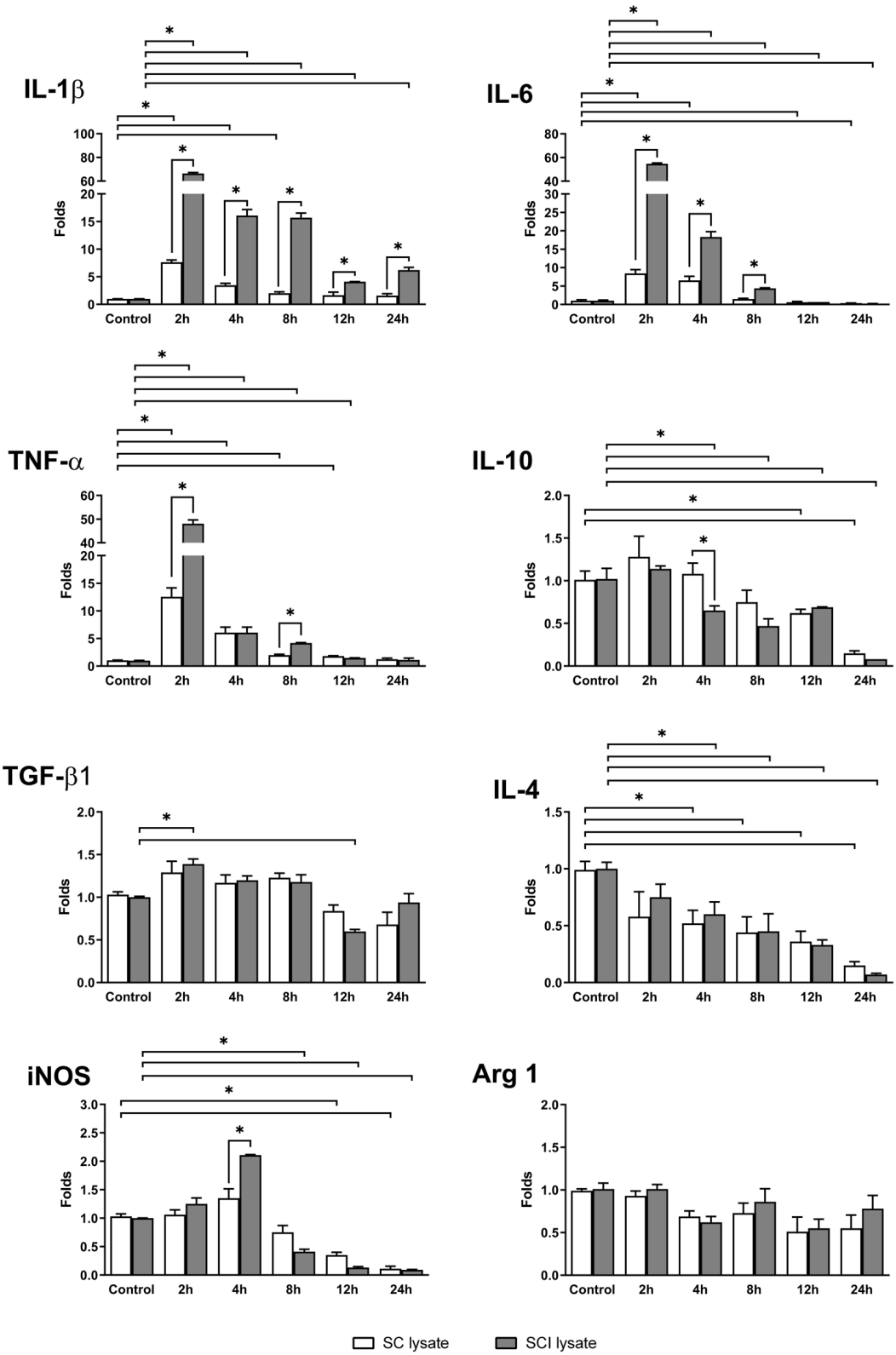

FIGURE 6 | mRNA expression from microglia cultures. Real-time PCR analyses of different mRNAs expressed in microglia cultures, with the addition of SC lysate and SCI lysate (at 50 μg/ml). Samples were taken in a time-course culture at 0, 2, 4, 8, 12 and 24 h after treatment. Values are expressed as mean and SEM (*$P < 0.05$). n = 3–5 biological replicates per condition.

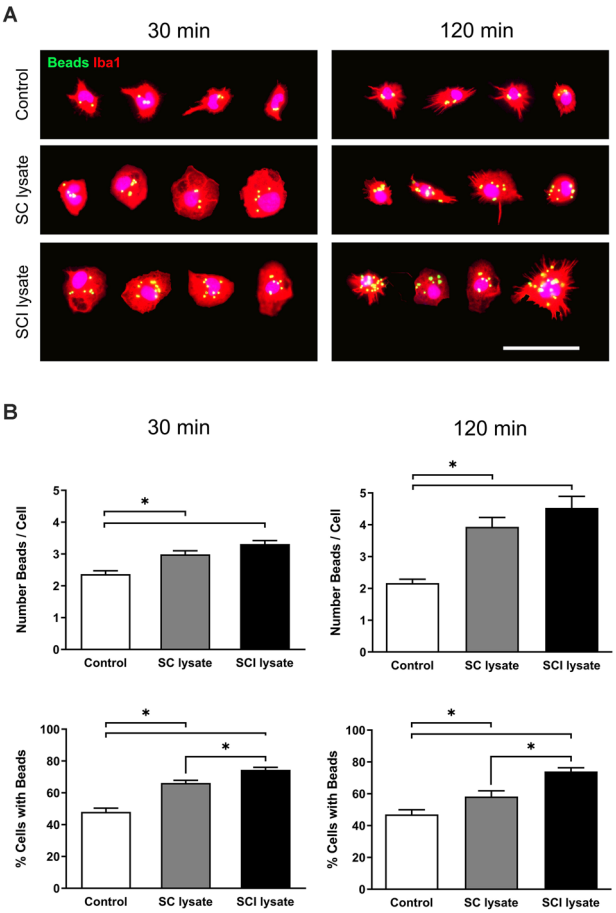

FIGURE 7 | Effects of SCI lysates in microglia phagocytosis. **(A)** Representative images of the phagocytic assay (at 30 and 120 min), showing microglial cells labeled against Iba1, and green-labeled beads inside. Cell images are from control, SC lysate and SCI lysate treatment (at 50 μg/ml). Scale bar: 50 μm. **(B)** Results from phagocytic assay expressed as the mean of beads engulfed per cell in each condition, and percentage of cells with ingested beads, at 30 and 120 min after treatments. Values are expressed as mean and SEM (*$P < 0.05$). $n = 3$ biological replicates per condition.

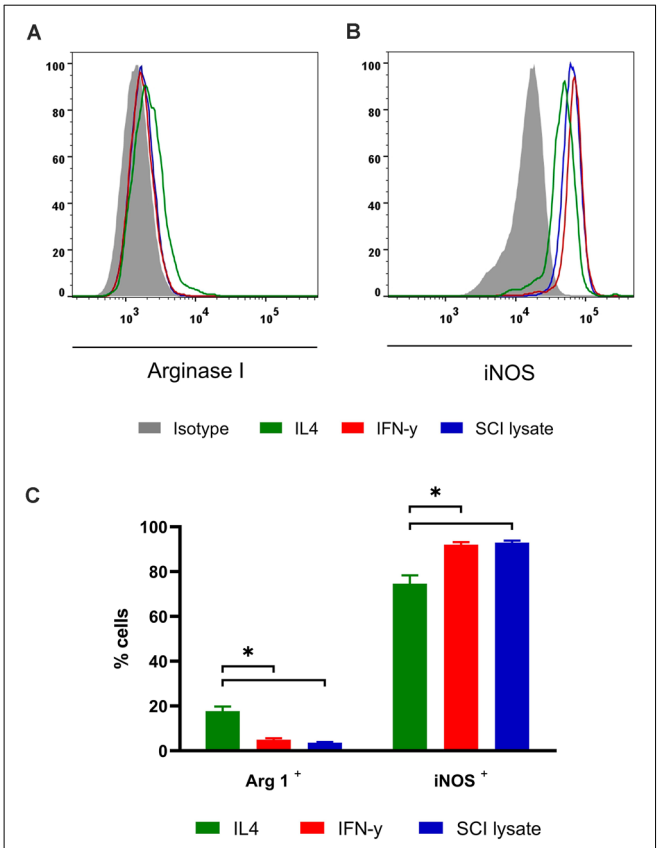

FIGURE 8 | Effects of SCI lysates in microglia phenotype *in vitro*. **(A,B)** Representative FACS plots Arg1 and iNOS levels in cultured microglial cells. **(C)** Graph showing the quantification of cultured microglial cells expressing Argl and iNOS after IFN-γ at 10 ng/ml, IL-4 at 10 ng/ml and SCI lysate at 50 μg/ml activation. Values are expressed as mean ± SEM ($n = 4$ biological replicates per condition; *$P < 0.05$).

To further analyze the proportion of microglial cells expressing each phenotypic marker we used flow cytometry analysis. Flow cytometry has been used in different studies to quantify or characterize microglia from *in vivo* samples. In one of the first studies, two cell-isolation methods based on mechanical dissociation and Percoll gradient separation were performed, and thereafter CD11b, CD45, and αβ T-cell receptor antibodies were employed for analysis (Campanella et al., 2002). An SCI model was used to analyze the resolution of acute inflammation by Prüss et al (Prüss et al., 2011), defining the existence of a resolution plateau index and characterizing the non-resolving aspects of inflammation after CNS injury. Some methods have been published to isolate microglia from mouse brain in order to assay expression profile, based in separation of microglia with discontinuous Percoll gradient and flow cytometry isolation using CD45 (Cardona et al., 2006), a modified protocol using magnetic bead purification and CD11b and CD45 markers by FACS (Chiu et al., 2013), or Percoll gradient plus CD11b staining with magnetic beads (Nikodemova and Watters, 2012). More recently, a modified method was published using Percoll gradient followed by CD11b staining to obtain an enriched neural cell suspension, in order to assess the ratio of proinflammatory and antiinflammatory cells, a useful tool to study neuroinflammation in traumatic CNS injury (Bedi et al., 2013). The cell suspension was identified by flow cytometry with CD11b+ $CD45^{lo}$ and categorized as proinflammatory or antiinflammatory macrophage/microglia based on CD206 and $F_c\gamma$RII/III expression.

Our studies on *in vivo* samples included CD11b and CD45 staining to gate properly the population of microglia ($CD45^{low}$, $CD11b^{+}$) or peripheral myeloid cells ($CD45^{high}$, $CD11b^{+}$), as in previous studies in mice (Francos-Quijorna et al., 2016). Macrophages were gated from the peripheral myeloid cells based on the expression of Iba1, since this marker is not expressed in neutrophils. Microglia and macrophages in mice express predominantly proinflammatory markers for the first 2 weeks after SCI, whereas the expression of M2 is scarce (Kigerl et al., 2009; Francos-Quijorna et al., 2016). Here, we observed that microglia/macrophages profile on day 7 after contusion injury

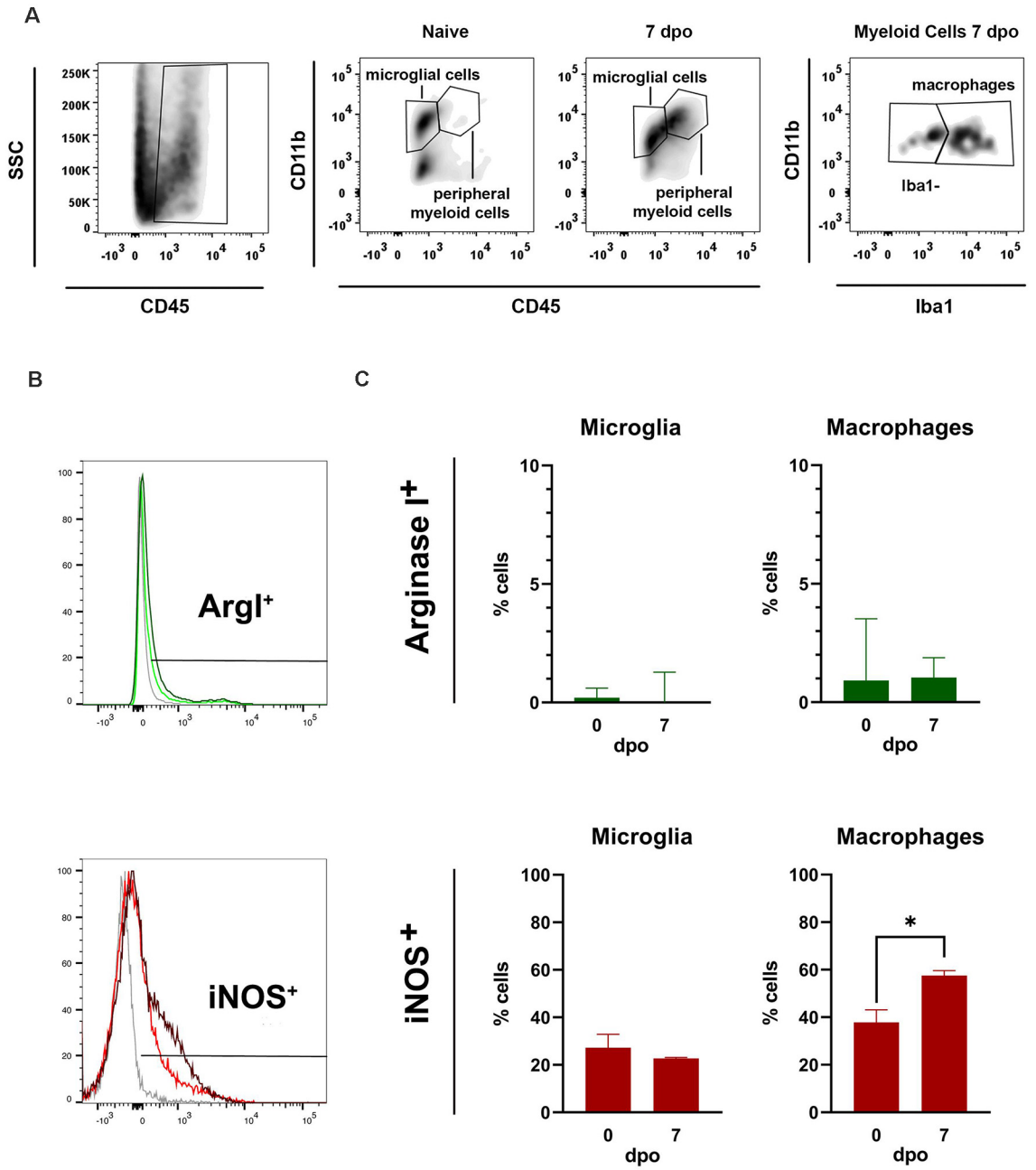

FIGURE 9 | Flow cytometer analysis of microglia *in vivo*. **(A)** Representative fluorescent activated cell sorting (FACS) density plots of naïve and injured spinal cord showing how microglia and macrophages were gated (>10,000 cells cd45+ cd11b+). **(B)** FACS histogram plots showing iNOS and Arg1 expression in microglia and macrophages. **(C)** Graphs showing the quantification of **(B)** microglia and **(C)** macrophages expressing Arg1 and iNOS markers 7 days post operation (dpo). Note that the percentage of microglia and macrophages expressing iNOS is markedly higher than those expressing Arg1. Values are expressed as mean ± SEM ($n = 3$ per group; $^*P < 0.05$).

in rats was characterized by an increased iNOS+ expression in macrophages, and minimal expression of Arg1+ macrophages and microglial cells, suggesting that these cells also adopt a proinflammatory phenotype similar to that observed after spinal cord injury in mice. In addition, this proinflammatory phenotype was also acquired *in vitro* when microglia were exposed to the SCI lysate.

Many endogenous factors appear involved in the phenotype switching of inflammatory cells after CNS injury, including cytokines, microRNA, or STAT molecules (Hu et al., 2014; Akhmetzyanova et al., 2019). Effective models to approach the SCI microenvironment will allow at investigating signaling pathways, and further identification of regulatory molecules and microglia profiles that could ultimately accelerate research

towards clinical applicability. Here, we show that SCI lysate could be an effective strategy to mimic the SCI milieu conditions and a useful tool for studying microglia activation.

DATA AVAILABILITY STATEMENT

The raw data supporting the conclusions of this article will be made available by the authors, without undue reservation.

ETHICS STATEMENT

The animal study was reviewed and approved by Ethical committee of the Universitat Autònoma de Barcelona in accordance with the European Directive 86/609/EEC.

AUTHOR CONTRIBUTIONS

JH, RL-V, and XN designed the study. JH, IF-Q, and ER-C performed the research, analyzed or interpreted results. JH, IF-Q, RL-V, and XN wrote the manuscript. All authors contributed to the article and approved the submitted version.

FUNDING

This research was supported by funds from Ministerio de Ciencia e Innovación, AEI and ERDF EU funds (PCI2018-093029, SAF2016-79774-R) to XN and RL-V. This research also received funds from Red de Terapia Celular (TERCEL, RD16/0011/0035) and CIBERNED (CB06/05/1105), both from the Instituto de Salud Carlos III of Spain, co-funded by European Union (ERDF funds).

ACKNOWLEDGMENTS

We thank Monica Espejo, Jessica Jaramillo, Marta Morell, and Cristina Gutiérrez from INc-UAB culture technological platform for excellence technical assistance.

REFERENCES

Ahuja, C. S., Wilson, J. R., Nori, S., Kotter, M. R. N., Druschel, C., Curt, A., et al. (2017). Traumatic spinal cord injury. *Nat. Rev. Dis. Primers* 3:17018. doi: 10.1038/nrdp.2017.18

Akhmetzyanova, E., Kletenkov, K., Mukhamedshina, Y., and Rizvanov, A. (2019). Different approaches to modulation of microglia phenotypes after spinal cord injury. *Front. Syst. Neurosci.* 13:37. doi: 10.3389/fnsys.2019.00037

Alé, A., Bruna, J., Herrando, M., Navarro, X., and Udina, E. (2015). Toxic effects of bortezomib on primary sensory neurons and schwann cells of adult mice. *Neurotox. Res.* 27, 430–440. doi: 10.1007/s12640-014-9514-8

Alexander, J. K., and Popovich, P. G. (2009). Neuroinflammation in spinal cord injury: therapeutic targets for neuroprotection and regeneration. *Prog. Brain Res.* 175, 125–137. doi: 10.1016/S0079-6123(09)17508-8

Bedi, S. S., Smith, P., Hetz, R. A., Xue, H., and Cox, C. S. (2013). Immunomagnetic enrichment and flow cytometric characterization of mouse microglia. *J. Neurosci. Methods* 219, 176–182. doi: 10.1016/j.jneumeth.2013.07.017

Blasco, A., Gras, S., Mòdol-Caballero, G., Tarabal, O., Casanovas, A., Piedrafita, L., et al. (2020). Motoneuron deafferentation and gliosis occur in association with neuromuscular regressive changes during ageing in mice. *J. Cachexia Sarcopenia Muscle* 11, 1628–1660. doi: 10.1002/jcsm.12599

Calderwood, S. K., and Prince, T. L. (Eds) (2018). *Methods and Protocols*. New York, NY: Springer Nature.

Campanella, M., Sciorati, C., Tarozzo, G., and Beltramo, M. (2002). Flow cytometric analysis of inflammatory cells in ischemic rat brain. *Stroke* 33, 586–592. doi: 10.1161/hs0202.103399

Cardona, A. E., Huang, D., Sasse, M. E., and Ransohoff, R. M. (2006). Isolation of murine microglial cells for RNA analysis or flow cytometry. *Nat. Protoc.* 1, 1947–1951. doi: 10.1038/nprot.2006.327

Chiu, I. M., Morimoto, E. T. A., Goodarzi, H., Liao, J. T., O'Keeffe, S., Phatnani, H. P., et al. (2013). A neurodegeneration-specific gene-expression signature of acutely isolated microglia from an amyotrophic lateral sclerosis mouse model. *Cell Rep.* 4, 385–401. doi: 10.1016/j.celrep.2013.06.018

David, S., Greenhalgh, A. D., and Kroner, A. (2015). Macrophage and microglial plasticity in the injured spinal cord. *Neuroscience* 307, 311–318. doi: 10.1016/j.neuroscience.2015.08.064

David, S., and Kroner, A. (2011). Repertoire of microglial and macrophage responses after spinal cord injury. *Nat. Rev. Neurosci.* 12, 388–399. doi: 10.1038/nrn3053

DiSabato, D. J., Quan, N., and Godbout, J. P. (2016). Neuroinflammation: the devil is in the details. *J. Neurochem.* 139, 136–153. doi: 10.1111/jnc.13607

Donnelly, D. J., and Popovich, P. G. (2008). Inflammation and its role in neuroprotection, axonal regeneration and functional recovery after spinal cord injury. *Exp. Neurol.* 209, 378–388. doi: 10.1016/j.expneurol.2007.06.009

Franco, R., and Fernández-Suárez, D. (2015). Alternatively activated microglia and macrophages in the central nervous system. *Prog. Neurobiol.* 131, 65–86. doi: 10.1016/j.pneurobio.2015.05.003

Francos-Quijorna, I., Amo-Aparicio, J., Martinez-Muriana, A., and López-Vales, R. (2016). IL-4 drives microglia and macrophages toward a phenotype conducive for tissue repair and functional recovery after spinal cord injury. *Glia* 64, 2079–2092. doi: 10.1002/glia.23041

Gensel, J. C., and Zhang, B. (2015). Macrophage activation and its role in repair and pathology after spinal cord injury. *Brain Res.* 1619, 1–11. doi: 10.1016/j.brainres.2014.12.045

Gordon, S., and Taylor, P. R. (2005). Monocyte and macrophage heterogeneity. *Nat. Rev. Immunol.* 5, 953–964. doi: 10.1038/nri1733

Greenhalgh, A. D., David, S., and Bennett, F. C. (2020). Immune cell regulation of glia during CNS injury and disease. *Nat. Rev. Neurosci.* 21, 139–152. doi: 10.1038/s41583-020-0263-9

Hu, X., Leak, R. K., Shi, Y., Suenaga, J., Gao, Y., Zheng, P., et al. (2014). Microglial and macrophage polarization—new prospects for brain repair. *Nat. Rev. Neurol.* 11, 56–64. doi: 10.1038/nrneurol.2014.207

Kigerl, K. A., Gensel, J. C., Ankeny, D. P., Alexander, J. K., Donnelly, D. J., and Popovich, P. G. (2009). Identification of two distinct macrophage subsets with divergent effects causing either neurotoxicity or regeneration in the injured mouse spinal cord. *J. Neurosci.* 29, 13435–13444. doi: 10.1523/JNEUROSCI.3257-09.2009

Livak, K. J., and Schmittgen, T. D. (2001). Analysis of relative gene expression data using real-time quantitative PCR and the $2^{-\Delta\Delta CT}$ method. *Methods* 25, 402–408. doi: 10.1006/meth.2001.1262

Lopez-Serrano, C., Torres-Espin, A., Hernandez, J., Alvarez-Palomo, A. B., Requena, J., Gasull, X., et al. (2016). Effects of the spinal cord injury environment on the differentiation capacity of human neural stem cells derived from induced pluripotent stem cells. *Cell Transplant.* 25, 1833–1852. doi: 10.3727/096368916X691312

Mantovani, A., Sica, A., Sozzani, S., Allavena, P., Vecchi, A., and Locati, M. (2004). The chemokine system in diverse forms of macrophage activation and polarization. *Trends Immunol.* 25, 677–686. doi: 10.1016/j.it.2004.09.015

Nikodemova, M., and Watters, J. J. (2012). Efficient isolation of live microglia with preserved phenotypes from adult mouse brain. *J. Neuroinflammation* 9:635. doi: 10.1186/1742-2094-9-147

Nimmerjahn, A. (2005). Resting microglial cells are highly dynamic surveillants of brain parenchyma *in vivo*. *Science* 308, 1314–1318. doi: 10.1126/science.1110647

Plemel, J. R., Wee Yong, V., and Stirling, D. P. (2014). Immune modulatory therapies for spinal cord injury—past, present and future. *Exp. Neurol.* 258, 91–104. doi: 10.1016/j.expneurol.2014.01.025

Popovich, P. G. (2014). Neuroimmunology of traumatic spinal cord injury: a brief history and overview. *Exp. Neurol.* 258, 1–4. doi: 10.1016/j.expneurol.2014.05.001

Prinz, M., Jung, S., and Priller, J. (2019). Microglia biology: one century of evolving concepts. *Cell* 179, 292–311. doi: 10.1016/j.cell.2019.08.053

Prüss, H., Kopp, M. A., Brommer, B., Gatzemeier, N., Laginha, I., Dirnagl, U., et al. (2011). Non-resolving aspects of acute inflammation after spinal cord injury (SCI): indices and resolution plateau. *Brain Pathol.* 21, 652–660. doi: 10.1111/j.1750-3639.2011.00488.x

Ransohoff, R. M. (2016). A polarizing question: do M1 and M2 microglia exist. *Nat. Neurosci.* 19, 987–991. doi: 10.1038/nn.4338

Ransohoff, R. M., and Perry, V. H. (2009). Microglial physiology: unique stimuli, specialized responses. *Annu. Rev. Immunol.* 27, 119–145. doi: 10.1146/annurev.immunol.021908.132528

Redondo-Castro, E., Hernández, J., Mahy, N., and Navarro, X. (2013). Phagocytic microglial phenotype induced by glibenclamide improves functional recovery but worsens hyperalgesia after spinal cord injury in adult rats. *Eur. J. Neurosci.* 38, 3786–3798. doi: 10.1111/ejn.12382

Redondo-Castro, E., and Navarro, X. (2014). Chronic ibuprofen administration reduces neuropathic pain but does not exert neuroprotection after spinal cord injury in adult rats. *Exp. Neurol.* 252, 95–103. doi: 10.1016/j.expneurol.2013.11.008

Salter, M. W., and Beggs, S. (2014). Sublime microglia: expanding roles for the guardians of the CNS. *Cell* 158, 15–24. doi: 10.1016/j.cell.2014.06.008

Siddiqui, A. M., Khazaei, M., and Fehlings, M. G. (2015). Translating mechanisms of neuroprotection, regeneration and repair to treatment of spinal cord injury. *Pro. Brain Res.* 218, 15–54. doi: 10.1016/bs.pbr.2014.12.007

Silva, S. L., Osório, C., Vaz, A. R., Barateiro, A., Falcão, A. S., Silva, R. F. M., et al. (2011). Dynamics of neuron-glia interplay upon exposure to unconjugated bilirubin. *J. Neurochem.* 117, 412–424. doi: 10.1111/j.1471-4159.2011.07200.x

Silver, J., Schwab, M. E., and Popovich, P. G. (2015). Central nervous system regenerative failure: role of oligodendrocytes, astrocytes and microglia. *Cold Spring Harb. Perspect. Biol.* 7:a020602. doi: 10.1101/cshperspect.a020602

Streit, W. J., Graeber, M. B., and Kreutzberg, G. W. (1988). Functional plasticity of microglia: a review. *Glia* 1, 301–307. doi: 10.1002/glia.440010502

Tator, C. H., and Fehlings, M. G. (1991). Review of the secondary injury theory of acute spinal cord trauma with emphasis on vascular mechanisms. *J. Neurosurg.* 75, 15–26. doi: 10.3171/jns.1991.75.1.0015

Vosler, P. S., Sun, D., Wang, S., Gao, Y., Kintner, D. B., Signore, A. P., et al. (2009). Calcium dysregulation induces apoptosis-inducing factor release: cross-talk between PARP-1- and calpain-signaling pathways. *Exp. Neurol.* 218, 213–220. doi: 10.1016/j.expneurol.2009.04.032

Wes, P. D., Holtman, I. R., Boddeke, E. W. G. M., Möller, T., and Eggen, B. J. L. (2016). Next generation transcriptomics and genomics elucidate biological complexity of microglia in health and disease. *Glia* 64, 197–213. doi: 10.1002/glia.22866

Young, K., and Morrison, H. (2018). Quantifying microglia morphology from photomicrographs of immunohistochemistry prepared tissue using ImageJ. *J. Vis. Exp.* 136, 1–9. doi: 10.3791/57648

Conflict of Interest: The authors declare that the research was conducted in the absence of any commercial or financial relationships that could be construed as a potential conflict of interest.

frontiers in Immunology

ORIGINAL RESEARCH
published: 01 June 2021
doi: 10.3389/fimmu.2021.684430

CD22 Blockage Restores Age-Related Impairments of Microglia Surveillance Capacity

Vanessa Aires[1,2,3], *Claire Coulon-Bainier*[1], *Anto Pavlovic*[1], *Martin Ebeling*[4], *Roland Schmucki*[4], *Christophe Schweitzer*[1], *Erich Kueng*[4], *Simon Gutbier*[5] *and Eva Harde*[1]*

[1] Roche Pharma Research and Early Development, Neuroscience and Rare Diseases Discovery and Translational Area, Roche Innovation Center Basel, F. Hoffmann-La Roche Ltd, Basel, Switzerland, [2] Department of Neurology, Medical Center – University of Freiburg, Freiburg, Germany, [3] Faculty of Biology, University of Freiburg, Freiburg, Germany, [4] Roche Pharma Research and Early Development, Pharmaceutical Sciences, Roche Innovation Center Basel, F. Hoffmann-La Roche Ltd, Basel, Switzerland, [5] Roche Pharma Research and Early Development, Therapeutic Modalities, Roche Innovation Center Basel, F. Hoffmann-La Roche Ltd, Basel, Switzerland

OPEN ACCESS

Edited by:
Amanda Sierra,
Achucarro Basque Center for Neuroscience, Spain

Reviewed by:
Rommy Von Bernhardi,
Pontificia Universidad Católica de chile, Chile
Daniel Erny,
University of Freiburg Medical Center, Germany
Delphine Boche,
University of Southampton, United Kingdom

***Correspondence:**
Eva Harde
Eva.harde@roche.com

Specialty section:
This article was submitted to Multiple Sclerosis and Neuroimmunology, a section of the journal Frontiers in Immunology

Received: 23 March 2021
Accepted: 17 May 2021
Published: 01 June 2021

Citation:
Aires V, Coulon-Bainier C, Pavlovic A, Ebeling M, Schmucki R, Schweitzer C, Kueng E, Gutbier S and Harde E (2021) CD22 Blockage Restores Age-Related Impairments of Microglia Surveillance Capacity. Front. Immunol. 12:684430. doi: 10.3389/fimmu.2021.684430

Microglia, the innate immune cells of the brain, are essential for maintaining homeostasis by their ramified, highly motile processes and for orchestrating the immune response to pathological stimuli. They are implicated in several neurodegenerative diseases like Alzheimer's and Parkinson's disease. One commonality of these diseases is their strong correlation with aging as the highest risk factor and studying age-related alterations in microglia physiology and associated signaling mechanism is indispensable for a better understanding of age-related pathomechanisms. CD22 has been identified as a modifier of microglia phagocytosis in a recent study, but not much is known about the function of CD22 in microglia. Here we show that CD22 surface levels are upregulated in aged versus adult microglia. Furthermore, in the amyloid mouse model PS2APP, Aβ-containing microglia also exhibit increased CD22 signal. To assess the impact of CD22 blockage on microglia morphology and dynamics, we have established a protocol to image microglia process motility in acutely prepared brain slices from CX3CR1-GFP reporter mice. We observed a significant reduction of microglial ramification and surveillance capacity in brain slices from aged versus adult mice. The age-related decrease in surveillance can be restored by antibody-mediated CD22 blockage in aged mice, whereas surveillance in adult mice is not affected by CD22 inhibition. Moreover to complement the results obtained in mice, we show that human iPSC-derived macrophages exhibit an increased phagocytic capacity upon CD22 blockage. Downstream analysis of antibody-mediated CD22 inhibition revealed an influence on BMP and TGFβ associated gene networks. Our results demonstrate CD22 as a broad age-associated modulator of microglia functionality with potential implications for neurodegenerative disorders.

Keywords: CD22, microglia, two-photon imaging, surveillance, iPSC macrophages, phagocytosis, aging, AD (Alzheimer's disease)

INTRODUCTION

Microglia are the resident immune cells of the brain and are manifold involved in shaping their surrounding tissue from development (1–3) till aging (4–6). Besides their role in pathogen recognition and immune response orchestration, microglia are also vital under homeostatic conditions. They contribute substantially to maintaining homeostasis in the brain, by removing cellular debris, aggregated proteins and apoptotic cells (2, 7). With their ramified and highly motile processes, microglia constantly monitor the brain parenchyma to sense and counteract disturbances in the central nervous system (8). During aging however, microglia undergo phenotypic changes, characterized by the reduced expression of cytoskeleton-regulating genes (9) consistent with the impaired surveillance and reduced lesion response of microglia (10). Moreover, during aging microglia loose their homeostatic signature (11) and adopt a pro-inflammatory state, accompanied by increased expression of pro-inflammatory cytokines (12), reduced phagocytic activity and the accumulation of insoluble cargo (13).

Aging is one of the biggest risk factors for neurodegenerative disorders (14) and age-related disturbances in microglia functionality could contribute to the initiation and progression of various neurodegenerative diseases. Therefore, understanding the effect of aging on microglial behavior and whether age-related dysfunctionality can be modulated is crucial to comprehend the ambiguous role of microglia in age-related neurodegenerative diseases. Ultimately, new findings in this area will be essential for the identification of new microglia-specific targets in drug discovery.

A recent study in murine cells identified CD22 as an age-associated modifier of microglial phagocytosis using a CRISPR-Cas9 knockout screen (15). *In vivo* antibody-mediated blockage of CD22 led to the restoration of phagocytosis, reprogrammed microglia toward a homeostatic transcriptional state and ultimately improved the cognitive functions of aged mice (15). CD22, a sialic-acid-binding immunoglobulin-like lectin (SIGLEC), is usually expressed on B-cells where it functions as an inhibitory co-receptor of the B-cell receptor (16). Besides its involvement in phagocytosis in murine phagocytosis, the function of CD22 in microglia is largely unknown.

Here, we report that CD22 is upregulated by microglia during aging and in plaque-associated microglia in the amyloid mouse model PS2APP. Investigating microglia can be challenging, since they are highly sensitive to changes in their environment and rapidly loose key characteristics upon isolation (17, 18). Therefore, it is essential to study microglia in their native tissue environment. Using two-photon live microscopy of acute brain slices prepared from CX3CR1-GFP reporter animals in combination with a nearly fully automated analysis pipeline, we show that microglial dynamic behavior can be reliably assessed by this technology. We demonstrate that surveillance is strongly reduced in aged versus adult microglia. Interestingly, antibody-mediated blockage of CD22 in brain slices of aged mice restores the age-related microglial hypo-ramification and the reduced surveillance capacity. To connect these murine based findings to human biology, we addressed the impact of CD22 blockage on human iPSC-derived macrophages by studying effects on phagocytosis and transcriptional regulation. Interestingly, in human iPSC macrophages inhibition of CD22 promoted the phagocytosis of Aβ-coated beads and modulated key regulatory networks at the gene expression level. By using a joint approach of murine and human model systems, we show that CD22 blockage acts as a broad age-related modifier of microglia functions.

MATERIALS AND METHODS

Animals

All animal experiments were performed with the permission of the Swiss Cantonal Veterinary Office. The mice used in this study were bred and maintained in temperature and humidity controlled facilities. Food and water was available *ad libitum*. The following lines were used in the study: CX3CR1-GFP (19) and a cross of CX3CR1-GFP to PS2APP (20). Both transgenes were kept in a heterozygous condition. To minimize gender-dependent heterogeneity of microglia phenotype (21, 22), only male mice were used in the study. CX3CR1-GFP animals were used at 6-8 months as adult mice and at 13-16 months as aged mice. PS2APP CX3CR1-GFP were around 10 months old.

Acute Slice Preparation

Animals were anesthetized in an isoflurane chamber and then sacrificed by decapitation. The brain was quickly removed and put in ice-cold NMDG-based artificial cerebral fluid solution (NMDG- ACSF) consisting of the following reagents: 110 mM NMDG, 3 mM KCl, 1.1 mM NaH_2PO_4, 25 mM $NaHCO_3$, 25 mM D-Glucose, 10 mM L-Ascorbic acid, 3 mM Pyruvic acid, 0.5 mM $CaCl_2$, 10 mM $MgCl_2$, 103.02 mM HCl; pH 7.3, 305-310 mOsm. Acute coronal hippocampal slices (300 µm thick) of adult (7-8 months) or aged (13-16 months) mice were sliced using a vibratome (VT1200, Leica). Dissection and slicing was performed in ice-cold NMDG-ACSF, which was constantly saturated with carbogen (95% O_2, 5% CO_2). After slicing and recovery in 37°C warm NMDG-ACSF for 15 min, acute slices were transferred to carbogenated ACSF (at room temperature), containing the following: 119 mM NaCl, 2.5 mM KCl, 2.5 mM $CaCl_2$, 1.3 mM $MgCl_2$, 1 mM NaH_2PO_4, 11 mM Glucose, 26.2 mM $NaHCO_3$; 290 mOsm. Slices were kept in ACSF until imaged, but stayed at least 30 min in ACSF for acclimatization.

For antibody treatment, ACSF acclimatization is followed by transfer to incubation chambers, containing carbogenated ACSF with either CD22 antibody (BioXcell, BE0011; 5 µg/ml) or IgG isotype control (BioXcell, BE0083; 5 µg/ml). Sections stayed in incubation chambers for at least 90 minutes.

Cranial Window Surgery

The animal was anaesthetized using a triple shot standard injection protocol consisting of a combination of Fentanyl (0.05 mg/kg), Medetomidine (0.5 mg/kg) and Midazolam (5 mg/kg) in a subcutaneous injection and the depth of

anesthesia was regularly assessed through toe pinching. Body temperature was maintained at 36.5–37.5°C using a heating pad connected to a controller, and the eyes were covered with eye protecting gel. During experimentation, heart rate (mouse = 300–450 beat/min) and O_2 saturation (SpO2; mouse >95%) were monitored using a pulse oximeter. The head was shaved on the surgical area and cleaned with Betadine, then firmly fixed with ear bars in a stereotaxic frame. The surgical area was locally numbed by s.c. injection of local anesthesia (bupivacaine).

An incision was carefully made over the skin. The periosteum was removed by gently scraping the skull with a scalpel blade and scratches were made on the skull for cement adherence. The skull was then degreased with H_2O_2 by cotton swabbing it and dried. All exposed skull bone was covered with 2 layers of I-bond (Kulzer I-Bond total etch) except for the area of the future cranial window and dried with an UV lamp. The area to drill was marked with a 3mm biopsy punch on the left parietal region. Tetric evoflow cement was applied on all the surface of the exposed skull, except the marked area. A circular thinning of the skull around the marked area for the cranial window was created. Bone crumbles were periodically blown away, the drilling region washed with cold saline to avoid heating and dried before restarting drilling. Thickness of the skull in the central groove was regularly checked by gently pushing on the central area of the cranial bone with a fine probe. When the thinned skull moved upon being lightly touched, it was ready to be removed. A large drop of cold saline was added on the thinned skull and the groove was gently pinched with sharp forceps and lifted away. The groove must be kept parallel to the skull's surface to avoid direct perforation of the dura mater. The cranial window was filled with a drop of ACSF and the 3mm coverslip covered with ACSF was placed in the hole. Tetric Evoflow cement was then applied all around the coverslip to seal the coverslip to the skull and slightly under it, so it is well maintained. The cement is then dried with an UV lamp. The animal was removed from the ear bars and we used an alignment tool to orient the mouse head so the coverslip is horizontal (laser coming vertically from the top of the animal to the coverslip is reflected on it and the reflection is indicating the angle of the coverslip). Then the metal head plate was placed parallel to the cover slip, fixed with Tetric Evoflow cement and dried with UV light.

Two-Photon Microscopy

Acute slices were imaged with a two-photon imaging system (Scientifica) equipped with a tunable Ti : Sapphire MaiTai DeepSee laser (Spectra Physics) using an excitation wavelength of 850 nm and the following bandpass filters: 450/50 nm for methoxy-X04 and 525/50 nm for GFP. After placing the acute slice on a cover slip, it was positioned under the 20x objective (XLUMPLFLN; Olympus) where it was constantly perfused with carbogenated ACSF. After identifying the CA1 region, one microglia was selected for time-lapse image acquisition. To avoid activated microglia at the borders of the slice, microglia were exclusively imaged at a depth of >80 µm. With a 6x optical zoom, the cell was centered and the soma was focused. Z-dimensions were set ±30 µm of the soma. Microglia selection was based on unbiased criteria such as clear soma recognition and distinction from neighboring cells. In average 8 stacks were recorded consecutively with the dimensions 129.5 µm*129.5 µm*60 µm (X*Y*Z), a resolution of 512px*512px per plane and a step size of 1 µm. Two images were acquired per plane, which were averaged during image processing. One cell per slice was imaged.

For *in vivo* imaging, the animal was transferred to the two-photon microscope right after surgery on a heating plate. Medetomidine (0.25mg/kg every hour) was injected to prolong the anesthesia. The head was fixed through the implanted head plate to the stage. A drop of water was added on the window and the bright field mode was used to center the window in the 10x objective. The 20x objective (XLUMPLFLN; Olympus) was then used with an excitation wavelength of 850 nm and the 525/50 nm bandpass filter to collect the GFP signal. We recorded cells at least 50 µm deep in a stack going ±30 µm with a 6x optical zoom, in the same way we recorded on slices.

Image Processing & Analysis

Image processing and analysis (**Figures S1A, B**) was performed using ImageJ by custom-written macros (available upon request). For the time-lapse, the maximum intensity Z-projection for each stack was created followed by the x,y registration using the StackReg plugin (23). After cropping the cell using the temporal color code image overlaying all timepoints, automated image correction steps were applied, including background removal, a 2px median filter, photobleaching correction and contrast enhancement. The resulting binarized images were used for analysis. The relative retraction area is the number of pixels in image t_n subtracted with the number of pixels from the consecutive image t_{n+1} relative to the total pixel number of t_n. The relative retraction reflects the percentage of the cell area, which retracted from t_n to t_{n+1}. For the extension area, the number of pixels in image t_{n+1} were subtracted with the number of pixels from the image t_n relative to the pixel number of t_n. The relative extension area reflects the percentage of pixels in a new location from t_n to t_{n+1}. The reported motility index is the sum of the relative retractions and extensions and is used as a readout for the process motility of the microglia. By summing up the absolute retraction and extension area, the surveillance index indicates the surveillance capacity of the microglia and reflects the surveilled area.

Microglia Activation in the Slice Preparation

At the slice surface, microglia morphology resembles an activated phenotype with rounded cell shape and fine, quickly moving processes (**Video S1**) due to tissue damage induced by the slicing. However, within the slice, homeostatic microglia with fine and highly branched processes are observed (for a scan through the slice see **Video S2**). Compounds of choice can be either applied prior (pre-incubation) or during (wash-in) imaging. To assess if the age of the slice after preparation has an effect on microglia behavior, we have plotted the relative motility, surveillance and area values of untreated slices (from experiment in **Figure 3**) versus the time after slice preparation (**Figures S1C–E**). We did not observe any correlation between our readouts and the age of

the slice after preparation. Therefore, these results indicate a stable slice preparation with no aberrant activation of microglia observed over time.

Tracing of Microglia Processes and Sholl Analysis

To trace microglial processes, the maximum intensity Z-projection from the t_0 time point of each recorded cell was selected. Using Fiji's SNT (Simple Neurite Tracer) plugin, processes were traced for subsequent Sholl analysis. With a step size of 1 µm, the number of processes crossing the concentric circles, which were arranged around the soma, were counted. This analysis reflects the ramification of microglia.

Primary Microglia Isolation

After mice were transcardially perfused with ice-cold PBS, whole brains were isolated to obtain single cell suspensions using the Adults Brain Dissociation Kit, mouse and rat (Miltenyi Biotec, 130-107-677) according to the manufacturer's protocol. Briefly, the brains were chopped into pieces in cold PBS, transferred into gentleMACS™ C Tubes (Miltenyi Biotec, 130-093-237) and digested using the provided enzymes with the gentleMACS™ Dissociator with Heaters (Miltenyi Biotec, 130-096-427). Tissue lysates were resuspended and filtered through 70µm cell strainers, which were subsequently rinsed with PBS. Samples were centrifuged at 1500 rpm for 10min and the supernatant was decanted. This was followed by gradient centrifugation with 30% Percoll (GE Healthcare Life Sciences, 17-0891-01) in PBS (v/v) (2750 rpm for 30 minutes, at 4°C, no brakes). Myelin was removed with a suction pump and the suspensions were filtered through 70 µm cell strainers and centrifuged at 1500 rpm, 4°C for 10 minutes. The samples were then ready for flow cytometry staining.

Flow Cytometry

Single cell suspensions were incubated with primary antibodies against CD11b (1:400, clone M1/70, BD Biosciences, 565976), CD45 (1:800, clone 30-F11, BD Biosciences, 563890) or CD45 (1:400, clone 30-F11, BD Biosciences, 565079), CD22 (1:100, clone OX-97, Biolegend, 126112) as well as live cell identification using Zombie NIR™ (1:500, Biolegend, 423106) in PBS for 30 min at 4°C. After washing once with PBS, samples were resuspended in 200 µl PBS and analyzed by flow cytometry with a BD LSRFortessa (BD Biosciences) or a BD FACSymphony flow Cytometer (BD Biosciences). To reduce fluorescent spillover, PMT voltages were adjusted with single-stain controls prepared with VersaComp Antibody Capture Bead Kit (Beckman Coulter, B22804) before sample acquisition. Acquired.fcs files were uploaded in FlowJo software (Tree Star), where artefacts arisen from incorrect compensation-matrix calculation were manually corrected.

In Vivo Amyloid-β Plaque Labeling

18h prior microglia isolation or imaging, PS2APP CX3CR1-GFP mice were injected intraperitoneally with methoxy-X04 (5mg/kg), a blood-brain-barrier penetrating dye, which labels amyloid plaques (24).

Human iPSC-Derived Macrophages

All work with human iPSC-derived macrophages was performed under the respective Swiss legislation, ethical guidelines, and approval. Production and maintenance of human iPSC-derived macrophages was done according to our recently published adapted protocol from van Wilgenburg et al. (25, 26).

Briefly, iPSC maintenance culture dishes (Corning) were coated with 12.5 µg/ml rhLaminin-521 (BioLamina) prior usage. Cells from the utilized human iPSC cell line Bioneer WT (BIONi010-C; Bioneer) were seeded and cultured in mTesR1 media (StemCell Technologies) at 37°C with 5% CO_2 with daily media changes. At 90% confluency, cells were passaged by washing the cells once with PBS and detaching with Accutase™ (Innovative Cell Technologies) for 2 to 5 min at 37°. After removal of Accutase™ by centrifugation, cells were either used for maintenance or induction of differentiation. Cell quality was controlled by STR profiling, SNP phenotyping and karyotyping after banking. Sub-culturing was reduced to an absolute minimum to avoid genetic drift.

To initiate macrophage differentiation, embryoid bodies (EBs) were generated as described previously (25). For EB generation, iPSCs were seeded onto AggreWell 800 plates (StemCell Technologies). Per well, 2 ml of a single cell suspension of $4*10^6$ cells in mTesR1, supplemented with 10 mM ROCK inhibitor (Y27632, StemCell Technologies), were added. Centrifugation at 100 g for 3 min assured an even cell distribution. The following day, 75% of the mTeSR1 media were exchanged with mTeSR1 media supplemented with 50 ng/ml rhBMP4 (Biotechne), 50 ng/ml rhVEGF (Biotechne), and 20 ng/ml rhSCF (Biotechne) to start mesoderm and subsequent hemogenic endothelium induction. This medium exchange was repeated for the next 2 days. On day 4 of differentiation, EBs were harvested and transferred to factory medium, consisting of X-VIVO 15 medium (Lonza) supplemented with 2 mM GlutaMAX (Thermo Fisher Scientific), 10 U/ml Penicillin/Streptomycin (Thermo Fisher Scientific), 50 µg/ml Mercaptoethanol (Thermo Fisher Scientific), 100 ng/ml rhMCSF (Miltenyi Biotech), and 25 ng/ml rhIL3 (Miltenyi Biotech). EBs were plated in growth factor reduced Matrigel (Corning) precoated cell culture vessels at a density of 1 EB/cm^2. Myeloid factories were matured as reported (25).

In Vitro Phagocytosis Assay

iPSC-derived macrophages were plated onto a 96 well plate (Falcon, 353219) at a density of 30000 cells per well. The following compounds were added respectively to assess their impact on phagocytosis: CD22 antibody (BioXcell, BE0011; 5 µg/ml), IgG isotype control (BioXcell, BE0083; 5 µg/ml) and Cytochalasin D (MCE, HY-N6682, 10 µM). Preparation of Aβ-coated, pHrodo-labelled beads was performed as previously described (27). After addition of the beads, phagocytosis was monitored with the IncuCyte S3 live-cell analysis system by acquiring 3-4 brightfield and red fluorescence images every 45 minutes for 12h. For cell recognition and quantification of red-positive cells, the IncuCyte software with its adherent cell-by-cell classification tool was utilized.

Molecular Phenotyping

Molecular phenotyping was performed as described previously (28–30). Expression levels of about 1,000 pre-selected "pathway reporter genes" are monitored using a targeted, parallelized, amplicon-based approach. Briefly, macrophages were treated for 4 hours with either anti-CD22 blocking antibody or the corresponding IgG control antibody at 5µg/ml. After incubation cells were lysed in 350 µl MagNA Pure LC RNA Buffer (Roche Diagnostics, 03604721001) and purified using the MagNA Pure 96 System (Roche Diagnostics). RNA was quantified using the Qubit RNA Assay Kit (Thermo Fisher Q32852) on the Fluorometer Glomax (Promega).

Amplicon Library Construction

10 ng of total RNA from each biological replicate were reverse transcribed to cDNA using Super Script IV Vilo (Thermo Fisher, 11766500, user guide MAN0015862). Libraries were generated with the AmpliSeq Library Plus Kit (Illumina Catalog number 20019103) according to the Reference Guide. Pipetting Steps for target amplification, primer digestion and adapter ligation were done with the mosquito automatic pipettor (ttp labtech) in a miniaturisation fashion. For the purifications before and after final library amplification, SPRI magnetic bead purification was chosen (Clean NGS, LABGENE Scientific SA) semi automated on multidrop (Thermo Fisher). Amplicon size and DNA concentration were measured using an Agilent High Sensitivity DNA Kit (Agilent Technologies, Waldbronn, Germany) according to the manufacturer's recommendation. Prior sequencing samples have to be normalized and pooled to 2nM final concentration on Biomek FXP workstation.

Illumina Sequencing

Pooled libraries were sequenced on the Illumina NovaSeq 6000 Instrument, SBS (sequencing by synthesis) technology. 75 cycles end up with a minimum of 2 Mio SR per sample for analyzing.

Read Mapping and Quantification

As every transcript is represented by a single, specific amplicon from the Molecular Phenotyping panel, the mapping results provide a direct quantification measure in "counts per amplicon" that is used for downstream analysis. Reads were mapped to the amplicon sequences of the panel using Bowtie2 (31).

Detection of Differentially Expressed Genes, Gene Set Enrichment

Counts per amplicon were used for the downstream analyses, greatly simplifying the data processing. Differentially expressed genes (DEGs) were identified from the amplicon sequencing data using edgeR based on negative binomial distribution (28). Gene set enrichment was performed using CAMERA (32).

Microglia Expression Modules

Microglia expression modules were derived from the publication of Friedman et al. (33) and complemented by two modules (DAM signatures TREM2 dependent and TREM2 independent) derived from the publication of Keren-Shaul et al. (34). Differences between two groups in these expression modules were visualized in a Radar plot using python.

Statistics

GraphPad Prism was used for statistical analysis. Data sets were tested for normality (D'Agostino-Pearson Omnibus K^2 normality test; significance level P=0.05) before employing the appropriate parametric or nonparametric statistical comparison test, which is depicted in the respective figure legend. If not stated otherwise, mean values ± SEM were reported. For outlier recognition, the Robust regression and Outlier removal (ROUT) method was utilized with an aggressiveness of Q=1. The Pearson correlation analysis was used to assess correlation.

RESULTS

CD22 Expression Is Enhanced in Aged Microglia and Microglia With Internalized Aβ

During aging, microglia undergo significant transcriptional changes (11). However, the consequences for microglial physiology due to age-associated altered expression levels and implicated signaling pathways are not well understood yet. To address the role of microglial CD22 during aging, we started as a first step by comparing microglial CD22 expression between adult (6 months) and aged (14-16 months) mice. Microglia were isolated from CX3CR1-GFP reporter mice, sorted by flow cytometry and mean fluorescent intensity were measured to determine CD22 levels (**Figure S2A**). To exclude any potential impact of autofluorescence signal in the CD22 channel, a FMO (fluorescence minus one, including all antibodies except anti-CD22) control was included on pooled samples and used to set the gate for CD22 signal (**Figure S2B**). In 14-16 month aged mice, we found the level of CD22 in microglia to be significantly upregulated compared to the adult animals at 6 month of age (**Figures 1A, B**). With this observation we strengthen not only previous findings (15), but also narrow down the time window, in which an evident increase in CD22 expression can be observed.

Since also distinct transcriptional microglia states e.g. DAMs (disease-associated microglia) have been identified in amyloid mouse models of age-related neurodegenerative disorders (34), we wondered whether CD22 is differentially expressed in these subpopulations. To evaluate the relevance of CD22 in an AD-related context, we used the transgenic amyloid mouse model PS2APP (20). We compared CD22 expression of isolated microglia from aged-matched CX3CR1-GFP and PS2APP CX3CR1-GFP double-transgenic mice by flow cytometry, but did not observe a change in mean CD22 levels of all GFP-positive isolated microglia (**Figures 1C, D**). Since DAMs are often located in the vicinity of, or associated to Aβ-plaques, we injected PS2APP CX3CR1-GFP mice with methoxy-X04 prior to microglia isolation to label intracellular Aβ-material (35). When discriminating between microglia subpopulations in the

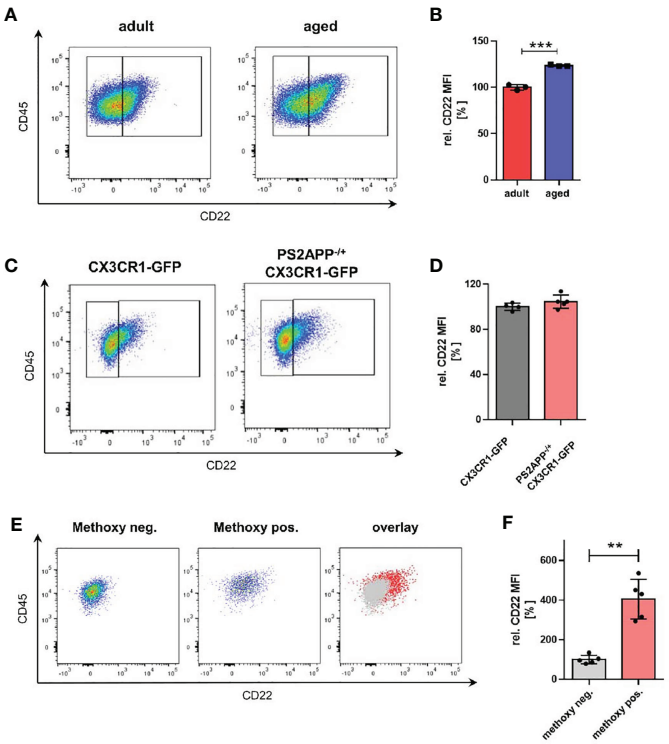

FIGURE 1 | Microglia from aged mice as well as Aβ-containing microglia exhibit an increased CD22 expression. **(A)** Representative flow cytometry scatter plots and **(B)** respective quantification showing the relative CD22 MFI of isolated microglia from adult (6 months) and aged (14-16 months) mice. n=3 mice per age. **(C)** Representative scatter plots and **(D)** quantification of the CD22 expression in isolated microglia from 13 months old PS2APP$^{-/+}$ CX3CR1-GFP and age-matched CX3CR1-GFP mice. n=4-5 mice. **(E)** Scatter plots of CD22 expression in methoxy-X04 negative microglia, methoxy-04 positive microglia and an overlay visualizing the differences in CD22 signal between both subsets. **(F)** Relative CD22 MFI of methoxy-X04 negative and methoxy-04 positive microglia from 13 months old PS2APP CX3CR1-GFP mice. n=5, mean ± SEM. For **(B, D)** and **(F)** mean ± SEM, unpaired nonparametric t-test (Mann-Whitney). **p<0.01, ***p<0.001.

PS2APP CX3CR1-GFP mice, Aβ-containing microglia (methoxy-positive cells) exhibited a significant 4-fold increase in CD22 levels in comparison to the methoxy-negative cells (**Figures 1E, F**), indicating an increased expression of CD22 in plaque-associated microglia.

Next, we were interested in how the increase in CD22 expression in aged and Aβ-containing microglia correlates with the physiological function, and more specifically surveillance capacity of these states.

Two-Photon Imaging Based Slice Assay to Study Microglia Dynamics Upon CD22 Blockage

Microglia are continuously surveilling their parenchymal environment with their highly branched and motile processes (**Video S3**). They are extremely sensitive to small alterations in their surrounding environment and change their phenotype dramatically after isolation from the tissue (17, 18). Therefore, to assess microglial phenotypic modulation by CD22, it is essential to develop assays that are as close as possible to the natural microglial environment. In order to measure CD22 and other compound-mediated effects on microglia surveillance and motility, we performed live imaging by two-photon microscopy in *ex vivo* acute slices (**Figure 2A** and **Video S4**) of the CX3CR1-GFP transgenic mouse model (19). We have established a semi-automated image processing and analysis pipeline to quantify microglia dynamics (**Figure S1** and methods).

To determine if continuous imaging by the pulsed laser induces alterations in microglia dynamics, we have measured motility of single microglia over a period of 80 minutes (**Figure 2B**). We did not observe any change with stable motility values over time, indicating that the continuous imaging does not lead to tissue damage and associated microglia response. To evaluate the noise of our image processing and analysis pipeline, we have imaged PFA-fixed acute slices in the imaging chamber. The motility index is strongly reduced in fixed slices in comparison to *ex vivo* acute slices (**Figure 2D**). The residual minimal motility signal results from slice movement in the imaging chamber due to continuous flow of ACSF. Interestingly, microglia imaged *in vivo* through a cranial window in anesthetized animals revealed a higher motility index as compared to the *ex vivo* acute slices (**Figure 2D** and **Video S5**). The high sensitivity of microglia morphology and motility to spontaneous neuronal activity and neurotransmission (36, 37), that is reduced in the slice preparation, could explain these findings and correlates with

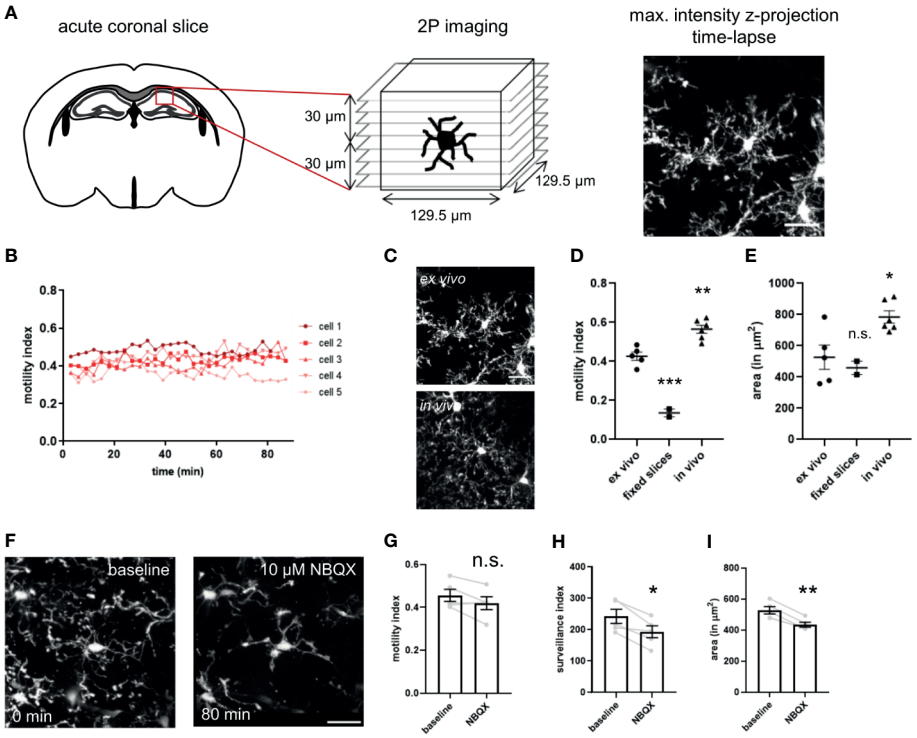

FIGURE 2 | Imaging setup of two-photon microscopy of *ex vivo* acutely prepared slices. **(A)** Freshly prepared acute coronal sections of CX3CR1-GFP mice are placed under the microscope and the region of interest is selected. After adjusting the parameters for stack acquisition, the time-lapse stack recording is initiated. **(B)** The motility index, calculated for each timepoint, is stable for a 80 min imaging period. **(C)** Representative images of microglia process complexity in the *ex vivo* and *in vivo* preparation **(D)** Motility index and **(E)** cell area of microglia imaged in *ex vivo* slices, PFA-fixed slices and *in vivo* through a cranial window. **(F)** The AMPA receptor blocker NBQX induces progressive decrease in size and complexity of the ramified processes. NBQX treatment leads to a marginal reduction in motility **(G)**, and a more severe decrease of the surveillance index **(H)** and microglia area **(I)**. For **(D, E)** and **(G–I)** One-way ANOVA multiple comparisons to *ex vivo*, *p<0.05, **p<0.01, ***p<0.001, n.s.>0.5 Scale bar: 20 µm.

the broader branched processes and increased covered area of microglia *in vivo* (**Figures 2C–E**).

For evaluation of our assay and assessment of its capability to detect microglial morphological changes, we used in a first step compounds to modulate microglial behavior. NBQX, an AMPA receptor antagonist, let to a slight drop in motility and more apparent in the surveillance index and occupied area (**Figures 2G–I**), and was concomitant with the observed de-ramification (**Figure 2F**) as seen in the time-lapse (**Video S6**). The sensitivity of the assay was further validated using the cytoskeleton blocker cytochalasin B and ATP (**Figure S3** and **Video S7, S8**). Taken together, we have established a microglia imaging and analysis platform that enables us to study their process dynamics in native tissue environment of the *ex vivo* slice preparation.

Microglia of Aged Mice Show Reduced Surveillance Capacity

Since we observed an upregulation of CD22 in microglia during aging and to address the question if CD22 is involved in age-related alterations of microglia physiology, we first compared dynamics of adult and aged microglia with the established two-photon based live imaging assay. We have prepared acute brain slices from 7-8 month old (adult) and 13-16 month old (aged) CX3CR1-GFP reporter mice. Microglia were live-imaged and the average surveillance, motility and area was calculated. Aged microglia exhibited a hypo-ramification as compared to microglia imaged from adult mice (**Figures 3A–E** and **Video S9, S10**). Strikingly, the hypo-ramification of aged microglia is accompanied by a significant reduction in their surveillance index as compared to adult microglia (**Figure 3B**). Microglia motility and cell area was reduced by 7% or 12%, respectively, but statistically there was no significant difference between the two groups (**Figures 3C, D**). Lastly, Sholl analysis reveals a significant reduction in ramification of aged compared to adult microglia (**Figure 3E**), thereby reflecting the age-associated morphological changes. These results show that aging of microglia is accompanied by a hypo-ramification and reduced surveillance of their parenchymal microenvironment.

Antibody-Induced CD22 Blockage Restores Age-Related Decline in Microglial Surveillance

CD22 deficiency leads to an enhanced motility as well as enhanced chemotaxis of B-cells (38). Therefore, we were

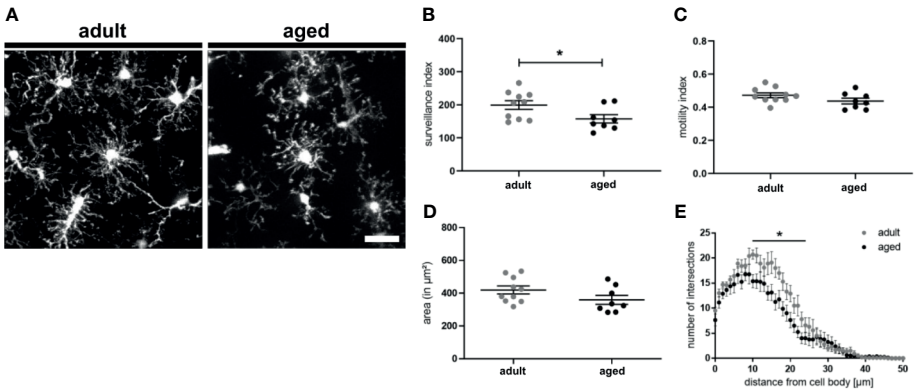

FIGURE 3 | Surveillance deficits and hypo-ramification in aged microglia. **(A)** Representative two-photon images of microglia from acute slices of adult (7-8 months) and aged (13-16 months) mice. Semi-automated analysis of **(B)** surveillance index, **(C)** motility index and **(D)** area of adult and aged microglia. **(E)** Sholl analysis using max. z-projections from time point t_0 of respective time-lapse recording showing the number of intersections in relation to the distance of the cell body. n=8-10 cells from n=7 mice each, mean ± SEM, unpaired nonparametric t-test (Mann-Whitney), *p<0.05. Scale bar: 20 µm.

asking if blockage of CD22 can also alter the morphology and dynamic activity of microglia. Since we observed a CD22 upregulation during aging of microglia, we were specifically interested if there is a differential effect on adult versus aged microglia. Thus, acute brain slices from adult (7-8 month old) and aged (13-16 month old) CX3CR1-GFP reporter animals were incubated with a CD22-blocking antibody or an isotype control antibody prior to imaging (**Figures 4A–F**). In adult microglia, antibody-mediated CD22 blockage did neither alter surveillance, motility and cell area, nor the ramification state as compared to IgG isotype control (**Figures 4B–E** and **Video S11, S12**). However, the evident de-ramification in aged microglia was reverted upon CD22 inhibition (**Figures 4A–J** and **Video S13, S14**) and an increase in overall cell area was observed (**Figure 4I**). Furthermore, the CD22-related morphological changes were accompanied by a significant increase of both surveillance and motility (**Figures 4G, H**). Ultimately, Sholl analysis revealed that microglial process ramification was restored by CD22 inhibition (**Figure 4J**). These results clearly demonstrate that in accordance with the upregulation of CD22 during aging, age-associated de-ramification and declining surveillance capacity can be restored *via* antibody-mediated inhibition of CD22 specifically in aged microglia and suggest CD22 as a negative regulator of microglia surveillance.

In addition to aging, we also observed a specific upregulation of CD22 in Aβ-containing microglia in the amyloid mouse model PS2APP CX3CR1-GFP. Extracellular accumulation of Aβ, a pathological hallmark of Alzheimer's disease, is associated with neuroinflammation and aberrantly activated microglia, referred to as disease-associated microglia (DAM) (34), that are specifically found around plaques. These DAMs exhibit a modified transcriptional signature, such as the upregulation of AD risk genes and the downregulation of homeostatic genes. Furthermore, plaque-associated microglia exhibit a reduced process motility (39). We therefore tested if CD22 blockage can also alter surveillance and motility of plaque-associated microglia. To analyze the effects of CD22 inhibition on plaque-associated microglia, two-photon live imaging was performed on brain slices prepared from methoxy-X04 injected PS2APP CX3CR1-GFP animals to label the plaques (**Figure S4A**). Since this amyloid mouse model develops plaques first in the frontal cortex, we selected this region for further evaluation. In contrast to homeostatic microglia, plaque-associated microglia exhibit a reduced surveillance and motility index of around 73 and 0.4, respectively. Upon blockage with the CD22 antibody, the surveillance index increased to 85, but statistically there was no significant difference to the IgG isotype control (**Figure S4B**). Motility of plaque-associated microglia was not affected by CD22 inhibition (**Figure S4C**). Although CD22 expression is strongly increased in methoxy-positive microglia, antibody-mediated blockage of CD22 did not significantly alter the surveillance of plaque-associated microglia.

Summarizing, with two-photon imaging of microglial dynamics in acutely prepared slices we show that the inhibition of CD22 signaling can enhance microglial motility as well as restore age-related decline in microglia surveillance and ramification in the non-diseased brain. In a disease context, plaque-associated microglia did not display significant changes upon antibody-mediated blockage of CD22, although a trend towards an increased surveillance capacity is visible.

CD22 Blockage Enhances Phagocytosis of Aβ-Coated Beads in Human iPSC-Derived Macrophages

CD22 has recently been identified as a modulator of microglial phagocytosis in a CRISPR screen based on Cas9 expressing murine BV2 cells (15). To connect observations from this study and our mouse *ex vivo* slices to human biology, we derived primitive macrophages from iPSC cells and assessed the effect of

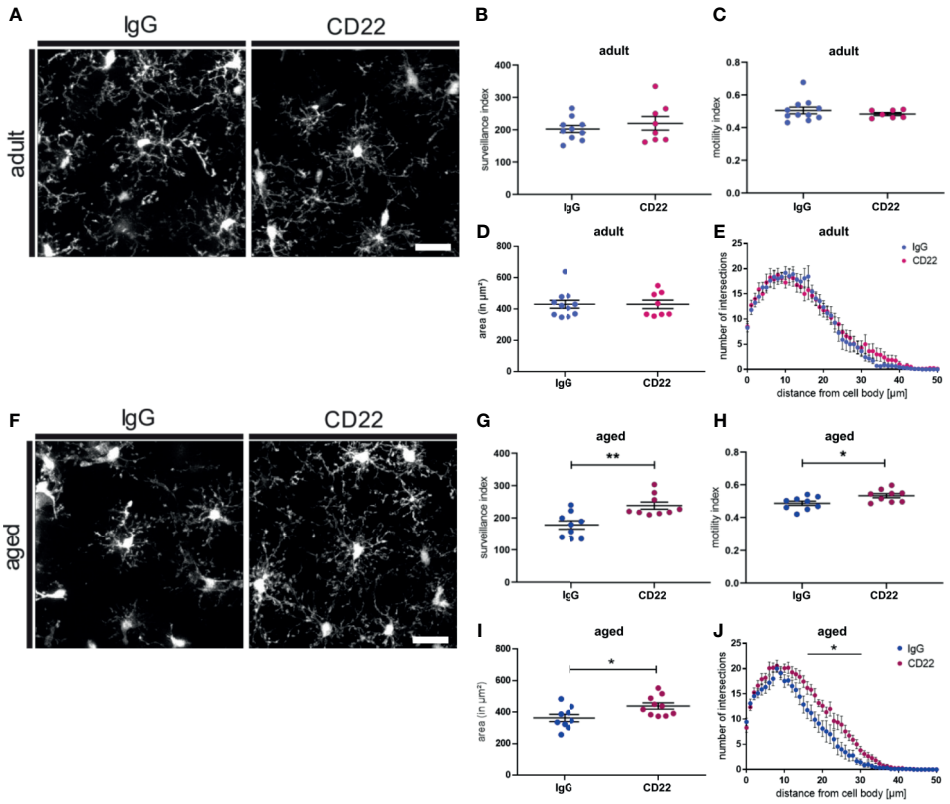

FIGURE 4 | Blockage of CD22 restores age-associated deficits in surveillance and ramification. **(A)** Representative two-photon images of microglia from acute slices prepared from adult (7-8 months) mice, which were either treated with a CD22 or an IgG isotype control antibody. Respective analysis of the **(B)** surveillance index and **(C)** motility index as well as the **(D)** area and the **(E)** sholl analysis reflecting the microglial ramification. **(F)** Two-photon images of microglia from aged (13-16 months) mice demonstrating the effect of treatment with CD22-blocking antibody. Quantification of the **(G)** surveillance index **(H)** motility index, **(I)** area and **(J)** sholl analysis comparing the antibody treatments. For **(B–E)** and **(G–J)** n=7-11 cells from n=7 mice each, mean ± SEM, unpaired nonparametric t-test (Mann-Whitney), *p<0.05, **p<0.01. Scale bar: 20 µm.

CD22 blockage on phagocytic activity. For the generation of the iPSC-derived macrophages we used a previously published protocol (25, 26) that resembles the correct ontogeny of yolk-sac-derived myb-independent primitive macrophages. Since macrophages are highly phagocytic cells with similar molecular mechanisms involved in phagocytosis as in microglia and we already established a variety of functional readouts using these cells previously we decided to use these cells as surrogate for microglial phagocytosis. To assess the phagocytic activity of the macrophages, we monitored the uptake of pHrodo-labelled Aβ-coated beads (27), which were added to the respective treatments. Upon treatment with the IgG isotype control antibody the amount of red-positive cells, which reflect the amount of phagocytic cells, does not differ over time compared to the control condition, whereas the phagocytic activity is completely abolished by cytochalasin D, a known actin polymerization inhibitor (**Figure 5B**). However, antibody-mediated CD22 blockage leads to a significant increase in red-positive cells over time compared to the isotype control (**Figures 5A–C**), indicating an increased phagocytic activity. Thus we conclude that CD22 negatively regulates phagocytosis in human macrophages *in vitro*, similar to previous findings reported in murine microglia-like cells (15).

CD22 Blockage Effects on Gene Expression in Human iPSC-Derived Macrophages

Since the observation of increased phagocytosis pointed to a specific effect of CD22 blockage on macrophages we used molecular phenotyping (28–30) to further characterize downstream pathways that are affected by CD22 blockage. **Figures 6A, B** shows volcano plots for the comparisons of control IgG-treated cells to untreated cells, and of anti-CD22-treated cells to IgG-treated cells. The horizontal red dashed line corresponds to a p value cutoff of p=0.05. Even for a panel of around 1,000 genes, the number and size of effects at the transcriptional level are small, and are comparable for the two tested treatments. Obviously, signaling events at the protein level are not captured in a differential gene expression analysis. We note that effects on phagocytosis and motility may well be regulated at the protein level and not be reflected in the gene

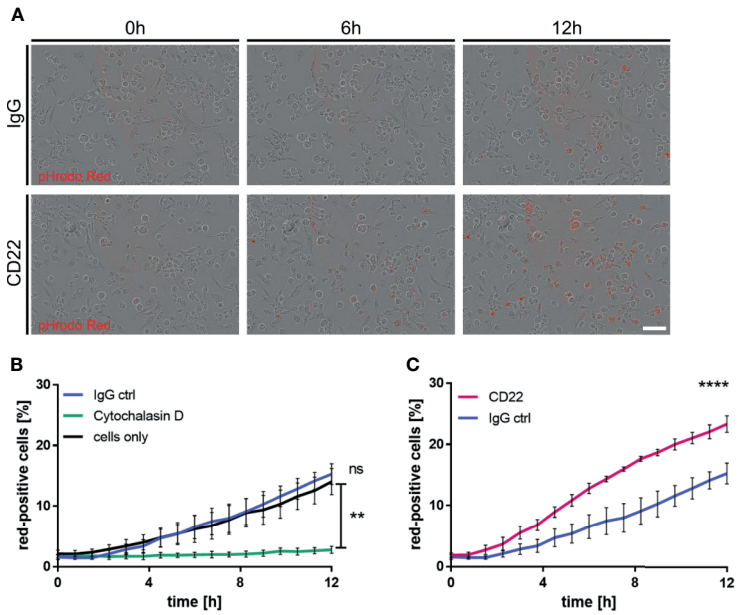

FIGURE 5 | CD22 blockage increases phagocytic capacity of human iPSC-derived macrophages. **(A)** Representative images of iPSC macrophages treated either with CD22 blocking antibody or IgG isotype control. Red signal indicates pH-rodo labeled Aβ-coated beads, which are located in the lysosomes. **(B)** Increase of phagocytosis-positive cells over time in untreated cells and cells treated with 5 µg/ml IgG isotype control, while no significant change is visible in cells treated with 10 µM Cytochalasin D. Cells were monitored using IncuCyte S3 and analyzed using IncuCyte cell by cell analysis. **(C)** Raise in phagocytosis positive cells over time in cells treated with 5 µg/ml CD22 blocking antibody or 5 µg/ml IgG isotype control. Cells were monitored using IncuCyte S3 and analyzed using IncuCyte cell by cell analysis. n=3, mean ± SEM, unpaired nonparametric t-test (Mann-Whitney), **p<0.01, ****p<0.0001. ns>0.05.

expression data. **Figures 6A, B** shows that several of the genes that are down-regulated in response to the generic IgG antibody (left: ITGB4, BMP4, HTRA1, CDH2) are up-regulated by anti-CD22 treatment compared to IgG.

Given the small number of clearly significant effects, we apply a gene set enrichment analysis approach to identify effects that are significant at the gene set level even though non-significant at the gene level. We assessed a total of about 3,000 gene sets obtained from the public domain as described in (28–30). **Figures 6C–F** illustrates two very clear findings.

First, the interferon response network is characterized here by annotated targets of interferon alpha (IFNA1). As the diagram in **Figure 6C** shows, for IgG controls, two IFNA1 target genes are up-regulated at the p=0.05 significance level (TRIM5, MX1, compare **Figure 6A**), but the majority of other IFNA1 target genes also show an upward trend, rendering this gene set as a whole significantly up-regulated. In **Figure 6D**, the same gene set is shown for the anti-CD22 treatment compared to IgG treatment. The set is overall balanced, and none of the member genes is significantly affected anymore, and there is no overall effect on this set of genes, suggesting that the anti-CD22 effect in this context alleviated the interferon response induced by the control antibody.

For another gene set of interest, genes annotated as involved in BMP/TGFB signaling, the situation is even more dramatic. **Figure 6E** suggests that, while only one of its member genes (BMP4) is statistically significantly down-regulated by treatment with IgG, the majority of member genes measured in our panel show a downward trend. As **Figure 6F** shows, this trend is reversed by treatment with anti-CD22. The majority of BMP/TGFB signaling genes now show upward trends, and three of them are individually significant at the p=0.05 level (SREBF1, FOXC1, BMP4). TGF-β signaling was associated with homeostasis of microglia (40).

For comparison with our previous work, we also used the previously described microglial gene modules (27) and compared the effect of CD22 blockage on these modules to untreated cells and isotype control antibody treated cells (**Figures 6G, H**). We note that CD22 itself is part of the "neurodegeneration" module analyzed by Friedman et al. (33). When compared to untreated cells, an up-regulation of the monocyte module and the interferon module could be observed (**Figure 6G**). As explained in more detail above (**Figures 6C, D**), the effect on the interferon module was not observed when the CD22 blockage was compared to isotype control. However, the monocyte module was still affected.

Overall, while we do not observe any clear gene expression effects related to phagocytosis or cell motility, blockage of CD22 signaling is shown to affect gene networks involved in modulating overall microglia activation and behavior.

DISCUSSION

Here we describe a novel function of microglial expressed CD22 in regulating process surveillance and ramification. We have

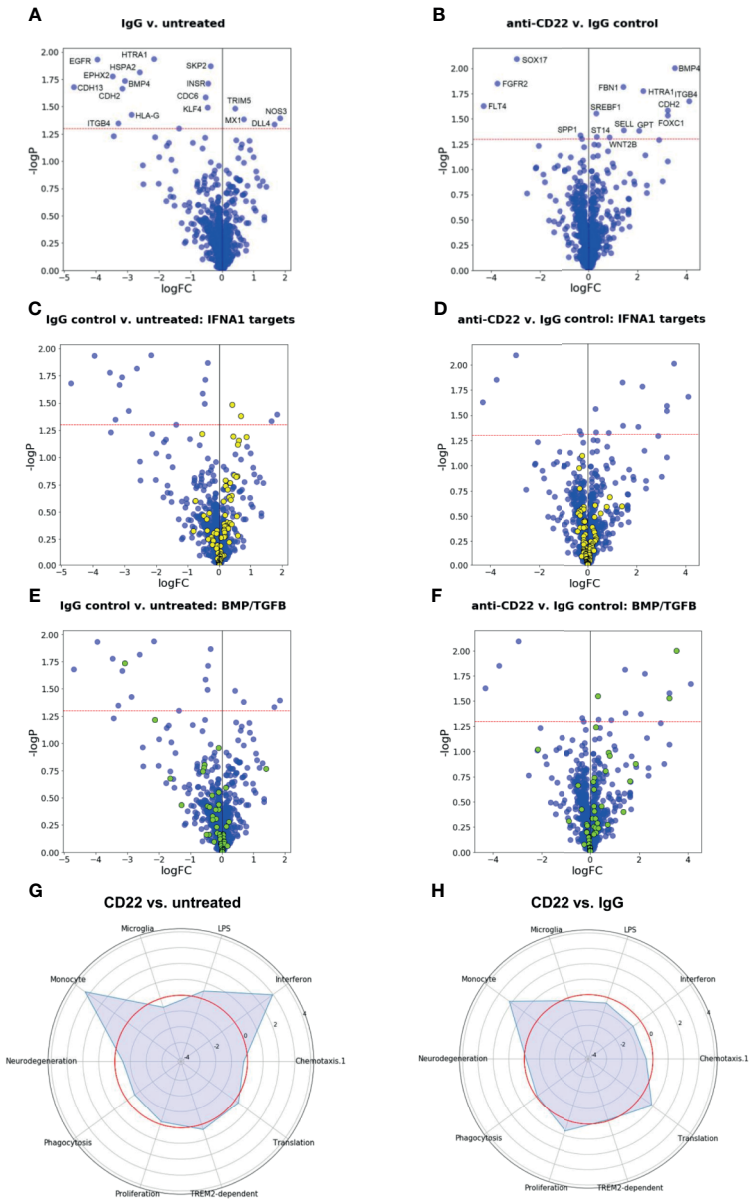

FIGURE 6 | Gene expression and gene set enrichment analyses. **(A, B)** Volcano plots of treatment effects on gene expression levels in iPSC-derived macrophages. Each point represents one of the 1,062 measured pathway reporter genes. The x axis shows log2 fold changes, the y axis has negative log10 of p values. The red horizontal line indicates a p value cutoff of 5 percent. All genes above the cutoff are indicated by their official gene symbols. **(A)** Effects of generic IgG antibody on untreated cells. **(B)** Effects of anti-CD22 antibody treatment compared to IgG treatment. **(C, D)** Volcano plots as in **(A, B)**, with genes annotated as targets of interferon alpha (IFNA) highlighted in yellow. **(E, F)** Volcano plots as in **(A, B)**, with genes belonging to BMP/TGFB signaling highlighted in yellow. **(G)** Radar plot to visualize changes in gene expression in gene modules relevant for microglia induced by CD22 blockage. Plotted values are enrichment scores calculated using CAMERA (32). The red circle indicates the reference level as detected in untreated macrophages. Peaks outside the red circle indicate up-regulation of a module in cells treated with CD22 blocking antibody and modules closer to the center indicate down-regulated modules compared to untreated macrophages. **(H)** Radar plot to visualize changes in gene expression in microglial modules induced by CD22 blockage in comparison to Isotype treated cells. The red circle indicates the reference level as detected in Isotype treated macrophages.

assessed microglial motility, surveillance and ramification *ex vivo* in acutely prepared brain slices using two-photon microscopy. Utilizing this technology, we were able to demonstrate age-related decrease in microglial surveillance and altered morphology comparing microglia from adult and aged CX3CR1-GFP reporter mice, which are consistent with the de-ramification of aged microglia observed in human studies (41). Importantly, the blockage of CD22 in acute brain slices of aged

mice restored age-related microglial hypo-ramification and the reduced surveillance capacity. Moreover, CD22 blockage results in increased phagocytosis of Aβ-coated beads in iPSC-derived macrophages and reprograms transcriptional state inducing an upregulation of BMP/TGFβ gene networks and a dampening of the interferon response.

Two-Photon Microglia Imaging

To evaluate dynamic and morphological changes in microglia upon blockage of CD22, we describe a two-photon imaging and analysis platform. While already various approaches were reported to study microglia dynamics *in vivo*, most of them are dependent on manual selections, which are more prone to bias and which we aimed to avoid with our semi-automated pipeline. An additional advantage of our analysis platform is its compatibility with both *in vivo* and *ex vivo* imaging, making it more versatile. A recently published review summarized different approaches on studying microglia dynamics (42) and in contrast to our data, when comparing the microglial process speed of different conditions, published data suggests an enhanced process speed in *ex vivo* acute slice recordings compared to *in vivo* imaging. However, the authors also illustrate that caution has to be taken by comparing values from different studies since the experimental settings often differ. We observe increased motility by *in vivo* imaging in anesthetized mice compared to *ex vivo* acute brain slices with the same acquisition and analysis pipeline, which is in line with a higher complexity of the microglial processes *in vivo*. Since our platform can be utilized for an *in vivo* and *ex vivo* setup, the obtained data is more comparable. Overall, this platform does not only help to further understand microglia dynamics and physiology, but also allows to dissect molecular pathways which control phenotypic alterations and subsequently to develop new therapeutic strategies to manipulate microglia behavior.

Aging and CD22

Numerous studies are linking aging with microglia deficits, making further research in understanding those impairments and their relevance for neurodegeneration indispensable. Our study for instance shows that CD22 blockage also restores the surveillance capacity and ramification of aged microglia in addition to the previously published effects on age-associated suppression of microglial phagocytosis (15). Since we and others have shown that murine CD22 levels are upregulated during aging (43), this potentially uncovers CD22 as a broad age-related modifier of microglial behavior. While we were able to show significant age-associated reductions in surveillance and ramification, only a trend towards a reduced area and motility was observed. Although previous studies robustly demonstrated age-related changes in microglial motility (42), it is important to emphasize that the age difference in our study is intentionally small (adult versus aged) and therefore we expect that the effects would be even more prominent with bigger age differences. Nevertheless, we provide valuable data on how to potentially modulate microglial malfunction observed during aging.

CD22 and Neurodegeneration

Despite RNASeq data indicating an increased CD22 expression in AD brains (33), little is known about the presumed role of CD22 in neurodegeneration. However, CD33, a member of the SIGLEC-family and an AD risk-gene (44), was shown to impair microglial Aβ-uptake and clearance (45, 46). Moreover, a SNP in INPP5D, the gene coding for the CD22 downstream signaling partner SHIP-1, was associated with late-onset Alzheimer's disease (LOAD) (47). By using the amyloid mouse model PS2APP, we evaluated the effects of CD22 blockage in an amyloid context. While CD22 overall expression comparing CX3CR1-GFP and PS2APP CX3CR1-GFP animals did not significantly differ, methoxy-positive microglia show considerably increased protein levels of CD22. This is in line with previously published scRNAseq data that show upregulation of CD22 mRNA in DAM state microglia (34). As plaque-associated microglia display an altered transcriptomic signature (34, 48), we could speculate that the uptake of Aβ or their transformation into a DAM state might cause an enhanced CD22 expression. While we observed clear morphological changes in aged microglia after blockage of CD22, data on process dynamics of plaque-associated microglia of PS2APP CX3CR1-GFP mice was more heterogeneous. The transcriptional signature of microglia is highly diverse between homeostatic versus plaque-associated microglia and throughout the different brain regions (11). This heterogeneity and differential expression of CD22 signaling partners could generally influence the susceptibility of microglia for targeted inhibitions like CD22 blockage. Since the plaque-associated microglia of PS2APP CX3CR1-GFP were imaged exclusively in the frontal cortex, evaluating the potential region-specificity of effects on microglial CD22 blockage might therefore be of interest for future experiments. Nevertheless, the option remains, that CD22 is mainly an age-associated modifier of microglial surveillance rather than disease-associated.

CD22 Downstream Signaling and Molecular Phenotypes

Transcriptomics studies emphasize differences between human and mouse microglia during aging and Alzheimer's disease (9, 49), underlining the importance of translational studies with human tissue or cells. By demonstrating a modulatory effect of CD22 blockage on Aβ phagocytosis in human iPSC-derived macrophages, we show the relevance of CD22 targeting for human biology. Further dissection of the microglial CD22 pathway will be necessary to fully understand the observed effects upon its inhibition, for instance elucidating the mechanisms underlying the increased CD22 expression during aging or the direct downstream effects on intracellular signaling pathways. The CD22 intracellular domain consists of ITIMs (immunoreceptor tyrosine-based inhibition motif), which, by recruiting the protein tyrosine phosphatase SHP-1, can counteract signals arising from ITAM (immunoreceptor tyrosine-based activation motif) receptors (50). DAP12, the TREM2 adaptor protein, presents an example of ITAM containing receptors in microglia and latest research indicates that ITAM signaling plays an important role in the phagocytosis

process (51). We have observed an increased phagocytosis upon CD22 blockage, which might be mediated by disinhibition and the release of ITAM signaling. Especially interesting would be the association with TREM2 signaling, which has been identified as a key receptor promoting microglial phagocytosis (52). Indeed, CD33, another ITIM siglec receptor, opposes TREM2 signaling and inhibits phagocytosis (46).

In addition to increased phagocytosis, we have also observed that inhibition of CD22 leads to enhanced surveillance and motility of microglia. A higher overall cell motility could also explain the finding of increased phagocytosis. CD22 signaling pathways have been characterized in other cell types including B-cells where it regulates B-cell receptor signaling *via* recruiting protein tyrosine phosphatase SHP-1 and SHP-2 (50). They in turn modulate the function of various signaling pathways and thereby control several cellular functions like chemotaxis or inflammation (53). Both SHP-1 and SHP-2 are also highly expressed in microglia (53), which suggest CD22 signaling *via* these protein tyrosine phosphatases during microglial phagocytosis as well. For instance, inhibition of SHP-1 was shown to rescue α-synuclein-associated inhibition of phagocytosis in rat primary microglia (54).

Here we already took one further step in dissecting the effects of CD22 blockage, by analyzing its transcriptional effects on human iPSC-derived macrophages. As expected for non Fc-silent antibodies, the CD22 blocking antibody as well as its isotype control showed some overlapping effects on signaling networks (55, 56). Overall, differential effects on a panel of "pathway reporter genes" were mild, but gene set enrichment analysis revealed interesting network-level effects. Strikingly, in comparison to previously published RNAseq on CD22 inhibition, we also observed an enrichment in TGF-β signaling (15). CD22 could influence the balance between the two major microglial survival pathways, the MCSF and TGF-β signaling (57). The latter, upregulated by CD22 blockage in our study, has previously been reported to influence microglial morphology (58). Therefore, the transcriptional effects observed in the human macrophages correlate with our observation of the morphology changes in the *ex vivo* slices. Furthermore, TGF-β signaling in microglia is central in the prevention of excessive activation of mature microglia, whereas homeostatic gene expression signature is not affected by TGF-β (59). Microglial activation is generally considered to be associated with aging. Thereby, CD22-blockage induced TGF-β signaling could present a mechanistic link of the observed age-dependent effects of CD22 inhibition on microglial surveillance. In addition we clearly saw an effect of CD22 blockage dampening the IgG-induced interferon response. *In vivo*, the microglia interferon response drives microglia away from the homeostatic stage towards a pro-inflammatory stage (33). The interferon module was found to be induced in disease and CD22 could play a role in inducing this module.

Summarizing, we have identified CD22 as a novel age-related modifier of microglial surveillance. The significance of CD22 signaling in human biology was confirmed in iPSC-derived macrophages, where CD22 blockage increases phagocytosis and modulates key gene networks implicated in microglial function.

DATA AVAILABILITY STATEMENT

The datasets presented in this study can be found in online repositories. The names of the repository/repositories and accession number(s) can be found below: https://www.ncbi.nlm.nih.gov/geo/, GSE169252.

ETHICS STATEMENT

The animal study was reviewed and approved by the Cantonal Ethical Committee for Animal Research and the Swiss Cantonal Veterinary Office.

AUTHOR CONTRIBUTIONS

EH and SG conceived, designed, and supervised the study. EH and CC-B established the two-photon imaging-based brain slice assay. VA conducted the *ex vivo* imaging experiments. AP and VA performed the flow cytometry and AP analyzed the data. VA and CS did the cellular experiments. ME, RS, and EK conducted the molecular phenotyping analysis and evaluated the data. VA drafted the article and co-wrote the paper with SG and EH. CC-B, AP, ME, RS, CS, and EK revised the article critically. All authors contributed to the article and approved the submitted version.

FUNDING

VA was supported by the Roche Internships for Scientific Exchange (RiSE) program.

ACKNOWLEDGMENTS

We thank Alicia M. Kemble, Linda Koene, Anja Gundlfinger, Beatriz Furones Cuadrado and Roberta Lauria for experimental advice, and Jitao D. Zhang for support with the data processing. Furthermore, we would like to acknowledge Benjamin Hall, Roger Redondo, Eva Mracsko, Ludovic Collin, Ravi Jagasia, Markus Britschgi and their respective teams for valuable support, advice, data discussion and feedback.

SUPPLEMENTARY MATERIAL

The Supplementary Material for this article can be found online at: https://www.frontiersin.org/articles/10.3389/fimmu.2021.684430/full#supplementary-material

Supplementary Figure 1 | Image processing and quantification of two-photon recordings. **(A)** A maximum intensity projection of the acquired stacks for each timepoint is used to generate the time-lapse. After x,y registration and manual cropping of the cell, an automated series of filters for image correction is applied for thresholding and binarization of the images. **(B)** To assess the process retractions, image tn is subtracted with tn+1. The results represent the amount of processes in tn which retracted in the following image tn+1. For the process extensions, image tn is subtracted from tn+1, describing the amount of processes which extended from tn to tn+1. While the motility index indicates the microglia process dynamics, the surveillance index serves as a readout for microglial surveillance. Correlation plots of the **(C)** relative motility, **(D)** relative surveillance and **(E)** relative area against the time after slice preparation to evaluate the stability of the measured readouts over time in untreated adult and aged microglia, which were used for experiment in Figure 3.

Supplementary Figure 2 | Supplementary flow cytometry data. **(A)** Gating strategy to assess microglial CD22 expression. Cells were gated based on their location on the FCS-A vs SSC-A plot and doublets were excluded consequently (FSC-A vs FCS-H). Live single cells were assessed for CD45 positivity and myeloid cells were gated ($CD11b^{+}CD45^{+}$ cells). Finally, CD22 expression in CX3CR1 positive myeloid cells (GFP+ cells) was analyzed. **(B)** Scatter plots to visualize acquired CD22 signal per sample. FMO: Fluorescence Minus One. As control, one sample was stained with all antibodies except the CD22-PE. This sample was used to set the CD22 negative and positive gates, which was then applied on all samples.

Supplementary Figure 3 | Application of other known microglia modulators induce distinct dynamic responses. **(A)** Wash-in of the actin polymerization inhibitor cytochalasin B diminishes the process speed **(B)** and the surveilled area **(C)**, while the total area remains stable **(D)**. **(E)** ATP evokes an increase in size and complexity of the processes and the development of bulbous tips. Upon application of ATP, a reversible increase of motility **(E)** and surveillance **(F)** followed by a recovery to steady state, whereas a constant increase of microglia area was measured **(G)**. n=5-6 cells per treatment. Mean ± SEM, (B)-(D) paired t-test, (F)-(H) one-way ANOVA multiple comparisons to baseline, * $p<0.05$, ** $p<0.01$, n.s.>0.05. Scale bar: 20 µm.

Supplementary Figure 4 | Plaque-associated microglia trend towards an increased surveillance capability upon CD22 blockage. **(A)** Representative two-photon images of plaque-associated microglia in 8-12 months old PS2APP x CX3CR1-GFP mice, which were either treated with a CD22 or an IgG isotype control antibody. Respective surveillance **(B)** and motility **(C)** analysis. n=8 cells from n=8 mice, mean ± SEM, unpaired nonparametric t-test (Mann-Whitney), Scale bar: 20 µm.

Supplementary Video 1 | Time-lapse of activated microglia at the slice surface. Scale bar: 20 µm.

Supplementary Video 2 | Two-photon Z-scan through the acute slice, starting at the slice surface until a depth of -111 µm. Scale bar: 20 µm.

Supplementary Video 3 | Montage of time-lapse (left) and cumulative surveilled area over time (right) of a homeostatic microglia. Scale bar: 20 µm.

Supplementary Video 4 | Two-photon recording of homeostatic microglia at a depth of -80 µm. Scale bar: 20 µm.

Supplementary Video 5 | Two-photon time-lapse of homeostatic microglia in vivo. Scale bar: 20 µm.

Supplementary Video 6 | 10µM NBQX provokes a severe microglial de-ramification when applied on the acute slice. Scale bar: 20 µm.

Supplementary Video 7 | Time-lapse of microglia experiencing abolishment of process dynamics upon wash-in of 1µM cytochalasin B. Scale bar: 20 µm.

Supplementary Video 8 | During wash-in of 1mM ATP, microglia react immediately by hyper-ramification and temporal development of bulbous tips. Scale bar: 20 µm.

Supplementary Video 9 | Two-photon recording of microglia from an adult mouse under steady-state conditions. Scale bar: 20 µm.

Supplementary Video 10 | Time-lapse of an aged microglia demonstrating age-associated hypo-ramification. Scale bar: 20 µm.

Supplementary Video 11 | No evident differences can be observed in adult microglia after treatment with IgG antibody. Scale bar: 20 µm.

Supplementary Video 12 | Upon pre-treatment with the CD22 antibody, no changes in microglia dynamics are visible in microglia from adult mice. Scale bar: 20 µm.

Supplementary Video 13 | After IgG control antibody incubation, reduced ramification of aged microglia remains unaffected. Scale bar: 20 µm.

Supplementary Video 14 | Antibody-mediated CD22-blockage reverses the age-related hypo-ramification of aged microglia. Scale bar: 20 µm.

REFERENCES

1. Thion MS, Ginhoux F, Garel S. Microglia and Early Brain Development: An Intimate Journey. *Science* (2018) 362:185–9. doi: 10.1016/j.stem.2010.08.014
2. Sierra A, Encinas JM, Deudero JJP, Chancey JH, Enikolopov G, Overstreet-Wadiche LS, et al. Microglia Shape Adult Hippocampal Neurogenesis through Apoptosis-Coupled Phagocytosis. *Cell Stem Cell* (2010) 7:483–95. doi: 10.1016/j.stem.2010.08.014
3. Bilimoria PM, Stevens B. Microglia Function During Brain Development: New Insights From Animal Models. *Brain Res* (2015) 1617:7–17. doi: 10.1016/j.brainres.2014.11.032
4. Tremblay M, Zettel ML, Ison JR, Allen PD, Majewska AK. Effects of Aging and Sensory Loss on Glial Cells in Mouse Visual and Auditory Cortices. *Glia* (2012) 60:541–58. doi: 10.1002/glia.22287
5. Wolf SA, Boddeke HWGM, Kettenmann H. Microglia in Physiology and Disease. *Annu Rev Physiol* (2016) 79:619–43. doi: 10.1146/annurev-physiol-022516-034406
6. Colonna M, Butovsky O. Microglia Function in the Central Nervous System During Health and Neurodegeneration. *Annu Rev Immunol* (2016) 35:1–28. doi: 10.1146/annurev-immunol-051116-052358
7. Chan A, Magnus T, Gold R. Phagocytosis of Apoptotic Inflammatory Cells by Microglia and Modulation by Different Cytokines: Mechanism for Removal of Apoptotic Cells in the Inflamed Nervous System. *Glia* (2001) 33:87–95. doi: 10.1002/1098-1136(20010101)33:1<87::aid-glia1008>3.0.co;2-s
8. Nimmerjahn A, Kirchhoff F, Helmchen F. Resting Microglial Cells Are Highly Dynamic Surveillants of Brain Parenchyma In Vivo. *Science* (2005) 308:1314–8. doi: 10.1126/science.1110647
9. Galatro TF, Holtman IR, Lerario AM, Vainchtein ID, Brouwer N, Sola PR, et al. Transcriptomic Analysis of Purified Human Cortical Microglia Reveals Age-Associated Changes. *Nat Neurosci* (2017) 20:1162–71. doi: 10.1038/nn.4597
10. Hefendehl JK, Neher JJ, Sühs RB, Kohsaka S, Skodras A, Jucker M. Homeostatic and Injury-Induced Microglia Behavior in the Aging Brain. *Aging Cell* (2014) 13:60–9. doi: 10.1111/acel.12149
11. Grabert K, Michoel T, Karavolos MH, Clohisey S, Baillie JK, Stevens MP, et al. Microglial Brain Region–Dependent Diversity and Selective Regional Sensitivities to Aging. *Nat Neurosci* (2016) 19:504–16. doi: 10.1038/nn.4222
12. Sierra A, Gottfried-Blackmore AC, McEwen BS, Bulloch K. Microglia Derived From Aging Mice Exhibit an Altered Inflammatory Profile. *Glia* (2007) 55:412–24. doi: 10.1002/glia.20468
13. Safaiyan S, Kannaiyan N, Snaidero N, Brioschi S, Biber K, Yona S, et al. Age-Related Myelin Degradation Burdens the Clearance Function of Microglia During Aging. *Nat Neurosci* (2016) 19:995–8. doi: 10.1038/nn.4325
14. Hou Y, Dan X, Babbar M, Wei Y, Hasselbalch SG, Croteau DL, et al. Ageing as a Risk Factor for Neurodegenerative Disease. *Nat Rev Neurol* (2019) 15:565–81. doi: 10.1038/s41582-019-0244-7
15. Pluvinage JV, Haney MS, Smith BAH, Sun J, Iram T, Bonanno L, et al. CD22 Blockade Restores Homeostatic Microglial Phagocytosis in Ageing Brains. *Nature* (2019) 568:187–92. doi: 10.1038/s41586-019-1088-4

16. Müller J, Nitschke L. The Role of CD22 and Siglec-G in B-cell Tolerance and Autoimmune Disease. *Nat Rev Rheumatol* (2014) 10:422–8. doi: 10.1038/nrrheum.2014.54
17. Bohlen CJ, Bennett FC, Tucker AF, Collins HY, Mulinyawe SB, Barres BA. Diverse Requirements for Microglial Survival, Specification, and Function Revealed by Defined-Medium Cultures. *Neuron* (2017) 94:759–73.e8. doi: 10.1016/j.neuron.2017.04.043
18. Sierra A, Paolicelli RC, Kettenmann H. Cien Años De Microglía: Milestones in a Century of Microglial Research. *Trends Neurosci* (2019) 42:778–92. doi: 10.1016/j.tins.2019.09.004
19. Jung S, Aliberti J, Graemmel P, Sunshine MJ, Kreutzberg GW, Sher A, et al. Analysis of Fractalkine Receptor CX3CR1 Function by Targeted Deletion and Green Fluorescent Protein Reporter Gene Insertion. *Mol Cell Biol* (2000) 20:4106–14. doi: 10.1128/mcb.20.11.4106-4114.2000
20. Ozmen L, Albientz A, Czech C, Jacobsen H. Expression of Transgenic APP Mrna Is the Key Determinant for Beta-Amyloid Deposition in PS2APP Transgenic Mice. *Neurodegener Dis* (2008) 6:29–36. doi: 10.1159/000170884
21. Nissen JC. Microglial Function Across the Spectrum of Age and Gender. *Int J Mol Sci* (2017) 18:561. doi: 10.3390/ijms18030561
22. Villa A, Torre SD, Maggi A. Sexual Differentiation of Microglia. *Front Neuroendocrin* (2018) 52:156–64. doi: 10.1016/j.yfrne.2018.11.003
23. Thevenaz P, Ruttimann UE, Unser M. A Pyramid Approach to Subpixel Registration Based on Intensity. *IEEE T Image Process* (1998) 7:27–41. doi: 10.1109/83.650848
24. Klunk WE, Bacskai BJ, Mathis CA, Kajdasz ST, McLellan ME, Frosch MP, et al. Imaging Aβ Plaques in Living Transgenic Mice With Multiphoton Microscopy and Methoxy-X04, a Systemically Administered Congo Red Derivative. *J Neuropathol Exp Neurol* (2002) 61:797–805. doi: 10.1093/jnen/61.9.797
25. Gutbier S, Wanke F, Dahm N, Rümmelin A, Zimmermann S, Christensen K, et al. Large-Scale Production of Human iPSC-Derived Macrophages for Drug Screening. *Int J Mol Sci* (2020) 21:4808. doi: 10.3390/ijms21134808
26. Wilgenburg BV, Browne C, Vowles J, Cowley SA. Efficient, Long Term Production of Monocyte-Derived Macrophages From Human Pluripotent Stem Cells Under Partly-Defined and Fully-Defined Conditions. *PloS One* (2013) 8:e71098. doi: 10.1371/journal.pone.0071098
27. Reich M, Paris I, Ebeling M, Dahm N, Schweitzer C, Reinhardt D, et al. Alzheimer's Risk Gene TREM2 Determines Functional Properties of New Type of Human iPSC-Derived Microglia. *Front Immunol* (2021) 11:617860. doi: 10.3389/fimmu.2020.617860
28. Zhang JD, Schindler T, Küng E, Ebeling M, Certa U. Highly Sensitive Amplicon-Based Transcript Quantification by Semiconductor Sequencing. *BMC Genomics* (2014) 15:565. doi: 10.1186/1471-2164-15-565
29. Drawnel FM, Zhang JD, Küng E, Aoyama N, Benmansour F, Rosario AAD, et al. Molecular Phenotyping Combines Molecular Information, Biological Relevance, and Patient Data to Improve Productivity of Early Drug Discovery. *Cell Chem Biol* (2017) 24:624–34.e3. doi: 10.1016/j.chembiol.2017.03.016
30. Zhang JD, Küng E, Boess F, Certa U, Ebeling M. Pathway Reporter Genes Define Molecular Phenotypes of Human Cells. *BMC Genomics* (2015) 16:342. doi: 10.1186/s12864-015-1532-2
31. Langmead B, Salzberg SL. Fast Gapped-Read Alignment With Bowtie 2. *Nat Methods* (2012) 9:357–9. doi: 10.1038/nmeth.1923
32. Wu D, Smyth GK. Camera: A Competitive Gene Set Test Accounting for Inter-Gene Correlation. *Nucleic Acids Res* (2012) 40:e133–3. doi: 10.1093/nar/gks461
33. Friedman BA, Srinivasan K, Ayalon G, Meilandt WJ, Lin H, Huntley MA, et al. Diverse Brain Myeloid Expression Profiles Reveal Distinct Microglial Activation States and Aspects of Alzheimer's Disease Not Evident in Mouse Models. *Cell Rep* (2018) 22:832–47. doi: 10.1016/j.celrep.2017.12.066
34. Keren-Shaul H, Spinrad A, Weiner A, Matcovitch-Natan O, Dvir-Szternfeld R, Ulland TK, et al. A Unique Microglia Type Associated With Restricting Development of Alzheimer's Disease. *Cell* (2017) 169:1276–90.e17. doi: 10.1016/j.cell.2017.05.018
35. Heneka MT, Kummer MP, Stutz A, Delekate A, Schwartz S, Vieira-Saecker A, et al. NLRP3 Is Activated in Alzheimer's Disease and Contributes to Pathology in APP/PS1 Mice. *Nature* (2013) 493:674–8. doi: 10.1038/nature11729
36. Fontainhas AM, Wang M, Liang KJ, Chen S, Mettu P, Damani M, et al. Microglial Morphology and Dynamic Behavior Is Regulated by Ionotropic Glutamatergic and GABAergic Neurotransmission. *PloS One* (2011) 6:e15973. doi: 10.1371/journal.pone.0015973
37. Liu YU, Ying Y, Li Y, Eyo UB, Chen T, Zheng J, et al. Neuronal Network Activity Controls Microglial Process Surveillance in Awake Mice *Via* Norepinephrine Signaling. *Nat Neurosci* (2019) 22:1771–81. doi: 10.1038/s41593-019-0511-3
38. Samardzic T, Marinkovic D, Danzer C, Gerlach J, Nitschke L, Wirth T. Reduction of Marginal Zone B Cells in CD22-Deficient Mice. *Eur J Immunol* (2002) 32:561–7. doi: 10.1002/1521-4141(200202)32:2<561::aid-immu561>3.0.co;2-h
39. Bolmont T, Haiss F, Eicke D, Radde R, Mathis CA, Klunk WE, et al. Dynamics of the Microglial/Amyloid Interaction Indicate a Role in Plaque Maintenance. *J Neurosci* (2008) 28:4283–92. doi: 10.1523/jneurosci.4814-07.2008
40. Zöller T, Schneider A, Kleimeyer C, Masuda T, Potru PS, Pfeifer D, et al. Silencing of TGFβ Signalling in Microglia Results in Impaired Homeostasis. *Nat Commun* (2018) 9:4011. doi: 10.1038/s41467-018-06224-y
41. Streit WJ, Sammons NW, Kuhns AJ, Sparks DL. Dystrophic Microglia in the Aging Human Brain. *Glia* (2004) 45:208–12. doi: 10.1002/glia.10319
42. Damani MR, Zhao L, Fontainhas AM, Amaral J, Fariss RN, Wong WT. Age-Related Alterations in the Dynamic Behavior of Microglia. *Aging Cell* (2011) 10:263–76. doi: 10.1111/j.1474-9726.2010.00660.x
43. Almanzar N, Antony J, Baghel AS, Bakerman I, Bansal I, Barres BA, et al. A Single-Cell Transcriptomic Atlas Characterizes Ageing Tissues in the Mouse. *Nature* (2020) 583:590–5. doi: 10.1038/s41586-020-2496-1
44. Naj AC, Jun G, Beecham GW, Wang L-S, Vardarajan BN, Buros J, et al. Common Variants at MS4A4/MS4A6E, CD2AP, CD33 and EPHA1 Are Associated With Late-Onset Alzheimer's Disease. *Nat Genet* (2011) 43:436–41. doi: 10.1038/ng.801
45. Initiative TADN, Bradshaw EM, Chibnik LB, Keenan BT, Ottoboni L, Raj T, et al. CD33 Alzheimer's Disease Locus: Altered Monocyte Function and Amyloid Biology. *Nat Neurosci* (2013) 16:848–50. doi: 10.1038/nn.3435
46. Griciuc A, Serrano-Pozo A, Parrado AR, Lesinski AN, Asselin CN, Mullin K, et al. Alzheimer's Disease Risk Gene CD33 Inhibits Microglial Uptake of Amyloid Beta. *Neuron* (2013) 78:631–43. doi: 10.1016/j.neuron.2013.04.014
47. (ADGC), ADGC, (EADI), TEADI, (CHARGE), C for H and AR in GEC, (GERAD/PERADES), G and ER in AG Polygenic and Environmental Risk for Alzheimer's Disease Consortium, Kunkle BW, Grenier-Boley B, Sims R, Bis JC, Damotte V, et al. Genetic Meta-Analysis of Diagnosed Alzheimer's Disease Identifies New Risk Loci and Implicates Aβ, Tau, Immunity and Lipid Processing. *Nat Genet* (2019) 51:414–30. doi: 10.1038/s41588-019-0358-2
48. Mrdjen D, Pavlovic A, Hartmann FJ, Schreiner B, Utz SG, Leung BP, et al. High-Dimensional Single-Cell Mapping of Central Nervous System Immune Cells Reveals Distinct Myeloid Subsets in Health, Aging, and Disease. *Immunity* (2018) 48:380–95.e6. doi: 10.1016/j.immuni.2018.01.011
49. Zhou Y, Song WM, Andhey PS, Swain A, Levy T, Miller KR, et al. Human and Mouse Single-Nucleus Transcriptomics Reveal TREM2-Dependent and TREM2-independent Cellular Responses in Alzheimer's Disease. *Nat Med* (2020) 26:131–42. doi: 10.1038/s41591-019-0695-9
50. Clark EA, Giltiay NV. CD22: A Regulator of Innate and Adaptive B Cell Responses and Autoimmunity. *Front Immunol* (2018) 9:2235. doi: 10.3389/fimmu.2018.02235
51. Linnartz B, Wang Y, Neumann H. Microglial Immunoreceptor Tyrosine-Based Activation and Inhibition Motif Signaling in Neuroinflammation. *Int J Alzheimer's Dis* (2010) 2010:587463. doi: 10.4061/2010/587463
52. Kleinberger G, Yamanishi Y, Suárez-Calvet M, Czirr E, Lohmann E, Cuyvers E, et al. TREM2 Mutations Implicated in Neurodegeneration Impair Cell Surface Transport and Phagocytosis. *Sci Transl Med* (2014) 6:243ra86–243ra86. doi: 10.1126/scitranslmed.3009093
53. Chong ZZ, Maiese K. The Src Homology 2 Domain Tyrosine Phosphatases SHP-1 and SHP-2: Diversified Control of Cell Growth, Inflammation, and Injury. *Histol Histopathol* (2007) 22:1251–67. doi: 10.14670/hh-22.1251
54. Choi YR, Kang S-J, Kim J-M, Lee S-J, Jou I, Joe E-H, et al. FcγRIIB Mediates the Inhibitory Effect of Aggregated α-Synuclein on Microglial Phagocytosis. *Neurobiol Dis* (2015) 83:90–9. doi: 10.1016/j.nbd.2015.08.025
55. Zhang L, Xia Y, Li W, Sun Y, Kong L, Xu P, et al. Activation of Fc Gamma Receptor IIb Up-Regulates the Production of Interferon-Alpha and

Interferon-Gamma in Porcine Alveolar Macrophages During PRRSV Infection. *Dev Comp Immunol* (2020) 109:103696. doi: 10.1007/s13238-017-0473-8

56. Wang X, Mathieu M, Brezski RJ. IgG Fc engineering to modulate antibody effector functions. *Protein Cell* (2018) 9:63–73. doi: 10.1007/s13238-017-0473-8
57. Taracha A, Kotarba G, Wilanowski T. Neglected Functions of TFCP2/TFCP2L1/UBP1 Transcription Factors may Offer Valuable Insights Into Their Mechanisms of Action. *Int J Mol Sci* (2018) 19:2852. doi: 10.3390/ijms19102852
58. Butovsky O, Jedrychowski MP, Moore CS, Cialic R, Lanser AJ, Gabriely G, et al. Identification of a Unique TGF-β–Dependent Molecular and Functional Signature in Microglia. *Nat Neurosci* (2014) 17:131–43. doi: 10.1038/nn.3599
59. Spittau B, Dokalis N, Prinz M. The Role of TGFβ Signaling in Microglia Maturation and Activation. *Trends Immunol* (2020) 41:836–48. doi: 10.1016/j.it.2020.07.003

Conflict of Interest: During the course of this study, all authors are or were full time employees or trainees at Roche and they may additionally hold Roche stock/stock options.

The reviewer DE declared a shared affiliation with one of the authors VA to the handling editor at the time of the review.

Advantages of publishing in Frontiers

OPEN ACCESS
Articles are free to read for greatest visibility and readership

FAST PUBLICATION
Around 90 days from submission to decision

HIGH QUALITY PEER-REVIEW
Rigorous, collaborative, and constructive peer-review

TRANSPARENT PEER-REVIEW
Editors and reviewers acknowledged by name on published articles

Frontiers
Avenue du Tribunal-Fédéral 34
1005 Lausanne | Switzerland

Visit us: www.frontiersin.org
Contact us: frontiersin.org/about/contact

REPRODUCIBILITY OF RESEARCH
Support open data and methods to enhance research reproducibility

DIGITAL PUBLISHING
Articles designed for optimal readership across devices

FOLLOW US
@frontiersin

IMPACT METRICS
Advanced article metrics track visibility across digital media

EXTENSIVE PROMOTION
Marketing and promotion of impactful research

LOOP RESEARCH NETWORK
Our network increases your article's readership